Circulating disease-specific CD8 T cells in Merkel cell carcinoma and COVID-19: Prognostic significance and improved approaches for their detection

Saumya Jani

A dissertation
submitted in partial fulfillment of the
requirements for the degree of

Doctor of Philosophy

University of Washington

2024

Reading Committee:
Paul Nghiem, Chair
Evan Newell
Phil Bradley

Program authorized to offer degree:
Molecular Medicine and Mechanisms of Disease

University of Washington

Abstract

Circulating disease-specific CD8 T cells in Merkel cell carcinoma and COVID-19: Prognostic significance and improved approaches for their detection

Saumya Jani

Chair of the Supervisory Committee:
Paul Nghiem
Department of Dermatology

Immune checkpoint inhibition (ICI) that targets the programmed death-1 (PD-1) pathway has made great strides in improving cancer patient outcomes and is the most successful immunotherapy to date, but only a subset of treated patients benefits. Predicting which patients are likely to respond to ICI and understanding the underlying mechanisms are of critical importance to prioritize patients for alternate or synergistic therapies and to avoid toxicities in patients who would not benefit. Because PD-1 pathway blockade targets T cells, it is feasible that patient-specific T cell characteristics could serve as predictive biomarkers of response. However, few studies can directly assess the numerically lower, but more functionally relevant population of cancer-specific T cells. This is because most cancers arise due to unique patient-specific mutations, which makes it extremely difficult to identify infrequent cancer-specific T cells. However, 80% of Merkel cell carcinoma (MCC) cases are virally-driven, persistently express conserved Merkel cell polyomavirus (MCPyV) oncoproteins, and have extraordinarily few amino acid-coding tumor mutations. This allows us to have a common set of target antigens that can be used to study MCPyV-specific T cells and gain insights that can be extended to other cancers.

In **chapter 1**, we review limitations encountered in studying tumor-specific CD8 T cells, propose virus-driven MCC as a model tumor, summarize current knowledge of mechanisms of response and resistance to ICI.

In **chapter 2**, we find that baseline abundance of MCPyV-specific CD8 T cells in blood can predict ICI response in two different clinical trials. However, this does not seem to be the case for intratumoral tumor-specific CD8 T cells. This difference may be attributable to our observation that tumor-specific CD8 T cells in the blood are less dysfunctional than their intratumoral counterparts. In **chapter 3**, we confirm our finding that baseline frequency of MCPyV-specific CD8 T cells associates with response to ICI in an independent patient cohort. And we additionally find that the frequency of $CD39^{+}CLA^{+}$ CD8 T cells can predict response to ICI.

However, current methods to quantify cancer-specific T cells require freshly acquired (non-archival) tissue, labile expensive custom reagents (peptide-HLA tetramers), and significant technical expertise, and are therefore not well suited for routine clinical care. Thus, in **chapters 4 and 5**, we explore methods to identify cancer-specific CD8 T cells more easily. In **chapter 4**, we characterize MCPyV-specific CD8 T cells in blood and identify a set of 98 genes that are enriched in these cells compared to other T cells. We find that this gene set can accurately identify tumor-specific CD8 T cells in both MCC and various mutationally-driven cancers. In **chapter 5**, we explore the feasibility of generating a library of T cell receptors (TCR) specific to MCPyV oncoproteins and using this library in combination with existing TCR similarity algorithms to identify cancer-specific CD8 T cells.

Given that significantly more TCR sequences were publicly available from patients with COVID infection than MCC, we tested the ability of TCR similarity algorithms to identify SARS-

CoV-2-specific CD8 T cells in COVID vaccine recipients in **chapters 6 and 7**. In **chapter 6**, we compared the phenotype and repertoire of SARS-CoV-2 specific CD8 T cells from the breastmilk and blood of lactating individuals who received a spike-specific mRNA vaccination post-delivery. We used a TCR similarity algorithm, tcrdist3, to identify novel potential SARS-CoV-2-specific CD8 T cells. In **chapter 7**, we used tcrdist3 to track the frequency of SARS-CoV-2-specific CD8 T cells in longitudinal blood samples from patients with a history of COVID infection, who subsequently received SARS-CoV-2 vaccines. We observed large expansions in response to vaccination and identified novel, functionally-proven SARS-CoV-2-specific CD8 T cells. Being able to accurately track and identify novel COVID-specific CD8 T cells with TCR similarity metrics in these studies increases our confidence in using similar methods for identifying cancer-specific CD8 T cells and justify efforts to create libraries of TCRs that target common oncogenic viruses and mutations.

Finally, in **chapter 8**, we investigate a case of secondary resistance to ICI, despite an abundance of tumor-specific CD8 T cells. We demonstrate that this patient’s tumor lacked HLA-I expression, preventing anti-tumor CD8 T cells from recognizing the tumor cells. Treatment with an intralesional stimulator of interferon genes (STING) agonist partially restored HLA-I expression via induction of an inflammatory tumor microenvironment, allowing to patient to experience an abscopal, partial response.

The studies detailed in chapters 2, 3, and 8 have made key advances in identifying mechanisms of response and resistance to PD-(L)1 pathway blockade in Merkel cell carcinoma. Additionally, the studies detailed in chapters 4, 5, 6, and 7 have made important advances in translating the identified mechanisms to more common, mutationally-driven cancers via gene expression profiling and bulk T cell receptor sequencing. We believe that use of these methods will translate to improving outcomes for all patients with cancer.

Acknowledgments

First and foremost, I would like to express my deepest gratitude to my advisor, Dr. Paul Nghiem, for his tireless support and guidance throughout my PhD. From framing every discussion about a new project with “How will this help patients?” to the very rewarding annual dinner with patients and their families, I could not have had a better physician-scientist role model. Thank you for fostering my passion for clear science communication and for giving me a seat at many tables that graduate students are typically not afforded (e.g., meetings with grant program officers, all communications with journal editors, and collaborations with pharmaceutical companies).

I am also extremely grateful to my committee members for their critical advice and direction: Dr. David Koelle for reading many drafts of my grant applications, developing reagents needed to identify antigen-specific CD8 T cells, and countless discussions about T cell receptors; Dr. Evan Newell for welcoming me into his lab, making sure I received the bioinformatics help I needed, and for freely sharing his wealth of knowledge about T cell phenotypes; Dr. Phil Bradley for facilitating my learning of T cell receptor similarity algorithms and timely help de-bugging code; Dr. Whitney Harrington for allowing me to participate in your projects, helping me think about how my work could extend to the immunology of pregnancy, and fostering my interest in maternal health; and to Dr. Michael Gerner for sharing his vast knowledge of immunology from recommending courses to take to deepen my knowledge base to sharing analogous and informative mouse studies.

I am also deeply indebted to Thomas Pulliam for teaching me everything I needed to know about single-cell RNA sequencing (from wet lab methods to data analysis pipelines) and T cell exhaustion. I have really appreciated how freely you shared your time – your repeated offers to help ensured that I never hesitated to ask when I had a question, and this is something I hope to emulate.

Many thanks to Tomas Bencomo for being patient with me as I learned how to be a mentor and for your excellent scientific judgement. I really appreciate your enthusiasm and willingness to help wherever you can.

I would also like to thank my colleagues in the Nghiem lab and collaborators at the Fred Hutch Cancer Center and the German Cancer Research Center, especially: Dr. Candice Church for reading the very first drafts of my writing, listening to the first iterations of my presentations, and all the moral support; Dr. Koshlan Mayer-Blackwell for writing critical code for me as I learned how to use TCRdist and for sharing your advice on how to learn how to code; Dr. Carolyn Shasha for verifying numerous of my single-cell analyses and for your critical insights on merging datasets and calculate gene set enrichment scores; and Dr. Jürgen Becker for your crucial feedback and for your willingness to share data and experiences of what worked and, importantly, what did not work.

Special thanks to past and present members of University of Washington's Engage group for building and teaching an excellent course in the basics of science communication, especially the class of Winter 2022 and Kevin Bishop for being our fearless leader. By engaging with different disciplines – acting, improv, graphic design, journalism – I learned so much about how to communicate science more effectively to a lay audience, and discovering this community has been one of the greatest joys of my PhD career. Thank you for learning and growing with me.

This work would not have been possible without patients who participated in clinical trials and donated their blood and tumor samples to us. I am also grateful to our funding sources, particularly the Interdisciplinary Training in Cancer Research program for my T32 fellowship and our philanthropic supporters.

I would also like to offer special thanks to my family – parents, Kajal and Kandarp; aunt, Kanal; and brother, Digvijay – for never letting me believe there was anything I could not do. Your encouragement, support, and love mean everything to me.

To Gladys and Gertrude, my feline friends, I do not know what I would do without you screaming at me and walking over my computer every day. Many days have been made by your persistent presence at all my Zoom meetings and your well-intentioned, but misguided, attempts to help me write.

Many thanks to my friends for the numerous vacations, game nights, and food adventures that have prevented me from burning out and allowed me to keep thinking about science at my best.

And finally, thank you to my Flight Room community for being one of the best parts of my day. You have all made it so easy for me to work towards my goal of preventing osteoporosis with your fun and welcoming personalities. I have cherished our adventures outsides of the aerial studio as well and am so grateful for the friendships we have developed.

Table of Contents

Appendix

*Equal contributors

Chapter 1: Insights into anti-tumor immunity via the polyomavirus shared across human Merkel cell carcinomas

Saumya Jani*, Candice Church*, Paul Nghiem

Frontiers in Immunology, May 2023

CHAPTER SUMMARY: In this chapter, we introduce Merkel cell carcinoma (MCC), the role of Merkel cell polyomavirus (MCPyV) in oncogenesis, and PD-1 pathway blockade as a pillar of cancer treatment. We then summarize the knowledge gained by studying T cells that target MCPyV oncoproteins, in addition to describing mechanisms of immunotherapy response and resistance gleaned from other cancers. Finally, we identify current gaps in knowledge and propose ways virus-driven MCC may be used as a model cancer to fill in those gaps.

Frontiers in Immunology

TYPE Review
PUBLISHED 23 May 2023
DOI 10.3389/fimmu.2023.1172913

OPEN ACCESS

EDITED BY
Vandana Kalia,
University of Washington, United States

REVIEWED BY
Kyra Zens,
University of Zurich, Switzerland
Claude-Agnes Reynaud,
INSERM U1151 Institut Necker Enfants Malades, France

*CORRESPONDENCE
Candice D. Church
✉ cdchurch@uw.edu

[†]These authors have contributed equally to this work and share first authorship

RECEIVED 24 February 2023
ACCEPTED 27 April 2023
PUBLISHED 23 May 2023

CITATION
Jani S, Church CD and Nghiem P (2023) Insights into anti-tumor immunity *via* the polyomavirus shared across human Merkel cell carcinomas. *Front. Immunol.* 14:1172913. doi: 10.3389/fimmu.2023.1172913

Insights into anti-tumor immunity *via* the polyomavirus shared across human Merkel cell carcinomas

Saumya Jani[1†], Candice D. Church[1*†] and Paul Nghiem[1,2]

[1]Department of Medicine, University of Washington, Seattle, WA, United States, [2]Fred Hutchinson Cancer Center, Seattle, WA, United States

Understanding and augmenting cancer-specific immunity is impeded by the fact that most tumors are driven by patient-specific mutations that encode unique antigenic epitopes. The shared antigens in virus-driven tumors can help overcome this limitation. Merkel cell carcinoma (MCC) is a particularly interesting tumor immunity model because (1) 80% of cases are driven by Merkel cell polyomavirus (MCPyV) oncoproteins that must be continually expressed for tumor survival; (2) MCPyV oncoproteins are only ~400 amino acids in length and are essentially invariant between tumors; (3) MCPyV-specific T cell responses are robust and strongly linked to patient outcomes; (4) anti-MCPyV antibodies reliably increase with MCC recurrence, forming the basis of a standard clinical surveillance test; and (5) MCC has one of the highest response rates to PD-1 pathway blockade among all solid cancers. Leveraging these well-defined viral oncoproteins, a set of tools that includes over 20 peptide-MHC class I tetramers has been developed to facilitate the study of anti-tumor immunity across MCC patients. Additionally, the highly immunogenic nature of MCPyV oncoproteins forces MCC tumors to develop robust immune evasion mechanisms to survive. Indeed, several immune evasion mechanisms are active in MCC, including transcriptional downregulation of MHC expression by tumor cells and upregulation of inhibitory molecules including PD-L1 and immunosuppressive cytokines. About half of patients with advanced MCC do not persistently benefit from PD-1 pathway blockade. Herein, we (1) summarize the lessons learned from studying the anti-tumor T cell response to virus-positive MCC; (2) review immune evasion mechanisms in MCC; (3) review mechanisms of resistance to immune-based therapies in MCC and other cancers; and (4) discuss how recently developed tools can be used to address open questions in cancer immunotherapy. We believe detailed investigation of this model cancer will provide insight into tumor immunity that will likely also be applicable to more common cancers without shared tumor antigens.

KEYWORDS

Merkel cell carcinoma, Merkel cell polyomavirus, skin cancer, anti-tumor T cells, immunotherapy, oncoproteins

1 Introduction

It is well established that the ability of T cells to target tumor cells is central to controlling and eliminating cancer (1). In contrast, details of the relative roles of cancer-specific lymphocytes and innate immune cells in the short- and long-term control of cancer is highly complex and not fully understood. Cancer immunotherapy has dramatically transitioned in the past decade from an understudied, empiric field to a dominant and mainstream scientific discipline. Nevertheless, enormous challenges remain. A major roadblock to improved understanding of cancer immunology is an inability to readily identify cancer-specific T cells due to the "private" (patient specific) nature of most tumor antigens. Personalized mutations and unique neoantigens expressed by most tumors require custom reagents for each tumor to study cancer-specific T cells between patients, making this process tedious and not readily amenable to studying a larger cohort of patients.

We propose that Merkel cell carcinoma (MCC) is a model cancer in which to study T cell and B cell responses because of the shared, highly immunogenic oncoproteins that drive this cancer. MCC is a rare but aggressive cutaneous neuroendocrine carcinoma with an incidence of about 3,200 new cases per year in the US (2). Initial observations that HIV+ patients had a >10-fold increased risk of MCC, suggested that this was an immune sensitive cancer and might be driven by a pathogen (3–5). In 2008, the Pittsburgh-based laboratory of Patrick Moore and Yuan Chang made the landmark discovery of a novel human DNA polyomavirus that was clonally integrated into a chromosome of the host (tumor) cell (6).

Merkel cell polyomavirus (MCPyV) is one of about a dozen human polyomaviruses, all of which show evidence of largely asymptomatic infection of more than half of healthy persons by adulthood (7). Accordingly, the majority of MCC cases (70-80%) are driven by MCPyV oncoproteins (8, 9). Of note, MCPyV is highly conserved across individuals, with very minimal amino acid polymorphisms. This also holds true across MCC tumors, meaning there is minimal antigenic variability between patient tumors (10, 11). The remaining ~20% of MCCs are caused by extensive ultraviolet (UV)-induced mutations (median of 1121 protein-coding somatic single nucleotide variants per exome) resulting in numerous immunogenic neoantigens expressed by tumor cells (12–14). Strikingly, both MCPyV-driven and UV-driven MCCs have a high (~50%) response rate to anti-PD-(L)1 therapies, suggesting that both etiologies are immunogenic in nature (15–17). The fact that two very distinct processes (UV-mutational and virus-induced) can lead to a histologically identical, aggressive, fast growing, immune-sensitive tumor provides numerous opportunities for insight into cancer immunobiology.

Several lines of evidence have demonstrated that expression of small and large T antigens of MCPyV is necessary in an ongoing way for virus-driven MCC growth and survival, essentially rendering the tumor cells "addicted" to these oncoproteins, which can therefore not be lost (18). This unique situation provides several advantages relevant to cancer immunobiology. Like any tumor antigen, viral oncoproteins are processed into peptides that are then presented by major histocompatibility complexes (MHCs) on the surface of tumor cells. These MHC-peptide complexes are in turn recognized by cancer-specific T cells. The fact that MCPyV oncoproteins are shared between patients allows for development of a suite of reagents that can identify tumor-specific immune responses among an entire cohort. Because the immune response can be studied across multiple patients, data gathered in virus-driven MCC can be linked to the patients' clinical outcomes and the relative significance of various immune-associated characteristics of interest can be determined.

Herein, we describe insights gleaned from virus-driven MCC by comparing the tumor microenvironments (TME) and T cell characteristics of patients who experience different outcomes. We will also review immune evasion and immunotherapy resistance mechanisms in MCC and solid tumors more broadly, as well as explore new therapeutic opportunities. Finally, we will discuss recent and anticipated technologies that help address open questions in cancer immunology.

2 Study of virus-driven MCC overcomes typical limitations imposed by private tumor antigens

Most cancers are driven by patient-specific mutations, and the resulting neoantigens are unique to each patient and vary in immunogenicity. While neoantigens can be rapidly identified by current whole exome sequencing (WES) and bioinformatic tools, extending this to create and validate tools (peptide-MHC tetramers, described below) that identify T cells that can recognize these neoantigens remains cumbersome and logistically infeasible. This is relevant as most predicted peptides are not immunogenic and do not identify cancer-specific T cells, requiring screening of large amounts of epitopes to identify T cells (19, 20). Additionally, the unpredictable and varied levels of immunogenicity prevent comparisons of cancer-specific T cells across patients. To avoid the complications related to personalized tetramer-based identification of cancer-specific T cells, approaches involving response to *in vitro* stimulation and expression of activation markers have been developed (21, 22). While identification of cells with such activation markers is relatively easy, they are not limited to tumor antigens, resulting in capture of activated bystander T cells within the target population. Together, the inability to reliably identify tumor neoantigen-specific T cells between patients prevents the use of high-throughput or bulk approaches that would be feasible for clinical use.

MCC, on the other hand, is driven by MCPyV in 80% of cases and has an exceptionally low tumor mutational burden (TMB) (23). This means that MCPyV oncoproteins are largely responsible for driving tumorigenesis and most cancer-specific T cells recognize MCPyV oncoproteins. In addition, MCPyV oncoproteins are small (approximately 400 amino acids in length) and invariant between patients (Figure 1A). Careful annotation of the integrated sequence has allowed for functional studies that identified MHC-restricted epitopes (Figure 1B) (21). Initial characterization of MCPyV immunogenicity was accomplished by stimulating blood and

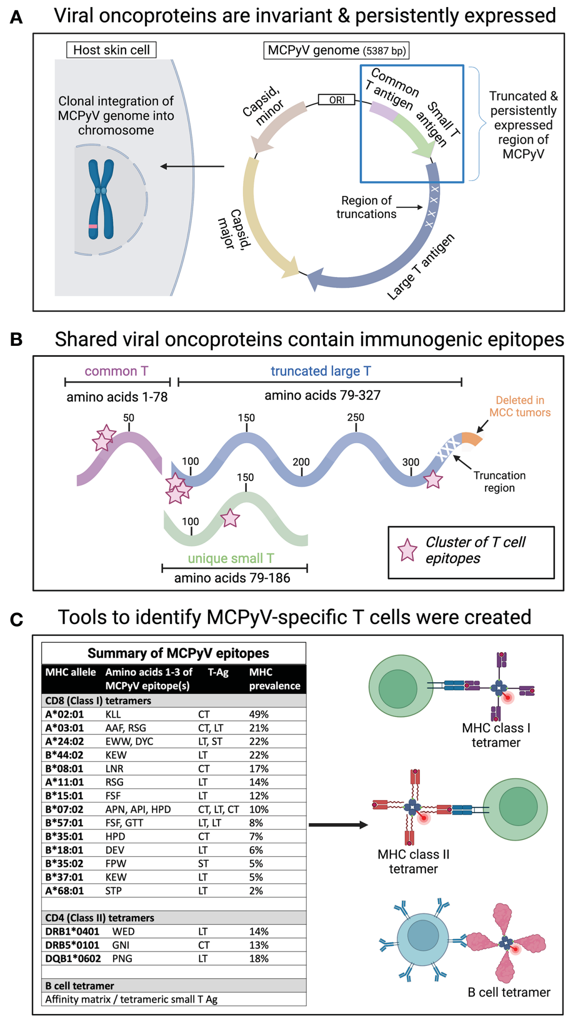

Summary of MCPyV epitopes

MHC allele	Amino acids 1-3 of MCPyV epitope(s)	T-Ag	MHC prevalence
CD8 (Class I) tetramers			
A*02:01	KLL	CT	49%
A*03:01	AAF, RSG	CT, LT	21%
A*24:02	EWW, DYC	LT, ST	22%
B*44:02	KEW	LT	22%
B*08:01	LNR	CT	17%
A*11:01	RSG	LT	14%
B*15:01	FSF	LT	12%
B*07:02	APN, API, HPD	CT, LT, CT	10%
B*57:01	FSF, GTT	LT, LT	8%
B*35:01	HPD	CT	7%
B*18:01	DEV	LT	6%
B*35:02	FPW	ST	5%
B*37:01	KEW	LT	5%
A*68:01	STP	LT	2%
CD4 (Class II) tetramers			
DRB1*0401	WED	LT	14%
DRB5*0101	GNI	CT	13%
DQB1*0602	PNG	LT	18%
B cell tetramer			
Affinity matrix / tetrameric small T Ag			

FIGURE 1
Virus-driven MCC is a unique model cancer for studying anti-tumor T cell responses. **(A)** Virus-driven MCC arises when MCPyV undergoes a truncation and integrates into the host genome. The integration site is thought to be random as it varies greatly among patients. Following the truncation and integration, two oncoproteins (large and small T antigens), which share a common region, are persistently expressed and drive tumorigenesis. **(B)** These viral oncoproteins are small (~400 amino acids), and this antigenic space has been rigorously studied to identify immunogenic peptides presented by common MHC types. The areas of immunogenicity are highlighted with pink stars. **(C)** Based on these functional studies, multimer tools to identify cancer-specific T and B cells have been developed and validated. The immunogenic peptides, the MHC molecules that can present them, the relevant oncoprotein region, and an approximation of the prevalence of these MHC molecules in patients with MCC are summarized in the table.

tumor samples from MCC patients with T antigen peptides. These studies revealed T cell responses to shared antigens across MCC patients. Based on these data, tetramer reagents were created. Tetramers consist of four MHC molecules containing a previously identified MCPyV peptide conjugated to a tetrameric streptavidin-biotin scaffold (Figure 1C). These molecules bind to MCPyV-specific T cells in a highly avid and sensitive manner and allow study of T cell responses across MCC patients in an efficient and reproducible way.

Tetramers offer additional advantages. By relying on T cell receptor (TCR) specificity, instead of functional readout to identify cancer-specific T cells, tetramers allow recognition of T cells that have lost cytotoxic capabilities due to chronic antigen stimulation. Indeed, in patients with a persistent or heavy disease burden, T cells are often identifiable with tetramers, but not through stimulation assays that measure interferon-gamma (IFN-γ) or interleukin-2 (IL-2) secretion as a means of detecting the presence of cancer-specific T cells (24). This is because cancer-specific T cells are often dysfunctional and incapable of expressing the activation markers or secreted effector cytokines used to detect them in such activation-based assays (24). Furthermore, they can be combined with other technologies to more deeply characterize cancer-specific T cells. Adding fluorophore-conjugated tetramers to flow cytometry panels has shown that tetramer-positive cells express higher levels of immune checkpoint markers such as programmed cell death protein 1 (PD-1) and T cell immunoglobulin and mucin domain (TIM-3), providing further evidence of dysfunction (25). Adding DNA barcode-conjugated tetramers facilitates identification of T cell specificity and links this data to single-cell sequencing-based approaches. This can allow us to characterize the epigenetic and transcriptional state of tumor-specific T cells (26–28). The next section summarizes what we have learned about the importance of cancer-specific T cells in MCC using these tools.

3 Lessons learned from tumor-specific lymphocytes in MCC

Given that the risk of MCC is often more than 10-fold higher in immune suppressed patients (while it is only ~2-fold higher than patients with malignant melanoma), the role of the immune system in responding to this cancer was of particular interest (29). In 2010, brisk infiltration of CD8+ T cells into MCC tumors was found to be predictive of improved MCC-specific survival, helping to explain the importance of tumor-specific immune responses for this cancer (30). However, it was not known whether the infiltrating T cells were capable of recognizing MCPyV oncoproteins. Once the viral sequence for MCPyV was described, investigation of patient blood and tumors demonstrated that T cells specific for the oncoproteins were present in MCC patients, but absent in corresponding specimens from healthy controls (31, 32). Furthermore, it has been observed that when tumors are effectively treated (surgically removed or fully respond to treatment) and the source of tumor antigens is no longer present, the number of MCPyV-specific T cells quickly drops (25). Considering that MCPyV-driven MCC has a low TMB (~12.5 mutations per exome versus 1,121 for UV-driven MCC), these data suggest that the relevant tumor antigens for the immune system to effectively target are indeed the viral antigens (12).

It is well established that chronic exposure to an antigen, and consequent activating signals, can cause T cells to become dysfunctional (33). Dysfunctional T cells can be identified by their expression of activation and exhaustion markers, including co-expression of PD-1, TIM-3 and others. When PD-1 on a T cell is engaged by its ligand, it significantly restrains the function of that cell. Consistent with this being a dominant immune evasion mechanism in MCC, oncoprotein-specific T cells in MCC patients often express PD-1. In over half of MCC tumors, programmed death-ligand 1 (PD-L1) is expressed by tumor cells and/or antigen presenting cells (25, 34). These data suggested that MCC tumors should be amenable to PD-1 pathway blockade therapies and provided a strong rationale for clinical trials to test this approach. Indeed, clinical trials of anti-PD-(L)1 as first-line treatment in MCC patients resulted in very high objective response rates of 56–62% (16, 17, 35). While many of these responses were durable, in the end, fewer than half of MCCs patients have persistent benefit from PD-1 pathway blockade. Because of the highly immunogenic nature of this cancer and its shared tumor antigens, this is an excellent opportunity to characterize the basis of primary and acquired resistance to immunotherapy.

3.1 Characteristics of tumor-infiltrating MCPyV oncoprotein-specific CD8 T cells linked to improved outcomes

To determine the link between MCPyV oncoprotein-specific CD8 T cells and clinical outcomes, T cells from patient tumors and blood were characterized, and differences between patients with divergent outcomes were assessed (36). Intratumoral T cell clones specific for a single MCPyV oncoprotein epitope (KLLEIAPNC) were tracked in a patient cohort by their unique complementarity determining region 3 sequences of the TCRβ chain (Figure 2A) (36). Frequency of T cell clones specific for this KLL epitope found within tumors was significantly greater in patients with extended survival compared to those with fewer clonotypes (36). Patients with >5 unique clonotypes had greater survival ($p = 0.0051$) and a higher chance of recurrence-free survival after definitive treatment than patients without diverse cancer-specific T cells (36). Additionally, patients who did not experience recurrences had more avid T cells (T cell clones that could respond well to low concentrations of peptide in a functional IFN-γ assay) compared to patients who experienced recurrence (36). Taken together, these data suggest that the presence of diverse, prevalent, and highly functional T cells that target tumor antigens are linked to improved patient outcomes. One approach to directly test the efficacy of these cancer-specific cells is being explored in a clinical trial of autologous, TCR-transgenic T cells that employ a highly avid A02-KLL-specific TCR (NCT03747484).

3.2 Links between peripheral blood circulating T cells and immune checkpoint inhibitor responses

A predictive biomarker for responsiveness to immunotherapy is needed to help determine the best therapeutic agents for a patient to experience long term control of their cancer. While expression of PD-L1 in the tumor, microsatellite instability (MSI) and TMB are used as predictive biomarkers of response to anti-PD-1 agents for various cancers, none have been shown to be clinically relevant for MCC (37). In a study of advanced MCC patients who received first-line pembrolizumab (NCT02267603), oncoprotein-specific CD8 T cells tracked with responsiveness wherein responders ($n = 13$) had more abundant cancer-specific T cells in blood at baseline compared to non-responders ($n = 4$) (38). Analogously, it was also reported that the presence of baseline circulating oncoprotein-specific CD8 T cells significantly correlated with progression-free survival in patients receiving neoadjuvant anti-PD-1 (NCT02488759) (Figure 2B) (39). Although both of these studies had a small number of available specimens and additional cohort(s) are needed to confirm these findings, both suggest improved outcomes for MCC patients who have more circulating oncoprotein-specific T cells at baseline. While it has long been appreciated that anti-tumor CD8 T cells are critical for control of cancer, these two studies are the first to show that MCC patients who have existing MCPyV oncoprotein-specific T cells at the start of therapy were more likely to respond. For patients who don't have circulating MCC-specific T cells prior to initiation of anti-PD-(L)1 therapies, adoptive cell therapies and therapeutic vaccines could be administered to increase the chances of a favorable response.

4 MCC requires multiple immune escape mechanisms at play

As discussed in the introduction, there are numerous lines of evidence that suggest that MCC is an immunogenic cancer, regardless of whether it was induced by MCPyV (viral epitopes) or UV exposure (neoantigens). This immunogenicity suggests that the immune system will detect the tumor at an early stage of development and deploy effective anti-tumor strategies, if robust immune evasion mechanisms are not employed. Indeed, individuals with a compromised or suppressed immune system are at a 10-50-fold greater risk of developing MCC, depending on the types and severity of immunosuppression (5, 40, 41). However, at least 90% of MCC cases arise in immune competent persons, suggesting that a vast majority of these tumors do have the capacity to evade an intact immune system. Indeed, MCC tumors have been observed to use one or more of these immune evasion approaches detailed below: (1) induce an immunosuppressive TME; (2) prevent T cell infiltration into the tumor; (3) inhibit tumor engagement with T cells; and (4) induce T cell dysfunction.

4.1 Immunosuppressive tumor microenvironment

Mechanisms by which MCC tumors induce an immunosuppressive microenvironment include suppression of innate immune danger signals and the presence of immune suppressive cells. Toll-like receptor 9 (TLR9) is an intracellular toll-like receptor that activates an inflammatory immune response upon recognizing foreign DNA, a potent danger signal to indicate a cell has been infected by a virus (42). MCPyV T antigens inhibit CCAAT/enhancer binding protein (C/EBP)

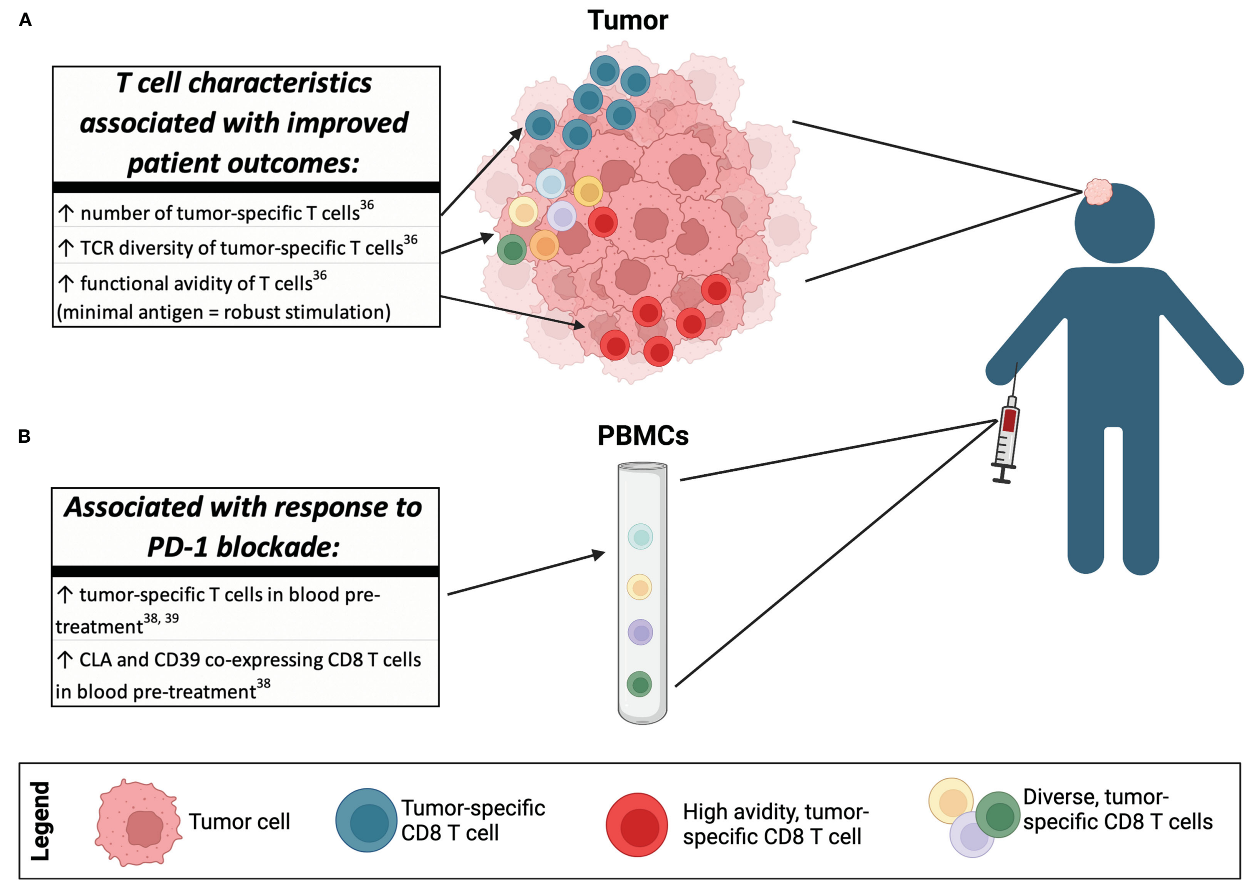

FIGURE 2
Insights into anti-tumor T cell responses gained by studying virus-driven MCC. Several lines of evidence have shown that virus-driven MCC is targetable by CD8 T cells and the presence of the MCPyV oncoprotein-specific T cells in patients can be linked to improved clinical outcomes. **(A)** Increased number of MCPyV oncoprotein-specific T cells, diverse T cell clonotypes that target MCPyV oncoprotein antigens, and CD8 T cells with high functional avidity found in the tumor are linked to improved patient outcomes in the absence of immunotherapy. **(B)** Circulating peripheral blood T cell characteristics that are associated with response to immunotherapy include the presence of MCPyV oncoprotein-specific CD8 T cells before initiation of anti-PD-1 therapy as assessed by MHC-peptide tetramer, and the presence of CD8 T cells that co-express CD39 and CLA before initiation of anti-PD-1 therapy.

transcription factor, which leads to downregulation of TLR9 (43). Indeed, a clinical study of cystic fibrosis patients demonstrated lower levels of TLR9 in patients harboring MCPyV (44). Thus, downregulation of TLR9 in MCC tumors could prevent recruitment of immune cells and may contribute to tumor survival. Additionally, the TME can induce immunosuppressive phenotypes in infiltrating immune cells, including macrophages and T regulatory cells.

While complex and controversial, macrophages can be grouped into two broad categories, M1 and M2. M1 macrophages are classically activated by IFN-γ or lipopolysaccharide (LPS) and secrete proinflammatory cytokines to protect against pathogens. M2 macrophages, on the other hand, are activated by exposure to other cytokines, including interleukin-4 (IL-4), interleukin-10 (IL-10), and transforming growth factor beta 1 (TGF-β1), and secrete immunosuppressive cytokines and factors that promote angiogenesis and tissue repair (45, 46). M2 macrophages are frequently found in MCC tumors and support tumor growth (46, 47). Furthermore, tumor cells and innate immune cells in the TME also secrete chemokines that recruit T regulatory cells (CCL17/22, CCL5, CCL28 and CXCL9/10/11), expand T regulatory cells (TGF-β, IL-10), and convert conventional T cells into T regulatory cells (TGF-β and adenosine) (48). These cells typically inactivate CD8 T cells and antigen-presenting cells to suppress an overactive immune response and prevent immune-mediated damage. While T regulatory cells are enriched in MCC tumors, their role in tumorigenesis and patient outcome is unclear, as there is no striking association between their presence and altered outcomes (47, 49).

4.2 Lack of T cell infiltration

In addition to creating an immunosuppressive environment, tumors can also employ strategies that prevent T cell infiltration (Figure 3B), such as downregulation of stimulator of interferon genes (STING) and E-selectin. MCC tumors silence STING, a molecule that senses DNA damage, activates a cytokine response, and recruits cancer-specific T cells to the TME. When STING expression was artificially restored in a human MCC cell line that was then co-cultured with MCPyV-specific T cells, the cancer-

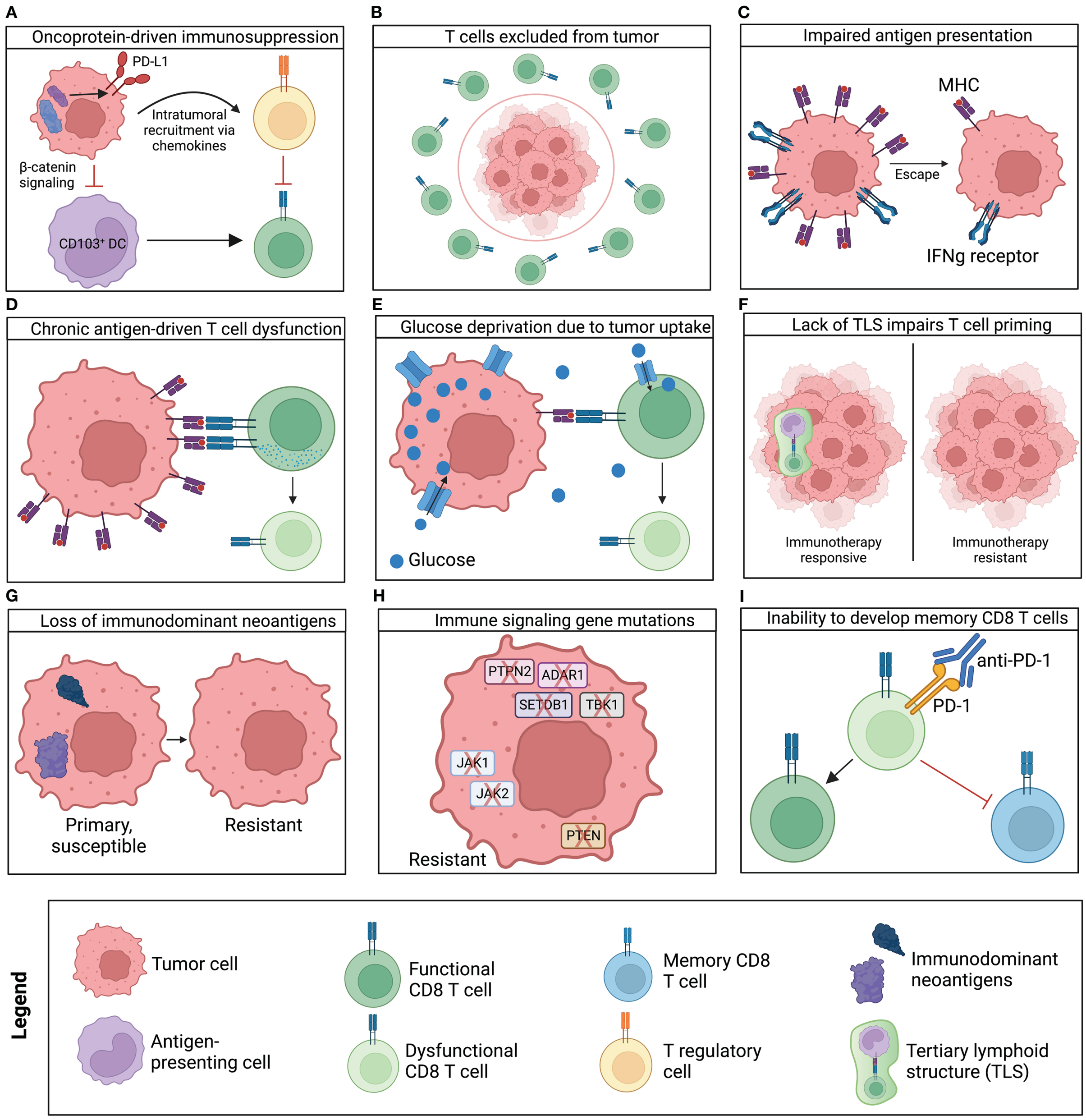

FIGURE 3

Summary of mechanisms of resistance to immunotherapy identified to-date. Several mechanisms can prevent response to immunotherapy altogether (primary resistance), while other mechanisms are acquired later in the disease course and lead to tumor relapse (secondary resistance). **(A)** Oncoproteins can induce immune suppressive environments that recruit tumor-promoting macrophages and T regulatory cells, prevent infiltration of antigen-presenting cells, and prevent infiltration and priming of effector T cells. **(B)** Tumor cells can prevent T cell recruitment *via* downregulation of inflammatory pathways and cell surface integrins (e.g., E-selectin) that mediate T cell entry into inflamed tissues. **(C)** Tumors often downregulate or develop mutations in genes responsible for antigen presentation (e.g., MHC, IFN-γ receptor), preventing tumor engagement with T cells. **(D)** Chronic exposure to their cognate antigens leads to activation of evolutionarily protective, immunosuppressive mechanisms that convert effector T cells to a hypofunctional phenotype. **(E)** Increased glucose uptake by the tumor leads to T cell activation in a nutrient-poor environment, which seems to prime T cells to attain a hyporesponsive phenotype. This phenotype cannot be reversed even if T cells are subsequently stimulated in nutrient-rich conditions. **(F)** Lack of TLS can prevent appropriate T cell priming and is linked to poor outcomes and poor response to immunotherapy. **(G)** Cancer and immune cells co-exist in balance with each other. Thus, immune pressure can lead to deletion of immunogenic neoantigens not required for tumor survival. This "hides" the tumor from the immune system. **(H)** Tumors can also downregulate or mutate cell surface receptors and intracellular proteins responsible for recognizing and responding to immune effector signals (e.g., PTPN2, ADAR1, SETDB1, TBK1, JAK1/2, and PTEN), thus preventing immune-mediated cancer cell death. **(I)** ICI has been demonstrated to re-invigorate the effector functions of T cells but may not induce memory cell formation. This would allow metastases and microtumors to grow after initial disease has been controlled.

specific T cells demonstrated increased cytokine production, migration, and tumor cell killing. This implies that downregulating STING allows the tumor to prevent a significant innate immune mechanism of T cell recruitment (50). In an actual human tumor, injection of a small molecule agonist of STING signaling induced infiltration of MCPyV-specific T cells and regression of multiple injected and non-injected tumors (51). MCC tumors have also been shown to downregulate E-selectin, an integrin critical for T cell homing to the skin, *via* local nitric oxide production. Tumors with increased amounts of nitrotyrosine, a stable biomarker of nitric oxide-induced reactive nitrogen species, had lower E-selectin expression, and consequently, lower T cell infiltration (52). The expression of the ligand for E-selectin, cutaneous lymphocyte antigen (CLA), needs to be further elucidated. Some studies found that a higher percentage of MCPyV-specific T cells express CLA when compared to T cells that target viruses that do not infect the skin (38, 52). A different study found low expression of CLA in cancer-specific T cells and corresponding reduced T cell infiltration into the TME of these patients (49).

4.3 Inhibition of immune cell engagement with the tumor

If efforts to prevent T cells from entering the TME are unsuccessful, MCC tumors can downregulate cell surface receptors that engage cytotoxic immune cells (Figure 3C). Cytotoxic CD8 T cells detect infected or cancerous cells by their TCRs binding to peptides presented on MHC complexes on the cells of interest or professional antigen-presenting cells. Typically, these peptide-MHC complexes are translocated to the cell surface after intracellular proteins are degraded, bound to MHC class I proteins (53). MCPyV oncoproteins interfere with this process by downregulating immunoproteasome genes (LMP2 and LMP7), transporters associated with antigen processing (TAP1 and TAP2), and antigen presentation molecules (MHC class I and β2 microglobulin) (54). The vast majority of MCC tumors (85%) have partial or complete downregulation of class I MHC on their surface relative to surrounding stromal structures (55). Specifically, MHC class I molecules are transcriptionally downregulated by L-Myc, the levels of which are markedly upregulated by the MCPyV oncoproteins (56). The small T antigen binds to L-Myc and recruits it to the EP400 histone acetyltransferase and chromatin remodeling complex to block expression of class I MHC (56). Class I MHC downregulation also confers transcription level resistance to adoptive T cell therapies reliant on presentation of peptide-MHC on MCC tumor cells for anti-tumor responses (57). Correspondingly, this class I MHC downregulation can be pharmacologically reversed by histone deacetylase inhibitors and interferons (54, 55, 58).

In addition to T cells, natural killer (NK) cells also possess cytotoxic potential. This is of particular importance because of the high frequency of class I MHC downregulation in MCC and the fact that NK cells are typically activated by lack of class I MHC on the surface of target cells. NK cells engage target cells based on a balance of activating and inhibitory cell surface receptors and costimulatory molecules (CD40, CD80, and CD86) (59, 60). MCC tumors epigenetically inhibit transcription and translation of two key natural killer group D ligands, MICA and MICB (61). Expression of these ligands on a cell's surface normally sends a "kill me" signal to NK cells. MICA and MICB can also be upregulated by histone deacetylase inhibitors, which have been explored as therapeutic targets in MCC due to their ability to upregulate both "kill me" signals and class I MHC (61). Indeed, in a small clinical trial of NK cells +/- IL-15, 2 of 6 MCC patients with immunotherapy refractory disease experienced clinical benefit and had indications of increased inflammation in their tumors (62). These data suggest that MCC can be sensitive to NK cell killing and therapeutics that recruit NKs cells into the TME should be further explored.

4.4 Induction of T cell dysfunction

To prevent tissue damage based on an immune response that persists unabated, immune cells express inhibitory receptors during activation, allowing inflammation to be attenuated after the acute response (Figure 3D). Chronic signaling through the TCR leads to elevated expression of these inhibitory receptors and facilitates irreversible differentiation to a hyporesponsive state *via* epigenetic alterations. This dysfunctional phenotype interferes with both mounting of an effective inflammatory response and developing stem-like and memory T cells. Indeed, MCC-specific T cells express greater levels of inhibitory receptors (PD-1, cytotoxic T lymphocyte-associated protein-4 (CTLA-4), TIM3, lymphocyte activation gene-3 (LAG-3), and T cell immunoreceptor with Ig and ITIM domains (TIGIT)) and lower levels of activation markers (CD25 and CD69) than bystander T cells (49). Bystander T cells are defined as either T cells present in healthy skin or T cells specific to other common viruses. MCC tumors take advantage of this mechanism by expressing immune checkpoint molecules, specifically PD-L1 and PD-L2, that can inactivate T cells that recognize the tumor (34, 49, 63). Along the same lines, several groups have discovered that a specific subset of PD-1+ cancer-specific T cells (expressing stem cell markers, TCF1 and CXCR5) do expand in response to anti-PD-1 therapy and are largely responsible for controlling the tumor (64–70). It is postulated that these progenitor exhausted cancer-specific T cells recognize antigens that may be expressed at lower levels or do not bind class I MHC as avidly, allowing these T cells to receive fewer activation signals and avoid a more irreversible dysfunctional phenotype (69, 71). It would be pertinent to determine whether this subset of cells could serve as a biomarker of response to immunotherapy in MCC.

5 A major open question: Why do some patients not benefit from immunotherapy?

Although MCC-specific T cells typically express inhibitory receptors targeted by immunotherapy (i.e., PD-1, CTLA-4, TIM-3, LAG-3), only about half of patients persistently respond to immune checkpoint inhibition (ICI). To address immunotherapy-refractory disease, it is critical to understand the mechanisms underlying response or resistance to immunotherapy. In addition to the previously reported MCC-specific immune evasion mechanisms described above, several resistance mechanisms have been demonstrated in other cancers and may also underlie immunotherapy resistance in MCC. Below is a summary of such mechanisms documented in other cancers to underlie primary resistance (no response at all) and secondary resistance (relapse of tumor following a response) (Figure 3).

5.1 Primary resistance

Many of the identified mechanisms of primary resistance involve anti-tumor T cells: (1) lack of cancer-specific T cells in the right place; (2) inability of existing T cells to mount anti-tumor immune responses; (3) inability to generate new T cell responses; and (4) tumor resistance to effector cytokines.

5.1.1 Lack of cancer-specific T cells in the right place

Given that a key target of PD-(L)1 blockade is cancer-specific T cells, it is imperative that such T cells are in fact present in the patient. Indeed, a randomized controlled clinical trial studied the efficacy of neoadjuvant vs. adjuvant treatment in 313 patients with resectable stage III-IV melanoma. Event-free survival was significantly higher in the neoadjuvant group 2 years after treatment (72). Both intratumoral T cells and the source of relevant cancer antigens (tumor cells) are removed during surgical resection and are thus absent when ICI is given in the adjuvant setting. The simplest explanation is that the presence of tumor at the time of immunotherapy initiation elicits a more robust immune response than if the tumor had already been removed. In contrast, other studies have found that chronic antigen stimulation by the tumor drives intratumoral T cells to dysfunction and that peripheral T cells may play a larger role in responding to anti-PD-(L)1 treatment (73, 74).

In a study of 11 patients with basal cell carcinoma, sequential biopsies of a patient's tumor before and after immunotherapy were analyzed, revealing that expanded T cell clones in post-therapy samples were not present in the pre-treatment sample (73). This suggests that the T cells that respond to ICI may have recently infiltrated the tumor. In addition, recent studies demonstrated that the degree of expansion of cancer-specific CD8 T cells in peripheral blood predicts response to PD-L1 blockade in patients with metastatic urothelial carcinoma (74). Similarly, the frequency of activated (PD-1+, KLRG1-) peripheral CD8 T cells predicts pathologic response in oral cancer (75). This implies that peripheral blood could serve as a reservoir of cancer-specific T cells that infiltrate the tumor after immunotherapy. It is likely a combination of intratumoral and peripheral cancer-specific T cells that respond to ICI, a balance that likely differs between patients.

Finally, it is possible that some patients do not have functional peripheral or intratumoral cancer-specific T cells. It has been observed that patients who do not respond to immunotherapy have more turnover of intratumoral T cells, implying that their T cells are not recognizing the cancer and receiving signals to stay/proliferate and fight (76). Additionally, this lack of T cells may be a consequence of minimally immunogenic neoantigens. Indeed, cancers that have a high TMB, either because of non-synonymous mutations or MSI as a result of inability to repair DNA mismatches, are more responsive to immunotherapy (77–81).

5.1.2 T cell generation and priming

If cancer-specific T cells are not present or are terminally exhausted, new T cells recruited from a naïve population could be primed and expanded to exert anti-tumor immunity. Given that thymic function gradually decreases with age and new T cells are rarely produced in older persons, this may contribute to a lack of T cells capable of responding to PD-(L)1 blockade (82). Additionally, existing naïve cancer-specific T cells may not be primed and activated appropriately due to TME or tumor draining lymph node conditions (Figure 3F). For example, it has been observed that β-catenin signaling decreases the recruitment of antigen-presenting CD103+ dendritic cells, which in turn reduces priming and activation of naïve cancer-specific T cells that enter the TME (83). Additionally, several studies have shown that formation of tertiary lymphoid structures (TLS) within the tumor correlates to improved response to immunotherapies (84–86). It is possible that TLS are where primary or secondary immune responses are generated and thus play a role in the priming and clonal expansion of cytotoxic CD8 T cells (87, 88). Thus, deficiencies of cytokines that promote formation of effective TLS could contribute to resistance to cancer immunotherapy. Both antibody and T cell frequencies track with MCC tumor burden (25, 89) suggesting a coordinated immune response and that the presence of TLS in MCC could be predictive of response.

5.1.3 Tumor resistance to effector cytokines

Four genes have been implicated in aiding immune evasion or conferring resistance to anti-PD-1 treatment: protein tyrosine phosphatase non-receptor 2 (PTPN2), RNA editing enzyme ADAR1 (Adenosine Deaminase Acting on RNA 1), H3K9 methyltransferase SETDB1 (SET Domain Bifurcated Histone Lysine Methyltransferase 1), and tank-binding kinase 1 (TBK1) (Figure 3H) (90–93). The PTPN2 phosphatase is involved in multiple signaling pathways, including negative regulation of IFN-γ signaling (90). Loss of PTPN2 increases IFN-γ mediated antigen presentation and growth suppression in melanoma and colon carcinoma murine models (90). Additionally, tumors lacking PTPN2 contain CD8 T cells with increased expression of granzyme B, a marker of activated, cytotoxic T cells (90). ADAR1 is an adenosine deaminase that prevents the sensing of endogenous double-stranded RNA (91). Thus, loss of ADAR1 increases cellular sensing of double-stranded RNA, and consequently inhibits tumor growth and increases inflammation (91). ADAR1 loss sensitizes tumors to IFN-γ signaling and overcomes resistance to anti-PD-1 immunotherapy (91). SETDB1, a histone methyltransferase, represses domains within the open gene compartment that contain transposable elements and immune genes (92). Loss of SETDB1 increases the activity of transposable element-mediated regulatory and immune stimulatory genes, in addition to increasing transposable element-specific cytotoxic T cell responses (92). TBK1 kinase coordinates the innate immune response to viruses by integrating signals from pattern recognition receptors and cytosolic nucleic acid sensors, and regulating activation of type I interferons and interferon-stimulated genes (93). Using PDX and organoid models, the authors demonstrated that loss of TBK1 lowered the threshold of immune cell-secreted effector cytokines needed to kill tumor cells and sensitized tumors to anti-PD-1 therapy (93). While these genes have not been studied in the context of MCC, these may be effective immunotherapy targets or might synergize with existing immunotherapies. Additional studies of MCC patient tumor biopsies are needed.

5.1.4 Emerging mechanisms: Physical removal of anti-PD-1 antibodies, gut microbiome, and cytotoxic CD4+ T cells

In addition to the CD8 T cell-based mechanisms described above, additional insights are emerging from analyses of specimens collected from clinical trials and mouse models. Three promising findings regarding primary immune resistance are summarized here.

In mouse models derived from colon carcinoma, melanoma, or lung adenocarcinoma cell lines, *in vivo* imaging revealed that PD-1- macrophages stripped anti-PD-1 antibodies from the surface of CD8+ T cells (94). This removal was dependent on the Fcγ receptors present on the macrophages and Fc region of the antibodies, suggesting that engineering the Fc region of anti-PD-1 treatments could increase the time of antibody engagement with cancer-specific CD8 T cells (94).

The gut microbiome is known to influence immune responses, and recent studies have shown that the microbiome also influences response to immunotherapy (95–97). Indeed, microbiome profiling has revealed that gut microbiome with high bacterial diversity and certain commensal pathogens (Faecalibacterium, *Akkermansia muciniphila*, and Ruminococcaceae family) correlates to T cell phenotypes that translate to favorable responses to ICI (98–101). Antibiotics can decrease microbiome diversity, and use of these agents prior to ICI decreases the likelihood of a favorable response to treatment in multiple cancers (102–104). The mechanism of action of the gut microbiome on responses to immunotherapy needs to be further elucidated.

Single-cell RNA sequencing revealed several subsets of T regulatory and cytotoxic, clonally expanded CD4 T cells in bladder cancer that were absent in patient-matched non-malignant tissue samples (105). The cytotoxic CD4 T cells were able to kill tumor cells in an MHC class II-dependent manner in cell culture (105). Additionally, a gene signature of cytotoxic CD4 T cells predicted response to PD-(L)1 blockade in a large cohort of metastatic bladder cancer patients (105).

5.2 Secondary resistance

5.2.1 Gene mutations and loss of immunodominant neoantigens

Gene mutations leading to loss of immunodominant neoantigens or disruptions in immune effector signaling pathways are two major reasons for disease progression or relapse after initial response to ICI (Figures 3G, H). Comparison of pre-treatment and resistant tumors revealed that acquired resistance can be mediated by tumor cells that lose expression of immunodominant neoantigens or by an outgrowth of a subset of the tumor population that never expressed immunogenic neoantigens (106). Thus, epitope spreading (expanding the breadth of cancer antigens recognized by T cells) should combat secondary resistance by reducing immune pressure on a narrow set of antigens. Additionally, as summarized below, there are examples of several immune effector genes that have been rendered non-functional in patients who acquired resistance to PD-1 blockade. Specifically, in a study of four patients with melanoma whose disease initially responded to anti-PD-1 treatment but relapsed months to years later, two patients had homozygous loss-of-function mutations in their Janus kinase 1 (JAK1) or JAK2 genes (107). In the same study, a third patient had a truncating mutation in their β2-microglobulin gene (107). In another study, a patient who had metastatic uterine leiomyosarcoma experienced complete tumor regression in all but one lesion (108). Analysis of the germline tissue, responding tumors, and the resistant tumors revealed decreased gene expression of immunodominant neoantigens and homozygous loss of phosphatase and tensin homolog (PTEN) in the resistant tumor (108). This is significant because PTEN genetic deletion in a mouse model of melanoma led to increased levels of immunosuppressive cytokines and angiogenic factors (Vascular endothelial growth factor, VEGF), decreased T cell infiltration, decreased autophagy, and resistance to PD-(L)1 blockade (109). CRISPR-based screens could be a useful tool to identify immune evasion mechanisms in MCC.

5.2.2 Lack of memory T cells

While this finding has been characterized in chronic viral infection and needs to be investigated in the context of cancer, it has been postulated that effector T cells that are responsible for initially controlling tumors do not differentiate into memory T cells (Figure 3I). Thus, the lack of cancer-specific memory T cells could mean that micro-metastases go unchecked and can give rise to new tumors. Indeed, MCC-specific T cells drop to very low or undetectable levels after effective disease control (21). This could be because cancer-specific T cells, similar to T cells that fight chronic infections, are antigen-addicted and cannot survive without disease burden and ongoing presentation of cognate peptide to TCRs. In a study of *Toxoplasma gondii* infection, a unique ‘transitional’ subset of T cells has been identified that possesses (1) hybrid effector and memory properties and (2) strong dependence on antigen for survival and proliferation to sustain the ongoing effector response (110). Additionally, while dysfunctional T cells can regain effector function *via* ICI, they are unable to differentiate into memory T cells (111, 112).

5.2.3 Emerging mechanism: Cell-in-cell formations

A recent study demonstrated that cancer cells form transient cell-in-cell formations, where one tumor cell “hides” inside another tumor cell. This is in response to granules secreted by and cell surface proteins expressed on IFN-γ-activated CD8 T cells. The T cell cytokines and surface molecules induce upregulation of signal transducer and activator of transcription 3 (STAT3) and early growth response factor 1 (EGR1) transcriptional programs, which are necessary and sufficient for generating cell-in-cell formations. While the outer cell is killed by CD8 T cells, the inner cell is not susceptible to lytic granules secreted by cytotoxic T cells. Therefore, the inner cells can escape when the CD8 T cells are no longer in the microenvironment and give rise to new tumor cells, leading to resistance or partial responses to immunotherapy (113).

6 Discussion and future directions

Cancer-specific T cells are crucial for effective anti-tumor immunity and response to immunotherapy, but patient-specific mutations that drive most cancers make it difficult to develop reagents to identify and directly study the relevant cells. Given that virus-driven MCC contains compact, immunogenic oncoproteins and a low TMB, it offers a unique opportunity to relatively comprehensively identify cancer-specific T cells (Figure 1). Indeed, detailed functional studies have identified 20 immunogenic epitopes that can be presented by a variety of MHC alleles. Tetramers corresponding to the identified immunogenic epitopes have been used to identify cancer-specific T cells. These reagents have led to the discoveries that increased number, diversity, and functional avidity of cancer-specific T cells correlates to improved survival in MCC (Figure 2) (36).

While immunotherapies that target T cell function have become a pillar of cancer treatment, only a subset of patients experience durable responses to PD-(L)1 pathway blockade (114). It is crucial to more fully understand the differences between patients who respond and those who do not to improve immunotherapies and prioritize patients for clinical trials of alternate and synergistic treatments. Many resistance mechanisms have been identified in MCC and other cancers, as discussed above (Figure 3). Specifically, MCPyV tetramer reagents have enabled studies that found that the frequency of circulating cancer-specific T cells before anti-PD-1 treatment predicts response (Figure 2) (38, 39).

While PDX models have allowed pre-clinical testing of proposed treatments in immune-deficient mice, the fact that MCPyV oncoproteins are not capable of inducing tumors in mice has prevented basic cancer immunology studies. Importantly, more than a decade of effort has identified other conditions needed for MCC development in mice (induction of MCPyV oncoproteins, induction of neuroendocrine differentiation factor ATOH1, and deletion of one copy of tumor suppressor gene p53) (115). Using these findings, an immune competent mouse model of MCC has recently been developed (115). This mouse model can now synergize with a suite of improved bio-technological developments including better resolution for spatial transcriptomics, improved cancer-specific T cell identification methods *via* genetic and bioinformatic means, and increased integration of single-cell RNA sequencing with other cell state assays. As summarized below, these combined approaches should now allow us to: (1) further identify immune evasion mechanisms utilized by this immunogenic cancer; (2) characterize the cellular and signaling requirements of an effective anti-tumor response; and (3) determine the efficacy of novel and/or synergistic treatments.

6.1 Future direction: Identify additional immune evasion mechanisms

Many studies have suggested that infiltration of functional, cancer-specific T cells is linked to patient survival and response to immune-based treatments. Thus, one goal of identifying immune evasion mechanisms is to enhance the recruitment and activation of cytotoxic T cells that can kill tumor cells, effectively a turning a cold tumor (no immune cells) into a hot tumor (immune infiltrated). A recent study showed that pre-existing, clonally expanded, tissue resident memory T cells are early responders to neoadjuvant immunotherapy (75). However, the responding tumor-specific T cells are also present in patients who do not respond to immunotherapy (116). Spatial transcriptomic technologies are actively being improved to provide better resolution and obtain data at a single-cell level (117–119). Comparison of TMEs between responders and non-responders using these spatial technologies has the potential to reveal immune cells and secreted factors that are necessary for priming, activating, and supporting the cytotoxic function of cancer-specific T cells. Additionally, CRISPR-based genetic screens have identified a few immune evasion genes (summarized above in sections 5.1.3 and 5.2.1). Given the rapid rate of progress in the field, it may be possible in the near future to use CRISPR to both identify genes with loss-of-function mutations and then restore the function of these genes in a patient-specific manner, overcoming resistance to immunotherapy (120).

6.2 Future direction: Characterize the cellular and signaling requirements of an effective anti-tumor response

The rapid paced technological improvements in single-cell transcriptomics, especially the ability to generate multimodal data (e.g., RNA expression, cell surface protein expression, and assessing chromosome accessibility for the same cell) and associated analytical packages, have the potential to thoroughly characterize and compare cancer-specific immune cells across patients. Using these techniques, we can seek to (1) understand the phenotypic and TCR affinity differences between cancer-specific T cells that expand or contract over treatment; (2) uncover master regulator(s) of dysfunction and stem-ness for chronically activated T cells; and (3) better understand the influence of the microbiome on response to immunotherapy.

While peptide-MHC tetramers have been used for years to identify antigen-specific T cells, these reagents have several limitations: (1) they miss low-affinity TCRs that may be activated *in vivo* based on secondary signals that are not present *in vitro*; and (2) they may disassociate from the cell of interest prior to its detection in the assay, making it harder to distinguish signal from noise especially in single-cell sequencing applications. To counteract these limitations, new assays and bioinformatic tools that can rapidly identify cancer-specific T cells *via* expansion-based assays (22, 121), gene expression profiles (122, 123), and lentiviral fusion (27) are also being developed. However, these methods still require significant time and experimental expertise, in addition to large amounts of patient samples, and are thus unsuitable for clinical use. To extend these techniques for clinical use, it may be possible to draw from the fields of viral and bacterial immunology.

To identify T cells that are specific for CMV, SARS-CoV-2, and *Borrelia burgdorferi*, a bioinformatic "predictor" of TCR antigen specificity was developed for each of these pathogens (124–126). These classifiers were generated by comparing bulk TCRβ chain sequences from persons with or without the infection of interest. Statistical methods were used to identify T cells enriched in the patients harboring the infection, on the assumption that the expanded T cells recognize the pathogen of interest. However, without laboratory confirmation, statistical enrichment does not prove antigen specificity. By combining tetramer-, ENTER-, expansion-, or gene expression-based methods of identifying antigen-specific T cells, it should be feasible to develop predictors that can identify antigen-specific T cells from MCC patient samples in a clinically feasible manner.

6.3 Future direction: Determine the efficacy of novel and/or synergistic treatments

Understanding immune evasion and immunotherapy resistance mechanisms provides insight into potential alternate and synergistic treatments for patients unlikely to respond to individual agent immunotherapy. Indeed, several such clinical trials are already planned or under way, and advances in immunology techniques and bioinformatic tools will be crucial in determining the efficacy of these treatments for augmenting the number and/or function of cytotoxic CD8 T cells.

Given recent observations that the frequency of circulating cancer-specific T cells correlates with response to immunotherapy (38, 39), several potential therapeutic approaches can be considered: therapeutic vaccines, TCR-transgenic T cells, and *in vitro*-expanded cancer-specific T cells isolated from the blood or the tumor. Therapeutic vaccines are designed to induce an adaptive immune response against tumor antigens to effect tumor regression and eliminate minimal residual disease (127). Clinical trials targeting a variety of tumors are ongoing based on (1) sophisticated new approaches to select immunogenic tumor antigens *via* improved prediction algorithms and (2) advanced vaccine technologies (e.g., modified viral vector-based vaccines that co-express target antigens and immunostimulatory molecules) (128). Current therapeutic vaccine trials include one that targets virus-driven MCC (NCT05422781). This is a DNA vaccine that fuses an MCPyV oncoprotein with lysosomal-associated membrane protein-1 (LAMP1) to increase MHC class II antigen presentation and consequent priming of MCPyV-specific CD4 T cell responses (129). In addition to therapeutic vaccines, it may be possible to infuse *ex vivo* expanded or engineered tumor-specific lymphocytes. Indeed, T cells with a transgenic, high-affinity TCR for an MCPyV epitope are currently being tested in combination with standard-of-care immunotherapy and MHC class I upregulation (NCT03747484) (130). A recent study also tested the efficacy of *in vitro* expanded tumor-infiltrating lymphocytes (TIL) versus anti-CTLA-4 therapy in unresectable, late-stage melanoma (131). In this study, resected tumor samples were dissected, and TILs were expanded with anti-CD3 and IL-2. Patients who received TIL therapy experienced progression-free survival for 4 more months and overall survival for 7 more months compared to those treated with anti-CTLA-4 treatment (131). It remains to be seen whether TIL therapy has better efficacy than PD-1 pathway blockade.

In combination with checkpoint blockade, options that either increase the number of neoantigens to be targeted (via inhibition of DNA repair) or increase the number of cancer-specific T cells (via therapeutic vaccination) are being investigated. DNA damage response proteins have long been intriguing therapeutic targets as inhibiting their function could trigger cell death (132). Excitingly, preclinical studies of DNA damage response inhibitors also indicate that they induce cell death in an immunogenic manner and increase recruitment and activation of antigen-presenting cells (132–139). Recruitment of these antigen-presenting cells could prime adaptive immune responses to tumor antigens and, combined with ICI, lead to an enhanced anti-tumor cytotoxic response (132). Four different DNA damage response inhibitors (three of which target ataxia telangiectasia and Rad3-related, ATR) are currently being tested in combination with ICI in multiple cancers, and a clinical trial of an ATR inhibitor for MCC is upcoming (132). As discussed above, vaccine modalities have greatly improved, and several tumor vaccines are in preclinical and clinical stages of development (128). However, they often fail to provide clinical benefit due to immune evasion mechanisms employed by the tumor. Combination with immune checkpoint inhibitors could improve the ability of cancer-specific T cells elicited by the vaccine to exert anti-tumor effects (140).

It has also been observed that PD-1 pathway blockade often upregulates the expression of other immune checkpoint molecules (141, 142). Indeed, combination anti-CTLA-4 and anti-PD-1 treatment is currently offered to and beneficial for some patients who do not respond to anti-PD-1 monotherapy (143). However, anti-CTLA-4 treatment poses a higher risk of immune-related adverse events (144). Thus, alternate immune checkpoint targets have been identified and clinical trials testing the efficacy of combination treatments are underway (145). Specifically, the field is focusing on the immune checkpoint molecules LAG-3 and TIM-3. LAG-3 downregulates CD4+ T cell and myeloid cell responses *via* interaction with class II MHC on tumor cells and dendritic cells (146, 147). TIM-3 binding to galactin-9, a C-type lectin expressed on hematopoietic cells, leads to increased calcium influx-mediated cell death in TIM-3+ T cells (148). Thus, blocking these inhibitory cell surface proteins has the potential to rescue immune function in patients who do not respond to anti-PD-1 monotherapy. Indeed, numerous clinical trials are testing the efficacy of anti-TIM-3/anti-PD-1 or anti-LAG-3/anti-PD-1 therapies in a variety of solid tumors, with one of the anti-LAG-3 and anti-PD-1 combinations approved for first-line treatment of advanced melanoma in early 2022 (121, 149–151). Building on the success of dual checkpoint inhibition in other cancers, a clinical trial studying the efficacy of dual and/or triple ICI in MCC could also prove beneficial.

6.4 Concluding remarks

In contrast to most cancers driven by private, patient-specific mutations, Merkel cell carcinoma is driven by Merkel cell polyomavirus in most cases. Additionally, the MCPyV oncoproteins are highly immunogenic and thus tumors need to develop robust immune evasion mechanisms to ensure their own survival, often including dependence on PD-1 pathway activation. Indeed, anti-PD-1 immunotherapies are more effective in MCC than in any other solid cancer (152). The invariant, shared oncoproteins have allowed the development of tetramer reagents to identify cancer-specific T and B cells across patients. These reagents allow investigators to bypass the need for tumor antigen identification and to extract valuable information from small biological specimens. Thus, MCC is an excellent model for answering open questions in cancer immunology and immunotherapy. Specifically, recent improvements in single-cell RNA sequencing modalities, spatial transcriptomics, T cell identification methods, and the recently developed mouse model with an intact immune system should allow identification of additional immune evasion mechanisms and determination of efficacy of immunotherapies in pre-clinical studies. Virus-driven MCC provides a rich environment in which to study the intrinsic immune response to cancer as well as help understand why patients do and do not respond to current immunotherapy. The lessons learned from studying this tractable, immunogenic cancer may prove applicable to other cancers and yield significant benefits for cancer patients more broadly.

Author contributions

CC and SJ performed literature search and manuscript preparation. CC, SJ and PN contributed to the article and performed editing. All authors approve the submitted version.

Funding

National Cancer Institute funding P01 CA225517 (PN), and T32 CA080416 (SJ); Odyssey Group Foundation Kelsey Dickson Team Science Courage Research Award: Advancing New Therapies for Merkel Cell Carcinoma (MCC) (A187769) (PN); and the Merkel cell carcinoma (MCC) patient gift fund at the University of Washington (PN).

Acknowledgments

We thank all members of the Nghiem lab for their assistance and critical feedback during manuscript preparation. All figures were created with Biorender.com.

Conflict of interest

PN's institution has received grant support from EMD Serono and Bristol Myers Squibb as well as honoraria from Merck and EMD-Serono. The remaining authors declare that the research was conducted in the absence of any commercial or financial relationships that could be construed as a potential conflict of interest. The handling editor VK declared a past co-authorship with the authors CC, PN.

Publisher's note

References

1. Schreiber RD, Old LJ, Smyth MJ. Cancer immunoediting: integrating immunity's roles in cancer suppression and promotion. *Science* (2011) 331(6024):1565–70. doi: 10.1126/science.1203486

2. Paulson KG, Park SY, Vandeven NA, Lachance K, Thomas H, Chapuis AG, et al. Merkel cell carcinoma: Current US incidence and projected increases based on changing demographics. *J Am Acad Dermatol* (2018) 78(3):457–63 e2. doi: 10.1016/j.jaad.2017.10

3. Engels EA, Frisch M, Goedert JJ, Biggar RJ, Miller RW. Merkel cell carcinoma and HIV infection. *Lancet* (2002) 359(9305):497–8. doi: 10.1016/S0140-6736(02)07668-7

4. Paulson KG, Iyer JG, Blom A, Warton EM, Sokil M, Yelistratova L, et al. Systemic immune suppression predicts diminished merkel cell carcinoma-specific survival independent of stage. *J Invest Dermatol* (2013) 133(3):642–46. doi: 10.1038/jid.2012.388

5. Heath M, Jaimes N, Lemos B, Mostaghimi A, Wang LC, Penas PF, et al. Clinical characteristics of merkel cell carcinoma at diagnosis in 195 patients: the AEIOU features. *J Am Acad Dermatol* (2008) 58(3):375–81. doi: 10.1016/j.jaad.2007.11.020

6. Feng H, Shuda M, Chang Y, Moore PS. Clonal integration of a polyomavirus in human merkel cell carcinoma. *Science* (2008) 319(5866):1096–100. doi: 10.1126/science.1152586

7. Viscidi RP, Rollison DE, Sondak VK, Silver B, Messina JL, Giuliano AR, et al. Age-specific seroprevalence of merkel cell polyomavirus, BK virus, and JC virus. *Clin Vaccine Immunol* (2011) 18(10):1737–43. doi: 10.1128/CVI.05175-11

8. Sihto H, Kukko H, Koljonen V, Sankila R, Bohling T, Joensuu H. Clinical factors associated with merkel cell polyomavirus infection in merkel cell carcinoma. *J Natl Cancer Inst* (2009) 101(13):938–45. doi: 10.1093/jnci/djp139

9. Garneski KM, Warcola AH, Feng Q, Kiviat NB, Leonard JH, Nghiem P. Merkel cell polyomavirus is more frequently present in north american than australian merkel cell carcinoma tumors. *J Invest Dermatol* (2009) 129(1):246–8. doi: 10.1038/jid.2008.229

10. Shuda M, Feng H, Kwun HJ, Rosen ST, Gjoerup O, Moore PS, et al. T antigen mutations are a human tumor-specific signature for merkel cell polyomavirus. *Proc Natl Acad Sci U.S.A.* (2008) 105(42):16272–7. doi: 10.1073/pnas.0806526105

11. Feng H, Kwun HJ, Liu X, Gjoerup O, Stolz DB, Chang Y, et al. Cellular and viral factors regulating merkel cell polyomavirus replication. *PloS One* (2011) 6(7):e22468. doi: 10.1371/journal.pone.0022468

12. Goh G, Walradt T, Markarov V, Blom A, Riaz N, Doumani R, et al. Mutational landscape of MCPyV-positive and MCPyV-negative merkel cell carcinomas with implications for immunotherapy. *Oncotarget* (2016) 7(3):3403–15. doi: 10.18632/oncotarget.6494

13. Wong SQ, Waldeck K, Vergara IA, Schroder J, Madore J, Wilmott JS, et al. UV-associated mutations underlie the etiology of MCV-negative merkel cell carcinomas. *Cancer Res* (2015) 75(24):5228–34. doi: 10.1158/0008-5472.CAN-15-1877

14. Church C, Pulliam T, Longino N, Park SY, Smythe KS, Makarov V, et al. Transcriptional and functional analyses of neoantigen-specific CD4 t cells during a profound response to anti-PD-L1 in metastatic merkel cell carcinoma. *J Immunother Cancer* (2022) 10(9). doi: 10.1136/jitc-2022-005328

15. Nghiem PT, Bhatia S, Lipson EJ, Kudchadkar RR, Miller NJ, Annamalai L, et al. PD-1 blockade with pembrolizumab in advanced merkel-cell carcinoma. *N Engl J Med* (2016) 374(26):2542–52. doi: 10.1056/NEJMoa1603702

16. D'Angelo SP, Russell J, Lebbe C, Chmielowski B, Gambichler T, Grob JJ, et al. Efficacy and safety of first-line avelumab treatment in patients with stage IV metastatic merkel cell carcinoma: A preplanned interim analysis of a clinical trial. *JAMA Oncol* (2018) 4(9):e180077. doi: 10.1001/jamaoncol.2018.0077

17. Topalian SL, Bhatia S, Amin A, Kudchadkar RR, Sharfman WH, Lebbe C, et al. Neoadjuvant nivolumab for patients with resectable merkel cell carcinoma in the CheckMate 358 trial. *J Clin Oncol* (2020) 38(22):2476–87. doi: 10.1200/JCO.20.00201

18. Houben R, Shuda M, Weinkam R, Schrama D, Feng H, Chang Y, et al. Merkel cell polyomavirus-infected merkel cell carcinoma cells require expression of viral t antigens. *J Virol* (2010) 84(14):7064–72. doi: 10.1128/JVI.02400-09

19. The problem with neoantigen prediction. *Nat Biotechnol* (2017) 35(2):97. doi: 10.1038/nbt.3800

20. Vitiello A, Zanetti M. Neoantigen prediction and the need for validation. *Nat Biotechnol* (2017) 35(9):815–17. doi: 10.1038/nbt.3932

21. Jing L, Ott M, Church CD, Kulikauskas RM, Ibrani D, Iyer JG, et al. Prevalent and diverse intratumoral oncoprotein-specific CD8(+) t cells within polyomavirus-driven merkel cell carcinomas. *Cancer Immunol Res* (2020) 8(5):648–59. doi: 10.1158/2326-6066.CIR-19-0647

22. Danilova L, Anagnostou V, Caushi JX, Sidhom JW, Guo H, Chan HY, et al. The mutation-associated neoantigen functional expansion of specific t cells (MANAFEST) assay: A sensitive platform for monitoring antitumor immunity. *Cancer Immunol Res* (2018) 6(8):888–99. doi: 10.1158/2326-6066.CIR-18-0129

23. Harms PW, Harms KL, Moore PS, DeCaprio JA, Nghiem P, Wong MKK, et al. The biology and treatment of merkel cell carcinoma: current understanding and research priorities. *Nat Rev Clin Oncol* (2018) 15(12):763–76. doi: 10.1038/s41571-018-0103-2

24. Yi JS, Cox MA, Zajac AJ. T-cell exhaustion: characteristics, causes and conversion. *Immunology* (2010) 129(4):474–81. doi: 10.1111/j.1365-2567.2010.03255.x

25. Afanasiev OK, Yelistratova L, Miller N, Nagase K, Paulson K, Iyer JG, et al. Merkel polyomavirus-specific t cells fluctuate with merkel cell carcinoma burden and express therapeutically targetable PD-1 and tim-3 exhaustion markers. *Clin Cancer Res* (2013) 19(19):5351–60. doi: 10.1158/1078-0432.CCR-13-0035

26. Zhang SQ, Ma KY, Schonnesen AA, Zhang M, He C, Sun E, et al. High-throughput determination of the antigen specificities of t cell receptors in single cells. *Nat Biotechnol* (2018) 36:1156–59. doi: 10.1038/nbt.4282

27. Yu B, Shi Q, Belk JA, Yost KE, Parker KR, Li R, et al. Engineered cell entry links receptor biology with single-cell genomics. *Cell* (2022) 185(26):4904–20 e22. doi: 10.1016/j.cell.2022.11.016

28. Swanson E, Lord C, Reading J, Heubeck AT, Genge PC, Thomson Z, et al. Simultaneous trimodal single-cell measurement of transcripts, epitopes, and chromatin accessibility using TEA-seq. *Elife* (2021). doi: 10.7554/eLife.63632

29. Kubica AW, Brewer JD. Melanoma in immunosuppressed patients. *Mayo Clin Proc* (2012) 87(10):991–1003. doi: 10.1016/j.mayocp.2012.04.018

30. Paulson KG, Iyer JG, Tegeder AR, Thibodeau R, Schelter J, Koba S, et al. Transcriptome-wide studies of merkel cell carcinoma and validation of intratumoral CD8+ lymphocyte invasion as an independent predictor of survival. *J Clin Oncol* (2011) 29(12):1539–46. doi: 10.1200/JCO.2010.30.6308

31. Iyer JG, Afanasiev OK, McClurkan C, Paulson K, Nagase K, Jing L, et al. Merkel cell polyomavirus-specific CD8(+) and CD4(+) t-cell responses identified in merkel cell carcinomas and blood. *Clin Cancer Res* (2011) 17(21):6671–80. doi: 10.1158/1078-0432.CCR-11-1513

32. Lyngaa R, Pedersen NW, Schrama D, Thrue CA, Ibrani D, Met O, et al. T-cell responses to oncogenic merkel cell polyomavirus proteins distinguish patients with merkel cell carcinoma from healthy donors. *Clin Cancer Res* (2014) 20(7):1768–78. doi: 10.1158/1078-0432.CCR-13-2697

33. Wherry EJ. T cell exhaustion. *Nat Immunol* (2011) 12(6):492–9. doi: 10.1038/ni.2035

34. Lipson EJ, Vincent JG, Loyo M, Kagohara LT, Luber BS, Wang H, et al. PD-L1 expression in the merkel cell carcinoma microenvironment: association with inflammation, merkel cell polyomavirus and overall survival. *Cancer Immunol Res* (2013) 1(1):54–63. doi: 10.1158/2326-6066.CIR-13-0034

35. Nghiem P, Bhatia S, Lipson EJ, Sharfman WH, Kudchadkar RR, Brohl AS, et al. Three-year survival, correlates and salvage therapies in patients receiving first-line pembrolizumab for advanced merkel cell carcinoma. *J Immunother Cancer* (2021). doi: 10.1136/jitc-2021-002478

36. Miller NJ, Church CD, Dong L, Crispin D, Fitzgibbon MP, Lachance K, et al. Tumor-infiltrating merkel cell polyomavirus-specific t cells are diverse and associated with improved patient survival. *Cancer Immunol Res* (2017) 5(2):137–47. doi: 10.1158/2326-6066.CIR-16-0210

37. Wang Y, Tong Z, Zhang W, Zhang W, Buzdin A, Mu X, et al. FDA-approved and emerging next generation predictive biomarkers for immune checkpoint inhibitors in cancer patients. *Front Oncol* (2021) 11:683419. doi: 10.3389/fonc.2021.683419

38. Ryu H, Bi T, Sarkar K, Church C, Ramchurren N, Pulliam T, et al. High dimensional profiling of merkel cell polyomavirus-specific t cells in response to anti-PD-1 immunotherapy. *Soc Immunotherapy Cancer* (1045) 2022:10. doi: 10.1136/jitc-2022-SITC2022.1045

39. Pulliam T, Jani SH, Jing L, Zhang J, Kulikauskas R, Church C, et al. 50 merkel cell polyomavirus-specific CD8 t cells in blood, but not in tumors, correlate with immunotherapy response in merkel cell carcinoma. *Soc Immunotherapy Cancer* (2022) 10. doi: 10.1136/jitc-2022-SITC2022.0050

40. Harms PW. Update on merkel cell carcinoma. *Clin Lab Med* (2017) 37(3):485–501. doi: 10.1016/j.cll.2017.05.004

41. Schadendorf D, Lebbe C, Zur Hausen A, Avril MF, Hariharan S, Bharmal M, et al. Merkel cell carcinoma: Epidemiology, prognosis, therapy and unmet medical needs. *Eur J Cancer* (2017) 71:53–69. doi: 10.1016/j.ejca.2016.10.022

42. Douzandeh-Mobarrez B, Kariminik A, Kazemi Arababadi M, Kheirkhah B. TLR9 in the human papilloma virus infections: Friend or foe? *Viral Immunol* (2022) 15:457–64. doi: 10.1089/vim.2021.0223

43. Shahzad N, Shuda M, Gheit T, Kwun HJ, Cornet I, Saidj D, et al. The t antigen locus of merkel cell polyomavirus downregulates human toll-like receptor 9 expression. *J Virol* (2013) 87(23):13009–19. doi: 10.1128/JVI.01786-13

44. Bitossi C, Viscido A, Prezioso C, Brazzini G, Trancassini M, Borrazzo C, et al. High prevalence of merkel cell polyomavirus is associated with dysregulation in transcript levels of TLR9 and type i IFNs in a large cohort of CF patients from the italian (Lazio) reference center for cystic fibrosis. *Microb Pathog* (2022) 169:105644. doi: 10.1016/j.micpath.2022.105644

45. Liu J, Geng X, Hou J, Wu G. New insights into M1/M2 macrophages: key modulators in cancer progression. *Cancer Cell Int* (2021) 21(1):389. doi: 10.1186/s12935-021-02089-2

46. Zhou J, Tang Z, Gao S, Li C, Feng Y, Zhou X. Tumor-associated macrophages: Recent insights and therapies. *Front Oncol* (2020) 10:188. doi: 10.3389/fonc.2020.00188

47. Sihto H, Bohling T, Kavola H, Koljonen V, Salmi M, Jalkanen S, et al. Tumor infiltrating immune cells and outcome of merkel cell carcinoma: a population-based study. *Clin Cancer Res* (2012) 18(10):2872–81. doi: 10.1158/1078-0432.CCR-11-3020

48. Chaudhary B, Elkord E. Regulatory t cells in the tumor microenvironment and cancer progression: Role and therapeutic targeting. *Vaccines (Basel)* (2016). doi: 10.3390/vaccines4030028

49. Dowlatshahi M, Huang V, Gehad AE, Jiang Y, Calarese A, Teague JE, et al. Tumor-specific t cells in human merkel cell carcinomas: a possible role for tregs and t-cell exhaustion in reducing t-cell responses. *J Invest Dermatol* (2013) 133(7):1879–89. doi: 10.1038/jid.2013.75

50. Liu W, Kim GB, Krump NA, Zhou Y, Riley JL, You J. Selective reactivation of STING signaling to target merkel cell carcinoma. *Proc Natl Acad Sci U.S.A.* (2020) 117 (24):13730–39. doi: 10.1073/pnas.1919690117

51. Pulliam TH, Bhakuni R, Jani S, Smythe K, Seaton B, Tachiki L, et al. An intratumoral STING agonist-mediated clinical response in PD-L1-refractory MCC via an unexpected mechanism of action. *J Invest Dermatol* (2022) 142(10). doi: 10.1016/j.jid.2022.08.019

52. Afanasiev OK, Nagase K, Simonson W, Vandeven N, Blom A, Koelle DM, et al. Vascular e-selectin expression correlates with CD8 lymphocyte infiltration and improved outcome in merkel cell carcinoma. *J Invest Dermatol* (2013) 133(8):2065–73. doi: 10.1038/jid.2013.36

53. Hewitt EW. The MHC class i antigen presentation pathway: strategies for viral immune evasion. *Immunology* (2003) 110(2):163–9. doi: 10.1046/j.1365-2567.2003.01738.x

54. Ritter C, Fan K, Paschen A, Reker Hardrup S, Ferrone S, Nghiem P, et al. Epigenetic priming restores the HLA class-i antigen processing machinery expression in merkel cell carcinoma. *Sci Rep* (2017) 7(1):2290. doi: 10.1038/s41598-017-02608-0

55. Paulson KG, Tegeder A, Willmes C, Iyer JG, Afanasiev OK, Schrama D, et al. Downregulation of MHC-i expression is prevalent but reversible in merkel cell carcinoma. *Cancer Immunol Res* (2014) 2(11):1071–9. doi: 10.1158/2326-6066.CIR-14-0005

56. Cheng J, Park DE, Berrios C, White EA, Arora R, Yoon R, et al. Merkel cell polyomavirus recruits MYCL to the EP400 complex to promote oncogenesis. *PloS Pathog* (2017) 13(10):e1006668. doi: 10.1371/journal.ppat.1006668

57. Paulson KG, Voillet V, McAfee MS, Hunter DS, Wagener FD, Perdicchio M, et al. Acquired cancer resistance to combination immunotherapy from transcriptional loss of class i HLA. *Nat Commun* (2018) 9(1):3868. doi: 10.1038/s41467-018-06300-3

58. Lee PC, Klaeger S, Le PM, Korthauer K, Cheng J, Ananthapadmanabhan V, et al. Reversal of viral and epigenetic HLA class i repression in merkel cell carcinoma. *J Clin Invest* (2022). doi: 10.1172/JCI151666

59. Wu J, Lanier LL. Natural killer cells and cancer. *Adv Cancer Res* (2003) 90:127–56. doi: 10.1016/s0065-230x(03)90004-2

60. Wilson JL, Charo J, Martin-Fontecha A, Dellabona P, Casorati G, Chambers BJ, et al. NK cell triggering by the human costimulatory molecules CD80 and CD86. *J Immunol* (1999) 163(8):4207–12. doi: 10.4049/jimmunol.163.8.4207

61. Ritter C, Fan K, Paulson KG, Nghiem P, Schrama D, Becker JC. Reversal of epigenetic silencing of MHC class i chain-related protein a and b improves immune recognition of merkel cell carcinoma. *Sci Rep* (2016) 6:21678. doi: 10.1038/srep21678

62. Bhatia S, Church C, Paulson KG, Pierce RH, Nghiem P, Lee JH, et al. O19 final results from a phase 2 study using off-the-shelf activated natural killer (aNK) cells in combination with n-803, an IL-15 superagonist, in patients with metastatic merkel cell carcinoma (MCC). *Soc Immunotherapy Cancer* (2019).

63. Hanna GJ, Kacew AJ, Tanguturi AR, Grote HJ, Vergara V, Brunkhorst B, et al. Association of programmed death 1 protein ligand (PD-L1) expression with prognosis in merkel cell carcinoma. *Front Med (Lausanne)* (2020) 7:198. doi: 10.3389/fmed.2020.00198

64. Im SJ, Hashimoto M, Gerner MY, Lee J, Kissick HT, Burger MC, et al. Defining CD8+ t cells that provide the proliferative burst after PD-1 therapy. *Nature* (2016) 537 (7620):417–21. doi: 10.1038/nature19330

65. Sade-Feldman M, Yizhak K, Bjorgaard SL, Ray JP, de Boer CG, Jenkins RW, et al. Defining t cell states associated with response to checkpoint immunotherapy in melanoma. *Cell* (2018) 175(4):998–1013 e20. doi: 10.1016/j.cell.2018.10.038

66. Siddiqui I, Schaeuble K, Chennupati V, Fuertes Marraco SA, Calderon-Copete S, Pais Ferreira D, et al. Intratumoral Tcf1(+)PD-1(+)CD8(+) t cells with stem-like properties promote tumor control in response to vaccination and checkpoint blockade immunotherapy. *Immunity* (2019) 50(1):195–211 e10. doi: 10.1016/j.immuni.2018.12.021

67. Kurtulus S, Madi A, Escobar G, Klapholz M, Nyman J, Christian E, et al. Checkpoint blockade immunotherapy induces dynamic changes in PD-1(-)CD8(+) tumor-infiltrating t cells. *Immunity* (2019) 50(1):181–94 e6. doi: 10.1016/j.immuni.2018.11.014

68. Miller BC, Sen DR, Al Abosy R, Bi K, Virkud YV, LaFleur MW, et al. Subsets of exhausted CD8(+) t cells differentially mediate tumor control and respond to checkpoint blockade. *Nat Immunol* (2019) 20(3):326–36. doi: 10.1038/s41590-019-0312-6

69. Burger ML, Cruz AM, Crossland GE, Gaglia G, Ritch CC, Blatt SE, et al. Antigen dominance hierarchies shape TCF1(+) progenitor CD8 t cell phenotypes in tumors. *Cell* (2021) 184(19):4996–5014 e26. doi: 10.1016/j.cell.2021.08.020

70. Qiu J, Xu B, Ye D, Ren D, Wang S, Benci JL, et al. Cancer cells resistant to immune checkpoint blockade acquire interferon-associated epigenetic memory to sustain t cell dysfunction. *Nat Cancer* (2023) 4(1):43–61. doi: 10.1038/s43018-022-00490-y

71. Hay ZLZ, Knapp JR, Magallon RE, O'Connor BP, Slansky JE. Low TCR binding strength results in increased progenitor-like CD8+ tumor-infiltrating lymphocytes. *Cancer Immunol Res* (2023). doi: 10.1158/2326-6066.CIR-22-0761

72. Patel S, Othus M, Prieto V, Lowe M, Buchbinder E, Chen Y, et al. LBA6 neoadjvuant versus adjuvant pembrolizumab for resected stage III-IV melanoma (SWOG S1801). *Ann Oncol* (2022). doi: 10.1016/j.annonc.2022.08.039

73. Yost KE, Satpathy AT, Wells DK, Qi Y, Wang C, Kageyama R, et al. Clonal replacement of tumor-specific t cells following PD-1 blockade. *Nat Med* (2019) 25 (8):1251–59. doi: 10.1038/s41591-019-0522-3

74. Holm JS, Funt SA, Borch A, Munk KK, Bjerregaard AM, Reading JL, et al. Neoantigen-specific CD8 t cell responses in the peripheral blood following PD-L1 blockade might predict therapy outcome in metastatic urothelial carcinoma. *Nat Commun* (2022) 13(1):1935. doi: 10.1038/s41467-022-29342-0

75. Luoma AM, Suo S, Wang Y, Gunasti L, Porter CBM, Nabilsi N, et al. Tissue-resident memory and circulating t cells are early responders to pre-surgical cancer immunotherapy. *Cell* (2022) 185(16):2918–35e29. doi: 10.1016/j.cell.2022.06.018

76. Sidhom JW, Oliveira G, Ross-MacDonald P, Wind-Rotolo M, Wu CJ, Pardoll DM, et al. Deep learning reveals predictive sequence concepts within immune repertoires to immunotherapy. *Sci Adv* (2022) 8(37)::eabq5089. doi: 10.1126/sciadv.abq5089

77. Schumacher TN, Schreiber RD. Neoantigens in cancer immunotherapy. *Science* (2015) 348(6230):69–74. doi: 10.1126/science.aaa4971

78. Van Allen EM, Miao D, Schilling B, Shukla SA, Blank C, Zimmer L, et al. Genomic correlates of response to CTLA-4 blockade in metastatic melanoma. *Science* (2015) 350(6257):207–11. doi: 10.1126/science.aad0095

79. Lawrence MS, Stojanov P, Polak P, Kryukov GV, Cibulskis K, Sivachenko A, et al. Mutational heterogeneity in cancer and the search for new cancer-associated genes. *Nature* (2013) 499(7457):214–18. doi: 10.1038/nature12213

80. Le DT, Durham JN, Smith KN, Wang H, Bartlett BR, Aulakh LK, et al. Mismatch repair deficiency predicts response of solid tumors to PD-1 blockade. *Science* (2017) 357(6349):409–13. doi: 10.1126/science.aan6733

81. Le DT, Uram JN, Wang H, Bartlett BR, Kemberling H, Eyring AD, et al. PD-1 blockade in tumors with mismatch-repair deficiency. *N Engl J Med* (2015) 372 (26):2509–20. doi: 10.1056/NEJMoa1500596

82. Palmer DB. The effect of age on thymic function. *Front Immunol* (2013) 4:316. doi: 10.3389/fimmu.2013.00316

83. Spranger S, Bao R, Gajewski TF. Melanoma-intrinsic beta-catenin signalling prevents anti-tumour immunity. *Nature* (2015) 523(7559):231–5. doi: 10.1038/nature14404

84. Petitprez F, de Reynies A, Keung EZ, Chen TW, Sun CM, Calderaro J, et al. B cells are associated with survival and immunotherapy response in sarcoma. *Nature* (2020) 577(7791):556–60. doi: 10.1038/s41586-019-1906-8

85. Cabrita R, Lauss M, Sanna A, Donia M, Skaarup Larsen M, Mitra S, et al. Tertiary lymphoid structures improve immunotherapy and survival in melanoma. *Nature* (2020) 577(7791):561–65. doi: 10.1038/s41586-019-1914-8

86. Helmink BA, Reddy SM, Gao J, Zhang S, Basar R, Thakur R, et al. B cells and tertiary lymphoid structures promote immunotherapy response. *Nature* (2020) 577 (7791):549–55. doi: 10.1038/s41586-019-1922-8

87. Fridman WH, Pages F, Sautes-Fridman C, Galon J. The immune contexture in human tumours: impact on clinical outcome. *Nat Rev Cancer* (2012) 12(4):298–306. doi: 10.1038/nrc3245

88. Thommen DS, Schumacher TN. T cell dysfunction in cancer. *Cancer Cell* (2018) 33(4):547–62. doi: 10.1016/j.ccell.2018.03.012

89. Paulson KG, Carter JJ, Johnson LG, Cahill KW, Iyer JG, Schrama D, et al. Antibodies to merkel cell polyomavirus t antigen oncoproteins reflect tumor burden in merkel cell carcinoma patients. *Cancer Res* (2010) 70(21):8388–97. doi: 10.1158/0008-5472.CAN-10-2128

90. Manguso RT, Pope HW, Zimmer MD, Brown FD, Yates KB, Miller BC, et al. *In vivo* CRISPR screening identifies Ptpn2 as a cancer immunotherapy target. *Nature* (2017) 547(7664):413–18. doi: 10.1038/nature23270

91. Ishizuka JJ, Manguso RT, Cheruiyot CK, Bi K, Panda A, Iracheta-Vellve A, et al. Loss of ADAR1 in tumours overcomes resistance to immune checkpoint blockade. *Nature* (2019) 565(7737):43–8. doi: 10.1038/s41586-018-0768-9

92. Griffin GK, Wu J, Iracheta-Vellve A, Patti JC, Hsu J, Davis T, et al. Epigenetic silencing by SETDB1 suppresses tumour intrinsic immunogenicity. *Nature* (2021) 595 (7866):309–14. doi: 10.1038/s41586-021-03520-4

93. Sun Y, Revach OY, Anderson S, Kessler EA, Wolfe CH, Jenney A, et al. Targeting TBK1 to overcome resistance to cancer immunotherapy. *Nature* (2023) 615:158–67. doi: 10.1038/s41586-023-05704-6

94. Arlauckas SP, Garris CS, Kohler RH, Kitaoka M, Cuccarese MF, Yang KS, et al. *In vivo* imaging reveals a tumor-associated macrophage-mediated resistance pathway in anti-PD-1 therapy. *Sci Transl Med* (2017) 9(389). doi: 10.1126/scitranslmed.aal3604

95. Hakozaki T, Richard C, Elkrief A, Hosomi Y, Benlaifaoui M, Mimpen I, et al. The gut microbiome associates with immune checkpoint inhibition outcomes in patients with advanced non-small cell lung cancer. *Cancer Immunol Res* (2020) 8 (10):1243–50. doi: 10.1158/2326-6066.CIR-20-0196

96. Vetizou M, Pitt JM, Daillere R, Lepage P, Waldschmitt N, Flament C, et al. Anticancer immunotherapy by CTLA-4 blockade relies on the gut microbiota. *Science* (2015) 350(6264):1079–84. doi: 10.1126/science.aad1329

97. Matson V, Fessler J, Bao R, Chongsuwat T, Zha Y, Alegre ML, et al. The commensal microbiome is associated with anti-PD-1 efficacy in metastatic melanoma patients. *Science* (2018) 359(6371):104–08. doi: 10.1126/science.aao3290

98. Chaput N, Lepage P, Coutzac C, Soularue E, Le Roux K, Monot C, et al. Baseline gut microbiota predicts clinical response and colitis in metastatic melanoma patients treated with ipilimumab. *Ann Oncol* (2017) 28(6):1368–79. doi: 10.1093/annonc/mdx108

99. Routy B, Le Chatelier E, Derosa L, Duong CPM, Alou MT, Daillere R, et al. Gut microbiome influences efficacy of PD-1-based immunotherapy against epithelial tumors. *Science* (2018) 359(6371):91–7. doi: 10.1126/science.aan3706

100. Gopalakrishnan V, Spencer CN, Nezi L, Reuben A, Andrews MC, Karpinets TV, et al. Gut microbiome modulates response to anti-PD-1 immunotherapy in melanoma patients. *Science* (2018) 359(6371):97–103. doi: 10.1126/science.aan4236

101. Zheng Y, Wang T, Tu X, Huang Y, Zhang H, Tan D, et al. Gut microbiome affects the response to anti-PD-1 immunotherapy in patients with hepatocellular carcinoma. *J Immunother Cancer* (2019) 7(1):193. doi: 10.1186/s40425-019-0650-9

102. Elkrief A, Derosa L, Kroemer G, Zitvogel L, Routy B. The negative impact of antibiotics on outcomes in cancer patients treated with immunotherapy: a new independent prognostic factor? *Ann Oncol* (2019) 30(10):1572–79. doi: 10.1093/annonc/mdz206

103. Wilson BE, Routy B, Nagrial A, Chin VT. The effect of antibiotics on clinical outcomes in immune-checkpoint blockade: a systematic review and meta-analysis of observational studies. *Cancer Immunol Immunother* (2020) 69(3):343–54. doi: 10.1007/s00262-019-02453-2

104. Pinato DJ, Howlett S, Ottaviani D, Urus H, Patel A, Mineo T, et al. Association of prior antibiotic treatment with survival and response to immune checkpoint inhibitor therapy in patients with cancer. *JAMA Oncol* (2019) 5(12):1774–78. doi: 10.1001/jamaoncol.2019.2785

105. Oh DY, Kwek SS, Raju SS, Li T, McCarthy E, Chow E, et al. Intratumoral CD4 (+) t cells mediate anti-tumor cytotoxicity in human bladder cancer. *Cell* (2020) 181 (7):1612–25e13. doi: 10.1016/j.cell.2020.05.017

106. Anagnostou V, Smith KN, Forde PM, Niknafs N, Bhattacharya R, White J, et al. Evolution of neoantigen landscape during immune checkpoint blockade in non-small cell lung cancer. *Cancer Discovery* (2017) 7(3):264–76. doi: 10.1158/2159-8290.CD-16-0828

107. Zaretsky JM, Garcia-Diaz A, Shin DS, Escuin-Ordinas H, Hugo W, Hu-Lieskovan S, et al. Mutations associated with acquired resistance to PD-1 blockade in melanoma. *N Engl J Med* (2016) 375(9):819–29. doi: 10.1056/NEJMoa1604958

108. George S, Miao D, Demetri GD, Adeegbe D, Rodig SJ, Shukla S, et al. Loss of PTEN is associated with resistance to anti-PD-1 checkpoint blockade therapy in

metastatic uterine leiomyosarcoma. *Immunity* (2017) 46(2):197–204. doi: 10.1016/j.immuni.2017.02.001

109. Peng W, Chen JQ, Liu C, Malu S, Creasy C, Tetzlaff MT, et al. Loss of PTEN promotes resistance to t cell-mediated immunotherapy. *Cancer Discovery* (2016) 6 (2):202–16. doi: 10.1158/2159-8290.CD-15-0283

110. Kalia V, Sarkar S. Antigen-addicted t cell reserves trickle charge the frontline killers. *Immunity* (2016) 45(1):10–2. doi: 10.1016/j.immuni.2016.07.004

111. Pauken KE, Sammons MA, Odorizzi PM, Manne S, Godec J, Khan O, et al. Epigenetic stability of exhausted t cells limits durability of reinvigoration by PD-1 blockade. *Science* (2016) 354(6316):1160–65. doi: 10.1126/science.aaf2807

112. Huang AC, Postow MA, Orlowski RJ, Mick R, Bengsch B, Manne S, et al. T-cell invigoration to tumour burden ratio associated with anti-PD-1 response. *Nature* (2017) 545(7652):60–5. doi: 10.1038/nature22079

113. Gutwillig A, Santana-Magal N, Farhat-Younis L, Rasoulouniriana D, Madi A, Luxenburg C, et al. Transient cell-in-cell formation underlies tumor relapse and resistance to immunotherapy. *Elife* (2022). doi: 10.7554/eLife.80315

114. Haslam A, Prasad V. Estimation of the percentage of US patients with cancer who are eligible for and respond to checkpoint inhibitor immunotherapy drugs. *JAMA Netw Open* (2019) 2(5):e192535. doi: 10.1001/jamanetworkopen.2019.2535

115. Verhaegen ME, Harms PW, Van Goor JJ, Arche J, Patrick MT, Wilbert D, et al. Direct cellular reprogramming enables development of viral t antigen-driven merkel cell carcinoma in mice. *J Clin Invest* (2022) 132(7). doi: 10.1172/JCI152069

116. Veatch JR, Riddell SR. Immune checkpoint blockade provokes resident memory t cells to eliminate head and neck cancer. *Cell* (2022) 185(16):2848–49. doi: 10.1016/j.cell.2022.07.006

117. Stahl PL, Salmen F, Vickovic S, Lundmark A, Navarro JF, Magnusson J, et al. Visualization and analysis of gene expression in tissue sections by spatial transcriptomics. *Science* (2016) 353(6294):78–82. doi: 10.1126/science.aaf2403

118. Merritt CR, Ong GT, Church SE, Barker K, Danaher P, Geiss G, et al. Multiplex digital spatial profiling of proteins and RNA in fixed tissue. *Nat Biotechnol* (2020) 38 (5):586–99. doi: 10.1038/s41587-020-0472-9

119. Chen KH, Boettiger AN, Moffitt JR, Wang S, Zhuang X. RNA imaging. spatially resolved, highly multiplexed RNA profiling in single cells. *Science* (2015) 348(6233): aaa6090. doi: 10.1126/science.aaa6090

120. Chavez M, Chen X, Finn PB, Qi LS. Advances in CRISPR therapeutics. *Nat Rev Nephrol* (2023) 19(1):9–22. doi: 10.1038/s41581-022-00636-2

121. Chan HY, Zhang J, Garliss CC, Kwaa AK, Blankson JN, Smith KN. A t cell receptor sequencing-based assay identifies cross-reactive recall CD8(+) t cell clonotypes against autologous HIV-1 epitope variants. *Front Immunol* (2020) 11:591. doi: 10.3389/fimmu.2020.00591

122. Lowery FJ, Krishna S, Yossef R, Parikh NB, Chatani PD, Zacharakis N, et al. Molecular signatures of antitumor neoantigen-reactive t cells from metastatic human cancers. *Science* (2022) 375(6583):877–84. doi: 10.1126/science.abl5447

123. Zhang J, Caushi J, Oliveira G, Zhang B, Ji Z , Naidoo J, et al. Development and validation of a neoantigen-specific t cell gene signature to identify antitumor t cells in lung cancer and melanoma. *Soc Immunotherapy Cancer* (2021) 9(Suppl 2). doi: 10.1136/jitc-2021-SITC2021.327

124. Emerson RO, DeWitt WS, Vignali M, Gravley J, Hu JK, Osborne EJ, et al. Immunosequencing identifies signatures of cytomegalovirus exposure history and HLA-mediated effects on the t cell repertoire. *Nat Genet* (2017) 49(5):659–65. doi: 10.1038/ng.3822

125. Elyanow R, Snyder TM, Dalai SC, Gittelman RM, Boonyaratanakornkit J, Wald A, et al. T cell receptor sequencing identifies prior SARS-CoV-2 infection and correlates with neutralizing antibodies and disease severity. *JCI Insight* (2022) 7(10). doi: 10.1172/jci.insight.150070

126. Greissl J, Pesesky M, Dalai SC, Rebman AW, Soloski MJ, Horn EJ, et al. Immunosequencing of the t-cell receptor repertoire reveals signatures specific for identification and characterization of early lyme disease. *MedRxiv* (2022). doi: 10.1101/2021.07.30.21261353

127. Saxena M, van der Burg SH, Melief CJM, Bhardwaj N. Therapeutic cancer vaccines. *Nat Rev Cancer* (2021) 21(6):360–78. doi: 10.1038/s41568-021-00346-0

128. Mougel A, Terme M, Tanchot C. Therapeutic cancer vaccine and combinations with antiangiogenic therapies and immune checkpoint blockade. *Front Immunol* (2019) 10:467. doi: 10.3389/fimmu.2019.00467

129. Rosean CB, Karkada M, Koelle DM, Nghiem P , Heiland T. LAMP1 targeting of the large t antigen of merkel cell polyomavirus elicits potent CD4+ t cell responses, tumor inhibition, and provides rationale for first-in-human trial. *Cancer Res* (2022) 82 (12_Supplement). doi: 10.1158/1538-7445.AM2022-2052

130. Veatch J, Akkiraju A, Darwanto A, Garrity S, Hallet D , Nguyen K, et al. ATTAC-MCC: Phase I/II study of autologous CD8+ and CD4+ transgenic t cells expressing a high affinity MCPyV-specific TCR combined with checkpoint inhibitors and class i MHC-upregulation in patients with metastatic MCC refractory to PD-1 axis blockade. *ASCO Annu Meeting* (2022) 40(16_Suppl). oi: 10.1200/JCO.2022.40.16_suppl.TPS9596

131. Rohaan MW, Borch TH, van den Berg JH, Met O, Kessels R, Geukes Foppen MH, et al. Tumor-infiltrating lymphocyte therapy or ipilimumab in advanced melanoma. *N Engl J Med* (2022) 387(23):2113–25. doi: 10.1056/NEJMoa2210233

132. Goff PH, Bhakuni R, Pulliam T, Lee JH, Hall ET, Nghiem P. Intersection of two checkpoints: Could inhibiting the DNA damage response checkpoint rescue immune checkpoint-refractory cancer? *Cancers (Basel)* (2021) 13(14). doi: 10.3390/cancers13143415

133. Vendetti FP, Karukonda P, Clump DA, Teo T, Lalonde R, Nugent K, et al. ATR kinase inhibitor AZD6738 potentiates CD8+ t cell-dependent antitumor activity following radiation. *J Clin Invest* (2018) 128(9):3926–40. doi: 10.1172/JCI96519

134. Combes E, Andrade AF, Tosi D, Michaud HA, Coquel F, Garambois V, et al. Inhibition of ataxia-telangiectasia mutated and RAD3-related (ATR) overcomes oxaliplatin resistance and promotes antitumor immunity in colorectal cancer. *Cancer Res* (2019) 79(11):2933–46. doi: 10.1158/0008-5472.CAN-18-2807

135. Sheng H, Huang Y, Xiao Y, Zhu Z, Shen M, Zhou P, et al. ATR inhibitor AZD6738 enhances the antitumor activity of radiotherapy and immune checkpoint inhibitors by potentiating the tumor immune microenvironment in hepatocellular carcinoma. *J Immunother Cancer* (2020) 8(1). doi: 10.1136/jitc-2019-000340

136. Sun LL, Yang RY, Li CW, Chen MK, Shao B, Hsu JM, et al. Inhibition of ATR downregulates PD-L1 and sensitizes tumor cells to t cell-mediated killing. *Am J Cancer Res* (2018) 8(7):1307–16.

137. Lopez-Pelaez M, Young L, Vazquez-Chantada M, Nelson N, Durant S, Wilkinson RW, et al. Targeting DNA damage response components induces enhanced STING-dependent type-i IFN response in ATM deficient cancer cells and drives dendritic cell activation. *Oncoimmunology* (2022) 11(1):2117321. doi: 10.1080/2162402X.2022.2117321

138. Zhang Q, Green MD, Lang X, Lazarus J, Parsels JD, Wei S, et al. Inhibition of ATM increases interferon signaling and sensitizes pancreatic cancer to immune checkpoint blockade therapy. *Cancer Res* (2019) 79(15):3940–51. doi: 10.1158/0008-5472.CAN-19-0761

139. Tsai AK, Khan AY, Worgo CE, Wang LL, Liang Y, Davila E. A multikinase and DNA-PK inhibitor combination immunomodulates melanomas, suppresses tumor progression, and enhances immunotherapies. *Cancer Immunol Res* (2017) 5(9):790–803. doi: 10.1158/2326-6066.CIR-17-0009

140. Tabachnick-Cherny S, Pulliam T, Church C, Koelle DM, Nghiem P. Polyomavirus-driven merkel cell carcinoma: Prospects for therapeutic vaccine development. *Mol Carcinog* (2020) 59(7):807–21. doi: 10.1002/mc.23190

141. Qin S, Xu L, Yi M, Yu S, Wu K, Luo S. Novel immune checkpoint targets: moving beyond PD-1 and CTLA-4. *Mol Cancer* (2019) 18(1):155. doi: 10.1186/s12943-019-1091-2

142. Badoual C, Hans S, Merillon N, Van Ryswick C, Ravel P, Benhamouda N, et al. PD-1-expressing tumor-infiltrating t cells are a favorable prognostic biomarker in HPV-associated head and neck cancer. *Cancer Res* (2013) 73(1):128–38. doi: 10.1158/0008-5472.CAN-12-2606

143. Saiag P, Blom A. Combined nivolumab and ipilimumab in non-resectable merkel cell carcinoma. *Lancet* (2022) 400(10357):976–77. doi: 10.1016/S0140-6736(22)01749-4

144. Bertrand A, Kostine M, Barnetche T, Truchetet ME, Schaeverbeke T. Immune related adverse events associated with anti-CTLA-4 antibodies: systematic review and meta-analysis. *BMC Med* (2015) 13:211. doi: 10.1186/s12916-015-0455-8

145. Khair DO, Bax HJ, Mele S, Crescioli S, Pellizzari G, Khiabany A, et al. Combining immune checkpoint inhibitors: Established and emerging targets and strategies to improve outcomes in melanoma. *Front Immunol* (2019) 10:453. doi: 10.3389/fimmu.2019.00453

146. He Y, Rivard CJ, Rozeboom L, Yu H, Ellison K, Kowalewski A, et al. Lymphocyte-activation gene-3, an important immune checkpoint in cancer. *Cancer Sci* (2016) 107(9):1193–7. doi: 10.1111/cas.12986

147. Huard B, Prigent P, Pages F, Bruniquel D, Triebel F. T cell major histocompatibility complex class II molecules down-regulate CD4+ t cell clone responses following LAG-3 binding. *Eur J Immunol* (1996) 26(5):1180–6. doi: 10.1002/eji.1830260533

148. Wolf Y, Anderson AC, Kuchroo VK. TIM3 comes of age as an inhibitory receptor. *Nat Rev Immunol* (2020) 20(3):173–85. doi: 10.1038/s41577-019-0224-6

149. Tian T, Li Z. Targeting tim-3 in cancer with resistance to PD-1/PD-L1 blockade. *Front Oncol* (2021) 11:731175. doi: 10.3389/fonc.2021.731175

150. Chocarro L, Blanco E, Arasanz H, Fernandez-Rubio L, Bocanegra A, Echaide M, et al. Clinical landscape of LAG-3-targeted therapy. *Immunooncol Technol* (2022) 14:100079. doi: 10.1016/j.iotech.2022.100079

151. Tawbi HA, Schadendorf D, Lipson EJ, Ascierto PA, Matamala L, Castillo Gutierrez E, et al. Relatlimab and nivolumab versus nivolumab in untreated advanced melanoma. *N Engl J Med* (2022) 386(1):24–34. doi: 10.1056/NEJMoa2109970

152. Yarchoan M, Hopkins A, Jaffee EM. Tumor mutational burden and response rate to PD-1 inhibition. *N Engl J Med* (2017) 377(25):2500–01. doi: 10.1056/NEJMc1713444

Glossary

ADAR1	Adenosine Deaminase Acting on RNA 1
ATR	Ataxia telangiectasia and Rad3-related
C/EBP	CCAAT/enhancer binding protein
CLA	Cutaneous lymphocyte antigen
CTLA-4	Cytotoxic T lymphocyte-associated protein 4
EGR1	Early growth response factor 1
ER	Endoplasmic reticulum
HPV	Human papillomavirus
ICI	Immune checkpoint inhibition
IFN-γ	Interferon gamma
IL-2	Interleukin-2
IL-4	Interleukin-4
IL-10	Interleukin-10
JAK	Janus kinase
LAG-3	Lymphocyte activation gene 3
LPS	Lipopolysaccharide
MCC	Merkel cell carcinoma
MCPyV	Merkel cell polyomavirus
MHC	Major histocompatibility complex
MSI	Microsatellite instability
NK	Natural killer
PD-1	Programmed cell death protein 1
PD-L1	Programmed death ligand 1
PTEN	Phosphatase and tensin homolog
PTPN2	Protein tyrosine phosphatase non-receptor 2
PDX	Patient-derived xenograft
SETDB1	SET Domain Bifurcated Histone Lysine Methyltransferase 1
STAT3	Signal transducer and activator of transcription 3
STING	Stimulator of interferon genes
TAP	Transporter associated with antigen presentation
TBK1	Tank-binding kinase 1
TCR	T cell receptor
TGF-β1	Transforming growth factor beta 1
TIGIT	T cell immunoreceptor with Ig and ITIM domains
TIL	Tumor-infiltrating lymphocytes
TIM-3	T cell immunoglobulin and mucin domain 3
TLR9	Toll-like receptor 9
TLS	Tertiary lymphoid structures
TME	Tumor microenvironment
TMB	Tumor mutational burden
UV	Ultraviolet
VEGF	Vascular endothelial growth factor
WES	Whole exome sequencing

Chapter 2: Circulating cancer-specific CD8 T cell frequency is associated with response to PD-1 blockade in Merkel cell carcinoma

Thomas Pulliam*, Saumya Jani*, Lichen Jing, Heeju Ryu, Ana Jojic, Carolyn Shasha, Jiajia Zhang, Rima Kulikauskas, Candice Church, Charlie Garnett-Benson, Ted Gooley, Aude Chapuis, Kelly Paulson, Kellie N. Smith, Drew M. Pardoll, Evan W. Newell, David M. Koelle, Suzanne L. Topalian, Paul Nghiem

Cell Reports Medicine, February 2024

CHAPTER SUMMARY: In this chapter, we use virus-driven Merkel cell carcinoma (MCC) to elucidate mechanisms of response and resistance to anti-PD-(L)1 therapies. We learn that the frequency of tumor-specific CD8 T cells in the blood before treatment strongly associates with recurrence-free survival after PD-1 blockade. However, the frequency of these cells in the tumor does not. In interrogating this discrepancy, we learn that the tumor-specific CD8 T cells in the blood are less dysfunctional than their intratumoral counterparts, suggesting that they may be more amenable to activation by immunotherapy and crucial in mediating disease regression.

An excellent lay summary of this chapter (as well as Chapter 3) can be found here: https://www.fredhutch.org/en/news/center-news/2024/02/biomarker-immune-checkpoint-inhibitor-merkel-cell-carcinoma.html

Cell Reports
Medicine

Article

Circulating cancer-specific CD8 T cell frequency is associated with response to PD-1 blockade in Merkel cell carcinoma

Graphical abstract

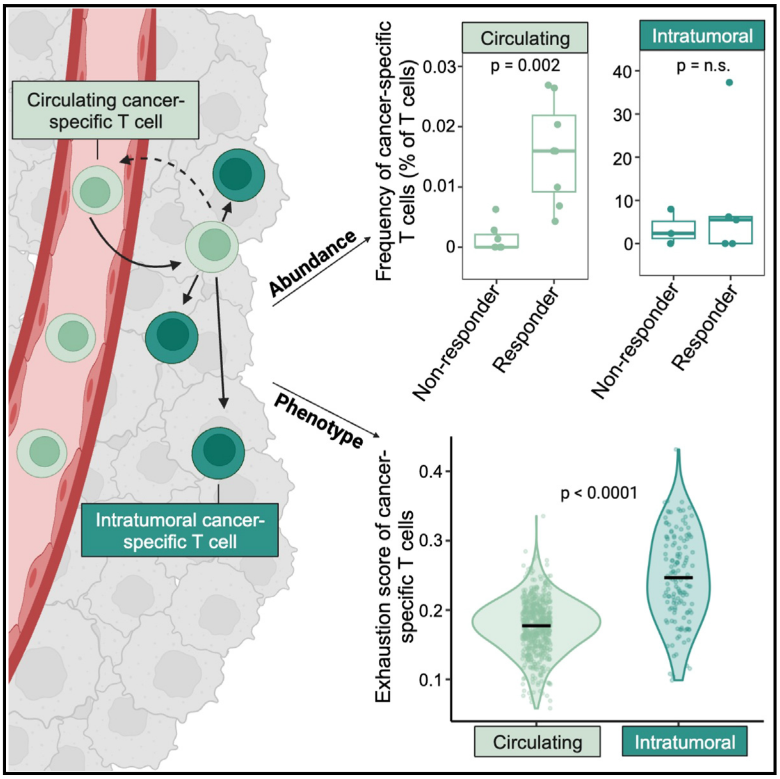

Highlights

- Frequency of anti-tumor CD8 T cells at baseline in blood predicts anti-PD-1 response
- Frequency of anti-tumor CD8 T cells in the tumor does not predict anti-PD-1 response
- Intratumoral CD8 T cells are more dysfunctional than their peripheral counterparts
- HLA-I downregulation is a mechanism of secondary resistance to anti-PD-1 in MCC

Authors

Thomas Pulliam, Saumya Jani, Lichen Jing, ..., David M. Koelle, Suzanne L. Topalian, Paul Nghiem

Correspondence

pnghiem@uw.edu

In brief

Pulliam et al. identified that the frequency of anti-tumor CD8 T cells in the blood is associated with response to anti-PD-1 treatment but the frequency of these cells in the tumor is not. Anti-tumor T cells in the blood are less dysfunctional than their intratumoral counterparts, which may contribute to this difference.

Pulliam et al., 2024, Cell Reports Medicine *5*, 101412
February 20, 2024
https://doi.org/10.1016/j.xcrm.2024.101412

CellPress

Please cite this article in press as: Pulliam et al., Circulating cancer-specific CD8 T cell frequency is associated with response to PD-1 blockade in Merkel cell carcinoma, Cell Reports Medicine (2024), https://doi.org/10.1016/j.xcrm.2024.101412

Cell Reports Medicine

CellPress
OPEN ACCESS

Article

Circulating cancer-specific CD8 T cell frequency is associated with response to PD-1 blockade in Merkel cell carcinoma

Thomas Pulliam,[1,15] Saumya Jani,[1,2,15] Lichen Jing,[3] Heeju Ryu,[4] Ana Jojic,[4] Carolyn Shasha,[4] Jiajia Zhang,[5,6,14] Rima Kulikauskas,[1] Candice Church,[1] Charlie Garnett-Benson,[7] Ted Gooley,[8] Aude Chapuis,[3,8] Kelly Paulson,[9,10] Kellie N. Smith,[5,6] Drew M. Pardoll,[5,6] Evan W. Newell,[2,4] David M. Koelle,[2,3,4,11,12] Suzanne L. Topalian,[6,13] and Paul Nghiem[1,16,*]

[1]Division of Dermatology, Department of Medicine, University of Washington, Seattle, WA 98109, USA
[2]Department of Laboratory Medicine and Pathology, University of Washington, Seattle, WA 98109, USA
[3]Department of Medicine, University of Washington, Seattle, WA 98109, USA
[4]Vaccine and Infectious Disease Department, Fred Hutchinson Cancer Center, Seattle, WA 98109, USA
[5]Department of Oncology, Johns Hopkins University, Baltimore, MD 21827, USA
[6]The Bloomberg-Kimmel Institute for Cancer Immunotherapy, Johns Hopkins University, Baltimore, MD 21287, USA
[7]Bristol Myers Squibb, Princeton, NJ 08540, USA
[8]Clinical Research Division, Fred Hutchinson Cancer Center, Seattle, WA 98109, USA
[9]Paul G. Allen Research Center, Providence-Swedish Cancer Institute, Seattle, WA 98104, USA
[10]Elson S. Floyd College of Medicine, Washington State University, Spokane, WA 99202, USA
[11]Department of Global Health, University of Washington, Seattle, WA 98109, USA
[12]Benaroya Research Institute, Seattle, WA 98101, USA
[13]Department of Surgery, Johns Hopkins University, Baltimore, MD 21287, USA
[14]Present address: Department of Medicine, University of California, Los Angeles, Los Angeles, CA, USA
[15]These authors contributed equally
[16]Lead contact
*Correspondence: pnghiem@uw.edu

https://doi.org/10.1016/j.xcrm.2024.101412

SUMMARY

Understanding cancer immunobiology has been hampered by difficulty identifying cancer-specific T cells. Merkel cell polyomavirus (MCPyV) causes most Merkel cell carcinomas (MCCs). All patients with virus-driven MCC express MCPyV oncoproteins, facilitating identification of virus (cancer)-specific T cells. We studied MCPyV-specific T cells from 27 patients with MCC using MCPyV peptide-HLA-I multimers, 26-color flow cytometry, single-cell transcriptomics, and T cell receptor (TCR) sequencing. In a prospective clinical trial, higher circulating MCPyV-specific CD8 T cell frequency before anti-PD-1 treatment was strongly associated with 2-year recurrence-free survival (75% if detectable, 0% if undetectable, $p = 0.0018$; ClinicalTrial.gov: NCT02488759). Intratumorally, such T cells were typically present, but their frequency did not significantly associate with response. Circulating MCPyV-specific CD8 T cells had increased stem/memory and decreased exhaustion signatures relative to their intratumoral counterparts. These results suggest that cancer-specific CD8 T cells in the blood may play a role in anti-PD-1 responses. Thus, strategies that augment their number or mobilize them into tumors could improve outcomes.

INTRODUCTION

Immunotherapies that inhibit the PD-1 pathway have revolutionized oncology, but PD-(L)1 blockade is not effective for many patients with metastatic cancers.[1,2] Multiple immunotherapy resistance mechanisms involving diverse pathways and cell types have been identified.[3] However, these mechanisms are thought to ultimately work by disrupting the recognition of cancer cells by tumor-specific T cells and/or inhibiting their function. Tumor recognition can be disrupted if (1) immunogenic cancer antigens are downregulated by cancer cells, (2) the cancer antigens are not presented on the cell surface due to loss of major histocompatibility complex (MHC) molecules or antigen presentation machinery, or (3) there is a lack of functional cancer-specific T cells.

Difficulties in identifying cancer-specific T cells have significantly limited direct studies of these mechanisms. The paucity of studies of cancer-specific CD8 T cells in humans is due in part to challenges in identifying these cells and their cognate antigens. In most cancers, adaptive immune responses develop against mutated proteins (neoantigens) or against self-proteins selectively overexpressed within the tumor (tumor-associated antigens [TAAs]). Since most neoantigens are not shared across

Please cite this article in press as: Pulliam et al., Circulating cancer-specific CD8 T cell frequency is associated with response to PD-1 blockade in Merkel cell carcinoma, Cell Reports Medicine (2024), https://doi.org/10.1016/j.xcrm.2024.101412

patients, customized immune reagents must be developed to study each patient's anti-tumor immune response. While TAAs are often shared across patients, they are less desirable to study relative to neoantigens or oncoviral antigens. Because they are self-proteins, both central and peripheral tolerance have resulted in deletion or anergy of many TAA-specific T cells.[4,5] Additionally, the TAA-specific T cells that are present have much lower functional avidity than neoantigen-specific T cells.[6] These limitations make it difficult to identify associations between clinical outcomes and cancer-specific T cell phenotypes across patients for most cancers.

During chronic antigen stimulation (originally studied in mouse models of acute and chronic LCMV[7,8]), T cell immune function progresses in a characteristic manner but ultimately reaches a state where virus-specific T cells are functionally unable to fully eliminate residual virus.[9–11] While controversial, and precise definitions vary,[12] a set of gene expression patterns and labels (precursor exhausted, terminally exhausted, etc.) is frequently used.[13] Because cancer-specific T cells are enriched in tumors, most studies of cancer-specific T cells in human cancers have focused on intratumoral CD8 T effector cells. Recent studies suggest that CD8 T cells in tumor-draining lymph nodes and blood may also play a key role in mediating systemic immunotherapy responses. Murine models have shown that cancer-specific CD8 T cells in lymph nodes are less dysfunctional/exhausted than their intratumoral counterparts.[14] Moreover, blocking the egress of these cells from tumor-draining lymph nodes abrogates anti-PD-(L)1 efficacy.[15] In mouse models, these less exhausted T cell subsets undergo expansion during anti-PD-(L)1 treatment and maintain a degree of effector capacity.[16–18] Other studies in humans have shown that there is substantial trafficking of CD8 T cell clones (some of which are likely cancer specific) between blood and tumor during immunotherapy,[19–21] suggesting that peripheral blood may be an important source of CD8 T cells that ultimately mediate tumor regression. Indeed, in a study of head and neck cancer, patients with higher levels of activated CD8 T cells (CD38$^+$, HLA-DR$^+$) in their blood were more likely to respond to immunotherapy.[22] However, the antigen specificities of these activated cells in the blood was not determined.

The paucity of studies of cancer-specific CD8 T cells in humans is due in part to difficulties in identifying these cells and their cognate antigens. While sparse, studies that have identified and profiled intratumoral cancer-specific CD8 T cells show epigenetically driven, sustained increases in expression of inhibitory co-receptors on these cells, corresponding to an exhausted phenotype.[6,23,24] Meanwhile, studies of TAA-specific CD8 T cells have shown an inconsistent relationship between their frequency and clinical outcomes.[25–28] In contrast to the challenges involved in studying mutationally driven cancers, virally driven cancers can facilitate the study of cancer-specific immune responses since viral oncoproteins are non-self, required for tumor growth, and shared across multiple patients.

To study cancer-specific CD8 T cells, we focused on Merkel cell carcinoma (MCC), a rare neuroendocrine skin cancer with a high initial response rate (>50%) to first-line anti-PD-(L)1 treatment.[29] These tumors are driven by the Merkel cell polyomavirus (MCPyV) in ∼80% of cases.[30] Oncogenesis by MCPyV requires two rare mutagenic events: truncation of the large T (LT) antigen and integration of the MCPyV genome into a human chromosome.[30] Importantly, these viral oncoproteins are persistently expressed in MCC and are absent in normal tissues, providing ideal targets for adaptive anti-cancer immune responses. MCPyV oncoproteins are also small (∼400 amino acids after integration and truncation), allowing more comprehensive *in vitro* profiling of virus-specific T cells than what is possible for larger oncogenic viruses, which can be more than 10 times larger.[29] Of note, readily detectable immune responses to MCPyV oncoproteins are rare (<1 of 10,000 circulating CD8 T cells) in healthy persons and in patients with virus-negative MCC (VN-MCC).[31,32]

These findings suggest that immune responses against MCPyV oncoproteins are cancer specific and not a response to background levels of MCPyV, which is frequently present on normal human skin.[33] Furthermore, the very low tumor mutation burden (TMB) in virally driven MCC (median of 13 somatic single nucleotide variants per exome compared with 1,121 in VN-MCC[34]) suggests that MCPyV oncoproteins are the likely targets of most anti-tumor immune responses in virus-positive MCC (VP-MCC). Given that antigen loss cannot be a mechanism of immunotherapy resistance in VP-MCC (ongoing expression of MCPyV oncoproteins is required for tumor cell growth),[35] we focused on the other two leading mechanisms: loss of antigen presentation and lack of cancer-specific T cells.

In the current study, we use HLA-I multimers incorporating MCPyV peptides to study cancer-specific CD8 T cells in the tumor and blood of MCC patients treated with anti-PD-(L)1 immunotherapy and correlate their frequencies with clinical outcomes. This was done using two independent patient groups, summarized in Figure 1. Cohort 1 consisted of 39 MCC patients with surgically resectable disease who were treated with a clinical trial of neoadjuvant (pre-surgical) nivolumab (ClinicalTrials.gov: NCT02488759[36]), and cohort 2 consisted of 8 patients with advanced MCPyV-positive MCC who had available tumor and blood specimens, three of whom had received immune checkpoint blockade during their treatment course. We found that the frequency of cancer-specific T cells in the blood is associated with PD-1 treatment, while the frequency of such cells in the tumor is not significantly associated. We investigated differences between peripheral and intratumoral cancer-specific T cells using single-cell RNA sequencing and found that the cancer-specific T cells in the blood are more functional than those in tumors.

RESULTS

The frequency of MCPyV-specific CD8 T cells in the blood is strongly associated with anti-PD-1 treatment response

The major oncogenic drivers of MCC, MCPyV small and LT antigens, are the result of alternative splicing and share a common amino terminus region.[37] A panel of HLA-I multimers containing peptides from these oncoproteins was assembled to identify cancer-specific T cells from patients with VP-MCC. To augment the panel of existing MCPyV-specific multimers,[38] tumor-infiltrating lymphocytes (TILs) from pre- and post-nivolumab-treated

Please cite this article in press as: Pulliam et al., Circulating cancer-specific CD8 T cell frequency is associated with response to PD-1 blockade in Merkel cell carcinoma, Cell Reports Medicine (2024), https://doi.org/10.1016/j.xcrm.2024.101412

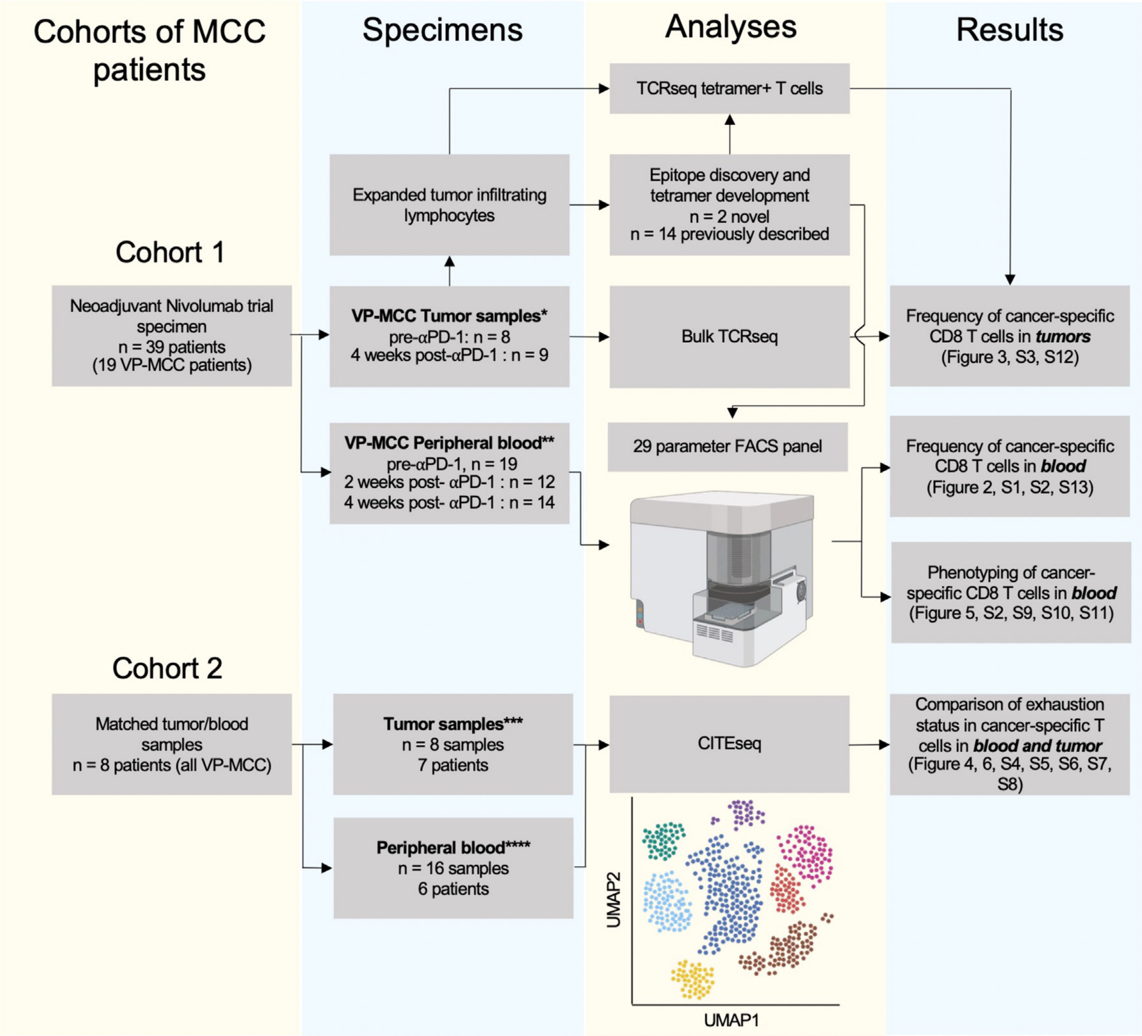

Figure 1. Overview of patient cohorts studied, analyses performed, result outputs, and relevant figures

27 patients with virus-positive tumors (VP-MCC) were studied. *Matched pre-and post-tumor samples were available from 9 patients. **Matched PBMC samples from all three time points were available from 16 patients. ***Matched pre- and post-tumor samples were available from 1 patient. ****Matched pre- and post-tumor samples were available from 3 patients.

patients were expanded *in vitro* and co-cultured with artificial antigen-presenting cells transfected with relevant patient-matched HLA-I alleles and MCPyV T antigen vectors (STAR Methods). TILs that produced IFN-γ in response to stimulation with MCPyV T antigens presented by patient-matched HLAs were then assayed with overlapping synthetic peptide pools to identify minimal epitopes.

This approach led to the identification of 2 novel epitopes (one A*68:01 restricted, one B*57:01 restricted; Figure S1) that were then combined with previously known MCPyV-epitopes[39] to create a panel of 16 HLA-I/MCPyV peptide multimers covering 15 unique HLA alleles (Table S1). These reagents were used to stain fresh-frozen peripheral blood mononuclear cells (PBMCs) from pre- and on-treatment blood collections from patients with resectable high-risk MCC who received neoadjuvant nivolumab for ~4 weeks before surgery (Figures 2A and S1; ClinicalTrials.gov: NCT02488759; see STAR Methods and Topalian et al.[36] for details). Pathologic scoring methods designed specifically to evaluate residual viable tumor following immunotherapy were applied to resected tumor tissues (see STAR Methods, DeCaprio,[37] and Jing et al.[38] for details). Patients whose tumor beds and draining lymph nodes no longer contained any viable tumor cells were designated to have had a "pathological complete response" (pCR). Patients whose tumor beds contained any residual viable tumor cells, even if markedly decreased, were defined as having a "non-PCR."

The presence of circulating MCPyV-specific CD8 T cells was highly associated with a pCR. Of the patients with available response data and MCPyV-specific CD8 T cells above the limit of reliable detection (frequency $\geq$ 0.01%, n = 10), 80% had a pCR. In contrast, none of the 5 patients with MCPyV-specific T cells below the limit of reliable detection had a pCR

Please cite this article in press as: Pulliam et al., Circulating cancer-specific CD8 T cell frequency is associated with response to PD-1 blockade in Merkel cell carcinoma, Cell Reports Medicine (2024), https://doi.org/10.1016/j.xcrm.2024.101412

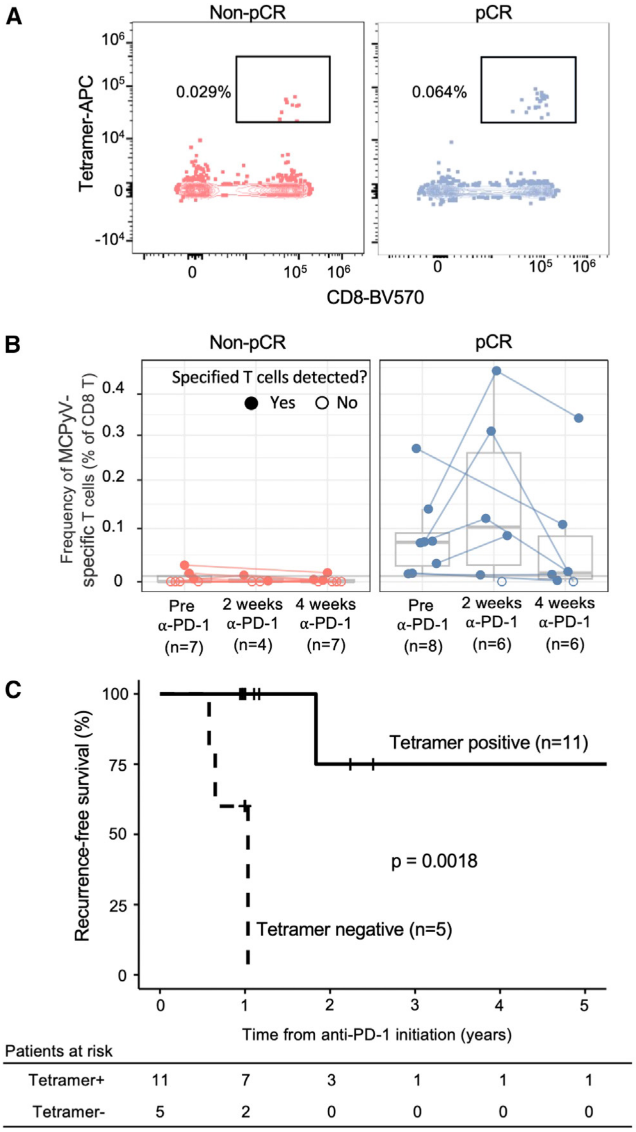

Figure 2. Associations between clinical outcome and relative frequency of MCPyV-specific CD8 T cells in the blood

(A) Representative example of the MCPyV-specific B*18:01 tetramer binding to pre-treatment CD8 T cells from a patient who later did not have a complete response (non-pCR; left) and a patient who later did have a pathological complete response (pCR; right). Frequencies shown represent the proportion of tetramer-binding T cells among all CD8 T cells.

(B) Comparison of MCPyV-specific CD8 T cell frequencies in patients who did or did not have a pCR. Open circles represent no detectable MCPyV-specific CD8 T cells. Statistical differences in MCPyV-specific T cell frequency prior to treatment were calculated using two-sided Wilcoxon rank-sum test.

(C) Kaplan-Meier plot of RFS in patients with MCPyV-specific CD8 T cells above the limit of reliable detection (tetramer positive) vs. those without such T cells (tetramer negative). The limit of reliable detection was set at 1 in 10,000 CD8 T cells (STAR Methods; Figure S1). Recurrence events included tumor recurrence or death due to any cause as in the original trial protocol.[36] Statistical differences in RFS were measured by log-rank test.

See also Figure S1 and Tables S1 and S2.

(p = 0.007, Fisher's exact test; Table S2). In addition to presence/absence, the relative frequency of these cells was also highly associated with response. The median pre-treatment frequency of MCPyV-specific CD8 T cells was 30-fold higher in the 8 patients with a pCR (0.073% of peripheral CD8 T cells) compared with the 7 patients with a non-pCR (0.0024%, p = 0.005 Wilcoxon test; Figure 2B). These findings suggest that pooled tetramer staining of peripheral blood for quantification of MCPyV-specific CD8 T cells may be a predictive biomarker for response to single-agent anti-PD-1 treatment. This approach also identifies patients who may require alternative or combination therapy.

The presence of MCPyV-specific CD8 T cells in the blood was also associated with recurrence-free survival (RFS). Patients who had MCPyV-specific CD8 T cells above the limit of reliable detection in their blood prior to initiation of nivolumab treatment had 75% RFS at 2 years compared with 0% RFS in patients who did not (Figure 2C; p = 0.0018 log rank test over the entire treatment period).

MCPyV CD8 T cells are present in tumors regardless of anti-PD-1 response

Given that the frequency of circulating MCPyV-specific CD8 T cells was associated with response, we next assessed if the frequency of intratumoral MCPyV-specific CD8 T cells and response were associated as well. To explore this, we quantified these cells in pre- and post-treatment tumor specimens. Due to limited sample quantity, we used an alternative approach to quantify MCPyV-specific CD8 T cells in tumor specimens. We used HLA-I multimers for MCPyV and selected other control viruses (CMV, EBV, and influenza virus [flu]) to isolate antigen-specific T cells from bulk-expanded tumor-infiltrating lymphocytes and determined the unique paired α-β T cell receptor (TCR) sequences of sorted antigen-specific CD8 T cells in individual patients at single cell-resolution. TCR chains identified from *ex vivo*-expanded TILs via multimer staining and single-cell TCRα/β sequencing were then matched to bulk TCR Vβ sequencing of the unmanipulated tumor specimen, allowing us to study the endogenous frequency of these MCPyV-specific TILs (see Table S3 for a list of all epitopes used; Figure 3A). Paired α-β TCRseq identified 152 unique TCRs with known specificity for a viral antigen (Figure 3B; Table S4). To validate our tetramer-based specificity assignments, we compared the biochemical similarity of these TCRs of known specificity using TCRdist3. TCRs that bound the same HLA-I multimer (nodes with the same color) were more likely to share similar TCR sequences (connection via a gray line) than TCRs that bound a different HLA-I multimer. MCPyV-specific T cell clones were detected in 7 of the 8 available pre-treatment tumors (colored in red in Figure 3C). Remarkably, in 5 of these tumors, the most frequent clonotype (different in each patient) was specific for an MCPyV oncoprotein epitope (depicted in Figure 3C as a red bar at the bottom of the columns for patients 1, 2, 4, 5, and 7).

Unlike in peripheral blood, the frequency of MCPyV-specific CD8 T cells in tumor tissues was not significantly associated with pathologic response. In pre-treatment tumors with a pCR, a mean of 0.86% (±0.41% SEM) of T cells were MCPyV specific compared with 0.25% (±0.13% SEM) in patients who did not

Please cite this article in press as: Pulliam et al., Circulating cancer-specific CD8 T cell frequency is associated with response to PD-1 blockade in Merkel cell carcinoma, Cell Reports Medicine (2024), https://doi.org/10.1016/j.xcrm.2024.101412

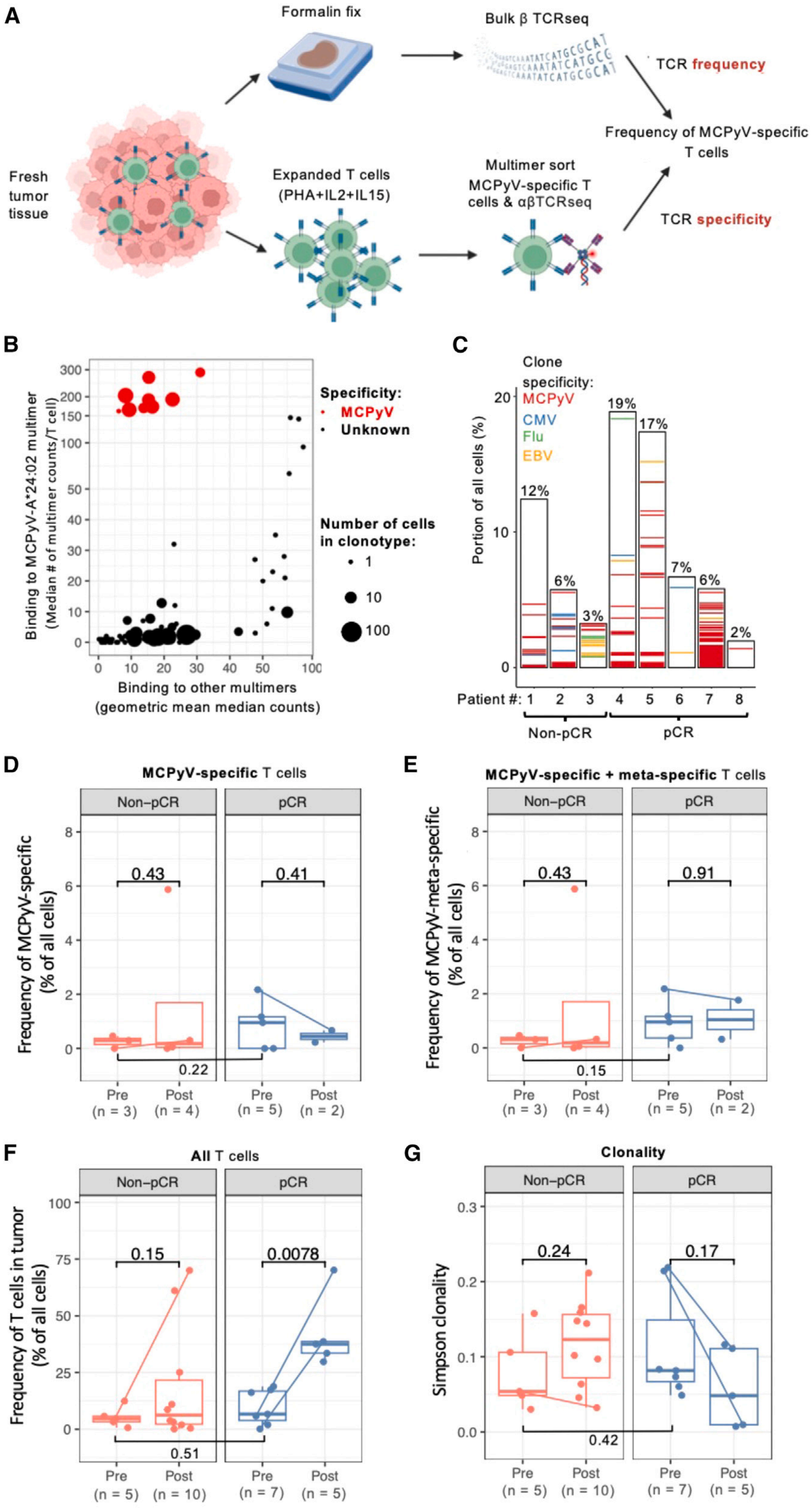

Figure 3. MCPyV-specific T cells are present in tumors regardless of anti-PD-1 therapy response

(A) Schematic describing the experimental approach to identifying antigen-specific intratumoral CD8 T cells.

(B) Representative plot of HLA-A*24:02 multimer binding to TILs expanded from a from a single patient's tumor. Cells with identical T cell receptor α (TCRα) and TCRβ chains (clonotypic) were grouped with number of cells per clonotype as indicated. Median multimer counts were calculated for each multimer and clonotype. Biexponential axis transformation was used for visualization.

(C) Extent of T cell infiltration and anti-viral specificity in pre-treatment tumors from 8 VP-MCC patients with a pCR or non-pCR as indicated. Bar height represents the proportion of all cells in the tumor mass that are T cells (indicated by the percentage at the top of the bar). The color of individual bars indicates viral specificity according to the legend (MCPyV, EBV, CMV, or influenza virus (flu), with white portions of each bar indicating T cells of unknown specificity). The thickness of each colored bar is proportional to the number of T cells in a virus-specific clonotype.

(D) Frequency of MCPyV-specific T cells as a fraction of T cells in tumor specimens before and after immunotherapy in patients who had a pCR (right) or not (left).

(E) Frequency of CD8 T cells with an exact match to a MCPyV-specific TCR or a similar TCR (TCRdist radius ≤ 9) as a fraction of all cells in tumor specimens before and after immunotherapy in patients who had a pCR (right) or not (left).

(F) Frequency of T cells with productive TCRs in tumor specimens before and after immunotherapy in patients who had a pCR (right) or not (left). Paired pre-treatment and post-treatment biopsy specimens from individual patients are indicated by connected lines.

(G) Simpson clonality of productive TCRs in tumor specimens before and after immunotherapy in patients who had a pCR (right) or not (left).

See also Tables S3 and S4.

Please cite this article in press as: Pulliam et al., Circulating cancer-specific CD8 T cell frequency is associated with response to PD-1 blockade in Merkel cell carcinoma, Cell Reports Medicine (2024), https://doi.org/10.1016/j.xcrm.2024.101412

achieve a pCR (p = 0.22; Figure 3D). In the post-treatment setting, a mean of 0.45% (±0.15% SEM) of T cells in tumors were MCPyV specific compared with 1.56% (±1.44% SEM) of cells in patients who did not achieve a pCR (Figure 3D). T cells with a TCR that was identical or highly similar (identified via TCRdist3[40]) to one of the known MCPyV-specific TCRs were categorized as meta-specific for MCPyV. Frequency of MCPyV-meta-specific T cells was also not significantly associated with response. In some cases, the meta-specificity analysis did not identify any additional "highly similar" T cells, and, thus, only T cells with TCRs identical to MCPyV multimer-binding T cells were included. Specifically, these MCPyV-meta-specific cells represented a mean of 0.94% (±0.38% SEM) and a mean of 1.0% (±0.72% SEM) of all intratumoral cells in pre- and post-treatment specimens from pCR patients. For non-pCR patients, MCPyV-meta-specific T cells represented a mean of 0.26% (±0.14% SEM) of all cells in pre-treatment and a mean of 1.56% (±1.44% SEM) of all cells in post-treatment tissues (Figure 3E). In contrast, for tumors with pCR, the mean frequency of intratumoral CD8 T cells (of any specificity) increased significantly from 10.1% of all cells (±3.36% SEM) prior to anti-PD-1 treatment to 50.0% (±20.2% SEM) 4 weeks following treatment (p = 0.0078; Figure 3F). In contrast, CD8 T cell frequency in patients with non-pCR underwent a statistically non-significant expansion from a mean of 7.14% (±2.73% SEM) to 35.4% (±17.5% SEM, p = 0.15; Figure 3F). A slight increase in Simpson productive clonality was noted in tumors with non-pCR from a mean of 0.06 (±0.02 SEM) to a mean of 0.12 (±0.03 SEM). In contrast, for tumors with pCR, clonality tended to decrease from a mean of 0.10 (±0.03 SEM) to a mean of 0.03 (±0.02 SEM). Neither of these changes in clonality was significant (Figure 3G).

MCPyV-specific CD8 T cells in the blood are less exhausted than intratumoral counterparts

To address why MCPyV-specific CD8 T cell frequency in the blood but not in the tumor was associated with response, we investigated phenotypic differences between cancer-specific T cells in the different compartments. Because fresh tumor digests (allowing MCPyV-specific T cells to be isolated) were not available from patients enrolled in the neoadjuvant nivolumab trial, we used matched tumor and blood samples from 8 patients with advanced MCC before and after treatment (cohort 2 in Figure 1). Cellular indexing of transcriptomes and epitopes by sequencing (CITEseq) was performed on these samples, together with staining with HLA-I multimers labeled with a unique DNA barcode and a fluorophore for identification of antigen-specific CD8 T cells (Figure 4A; STAR Methods). This led to identification of 51,555 unique single cells that passed quality control metrics (24,065 from tumors and 27,431 cells from blood; Figures S2A–S2C). Clustering revealed major lineages of natural killer (NK), CD4, CD8, B, myeloid, and tumor cells through expression of common genes and proteins (Figures S2A, S2D, and S2F). Blood specimens from two patients were not usable, and a third patient only had a small number of tumor-resident cells that passed quality control filters due to high necrosis in the tumor (Figure S2E), leaving 5 patients with paired and evaluable specimens from both tumor and blood.

Sub-clustering of CD8 T cells (8,151 cells of 51,555 unique single cells) revealed 7 clusters consisting of naive, memory, effector, senescent, γ-δ, precursor exhausted and terminally exhausted CD8 T cells (Figures 4B, S2G, and S2H). Precursor and terminally exhausted clusters represented most of the intratumoral CD8 T cells, with the less exhausted cell populations being more dominant in the blood (Figures 4C; S2H, S2D, and S2G). In intratumoral CD8 T cells, gene signature scores showed predominance of an exhaustion phenotype (e.g., *PD1*, *TOX*, and *LAG3*). For circulating T cells, memory (e.g., *TCF7*, *CCR7*, and *LEF1*) and senescent (*CD57*$^+$ and *CD28*$^-$) phenotypes were dominant (Figure 4D; Table S5; STAR Methods). MCPyV-specific CD8 T cells from tumors were most likely to be present in the precursor exhausted or terminally exhausted clusters (90%–100% of intratumoral MCPyV-specific CD8 T cells; Figure 4E). Compared with MCPyV-specific CD8 T cells from tumors, in the blood, these cells were more likely to be in the effector cluster (33%–100% of circulating MCPyV-specific CD8 T cells; Figure 4E) and less likely to fall into exhausted clusters (p = 0.0016; Figure 4F).

These differentiation patterns were also supported by pseudotime analyses that showed a "tumor path" and "blood path" corresponding to the site from which these cells were obtained (Figures S2I and S2J). The tumor path was characterized by increases in CD39 and decreases in CD127 protein expression, consistent with development of an exhausted phenotype. In contrast, the blood path was associated with increased CD57 expression and decreased CD28 expression, consistent with development of a senescent phenotype[41] (Figures S2K and S2L). These findings were further supported by expression of an extensive set of exhaustion-associated genes on the tumor path, while the blood path was characterized by senescence-associated genes on the blood path (Figures S2M–S2O).

Direct comparison of antigen-specific CD8 T cells showed that intratumoral MCPyV-specific CD8 T cells expressed significantly higher levels of checkpoint molecules (*PD-1*, *TIM-3*, *LAG-3*, and *CTLA-4*) than intratumoral CMV-specific T cells or peripheral MCPyV-specific T cells (Figure 4G). In contrast, the stem/memory markers *TCF7*, *SELL* (CD62L), and *LEF1* were all more highly expressed in MCPyV-specific CD8 T cells in the blood than in MCPyV-specific T cells in tumors (Figure 4G). We also observed higher levels of AP-1 subunits (*FOS* and *JUN*) and lower levels of NFAT1 subunits (*NFAT1C1* and *NFATC2*) in circulating MCPyV-specific CD8 T cells compared with intratumoral MCPyV-specific CD8 T cells, consistent with a more exhausted state in intratumoral cells[42,43] (Figure 4G). Differences in effector molecules were also seen between MCPyV-specific T cells in the blood compared with in tumors. Specifically, granzyme expression was higher in circulating CD8 T cells than in their intratumoral counterparts (Figure 4G). Notably, *CXCL13* was exclusively expressed by intratumoral MCPyV-specific CD8 T cells (Figure 4G). This observation has also been made in other tumor types[24,44] and suggests *CXCL13* as a particularly accurate indicator of T cell specificity within tumors.

To compare MCPyV-specific CD8 T cells with cancer-specific T cells from other virally driven malignancies, we used analogous data from HPV-specific CD8 T cells infiltrating head and neck tumors.[23] Cells from both studies were clustered into

Please cite this article in press as: Pulliam et al., Circulating cancer-specific CD8 T cell frequency is associated with response to PD-1 blockade in Merkel cell carcinoma, Cell Reports Medicine (2024), https://doi.org/10.1016/j.xcrm.2024.101412

stem, transitory, and terminally differentiated populations (as described by Eberhardt et al.[23]; Figures S3A and S3D). MCPyV-specific CD8 T cells overlapped with HPV-specific T cells in uniform manifold approximation and projection (UMAP) space (Figure S3B). Approximately 75% of MCPyV-specific T cells from both blood and tumor fell within the terminally differentiated cluster (Figures S3B and S3C). Of the remaining MCPyV-specific CD8 T cells, the majority of cells from blood fell within the stem cluster, while the majority of cells from tumor fell within the transitory cluster (Figures S3B and S3C). This is consistent with our finding that the tumor-specific CD8 T cells in the blood are overall more stem like and less dysfunctional than their intratumoral counterparts. To determine whether these findings extend to more common, mutationally driven cancers, we integrated CD8 T cell data from our study and that from patients with non-small cell lung cancer (as studied in Caushi et al.[24]; Figures S3E and S3F). Mutation-associated neoantigen (MANA)-specific CD8 T cells were identified in this study. We observed that MCPyV-specific CD8 T cells clustered with MANA-specific CD8 T cells in UMAP space in both tumor and blood (Figures S3G and S3H). Tumor-derived MANA- and MCPyV-specific CD8 T cells expressed higher levels of exhaustion and checkpoint genes and lower levels of stem-like and memory genes. Taken together, these data are consistent with cancer-specific T cells being more functional in blood than in tumor.

Transcriptional regulatory network analysis via SCENIC[45] was performed on CD8 T cells and identified 535 regulatory networks (regulons) associated with transcription factors. Regulons associated with the AP-1 complex (*FOS* and *JUN*) were more highly expressed in naive and memory CD8 T cells, whereas regulons associated with effector function and terminal differentiation (*EOMES*,[46,47] *TBX21*,[47] *IRF1*, *IRF8*, *STAT3*, and *CREM*) were more associated with terminally differentiated clusters of exhausted and senescent cells. MCPyV-specific CD8 T cells in tumors exhibited higher expression of the exhaustion-associated regulons *IRF4*, *BATF*, and *PRDM1* than CMV-specific CD8 T cells or MCPyV-specific CD8 T cells in the blood.

MCPyV-specific CD8 T cells in blood express protein markers of activation/exhaustion

Since we observed a strong correlation between cancer-specific CD8 T cell frequency in blood and clinical response, we next

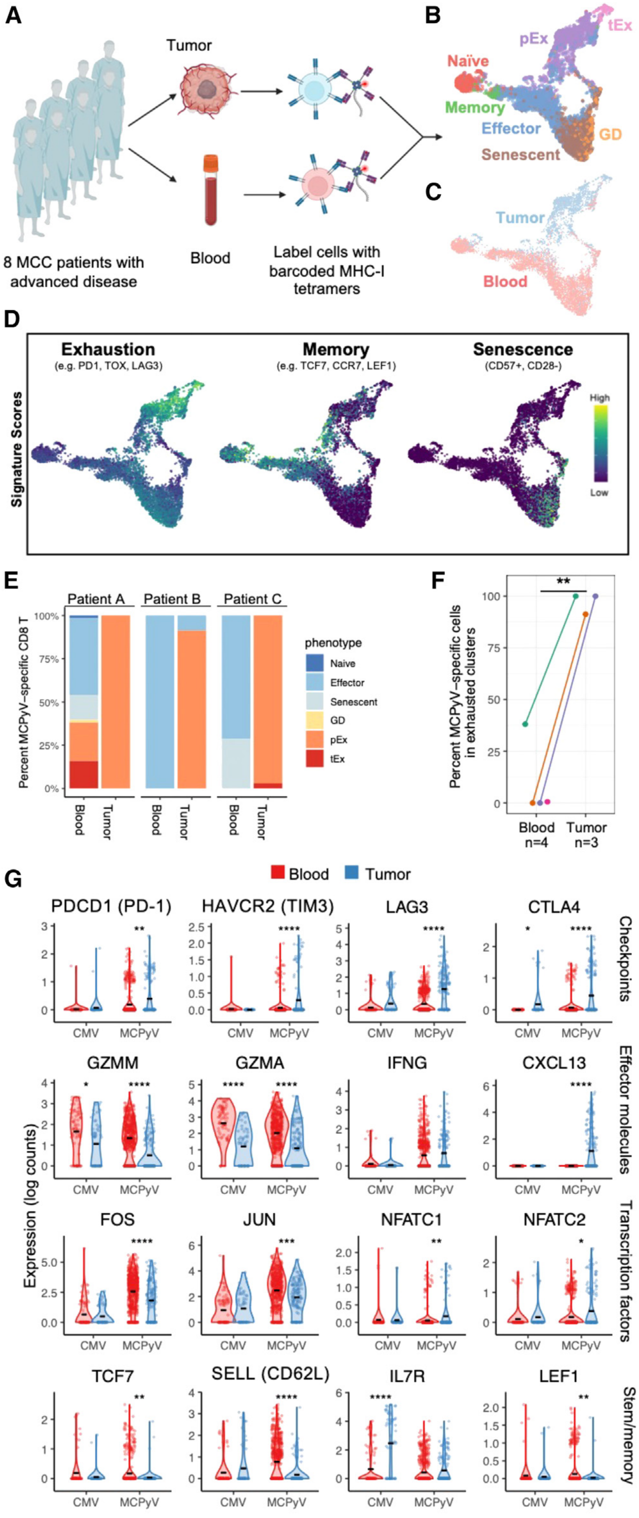

Figure 4. Transcriptomic and proteomic profiling of antigen-specific CD8 T cells in matched tumor and blood specimens

(A) Schematic of the experimental design. Matched pre- and post-treatment tumor and blood specimens from 8 patients (cohort 2 in Figure 1) were labeled with barcoded HLA-I multimers, and CITEseq was performed.

(B) UMAP plot of CD8 T cells colored by cluster: naive (red), memory (green), effector (blue), senescent (brown), γ-δ T cells (Gamma-Delta; orange), precursor exhausted (pEx; purple), and terminally exhausted (tEx; pink).

(C) UMAP plot of CD8 T cells colored by origin from blood (pink) or tumor (blue).

(D) UMAP plots (green/yellow, high expression) of the indicated gene signatures for different T cell programs of interest.

(E) Portions of MCPyV-specific T cells in each cluster as in (B).

(F) Comparison of frequency of MCPyV-specific CD8 T cells in exhausted clusters (as in D). p = 0.0016 using unpaired t test.

(G) Violin plots of exhaustion, memory, and checkpoint gene sets for MCPyV-specific and CMV-specific CD8 T cells from tumor or blood. T tests were performed between tumor and blood specimens for MCPyV-specific vs. CMV-specific T cells. Benjamini-Hochberg correction for multiple comparisons.

$^{*}p \leq 0.05$, $^{**}p \leq 0.01$, $^{***}p \leq 0.001$, $^{****}p \leq 0.0001$. See also Figures S2 and S3 and Tables S3, S4, and S5.

Please cite this article in press as: Pulliam et al., Circulating cancer-specific CD8 T cell frequency is associated with response to PD-1 blockade in Merkel cell carcinoma, Cell Reports Medicine (2024), https://doi.org/10.1016/j.xcrm.2024.101412

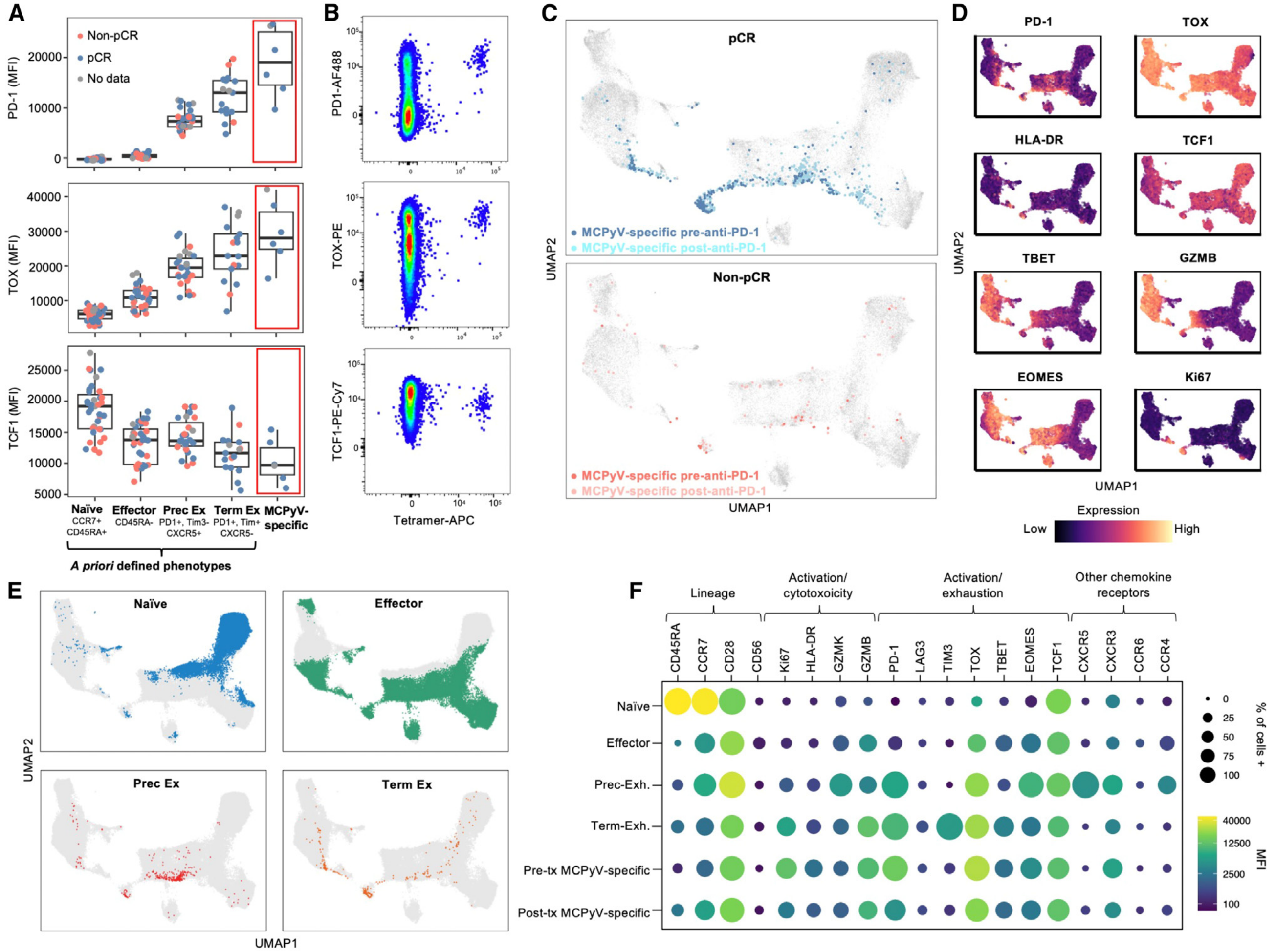

Figure 5. Assessment of exhaustion/dysfunction status of cancer-specific CD8 T cells within the blood via high-dimensional flow cytometry

(A) Expression of key exhaustion markers (PD-1, TOX, and TCF1) in the indicated CD8 T cell subsets from before immunotherapy. Populations with less than 10 cells were excluded. Red boxes indicate MCPyV-specific CD8 T cells.

|(B) Representative fluorescence-activated cell sorting (FACS) plot of CD8 T cells, showing tetramer binding versus PD-1, TOX, and TCF1 expression.

(C) UMAP plots of CD8 T cells. Shown are MCPyV-specific T cells in patients who did (top) or did not (bottom) achieve a pCR.

(D) Expression of 8 differentiation-related proteins using the same projection as in (C) and (E). Cancer-specific T cells are grouped in regions positive (orange/yellow) for exhaustion (PD-1, TOX, and EOMES), proliferation (Ki67 and HLA-DR), and effector function (granzyme B).

(E) UMAP plots of CD8 T cells from blood. Cells are grouped, colored, and labeled using *a priori*-defined phenotypes.

(F) Comprehensive representation of expression of differentiation proteins across T cell subsets that were *a priori*-defined (naive, effector, precursor exhausted, and terminally exhausted) compared with MCPyV-specific CD8 T cells before and after immunotherapy (bottom two rows, red box). As indicated in the legends, the size of each circle represents the proportion of cells positive for that marker via flow cytometry. The color represents the median fluorescence intensity of each protein in each population. Of note, the rare cancer-specific T cells identified in patients without a pCR were present at fewer than 10 cells per sample. Therefore, these results reflect only cancer-specific T cells in patients with pCRs.

MFI, median fluorescence intensity; AF488, Alexa Fluor 488; PE, phycoerythrin; APC, allophycoerythrin, UMAP; uniform manifold approximation and projection; GZMB, granzyme B; Prec Ex, precursor exhausted; Term Ex, terminal exhausted; MCPyV, Merkel cell polyomavirus; EMRA, effector-memory RA positive; Activ/exh, activated/exhausted; tx, treatment. See also Figures S4–S6 and Table S1.

sought to better understand the functional state of these cells. To address the high rate of cell loss in the single-cell RNA sequencing pipeline, we also used high-dimensional flow cytometry to study CD8 T cell phenotype and functional states from patients enrolled in the neoadjuvant nivolumab trial in a more comprehensive manner. MCPyV-specific CD8 T cells in the blood expressed high levels of PD-1 and the exhaustion-associated transcription factor TOX, low levels of the stem-promoting transcription factor TCF1, and similar levels of TBET and EOMES compared with CD8 T cells of unknown specificity that demonstrated canonical patterns of exhaustion (PD-1^{+}, TIM3$^{+/-}$, and CXCR5$^{+/-}$; Figures 5A, 5B, 5E, 5F, S4A, and S4B).[16–18]) While responding patients had larger numbers of MCPyV-specific CD8 T cells, unbiased analyses showed that these cancer-specific T cells shared a highly similar phenotype across pre- and post-nivolumab time points and patient

Please cite this article in press as: Pulliam et al., Circulating cancer-specific CD8 T cell frequency is associated with response to PD-1 blockade in Merkel cell carcinoma, Cell Reports Medicine (2024), https://doi.org/10.1016/j.xcrm.2024.101412

outcomes (Figures 5C and 5F). These MCPyV-specific cells mapped to exhausted/activated clusters (Figures S4D–S4F), corresponding to areas of high PD-1, Ki67, and HLA-DR expression within UMAP plots (Figures 5D and 5E).

The expression pattern of exhaustion-associated markers in circulating cancer-specific CD8 T cells was stable over the course of immunotherapy (Figures 5C–5F, S4B, S4D, and S4E). However, there was significant downregulation of PD-1 on MCPyV-specific CD8 T cells after anti-PD-1 therapy initiation (Figures S4B and S4C). Of note, this was not due to competition between nivolumab and the fluorescently labeled anti-PD-1 antibody, as a clone known to bind an epitope distinct from that of nivolumab was used for flow cytometry (clone MIH4[48]).

An unbiased analysis of T and NK cells showed expansion of proliferating CD4 and CD8 T cells 2 weeks after the start of immunotherapy in patients with pCR (CD4 $p = 0.0015$ and CD8 $p = 0.021$ in pCR; CD4 $p = 0.47$ and CD8 $p = 0.13$ in non-pCR; Figure S5).

Concentrations of 20 inflammation-related serum proteins from nivolumab-treated patients were also measured, but no association was observed with either response or drug treatment status (pre vs. post treatment; Figure S6A). Similarly, there was no correlation between clinical response and MCPyV oncoprotein-specific antibody titer, MCPyV capsid-specific antibody titer, or frequency of circulating myeloid-derived suppressor cells (MDSCs; CD14$^+$, lineage negative, HLA-DR negative/low; Figures S6B–S6D). MCC viral status and proportion of MCPyV-specific CD8 T cells were also associated with MDSC frequency (Figures S6E and S6F).

Tumor cell HLA-I downregulation during acquired resistance to PD-1 pathway blockade

Given that our initial analyses focused on initial (primary) response/resistance in previously untreated patients receiving neoadjuvant anti-PD-1, we next sought to assess the role of circulating MCPyV-specific CD8 T cells in acquired (secondary) resistance. We identified a patient from cohort 2 who received anti-PD-L1 therapy with an initial partial response according to RECIST1.1 radiographic criteria.[49] This patient continued treatment for 1 year and then electively stopped treatment. 6 months after discontinuing anti-PD-L1 therapy, the patient experienced tumor progression, but no response was observed after resuming anti-PD-L1 (Figure 6A). CITEseq with DNA-barcoded HLA-I multimers was performed on the peripheral blood of this patient to identify MCPyV-specific CD8 T cells, which identified TCR sequences of 49 unique clonotypes specific for a B*37:01-restricted epitope (Figure 6B). Bulk TCRseq of blood at 6 time points along the disease course showed the dynamics of these cancer-specific CD8 T cells. Specifically, they were present at 0.04% of all T cells in the blood before treatment, expanded to 0.15% following treatment initiation, and further expanded to 0.53% after anti-PD-L1 re-initiation for progressive disease (Figure 6C). Additionally, 21 novel clones expanded following initial treatment (blue shades, Figures 6C and 6D) including the two most frequent cancer-specific TCRs at the time of recurrence. Immunohistochemistry of the tumor before treatment shows an "immune-excluded" tumor (T cells present at the tumor margins) expressing ample MCPyV oncoproteins and HLA-I on 46% of tumor cells (Figures 6E and 6F). In contrast, at the time of progression, histology showed a "cold" tumor (no T cells present within or near the tumor), and HLA-I expression detected on only 5% of tumor cells (Figures 6E and 6F). This suggests that resistance to anti-PD-L1 at treatment re-initiation was not due to a lack of cancer-specific T cells in the blood but instead coincided with downregulation of HLA-I on tumor cells.

DISCUSSION

Only a small subset of T cells found in patients with cancer recognizes cancer antigens, and the unique nature of tumor antigens in most patients' cancers makes identification of such T cells difficult. However, cancer-specific T cells are likely critical in mediating response to anti-PD-(L)1 therapy. In this study, we leveraged the fact that tumor antigens are shared among patients with VP-MCC to study cancer-specific T cell responses in 27 patients. This allowed us to identify associations between cancer-specific CD8 T cells and objective tumor regression in patients treated with anti-PD-1 therapy.

Through analyzing many parameters, we found that the feature most strongly associated with response to anti-PD-(L)1 was a higher frequency of MCPyV-specific CD8 T cells in peripheral blood at baseline. Patients with complete pathological responses had a 30-fold higher frequency of MCPyV-specific CD8 T cells relative to patients without complete pathological responses (median frequency of 0.073% in patients with a pCR and 0.002% in patients with a non-pCR). Patients with complete pathological responses were also likely to have longer RFS.[36] We also observed an upward trend in the number of peripheral cancer-specific CD8 T cells at 2 weeks in patients who achieved a pCR, followed by a drop in the number of cancer-specific CD8 T cells at 4 weeks. This is consistent with findings in resectable non-small cell lung cancer[50,51] and melanoma.[52] Although the number of relevant human studies is limited, some other groups have also suggested that the presence and/or diversity of cancer-specific T cells in the blood is relevant to immunotherapy response. A recent study of urothelial carcinoma found that patients whose T cells recognized more neoantigen epitopes 3 weeks post immunotherapy initiation trended toward a higher likelihood of objective responses; however, this trend was not statistically significant ($p = 0.067$).[44] Similarly, a separate study from Puig-Saus et al.[53] showed that melanoma patients who responded to immunotherapy had more unique T cell clonotypes per neoantigen than patients who did not respond to immunotherapy. In aggregate, the data appear to suggest that the number, kinetics, and diversity of cancer-specific T cells in blood are associated with response to anti-PD-(L)1 treatment.

In contrast to the correlation between MCC response to anti-PD-1- and MCPyV-specific T cell frequency in blood, the frequency of these cells in tumors was not significantly associated with response in this study. It is possible that, in a larger cohort or a cohort where viable tumor digest samples could be directly stained with peptide-HLA multimer reagents, intratumoral T cells would be significantly associated with response as opposed to the modest trend we observed (Figure 3D). Indeed, a sophisticated study of melanoma-associated antigens did see a correlation between pre-treatment MART-1-specific

Please cite this article in press as: Pulliam et al., Circulating cancer-specific CD8 T cell frequency is associated with response to PD-1 blockade in Merkel cell carcinoma, Cell Reports Medicine (2024), https://doi.org/10.1016/j.xcrm.2024.101412

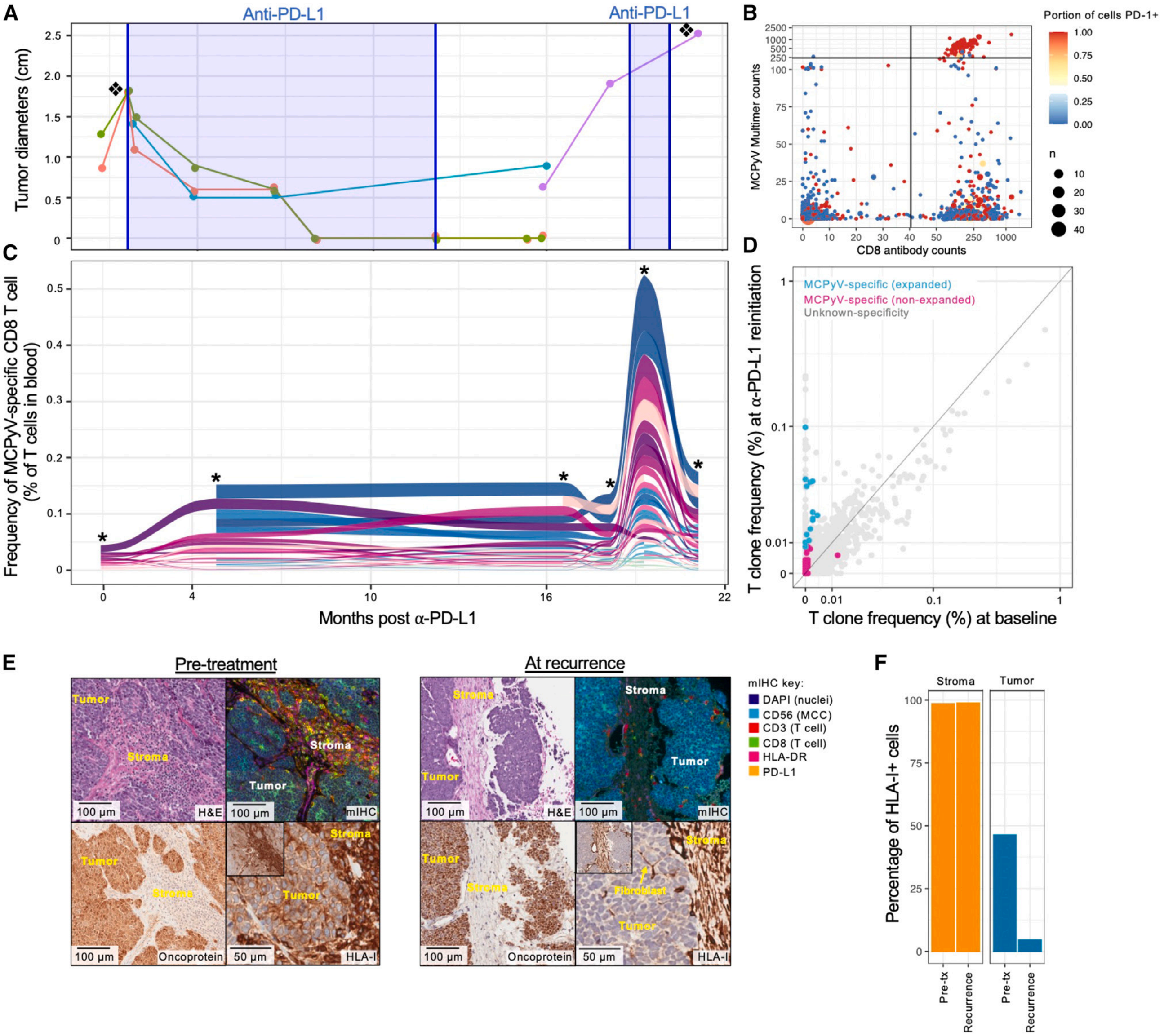

Figure 6. MHC class I downregulation during secondary resistance to PD-1 pathway blockade

(A) Clinical course of a patient with advanced unresectable MCC. The patient had an initial partial response to anti-PD-L1 treatment per RESIST1.1 radiographic criteria, discontinued treatment, and then developed recurrent disease. Each line represents the diameter of an individual tumor lesion (each lesion is assigned a different color) tracked over time. Lesions in red and green were not appreciated 7 months after anti-PD-1 initiation. A new lesion appeared at 16 months during a treatment-free interval. Periods of anti-PD-L1 treatment are shaded in blue. Diagonal squares indicate tumor collection time points for samples shown in (E).

(B) Gating of MCPyV-specific CD8 T cells via CITEseq. The y axis represents the number of unique molecular identifier (UMI) counts for an MHC B*37:01 restricted epitope containing an MCPyV peptide. The x axis represents UMI counts of CD8 antibodies. Each point represents a clonal TCR. The point size represents the number of cells detected per clonotype. Cell color represents the portion of cells positive for PD-1. Only cells with productive TCRs are shown.

(C) Alluvial plot of MCPyV-specific CD8 T cell clones as a portion of all T cells in the blood. Cells present prior to anti-PD-L1 therapy are colored in magenta shades. Cells appearing following anti-PD-L1 initiation are shaded blue. Asterisks represent time points where bulk blood TCR beta sequencing was performed.

(D) Frequency of MCPyV-specific T cell clones in the blood prior to immunotherapy compared with at the time of secondary resistance. Expanded clones were determined via statistical difference between pre-immunotherapy samples and immunotherapy reinitiation samples (β binomial test, $p < 0.01$).

(E) MCPyV T antigen and MHC-I expression on pre-treatment and secondarily resistant tumors. The top left square shows H&E staining. The top right square shows a multiplexed immunofluorescence image with a color key on the right. The bottom left shows T antigen oncoprotein expression with IHC. The bottom right shows MHC class I expression with IHC (with a low-magnification inset). Scale bars vary by sample and are embedded in each image.

(F) Quantification of MHC expression on stromal and tumor cells shown in (E).

Please cite this article in press as: Pulliam et al., Circulating cancer-specific CD8 T cell frequency is associated with response to PD-1 blockade in Merkel cell carcinoma, Cell Reports Medicine (2024), https://doi.org/10.1016/j.xcrm.2024.101412

T cell frequency in tumors and immunotherapy response among 60 melanoma patients ($p = 0.041$).[54] Regardless, the strong association with response we observed for MCPyV-specific CD8 T cell frequency in blood suggested that these cells may be playing a unique role in the immunotherapy response, which we explored using single-cell RNA sequencing (RNA-seq). We used barcoded HLA-I multimers to identify tumor-specific CD8 cells from tumor and blood samples of MCC patients for further transcriptional analyses. MCPyV-specific T cells in tumors exhibited characteristics of terminal exhaustion, including high expression of immune checkpoint genes, *PRDM1*, *IRF4*, and high *AP-1* subunit expression in the setting of low *NFAT* expression.[55–57] In contrast to MCPyV-specific CD8 T cells within tumors, MCPyV-specific T cells in blood expressed fewer genes associated with exhaustion and more genes associated with a stem-like phenotype, including expression of lymph homing receptors and *TCF7* (encodes TCF1). In murine studies of dysfunctional CD8 T cells in chronic viral infections, TCF1-expressing cells undergo proliferation following anti-PD-(L)1 treatment and maintain more effector capacity than TCF1-negative cells.[16–18] Furthermore, the presence of TCF1-expressing CD8 T cells in human tumors has been reported to correlate positively with anti-PD-1 response.[58]

Of note, the 168 unique MCPyV-specific TCRs (listed in Table S4, includes both cohorts) could serve as the basis for developing transgenic T cell therapy or TCR-based bispecific agents. These TCRs represent broad HLA diversity across 9 HLA-I alleles. Based on the HLA-I alleles covered by these TCRs, 87% of VP-MCC patients have at least one of these HLA-I alleles, and 37% of patients have 2 of these alleles, for which MCPyV-specific TCRs were identified. TCR therapies that target more than one HLA allele could protect against immune evasion by allele-specific HLA downregulation, a known immune evasion mechanism in MCC[59] (Figure S6).

These data support a model where blood contains a significant number of cancer-specific CD8 T cells that are at an early stage of exhaustion and capable of expanding and mediating clinical responses. The current study was focused on responses to initial therapy with anti-PD-1 agents. Our longitudinal case study of a patient with acquired (secondary) resistance to anti-PD-(L)1 showed a persistently high frequency of peripheral cancer-specific CD8 T cells. Notably, eventual tumor progression was associated with tumor cell downregulation of HLA-I, allowing evasion from CD8 T cell recognition and suggesting that reinduction of HLA-I expression could be beneficial in some patients with abundant cancer-specific CD8 T cells.

The unique nature of neoantigens in mutationally driven tumors has hampered the detailed study of cancer-specific immune responses in patients. By leveraging VP-MCC, we characterized cancer-specific CD8 T cells in 27 patients. We found that cancer-specific T cells in the blood were less exhausted and that their frequency was associated with response to immunotherapy, while intratumoral CD8 T cells were more exhausted, and their frequency did not predict response. These data suggest that the blood contains significant numbers of functional anti-cancer CD8 T cells and that these cells are relevant for response to PD-1 pathway blockade. Further, they raise the possibility that a subset of patients lacking circulating cancer-specific T cells may particularly benefit from approaches such as adoptive cellular therapy or therapeutic vaccination.

Limitations of the study

We were limited by the number of patients, particularly when studying the frequency of intratumoral cancer-specific CD8 T cells. Additionally, investigation of trafficking between blood and tumor was not possible due to limited sample quantity. Given that a small subset of the TCR repertoire is shared between tumor and blood, a large amount of each sample type is usually required to find shared T cell clones. It is likely that some cancer-specific epitopes were not included in these analyses; thus, cancer-specific T cell identification was not exhaustive.

STAR★METHODS

Detailed methods are provided in the online version of this paper and include the following:

- KEY RESOURCES TABLE
- RESOURCE AVAILABILITY
  - ○ Lead contact
  - ○ Materials availability
  - ○ Data and code availability
- EXPERIMENTAL MODEL AND STUDY PARTICIPANT DETAILS
- METHOD DETAILS
  - ○ Blood collection and processing
  - ○ Tumor digestion and processing
  - ○ MCPyV epitope discovery and epitope mapping
  - ○ Flow cytometry
  - ○ Single cell RNAseq sample preparation
  - ○ scRNA-seq and scV(D)J-seq library preparation and sequencing
  - ○ TCRβ receptor profiling
  - ○ Immunohistochemistry
  - ○ HLA multimer preparation
  - ○ HLA multimer gating and analysis
  - ○ Flow cytometry data analysis
  - ○ Single-cell RNA sequencing data analysis
  - ○ Gene set derivation from previous studies
- QUANTIFICATION AND STATISTICAL ANALYSIS
- ADDITIONAL RESOURCES

SUPPLEMENTAL INFORMATION

Supplemental information can be found online at https://doi.org/10.1016/j.xcrm.2024.101412.

ACKNOWLEDGMENTS

This study was funded by National Institutes of Health (NIH) National Cancer Institute (NCI) grants P01 CA225517 (to P.N.), F30 CA254168 (to T.P.), T32 CA080416 (to S.J.), R37 CA251447 (to K.N.S.), R01 CA142779 (to S.L.T. and D.M.P.), and P30 CA015704 (to P.N.); the Odyssey Group Foundation Kelsey Dickson Team Science Courage Research Award: Advancing New Therapies for Merkel Cell Carcinoma (MCC) (A187769 to P.N.); Bristol-Myers Squibb (to S.L.T.); the National Foundation for Cancer Research (to S.L.T. and P.N.); and the Merkel Cell Carcinoma (MCC) Patient Gift Fund at the University of Washington (to P.N.). This research was supported by the Cell Analysis Facility Flow Cytometry Shared Resource Lab in the Department of Immunology at the University of Washington. We thank Victoria L. Campbell for depositing epitopes into IEDB. Some figures were created with BioRender.

AUTHOR CONTRIBUTIONS

Conceptualization, D.M.K., P.N., T.P., and S.L.T.; methodology, D.M.K., P.N., K.P., and T.P., and S.L.T.; validation, C.C., A.J., S.J., H.R., C.S., and J.Z.; formal analysis, T.G. and T.P.; investigation, L.J., R.K., and T.P.; resources, C.G.-B.; data curation, T.P.; writing – original draft, T.P.; writing – review & editing, all authors; visualization, S.J. and T.P.; supervision, A.C., D.M.K., E.W.N., P.N., D.M.P., K.N.S., and S.L.T.; funding acquisition, S.J., P.N., D.M.P., T.P., K.N.S., and S.L.T.

DECLARATION OF INTERESTS

P.N.'s institution has received grant support from EMD Serono and Bristol Myers Squibb (BMS) as well as honoraria from Merck and EMD-Serono. D.M.K., P.N., and A.C. are co-inventors on institutionally owned patents concerning MCPyV-specific T cell receptors. K.N.S. has received honoraria/consultant fees from Adaptive Biotechnologies and research funding from BMS, AstraZeneca, and Enara Bio and holds founders' equity in ManaT Bio, Inc. S.L.T. has received research funding from BMS and consultant fees from PathAI. D.M.P. has received research funding from BMS and Compugen; consultant fees from Amgen, BMS, Compugen, Janssen Pharmaceuticals, Normunity, RAPT Therapeutics, Regeneron, and Tizona LLC; and patent royalties through institution from BMS and owns stocks of Compugen; Mana T Bio, Inc.; RAPT Therapeutics; Tizona LCC; and TRex Bio Ltd.

Received: July 3, 2023
Revised: December 1, 2023
Accepted: January 12, 2024
Published: February 9, 2024

REFERENCES

1. Yarchoan, M., Hopkins, A., and Jaffee, E.M. (2017). Tumor Mutational Burden and Response Rate to PD-1 Inhibition. N. Engl. J. Med. *377*, 2500–2501. https://doi.org/10.1056/NEJMc1713444.
2. Gandini, S., Massi, D., and Mandalà, M. (2016). PD-L1 expression in cancer patients receiving anti PD-1/PD-L1 antibodies: A systematic review and meta-analysis. Crit. Rev. Oncol. Hematol. *100*, 88–98. https://doi.org/10.1016/j.critrevonc.2016.02.001.
3. Vesely, M.D., Zhang, T., and Chen, L. (2022). Resistance Mechanisms to Anti-PD Cancer Immunotherapy. Annu. Rev. Immunol. *40*, 45–74. https://doi.org/10.1146/annurev-immunol-070621-030155.
4. Overwijk, W.W., Tsung, A., Irvine, K.R., Parkhurst, M.R., Goletz, T.J., Tsung, K., Carroll, M.W., Liu, C., Moss, B., Rosenberg, S.A., and Restifo, N.P. (1998). gp100/pmel 17 is a murine tumor rejection antigen: induction of "self"-reactive, tumoricidal T cells using high-affinity, altered peptide ligand. J. Exp. Med. *188*, 277–286. https://doi.org/10.1084/jem.188.2.277.
5. Alves, P.M.S., Viatte, S., Fagerberg, T., Michielin, O., Bricard, G., Bouzourene, H., Vuilleumier, H., Kruger, T., Givel, J.C., Lévy, F., et al. (2007). Immunogenicity of the carcinoembryonic antigen derived peptide 694 in HLA-A2 healthy donors and colorectal carcinoma patients. Cancer Immunol. Immunother. *56*, 1795–1805. https://doi.org/10.1007/s00262-007-0323-2.
6. Oliveira, G., Stromhaug, K., Klaeger, S., Kula, T., Frederick, D.T., Le, P.M., Forman, J., Huang, T., Li, S., Zhang, W., et al. (2021). Phenotype, specificity and avidity of antitumour CD8(+) T cells in melanoma. Nature *596*, 119–125. https://doi.org/10.1038/s41586-021-03704-y.
7. Zajac, A.J., Blattman, J.N., Murali-Krishna, K., Sourdive, D.J., Suresh, M., Altman, J.D., and Ahmed, R. (1998). Viral immune evasion due to persistence of activated T cells without effector function. J. Exp. Med. *188*, 2205–2213. https://doi.org/10.1084/jem.188.12.2205.
8. Gallimore, A., Glithero, A., Godkin, A., Tissot, A.C., Plückthun, A., Elliott, T., Hengartner, H., and Zinkernagel, R. (1998). Induction and exhaustion of lymphocytic choriomeningitis virus-specific cytotoxic T lymphocytes visualized using soluble tetrameric major histocompatibility complex class I-peptide complexes. J. Exp. Med. *187*, 1383–1393. https://doi.org/10.1084/jem.187.9.1383.
9. McLane, L.M., Abdel-Hakeem, M.S., and Wherry, E.J. (2019). CD8 T Cell Exhaustion During Chronic Viral Infection and Cancer. Annu. Rev. Immunol. *37*, 457–495. https://doi.org/10.1146/annurev-immunol-041015-055318.
10. Kahan, S.M., Wherry, E.J., and Zajac, A.J. (2015). T cell exhaustion during persistent viral infections. Virology *479–480*, 180–193. https://doi.org/10.1016/j.virol.2014.12.033.
11. Paley, M.A., Kroy, D.C., Odorizzi, P.M., Johnnidis, J.B., Dolfi, D.V., Barnett, B.E., Bikoff, E.K., Robertson, E.J., Lauer, G.M., Reiner, S.L., and Wherry, E.J. (2012). Progenitor and terminal subsets of CD8+ T cells cooperate to contain chronic viral infection. Science *338*, 1220–1225. https://doi.org/10.1126/science.1229620.
12. Blank, C.U., Haining, W.N., Held, W., Hogan, P.G., Kallies, A., Lugli, E., Lynn, R.C., Philip, M., Rao, A., Restifo, N.P., et al. (2019). Defining 'T cell exhaustion'. Nat. Rev. Immunol. *19*, 665–674. https://doi.org/10.1038/s41577-019-0221-9.
13. Kallies, A., Zehn, D., and Utzschneider, D.T. (2020). Precursor exhausted T cells: key to successful immunotherapy? Nat. Rev. Immunol. *20*, 128–136. https://doi.org/10.1038/s41577-019-0223-7.
14. Huang, Q., Wu, X., Wang, Z., Chen, X., Wang, L., Lu, Y., Xiong, D., Liu, Q., Tian, Y., Lin, H., et al. (2022). The primordial differentiation of tumor-specific memory CD8(+) T cells as bona fide responders to PD-1/PD-L1 blockade in draining lymph nodes. Cell *185*, 4049–4066.e25. https://doi.org/10.1016/j.cell.2022.09.020.
15. Fransen, M.F., Schoonderwoerd, M., Knopf, P., Camps, M.G., Hawinkels, L.J., Kneilling, M., van Hall, T., and Ossendorp, F. (2018). Tumor-draining lymph nodes are pivotal in PD-1/PD-L1 checkpoint therapy. JCI Insight *3*, e124507. https://doi.org/10.1172/jci.insight.124507.
16. Utzschneider, D.T., Charmoy, M., Chennupati, V., Pousse, L., Ferreira, D.P., Calderon-Copete, S., Danilo, M., Alfei, F., Hofmann, M., Wieland, D., et al. (2016). T Cell Factor 1-Expressing Memory-like CD8(+) T Cells Sustain the Immune Response to Chronic Viral Infections. Immunity *45*, 415–427. https://doi.org/10.1016/j.immuni.2016.07.021.
17. He, R., Hou, S., Liu, C., Zhang, A., Bai, Q., Han, M., Yang, Y., Wei, G., Shen, T., Yang, X., et al. (2016). Follicular CXCR5- expressing CD8(+) T cells curtail chronic viral infection. Nature *537*, 412–428. https://doi.org/10.1038/nature19317.
18. Im, S.J., Hashimoto, M., Gerner, M.Y., Lee, J., Kissick, H.T., Burger, M.C., Shan, Q., Hale, J.S., Lee, J., Nasti, T.H., et al. (2016). Defining CD8+ T cells that provide the proliferative burst after PD-1 therapy. Nature *537*, 417–421. https://doi.org/10.1038/nature19330.
19. Sidhom, J.W., Oliveira, G., Ross-MacDonald, P., Wind-Rotolo, M., Wu, C.J., Pardoll, D.M., and Baras, A.S. (2022). Deep learning reveals predictive sequence concepts within immune repertoires to immunotherapy. Sci. Adv. *8*, eabq5089. https://doi.org/10.1126/sciadv.abq5089.
20. Wu, T.D., Madireddi, S., de Almeida, P.E., Banchereau, R., Chen, Y.J.J., Chitre, A.S., Chiang, E.Y., Iftikhar, H., O'Gorman, W.E., Au-Yeung, A., et al. (2020). Peripheral T cell expansion predicts tumour infiltration and clinical response. Nature *579*, 274–278. https://doi.org/10.1038/s41586-020-2056-8.
21. Yost, K.E., Satpathy, A.T., Wells, D.K., Qi, Y., Wang, C., Kageyama, R., McNamara, K.L., Granja, J.M., Sarin, K.Y., Brown, R.A., et al. (2019). Clonal replacement of tumor-specific T cells following PD-1 blockade. Nat. Med. *25*, 1251–1259. https://doi.org/10.1038/s41591-019-0522-3.

Please cite this article in press as: Pulliam et al., Circulating cancer-specific CD8 T cell frequency is associated with response to PD-1 blockade in Merkel cell carcinoma, Cell Reports Medicine (2024), https://doi.org/10.1016/j.xcrm.2024.101412

22. Luoma, A.M., Suo, S., Wang, Y., Gunasti, L., Porter, C.B.M., Nabilsi, N., Tadros, J., Ferretti, A.P., Liao, S., Gurer, C., et al. (2022). Tissue-resident memory and circulating T cells are early responders to pre-surgical cancer immunotherapy. Cell *185*, 2918–2935.e29. https://doi.org/10.1016/j.cell.2022.06.018.
23. Eberhardt, C.S., Kissick, H.T., Patel, M.R., Cardenas, M.A., Prokhnevska, N., Obeng, R.C., Nasti, T.H., Griffith, C.C., Im, S.J., Wang, X., et al. (2021). Functional HPV-specific PD-1(+) stem-like CD8 T cells in head and neck cancer. Nature *597*, 279–284. https://doi.org/10.1038/s41586-021-03862-z.
24. Caushi, J.X., Zhang, J., Ji, Z., Vaghasia, A., Zhang, B., Hsiue, E.H.C., Mog, B.J., Hou, W., Justesen, S., Blosser, R., et al. (2021). Transcriptional programs of neoantigen-specific TIL in anti-PD-1-treated lung cancers. Nature *596*, 126–132. https://doi.org/10.1038/s41586-021-03752-4.
25. Li, P., Chen, X., Ping, Y., Qin, G., Huang, L., Zhao, Q., Zhang, Z., Chen, H., Wang, L., Yang, S., and Zhang, Y. (2022). Clinical Correlation of Function and TCR vbeta Diversity of MAGE-C2-Specific CD8(+) T Cell Response in Esophageal Cancer. J. Immunol. *209*, 1039–1047. https://doi.org/10.4049/jimmunol.2101182.
26. Tauber, C., Schultheiss, M., Luca, R.D., Buettner, N., Llewellyn-Lacey, S., Emmerich, F., Zehe, S., Price, D.A., Neumann-Haefelin, C., Schmitt-Graeff, A., et al. (2019). Inefficient induction of circulating TAA-specific CD8+ T-cell responses in hepatocellular carcinoma. Oncotarget *10*, 5194–5206. https://doi.org/10.18632/oncotarget.27146.
27. Tada, H., Takahashi, H., Yamada, K., Masuda, K., Nagata, Y., Uchida, M., Shino, M., Ida, S., Mito, I., Matsuyama, T., et al. (2022). Dynamic alterations of circulating T lymphocytes and the clinical response in patients with head and neck squamous cell carcinoma treated with nivolumab. Cancer Immunol. Immunother. *71*, 851–863. https://doi.org/10.1007/s00262-021-03042-y.
28. Palata, O., Podzimkova Hradilova, N., Mysiková, D., Kutna, B., Mrazkova, H., Lischke, R., Spisek, R., and Adkins, I. (2020). Detection of tumor antigens and tumor-antigen specific T cells in NSCLC patients: Correlation of the quality of T cell responses with NSCLC subtype. Immunol. Lett. *219*, 46–53. https://doi.org/10.1016/j.imlet.2020.01.001.
29. Becker, J.C., Stang, A., DeCaprio, J.A., Cerroni, L., Lebbé, C., Veness, M., and Nghiem, P. (2017). Merkel cell carcinoma. Nat. Rev. Dis. Prim. *3*, 17077. https://doi.org/10.1038/nrdp.2017.77.
30. Feng, H., Shuda, M., Chang, Y., and Moore, P.S. (2008). Clonal integration of a polyomavirus in human Merkel cell carcinoma. Science *319*, 1096–1100. https://doi.org/10.1126/science.1152586.
31. Miller, N.J., Church, C.D., Dong, L., Crispin, D., Fitzgibbon, M.P., Lachance, K., Jing, L., Shinohara, M., Gavvovidis, I., Willimsky, G., et al. (2017). Tumor-Infiltrating Merkel Cell Polyomavirus-Specific T Cells Are Diverse and Associated with Improved Patient Survival. Cancer Immunol. Res. *5*, 137–147. https://doi.org/10.1158/2326-6066.CIR-16-0210.
32. Hansen, U.K., Lyngaa, R., Ibrani, D., Church, C., Verhaegen, M., Dlugosz, A.A., Becker, J.C., Straten, P.T., Nghiem, P., and Hadrup, S.R. (2022). Extended T-Cell Epitope Landscape in Merkel Cell Polyomavirus Large T and Small T Oncoproteins Identified Uniquely in Patients with Cancer. J. Invest. Dermatol. *142*, 239–243.e13. https://doi.org/10.1016/j.jid.2021.06.027.
33. Schowalter, R.M., Pastrana, D.V., Pumphrey, K.A., Moyer, A.L., and Buck, C.B. (2010). Merkel cell polyomavirus and two previously unknown polyomaviruses are chronically shed from human skin. Cell Host Microbe *7*, 509–515. https://doi.org/10.1016/j.chom.2010.05.006.
34. Goh, G., Walradt, T., Markarov, V., Blom, A., Riaz, N., Doumani, R., Stafstrom, K., Moshiri, A., Yelistratova, L., Levinsohn, J., et al. (2016). Mutational landscape of MCPyV-positive and MCPyV-negative Merkel cell carcinomas with implications for immunotherapy. Oncotarget *7*, 3403–3415. https://doi.org/10.18632/oncotarget.6494.
35. Houben, R., Shuda, M., Weinkam, R., Schrama, D., Feng, H., Chang, Y., Moore, P.S., and Becker, J.C. (2010). Merkel cell polyomavirus-infected Merkel cell carcinoma cells require expression of viral T antigens. J. Virol. *84*, 7064–7072. https://doi.org/10.1128/JVI.02400-09.
36. Topalian, S.L., Bhatia, S., Amin, A., Kudchadkar, R.R., Sharfman, W.H., Lebbé, C., Delord, J.P., Dunn, L.A., Shinohara, M.M., Kulikauskas, R., et al. (2020). Neoadjuvant Nivolumab for Patients With Resectable Merkel Cell Carcinoma in the CheckMate 358 Trial. J. Clin. Oncol. *38*, 2476–2487. https://doi.org/10.1200/JCO.20.00201.
37. DeCaprio, J.A. (2021). Molecular Pathogenesis of Merkel Cell Carcinoma. Annu. Rev. Pathol. *16*, 69–91. https://doi.org/10.1146/annurev-pathmechdis-012419-032817.
38. Jing, L., Ott, M., Church, C.D., Kulikauskas, R.M., Ibrani, D., Iyer, J.G., Afanasiev, O.K., Colunga, A., Cook, M.M., Xie, H., et al. (2020). Prevalent and Diverse Intratumoral Oncoprotein-Specific CD8. Cancer Immunol. Res. *8*, 648–659. https://doi.org/10.1158/2326-6066.CIR-19-0647.
39. Jing, L., Ott, M., Church, C.D., Kulikauskas, R.M., Ibrani, D., Iyer, J.G., Afanasiev, O.K., Colunga, A., Cook, M.M., Xie, H., et al. (2020). Prevalent and Diverse Intratumoral Oncoprotein-Specific CD8(+) T Cells within Polyomavirus-Driven Merkel Cell Carcinomas. Cancer Immunol. Res. *8*, 648–659. https://doi.org/10.1158/2326-6066.CIR-19-0647.
40. Mayer-Blackwell, K., Schattgen, S., Cohen-Lavi, L., Crawford, J.C., Souquette, A., Gaevert, J.A., Hertz, T., Thomas, P.G., Bradley, P., and Fiore-Gartland, A. (2021). TCR meta-clonotypes for biomarker discovery with tcrdist3 enabled identification of public, HLA-restricted clusters of SARS-CoV-2 TCRs. Elife *10*, e68605. https://doi.org/10.7554/eLife.68605.
41. Zhang, J., He, T., Xue, L., and Guo, H. (2021). Senescent T cells: a potential biomarker and target for cancer therapy. EBioMedicine *68*, 103409. https://doi.org/10.1016/j.ebiom.2021.103409.
42. Martinez, G.J., Pereira, R.M., Äijö, T., Kim, E.Y., Marangoni, F., Pipkin, M.E., Togher, S., Heissmeyer, V., Zhang, Y.C., Crotty, S., et al. (2015). The transcription factor NFAT promotes exhaustion of activated CD8(+) T cells. Immunity *42*, 265–278. https://doi.org/10.1016/j.immuni.2015.01.006.
43. Mognol, G.P., Spreafico, R., Wong, V., Scott-Browne, J.P., Togher, S., Hoffmann, A., Hogan, P.G., Rao, A., and Trifari, S. (2017). Exhaustion-associated regulatory regions in CD8(+) tumor-infiltrating T cells. Proc. Natl. Acad. Sci. USA *114*, E2776–E2785. https://doi.org/10.1073/pnas.1620498114.
44. Lowery, F.J., Krishna, S., Yossef, R., Parikh, N.B., Chatani, P.D., Zacharakis, N., Parkhurst, M.R., Levin, N., Sindiri, S., Sachs, A., et al. (2022). Molecular signatures of antitumor neoantigen-reactive T cells from metastatic human cancers. Science *375*, 877–884. https://doi.org/10.1126/science.abl5447.
45. Van de Sande, B., Flerin, C., Davie, K., De Waegeneer, M., Hulselmans, G., Aibar, S., Seurinck, R., Saelens, W., Cannoodt, R., Rouchon, Q., et al. (2020). A scalable SCENIC workflow for single-cell gene regulatory network analysis. Nat. Protoc. *15*, 2247–2276. https://doi.org/10.1038/s41596-020-0336-2.
46. Li, J., He, Y., Hao, J., Ni, L., and Dong, C. (2018). High Levels of Eomes Promote Exhaustion of Anti-tumor CD8(+) T Cells. Front. Immunol. *9*, 2981. https://doi.org/10.3389/fimmu.2018.02981.
47. Buggert, M., Tauriainen, J., Yamamoto, T., Frederiksen, J., Ivarsson, M.A., Michaëlsson, J., Lund, O., Hejdeman, B., Jansson, M., Sönnerborg, A., et al. (2014). T-bet and Eomes are differentially linked to the exhausted phenotype of CD8+ T cells in HIV infection. PLoS Pathog. *10*, e1004251. https://doi.org/10.1371/journal.ppat.1004251.
48. Zappasodi, R., Budhu, S., Hellmann, M.D., Postow, M.A., Senbabaoglu, Y., Manne, S., Gasmi, B., Liu, C., Zhong, H., Li, Y., et al. (2018). Non-conventional Inhibitory CD4(+)Foxp3(-)PD-1(hi) T Cells as a Biomarker of Immune Checkpoint Blockade Activity. Cancer Cell *33*, 1017–1032.e7. https://doi.org/10.1016/j.ccell.2018.05.009.
49. Eisenhauer, E.A., Therasse, P., Bogaerts, J., Schwartz, L.H., Sargent, D., Ford, R., Dancey, J., Arbuck, S., Gwyther, S., Mooney, M., et al. (2009). New response evaluation criteria in solid tumours: revised RECIST guideline (version 1.1). Eur. J. Cancer *45*, 228–247. https://doi.org/10.1016/j.ejca.2008.10.026.

Please cite this article in press as: Pulliam et al., Circulating cancer-specific CD8 T cell frequency is associated with response to PD-1 blockade in Merkel cell carcinoma, Cell Reports Medicine (2024), https://doi.org/10.1016/j.xcrm.2024.101412

50. Forde, P.M., Chaft, J.E., Smith, K.N., Anagnostou, V., Cottrell, T.R., Hellmann, M.D., Zahurak, M., Yang, S.C., Jones, D.R., Broderick, S., et al. (2018). Neoadjuvant PD-1 Blockade in Resectable Lung Cancer. N. Engl. J. Med. *378*, 1976–1986. https://doi.org/10.1056/NEJMoa1716078.
51. Zhang, J., Ji, Z., Caushi, J.X., El Asmar, M., Anagnostou, V., Cottrell, T.R., Chan, H.Y., Suri, P., Guo, H., Merghoub, T., et al. (2020). Compartmental Analysis of T-cell Clonal Dynamics as a Function of Pathologic Response to Neoadjuvant PD-1 Blockade in Resectable Non-Small Cell Lung Cancer. Clin. Cancer Res. *26*, 1327–1337. https://doi.org/10.1158/1078-0432.CCR-19-2931.
52. Veatch, J.R., Singhi, N., Jesernig, B., Paulson, K.G., Zalevsky, J., Iaccucci, E., Tykodi, S.S., and Riddell, S.R. (2020). Mobilization of pre-existing polyclonal T cells specific to neoantigens but not self-antigens during treatment of a patient with melanoma with bempegaldesleukin and nivolumab. J. Immunother. Cancer *8*, e001591. https://doi.org/10.1136/jitc-2020-001591.
53. Puig-Saus, C., Sennino, B., Peng, S., Wang, C.L., Pan, Z., Yuen, B., Purandare, B., An, D., Quach, B.B., Nguyen, D., et al. (2023). Neoantigen-targeted CD8(+) T cell responses with PD-1 blockade therapy. Nature *615*, 697–704. https://doi.org/10.1038/s41586-023-05787-1.
54. Huuhtanen, J., Chen, L., Jokinen, E., Kasanen, H., Lönnberg, T., Kreutzman, A., Peltola, K., Hernberg, M., Wang, C., Yee, C., et al. (2022). Evolution and modulation of antigen-specific T cell responses in melanoma patients. Nat. Commun. *13*, 5988. https://doi.org/10.1038/s41467-022-33720-z.
55. Jung, I.Y., Narayan, V., McDonald, S., Rech, A.J., Bartoszek, R., Hong, G., Davis, M.M., Xu, J., Boesteanu, A.C., Barber-Rotenberg, J.S., et al. (2022). BLIMP1 and NR4A3 transcription factors reciprocally regulate antitumor CAR T cell stemness and exhaustion. Sci. Transl. Med. *14*, eabn7336. https://doi.org/10.1126/scitranslmed.abn7336.
56. Shin, H., Blackburn, S.D., Intlekofer, A.M., Kao, C., Angelosanto, J.M., Reiner, S.L., and Wherry, E.J. (2009). A role for the transcriptional repressor Blimp-1 in CD8(+) T cell exhaustion during chronic viral infection. Immunity *31*, 309–320. https://doi.org/10.1016/j.immuni.2009.06.019.
57. Man, K., Gabriel, S.S., Liao, Y., Gloury, R., Preston, S., Henstridge, D.C., Pellegrini, M., Zehn, D., Berberich-Siebelt, F., Febbraio, M.A., et al. (2017). Transcription Factor IRF4 Promotes CD8(+) T Cell Exhaustion and Limits the Development of Memory-like T Cells during Chronic Infection. Immunity *47*, 1129–1141.e5. https://doi.org/10.1016/j.immuni.2017.11.021.
58. Sade-Feldman, M., Yizhak, K., Bjorgaard, S.L., Ray, J.P., de Boer, C.G., Jenkins, R.W., Lieb, D.J., Chen, J.H., Frederick, D.T., Barzily-Rokni, M., et al. (2018). Defining T Cell States Associated with Response to Checkpoint Immunotherapy in Melanoma. Cell *175*, 998–1013.e20. https://doi.org/10.1016/j.cell.2018.10.038.
59. Paulson, K.G., Voillet, V., McAfee, M.S., Hunter, D.S., Wagener, F.D., Perdicchio, M., Valente, W.J., Koelle, S.J., Church, C.D., Vandeven, N., et al. (2018). Acquired cancer resistance to combination immunotherapy from transcriptional loss of class I HLA. Nat. Commun. *9*, 3868. https://doi.org/10.1038/s41467-018-06300-3.
60. Cottrell, T.R., Thompson, E.D., Forde, P.M., Stein, J.E., Duffield, A.S., Anagnostou, V., Rekhtman, N., Anders, R.A., Cuda, J.D., Illei, P.B., et al. (2018). Pathologic features of response to neoadjuvant anti-PD-1 in resected non-small-cell lung carcinoma: a proposal for quantitative immune-related pathologic response criteria (irPRC). Ann. Oncol. *29*, 1853–1860. https://doi.org/10.1093/annonc/mdy218.
61. Stein, J.E., Lipson, E.J., Cottrell, T.R., Forde, P.M., Anders, R.A., Cimino-Mathews, A., Thompson, E.D., Allaf, M.E., Yarchoan, M., Feliciano, J., et al. (2020). Pan-Tumor Pathologic Scoring of Response to PD-(L)1 Blockade. Clin. Cancer Res. *26*, 545–551. https://doi.org/10.1158/1078-0432.CCR-19-2379.
62. Longino, N.V., Yang, J., Iyer, J.G., Ibrani, D., Chow, I.T., Laing, K.J., Campbell, V.L., Paulson, K.G., Kulikauskas, R.M., Church, C.D., et al. (2019). Human CD4(+) T Cells Specific for Merkel Cell Polyomavirus Localize to Merkel Cell Carcinomas and Target a Required Oncogenic Domain. Cancer Immunol. Res. *7*, 1727–1739. https://doi.org/10.1158/2326-6066.CIR-19-0103.
63. Jing, L., Haas, J., Chong, T.M., Bruckner, J.J., Dann, G.C., Dong, L., Marshak, J.O., McClurkan, C.L., Yamamoto, T.N., Bailer, S.M., et al. (2012). Cross-presentation and genome-wide screening reveal candidate T cells antigens for a herpes simplex virus type 1 vaccine. J. Clin. Invest. *122*, 654–673. https://doi.org/10.1172/JCI60556.
64. Koelle, D.M. (2003). Expression cloning for the discovery of viral antigens and epitopes recognized by T cells. Methods *29*, 213–226. https://doi.org/10.1016/s1046-2023(02)00344-4.
65. Petersdorf, E.W., Malkki, M., Hsu, K., Bardy, P., Cesbron, A., Dickinson, A., Dubois, V., Fleischhauer, K., Kawase, T., Madrigal, A., et al. (2013). 16th IHIW: international histocompatibility working group in hematopoietic cell transplantation. Int. J. Immunogenet. *40*, 2–10. https://doi.org/10.1111/iji.12022.
66. Williams, J.A. (2014). Improving DNA vaccine performance through vector design. Curr. Gene Ther. *14*, 170–189. https://doi.org/10.2174/156652321403140819122538.
67. Koelle, D.M., Chen, H.B., Gavin, M.A., Wald, A., Kwok, W.W., and Corey, L. (2001). CD8 CTL from genital herpes simplex lesions: recognition of viral tegument and immediate early proteins and lysis of infected cutaneous cells. J. Immunol. *166*, 4049–4058. https://doi.org/10.4049/jimmunol.166.6.4049.
68. Iyer, J.G., Afanasiev, O.K., McClurkan, C., Paulson, K., Nagase, K., Jing, L., Marshak, J.O., Dong, L., Carter, J., Lai, I., et al. (2011). Merkel cell polyomavirus-specific CD8(+) and CD4(+) T-cell responses identified in Merkel cell carcinomas and blood. Clin. Cancer Res. *17*, 6671–6680. https://doi.org/10.1158/1078-0432.CCR-11-1513.
69. Jurtz, V., Paul, S., Andreatta, M., Marcatili, P., Peters, B., and Nielsen, M. (2017). NetMHCpan-4.0: Improved Peptide-MHC Class I Interaction Predictions Integrating Eluted Ligand and Peptide Binding Affinity Data. J. Immunol. *199*, 3360–3368. https://doi.org/10.4049/jimmunol.1700893.
70. Robins, H.S., Campregher, P.V., Srivastava, S.K., Wacher, A., Turtle, C.J., Kahsai, O., Riddell, S.R., Warren, E.H., and Carlson, C.S. (2009). Comprehensive assessment of T-cell receptor beta-chain diversity in alphabeta T cells. Blood *114*, 4099–4107. https://doi.org/10.1182/blood-2009-04-217604.
71. Church, C., Pulliam, T., Longino, N., Park, S.Y., Smythe, K.S., Makarov, V., Riaz, N., Jing, L., Amezquita, R., Campbell, J.S., et al. (2022). Transcriptional and functional analyses of neoantigen-specific CD4 T cells during a profound response to anti-PD-L1 in metastatic Merkel cell carcinoma. J. Immunother. Cancer *10*, e005328. https://doi.org/10.1136/jitc-2022-005328.
72. Goncharov, M., Bagaev, D., Shcherbinin, D., Zvyagin, I., Bolotin, D., Thomas, P.G., Minervina, A.A., Pogorelyy, M.V., Ladell, K., McLaren, J.E., et al. (2022). VDJdb in the pandemic era: a compendium of T cell receptors specific for SARS-CoV-2. Nat. Methods *19*, 1017–1019. https://doi.org/10.1038/s41592-022-01578-0.
73. Guo, X., Zhang, Y., Zheng, L., Zheng, C., Song, J., Zhang, Q., Kang, B., Liu, Z., Jin, L., Xing, R., et al. (2018). Global characterization of T cells in non-small-cell lung cancer by single-cell sequencing. Nat. Med. *24*, 978–985. https://doi.org/10.1038/s41591-018-0045-3.
74. Oh, D.Y., Kwek, S.S., Raju, S.S., Li, T., McCarthy, E., Chow, E., Aran, D., Ilano, A., Pai, C.C.S., Rancan, C., et al. (2020). Intratumoral CD4(+) T Cells Mediate Anti-tumor Cytotoxicity in Human Bladder Cancer. Cell *181*, 1612–1625.e13. https://doi.org/10.1016/j.cell.2020.05.017.

Please cite this article in press as: Pulliam et al., Circulating cancer-specific CD8 T cell frequency is associated with response to PD-1 blockade in Merkel cell carcinoma, Cell Reports Medicine (2024), https://doi.org/10.1016/j.xcrm.2024.101412

STAR★METHODS

KEY RESOURCES TABLE

REAGENT or RESOURCE	SOURCE	IDENTIFIER
Antibodies		
CD3 Antibody, clone UCHT1, fluorophore AF532	Invitrogen	Cat# 58-0038-42; RRID: AB_11218675
CD4 Antibody, clone SK3, fluorophore BUV805	BD	Cat# 612888; RRID: AB_2870177
CD8 Antibody, clone RPA-T8, fluorophore BV570	Biolegend	Cat# 301038; RRID: AB_10933259
CD14 Antibody, clone MφP9, fluorophore BB700	BD	Cat# 566465; RRID: AB_2739737
CD19 Antibody, clone SJ25C1, fluorophore BB700	BD	Cat# 566396; RRID: AB_2744310
CCR7 (CD197) Antibody, clone GO43H7, fluorophore BV605	BD	Cat# 353223; RRID: AB_11124325
CD45RA Antibody, clone HI100, fluorophore BUV563	BD	Cat# 612927; RRID: AB_2870212
CXCR3 Antibody, clone G025H7, fluorophore Pacific blue	Biolegend	Cat# 353724; RRID: AB_2561441
CXCR5 Antibody, clone RF8B2, fluorophore BV480	BD	Cat# 566142; RRID: AB_2739540
Tbet Antibody, clone 4B10, fluorophore BV785	Biolegend	Cat# 644835; RRID: AB_2721566
PD1 (CD279) Antibody, clone MIH4, fluorophore AF488	Invitrogen	Cat# 53-9969-42; RRID: AB_2762480
Lag3 Antibody, clone 11C3C65, fluorophore BV421	Biolegend	Cat# 369314; RRID: AB_2629797
FoxP3 Antibody, clone PCH101, fluorophore PE-Cy5	Invitrogen	Cat# 15-4776-42; RRID: AB_1963595
Tim3 Antibody, clone 7D3, fluorophore BV650	BD	Cat# 565564; RRID: AB_2722547
GZMK Antibody, clone G3H69, fluorophore PerCP-eF710	Invitrogen	Cat# 46-8897-42; RRID: AB_2573854
Tox Antibody, clone TXRX10, fluorophore PE	Invitrogen	Cat# 12-6502-82; RRID: AB_10855034
Eomes Antibody, clone WD1928, fluorophore PE-eF610	Invitrogen	Cat# 61-4877-42; RRID: AB_2574616
GZMB Antibody, clone QA16A092, fluorophore APC-Fire750	Biolegend	Cat# 372210; RRID: AB_2728376
CD28 Antibody, clone CD28.2, fluorophore BUV737	BD	Cat# 612815; RRID: AB_2870140
CD56 Antibody, clone NCAM16.2, fluorophore BUV395	BD	Cat# 563555; RRID: AB_2687886
CCR6 Antibody, clone 11A9, fluorophore BUV496	BD	Cat# 612948; RRID: AB_2833076
Ki67 Antibody, clone B56, fluorophore AF700	BD	Cat# 561277; RRID: AB_10611571
CCR4 Antibody, clone 1G1, fluorophore BUV615	BD	Cat# 613000; RRID: AB_2870269
TCF7 Antibody, clone C63D9, fluorophore PE-Cy7	Cell Signaling Technology	Cat# 90511S; RRID: AB_3086656
HLA-DR Antibody, clone L243, fluorophore BV711	BD	Cat# 752490; RRID: AB_2917483
CD7 Antibody, clone M-T701, fluorophore APC	BD	Cat# 653312; RRID: AB_2870352
CD3 Antibody, clone Sk7, fluorophore AF488	Biolegend	Cat# 344810; RRID: AB_10576234
CD4 Antibody, clone, fluorophore AF700	Invitrogen	Cat# 56-0048-82; RRID: AB_657741
CD8 Antibody, clone SK1, fluorophore BV570	Biolegend	Cat# 344755; RRID: AB_2810546
CD19 Antibody, clone HIB19, fluorophore BV421	Biolegend	Cat# 302234; RRID: AB_10897802
CD56 Antibody, clone NCAM16.2, fluorophore PE-Cy7	BD	Cat# 335809; RRID: AB_399984
CM2B4 Clone	Santa Cruz	136172; RRID: AB_2013156
Anti-HLA-I antibody, EMR8-5 clone	MBL International	D367-3; RRID: AB_3086657
Anti-Cytokeratin 20, Clone Ks20.8	Agilent	GA77761-2; RRID: AB_3086658
Anti-CD8, Clone C8/144B	Agilent	GA62361-2; RRID: AB_3073940
Anti-CD3, clone SP7	Invitrogen	MA1-90582; RRID: AB_1956722
Anti-HLA-DR, clone EP96	Bio SB	BSB 6793; RRID: AB_3086660
Anti-CD56, clone 123.C3	Bio SB	BSB 5267; RRID: AB_3086661
Anti-PD-L1	Cell Signaling Technology	13684; RRID: AB_2687655
Biological samples		
Neoadjuvant Nivolumab PBMC	Bristol Myers Squibb	NCT02488759
MCC Tumor and PBMC samples	Nghiem lab repository, University of Washington	IRB Protocol 6585, Fred Hutch Cancer Center

(Continued on next page)

Please cite this article in press as: Pulliam et al., Circulating cancer-specific CD8 T cell frequency is associated with response to PD-1 blockade in Merkel cell carcinoma, Cell Reports Medicine (2024), https://doi.org/10.1016/j.xcrm.2024.101412

Continued

REAGENT or RESOURCE	SOURCE	IDENTIFIER
Chemicals, peptides, and recombinant proteins		
Peptides (See Tables S1, S3, and S6)	Genscript, Piscataway, NJ	Custom
Human Serum	Valley Biomedical	HS1004
RPMI 1640	Corning	15-040-CV
DMSO	Millipore Sigma	20–139
Remel phytohemagglutinin-purified mitogen	Thermofisher	R30852801
human recombinant IL-15	R&D systems	BT-015-025
natural interleukin IL-2	Hemagen	906011
MHC-I tetramers	International Histocompatibility Working Group, Fred Hutch Cancer Center, Seattle WA	Custom
DNAse I	Worthington Biochemical	LS002139
dasatinib	Selleck Chem	S1021
LIVE/DEAD^{TM} Fixable Blue Dead Cell Stain Kit	Invitrogen	L23105
autoMACS® Running Buffer	Miltenyi	130-091-221
eBioscience^{TM} Foxp3/Transcription Factor Staining Buffer Set	Invitrogen	00-5523-00
AbC^{TM} Total Antibody Compensation Bead Kit	Invitrogen	A10497
ArC^{TM} Amine Reactive Compensation Bead Kit	Invitrogen	A10346
Fixable Viability Stain 780	BD	565388
MHC-I dextramers	Immudex	Custiom
Critical commercial assays		
Chromium i7 Multiplex Kit, 96 rxns	10× Genomics	120262
Chromium Single Cell 5′ Library & Gel Bead Kit	10× Genomics	1000014
Chromium Single Cell 5′ Library Construction Kit	10× Genomics	1000020
Chromium Single Cell V(D)J Enrichment Kit, Human T cell	10× Genomics	1000005
Chromium Single Cell 5′ Feature Barcode Library Kit	10× Genomics	1000080
Chromium i7 Multiplex Kit N Set A	10× Genomics	1000084
Chromium Next GEM Chip G Single Cell Kit	10× Genomics	1000127
Chromium Next GEM Single Cell 5′ Library and Gel Bead Kit v1.1	10× Genomics	1000167
QIAamp DNA FFPE tissue kit	Qiagen	56404
QIAamp DNA Blood Mini Kit	Qiagen	51104
Deposited data		
CITEseq data	This study	GSE227054
Alpha-beta TCRseq	This study	GSE227708
CITEseq data, Patient A	This study	GSE227709
Eberhardt et al. scRNAseq dataset	Eberhardt et al. 2021	GSE180268
Caushi et al. scRNAseq dataset	Caushi et al. 2021	GSE173351
Experimental models: Cell lines		
Cos-7 cells	ATCC	Cat#CRL-1651
Software and algorithms		
CellRanger	10× Genomics	V3.10
R	CRAN	v.4.1.2
FlowJo	FlowJo	v.10.8.1
scater	CRAN	v.1.22.
Seurat	CRAN	v.4.3.
ggplot2	CRAN	3.4.0)
SCENIC	CRAN	v.1.2.4
UCell	CRAN	v.1.99.1
slingshot	CRAN	v.2.2.1

(*Continued on next page*)

Please cite this article in press as: Pulliam et al., Circulating cancer-specific CD8 T cell frequency is associated with response to PD-1 blockade in Merkel cell carcinoma, Cell Reports Medicine (2024), https://doi.org/10.1016/j.xcrm.2024.101412

Continued

REAGENT or RESOURCE	SOURCE	IDENTIFIER
clustree	CRAN	v.0.5.
scran	CRAN	v.1.22.1
batchelor	CRAN	v1.10.0
scuttle	CRAN	v.1.4.0
DropletUtils	CRAN	v.1.14.2
scds	CRAN	v.1.10.0
phenograph	CRAN	v.0.99.1
uwot	CRAN	v.0.1.14
survminer	CRAN	v0.4.
netMHCpan	DTU Health Tech	v4.0

RESOURCE AVAILABILITY

Lead contact

Further information and requests for resources and reagents should be directed to and will be fulfilled by the lead contact, Paul Nghiem (pnghiem@uw.edu).

Materials availability

This study did not generate new unique reagents.

Data and code availability

The expression data obtained in this study has been uploaded to the GEO database with accession nos. GSE227054 (TCRseq data) and GSE227708 (CITEseq). One patient in cohort 2 (patient A) was performed as part of a separate study and was uploaded to the GEO database with accession no. GSE227709. Any requests for the raw data will be reviewed by the corresponding authors to ensure patient confidentiality is maintained. If possible, the data will be shared under a material transfer agreement. Data previously published and analyzed here are available on GEO with accession numbers GSE180268 and GSE173351. ImmunoSEQ data can be found at on the Adaptive biotechnologies' ImmuneAccess repository under https://doi.org/10.21417/TP2024CRM. Additional data supporting the study's findings can be found in the main text, figures, extended data, and Supplemental files.This paper does not report original code, however, code needed to reproduce any of the analyses will be made available upon reasonable request. Any additional information required to reanalyze the data reported in this work paper is available from the lead contact upon request.

EXPERIMENTAL MODEL AND STUDY PARTICIPANT DETAILS

The samples in cohort 1 (Figure 1) were collected as part of a neoadjuvant nivolumab trial (NCT02488759; ref. [36]). Briefly, eligible patients were at least 18 years old, had an Eastern Cooperative Oncology Group performance score of 0 or 1, and had MCC pathologically confirmed. Patients had stage IIA-IIIB MCC that could be biopsied before treatment and was considered surgically resectable. After 2 doses of nivolumab (4 weeks after initial dose), surgery was carried out and the extent of pathological response was determined, according to criteria described by Stein et al.,[36] wherein a pathological complete response (pCR) was defined as "absence of residual viable invasive cancer on hematoxylin and eosin evaluation of completely resected tumor specimens including all sampled lymph nodes".[60,61] Resection specimens with any viable tumor cells remaining were categorized as non-pathological complete response (non-pCR).

Samples in cohort 2 (Figure 1) were collected with informed consent for research use and were approved by the Fred Hutchinson Cancer Center (FHCC) institutional review board, in accordance with the Declaration of Helsinki (2013) as part of observational registry studies focusing on Merkel cell carcinoma. Patient samples for cohort 2 were selected based on availability of frozen viable tumor tissues, and corresponding PBMCs collected within 30 days of tumor resection. Patient samples were further selected to only include MCPyV positive tumors and those from immune competent patients.

METHOD DETAILS

Blood collection and processing

Heparinized whole blood from MCC patients was processed at the Specimen Processing Lab (FHCC). PBMC were isolated by routine Ficoll density gradient centrifugation and cryopreserved in liquid nitrogen.

Please cite this article in press as: Pulliam et al., Circulating cancer-specific CD8 T cell frequency is associated with response to PD-1 blockade in Merkel cell carcinoma, Cell Reports Medicine (2024), https://doi.org/10.1016/j.xcrm.2024.101412

Tumor digestion and processing

Fresh MCC tumor specimens from needle cores, punch biopsies, or surgical excisions were enzymatically digested as described.[62] All single-cell suspensions were cryopreserved in Freezing Medium [50% human serum (Valley Biomedical), 40% RPMI (Corning), and 10% DMSO (Sigma-Aldrich)] and stored in liquid nitrogen.

To expand T cells from tumors, tumor tissue was chopped into small pieces and placed in culture along with 10^6 allogenic irradiated PBMCs, Remel phytohemagglutinin-purified mitogen (1.6 μg/mL; ThermoFisher), human recombinant IL-15 (10 ng/mL; R&D Systems), and human natural interleukin IL-2 (32 U/mL; Hemagen, Columbia, MD).

MCPyV epitope discovery and epitope mapping

We used previously described methods to discover novel MCPyV epitopes in expanded T cells.[39,63,64] In brief, HLA cDNA was either cloned from PBMC of HLA-typed persons or obtained ready-to-use from the International Histocompatibility Working Group gene bank housed at FHCC (Seattle, WA).[65] The protocol for cloning of HLA cDNA from PBMC has been previously detailed.

MCPyV LT AA 1–327 or full-length ST AA 1–186 with a carboxy-terminus six-histidine addition were cloned into the Nature Technology Corporation (NTC) 9385R vector.[66] These plasmids encode an identical 78 AA N-terminal CT domain. The NTC plasmids were based on GenBank HM011538.1. LT AA 1–259 from MCVw156 (GenBank HM355825.1) was separately cloned into pDEST103, a vector constructed in our laboratory.[63]

To screen TIL for reactivity to MCPyV epitopes, 10^4 COS-7 cells (ATCC) were seeded into each well of a 96-well flat-bottom plate. After 24 h, the COS-7 cells were co-transfected with HLA and MCPyV plasmids to create artificial antigen-presenting cells (aAPC). After two days, 10^5 TIL were added and supernatant IFNγ was measured 24–48 h later by ELISA.[67] IFNγ results were reported as the mean and standard deviation (SD) in figures. Fine epitope mapping was performed using 95 overlapping T-Ag peptides (OLP; Table S6; Genscript) as previously described.[68] Peptides covering LT AA 1–281 and the unique region of ST were 13 AA long with 9 AA overlap and based on MCPyV 350 (GenBank FJ173805.1; ref. [68]). Peptides were tested individually at 1 μg/mL final concentration by addition to Cos-7 cells 48 h after HLA transfection. TILs (10^5) were added 1–2 h later, and supernatants were tested for IFNγ by ELISA 24–48-h later as indicated above. Alternatively, OLP were matrix-pooled into rows and columns of 9–10 peptides/pool and tested at 1 μg/mL final concentration each. Peptides at positive pool intersection(s) (mean ELISA OD450 value >0.2) were retested for confirmation. For some assays, aAPCs were peptide-pulsed at 10 μg/mL for 1 h and PBS-washed before adding responder cells to reduce T cell auto-presentation. Positive pools were deconvoluted to identify individual reactive peptides in follow-up assays. The HLA-peptide binding prediction algorithm netMHCpan 4.0[69] was used to predict HLA binding peptides within reactive 13-mers. Short internal peptides within reactive 13-mer peptides were obtained (Genscript) and tested.

Flow cytometry

PBMCs from the neoadjuvant anti-PD-1 cohort (Figure 1) were analyzed by flow cytometry. Because cell viability and tetramer staining was sensitive to thawing conditions, after optimization, we carefully followed this procedure: frozen tubes of PBMC were thawed at 37 C, followed by dropwise addition of complete media (RPMI, 10% Fetal bovine serum, 1× penicillin/streptomycin, 1× l-glutamine). DNAse I (10 units/ml) was added, and cells were allowed to rest for 1 h. Cells were counted using a hemacytometer and split into tubes of 1–3 million cells. Cells were washed twice with PBS and then incubated with dasatinib (100 nM) and live dead staining buffer (Live dead Blue; ThermoFisher) at 37C for 10 min. HLA-I multimers were then added. If a sample had more potential HLA matches than tubes of 1–3 million cells, multiple HLA-I multimers for the same virus were added to a tube. The sample was first stained with antibodies against chemokine or cytokine receptors (See key resources table for antibodies used). After a 30-min incubation, antibodies against other cell surface receptors were added. Following another 30-min incubation, cells were washed twice with autoMACS running buffer (Miltenyi), permeabilized using the Foxp3/Transcription factor staining buffer set (eBioscience), and washed twice with the kit permeabilization buffer. Intracellular antibodies were then added after permeabilization, and the samples were incubated at room temperature for 1 h. Cells were washed twice with permeabilization buffer and fixed in 1% paraformaldehyde. Antibody capture beads or amine reactive beads (ThermoFisher) were used to compensate each fluorophore in the experiment. Stained cells were analyzed by the Cytek Aurora spectral analyzer at the University of Washington, Department of Immunology's Cell Analysis Facility. Spectral unmixing was performed using SpectroFlo software. Visualization and Initial gating selecting for single cells, lymphocytes and live cells was performed in FlowJo v.10 (FlowJo LLC). Subsequent analyses were performed in R (See below).

Single cell RNAseq sample preparation

Frozen tumor and PBMC single cell suspensions from cohort 2 (Figure 1) were analyzed by cellular indexing of transcripts and epitopes by sequencing (CITEseq). Frozen tubes were thawed at 37 C, followed by dropwise addition of 1 mL complete media (RPMI, 10% Fetal bovine serum, 1× penicillin/streptomycin, 1× l-glutamine). Equivolume of complete media was continuously added 4 additional times (dropwise with gentle mixing in between additions (total volume of 32 mL). Cells were then washed twice with 4 C PBS, counted using a hemacytometer and transferred to FACS tubes (Fisher Scientific). Live dead stain was then added (FVS780; BD Biosciences), followed by a blocking buffer to bring samples to 0.5% BSA, 5% TruStain FcX buffer (Biolegend), 100 nM dasatinib, and 50 μg salmon sperm. Samples were then incubated on ice for 10 min followed by the following reagents in order: DNA barcode-labeled HLA-matched HLA-I multimers, hashtag antibodies to identify sample origin in subsequent pooling

Please cite this article in press as: Pulliam et al., Circulating cancer-specific CD8 T cell frequency is associated with response to PD-1 blockade in Merkel cell carcinoma, Cell Reports Medicine (2024), https://doi.org/10.1016/j.xcrm.2024.101412

steps, fluorophore labeled antibodies, and DNA barcode-labeled antibodies. Cells were then incubated on ice for 30 min and washed three times. Cells were then sorted on an Aria II Cell sorter (BD Biosciences). Dead cells and debris were excluded, and samples were enriched for HLA multimer binding cells. Cells were sorted into cold complete media, pooled and immediately prepared for sequencing (see below).

scRNA-seq and scV(D)J-seq library preparation and sequencing

Single cell suspensions were collected from either tumor or blood samples and brought to a concentration of 700-1,200 viable cells per microliter using a hemacytometer. These single cell suspensions were then loaded into the appropriate microfluidic chip (chip G; 10× Genomics) and run through a Chromium controller to obtain Gel Beads-in-Emulsion (10× Genomics). Resulting cell suspensions then went through a library preparation process for single-cell RNA sequencing (scRNA-seq) along with paired scV(D)J-seq for T cell receptor (TCR) clonotypes using the 5′ transcriptome kit with feature barcoding (V1.1; 10× Genomics) per manufacturer guidelines. The complementary DNA libraries were then sequenced using a NovaSeq instrument (Illumina) with 2 × 92 base pair paired-end reads aiming for an average of 20,000 reads per cell per 10× Genomics guidelines.

TCRβ receptor profiling

DNA was extracted from frozen peripheral blood mononuclear cells or formalin-fixed paraffin-embedded (FFPE) tumor biopsy material (20 μm thick molecular curls or material scraped from pre-cut slides) using QIAamp DNA Blood Mini Kit or QIAamp DNA FFPE tissue kit, respectively (Qiagen). Resulting samples were submitted to Adaptive Biotechnologies for TCRβ sequencing and normalization, as previously described.[70]

Immunohistochemistry

Standard immunohistochemistry was performed on FFPE tissues with antibodies recognizing Merkel cell polyomavirus (CM2B4 clone at 1:50 dilution, Santa Cruz, CA, USA), class I HLA (EMR8-5 clone at 1:8000 dilution, MBL International, MA, USA), and cytokeratin 20 (Dako clone Ks20.8 at 1:200 dilution, Agilent, CA, USA). Multiplex immunohistochemistry was performed with a panel of antibodies including CD8 (clone 144B/Dako/fluor 520 opal/concentration 0.2 μg/mL), CD3 (Sp7/Thermo/fluor opal 650), HLA-DR (EP96/BSB/0.125 μg/mL/fluor opal 690), CD56 (123.C3/BSB 1 μg/mL/fluor 540), and PD-L1 (E1L3N 0.5 μg/mL) using a modified Akoya Opal Multiplex IHC assay.[71] We also attempted PD-1 staining with antibody clone D4W2J. However, non-specific staining was observed, and PD-1 was thus excluded from analysis. Quantitative image analysis was performed with HALO software.

HLA multimer preparation

Allophycocyanin (APC)-labeled HLA-I multimers were used for flow cytometry experiments and prepared by the Immune Monitoring Lab at Fred Hutchinson Cancer Center. Multimers were titered using samples of known positivity. HLA multimers used for scRNAseq were created using HLA-I easYmers (Immunaware) and PE or APC and DNA barcode-labeled streptavidins (Biolegend). DNA barcode- and fluorophore-labeled HLA-I dextramers were prepared by Immudex. These multimers were used for staining expanded T cells as directed. A full list of all epitopes used is provided in Tables S1 and S3.

HLA multimer gating and analysis

For HLA-I multimer gating on flow cytometry analyses, samples were grouped by HLA-I multimer. Gates were manually drawn for each sample while blinded to tumor viral status, response, and patient identity. If a sample was stained with more than one epitope, then the sample was included in all potential epitopes and then the gate was drawn at the maximum value of all potential epitopes. Median gate values were then calculated for each individual epitope and all gates were redrawn resulting in 144 FACS plots that were then reviewed by a second person with experience in tetramer staining (C.C., also blinded to tumor viral status, response, and patient identity). Any variations in gating values were then discussed and, if appropriate, gates were edited. Once final gate values were established, frequency of MCPyV-specific CD8 T cells in the blood of patients with virally driven or non-virally driven cancer were calculated (Figure S1D). These results supported accurate gating as no patients with non-MCPyV driven cancer had more than 1 in 10,000 CD8 T cells binding to HLA-I multimers containing MCPyV oncoprotein peptides. This limit of detection is similar to prior study of MCPyV-specific CD8 T cells in healthy controls.[31] Phenotypic similarity was also used to confirm gate values. Given *a priori* knowledge of the phenotype of MCPyV-specific CD8 T cells (naive, largely PD-1+[31]), the cumulative portion of cells that were naive or PD-1 positive were calculated as a function of decreased tetramer intensity (Figures S1B and S1C). These results further validated the gating of MCPyV-specific T cells. Since the gate values drawn were concordant with this approach, no further adjustments were made using this approach.

For gating of antigen-specific CD8 T cells in single cell RNAseq data, the counts of HLA-I multimer unique molecular identifiers (UMIs) were used. A similar approach was used as above where gates were manually drawn for each sample while blinded to tumor viral status, response, and patient identity and then reviewed by a second person (S.J.) who was also blinded to these factors. TCRβ sequences of multimer-positive cells were then compared to TCRs of known specificity in the VDJ database.[72] After comparison, 15/16 TCRβs that were found in the database were accurately matched. The non-matched TCR was reviewed and HLA-I count values appeared in ranges of other matched cells suggesting this TCR could recognize different peptides in different HLA context with a different TCRα. This clone was included as MCPyV-specific as per our HLA-I multimer binding data.

Please cite this article in press as: Pulliam et al., Circulating cancer-specific CD8 T cell frequency is associated with response to PD-1 blockade in Merkel cell carcinoma, Cell Reports Medicine (2024), https://doi.org/10.1016/j.xcrm.2024.101412

Flow cytometry data analysis

Live, CD19$^-$, CD14$^-$lymphocytes fcs files were loaded into a gating set object in R using flowWorkspace (v.4.6.0). Fluorescent data was transformed using the biexponential function. Fluorescent-minus-one samples were used to draw gates at the 99th percentile which were then used as the minimum gate for the markers CCR4, CCR6, CCR7, CD45RA, CD4, CD8, CXCR5 CD28, CD56, CD3, FOXP3, TCF1, and Ki67. Gates were adjusted upward as appropriate based on visual inspection. Markers of activated T cells including LAG3, TIM3, HLA-DR, TBET, EOMES, PD-1, Granzyme B, Granzyme K, and TOX were gated similarly with the 99th percentile of naive cells acting as an additional minimum gate. UMAP dimensionality reduction was performed using uwot (v.0.1.14). Clustering was performed using phenograph (v.0.99.1). Visualization was performed using ggplot2 (v.3.4.0) or FlowJo (v.10.8.1).

Single-cell RNA sequencing data analysis

Raw sequencing reads were aligned to the hg38 genome using Cell Ranger v.3.1. Filtered counts matrices of transcripts and feature barcoding counts were loaded into a SingleCellExperiment object for further analyses in R (v.4.1.2). Sample hash deconvolution was performed using DropletUtils (v.1.14.2). Doublets were detected using scds (v.1.10.0) and hash deconvolution, and subsequently removed. Cells that had fewer than 800 transcript reads, fewer than 250 genes detected or more than 10% mitochondrial DNA were excluded as low quality. Comparisons of excluded and kept cells were performed to ensure no cell populations were disproportionally removed. This showed mitochondrial genes, MALAT1 (a transcript associated with dying cells), and hemoglobin genes were the only genes disproportionally represented in the removed cells. Cells were size-normalized (to account for RNA capture efficiency) and log transformed using scuttle (v.1.4.0).

Cells from different runs were then integrated using the mutual nearest neighbor method though the batchelor package (v1.10.0). UMAP dimensionality reduction was performed using the integrated values. Clustering was performed using the integrated transcript values and feature barcoding reads through the walktrap algorithm on a nearest neighbor graph (scran v.1.22.1). Numbers of clusters was varied by scaling the number of nearest neighbors (k) during graph construction followed by analysis via clustree (v.0.5.0). Clusters were then labeled as major cell lineages of CD4 T cells, CD8 T cells, B cells, myeloid cells, erythrocytes, NK cells and tumor cells through expression of key genes including MS4A1, CD19, CD4, CD8A, CD3E, CD3D, GZMB, NCAM1, HLA-DRA, PTPRC, NKG7 and the MCPyV oncoproteins. Cluster labels were then validated by investigating the portion of cluster with productive BCR or TCR rearrangements. Cell lineages were then isolated in silico and dimensionality reduction and clustering was re-performed on CD8 T cells as above. Cells were scored for expression of memory and exhaustion gene sets (see below) using the UCell (v.1.99.1) package. Pseudotime analyses was performed using slingshot (v.2.2.1) with the naive CD8 T cell population as the starting population. Pseudotime heatmap was created by fitting a spline to each gene shown against pseudotime.

Single cell transcriptional regulatory networks in CD8 T cells were analyzed using SCENIC (v.1.2.4) as previously described.[45] Briefly, genes with more than 488 total counts across all CD8 T cells and cells with more than 163 genes were isolated for subsequent analysis. Correlations between transcription factors and genes were determined and GENIE3 was used to establish regulatory networks. SCENIC was then used to score the expression of these regulatory networks in each cell. UMAP dimensionality reduction was reperformed based on these regulons.

MCPyV-specific CD8 T cells were isolated and integrated into a large single cell RNAseq dataset of HPV-specific CD8 T cells from HPV driven head and neck cancer.[23] Each dataset was rescaled using SCTransform (Seurat). Integration features (genes) were selected based on their variability across both datasets followed by removal of TCR and BCR V, D and J genes and mitochondrial genes. Seurat was then used to integrate the datasets using the HPV dataset as an anchor and a k.weight of 40.

All CD8 T cell data from blood and tumor of MCC patients was similarly integrated with a dataset of CD8 T cells from patients with non-small cell lung cancer.[24]

Plots were made using scater (v.1.22.0), Seurat (v.4.3.0) or ggplot2 (3.4.0).

Gene set derivation from previous studies

Single cell RNAseq datasets from 4 studies containing diverse populations of CD8 T cells from human tumors[6,58,73,74] were used to create a compendium of labeled clusters along with genes positively or negatively associated with each cluster (Table S5). Clusters with synonymous labels were renamed and grouped. Genes associated with clusters with p values of less than 0.05 and average log fold changes greater than 0.5 were selected for further inclusion. An "exhaustion" gene signature was developed for genes that were associated with exhausted clusters (labeled as exhausted, precursor exhausted, terminally exhausted, exhausted cycling) in at least 3 of 4 datasets (74 total genes). Similarly, a "memory" gene signature was developed for genes that were associated with memory clusters (labeled as naive, memory or central memory) in at least 2 of 3 datasets that had these populations (12 total genes). Immune checkpoints included in the exhaustion gene set were manually identified as PDCD1, LAG3, TIGIT, HAVCR2, CD276, ENTPD1, CD73, ADORA2A, and CTLA4.

QUANTIFICATION AND STATISTICAL ANALYSIS

The statistical tests applied were two-sided unless specified otherwise. T tests were used to compare differences between two groups unless otherwise noted. When comparing more than two groups, the nonparametric Kruskal–Wallis test was used. Multiple

Please cite this article in press as: Pulliam et al., Circulating cancer-specific CD8 T cell frequency is associated with response to PD-1 blockade in Merkel cell carcinoma, Cell Reports Medicine (2024), https://doi.org/10.1016/j.xcrm.2024.101412

hypothesis testing was done with the Benjamini–Hochberg method unless noted differently. Fisher's exact test was used to evaluate differences between two categorical variables. The ROC analysis was used to measure classification accuracy, which was expressed as the AUC. Pearson (r) or Spearman (ρ) correlation was used to determine linear concordance, and a two-sided t-test was used to see if the result was significantly different from zero. The significance levels and HRs for Kaplan–Meier analyses were calculated using a two-sided log rank test. All statistical analysis was carried out using R v.4.1+.

ADDITIONAL RESOURCES

Further information relevant to the clinical trial under which Cohort 1 (Figure 1) samples were collected can be found at https://clinicaltrials.gov/study/NCT02488759.

Cell Reports Medicine, Volume *5*

Supplemental information

Circulating cancer-specific CD8 T cell frequency
is associated with response to PD-1 blockade
in Merkel cell carcinoma

Thomas Pulliam, Saumya Jani, Lichen Jing, Heeju Ryu, Ana Jojic, Carolyn Shasha, Jiajia Zhang, Rima Kulikauskas, Candice Church, Charlie Garnett-Benson, Ted Gooley, Aude Chapuis, Kelly Paulson, Kellie N. Smith, Drew M. Pardoll, Evan W. Newell, David M. Koelle, Suzanne L. Topalian, and Paul Nghiem

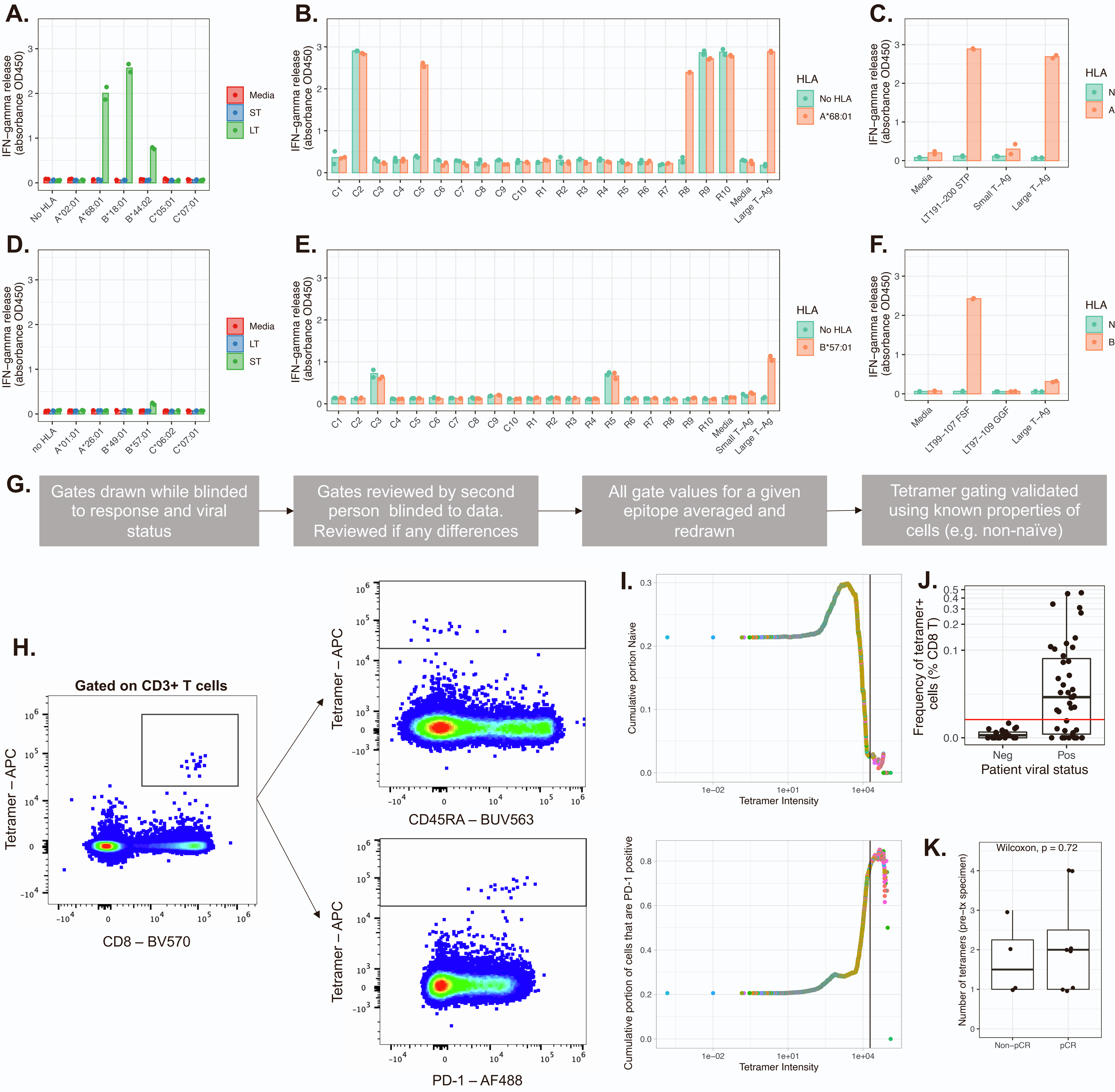
A.
IFN−gamma release (absorbance OD450)
No HLA
A*02:01
A*68:01
B*18:01
B*44:02
C*05:01
C*07:01
Media
ST
LT
B.
C1 C2 C3 C4 C5 C6 C7 C8 C9 C10 R1 R2 R3 R4 R5 R6 R7 R8 R9 R10 Media Large T−Ag
HLA
No HLA
A*68:01
C.
Media
LT191−200 STP
Small T−Ag
Large T−Ag
D.
no HLA
A*01:01
A*26:01
B*49:01
B*57:01
C*06:02
C*07:01
Media
LT
ST
E.
C1 C2 C3 C4 C5 C6 C7 C8 C9 C10 R1 R2 R3 R4 R5 R6 R7 R8 R9 R10 Media Small T−Ag Large T−Ag
No HLA
B*57:01
F.
Media
LT99−107 FSF
LT97−109 GGF
Large T−Ag
G.
Gates drawn while blinded to response and viral status
Gates reviewed by second person blinded to data. Reviewed if any differences
All gate values for a given epitope averaged and redrawn
Tetramer gating validated using known properties of cells (e.g. non-naïve)
H.
Gated on CD3+ T cells
Tetramer – APC
CD8 – BV570
CD45RA – BUV563
PD-1 – AF488
I.
Cumulative portion Naive
Cumulative portion of cells that are PD-1 positive
Tetramer Intensity
1e−02
1e+01
1e+04
J.
Frequency of tetramer+ cells (% CD8 T)
Neg
Pos
Patient viral status
K.
Wilcoxon, p = 0.72
Number of tetramers (pre−tx specimen)
Non−pCR
pCR

Supplemental Figure 1. MCPyV T-Ag CD8+ T-cell epitope discovery and validation of tetramer gating.
A, D. Reactivity of bulk-expanded TIL with aAPC expressing the indicated HLA alleles and MCPyV short T (ST) or long T (LT) antigens.
B, E. Reactivity of bulk-expanded TIL to aAPC expressing the indicated HLA alleles and MCPyV T antigen peptides arranged as column (C) or row (R) pools in a rectangular matrix. Positive and negative controls at right. Note that fine peptide mapping for HLA-B*18:01 and HLA-B*44:02-restricted responses have been previously reported.
C, F. Fine peptide mapping. Reactivity of bulk-expanded TIL to aAPC expressing the indicated HLA alleles with the indicated MCPyV T antigen peptide added. Numbers refer to amino acid positions in large T (LT) or small T (ST) isoforms of MCPyV T antigen. The indicated peptides are truncation internal peptides within peptides lying at the intersections of reactive pools in B and E. At right of both, controls show aAPC co-transfected with HLA and the indicated MCPyV T antigen plasmids. Data are OD_{450} values from IFN-γ ELISA of culture supernatants. Dots are raw data of technical duplicates and bars are means.
G. Flow chart of tetramer gating strategy.
H. Example FACS plots of PBMCs stained with multimers with tetramer gate shown (left). Tetramer gating was validated with expected biology (increased proportion of PD-1[60], decreased expression of CD45RA).
I. Representative cumulative density plot of portions of cells that are naïve (CCR7+, CD45RA+; top) or PD-1+ (bottom) as a function of fluorescence intensity in the tetramer channel. Cumulative density is calculated from high tetramer intensity to low (i.e., right to left). Each individual point represents a CD8 T cell colored by the sample of origin. Data concatenated from samples all samples stained with an A*02:01 restricted MCPyV-epitope. Vertical line represents MHC-I tetramer gate value as determined in panel A, blinded to all phenotypic and clinical data.
J. Frequency of total tetramer positive (MCPyV-specific) cells in virus negative (Neg) or virus positive (Pos) patients. Each point represents a single sample from pre- or post-nivolumab treatment. Red line depicts limit of detection at 1 in 10,000 CD8 T cells consistent with prior studies[31].
K. Comparison of the number of MHC-I tetramers available and used for patients that had complete pathological response or non-pathological complete responses.
See also Figure 2.

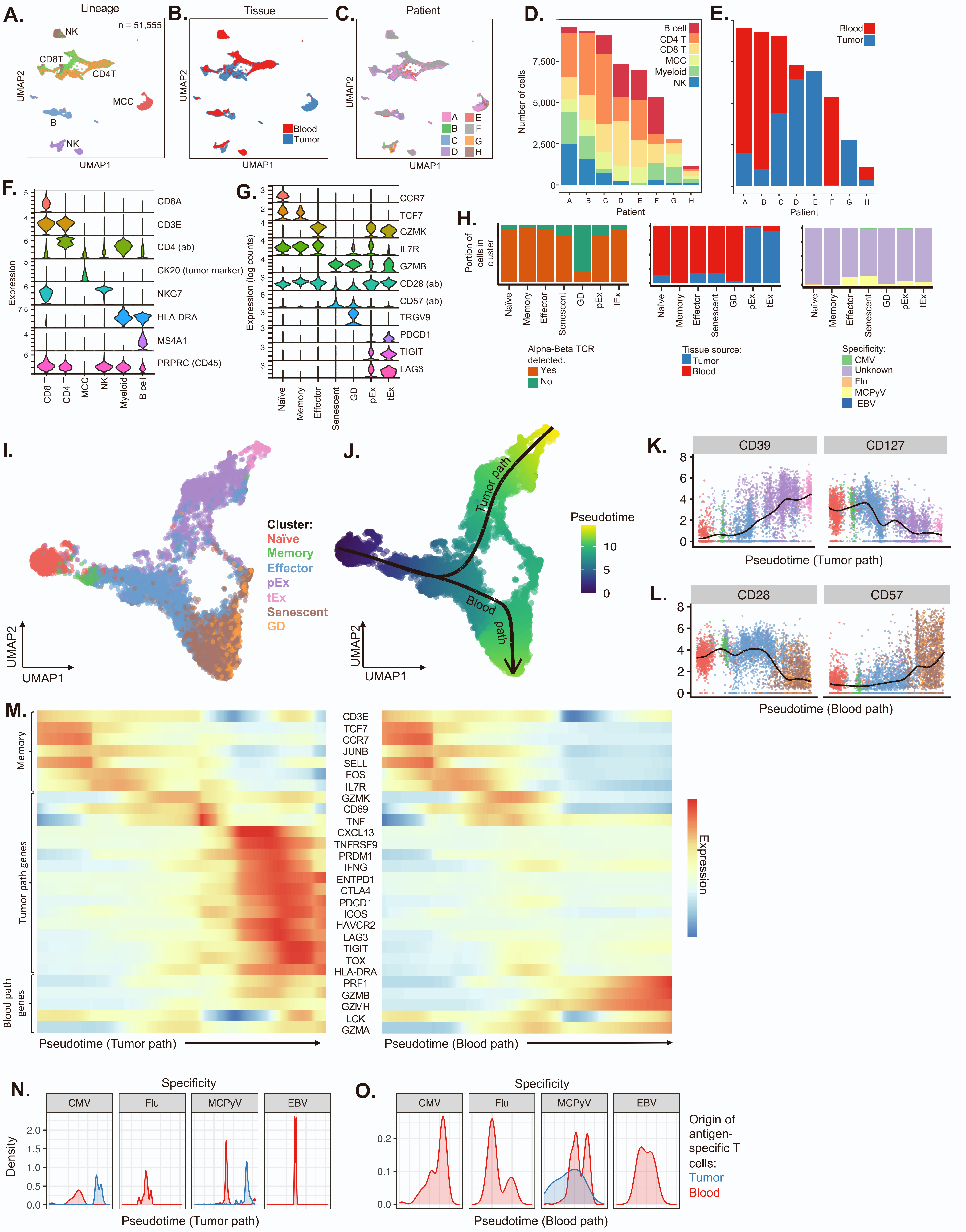
A.
Lineage
n = 51,555
NK
CD8T
CD4T
MCC
B
NK
UMAP2
UMAP1
B.
Tissue
Blood
Tumor
UMAP2
UMAP1
C.
Patient
A
B
C
D
E
F
G
H
UMAP2
UMAP1
D.
Number of cells
0
2,500
5,000
7,500
B cell
CD4 T
CD8 T
MCC
Myeloid
NK
A B C D E F G H
Patient
E.
Blood
Tumor
A B C D E F G H
Patient
F.
CD8A
CD3E
CD4 (ab)
CK20 (tumor marker)
NKG7
HLA-DRA
MS4A1
PRPRC (CD45)
Expression
CD8 T
CD4 T
MCC
NK
Myeloid
B cell
G.
CCR7
TCF7
GZMK
IL7R
GZMB
CD28 (ab)
CD57 (ab)
TRGV9
PDCD1
TIGIT
LAG3
Expression (log counts)
Naïve
Memory
Effector
Senescent
GD
pEx
tEx
H.
Portion of cells in cluster
Naïve
Memory
Effector
Senescent
GD
pEx
tEx
Alpha-Beta TCR detected:
Yes
No
Tissue source:
Tumor
Blood
Specificity:
CMV
Unknown
Flu
MCPyV
EBV
I.
Cluster:
Naïve
Memory
Effector
pEx
tEx
Senescent
GD
UMAP2
UMAP1
J.
Tumor path
Blood path
Pseudotime
10
5
0
UMAP2
UMAP1
K.
CD39
CD127
0
2
4
6
8
Pseudotime (Tumor path)
L.
CD28
CD57
0
2
4
6
8
Pseudotime (Blood path)
M.
Memory
Tumor path genes
Blood path genes
CD3E
TCF7
CCR7
JUNB
SELL
FOS
IL7R
GZMK
CD69
TNF
CXCL13
TNFRSF9
PRDM1
IFNG
ENTPD1
CTLA4
PDCD1
ICOS
HAVCR2
LAG3
TIGIT
TOX
HLA-DRA
PRF1
GZMB
GZMH
LCK
GZMA
Pseudotime (Tumor path)
Pseudotime (Blood path)
Expression
N.
Specificity
CMV
Flu
MCPyV
EBV
Density
0.0
0.5
1.0
1.5
2.0
Pseudotime (Tumor path)
O.
Specificity
CMV
Flu
MCPyV
EBV
0.0
0.1
0.2
Pseudotime (Blood path)
Origin of antigen-specific T cells:
Tumor
Blood

Supplemental Figure 2. Justification of single cell RNAseq clustering of bulk cells and subclustering of CD8 T cells in Figure 4 and pseudotime analysis of CD8 T cells.

A. UMAP plot of scRNAseq data from 51,555 cells isolated from tumor and blood samples from 8 patients. Cells were clustered and subsequently named according to the cell lineage (see panel F).
B. UMAP plot (as in panel A) colored by whether cells were isolated from tumor or blood specimens.
C. UMAP plot (as in panel A) colored by patient.
D. Bar plot of the number of cells contributed by each patient and colored by cell type combining blood and tumor.
E. Bar plot of the number of cells contributed by each patient and colored by portions of cells from tumor or blood.
F. Violin plots of cell lineage markers confirming cell types shown in panel A.
G. Violin plots of phenotypic genes in CD8 T cells isolated *in silico* from bulk population shown in Panel A.
H. Bar plots of the portions of cells in each phenotype in panel G by whether these cells had an α-β TCR (top), originated from the tumor or blood (middle), or the specificity of each T cell (bottom).
I. Data from single cell RNAseq of 8151 CD8 T cells. UMAP plot of CD8 T cells colored by the clustering and phenotypic identity (reproduced for clarity, from **Figure 4B**).
J. Trajectory analysis was performed on CD8 T cells shown in panel A which showed a bifurcated pathway with one pathway (tumor path) originated in in the naïve CD8 T cell cluster and terminating in the terminally exhausted T cell cluster while the other path (blood path) originated in the naïve CD8 T cell population and terminating in the γ-δ and senescent clusters. Plot is colored by pseudotime along these paths.
K. Plot of CD39 and CD127 (IL7R) cell surface protein levels against pseudotime along the tumor path. Points colored according to their cluster identity as in A. Spline (black) tracks average of these markers over pseudotime.
L. Plot of CD28 and CD57 cell surface protein levels against pseudotime along the blood path. Points colored according to their cluster identity as in A. Spline (black) tracks average of these markers over pseudotime.
M. Heatmaps of memory, exhaustion, and senescence genes along the tumor path pseudotime (left) or blood path pseudotime (right).
N. Histograms of tetramer-identified CMV, Flu, MCPyV and EBV-specific CD8 T cells and their positions along the tumor path pseudotime
O. Histograms of CMV, Flu, MCPyV and EBV-specific CD8 T cells and their positions along the blood path pseudotime.

Abbreviations: ab = antibody

See also Figure 4.

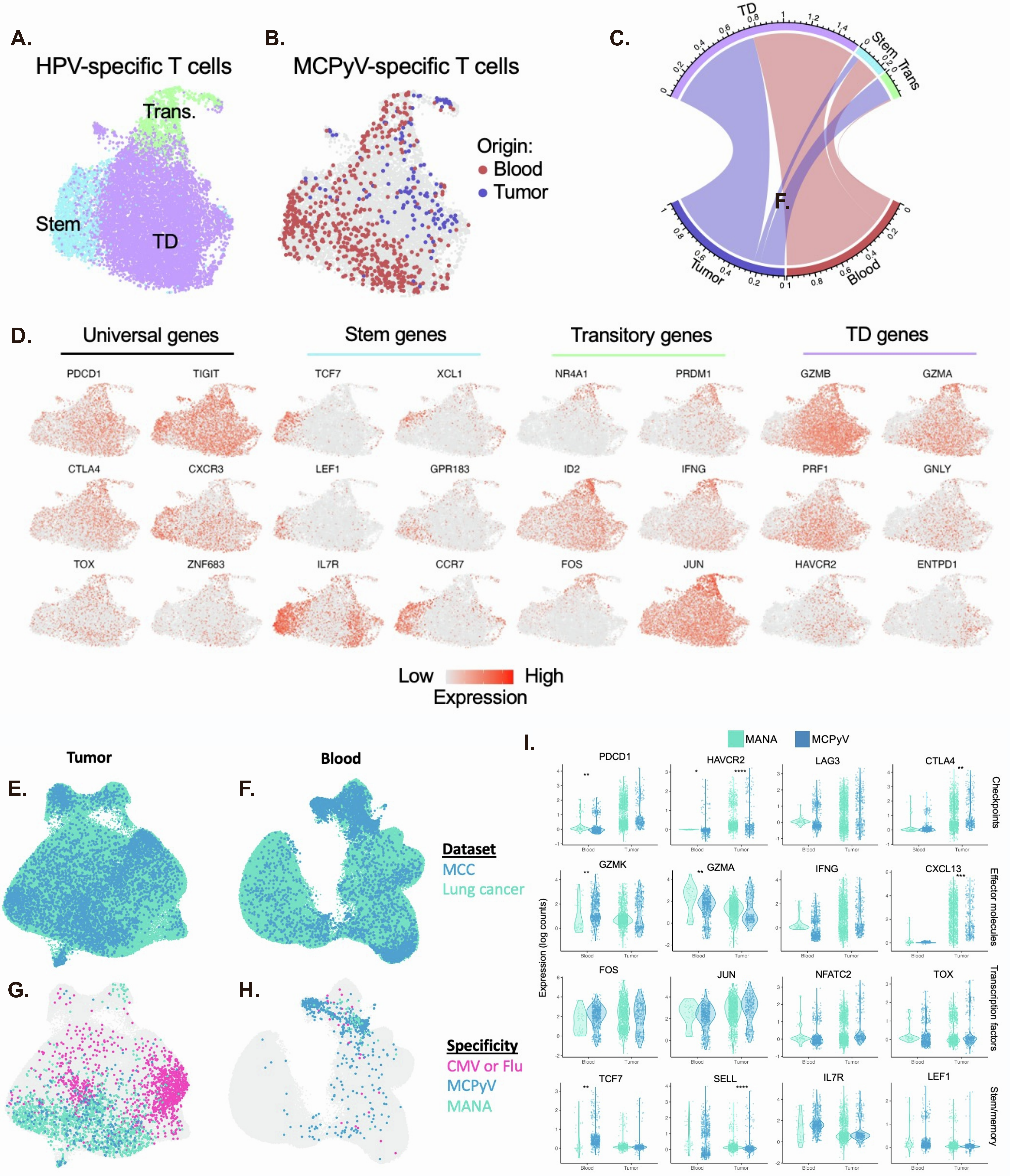
A.
HPV-specific T cells
Trans.
Stem
TD
B.
MCPyV-specific T cells
Origin:
● Blood
● Tumor
C.
TD
Stem
Trans
Tumor
Blood
D.
Universal genes
Stem genes
Transitory genes
TD genes
PDCD1
TIGIT
TCF7
XCL1
NR4A1
PRDM1
GZMB
GZMA
CTLA4
CXCR3
LEF1
GPR183
ID2
IFNG
PRF1
GNLY
TOX
ZNF683
IL7R
CCR7
FOS
JUN
HAVCR2
ENTPD1
Low
High
Expression
Tumor
Blood
E.
F.
Dataset
MCC
Lung cancer
G.
H.
Specificity
CMV or Flu
MCPyV
MANA
I.
MANA
MCPyV
Expression (log counts)
PDCD1
HAVCR2
LAG3
CTLA4
Checkpoints
GZMK
GZMA
IFNG
CXCL13
Effector molecules
FOS
JUN
NFATC2
TOX
Transcription factors
TCF7
SELL
IL7R
LEF1
Stem/memory
Blood
Tumor

Supplemental Figure 3. MCPyV-specific CD8 T cells in blood are phenotypically similar to stem-like HPV-specific CD8 T cells in virally-driven head and neck cancer and neoantigen-specific CD8 T cells from non-small cell lung cancer patients.

A. UMAP plot pseudo colored by cluster identity.
B. UMAP highlighting MCPyV-specific CD8 T cells and pseudocolored by anatomic origin of cells. HPV-specific cells are in grey in background.
C. Chord diagram showing cluster identities of MCPyV-specific CD8 T cells from tumor (bottom left) or blood (bottom right) and their corresponding cluster identities (top).
D. UMAP plots of expression of key genes as in Eberhardt *et al* but including MCPyV-specific CD8 T cells.
E. UMAP plot demonstrating integration of intratumoral CD8 T cells from patients with MCC (dark blue) or non-small-cell lung cancer (aquamarine).
F. UMAP plot demonstrating integration of circulating CD8 T cells from patients with MCC (dark blue) or non-small-cell lung cancer (aquamarine).
G. UMAP plot highlighting antigen-specificity of intratumoral CD8 T cells: MCPyV in dark blue; mutation-associated neoantigens (MANA) in aquamarine; and CMV, EBV, or Flu in pink. T cells of unknown specificity are in grey in the background.
H. UMAP plot highlighting antigen-specificity of circulating CD8 T cells: MCPyV in dark blue; mutation-associated neoantigens (MANA) in aquamarine; and CMV, EBV, or Flu in pink. T cells of unknown specificity are in grey in the background.
I. Violin plots of exhaustion, memory, and checkpoint gene sets for MCPyV-specific and MANA-specific CD8 T cells from tumor or blood. T tests performed between MCPyV-specific vs MANA-specific T cells within tumor and blood specimens. Benjamini–Hochberg correction was performed for multiple comparisons.

p values: * ≤0.05; **≤0.01, *** ≤0.001, ****≤0.0001

See also Figure 4.

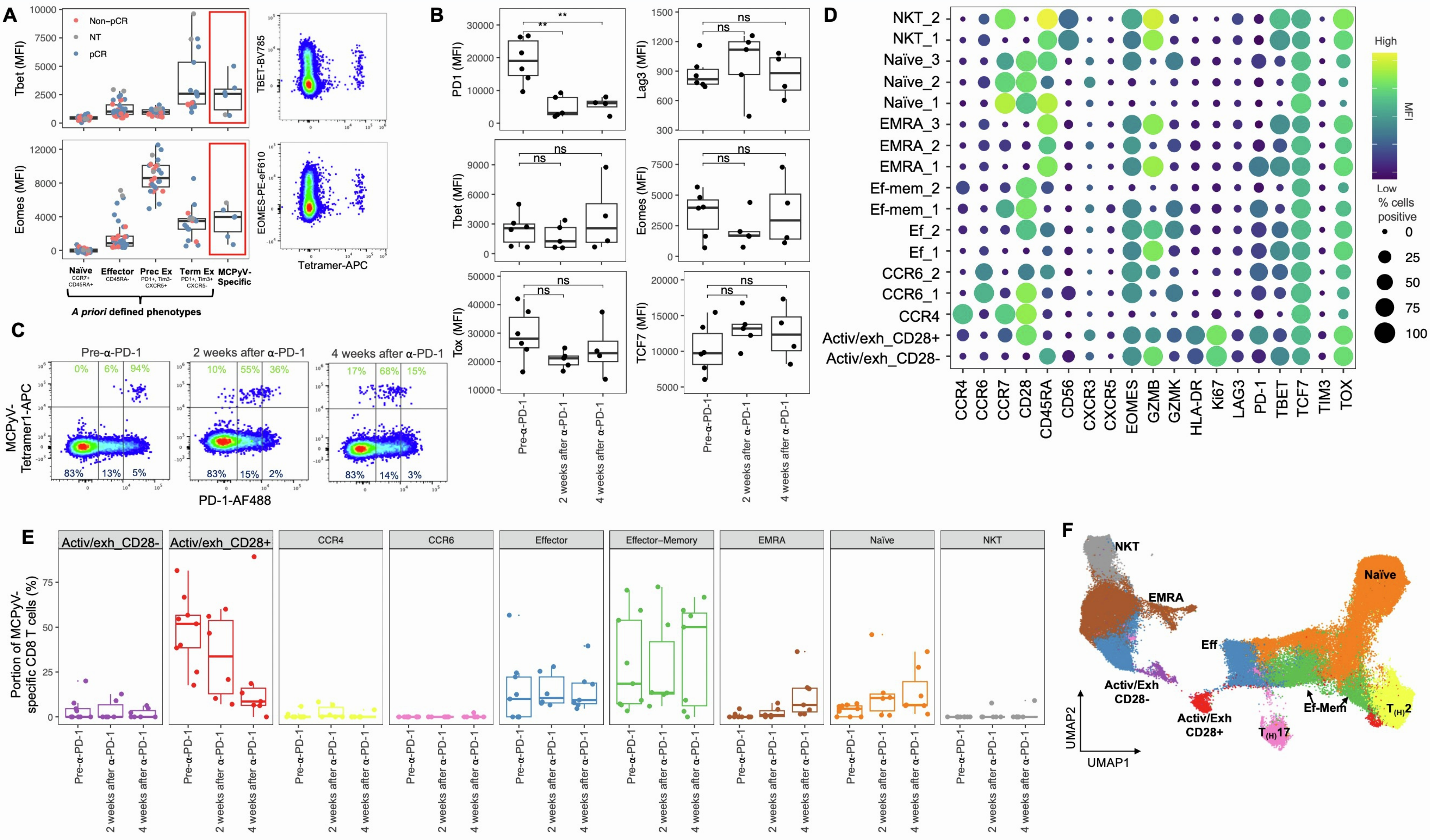

Supplemental Figure 4. MCPyV-specific CD8 T cells downregulate PD-1 over the course of anti-PD-1 therapy.

A. Expression of TBET and EOMES proteins in naïve, effector, precursor exhausted, terminally exhausted and MCPyV-specific T cells via flow cytometry. Each point represents MCPyV-specific T cells from one patient at the pre-treatment time point. If a patient has less than 10 cells for a given population, that patient was excluded.

B. Changes in expression of PD-1, LAG3, TBET, EOMES, TOX and TCF7 protein expression in MCPyV-specific CD8 T cells over the course of anti-PD-1 therapy. Each point represents MCPyV-specific T cells from one patient at that time point. T tests were used for statistical significance.

C. Representative Flow cytometry dot plots showing down regulation of PD-1 in MCPyV-specific CD8 T cells over the course of therapy. Gates drawn for PD-1 high, PD-1 middle and PD-1 negative cells. Percentages in top of plots (green) represent portion of tetramer+ (MCPyV-specific) cells. Percentages on bottom of plots (dark blue) represent portions of tetramer negative cells (unknown specificity).

D. Justification of phenograph clustering labels. CD8 T cells were clustered using flow cytometry data (panel E and F) to assign phenotypic labels to each cluster, the MFI and portion of cells positive for each marker were tabulated for each cluster and plotted. Phenotypic labels y-axis labels) were then assigned based on the expression of these makers.

E. Phenotypes of MCPyV-specific CD8 T cells and changes over course of therapy. Each point represents MCPyV-specific T cells from one patient at the designated time point. If a patient had less than 10 cells for a given population, that point was excluded.

F. UMAP plots of CD8 T cells from blood. Cells grouped, colored and labeled using phenograph clustering.

p values: ns = $p \geq 0.05$; * = $p < 0.05$; ** = $p < 0.01$; *** = $p < 0.001$; **** = $p < 0.0001$

See also Figure 5.

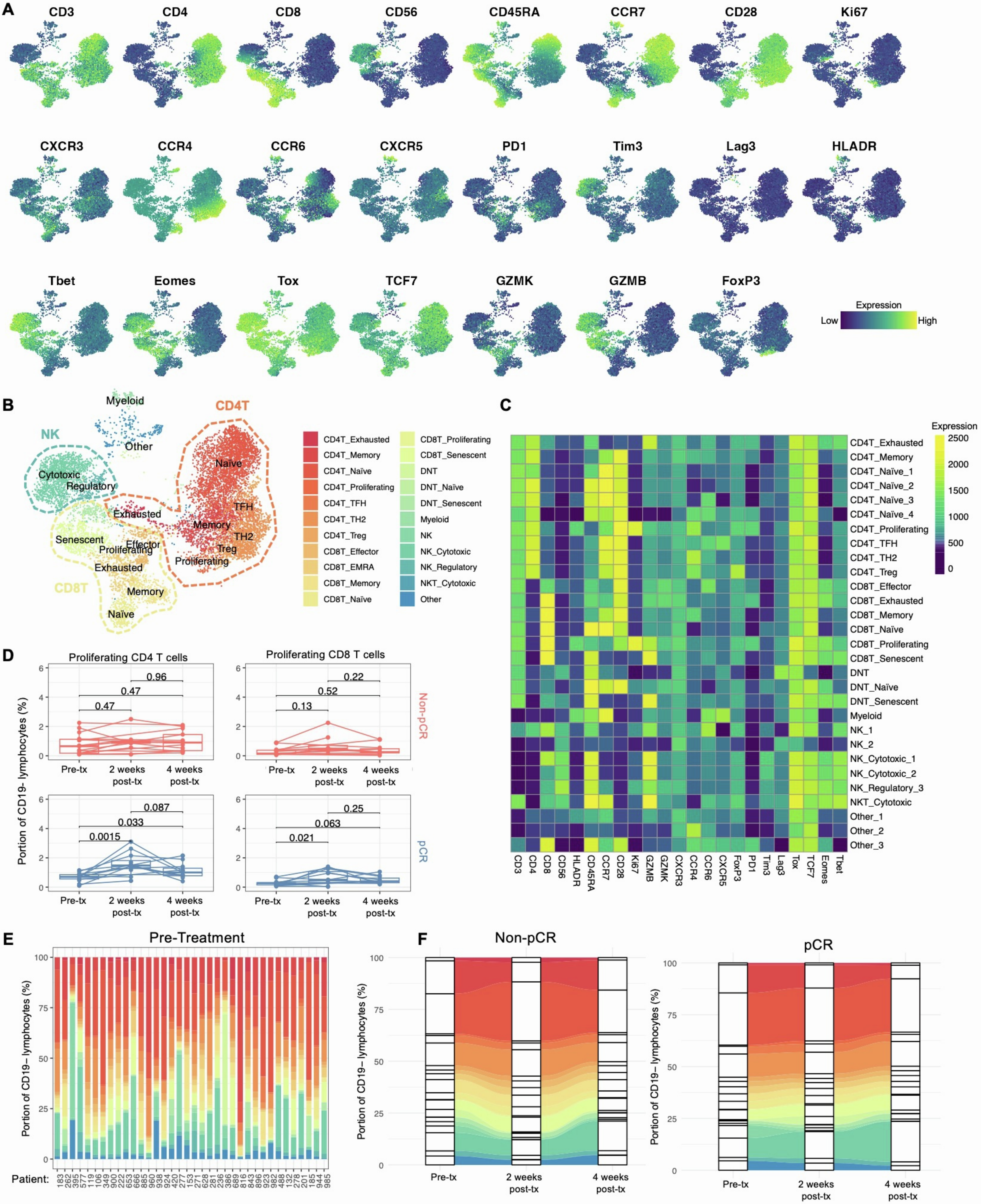
A
CD3
CD4
CD8
CD56
CD45RA
CCR7
CD28
Ki67
CXCR3
CCR4
CCR6
CXCR5
PD1
Tim3
Lag3
HLADR
Tbet
Eomes
Tox
TCF7
GZMK
GZMB
FoxP3
Expression
Low
High
B
Myeloid
CD4T
NK
Other
Cytotoxic
Regulatory
Naïve
TFH
Exhausted
Memory
TH2
Treg
Senescent
Effector
Proliferating
Proliferating
Exhausted
CD8T
Memory
Naïve
CD4T_Exhausted
CD4T_Memory
CD4T_Naïve
CD4T_Proliferating
CD4T_TFH
CD4T_TH2
CD4T_Treg
CD8T_Effector
CD8T_EMRA
CD8T_Memory
CD8T_Naïve
CD8T_Proliferating
CD8T_Senescent
DNT
DNT_Naïve
DNT_Senescent
Myeloid
NK
NK_Cytotoxic
NK_Regulatory
NKT_Cytotoxic
Other
C
Expression
2500
2000
1500
1000
500
0
CD4T_Exhausted
CD4T_Memory
CD4T_Naïve_1
CD4T_Naïve_2
CD4T_Naïve_3
CD4T_Naïve_4
CD4T_Proliferating
CD4T_TFH
CD4T_TH2
CD4T_Treg
CD8T_Effector
CD8T_Exhausted
CD8T_Memory
CD8T_Naïve
CD8T_Proliferating
CD8T_Senescent
DNT
DNT_Naïve
DNT_Senescent
Myeloid
NK_1
NK_2
NK_Cytotoxic_1
NK_Cytotoxic_2
NK_Regulatory_3
NKT_Cytotoxic
Other_1
Other_2
Other_3
CD3
CD4
CD8
CD56
HLADR
CD45RA
CCR7
CD28
Ki67
GZMB
GZMK
CXCR3
CCR4
CCR6
CXCR5
FoxP3
PD1
Tim3
Lag3
Tox
TCF7
Eomes
Tbet
D
Proliferating CD4 T cells
Proliferating CD8 T cells
Portion of CD19- lymphocytes (%)
6
4
2
0
0.96
0.47
0.47
0.22
0.52
0.13
Non-pCR
0.087
0.033
0.0015
0.25
0.063
0.021
pCR
Pre-tx
2 weeks post-tx
4 weeks post-tx
E
Pre-Treatment
Portion of CD19- lymphocytes (%)
100
75
50
25
0
Patient:
183
262
395
577
119
106
349
900
222
653
666
885
960
938
924
277
153
271
628
281
236
386
689
816
843
896
923
488
132
278
201
185
944
985
F
Non-pCR
pCR
Portion of CD19- lymphocytes (%)
100
75
50
25
0
Pre-tx
2 weeks post-tx
4 weeks post-tx

Supplemental Figure 5. Analyses of bulk lymphocyte flow cytometry show association between pathological response and increases in proliferating CD4 and CD8 T cells in blood following anti-PD-1 blockade.

A. UMAP plots of key markers of CD19- lymphocytes using 29 parameter flow cytometry data.
B. UMAP plot of same projection in A pseudo colored by phenograph clustering.
C. Heatmap of each phenograph cluster (y axis) and the median expression of markers (x axis).
D. Frequency of proliferating CD4 (left) or CD8 (right) T cells over the course of neoadjuvant PD-1 blockage grouped by patients with non-pCRs (top) or pCRs (bottom). T tests were used to establish statistical significance.
E. Proportion of each phenograph cluster in each patient prior to treatment (Same color scale as panel B).
F. Changes in proportions of phenograph clusters over the course of neoadjuvant PD-1 blockade. Proportions averaged across all patients with non-pCRs (left) or pCRs (right).

See also Figure 5.

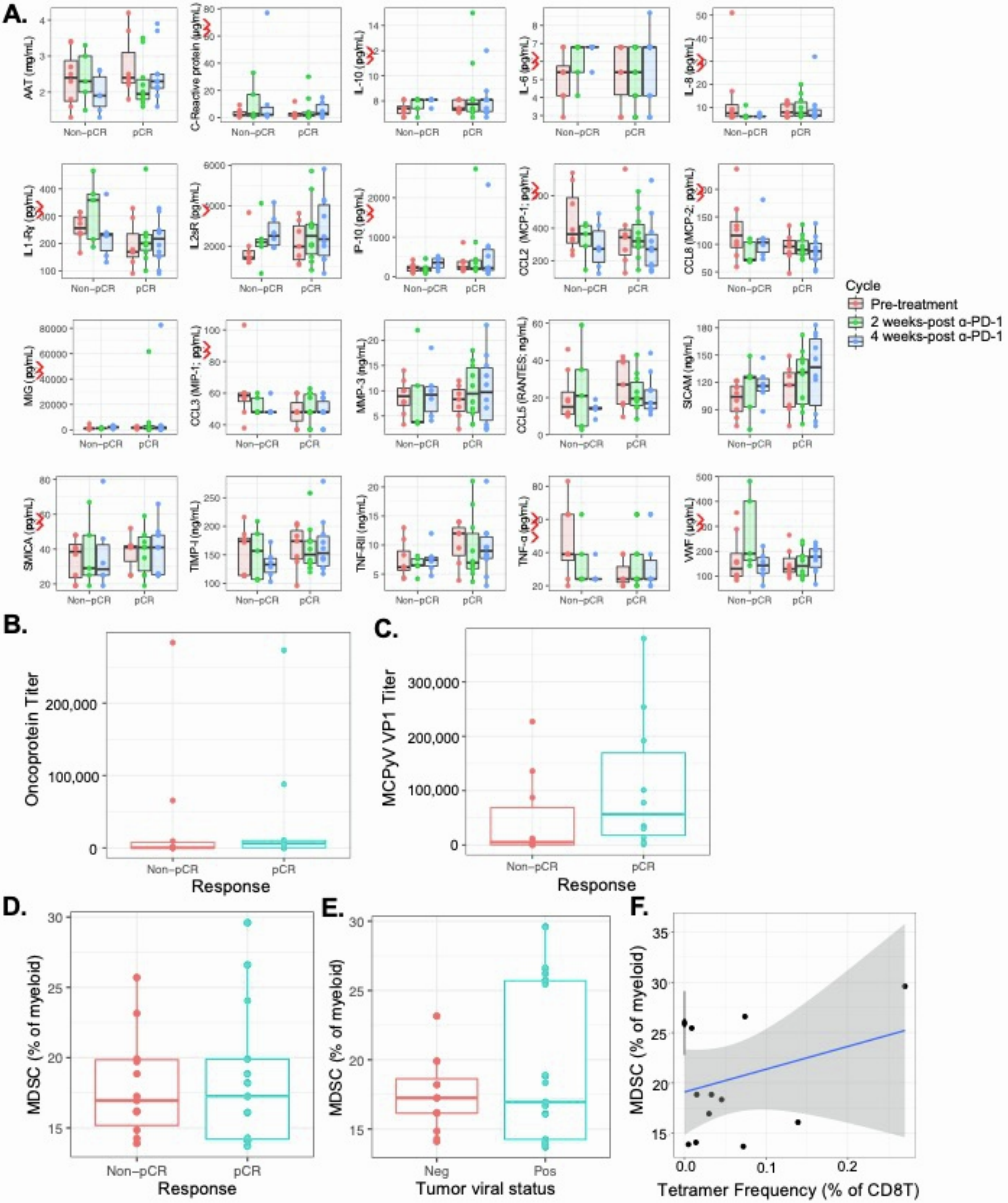
A.
AAT (mg/mL)
C-Reactive protein (μg/mL)
IL-10 (pg/mL)
IL-6 (pg/mL)
IL-8 (pg/mL)
IL1-Rγ (pg/mL)
IL2sR (pg/mL)
IP-10 (pg/mL)
CCL2 (MCP-1; pg/mL)
CCL8 (MCP-2; pg/mL)
MIG (pg/mL)
CCL3 (MIP-1; pg/mL)
MMP-3 (ng/mL)
CCL5 (RANTES; ng/mL)
SICAM (ng/mL)
SMICA (pg/mL)
TIMP-I (ng/mL)
TNF-RII (ng/mL)
TNF-α (pg/mL)
VWF (μg/mL)
Non−pCR
pCR
Cycle
Pre-treatment
2 weeks-post α-PD-1
4 weeks-post α-PD-1
B.
Oncoprotein Titer
0
100,000
200,000
Non−pCR
pCR
Response
C.
MCPyV VP1 Titer
0
100,000
200,000
300,000
Non−pCR
pCR
Response
D.
MDSC (% of myeloid)
15
20
25
30
Non−pCR
pCR
Response
E.
MDSC (% of myeloid)
15
20
25
30
Neg
Pos
Tumor viral status
F.
MDSC (% of myeloid)
15
20
25
30
35
0.0
0.1
0.2
Tetramer Frequency (% of CD8T)

Supplemental Figure 6. Association of pathological response and peripheral blood cytokines or myeloid derived suppressor cells (MDSC).

A. Concentrations of key cytokines in blood measured via Luminex assay in patients with pCRs (left) or non-pCRs (right) sub-grouped by timepoint.
B. MCPyV oncoprotein titer measured by the AMERK assay at the pre-treatment timepoint grouped by pathological response at the pre-treatment timepoint.
C. MCPyV viral capsid (VP1) titer measured by the AMERK assay at the pre-treatment timepoint grouped by pathological response at the pre-treatment timepoint.
D. Frequency of MDSCs as a portion of all myeloid cells in the peripheral blood at the pre-treatment timepoint grouped by pathological response at the pre-treatment timepoint.
E. Frequency of MDSCs as a portion of all myeloid cells in the peripheral blood at the pre-treatment timepoint grouped by tumor viral status.
F. Association of frequency of MDSCs and frequency of MCPyV-specific CD8 T cells in the peripheral blood at the pre-treatment timepoint.

See also Figure 5**.**

Chapter 3: Merkel cell polyomavirus-specific and CD39$^+$CLA$^+$ CD8 T cells as blood-based predictive biomarkers for PD-1 blockade in Merkel cell carcinoma

Heeju Ryu, Timothy M. Bi, Thomas H. Pulliam, Korok Sarkar, Candice D. Church, Nandita Kumar, Koshlan Mayer-Blackwell, Saumya Jani, Nirasha Ramchurren, Ulla K. Hansen, Sine R. Hadrup, Steven P. Fling, David M. Koelle, Paul Nghiem, Evan W. Newell

Cell Reports Medicine, February 2024

CHAPTER SUMMARY: In this chapter, we validate our finding that tumor-specific CD8 T cell frequency in blood correlates with survival, as well as quality of response (complete, partial, or progressive disease) using an independent cohort of virus-driven Merkel cell carcinoma (MCC) patients. Additionally, we find that the patients with a higher frequency of CD39$^+$CLA$^+$ CD8 T cells experience more durable responses to anti-PD-1 treatment. In contrast, patients with a higher frequency of CD39$^+$CD103$^+$ CD8 T cells experience poorer outcomes. This suggests that having T cells that can specifically home to the skin vs. establish broad tissue residence are more important in response to immunotherapy in MCC. Additionally, since these studies do not rely on identification of antigen-specific CD8 T cells, but rather a limited number of markers, they may be more easily translated to a clinical setting and predict response to immunotherapy.

An excellent lay summary of this chapter (as well as Chapter 2) can be found here: https://www.fredhutch.org/en/news/center-news/2024/02/biomarker-immune-checkpoint-inhibitor-merkel-cell-carcinoma.html

Cell Reports
Medicine

Article

Merkel cell polyomavirus-specific and CD39$^+$CLA$^+$ CD8 T cells as blood-based predictive biomarkers for PD-1 blockade in Merkel cell carcinoma

Graphical abstract

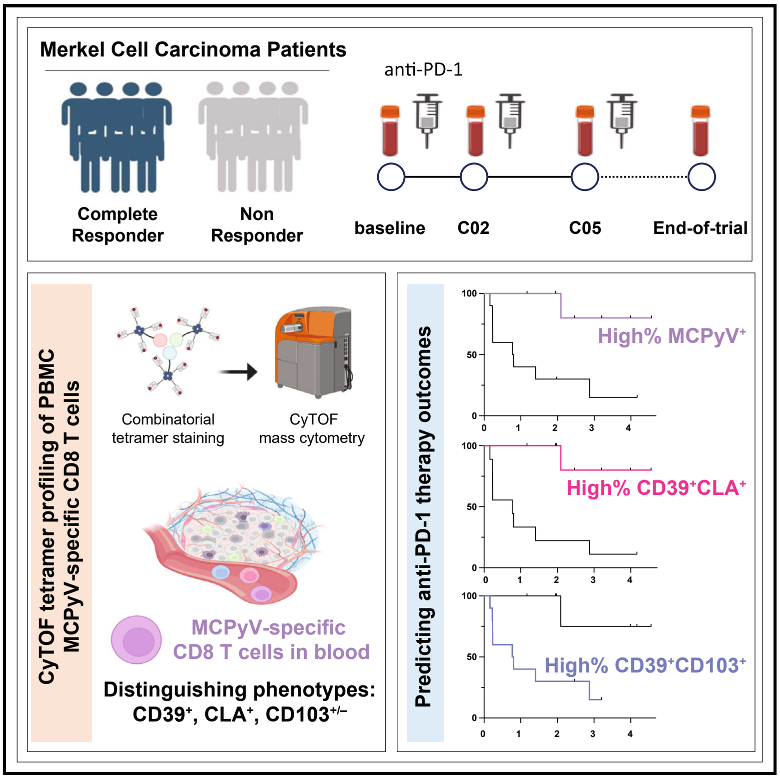

Authors

Heeju Ryu, Timothy M. Bi,
Thomas H. Pulliam, ..., David M. Koelle,
Paul Nghiem, Evan W. Newell

Correspondence

enewell@fredhutch.org

In brief

Ryu et al. profile MCC patient peripheral CD8 T cells and find that higher frequencies of MCPyV-specific cells predict response to anti-PD-1 therapy. Based on antigen-specific cell profiles, they identify CD39$^+$CLA$^+$ and CD39$^+$CD103$^+$ frequencies among total CD8 T cells as potential markers of tumor reactivity and as biomarkers for immunotherapy response.

Highlights

- MCPyV-specific CD8 T cells in blood predict MCC patient response to anti-PD-1
- Blood MCPyV-specific CD8 T cells often express CD39, CLA, or CD103
- Bulk CD39$^+$CLA$^+$ CD8 T cells predict response to anti-PD-1
- Bulk CD39$^+$CD103$^+$ CD8 T cells correlate with tumor burden and predict poor outcomes

Ryu et al., 2024, Cell Reports Medicine *5*, 101390
February 20, 2024
https://doi.org/10.1016/j.xcrm.2023.101390

CellPress

Please cite this article in press as: Ryu et al., Merkel cell polyomavirus-specific and CD39⁺CLA⁺ CD8 T cells as blood-based predictive biomarkers for PD-1 blockade in Merkel cell carcinoma, Cell Reports Medicine (2023), https://doi.org/10.1016/j.xcrm.2023.101390

Cell Reports Medicine

CellPress
OPEN ACCESS

Article

Merkel cell polyomavirus-specific and CD39$^+$CLA$^+$ CD8 T cells as blood-based predictive biomarkers for PD-1 blockade in Merkel cell carcinoma

Heeju Ryu,[1] Timothy M. Bi,[1] Thomas H. Pulliam,[2] Korok Sarkar,[1] Candice D. Church,[2] Nandita Kumar,[1,3]
Koshlan Mayer-Blackwell,[1] Saumya Jani,[2,3] Nirasha Ramchurren,[4] Ulla K. Hansen,[5] Sine R. Hadrup,[5] Steven P. Fling,[4]
David M. Koelle,[1,3,6,7,8] Paul Nghiem,[2] and Evan W. Newell[1,3,9,*]
[1]Vaccine and Infectious Disease Division, Fred Hutchinson Cancer Center, Seattle, WA, USA
[2]Department of Medicine, Division of Dermatology, University of Washington, Seattle, WA, USA
[3]Department of Lab Medicine and Pathology, University of Washington, Seattle, WA, USA
[4]Cancer Immunotherapy Trails Network, Fred Hutchinson Cancer Center, Seattle, WA, USA
[5]Department of Health Technology, Technical University of Denmark, Kongens Lyngby, Denmark
[6]Department of Medicine, Division of Allergy and Infectious Diseases, University of Washington, Seattle, WA, USA
[7]Department of Global Health, University of Washington, Seattle, WA, USA
[8]Benaroya Research Institute, Seattle, WA, USA
[9]Lead contact
*Correspondence: enewell@fredhutch.org
https://doi.org/10.1016/j.xcrm.2023.101390

SUMMARY

Merkel cell carcinoma is a skin cancer often driven by Merkel cell polyomavirus (MCPyV) with high rates of response to anti-PD-1 therapy despite low mutational burden. MCPyV-specific CD8 T cells are implicated in anti-PD-1-associated immune responses and provide a means to directly study tumor-specific T cell responses to treatment. Using mass cytometry and combinatorial tetramer staining, we find that baseline frequencies of blood MCPyV-specific cells correlated with response and survival. Frequencies of these cells decrease markedly during response to therapy. Phenotypes of MCPyV-specific CD8 T cells have distinct expression patterns of CD39, cutaneous lymphocyte-associated antigen (CLA), and CD103. Correspondingly, overall bulk CD39$^+$CLA$^+$ CD8 T cell frequencies in blood correlate with MCPyV-specific cell frequencies and similarly predicted favorable clinical outcomes. Conversely, frequencies of CD39$^+$CD103$^+$ CD8 T cells are associated with tumor burden and worse outcomes. These cell subsets can be useful as biomarkers and to isolate blood-derived tumor-specific T cells.

INTRODUCTION

Merkel cell carcinoma (MCC) is a rare and aggressive form of skin cancer with a high mortality rate. The etiology of MCC has been linked to both Merkel cell polyomavirus (MCPyV) and UV-induced mutagenesis.[1] The persistent expression of two MCPyV oncoprotein isoforms, large T antigen (LTA) and small T antigen (STA), is detectable in 80% of MCC cases in the US, which are categorized as virus positive (VP). The rest of cases where MCPyV cannot be detected are considered virus negative (VN).[2]

Involvement of immune cells in MCC is an important aspect of both disease progression and prognosis, and both VP and VN MCCs are known to be immunogenic.[3,4] Higher intratumoral T cell counts and robust CD8 T cell infiltration within the tumor have been associated with improved survival regardless of the tumor stage at diagnosis.[5] In contrast to many other solid tumors, treatment with the anti-PD-1 antibody has demonstrated remarkable efficacy in both VP and VN advanced MCCs.[6] Clinical studies, including the Cancer Immunotherapy Trials Network-09 (CITN-09)/KEYNOTE-017, have revealed that initial response rates reached up to 58%, with a notable 30% of treatment recipients achieving complete and durable response.[7,8] These promising outcomes provide strong motivation for further investigation into T cell-based biomarkers for MCC.

In particular, MCPyV-specific CD8 T cells play a major role in the immunopathogenesis of MCC. They are found at the site of the tumor and are enriched among tumor-infiltrating lymphocytes.[9] Major histocompatibility complex (MHC) class I-restricted MCPyV oncoprotein processing and presentation by mammalian cells have been shown to lead to CD8-mediated cytotoxicity, and a number of virally derived T cell epitopes have been characterized in the context of MCC.[10,11] Moreover, MCPyV-specific T cells have been identified in both MCC tumors and peripheral blood mononuclear cells (PBMCs) of patients with MCC but are more abundantly found in the former.[12] Even though MCPyV-specific T cells are implicated in immunotherapeutic responses, further qualitative and quantitative analyses of those cells among responders and non-responders are

Please cite this article in press as: Ryu et al., Merkel cell polyomavirus-specific and CD39$^+$CLA$^+$ CD8 T cells as blood-based predictive biomarkers for PD-1 blockade in Merkel cell carcinoma, Cell Reports Medicine (2023), https://doi.org/10.1016/j.xcrm.2023.101390

needed to understand why only some VP patients respond to anti-PD-1 checkpoint blockade immunotherapy.

Currently, very few predictive or prognostic biomarkers exist for the diagnosis or treatment of MCC. Prior to the use of checkpoint blockade as a therapy for MCC, it was found that the presence of tumor-infiltrating MCPyV-specific T cells was associated with improved patient survival[9] and that frequencies of peripheral virus-specific cells expressing PD-1 and Tim-3 are generally directly associated with disease burden.[12,13] Consistent with the association between MCPyV-specific CD8 T cell frequencies in the blood and tumor burden, levels of MCPyV-oncoprotein-specific antibodies are also associated with tumor mass. These antibody levels can be used as a prognostic marker for relapse in patients with advanced MCC, particularly those at high risk for recurrent disease.[14] Additionally, intratumoral T cell clonality has been found to be a differentiating characteristic between VP MCCs and VN MCCs, with the former showing higher clonality indices than the latter.[9] However, as of yet, there are no clear blood-based characteristics that can predict which patients are more likely to respond to anti-PD-1 therapy, and the mechanisms of response and resistance remain poorly understood.

Because of the high rates of complete initial responses and the consistent expression of viral antigens, VP MCC provides an ideal model system to track and evaluate T cell responses during anti-PD-1 checkpoint blockade immunotherapy. Using MHC class I tetramers against MCPyV oncoproteins, it is possible to explore shared tumor-specific T cell responses across patients with VP MCC without the requirement of identifying mutation-derived antigens or other tumor-associated antigens, which are often challenging to identify and typically not always shared among patients. Additionally, leveraging the ability to detect tumor-specific T cell responses in treatment-responsive patients with VP MCC may also help inform therapeutic strategies for patients with VN MCC, which are driven by less defined and likely more heterogeneous UV-induced neoantigens and are therefore more difficult to study. Ultimately, this could help identify correlates of anti-PD-1 response and inform strategies to improve efficacy.

In this study, we examine tumor-specific T cell dynamics in the blood of patients with MCC treated with an anti-PD-1 antibody, pembrolizumab. Taking advantage of the persistent expression of MCPyV oncoproteins in VP MCC tumors, we analyze CD8 T cells that target these proteins to directly study and measure tumor-specific T cell responses. We utilized a mass-cytometry-based multiplexed peptide-MHC class I-tetramer staining approach to first assess the frequencies and phenotypes of MCPyV-specific CD8 T cells in the blood of patients with MCC receiving pembrolizumab. Based on the phenotypes of the virus-specific cells, we identified that the frequencies of certain phenotypic subsets within total blood CD8 T cells were predictive of patient response to therapy, and these phenotypic signatures may be useful to indirectly identify tumor- and MCPyV-specific cells. Our findings provide valuable insights into tumor-specific immune responses in MCC and identify a potential biomarker for predicting immunotherapy response and isolating tumor-specific T cells from blood.

RESULTS

Identification and quantification of MCPyV-specific CD8 T cells in blood from patients with MCC

To examine the effect of pembrolizumab treatment on peripheral CD8 T cell responses in the context of MCC, we analyzed longitudinally collected PBMC samples from patients enrolled in the CITN-09 clinical trial (ClinicalTrials.gov: NCT02267603). We carefully selected a patient sample cohort that encompassed diverse clinical responses and viral status (complete response [CR], n = 13; partial response [PR], n = 6; and stable and progressive disease [SD/PD], n = 5; viral status: VP, n = 17; VN, n = 7). To ensure robust data collection and analysis, we considered human leukocyte antigen (HLA)-typing information and the availability of PBMCs for at least baseline and end-of-treatment time points (see method details). Specifically, we analyzed samples obtained prior to treatment (C01), at 3 weeks post-treatment (C02), at 12 weeks post-treatment (C05), and at the end of treatment (EOT) (Table S1).

To detect treatment-associated phenotypic changes in circulating MCPyV-specific T cells, we used mass cytometry (CyTOF) combined with multiplexed MHC class I-tetramer staining (as described previously) to screen 76 MCPyV-associated epitopes and 44 MCC-unrelated viral epitopes (spanning A*01:01, A*02:01, A*03:01, A*11:01, A*24:02, A*68:01, B*07:02, B*08:01, B*15:01, B*35:01, B*37:01, and B*57:01) (Figures S1A and S1B; Table S2).[15–17] Our MCPyV epitope panel allowed for the direct detection of tumor-specific CD8 T cells in VP MCC and included both previously known epitopes for both small and large T oncoproteins as well as epitopes that were computationally predicted to bind to HLA allelic variants in our cohort (see methods details).[11,12] The 35 markers in our phenotyping panel allowed us to detect broad immune compartment changes as well as T cell phenotypic markers to identify cell states such as differentiation, trafficking, activation, and exhaustion (Figure 1A; key resources table).[15] Ultimately, this enabled us to identify a total of 111 T cell populations that were specific for 16 MCPyV T oncoprotein-associated epitopes including 5 novel epitopes (based on epitope predictions) and 3 MCPyV capsid-protein-associated epitopes from 72 samples (n = 24 patient over 2–4 time points), which we could then further phenotypically characterize (Figure 1B). To comprehensively measure the overall changes to antigen-specific T cells, we combined the frequencies of cells detected by tetramers loaded with epitopes of the same antigen specificity within each patient across different time points (Figures 1C–1E).

First, we analyzed the frequencies of peripheral MCPyV-specific T cells and other MCC-unrelated virus-specific T cells at baseline to identify any correlations to response. As expected, VN patients had lower levels of MCPyV-specific CD8 T cells compared to VP patients (p = 0.0567 Mann-Whitney test) (Figures S1C and S1D). This is in line with previous reports that quantified MCPyV-specific CD8 T cells among tumor-infiltrating T cells (tumor-infiltrating lymphocytes [TILs]) in patients with VP MCC.[12] In addition, we found that the baseline frequency of circulating MCPyV-specific CD8 T cells summed across all MCPyV-epitope-specific T cell populations detected for each sample was associated with improved response (Figure 1C).

Please cite this article in press as: Ryu et al., Merkel cell polyomavirus-specific and CD39⁺CLA⁺ CD8 T cells as blood-based predictive biomarkers for PD-1 blockade in Merkel cell carcinoma, Cell Reports Medicine (2023), https://doi.org/10.1016/j.xcrm.2023.101390

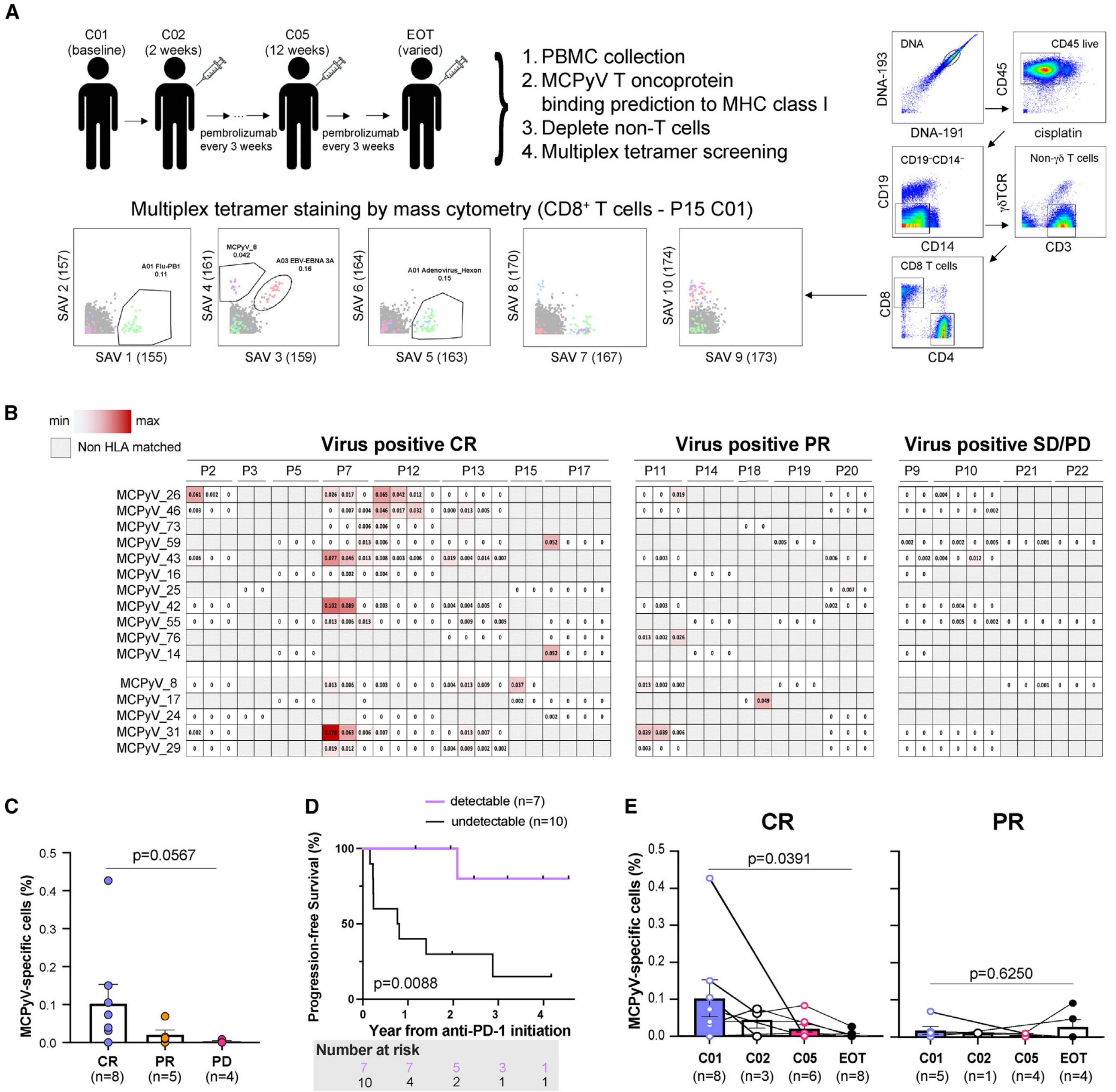

Figure 1. Identification of MCPyV-specific CD8 T cells and correlation with MCC pembrolizumab treatment clinical outcomes

(A) Experimental schematic and representative mass cytometry gating tree and dot plots of CD8 T cells showing the detection of MCPyV-specific and MCC-unrelated epitopes. Representative plots from one patient (P15) and one time point (C01, baseline).

(B) Heatmap of individual MCPyV epitopes detected across all VP patients with complete response (CR; n = 8), partial response (PR; n = 5), stable disease (SD; n = 1), and progressive disease (PD; n = 3).

(C) Integrated frequencies of MCPyV-specific CD8 T cells in PBMCs prior to the treatment. Data are represented as mean ± SEM; Mann-Whitney test.

(D) Kaplan-Meier curve of progression-free survival in patients with detectable (>0.01% of CD8 T cells, violet) or undetectable (<0.01% of CD8 T cells, black) MCPyV-specific CD8 T cells in PBMCs. Detection limit was determined by the highest frequency observed in VN patients. Log-rank test.

(E) Frequencies of MCPyV-specific CD8 T cells in PBMCs over the course of the therapy in patients with CR (left) and PR (right). Data are represented as mean ± SEM. Wilcoxon test. SAV, streptavidin.

Specifically, the mean frequency of MCPyV-specific CD8 T cells in CR patients was 5 times higher than in PR patients (mean = 0.1032 vs. 0.02077, p = 0.2199 Mann-Whitney test) and 38 times higher than in SD/PD patients (mean = 0.002654, p = 0.0727 Mann-Whitney test). Furthermore, patients with detectable (>0.01%) MCPyV-specific CD8 T cells in their blood at baseline

Please cite this article in press as: Ryu et al., Merkel cell polyomavirus-specific and CD39$^+$CLA$^+$ CD8 T cells as blood-based predictive biomarkers for PD-1 blockade in Merkel cell carcinoma, Cell Reports Medicine (2023), https://doi.org/10.1016/j.xcrm.2023.101390

had improved overall survival and progression-free survival compared to patients that did not (Figures 1D and S1E; p = 0.0088 and 0.0405, respectively, log-rank test).

When analyzing on-treatment kinetics in MCPyV-specific T cell frequencies in VP patients, we found that pembrolizumab treatment was associated with a significant decrease in frequencies of MCPyV-specific CD8 T cells in CR patients (p = 0.0391 Wilcoxon) but were only marginally different in PR and SD/PD patients across treatments (Figures 1E and S1F). The frequencies of MCC-unrelated virus-specific cells (e.g., cytomegalovirus [CMV], Epstein-Barr virus [EBV], herpes simplex virus [HSV], and influenza) remained unchanged over the course of the therapy (p = 0.5879 Wilcoxon), suggesting that MCPyV-specific cells in the blood are closely associated with tumor immune responses (Figure S1G). Taken together, these results indicate that tumor-associated MCPyV-specific CD8 T cells are present in the periphery and are closely linked to patient clinical outcomes.

Phenotypic characterization of tumor-specific CD8 T cells in patients with MCC

To further investigate peripheral tumor-associated MCPyV-specific CD8 T cells that correlate with patient clinical response, we performed deep immune phenotyping of these cells and compared their phenotypes to MCC-unrelated virus-specific T cells and the peripheral CD8 compartment as a whole. The bulk peripheral CD8 T cell compartment of patients with MCC is highly heterogeneous and comprised of cells with various distinct phenotypes including naive (CCR7$^+$CD45RA$^+$), effector memory (EM; CCR7$^-$CD45RA$^-$CD45RO$^+$), effector memory re-expressing CD45RA (TEMRA; CCR7$^-$CD45RA$^+$CD45RO$^-$), tissue resident-like (RM; CD103$^+$), and activated/exhausted (CD38$^+$PD-1$^+$HLA-DR$^+$CD39$^+$). To examine high-dimensional phenotypes of peripheral CD8 T cells, we embedded cell surface markers using UMAP (uniform manifold approximation and projection) and applied the Leiden algorithm based clustering to samples across the entire cohort (Figure 2A; see method details). In parallel, we also quantified the frequencies of each marker expression across all antigen-specific cells identified for each patient time point to corroborate these findings (exemplified in Figure S1H).

When comparing the phenotypes of MCPyV-specific and MCC-unrelated virus-specific CD8 T cells (CMV, HSV, and influenza), we identified unique phenotypic profiles that differentiate these cell populations based on their antigen specificity (Figures 2B and S1I). Our analysis of virus-specific T cells with MCC-unrelated specificities showed that CMV-specific T cells expressed high levels of CD45RA, CD57, and KLRG1, consistent with TEMRA-like phenotypes, and EBV-specific cells were enriched for CXCR5, CD27, and CD45RO (Figure 2C). As previously reported, HSV-specific cells expressed high levels of cutaneous lymphocyte-associated antigen (CLA), a skin-homing marker, and influenza-specific cells expressed high levels of CXCR3 and CCR5 (Figure 2C).[18]

In contrast, we found that MCPyV-oncoprotein-specific CD8 T cells (LTA and STA) expressed various co-stimulatory and inhibitory receptors, such as PD-1 and TIGIT, and were highly enriched for CD39, a marker previously reported to distinguish tumor-specific exhausted CD8 TILs (Figure 2C).[19–22] These cells also highly expressed proliferation, activation, and effector T cell markers, such as HLA-DR, CD38, CD71, and CXCR3. Interestingly, they also highly expressed the skin-homing marker CLA and sporadically expressed a tissue-recirculating marker CD103.[23–25] These observations were even more prominent when we quantified the marker expression of each epitope-specific cell population individually (i.e., when multiple epitope-specific populations for each patient time point were detected) (Figure 2D). Note that in this analysis, we observed some MCPyV-specific cell populations to be highly elevated for CD103 expression, which was not as readily apparent when MCPyV-specific cells were aggregated within samples. We also found that the expression levels of CD39, CLA, and CD103 on MCPyV-specific cells were maintained over the course of therapy (Figure 2C).

Notably, we also found that the phenotypes of CD8 T cells that were specific for the non-oncogenic MCPyV capsid protein were similar to MCPyV-oncoprotein-specific CD8 T cells. However, these cells exhibited lower levels of activation markers such as HLA-DR and CD71 and terminal differentiation markers such as CD45RA and KLRG1. Viral capsid-protein-specific CD8 T cells, like their oncoprotein-specific counterparts, expressed relatively high levels of CD39 in comparison to other bystander T cells, which might be a result of persistent MCPyV capsid expression in the tumor. To test this hypothesis, we analyzed public MCC tumor RNA sequencing datasets and aligned gene sequences of LTA, STA, and major capsid protein VP1 by employing the Basic Local Alignment Search Tool (BLAST).[26–28] Expression of LTA and STA transcripts were detectable in more than 90% of VP patients, with a much lower prevalence of detection in VN patients (Figures S1J and S1K). Interestingly, VP1 expression was identified in 30% of VP patients, whereas none of the VN patients expressed detectable VP1 transcripts (Figure S1L). This finding supports the notion that persistent MCPyV capsid expression may contribute to the observed phenotype of capsid-protein-specific CD8 T cells. Taken together, MCPyV-specific CD8 T cells display a unique phenotype characterized by elevated expression of co-stimulatory and inhibitory marker receptors and enrichment for CD39, CLA, and CD103. The maintenance of these phenotypes throughout the course of therapy suggests their potential as immune biomarkers and therapeutic targets.

CD39$^+$CLA$^+$ CD8 T cells in blood as predictive biomarkers for favorable clinical outcomes in patients with MCC

Since the phenotypes of MCPyV-specific CD8 T cells remained consistent across time points, we sought to explore if the decline in MCPyV-specific cell frequencies could be attributed to changes in the overall composition of the CD8 T cell compartment, independent of antigen specificities detected by MHC class I tetramers. In line with this, we observed notable alterations in the composition of bulk CD8 T cells, specifically within populations characterized by high expression levels of CD39, CLA, and CD103 (Figure S2A). This was one indication that we might be able to leverage our knowledge of the detailed phenotypes of MCPyV-specific cells to identify high-dimensional

Please cite this article in press as: Ryu et al., Merkel cell polyomavirus-specific and CD39$^+$CLA$^+$ CD8 T cells as blood-based predictive biomarkers for PD-1 blockade in Merkel cell carcinoma, Cell Reports Medicine (2023), https://doi.org/10.1016/j.xcrm.2023.101390

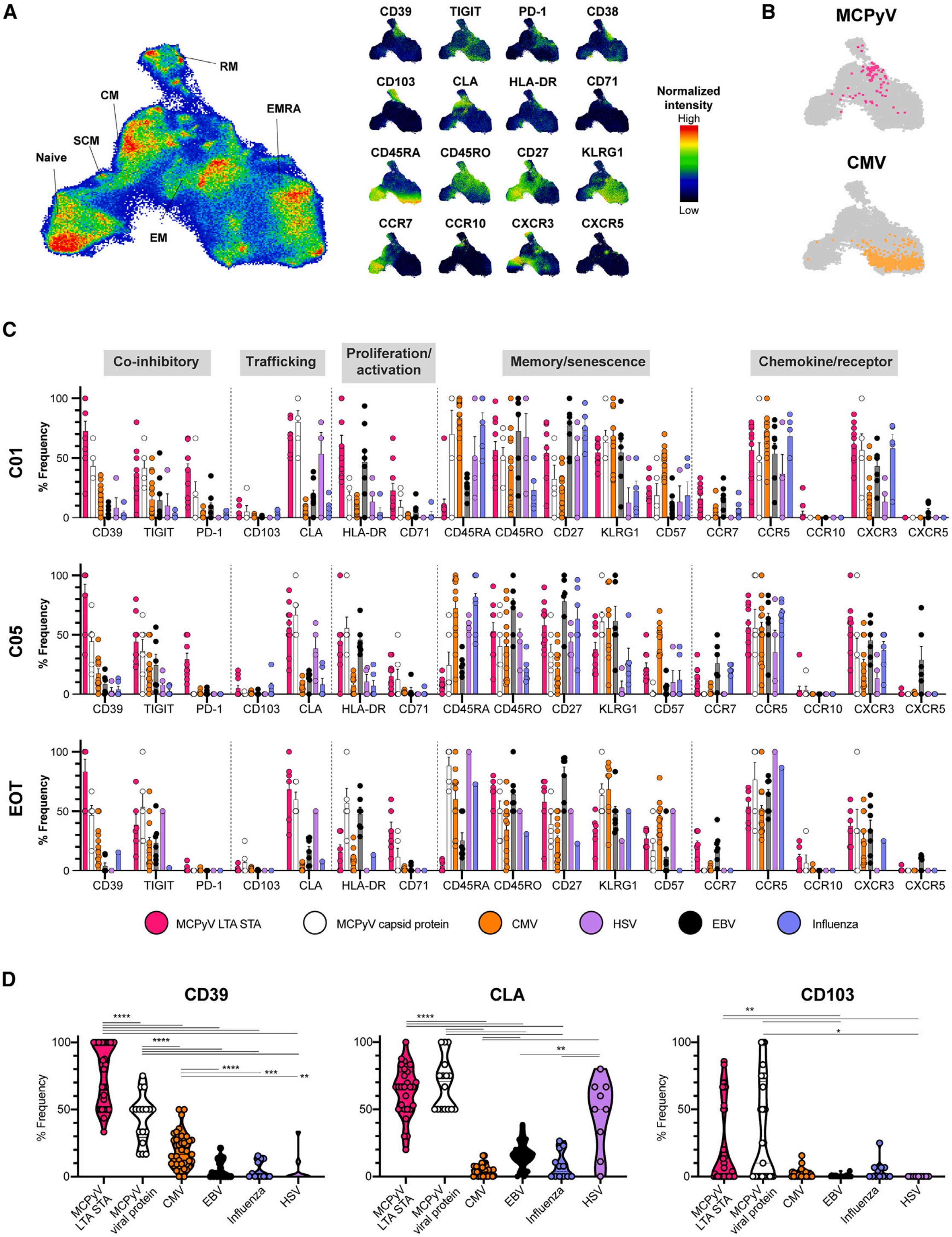

Figure 2. Phenotypic profiling of MCPyV-specific CD8 T cells in patients with MCC

(A) UMAP embedding of CD8 T cells from all patients (left). Normalized expression of selected markers defining CD8 T cell clusters (right).

(B) MCPyV-specific (top) and CMV-specific (bottom) cells projected onto a UMAP embedding. Manually gated individual tetramer$^+$ cells were concatenated.

(C) Expression of markers by indicated tetramer$^+$ cells within CD8 T cells from individual patients over the course of pembrolizumab (top: C01 or baseline, middle: C05, bottom: end of treatment [EOT]). Data are represented as mean ± SEM. LTA, large T antigen; STA, small T antigen; CMV, cytomegalovirus; HSV, herpes simplex virus; EBV, Epstein-Barr virus.

(D) Expression of CD39, CLA, and CD103 by individual tetramer$^+$ cells within CD8 T cells of MCPyV LTA and STA (n = 32), MCPyV viral protein (n = 17), CMV (n = 41), EBV (n = 21), influenza (n = 12), and HSV (n = 9). Mann-Whitney test, *$p < 0.05$, **$p < 0.01$, ***$p < 0.001$, and ****$p < 0.0001$.

Please cite this article in press as: Ryu et al., Merkel cell polyomavirus-specific and CD39$^+$CLA$^+$ CD8 T cells as blood-based predictive biomarkers for PD-1 blockade in Merkel cell carcinoma, Cell Reports Medicine (2023), https://doi.org/10.1016/j.xcrm.2023.101390

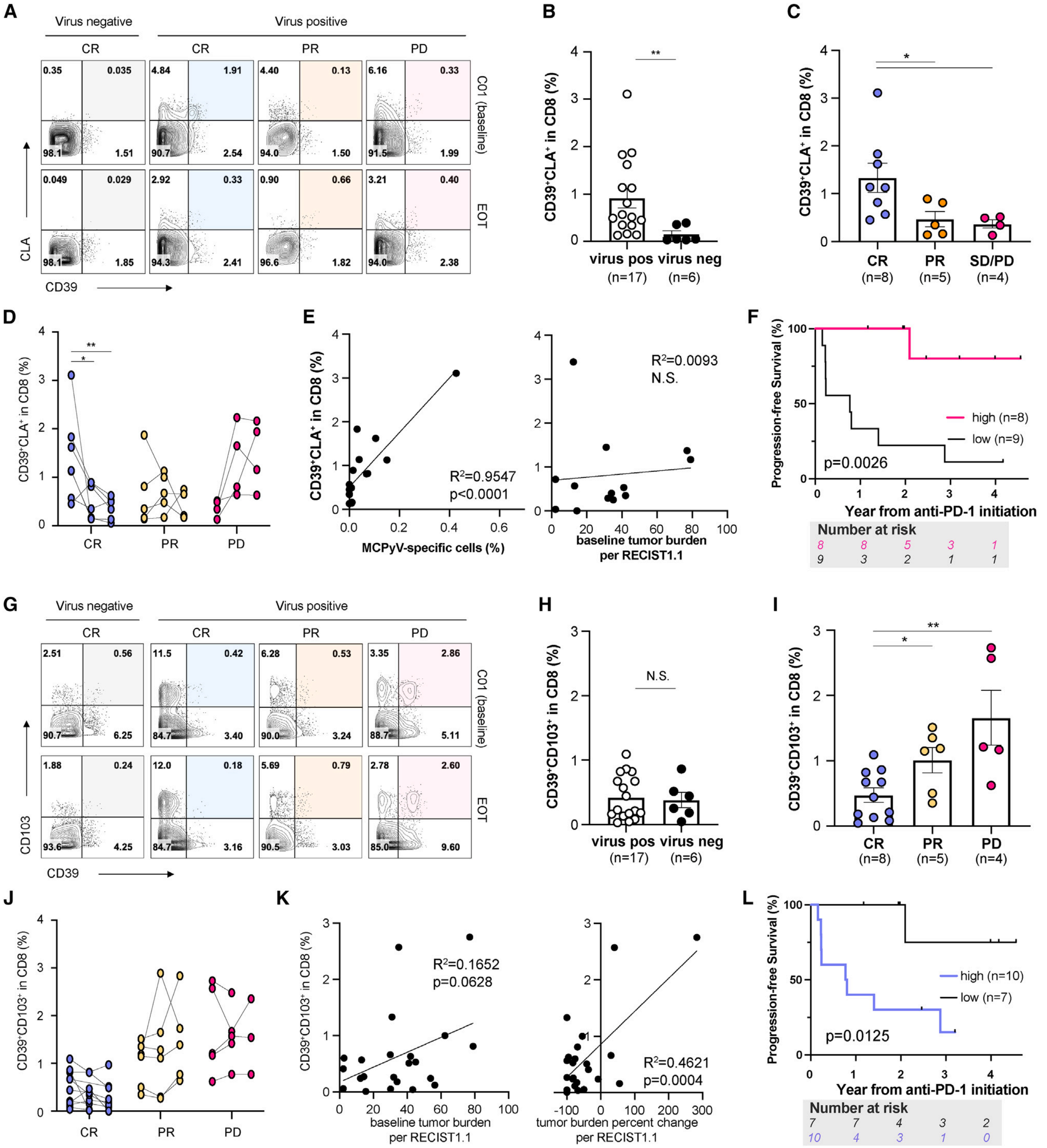

Figure 3. Prognostic potential of CD39, CLA, and CD103 expression among CD8 T cells in the peripheral blood of patients with MCC

(A) Contour plots identifying CD39$^+$CLA$^+$ CD8 T cells by mass cytometry. CD8 T cells were defined and pregated as live/CD45$^+$/CD19$^-$/CD14$^-$/CD3$^+$/$\gamma\delta$TCR$^-$/CD4$^-$/CD8$^+$. Representative data.

(B) Frequencies of CD39$^+$CLA$^+$ CD8 T cells prior to treatment in all patients. Data are represented as mean ± SEM; Mann-Whitney test.

(C) Frequencies of CD39$^+$CLA$^+$ CD8 T cells prior to treatment in VP patients. Data are represented as mean ± SEM; Mann-Whitney test.

(D) Frequencies of CD39$^+$CLA$^+$ CD8 T cells over the course of pembrolizumab in VP patients. Data are represented as mean ± SEM; Wilcoxon test.

(E) Linear regression analysis of frequencies of CD39$^+$CLA$^+$ CD8 T cells and frequencies of MCPyV-specific CD8 T cells (left) or baseline tumor burden (right) in VP patients.

(F) Kaplan-Meier curve of progression-free survival in VP patients with high or low CD39$^+$CLA$^+$ CD8 T cells. Log-rank test.

(legend continued on next page)

Please cite this article in press as: Ryu et al., Merkel cell polyomavirus-specific and CD39$^+$CLA$^+$ CD8 T cells as blood-based predictive biomarkers for PD-1 blockade in Merkel cell carcinoma, Cell Reports Medicine (2023), https://doi.org/10.1016/j.xcrm.2023.101390

clusters of bulk CD8 T cells that could also be useful as biomarkers for immunotherapeutic responses.

To identify unbiased correlates of clinical outcome, we conducted clustering analysis (Figures S2B and S2C) followed by regularized regression analysis using LASSO to identify high-dimensionally defined clusters of CD8 T cells with frequencies predictive of patient outcome (see STAR Methods). This analysis identified cluster 18 (CD39$^+$CLA$^+$) as a positive predictor of the patient's clinical outcome (Figure S2D). It is noteworthy that in CR patients, the frequency of cluster 18 increased shortly after the first post-therapy time point (C02) but declined post-treatment (EOT). However, in PR and SD/PD patients, these cells persisted at the same level or were even elevated (Figure S2E).

Since CD39 has been previously identified as a marker of tumor-specific, terminally exhausted CD8 TILs and is highly expressed by patient MCPyV-specific cells, we initially investigated whether the expression of CD39 in CD8 T cells alone could serve as a predictor of patient response to therapy.[19,20,29] We found that the baseline frequency of CD39$^+$ CD8 T cells in CR patients was associated with baseline tumor burden; however, it did not show any correlation with the clinical outcome or viral status of the patients (Figures S2F and S2G). After anti-PD-1 therapy, the frequencies of CD39$^+$ CD8 T cells decreased in patients who achieved CR but remained the same or decreased in patients who achieved PR and SD/PD (Figure S2H). Additionally, the frequencies of CD39$^+$ CD8 T cells in VP and VN patients correlated with the patients' baseline tumor burden (Figure S2I).

Further informed by the phenotypes of MCPyV-specific CD8 T cells, we hypothesized that CLA and CD103 could be used to better delineate CD39$^+$ CD8 T cells in blood samples, which could improve our ability to identify biomarkers for predicting the clinical prognosis of patients (Figure 3A). We found that the frequencies of CD39$^+$CLA$^+$ CD8 T cells were higher in VP patients than in VN patients, suggesting a potential association with MCPyV-driven tumors ($p = 0.0032$ Mann-Whitney test; Figure 3B). Similar to MCPyV-specific cells, the frequency of these cells was higher at baseline in patients with VP MCC who achieved a complete response to therapy ($p = 0.0295$ for CR vs. PR; $p = 0.0162$ for CR vs. PD, Mann-Whitney test; Figure 3C) and decreased over time, while the frequency of these cells remained the same or increased after the therapy in patients with PR or SD/PD ($p = 0.0469$ and $p = 0.0096$ Wilcoxon test; Figure 3D). This suggests that the presence of CD39$^+$CLA$^+$ cells at baseline may indicate a favorable treatment outcome in MCC. The frequencies of these cells were correlated with the frequency of MCPyV-tetramer-positive cells, but not with baseline tumor burden, unlike the total frequency of CD39$^+$ CD8 T cells (Figure 3E). This indicates a potential relationship between the presence of these cells and tumor-specific responses in patients with MCC that are not confounded by baseline tumor burden.

To validate the efficacy of CD39$^+$CLA$^+$ as a binary classifier that can distinguish between complete response (CR) and non-complete response (non-CR), we employed a receiver operating characteristic curve (ROC) to estimate an optimal threshold for classification (area under the curve [AUC] = 0.9028, $p = 0.0053$ for AUC > 0.5; Figure S3A). Note that the ROC analysis only included VP patients due to the scarcity of CD39$^+$CLA$^+$ CD8 T cells in VN patients. By utilizing a threshold of 0.81% as determined by ROC analysis, we found that patients with a higher frequency of CD39$^+$CLA$^+$ CD8 T cells prior to treatment achieved a 75% progression-free survival (PFS) rate at 3 years post-treatment. In contrast, patients that fell below this threshold exhibited a substantially lower PFS rate of 11% (Figure 3F; $p = 0.0026$ log-rank test). Furthermore, patients with high CD39$^+$CLA$^+$ levels demonstrated an overall survival rate of 100% at the 4 year mark, while only 40% patients below the threshold achieved a similar outcome (Figure S3B, left; $p = 0.0285$ log-rank test). Notably, the significance of this predictor was retained even when VN patients were included in the analysis, despite the threshold being initially determined using VP patients (Figure S3C, left; $p = 0.0026$ log-rank test). These findings underscore the potential utility and robustness of the frequency of CD39$^+$CLA$^+$ CD8 T cells as a predictive marker for therapeutic response.

CD39$^+$CD103$^+$ CD8 T cells in blood as a predictive biomarker for poor clinical outcomes in patients with MCC

A similar analysis of CD39$^+$CD103$^+$ CD8 T cells showed a different association with clinical outcomes. That is, these cells were present in both MCPyV-positive and -negative patients and were found to be higher in patients with MCC with a poor clinical outcome (Figures 3G–3I). The frequencies of these cells slightly decreased ($p = 0.0955$) over the course of pembrolizumab treatment in CR, but not in PR and SD/PD, patients (Figure 3J). Furthermore, frequencies of CD39$^+$CD103$^+$ among CD8 T cells were correlated with baseline tumor burden and changes in tumor burden (Figure 3K). Overall, this suggests that the presence of CD39$^+$CD103$^+$ CD8 T cells may associate with a less favorable response to treatment in MCC.

To validate the potential utility of CD39$^+$CD103$^+$ for binary classification of responsiveness to PD-1 blockade, we determined an optimal threshold of 0.82% through ROC analysis (AUC = 0.9444, $p = 0.002$ for AUC > 0.5; Figure S3A) for VP patients. Patients with a higher frequency of CD39$^+$CD103$^+$ CD8 T cells prior to treatment achieved a PFS rate of 10% at 3 years,

(G) Contour plots identifying CD39$^+$CD103$^+$ CD8 T cells by mass cytometry, CD8 T cells were defined and pregated as live/CD45$^+$/CD19$^-$/CD14$^-$/CD3$^+$/$\gamma\delta$TCR$^-$/CD4$^-$/CD8$^+$. Representative data.

(H) Frequencies of CD39$^+$CD103$^+$ CD8 T cells prior to treatment in all patients. Data are represented as mean ± SEM; Mann-Whitney test.

(I) Frequencies of CD39$^+$CD103$^+$ CD8 T cells prior to treatment in VP patients. Data are represented as mean ± SEM; Mann-Whitney test.

(J) Frequencies of CD39$^+$CD103$^+$ CD8 T cells over the course of pembrolizumab in VP patients. Data are represented as mean ± SEM; Wilcoxon test.

(K) Linear regression analysis of frequencies of CD39$^+$CD103$^+$ CD8 T cells and frequencies of MCPyV-specific CD8 T cells (left) or baseline tumor burden (right) in VP patients.

(L) Kaplan-Meier curve of progression-free survival in VP patients with high or low CD39$^+$CD103$^+$ CD8 T cells. Log-rank test. *$p < 0.05$ and **$p < 0.01$. Each symbol represents an individual patient.

Please cite this article in press as: Ryu et al., Merkel cell polyomavirus-specific and CD39$^+$CLA$^+$ CD8 T cells as blood-based predictive biomarkers for PD-1 blockade in Merkel cell carcinoma, Cell Reports Medicine (2023), https://doi.org/10.1016/j.xcrm.2023.101390

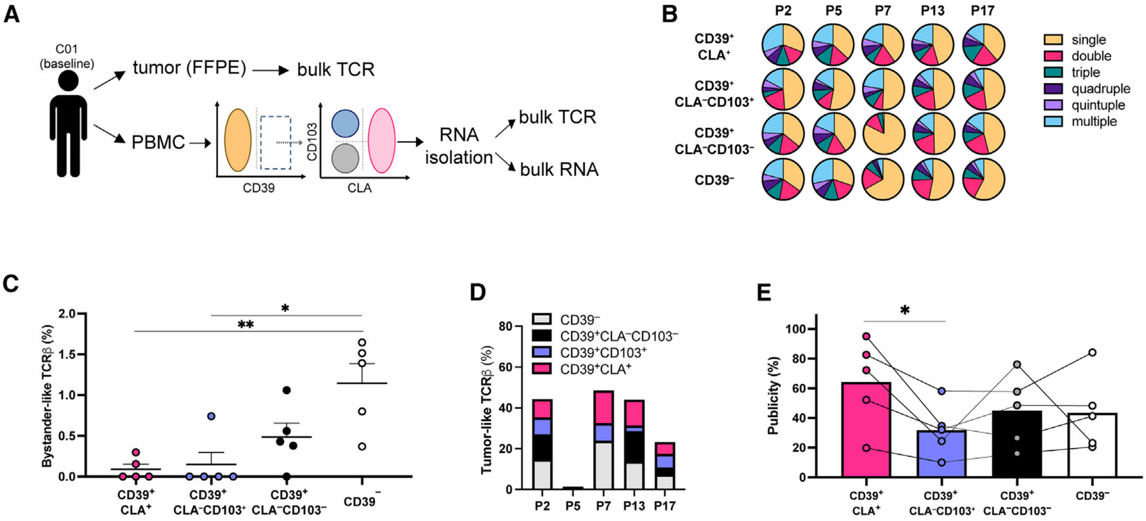

Figure 4. TCR repertoire analysis of circulating CD39$^+$CLA$^+$ and CD39$^+$CLA$^-$CD103$^+$ CD8 T cells from patients with MCC

(A) Experimental schematic. Bulk TCRβ sequencing was performed on FFPE tumor biopsy samples (n = 5) obtained from patients with a complete response. Patient-matched PBMC samples collected prior to treatment were subjected to flow-based sorting followed by RNA isolation, bulk TCRβ sequencing, and RNA sequencing.

(B) Pie chart illustrating the distribution of unique TCR clonotypes within each population of CD8 T cells.

(C) Frequency of bystander-like TCRβ from each CD8 population determined by clustering and quantifying their connection frequency with VDJ database based on sequence similarity (distance $\leq$ 12). Data are represented as mean ± SEM; Mann-Whitney test.

(D) Frequency of tumor-like TCRβ from each CD8 population determined by clustering and quantifying their connection frequency with patient-matched tumor TCRβ based on sequence similarity (distance $\leq$ 12).

(E) Frequency of publicity determined by clustering and quantifying their connection with other patients based on sequence similarity (distance $\leq$ 12). Data are represented as mean ± SEM, Wilcoxon test. $^*p < 0.05$ and $^{**}p < 0.01$. Each symbol represents an individual patient.

while patients falling below this threshold demonstrated a significantly higher PFS rate of 70% (Figure 4L; p = 0.0125 log-rank test). This observation also held true when analyzing overall survival (Figure S3B, right; p = 0.0453 log-rank test) and even when including VN patients (Figure S3C, right; p = 0.0048 log-rank test).

Since we discovered that these two phenotypically defined cell subsets predict patients' clinical outcomes in opposite directions, we hypothesized that the ratio of their frequencies would yield improved predictive accuracy. By employing an optimal threshold of 0.695, inferred from ROC analysis of the CD39$^+$CLA$^+$/CD39$^+$CD103$^+$ ratio (AUC = 0.9444, p = 0.0021 for AUC > 0.5), we found that this ratio can indeed predict improved PFS (Figure S3D) and overall survival (Figure S3E) in both VP (left) and VN patients (right). Altogether, these findings suggest that CD39$^+$ cells co-expressing CLA or CD103 in blood could serve as potential blood-based biomarkers of response to immunotherapy in patients with MCC.

Distinct tumor antigen-specificity of CD39$^+$CLA$^+$ and CD39$^+$CLA$^-$CD103$^+$ CD8 T cells in blood

Having identified two biomarkers with contrasting predictions for patient clinical outcomes, we next sought to assess the antigen specificity of these cells. Among VP patients at the baseline time point, we observed that within the CD39$^+$CLA$^+$ cell populations, approximately 5% of the cells bound to MCPyV tetramers. In contrast, only 0.05% of the CD39$^+$CD103$^+$ cells showed MCPyV tetramer positivity. This indicates that CD39$^+$CLA$^+$ CD8 T cells are significantly enriched for MCPyV reactivity, despite the possibility of false negatives affecting these frequencies (Figure S2J).

As an alternative method to test whether CD39$^+$CLA$^+$ and CD39$^+$CD103$^+$ populations were enriched for tumor reactivity, we used additional PBMC samples and sorted bulk CD8 T cells into four subpopulations: (1) CD39$^-$, (2) CD39$^+$CLA$^-$CD103$^-$, (3) CD39$^+$CLA$^+$CD103$^{+/-}$, and (4) CD39$^+$CLA$^-$CD103$^+$. These subpopulations were sorted from the baseline blood samples of VP CR patients (n = 5), and bulk T cell receptor (TCR) sequencing was performed on the sorted populations to assess the TCR repertoire. Depending on the sample, 5,000–100,000 cells were sorted for each population prior to bulk TCRα and -β sequencing (analysis was focused on TCRβ; see method details). Additionally, we obtained TCRβ clonotypes from patient-matched tumors (n = 5) preserved in formalin-fixed, paraffin-embedded (FFPE) samples (Figure 4A). All sorted populations contained a range of singleton and expanded clones (Figure 4B), and the number of detected clonotypes varied mostly as a function of the number of cells sorted (Figure S4A). However, when we corrected for sampling biases using the true diversity method, which considers both the number of clonotypes present and their relative abundances, the effective number of clonotypes was the lowest in CD39$^+$CLA$^+$ cells, followed by CD39$^+$CLA$^-$CD103$^+$.[30] This observation is consistent with some degree of clonal selection within these populations and indicates a more restricted diversity within CD39$^+$CLA$^+$ cells (Figure S4B). To explore antigen specificity, we compared the TCRβ sequences of each group to TCRs with known specificity in the VDJ database (see

Please cite this article in press as: Ryu et al., Merkel cell polyomavirus-specific and CD39$^+$CLA$^+$ CD8 T cells as blood-based predictive biomarkers for PD-1 blockade in Merkel cell carcinoma, Cell Reports Medicine (2023), https://doi.org/10.1016/j.xcrm.2023.101390

method details).[31] TCRβ sequences recovered from cells with CD39$^+$CLA$^+$ and CD39$^+$CLA$^-$CD103$^+$ phenotypes were less frequently matched with the database receptors compared to CD39$^-$ and CD39$^+$CLA$^-$CD103$^-$ cells (Figure 4C). This suggests that CD39$^+$CLA$^+$ and CD39$^+$CLA$^-$CD103$^+$ cells are less likely to represent MCC-unrelated bystander T cells.

Next, to examine potential overlap of similar TCRβ sequences between tumor and blood populations, we computed the Morisita-Horn indexes as well as the pairwise sequence distances (TCRdist) among receptors and grouped highly similar sequences into clusters of *meta*-clonotypes (Figures S4C–S4E).[32,33] The number of clones recovered varied greatly among T cell populations (Figure S4A). Thus, before clustering to identify sequence overlap, we normalized repertoires to the clone count of the smallest repertoires. After downsampling to correct for the variable numbers of clonotypes detected in each of the samples, we found that CD39$^+$CLA$^+$ and CD39$^+$CLA$^-$CD103$^+$ populations exhibited a similar degree of shared TCRβ sequences with tumors compared to CD39$^-$ and CD39$^+$CLA$^-$CD103$^-$ populations (Figure 4D). Comparable results were obtained using the Morisita-Horn index, a measure of sequence overlap, which corrects for the degree of sampling (Figure S4C). Considering that the CD39$^-$ population—but not the CD39$^+$CLA$^+$ or CD39$^+$CLA$^-$CD103$^+$ population—were found to be enriched for bystander activity in blood (Figure 4C) and in tumors,[19,20,34] we infer that CD39$^+$CLA$^+$ and CD39$^+$CLA$^-$CD103$^+$ populations play a role in recognizing non-bystander cells that infiltrate tumors, indicating their potential specificity toward tumor recognition.

Lastly, to compare the clonal sharing of the CD39$^+$CLA$^+$ cells (most correlated with MCPyV-specific cells and associated with favorable clinical outcomes) to the CD39$^+$CLA$^-$CD103$^+$ cells (less correlated with MCPyV-specific cell frequencies and associated with worse clinical outcomes), we calculated a publicity score for each sample (see method details) to determine the extent to which the clones within these two populations were shared between individuals. From this, we observed that the TCRs in T cells of CD39$^+$CLA$^-$CD103$^+$ had low publicity compared to TCRs in CD39$^+$CLA$^+$ (Figure 4E). This is consistent with the hypothesis that CD39$^+$CLA$^+$ cells are enriched for shared antigens such MCPyV-derived antigens, whereas CD39$^+$CLA$^-$CD103$^+$ might be more enriched for T cells that recognize a range of private or patient-specific antigens. Additionally, we constructed sequence similarity networks from TCRs derived from both the circulating CD39$^+$CLA$^+$ CD8 T cells and tumor samples to explore shared CDR3 motifs present within and across individuals (Figure S4F). Highly similar clusters of TCRs found across individuals can arise due to convergent selection for shared epitope specificity for shared viral antigens. Altogether, TCR sequence similarity analyses revealing large public clusters of TCRs between blood and tumor samples are consistent with the enrichment of T cells with viral or tumor specificity among CD39$^+$CLA$^+$ and CD39$^+$CLA$^-$CD103$^+$ CD8 T cell populations.

Differential transcriptional profiles of exhausted T cells categorized by CLA and CD103 expression

Next, to gain insights into the roles of blood-derived T cell populations with opposing predictive functions, we sought to perform a more detailed comparison of the phenotype and gene expression of profiles of CD39$^+$CLA$^+$ and CD39$^+$CLA$^-$CD103$^+$ CD8 T cells. We started by identifying differentially expressed protein markers in the mass cytometry data between these populations that delineated a response. By examining the ratio of median differential protein expression of these cells (CD39$^+$CLA$^+$/CD39$^+$CLA$^-$CD103$^+$) prior to treatment, we observed that the frequencies of CD71 expression on CD39$^+$CLA$^+$ cells were higher in CR patients compared to PR or SD/PD patients. Conversely, frequencies of TIM3 expression were higher in CD39$^+$CLA$^-$CD103$^+$ cells among patients with PR or SD/PD responses (Figure S2K).

To assess the functional states of these cells more comprehensively, we performed transcriptomic profiling on the same sorted populations described for the TCR sequencing analysis (Figure 4A). As expected, sorted populations with CD39 expression showed higher levels of *ENTPD1*, which encodes CD39 (Figure 5A), and CD39$^+$CLA$^-$CD103$^+$ cells expressed higher levels of *ITGAE*, which encodes the αE chain of CD103. CD39$^+$CLA$^+$ cells expressed slightly higher levels of *SELPLG*, which encodes one of the key components, PSGL-1, of CLA, as well as *ZNF683*, which encodes the tissue-resident T cell transcription factor HOBIT (Figure S5A).[35,36]

Pairwise comparison of defined differentially expressed genes (DEGs) and subset-specific transcriptional signatures was performed and summarized using principal-component analysis (PCA) to highlight a distinct transcriptional program of CD39$^+$CLA$^-$CD103$^+$ cells compared to other subpopulations (Figure 5B). CD39$^+$CLA$^+$ and CD39$^+$CLA$^-$CD103$^+$ cell subsets shared upregulated genes (DEG^{UP}) with each other but fewer with CD39$^-$ and CD39$^+$CLA$^-$CD103$^-$ subsets (Figure 5C). For example, ~40% of DEGs from CD39$^+$CLA$^+$ cells were also upregulated in CD39$^+$CLA$^-$CD103$^+$ cells, whereas less than 10% of these genes were shared by CD39$^-$ and CD39$^+$CLA$^-$CD103$^-$ subsets. This suggests that CD39$^+$CLA$^+$ and CD39$^+$CLA$^-$CD103$^+$ cells have a similar transcriptional program compared to other subsets.

To analyze subset-specific biology, we clustered DEGs and performed Gene Ontology analysis. Among the 5 clusters of DEGs identified, cluster 1, which was most enriched within CD39$^+$ populations, contained canonical exhaustion signatures such as *TOX* and *CXCL13* (Figure 5D). In addition, Gene Ontology (GO) biological pathway analysis revealed lymphocyte activation/differentiation and cell adhesion features in cluster 1 (Figure 5E). Clusters 2 and 3 contained genes that were preferentially upregulated in CD39$^+$CLA$^-$CD103$^+$ and were enriched for genes related to cell differentiation, activation, and apoptosis, which is a signature of T cell dysfunction. Cluster 4 captured genes that were downregulated in CD39$^+$CLA$^-$CD103$^+$ and included stemness/effector signature genes and cytokines. Lastly, cluster 5 contained genes at low levels across all CD39$^+$ cell populations, which included metabolic-related pathways (Figures 5D and 5E).

Overall, when comparing the transcriptional profiles of CD39$^+$CLA$^+$ and CD39$^+$CLA$^-$CD103$^+$ subpopulations, we found they both exhibited signs of exhaustion, which is in line with CD39 being a marker of terminal exhaustion (Figures S5B and S5C).[29] The exhaustion scores of CD39$^+$CLA$^+$ and

Please cite this article in press as: Ryu et al., Merkel cell polyomavirus-specific and CD39$^+$CLA$^+$ CD8 T cells as blood-based predictive biomarkers for PD-1 blockade in Merkel cell carcinoma, Cell Reports Medicine (2023), https://doi.org/10.1016/j.xcrm.2023.101390

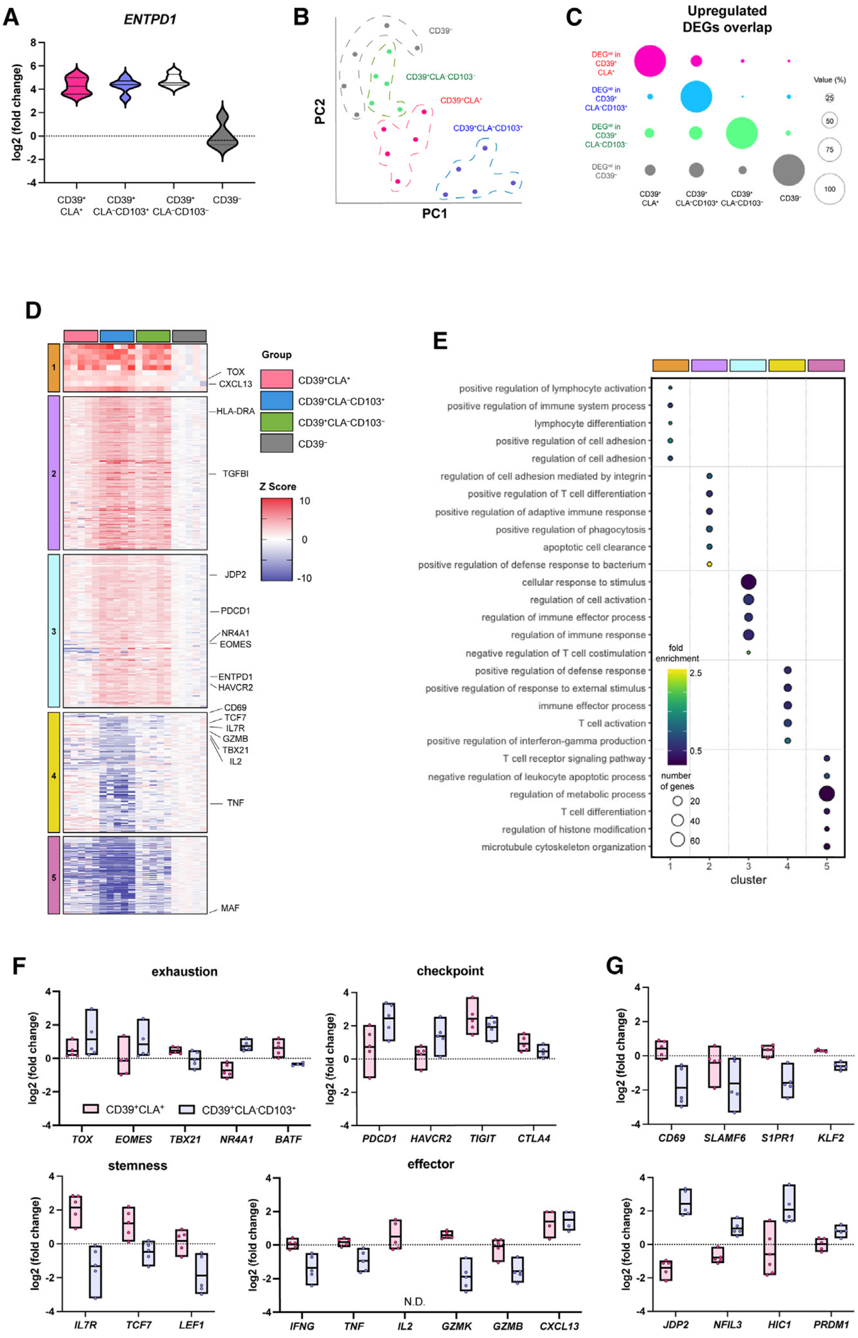

Figure 5. Distinct transcriptional signatures of circulating CD39$^+$CLA$^+$ and CD39$^+$CLA$^−$ CD103$^+$ CD8 T cells

(A) Expression of *ENTPD1* in each CD8 T cell population, normalized to those of CD39$^−$.

(B) PCA projection of sorted CD39$^+$CLA$^+$, CD39$^+$CLA$^−$CD103$^+$, CD39$^+$CLA$^−$CD103$^−$, and CD39$^−$ CD8 T cells from each patient. Each symbol represents an individual patient.

(C) DEG^{UP} overlaps between indicated populations. Bubble size represents the proportion of DEGs^{UP} from each population (y axis) also found to be upregulated in indicated subsets (x axis).

(D) Heatmap illustrating all DEGs (2-fold change, $p < 0.05$, and false discovery rate [FDR] < 0.1) clustered by using Pearson's correlation matrix. Color legend indicates *Z* scores.

(E) Pathway enrichment analysis of significantly enriched pathways by log(q value) for each cluster defined in Figure 4D. PCA, principal-component analysis; DEG, differentially expressed gene.

CD39$^+$CLA$^−$CD103$^+$ cells were also higher than those of CD39$^−$ and CD39$^+$CLA$^−$CD103$^−$ subsets (Figures 5F and S5D). When contrasting these populations, CD39$^+$CLA$^+$ cells showed higher signatures of stemness and effector function compared to CD39$^+$CLA$^-$CD103$^+$ cells (Figures 5F and S5E).[37–39] Specifically, CD39$^+$CLA$^+$ cells expressed higher levels of *TIGIT*, *CTLA4*, and *TBX21* than CD39$^+$CLA$^−$CD103$^+$ cells, which are often associated with effector function. Additionally, these cells expressed higher levels of *IL7R* and *CCR7*, which are associated with naive or central memory CD8 T cells.[40] Conversely, CD39$^+$CD103$^+$ cells expressed lower levels of effector cytokine production (*IFNG*, *TNF*, *IL2*, *GZMK*, *GZMB*) and stemness markers (*IL7R*, *TCF7*, *LEF1*). CD39$^+$CLA$^−$CD103$^+$ cells also upregulate the transforming growth factor β (TGF-β) signaling pathway, which leads to the CD39$^+$CLA$^−$CD103$^+$ expression in T cells needed for epithelial homing (Figure S5F).[41] Since CD39$^+$CLA$^−$CD103$^+$ cells exhibited both tissue-resident markers (CD103 and *ZNF683*) and exhaustion markers (*TOX*, *NR4A1*, *LAYN*, *CXCL13*, *HAVCR2*, and *TIGIT*), we hypothesize that CD39$^+$CLA$^−$CD103$^+$ cells are more closely related to recirculating resident T and terminally exhausted cells.[22,36,42–46] A recent study has shown novel transcription factors that distinguish resident and terminally exhausted cells.[47] Expression of *JDP2* and *NFIL3*, which is only found in exhaustion program rather than resident T cells, was significantly higher in CD39$^+$CLA$^−$CD103$^+$ than CD39$^+$CLA$^+$, suggesting that CD39$^+$CLA$^−$CD103$^+$ cells were terminally exhausted rather than originating from typical tissue-resident memory T cells (Figure 5G). Of note, CD39$^+$CLA$^+$ and CD39$^+$CLA$^−$CD103$^+$ cells had comparable levels of *CXCL13*, which is known to be associated with tumor reactivity (Figure 5F). Altogether, these results suggest that CD39$^+$CLA$^+$ and CD39$^+$CLA$^−$CD103$^+$ CD8 T cell populations have distinct transcriptional profiles and functional characteristics.

DISCUSSION

Immune checkpoint therapy has shown significant advancements in the treatment of patients with cancer; nevertheless,

Please cite this article in press as: Ryu et al., Merkel cell polyomavirus-specific and CD39^{+}CLA^{+} CD8 T cells as blood-based predictive biomarkers for PD-1 blockade in Merkel cell carcinoma, Cell Reports Medicine (2023), https://doi.org/10.1016/j.xcrm.2023.101390

the impact of treatment on tumor-specific T cells and the identification of predictive biomarkers for patient response are lacking. In this study, we utilized a mass-cytometry-based multiplexed peptide-MHC class I-tetramer staining approach to analyze MCPyV-oncoprotein-specific T cells longitudinally in the blood of 24 patients treated with PD-1 blockade. Our findings revealed that patients with a higher frequency of baseline MCPyV-specific cells have better clinical outcomes and that the frequency of MCPyV-specific CD8 T cells decreased during pembrolizumab treatment in complete responders. Additionally, we identified two distinct populations of tumor-specific cells that correlated with clinical outcomes: CD39^{+}CLA^{+} cells, which positively correlated with MCPyV-specific cell frequencies and the magnitude of clinical outcome, and CD39^{+}CD103^{+} CD8 T cells, which positively correlated with the baseline tumor burden and negatively correlated with the magnitude of clinical outcome. These findings suggest that MCPyV-specific cells, CD39^{+}CLA^{+} cells, and CD39^{+}CD103^{+} cells could serve as blood-based biomarkers for predicting response to immunotherapy and as targets for novel cellular therapeutic strategies in patients with MCC. Here, we discuss the potential reasons behind the correlation of these populations with patient response to therapy and their implications for the further development of therapy.

Previous studies have demonstrated the presence of MCPyV-specific T cells in the tumor microenvironment of patients with MCC, which is associated with improved clinical outcomes.[9] However, studies of tumor-specific T cells in blood are limited due to difficulties in identifying cancer-specific T cells and the rarity of these cells in blood. Herein, we show that frequency of tumor-specific T cells in blood positively correlated to response to anti-PD-1 therapy. Of note, these results are supported by a parallel study that showed that the frequency of MCPyV-specific CD8 T cells in the blood correlated with pathological response in a clinical trial of neoadjuvant anti-PD-1 therapy.[48] We further show that anti-PD-1 therapy reduced the frequency of MCPyV-specific CD8 T cells in patients with complete response over the course of pembrolizumab but had only a marginal change in patients with PR. Phenotyping of these cells showed that although MCPyV-specific cells in the blood were enriched for various protein and gene expression profiles associated with terminal exhaustion, they exhibited less exhaustion than would be expected for tumor-infiltrating T cells and expressed genes associated with a maintained effector function. Consistent with our findings, other studies have shown that MCPyV-specific cells found within tumors are at late stages of exhaustion and do not strongly correlate with patient response to immunotherapy.[48,49] Therefore, prior to initiating PD-1 blockade, MCPyV-specific CD8 T cells in the blood could serve as a non-invasive biomarker for predicting patient outcomes, as has been reported in other cancer types.[50,51]

Our multimodal analysis provided insights into the complex nature of CD8 T cells in patients with MCC, particularly those with tumor-specific phenotypes and distinct co-stimulatory and inhibitory receptor expression patterns. By comparing these cells to bystander CD8 T cells, those recognizing common non-MCC-associated viral antigens (e.g., CMV, EBV, HSV, and influenza), we elucidated specific features unique to MCPyV-specific cells. Notably, MCPyV-specific cells exhibited high expression of the activation/exhaustion marker CD39, the skin-homing receptor CLA, and the tissue-recirculating marker CD103. This observation suggests a potential role for these cells in the local immune response within the skin, which is particularly relevant since MCC is a skin cancer and the initial encounter of T cells with the antigen is in skin-draining lymph nodes. Previous research has linked CLA-expressing tumor-infiltrating T cells with increased total T cell infiltration and highlighted the association of MCC tumors lacking CLA expression with immune evasion and poorer clinical outcomes. Our study found that MCPyV-specific T cells expressed high levels of CLA, and the frequency of CD39^{+}CLA^{+} cells in the blood is associated with the frequency of MCPyV-specific cells and is predictive of favorable immunotherapy clinical outcomes.

The finding that the presence of CD39^{+}CLA^{+} CD8 T cells in the blood is associated with favorable clinical outcomes suggests that these cells play a crucial role in the immune response against MCC. It is possible that these cells possess a higher degree of tumor reactivity and that they retain their functional capacity, allowing them to effectively target and eliminate tumor cells. The elevated expression of inhibitory receptors, such as PD-1, TIGIT, and CTLA-4, in CD39^{+}CLA^{+} cells indicates that their activation and effector function may be regulated by immune checkpoint signaling, aligning with recent findings in patients with oral cancer.[52] Therefore, combination therapies targeting multiple inhibitory receptors could potentially enhance the anti-tumor immune response mediated by CD39^{+}CLA^{+} cells.

Interestingly, we identified a population of CD39^{+}CD103^{+} CD8 T cells with otherwise similar high-dimensional phenotypes to MCPyV-specific cells and CD39^{+}CLA^{+} cells. The presence of these cells in the tumor have been reported in various solid tumors, such as non-small cell lung cancer, melanoma, breast cancer, and ovarian cancer.[19,20,53–56] Notably, these cells have been demonstrated to be enriched for tumor reactivity and are associated with improved survival and increased response to PD-1 blockade. Tracking TCRs of these cells within tumors has revealed dynamic changes in circulating T cells in response to immunotherapy, with a higher frequency of these TCRs in patients with disease progression.[57–59] We extended our analysis beyond cell specificity and quantification, providing a comprehensive characterization of CD39^{+}CD103^{+} cells in the blood through CyTOF and bulk RNA sequencing. CD39^{+}CD103^{+} cells in the blood exhibited characteristics of terminal exhaustion, including expression of PD-1, lack of cytokine production, and stemness. These cells are associated with baseline tumor burden and a worse clinical outcome. The expression of TIM3, an inhibitory receptor, further supports their exhausted phenotype. Strategies aimed at reinvigorating these exhausted cells, such as dual or triple immune checkpoint blockade, may be necessary to enhance their functionality and improve patient responses to immunotherapy.

Understanding the phenotypic and functional characteristics of tumor-specific T cells and their correlation with patient response to immunotherapy has important implications for the further development of therapy for MCC and other immunogenic cancers. Our findings suggest that measuring the frequency of MCPyV-specific cells, CD39^{+}CLA^{+} cells, and CD39^{+}CD103^{+} cells in the blood could serve as non-invasive biomarkers to predict patient responses to immunotherapy. These biomarkers can aid in patient stratification and guide treatment decisions, facilitating personalized therapeutic approaches for MCC. Similar cell populations and CD8 T cell profiles might have comparable utility in other cancer types. Therefore, we think it could be worthwhile to monitor these or similar populations in other contexts. These cell populations could also be useful for rapid identification of patient-specific tumor-reactive T cells and TCRs that could be used for the design of novel cellular therapy strategies.[60]

Based on our findings, we propose that measuring CD8 T cells expressing both CD39 and CLA in the bloodstream prior to treatment can predict the frequency of MCPyV-specific cells and positive clinical response to pembrolizumab. CD39, known for its immunosuppressive role, has been suggested as a marker for T cell activation and exhaustion. Our study revealed that MCPyV-specific cells expressing CD39 and CLA associate with a favorable clinical outcome. CLA, which guides memory T cells back to the skin, has been associated with higher total T cell infiltration and better clinical outcomes in MCC.[61] In contrast, we also identified a CD39$^+$CD103$^+$ CD8 T cell population that is transcriptionally distinct and inversely correlated with patient response to pembrolizumab. CD103, a resident memory T cell marker that also mediates cell binding to epithelial and endothelial cells, has also been implicated as a marker for tumor reactivity in TILs[19,62,63] and in blood[64] in the context of other tumor types. The association between the frequencies of these cells and baseline tumor burden might partially explain their association with poor clinical outcomes. In addition, perhaps because of their more terminally exhausted profiles, these cells might be less receptive to disinhibition by PD-1 blockade. We believe this aligns well with a previous study showing that peripheral detection of TCR clonotypes corresponding to those of terminally exhausted tumor-infiltrating T cells was also associated with poor clinical outcomes after immunotherapy.[58]

TCR sequencing analysis provided insights into the antigen specificity of these T cell populations. Circulating CD8 T cells shared significant TCRβ sequences with tumor-infiltrating T cells, indicating dynamic movement of T cells between the bloodstream and the tumor. CD39$^+$CLA$^+$ cells showed a high degree of clonal sharing and were correlated with MCPyV-specific cells, suggesting their tracking of tumor-specific cells. CD39$^+$CD103$^+$ cells displayed lower clonal sharing among patients and were correlated with baseline tumor burden, suggesting that these cells might also be tumor reactive but possibly specific for private non-viral antigens such as mutation-derived neoantigens or other less ubiquitously expressed tumor-associated antigens. However, this would need to be tested in further studies.

In summary, our study highlights the significance of MCPyV-specific cells, CD39$^+$CLA$^+$ cells, and CD39$^+$CD103$^+$ cells as potential blood-based biomarkers for predicting patient responses to immunotherapy and as potential sources of tumor-specific T cells and TCRs in MCC. These subsets of tumor-specific cells exhibit distinct phenotypic and functional characteristics, which may contribute to their correlation with differential responses to immune checkpoint blockade. Understanding the implications of these populations in the context of immunotherapy response and their association with tumor burden and exhaustion status can guide the development of more effective and personalized treatment strategies for patients with MCC as well other cancers. Further investigation is warranted to validate these findings and explore the therapeutic potential of targeting these tumor-specific cell populations in MCC and other cancer types.

Limitations of the study

The study has some limitations that should be considered when interpreting the findings. Firstly, the study was based on a single trial and involved a relatively small number of patients, which may limit the generalizability of the results. An independent study (Pulliam, Jani et al., manuscript submitted) has demonstrated that the baseline MCPyV-specific cell frequencies can predict immunotherapy responses in a separate clinical trial. However, further validation of other predictive biomarkers is still required. Additionally, the study did not assess the functional activity of CD39$^+$CLA$^+$ or CD39$^+$CD103$^+$ CD8 T cells derived from blood against MCC tumors. Finally, as this study was cross-sectional in nature, it cannot establish causality or the direction of associations between the variables examined. Further mechanistic studies are required to investigate how CD39$^+$CLA$^+$ and CD39$^+$CD103$^+$ cells modulate the immune response to MCPyV by pembrolizumab treatment. These studies should also examine the detailed phenotypes and importance of MCPyV-specific CD4 or other immune subsets affected by anti-PD-1.

STAR★METHODS

Detailed methods are provided in the online version of this paper and include the following:

- KEY RESOURCES TABLE
- RESOURCE AVAILABILITY
    - ○ Lead contact
    - ○ Materials availability
    - ○ Data and code availability
- EXPERIMENTAL MODEL AND STUDY PARTICIPANT DETAILS
    - ○ Patients and patient samples
- METHOD DETAILS
    - ○ Epitope prediction and multiplexed peptide-MHC-I-tetramer preparation
    - ○ Mass cytometry staining
    - ○ Mass cytometry data analysis
    - ○ Cell sorting and RNA isolation
    - ○ Bulk TCR sequencing and data processing
    - ○ Tumor T cell receptor sequencing
    - ○ Bulk RNAseq and data processing
- QUANTIFICATION AND STATISTICAL ANALYSIS

SUPPLEMENTAL INFORMATION

Supplemental information can be found online at https://doi.org/10.1016/j.xcrm.2023.101390.

ACKNOWLEDGMENTS

This project was supported by funding from a CCSG pilot award (P30 CA015704 to E.W.N.), a Fred Hutchinson Cancer Center IIRC post-doctoral fellowship (to H.R.), a post-doctoral training fellowship from the National Research Foundation of Korea (2020R1A6A3A03037852 to H.R.), an NIH R01 grant (CA264646 to E.W.N.), an NIH N01 grant (75N93019C00063 to D.M.K.), a Kelsey Dickson Team Science Courage Research Award (to P.N., C.D.C., and S.J.), Merck & Co., and a NIH P01 grant (P01 CA225517 to P.N.). We thank all patients and participants in the CITN-09 clinical trial. We thank all other members of the Newell and Nghiem labs for their feedback and support for this project. We also thank Suzanne Topalian for critical feedback and contributions to the design of the pembrolizumab trial.

AUTHOR CONTRIBUTIONS

Conceptualization, H.R., T.M.B., T.H.P., S.J., S.R.H., D.M.K., P.N., and E.W.M.; methodology, H.R., T.M.B., T.H.P., and E.W.N.; formal analysis, H.R. and K.M.-B.; investigation, H.R., T.M.B., U.K.H., and K.S.; resources and data curation, C.D.C., N.R., and S.P.F.; writing – original draft, H.R.; writing – review & editing, H.R., T.M.B., T.H.P., K.S., C.D.C., N.K., K.M.-B., S.J., U.K.H., D.M.K., P.N., and E.W.N.; visualization, H.R. and K.M.-B.; supervision, S.R.H., D.M.K., P.N., and E.W.N.; project administration, H.R., T.H.P., C.D.C., N.R., S.P.F., P.N., and E.W.N.; funding acquisition, H.R., D.M.K., P.N., and E.W.N.

DECLARATION OF INTERESTS

E.W.N. is a co-founder, advisor, and shareholder for ImmunoScape Pte. Ltd., a scientific advisory board member and shareholder for Neogene Therapeutics, and a scientific advisory board member for Nanostring Biotechnologies and Trojan Biotechnologies. D.M.K. and P.N. are co-inventors on an institutionally owned patent concerning MCPyV-specific TCRs.

Received: July 3, 2023
Revised: November 29, 2023
Accepted: December 21, 2023
Published: February 9, 2024

REFERENCES

1. Becker, J.C., Stang, A., DeCaprio, J.A., Cerroni, L., Lebbé, C., Veness, M., and Nghiem, P. (2017). Merkel cell carcinoma. Nat. Rev. Dis. Primers *3*, 17077.
2. DeCaprio, J.A. (2021). Molecular Pathogenesis of Merkel Cell Carcinoma. Annu. Rev. Pathol. *16*, 69–91.
3. Bhatia, S., Afanasiev, O., and Nghiem, P. (2011). Immunobiology of Merkel Cell Carcinoma: Implications for Immunotherapy of a Polyomavirus-Associated Cancer. Curr. Oncol. Rep. *13*, 488–497.
4. Sihto, H., Böhling, T., Kavola, H., Koljonen, V., Salmi, M., Jalkanen, S., and Joensuu, H. (2012). Tumor Infiltrating Immune Cells and Outcome of Merkel Cell Carcinoma: A Population-Based Study. Clin. Cancer Res. *18*, 2872–2881.
5. Paulson, K.G., Iyer, J.G., Simonson, W.T., Blom, A., Thibodeau, R.M., Schmidt, M., Pietromonaco, S., Sokil, M., Warton, E.M., Asgari, M.M., and Nghiem, P. (2014). CD8+ Lymphocyte Intratumoral Infiltration as a Stage-Independent Predictor of Merkel Cell Carcinoma Survival: A Population-Based Study. Am. J. Clin. Pathol. *142*, 452–458.
6. Yarchoan, M., Hopkins, A., and Jaffee, E.M. (2017). Tumor Mutational Burden and Response Rate to PD-1 Inhibition. N. Engl. J. Med. *377*, 2500–2501.
7. Nghiem, P.T., Bhatia, S., Lipson, E.J., Kudchadkar, R.R., Miller, N.J., Annamalai, L., Berry, S., Chartash, E.K., Daud, A., Fling, S.P., et al. (2016). PD-1 Blockade with Pembrolizumab in Advanced Merkel-Cell Carcinoma. N. Engl. J. Med. *374*, 2542–2552.
8. Nghiem, P., Bhatia, S., Lipson, E.J., Sharfman, W.H., Kudchadkar, R.R., Brohl, A.S., Friedlander, P.A., Daud, A., Kluger, H.M., Reddy, S.A., et al. (2021). Three-year survival, correlates and salvage therapies in patients receiving first-line pembrolizumab for advanced Merkel cell carcinoma. J. Immunother. Cancer *9*, e002478.
9. Miller, N.J., Church, C.D., Dong, L., Crispin, D., Fitzgibbon, M.P., Lachance, K., Jing, L., Shinohara, M., Gavvovidis, I., Willimsky, G., et al. (2017). Tumor-Infiltrating Merkel Cell Polyomavirus-Specific T Cells Are Diverse and Associated with Improved Patient Survival. Cancer Immunol. Res. *5*, 137–147.
10. Iyer, J.G., Afanasiev, O.K., McClurkan, C., Paulson, K., Nagase, K., Jing, L., Marshak, J.O., Dong, L., Carter, J., Lai, I., et al. (2011). Merkel Cell Polyomavirus-Specific CD8+ and CD4+ T-cell Responses Identified in Merkel Cell Carcinomas and Blood. Clin. Cancer Res. *17*, 6671–6680.
11. Jing, L., Ott, M., Church, C.D., Kulikauskas, R.M., Ibrani, D., Iyer, J.G., Afanasiev, O.K., Colunga, A., Cook, M.M., Xie, H., et al. (2020). Prevalent and Diverse Intratumoral Oncoprotein-Specific CD8+ T Cells within Polyomavirus-Driven Merkel Cell Carcinomas. Cancer Immunol. Res. *8*, 648–659.
12. Miller, N.J., Church, C.D., Fling, S.P., Kulikauskas, R., Ramchurren, N., Shinohara, M.M., Kluger, H.M., Bhatia, S., Lundgren, L., Cheever, M.A., et al. (2018). Merkel cell polyomavirus-specific immune responses in patients with Merkel cell carcinoma receiving anti-PD-1 therapy. J. Immunother. Cancer *6*, 131.
13. Afanasiev, O.K., Yelistratova, L., Miller, N., Nagase, K., Paulson, K., Iyer, J.G., Ibrani, D., Koelle, D.M., and Nghiem, P. (2013). Merkel Polyomavirus-Specific T Cells Fluctuate with Merkel Cell Carcinoma Burden and Express Therapeutically Targetable PD-1 and Tim-3 Exhaustion Markers. Clin. Cancer Res. *19*, 5351–5360.
14. Samimi, M., Molet, L., Fleury, M., Laude, H., Carlotti, A., Gardair, C., Baudin, M., Gouguet, L., Maubec, E., Avenel-Audran, M., et al. (2016). Prognostic value of antibodies to Merkel cell polyomavirus T antigens and VP1 protein in patients with Merkel cell carcinoma. Br. J. Dermatol. *174*, 813–822.
15. Cheng, Y., Gunasegaran, B., Singh, H.D., Dutertre, C.-A., Loh, C.Y., Lim, J.Q., Crawford, J.C., Lee, H.K., Zhang, X., Lee, B., et al. (2021). Non-terminally exhausted tumor-resident memory HBV-specific T cell responses correlate with relapse-free survival in hepatocellular carcinoma. Immunity *54*, 1825–1840.e7.
16. Newell, E.W., Sigal, N., Bendall, S.C., Nolan, G.P., and Davis, M.M. (2012). Cytometry by Time-of-Flight Shows Combinatorial Cytokine Expression and Virus-Specific Cell Niches within a Continuum of CD8$^+$ T Cell Phenotypes. Immunity *36*, 142–152.
17. Newell, E.W., Sigal, N., Nair, N., Kidd, B.A., Greenberg, H.B., and Davis, M.M. (2013). Combinatorial tetramer staining and mass cytometry analysis facilitate T-cell epitope mapping and characterization. Nat. Biotechnol. *31*, 623–629.
18. Koelle, D.M., Liu, Z., McClurkan, C.M., Topp, M.S., Riddell, S.R., Pamer, E.G., Johnson, A.S., Wald, A., and Corey, L. (2002). Expression of cutaneous lymphocyte-associated antigen by CD8+ T cells specific for a skin-tropic virus. J. Clin. Invest. *110*, 537–548.
19. Duhen, T., Duhen, R., Montler, R., Moses, J., Moudgil, T., de Miranda, N.F., Goodall, C.P., Blair, T.C., Fox, B.A., McDermott, J.E., et al. (2018). Co-expression of CD39 and CD103 identifies tumor-reactive CD8 T cells in human solid tumors. Nat. Commun. *9*, 2724.
20. Simoni, Y., Becht, E., Fehlings, M., Loh, C.Y., Koo, S.-L., Teng, K.W.W., Yeong, J.P.S., Nahar, R., Zhang, T., Kared, H., et al. (2018). Bystander CD8+ T cells are abundant and phenotypically distinct in human tumour infiltrates. Nature *557*, 575–579.
21. Hanada, K.-i., Zhao, C., Gil-Hoyos, R., Gartner, J.J., Chow-Parmer, C., Lowery, F.J., Krishna, S., Prickett, T.D., Kivitz, S., Parkhurst, M.R., et al. (2022). A phenotypic signature that identifies neoantigen-reactive T cells in fresh human lung cancers. Cancer Cell *40*, 479–493.e6.
22. Veatch, J.R., Lee, S.M., Shasha, C., Singhi, N., Szeto, J.L., Moshiri, A.S., Kim, T.S., Smythe, K., Kong, P., Fitzgibbon, M., et al. (2022). Neoantigen-specific CD4+ T cells in human melanoma have diverse differentiation

states and correlate with CD8+ T cell, macrophage, and B cell function. Cancer Cell *40*, 393–409.e9.

23. Wijeyesinghe, S., Beura, L.K., Pierson, M.J., Stolley, J.M., Adam, O.A., Ruscher, R., Steinert, E.M., Rosato, P.C., Vezys, V., and Masopust, D. (2021). Expansible residence decentralizes immune homeostasis. Nature *592*, 457–462.
24. Yenyuwadee, S., Sanchez-Trincado Lopez, J.L., Shah, R., Rosato, P.C., and Boussiotis, V.A. (2022). The evolving role of tissue-resident memory T cells in infections and cancer. Sci. Adv. *8*, eabo5871.
25. Peng, C., Huggins, M.A., Wanhainen, K.M., Knutson, T.P., Lu, H., Georgiev, H., Mittelsteadt, K.L., Jarjour, N.N., Wang, H., Hogquist, K.A., et al. (2022). Engagement of the costimulatory molecule ICOS in tissues promotes establishment of CD8$^+$ tissue-resident memory T cells. Immunity *55*, 98–114.e5.
26. Das, B.K., Kannan, A., Velasco, G.J., Kunika, M.D., Lambrecht, N., Nguyen, Q., Zhao, H., Wu, J., and Gao, L. (2023). Single-cell dissection of Merkel cell carcinoma heterogeneity unveils transcriptomic plasticity and therapeutic vulnerabilities. Cell Rep. Med. *4*, 101101.
27. Salmikangas, M., Laaksonen, M., Edgren, H., Salgado, M., Suoranta, A., Mattila, P., Koljonen, V., Böhling, T., and Sihto, H. (2023). Neurocan expression associates with better survival and viral positivity in Merkel cell carcinoma. PLoS One *18*, e0285524.
28. Morgulis, A., Coulouris, G., Raytselis, Y., Madden, T.L., Agarwala, R., and Schäffer, A.A. (2008). Database indexing for production MegaBLAST searches. Bioinformatics *24*, 1757–1764.
29. Gupta, P.K., Godec, J., Wolski, D., Adland, E., Yates, K., Pauken, K.E., Cosgrove, C., Ledderose, C., Junger, W.G., Robson, S.C., et al. (2015). CD39 Expression Identifies Terminally Exhausted CD8+ T Cells. PLoS Pathog. *11*, e1005177.
30. Chiffelle, J., Genolet, R., Perez, M.A., Coukos, G., Zoete, V., and Harari, A. (2020). T-cell repertoire analysis and metrics of diversity and clonality. Curr. Opin. Biotechnol. *65*, 284–295.
31. Goncharov, M., Bagaev, D., Shcherbinin, D., Zvyagin, I., Bolotin, D., Thomas, P.G., Minervina, A.A., Pogorelyy, M.V., Ladell, K., McLaren, J.E., et al. (2022). VDJdb in the pandemic era: a compendium of T cell receptors specific for SARS-CoV-2. Nat. Methods *19*, 1017–1019.
32. Mayer-Blackwell, K., Schattgen, S., Cohen-Lavi, L., Crawford, J.C., Souquette, A., Gaevert, J.A., Hertz, T., Thomas, P.G., Bradley, P., and Fiore-Gartland, A. (2021). TCR meta-clonotypes for biomarker discovery with tcrdist3 enabled identification of public, HLA-restricted clusters of SARS-CoV-2 TCRs. Elife *10*, e68605.
33. Dash, P., Fiore-Gartland, A.J., Hertz, T., Wang, G.C., Sharma, S., Souquette, A., Crawford, J.C., Clemens, E.B., Nguyen, T.H.O., Kedzierska, K., et al. (2017). Quantifiable predictive features define epitope-specific T cell receptor repertoires. Nature *547*, 89–93.
34. Scheper, W., Kelderman, S., Fanchi, L.F., Linnemann, C., Bendle, G., de Rooij, M.A.J., Hirt, C., Mezzadra, R., Slagter, M., Dijkstra, K., et al. (2019). Low and variable tumor reactivity of the intratumoral TCR repertoire in human cancers. Nat. Med. *25*, 89–94.
35. Maverakis, E., Kim, K., Shimoda, M., Gershwin, M.E., Patel, F., Wilken, R., Raychaudhuri, S., Ruhaak, L.R., and Lebrilla, C.B. (2015). Glycans in the immune system and The Altered Glycan Theory of Autoimmunity: A critical review. J. Autoimmun. *57*, 1–13.
36. Parga-Vidal, L., Behr, F.M., Kragten, N.A.M., Nota, B., Wesselink, T.H., Kavazović, I., Covill, L.E., Schuller, M.B.P., Bryceson, Y.T., Wensveen, F.M., et al. (2021). Hobit identifies tissue-resident memory T cell precursors that are regulated by Eomes. Sci. Immunol. *6*, eabg3533.
37. Jansen, C.S., Prokhnevska, N., Master, V.A., Sanda, M.G., Carlisle, J.W., Bilen, M.A., Cardenas, M., Wilkinson, S., Lake, R., Sowalsky, A.G., et al. (2019). An intra-tumoral niche maintains and differentiates stem-like CD8 T cells. Nature *576*, 465–470.
38. Galletti, G., De Simone, G., Mazza, E.M.C., Puccio, S., Mezzanotte, C., Bi, T.M., Davydov, A.N., Metsger, M., Scamardella, E., Alvisi, G., et al. (2020). Two subsets of stem-like CD8+ memory T cell progenitors with distinct fate commitments in humans. Nat. Immunol. *21*, 1552–1562.
39. Apetoh, L., Smyth, M.J., Drake, C.G., Abastado, J.-P., Apte, R.N., Ayyoub, M., Blay, J.-Y., Bonneville, M., Butterfield, L.H., Caignard, A., et al. (2015). Consensus nomenclature for CD8+ T cell phenotypes in cancer. Oncoimmunology *4*, e998538.
40. van der Leun, A.M., Thommen, D.S., and Schumacher, T.N. (2020). CD8+ T cell states in human cancer: insights from single-cell analysis. Nat. Rev. Cancer *20*, 218–232.
41. El-Asady, R., Yuan, R., Liu, K., Wang, D., Gress, R.E., Lucas, P.J., Drachenberg, C.B., and Hadley, G.A. (2005). TGF-β–dependent CD103 expression by CD8+ T cells promotes selective destruction of the host intestinal epithelium during graft-versus-host disease. J. Exp. Med. *201*, 1647–1657.
42. Liu, X., Wang, Y., Lu, H., Li, J., Yan, X., Xiao, M., Hao, J., Alekseev, A., Khong, H., Chen, T., et al. (2019). Genome-wide analysis identifies NR4A1 as a key mediator of T cell dysfunction. Nature *567*, 525–529.
43. Chen, J., López-Moyado, I.F., Seo, H., Lio, C.-W.J., Hempleman, L.J., Sekiya, T., Yoshimura, A., Scott-Browne, J.P., and Rao, A. (2019). NR4A transcription factors limit CAR T cell function in solid tumours. Nature *567*, 530–534.
44. Seo, H., Chen, J., González-Avalos, E., Samaniego-Castruita, D., Das, A., Wang, Y.H., López-Moyado, I.F., Georges, R.O., Zhang, W., Onodera, A., et al. (2019). TOX and TOX2 transcription factors cooperate with NR4A transcription factors to impose CD8+ T cell exhaustion. Proc. Natl. Acad. Sci. USA *116*, 12410–12415.
45. Khan, O., Giles, J.R., McDonald, S., Manne, S., Ngiow, S.F., Patel, K.P., Werner, M.T., Huang, A.C., Alexander, K.A., Wu, J.E., et al. (2019). TOX transcriptionally and epigenetically programs CD8+ T cell exhaustion. Nature *571*, 211–218.
46. Scott, A.C., Dündar, F., Zumbo, P., Chandran, S.S., Klebanoff, C.A., Shakiba, M., Trivedi, P., Menocal, L., Appleby, H., Camara, S., et al. (2019). TOX is a critical regulator of tumour-specific T cell differentiation. Nature *571*, 270–274.
47. Chung, H.K., Cong, L., Eduardo, C., Brent, C., Bryan, M., Jun, W., Peixiang, H., Ming, S., Shixin, M., Qiyuan, Y., et al. (2023). Multiomics atlas-assisted discovery of transcription factors enables specific cell state programming. Preprint at bioRxiv, https://doi.org/10.1101/2023.01.03.522354.
48. Pulliam, T., Jani, S., Jing, L., Ryu, H., Jojic, A., Shasha, C., Zhang, J., Kulikauskas, R., Church, C., Garnett-Benson, C., et al. (2023). Circulating cancer-specific CD8 T cell frequency is associated with response to PD-1 blockade in Merkel cell carcinoma. Cell Rep Med *5* (*2*).
49. Lyngaa, R., Pedersen, N.W., Schrama, D., Thrue, C.A., Ibrani, D., Met, Ö., thor Straten, P., Nghiem, P., Becker, J.C., and Hadrup, S.R. (2014). T-cell Responses to Oncogenic Merkel Cell Polyomavirus Proteins Distinguish Patients with Merkel Cell Carcinoma from Healthy Donors. Clin. Cancer Res. *20*, 1768–1778.
50. Yamauchi, T., Hoki, T., Oba, T., Jain, V., Chen, H., Attwood, K., Battaglia, S., George, S., Chatta, G., Puzanov, I., et al. (2021). T-cell CX3CR1 expression as a dynamic blood-based biomarker of response to immune checkpoint inhibitors. Nat. Commun. *12*, 1402.
51. Fehlings, M., Jhunjhunwala, S., Kowanetz, M., O'Gorman, W.E., Hegde, P.S., Sumatoh, H., Lee, B.H., Nardin, A., Becht, E., Flynn, S., et al. (2019). Late-differentiated effector neoantigen-specific CD8+ T cells are enriched in peripheral blood of non-small cell lung carcinoma patients responding to atezolizumab treatment. J. Immunother. Cancer *7*, 249.
52. Luoma, A.M., Suo, S., Wang, Y., Gunasti, L., Porter, C.B.M., Nabilsi, N., Tadros, J., Ferretti, A.P., Liao, S., Gurer, C., et al. (2022). Tissue-resident memory and circulating T cells are early responders to pre-surgical cancer immunotherapy. Cell *185*, 2918–2935.e29.
53. Ganesan, A.-P., Clarke, J., Wood, O., Garrido-Martin, E.M., Chee, S.J., Mellows, T., Samaniego-Castruita, D., Singh, D., Seumois, G., Alzetani, A., et al. (2017). Tissue-resident memory features are linked to the

Please cite this article in press as: Ryu et al., Merkel cell polyomavirus-specific and CD39$^+$CLA$^+$ CD8 T cells as blood-based predictive biomarkers for PD-1 blockade in Merkel cell carcinoma, Cell Reports Medicine (2023), https://doi.org/10.1016/j.xcrm.2023.101390

magnitude of cytotoxic T cell responses in human lung cancer. Nat. Immunol. *18*, 940–950.

54. Edwards, J., Wilmott, J.S., Madore, J., Gide, T.N., Quek, C., Tasker, A., Ferguson, A., Chen, J., Hewavisenti, R., Hersey, P., et al. (2018). CD103+ Tumor-Resident CD8+ T Cells Are Associated with Improved Survival in Immunotherapy-Naïve Melanoma Patients and Expand Significantly During Anti–PD-1 Treatment. Clin. Cancer Res. *24*, 3036–3045.
55. Park, M.H., Kwon, S.Y., Choi, J.E., Gong, G., and Bae, Y.K. (2020). Intratumoral CD103-positive tumour-infiltrating lymphocytes are associated with favourable prognosis in patients with triple-negative breast cancer. Histopathology *77*, 560–569.
56. Webb, J.R., Milne, K., Watson, P., deLeeuw, R.J., and Nelson, B.H. (2014). Tumor-Infiltrating Lymphocytes Expressing the Tissue Resident Memory Marker CD103 Are Associated with Increased Survival in High-Grade Serous Ovarian Cancer. Clin. Cancer Res. *20*, 434–444.
57. Caushi, J.X., Zhang, J., Ji, Z., Vaghasia, A., Zhang, B., Hsiue, E.H.-C., Mog, B.J., Hou, W., Justesen, S., Blosser, R., et al. (2021). Transcriptional programs of neoantigen-specific TIL in anti-PD-1-treated lung cancers. Nature *596*, 126–132.
58. Oliveira, G., Stromhaug, K., Klaeger, S., Kula, T., Frederick, D.T., Le, P.M., Forman, J., Huang, T., Li, S., Zhang, W., et al. (2021). Phenotype, specificity and avidity of antitumour CD8+ T cells in melanoma. Nature *596*, 119–125.
59. Rahim, M.K., Okholm, T.L.H., Jones, K.B., McCarthy, E.E., Liu, C.C., Yee, J.L., Tamaki, S.J., Marquez, D.M., Tenvooren, I., Wai, K., et al. (2023). Dynamic CD8+ T cell responses to cancer immunotherapy in human regional lymph nodes are disrupted in metastatic lymph nodes. Cell *186*, 1127–1143.e18.
60. Norberg, S.M., and Hinrichs, C.S. (2023). Engineered T cell therapy for viral and non-viral epithelial cancers. Cancer Cell *41*, 58–69.
61. Dowlatshahi, M., Huang, V., Gehad, A.E., Jiang, Y., Calarese, A., Teague, J.E., Dorosario, A.A., Cheng, J., Nghiem, P., Schanbacher, C.F., et al. (2013). Tumor-Specific T Cells in Human Merkel Cell Carcinomas: A Possible Role for Tregs and T-Cell Exhaustion in Reducing T-Cell Responses. J. Invest. Dermatol. *133*, 1879–1889.
62. Banchereau, R., Chitre, A.S., Scherl, A., Wu, T.D., Patil, N.S., de Almeida, P., Kadel Iii, E.E., Madireddi, S., Au-Yeung, A., Takahashi, C., et al. (2021). Intratumoral CD103+ CD8+ T cells predict response to PD-L1 blockade. J. Immunother. Cancer *9*, e002231.
63. Lee, Y.J., Kim, J.Y., Jeon, S.H., Nam, H., Jung, J.H., Jeon, M., Kim, E.-S., Bae, S.J., Ahn, J., Yoo, T.-K., et al. (2022). CD39+ tissue-resident memory CD8+ T cells with a clonal overlap across compartments mediate antitumor immunity in breast cancer. Sci. Immunol. *7*, eabn8390.
64. Wang, Z., Ahmed, S., Labib, M., Wang, H., Wu, L., Bavaghar-Zaeimi, F., Shokri, N., Blanco, S., Karim, S., Czarnecka-Kujawa, K., et al. (2023). Isolation of tumour-reactive lymphocytes from peripheral blood via microfluidic immunomagnetic cell sorting. Nat. Biomed. Eng. *7*, 1188–1203.
65. Wagih, O. (2017). ggseqlogo: a versatile R package for drawing sequence logos. Bioinformatics *33*, 3645–3647.
66. Paulson, K.G., Carter, J.J., Johnson, L.G., Cahill, K.W., Iyer, J.G., Schrama, D., Becker, J.C., Madeleine, M.M., Nghiem, P., and Galloway, D.A. (2010). Antibodies to Merkel Cell Polyomavirus T Antigen Oncoproteins Reflect Tumor Burden in Merkel Cell Carcinoma Patients. Cancer Res. *70*, 8388–8397.
67. Shuda, M., Arora, R., Kwun, H.J., Feng, H., Sarid, R., Fernández-Figueras, M.T., Tolstov, Y., Gjoerup, O., Mansukhani, M.M., Swerdlow, S.H., et al. (2009). Human Merkel cell polyomavirus infection I. MCV T antigen expression in Merkel cell carcinoma, lymphoid tissues and lymphoid tumors. Int. J. Cancer *125*, 1243–1249.
68. Jurtz, V., Paul, S., Andreatta, M., Marcatili, P., Peters, B., and Nielsen, M. (2017). NetMHCpan-4.0: Improved Peptide–MHC Class I Interaction Predictions Integrating Eluted Ligand and Peptide Binding Affinity Data. J. Immunol. *199*, 3360–3368.
69. Cheng, Y., Zhu, Y.O., Becht, E., Aw, P., Chen, J., Poidinger, M., de Sessions, P.F., Hibberd, M.L., Bertoletti, A., Lim, S.G., and Newell, E.W. (2019). Multifactorial heterogeneity of virus-specific T cells and association with the progression of human chronic hepatitis B infection. Sci. Immunol. *4*, eaau6905.
70. Hagberg, A.A., Schult, D.A., and Swart, P. (2008). Exploring Network Structure, Dynamics, and Function Using NetworkX.
71. Britanova, O.V., Shugay, M., Merzlyak, E.M., Staroverov, D.B., Putintseva, E.V., Turchaninova, M.A., Mamedov, I.Z., Pogorelyy, M.V., Bolotin, D.A., Izraelson, M., et al. (2016). Dynamics of Individual T Cell Repertoires: From Cord Blood to Centenarians. J. Immunol. *196*, 5005–5013.
72. Samokhina, M.P., Aleksandr, I., Nazarov, V., immunarch.bot, Rumynskiy, E., gracecodeadventures, Zarodniuk, M., and tsvvas. (2019). Immunarch: an R package for painless bioinformatics analysis of T-cell and B-cell immune repertoires. Zenodo *10*, 5281.
73. Robins, H.S., Campregher, P.V., Srivastava, S.K., Wacher, A., Turtle, C.J., Kahsai, O., Riddell, S.R., Warren, E.H., and Carlson, C.S. (2009). Comprehensive assessment of T-cell receptor β-chain diversity in αβ T cells. Blood *114*, 4099–4107.
74. Dobin, A., Davis, C.A., Schlesinger, F., Drenkow, J., Zaleski, C., Jha, S., Batut, P., Chaisson, M., and Gingeras, T.R. (2013). STAR: ultrafast universal RNA-seq aligner. Bioinformatics *29*, 15–21.
75. Zhou, G., Soufan, O., Ewald, J., Hancock, R.E.W., Basu, N., and Xia, J. (2019). NetworkAnalyst 3.0: a visual analytics platform for comprehensive gene expression profiling and meta-analysis. Nucleic Acids Res. *47*, W234–W241.
76. Thomas, P.D., Ebert, D., Muruganujan, A., Mushayahama, T., Albou, L.-P., and Mi, H. (2022). PANTHER: Making genome-scale phylogenetics accessible to all. Protein Sci. *31*, 8–22.
77. Zhang, Z., Schwartz, S., Wagner, L., and Miller, W. (2000). A Greedy Algorithm for Aligning DNA Sequences. J. Comput. Biol. *7*, 203–214.

STAR★METHODS

KEY RESOURCES TABLE

REAGENT or RESOURCE	SOURCE	IDENTIFIER
Antibodies		
7-AAD	BD Biosciences	Cat# 559925, RRID:AB_2869266
APC/Cyanine7 anti-human CD14 Antibody (clone: M5E2)	Biolegend	Cat# 301820, RRID:AB_493695
APC/Cyanine7 anti-human CD19 Antibody (clone: HIB19)	Biolegend	Cat# 302218, RRID:AB_314247
BUV395 Mouse Anti-Human CD3 (clone: UCHT1)	BD Biosciences	Cat# 563546, RRID:AB_2744387
BUV805 CD4 Mouse anti-Human (clone: RPA-T4)	BD Biosciences	Cat# 742000, RRID:AB_2871299
BUV737 CD8 Mouse anti-Human (clone: RPA-T8)	BD Biosciences	Cat# 612755, RRID:AB_2870086
Brilliant Violet 711 anti-human CD39 Antibody (clone: A1)	Biolegend	Cat# 328228, RRID:AB_2632894
CD103 (Integrin alpha E) Monoclonal Antibody (B-Ly7), APC	eBioscience	Cat# 17-1038-42, RRID:AB_10670631
PE anti-human/mouse Cutaneous Lymphocyte Antigen (CLA) Antibody (clone: HECA-452)	Biolegend	Cat# 321312, RRID:AB_2565589
89 - CD45 (clone: HI30)	Fluidigm	Cat# 3089003, RRID:AB_2661851
110 - CD4 (clone: RPA-T4)	Biolegend	Cat# 300502, RRID:AB_314070
111 - CD8a (clone: RPA-T8)	Biolegend	Cat# 301002, RRID:AB_314120
112 - CD14 (clone: TuK4)	Thermofisher	Cat# MHCD1400, RRID:AB_10371749
113 - CD19 (clone: HIB19)	Biolegend	Cat# 302202, RRID:AB_314232
114 - CD56 (clone: REA196)	Miltenyi Biotec	Cat# 130-108-016, RRID:AB_2658728
115 - CD57 (clone: HNK-1)	Biolegend	Cat# 359602, RRID:AB_2562403
116 - CD3 (clone: UCHT1)	Biolegend	Cat# 300402, RRID:AB_314056
141 - CLA (HECA-452)	Biolegend	Cat# 321302, RRID:AB_492894
142 - HLA-DR (clone: L243)	Biolegend	Cat# 307602, RRID:AB_314680
143 - ITB7 (clone: FIB504)	BD Biosciences	Cat# 555943, RRID:AB_396240
144 - TIGIT (clone: MBSA-43)	Thermofisher	Cat# 16-9500-82, RRID:AB_10718831
145 - Granzyme K (clone: GM6C3)	Santa cruz	Cat# SC-56125, RRID:AB_2263772
TCR gamma/delta Monoclonal Antibody (clone: 5A6.E9)	Thermofisher	Cat# MHGD04, RRID:AB_1502165
146 - anti-PE (clone: PE001)	Biolegend	Cat# 408102, RRID:AB_2168924
147 - CCR10 (clone: 314305)	R&D	Cat# MAB3478, RRID:AB_2275692
148 - CD45RO (clone: UCHL1)	Biolegend	Cat# 304202, RRID:AB_314418
149 - CD161 (clone: HP-3G10)	Biolegend	Cat# 339902, RRID:AB_1501090
150 - KLRG1 (clone: 13F2F12)	Thermofisher	Cat# 16-9488-85, RRID:AB_2637116
151 - CD27 (clone: O323)	Biolegend	Cat# 302802, RRID:AB_314294
152 - ICOS (clone: C398.4A)	Thermofisher	Cat# 14-9949-82, RRID:AB_468637
153 - CD103 (clone: B-Ly7)	Thermofisher	Cat# 14-1038-80, RRID:AB_467411
154 - Granzyme B (clone: 2C5/F5)	BD Biosciences	Cat# 550558, RRID:AB_393751
156 - CD25 (clone: M-A251)	Biolegend	Cat# 356102, RRID:AB_2561751
158 - CXCR3 (clone: G025H7)	Biolegend	Cat# 353702, RRID:AB_10983073
160 - PD-1 (clone: eBioJ105)	Thermofisher	Cat# 14-2799-80, RRID:AB_763476
162 - TIM3 (clone: F38-2E2)	Biolegend	Cat# 345002, RRID:AB_2116574
165 - CXCR5 (clone: RF8B2)	BD Biosciences	Cat# 552032, RRID:AB_394324
168 - CCR7 (clone: 150503)	R&D	Cat# MAB197, RRID:AB_2072803
169 - CD45RA (clone: HI100)	Biolegend	Cat# 304102, RRID:AB_314406
171 - CCR5 (clone: HEK/1/85a)	BioRAD	Cat# MCA2175GA, RRID:AB_324205
172 - CD39 (clone: A1)	Biolegend	Cat# 328202, RRID:AB_940438

(*Continued on next page*)

Please cite this article in press as: Ryu et al., Merkel cell polyomavirus-specific and CD39^{+}CLA^{+} CD8 T cells as blood-based predictive biomarkers for PD-1 blockade in Merkel cell carcinoma, Cell Reports Medicine (2023), https://doi.org/10.1016/j.xcrm.2023.101390

Continued

REAGENT or RESOURCE	SOURCE	IDENTIFIER
175 - Perforin (clone: B-D48)	Fluidigm	Cat# 3175004B, RRID:AB_2895147
176 - CD38 (clone: HIT2)	Biolegend	Cat# 303502, RRID:AB_314354
209 - CD16 (clone: 3G8)	Fluidigm	Cat# 3209002B, RRID:AB_2756431
Chemicals, peptides, and recombinant proteins		
Merkel cell polyomavirus peptides	Mimotopes	Custom
Control viral peptides	Mimotopes	Custom
UV-cleavable MHC class I monomers	Fred Hutchinson Cancer Center	Custom
Streptavidin	Fred Hutchinson Cancer Center	Custom
Critical commercial assays		
NucleoSpin® RNA Plus XS	Takara Bio	740990
SMARTer® Human TCR a/b Profiling Kit v2	Takara Bio	634479
Illumina Truseq stranded mRNA library prep kit	Illumina	20020594
Deposited data		
Bulk TCR sequencing fastq	This paper	Zenodo: https://doi.org/10.5281/zenodo.8102089
Bulk RNA sequencing BAM	This paper	Zenodo: https://doi.org/10.5281/zenodo.8104398
Software and algorithms		
FlowJo	BD Biosciences	V9.9.4 and V10.8.0
R	R Foundation for Statistical Computing	V4.2.1
GraphPad Prism	GraphPad	V9
tcrdist3	Mayer-Blackwell et al.[32]	https://github.com/kmayerb/tcrdist3
ggseqlogo	Wagih et al.[65]	https://github.com/omarwagih/ggseqlogo

RESOURCE AVAILABILITY

Lead contact

Further information and requests for resources and regents should be directed to and will be fulfilled by the lead contact, Evan W. Newell (enewell@fredhutch.org).

Materials availability

All unique and stable reagents generated in this study are available to the scientific community upon request and following execution of materials transfer agreement by contacting the lead contact.

Data and code availability

Bulk TCR sequencing, bulk RNA sequencing data discussed in this study have been deposited on Zenodo (Zenodo: https://doi.org/10.5281/zenodo.8102089, https://doi.org/10.5281/zenodo.8104398). No original code was generated in this study. Further data that support the finding of this study are available from the corresponding authors upon reasonable request.

EXPERIMENTAL MODEL AND STUDY PARTICIPANT DETAILS

Patients and patient samples

All patients enrolled in this study provided written informed consent. Patients received pembrolizumab intravenously every 3 weeks at a dose of 2 mg/kg, for a maximum period of 2 years with radiologic assessment every 9 weeks. Investigators reported clinical responses based on CT scans per RECIST 1.1, as follows: complete response (CR), partial response (PR), stable disease (SD) or progressive disease (PD) based on imaging collected from time of enrollment to 08/01/2016. An initial response was confirmed by a serial CT scan showing the same result to be considered a confirmed response. Blood samples were drawn for correlative laboratory analyses. Peripheral blood mononuclear cells (PBMC) were cryopreserved after routine Ficoll preparation by a specimen processing facility at the Cancer Immunotherapy Trials Network. Tumor viral status was defined by expression of Large T-antigen within the tumor or by production of antibodies to small T-antigen as both are restricted to patients with MCPyV-positive tumors, as previously described.[66],[67] All patients were HLA class I genotyped to determine eligibility for CD8 T cell specific MCPyV-tetramer screening

Please cite this article in press as: Ryu et al., Merkel cell polyomavirus-specific and CD39$^+$CLA$^+$ CD8 T cells as blood-based predictive biomarkers for PD-1 blockade in Merkel cell carcinoma, Cell Reports Medicine (2023), https://doi.org/10.1016/j.xcrm.2023.101390

(Bloodworks Northwest, Seattle, WA). No statistical methods were used to predetermine sample size. The experiments were not randomized, and the investigators were not blinded to allocation during experiments and outcome assessment. The samples were provided by Cancer Immunotherapy Trails Network (trial registration: ClinicalTrials.gov NCT02267603) and the analysis was performed according to the IRB file/approval number IR File #10686 (Table S1).

METHOD DETAILS

Epitope prediction and multiplexed peptide-MHC-I-tetramer preparation

Binding of epitopes of MCPyV LTA and STA proteins to HLA-A*01:01, HLA-A*02:01, HLA-A*03:01, HLA-A*11:01, HLA-A*24:02, HLA-B*07:02 was predicted using the NetMHC4.0 algorithm.[68] Candidate epitopes (8–11 amino acids) with a predicted affinity <500 nM were selected and synthesized (Mimotopes). For MCPyV HLA-A*68:01, HLA-B*08:01, HLA-B*15:01, HLA-B*35:01, HLA-B*37:01, B*57:01, MHC-I easYmers were purchased from immuAware.[11] 34 common viral epitopes from HLA-A*01:01, HLA-A*02:01, HLA-A*03:01, HLA-A*11:01, HLA-A*24:02, HLA-B*07:02, HLA-B*08:01, HLA-B*35:01 were chosen based on the previous literatures (Table S2).[11,15,20,69]

For multiplex MHC-I-tetramer staining, each tetramer was labeled with a combination of three metal-labelled streptavidin (SAV).[17] Using ten different metal-labeled SAV, 120 possible combinations were generated. Each specific combination was associated with a different peptide and HLA allele. Each metal-labeled SAV (50 μg/mL) was mixed for each combination using an automated pipetting device (TECAN). In a 96 well plate, peptide (1 mM) was added to corresponding HLA monomer (100 μg/mL), with a different peptide in each well. The plate was exposed to UV (365 nm) for 10 min for peptide exchange and left overnight at 4 °C. For the tetramerization, each peptide–MHC-I complex–metal-labelled SAV combination (50 μg/mL) was added in three steps according to the coding scheme. Then, tetramerized peptide-MHC-I complexes were incubated with free biotin for 10 min (10 μM) (Sigma). All different tetramers were combined and concentrated using a 50-kDa Amicon filter (Millipore). Before staining, the tetramer cocktail was filtered using a 0.1-μm filter (Millipore).

Mass cytometry staining

Purified antibodies lacking carrier proteins were purchased according to the provided in the Key resources table. Antibody conjugation was performed according to the protocol provided by Fluidigm. SAV was expressed, purified and heavy-metal conjugated as previously described.[16] HLA-A*01:01, HLA-A*02:01, HLA-A*03:01, HLA-A*11:01, HLA-A*24:02 and HLA-B*07:02 monomer was refolded with appropriate UV-cleavable peptide and biotinylated as described. HLA-A*68:01, HLA-B*08:01, HLA-B*15:01, HLA-B*35:01, HLA-B*37:01, B*57:01 were purchased from immunAware. Tetramerization was performed with metal-labeled SAV as previously described. PBMCs were thawed and enriched for T cells by Pan T cell isolation kit (removing cells expressing CD14, CD15, CD16, CD19, CD34, CD36, CD56, CD123, and CD235a) using MACS LS columns (Miltenyi). Cells were then stained for cisplatin (5 mM) in PBS for 5 min on ice, washed and incubated for 1h at room temperature with tetramer cocktails in FACS buffer (PBS, 0.5% BSA, 0.02% sodium azide). Cells were then incubated with primary and secondary surface antibodies cocktails for 20min each on ice and fixed overnight in PFA 2%. The next day, cells were washed and permeabilized using permeabilization buffer (eBioscience) and stained with intracellular antibodies for 30 min at room temperature followed by DNA staining for 30 min at room temperature. Cells were washed three times with Cell Acquisition Solution (Fluidigm) and run on CyTOF (Helios, Fluidigm).

Mass cytometry data analysis

After CyTOF acquisition, which was performed as previously described,[20] any zero values were randomized using a uniform distribution of values between zero and −1 using an R script (as was the default operation of previous CyTOF software). Note also that all other integer values measured by the mass cytometer are randomized in a similar fashion by default. The signal of each parameter was then normalized based on the EQ beads (Fluidigm) as previously described. Cells were manually de-barcoded using FlowJo.

In line with the previously described method, we initially utilized an R script to identify tetramer positive cells.[69] In brief, we determined the thresholds for identifying tetramer positive events in CD8 T cells by manually gating out the SAV-metal channel in FlowJo. Based on the thresholds (Threshold X = Tx and Threshold Y = Ty) of every SAV-metal channel, the safety factors then automatically identify the tetramer positive population of CD8 T cells using the pre-set geometric criteria (Y/X Slope = k, X/Y Slope = k, and Width = w). The deconvolution algorithm excluded any tetramer positive cells that have less, or more than three SAV-metals coding. All events which were identified as tetramer positive cells underwent manual cross-checking of their three SAV-metal codes and HLA-allelic variants and then considered as validated antigen-specific CD8 T cells.

Samples were then used for UMAP analysis similar to that previously described using customized R scripts based on the 'flowCore' and 'uwot' R packages. In R, all data were transformed using the logicleTransform function (flowCore package) using parameters: w = 0.25, t = 16409, m = 4.5, a = 0 to roughly match scaling historically used in FlowJo. For heatmaps, median intensity corresponds to a logical data scale using the formula previously described. The colors in the heatmap represent the measured means intensity value of a given marker in each sample. A seven-color scale was used with black–blue indicating low expression values, green–yellow indicating intermediately expressed markers, and orange-red representing highly expressed markers. Samples were then used for UMAP analysis similar to that previously described[20] using customized R scripts based on the 'flowCore'

Please cite this article in press as: Ryu et al., Merkel cell polyomavirus-specific and CD39$^+$CLA$^+$ CD8 T cells as blood-based predictive biomarkers for PD-1 blockade in Merkel cell carcinoma, Cell Reports Medicine (2023), https://doi.org/10.1016/j.xcrm.2023.101390

and 'uwot' R packages. In R, all data were transformed using the logicleTransform function (flowCore package) using parameters: $w = 0.25$, $t = 16409$, $m = 4.5$, $a = 0$ to roughly match scaling historically used in FlowJo.

Cell sorting and RNA isolation

PBMCs were thawed and stained with Human TruStain FcX (Biolegend) for 10 min at room temperature followed by 20-min staining on ice with fluorescent antibody cocktails (Key resources table). CD8 T cells were isolated by FACS sorting (BD Bioscience) and subjected to RNA isolation (Takara). RNA purity was determined by assaying 1 μL of total RNA extract on a NanoDrop8000 spectrophotometer. Total RNA integrity was checked using an Agilent Technologies 2100 Bioanalyzer with an RNA Integrity Number (RIN) value.

Bulk TCR sequencing and data processing

RNA samples isolated from sorted CD8 T cell populations were subjected to TCR sequencing library preparation using SMARTer Human TCR a/b Profiling Kit v2 (Takara Bio USA). Briefly, after isolating mRNA from the sorted cells (NucleoSpin RNA Plus XS, Takara Bio USA), cDNA was synthesized and amplified following manufacturer's instructions. Quality of final libraries was assessed using Agilent 2200 TapeStation with High Sensitivity D5000 ScreenTape, quantified using a Qubit Fluorometer (ThermoFisher) and KAPA library quantification kit (Roche). The resulting libraries were sequenced on Illumina Miseq system (paired-end 300 bp). Raw reads of sequence data were aligned and assembled using Cogent NGS Immune Profiler Software (Takara Bio USA).

We computed TCR distances between all recovered TCRβ receptors using tcrdist3 software.[32,33] Retaining all distances $\leq$ 12 tcr distance units (corresponding roughly to an edit distance of 1–2), we visualized a similarity network using the Python package networkX.[70] We extracted the connected components within the sequence similarity network, and – for each connected component – we sampled a background set of TCRs from umbilical cord blood[71] with the same V- and J-gene usage to permit generation of background subtracted CDR3 motifs, which emphasize conserved non-germline encoded residues. We exported the aligned CDR3 motifs and used a custom R script (www.github.com/kmayerb/cdr3art/) to visualize each cluster CDR3 motif and gene usage using R packages ggseqlogo[65] (version 0.1.0) and ggsankey (https://github.com/davidsjoberg/ggsankey, version 0.0.9). True diversity and Morisita-Horn index were calculated using R package immunarch.[72] We used R 4.1.2.

Tumor T cell receptor sequencing

Pre-treatment formalin-fixed paraffin-embedded (FFPE) tumor biopsy material (20–25 μm thick molecular curls or material scraped from pre-cut slides) were submitted to Adaptive Biotechnologies for genomic DNA extraction of tissue, TCRβ sequencing and normalization as previously described.[73]

Bulk RNAseq and data processing

mRNA sequencing libraries were prepared according to the manufacturer's instructions (Illumina Truseq stranded mRNA library prep kit). mRNA was purified and fragmented from total RNA (1ug) using poly-T oligo-attached magnetic beads using two rounds of purification. Cleaved RNA Fragments primed with random hexamers were reverse transcribed into first strand cDNA using reverse transcriptase, random primers, dUTP in place of dTTP. (The incorporation of dUTP quenches the second strand during amplification, because the polymerase does not incorporate past this nucleotide.) These cDNA fragments then had the addition of a single 'A' base and subsequent ligation of the adapter. The products were purified and enriched with PCR to create the final strand specific cDNA library. The quality of the amplified libraries was verified by capillary electrophoresis (Bioanalyzer, Agilent). After qPCR using SYBR Green PCR Master Mix (Applied Biosystems), we combined libraries that index tagged in equimolar amounts in the pool and performed Nextseq 2000 sequencing system (Illumina) with 2 × 100bp read length. FASTQ files for each sample were mapped to the reference genome (human hg19) by STAR aligner.[74] The aligned results were further analyzed by NetworkAnalyst 3.0 to normalize data and report differentially expressed genes.[75] Genes with 2-fold change, p value < 0.05 and FDR<0.1 were selected for ontology analysis.[76] Data are visualized by R 4.1.2.

For LTA, STA, and viral capsid protein expression on tumor analysis, gene sequences of LTA, STA and VP1 were retrieved from the NCBI database (Gene ID: 10987417; 10987419; 10987416, respectively) and bulk RNA sequencing data of MCC cell lines and tumors were obtained from the SRA database.[26,27] To align and compare the expression patterns, we employed the MegaBLAST algorithm of the BLASTn suite from NCBI to identify highly similar sequences (Match/Mismatch Scores: 1, -2; Gap Costs: linear; suitable for 95% conserved) as previously reported.[28,77]

QUANTIFICATION AND STATISTICAL ANALYSIS

The statistical tests were conducted as per the specifications mentioned in each figure. To determine the optimal threshold for classifiers, ROC analysis was employed, which was represented as the distance from the linear line. Pearson (r) or Spearman (ρ) correlation was used to determine linear concordance, and a two-sided t-test was used to see if the result was significantly different from zero. All statistical analysis was carried out using R 4.1.2 or Prism 9.

Cell Reports Medicine, Volume *5*

Supplemental information

Merkel cell polyomavirus-specific and CD39$^+$CLA$^+$ CD8 T cells as blood-based predictive biomarkers for PD-1 blockade in Merkel cell carcinoma

Heeju Ryu, Timothy M. Bi, Thomas H. Pulliam, Korok Sarkar, Candice D. Church, Nandita Kumar, Koshlan Mayer-Blackwell, Saumya Jani, Nirasha Ramchurren, Ulla K. Hansen, Sine R. Hadrup, Steven P. Fling, David M. Koelle, Paul Nghiem, and Evan W. Newell

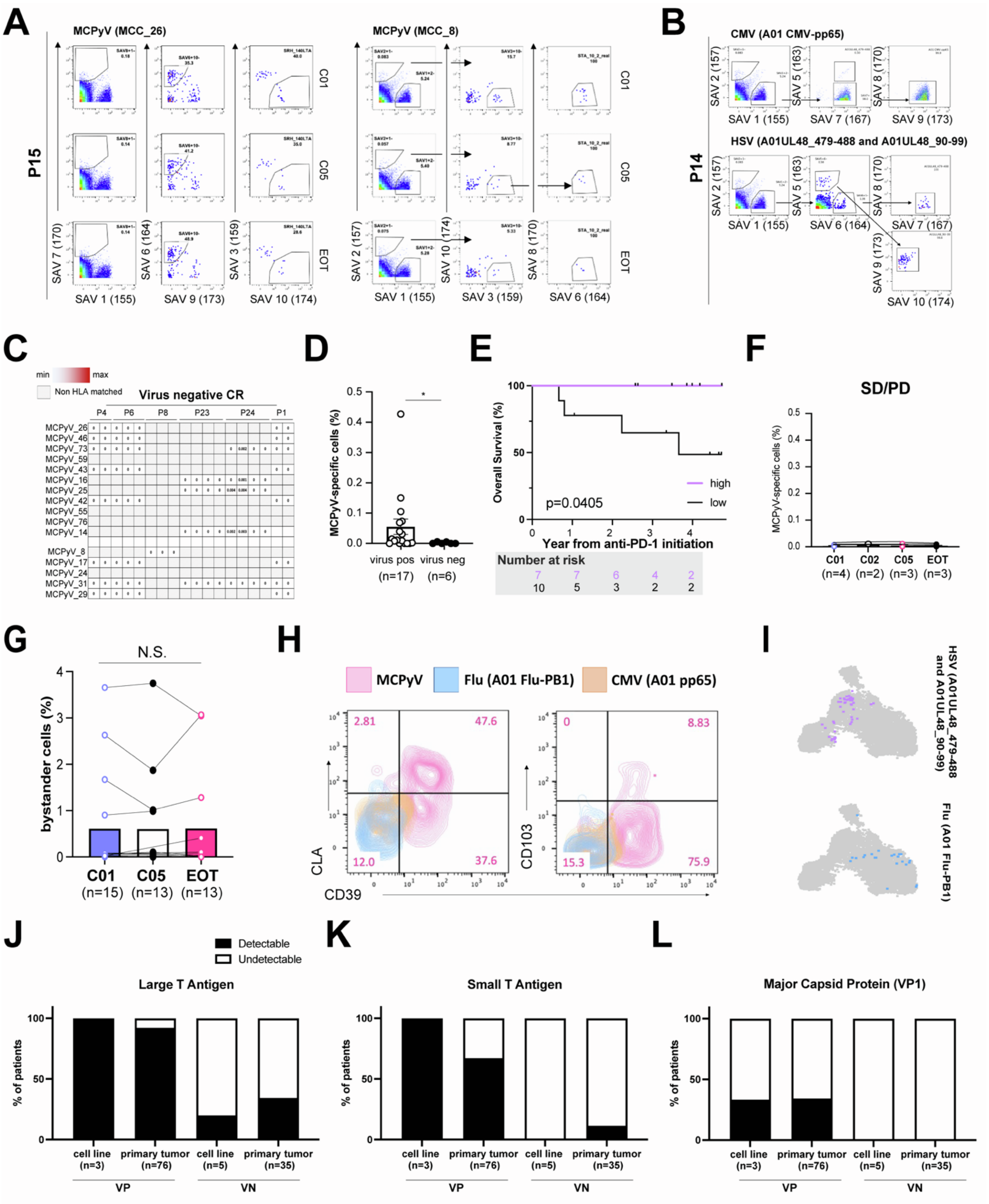

Figure S1. MCPyV-specific and MCC-unrelated antigen-specific CD8 T cell analysis, related to Figure 1 and 2.

(A and B) Gating strategy used for mass cytometry coupled to multiplex MHC class I-tetramer staining of MCPyV LTA (A, left, MCC_26) MCPyV STA (A, right, MCC_8), CMV (B, top) and HSV (B, bottom). Representative data from one patient, respectively. (C) Heatmap of individual MCPyV epitopes detected across all virus-negative patients (n=6).

(D) Frequencies of MCPyV-specific CD8 T cells amongst all VP and VN patients prior to the treatment. Data are represented as mean±S.E.M.. Mann-Whitney test. *p<0.05. Each symbol represents an individual patient.

(E) Kaplan-Meier curve of overall survival in VP patients with detectable (>0.01%, violet) or undetectable (<0.01%, black) MCPyV-specific CD8 T cells. Detection limit was determined by the highest frequency from virus-negative patients. Log-rank test.

(F) Frequencies of MCPyV-specific CD8 T cells over the course of the therapy in VP patients with SD and PD. Data are represented as mean±S.E.M.. Wilcoxon test.

(G) Frequencies of MCC-unrelated antigen-specific CD8 T cells over the course of the therapy in VP and VN patients. Wilcoxon test.

(H) Expression of CD39, CLA and CD103 by concatenated PBMC-derived MCPyV-, influenza-, and CMV-specific CD8 T cells from all patients.

(I) Representative UMAP embedding projections of HSV-specific (top) and influenza-specific (bottom) cells.

(J-L) Frequencies of samples with detectable or undetectable expression of LTA (J), STA (K), and major capsid protein (VP1, L) among VP and VN cell lines and primary tumors.

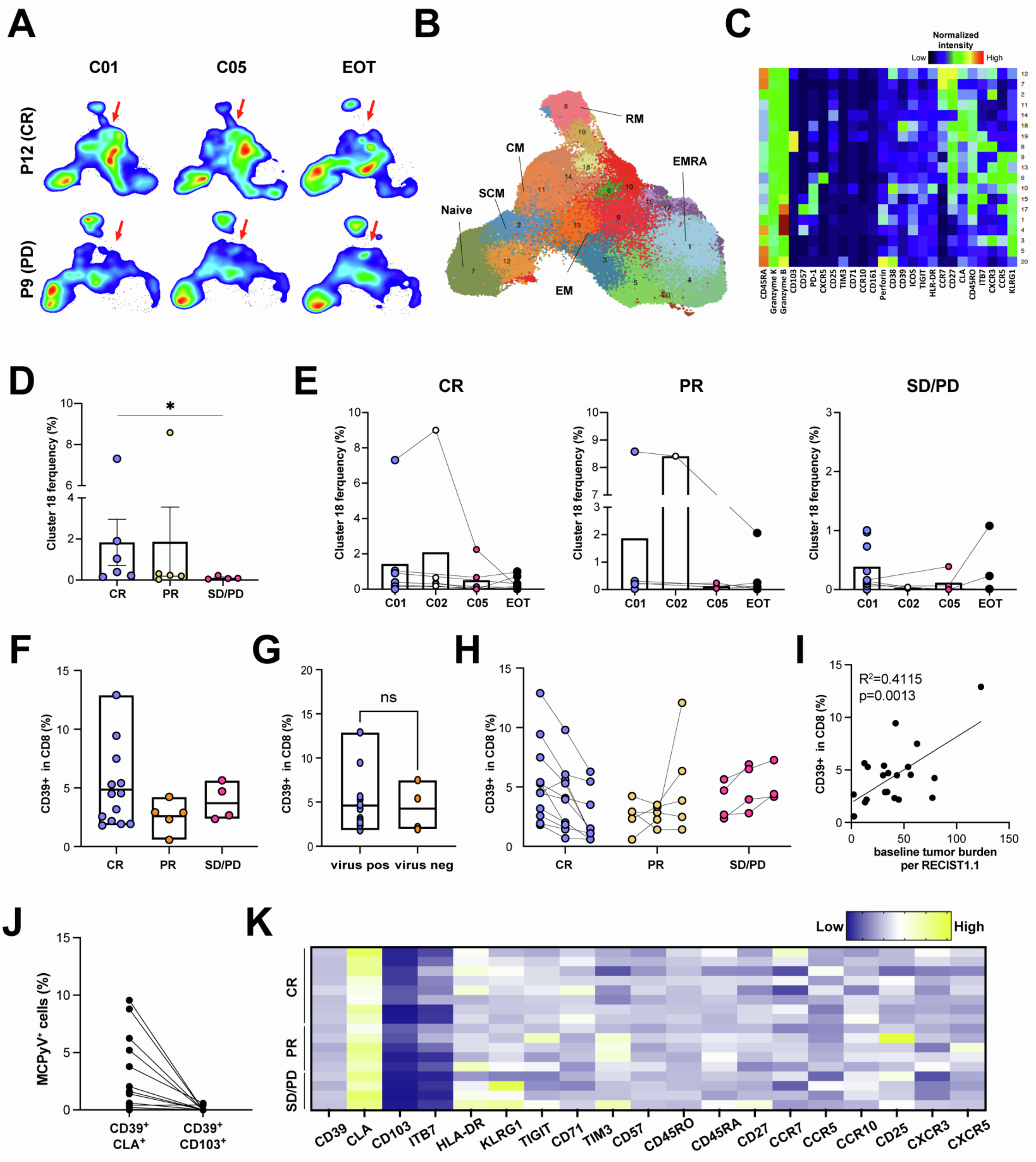

Figure S2. Phenotypic and high dimensional cluster analysis of CD8 T cells over the course of the therapy, related to Figure 3.

(A) UMAP projections of CD8 T cells from P12 (top) and P6 (bottom) over the course of the therapy. Red arrows indicate the dynamics of CD8 T cell population.

(B) UMAP embedding of CD8 T cells from all patients. Each cluster is shown in a different color.

(C) Heatmap plot of marker expression from each cluster of CD8 T cells.

(D) Frequencies of cluster 18 among VP patients. Mann-Whitney test. *p<0.05. Each symbol represents an individual patient.

(E) Frequencies of cluster 18 of CR (left), PR (middle), SD/PD (right) over the course of the therapy in VP patients.

(F) Frequencies of $CD39^+$ CD8 T cells among VP patients.

(G) Frequencies of $CD39^+$ CD8 T cells among all patients. Mann-Whitney test.

(H) Frequencies of $CD39^+$ CD8 T cells of CR (left), PR (middle), SD/PD (right) over the course of the therapy in VP patients.

(I) Linear-regression analysis of frequencies of $CD39^+$ CD8 T cells and baseline tumor burden in VP patients.

(J) Frequencies of MCPyV-specific cells among $CD39^+CLA^+$ and $CD39^+CD103^+$ CD8 T cells in VP patients at the baseline.

(K) Heatmap of relative marker expression of $CD39^+CLA^+$ CD8 T cells in comparison to $CD39^+CD103^+$ CD8 T cells.

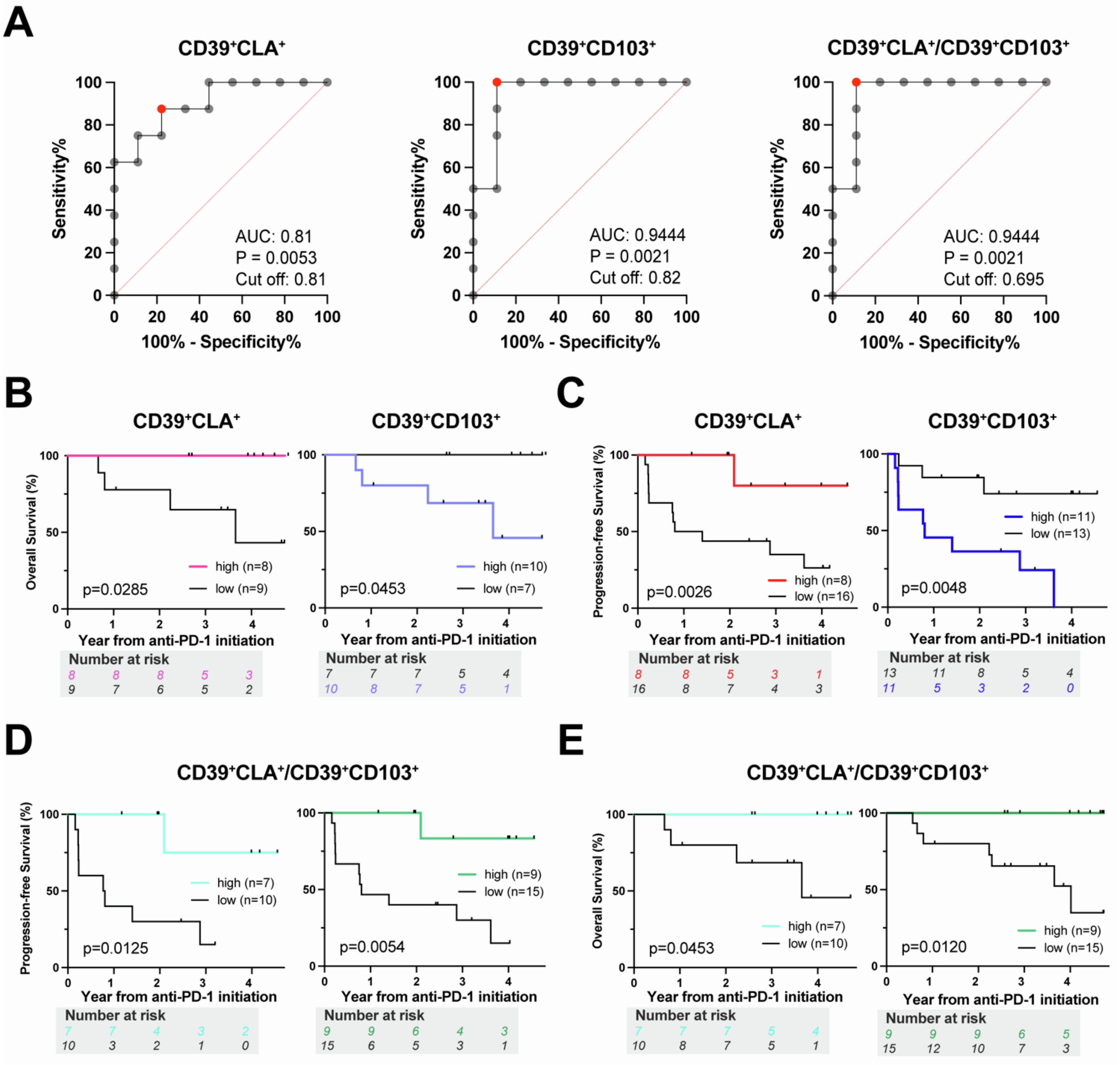

Figure S3. Receiver operating characteristic (ROC) curves and Kaplan-Meier curves of various markers in MCC patients, related to Figure 3.

(A) ROC curves for determining optimal threshold. Red dots indicate the optimal threshold chosen for classifiers. 95% confidence interval was determined by Wilson/Brown method.

(B) Kaplan-Meier curves of overall survival in VP patients with high or low CD39$^+$CLA$^+$ (left) or CD39$^+$CD103$^+$ (right) CD8 T cells. Log-rank test.

(C) Kaplan-Meier curves of progression-free survival in all patients with high or low CD39$^+$CLA$^+$ (left) or CD39$^+$CD103$^+$ (right) CD8 T cells. Log-rank test.

(D) Kaplan-Meier curves of progression-free survival in VP (left) or all (right) patients with high or low ratio of CD39$^+$CLA$^+$/CD39$^+$CD103$^+$ CD8 T cells. Log-rank test.

(E) (D) Kaplan-Meier curves of overall survival in VP (left) or all (right) patients with high or low ratio of CD39$^+$CLA$^+$/CD39$^+$CD103$^+$ CD8 T cells. Log-rank test.

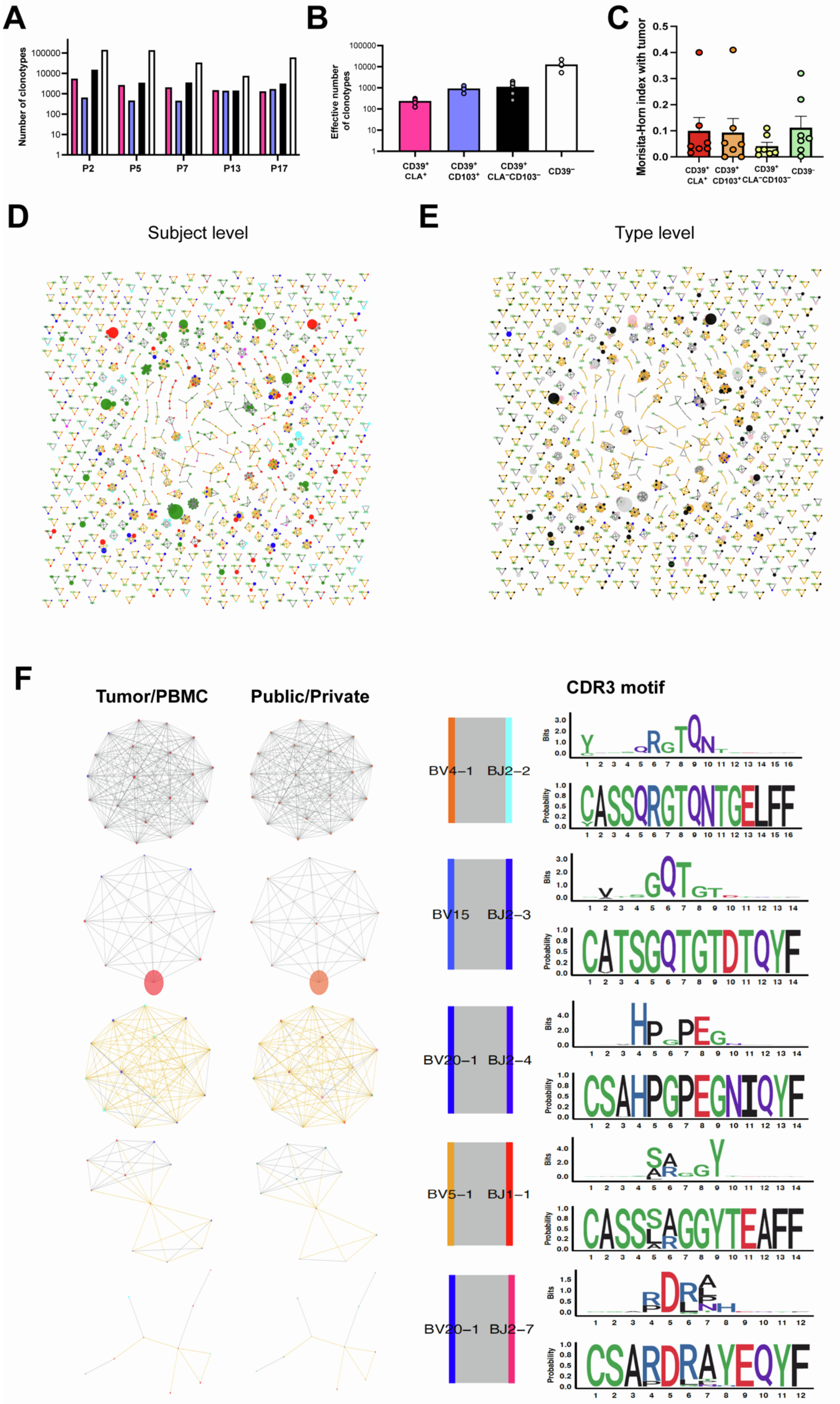
A
Number of clonotypes
100000
10000
1000
100
10
1
P2
P5
P7
P13
P17
B
Effective number of clonotypes
100000
10000
1000
100
10
1
CD39⁺ CLA⁺
CD39⁺ CD103⁺
CD39⁺ CLA⁻CD103⁻
CD39⁻
C
Morisita-Horn index with tumor
0.5
0.4
0.3
0.2
0.1
0.0
CD39⁺ CLA⁺
CD39⁺ CD103⁺
CD39⁺ CLA⁻CD103⁻
CD39⁻
D
Subject level
E
Type level
F
Tumor/PBMC
Public/Private
CDR3 motif
BV4−1
BJ2−2
Bits
Probability
CASSQRGTQNTGELFF
BV15
BJ2−3
CATSGQTGTDTQYF
BV20−1
BJ2−4
CSAHPGPEGNIQYF
BV5−1
BJ1−1
CASSSAGGYTEAFF
BV20−1
BJ2−7
CSARDRAYEQYF

Figure S4. TCRb sequence similarity network analysis of CD39, CLA and CD103 expressing subsets of CD8 T cells from MCC patients, related to Figure 4.

(A) Number of TCRb clonotypes recovered from TCR sequencing prior to down-sampling.

(B) True diversity indices of each CD8 T cell population.

(C) Morisita-Horn indices with tumor of each CD8 T cell population.

(D) Sequence similarity graphs from 5 patients colored by patients. Yellow lines indicate public edges and grey lines indicate private edges.

(E) Sequence similarity graphs from 5 patients colored by each CD8 subset. Yellow lines indicate public edges and grey lines indicate private edges. Tumor (light gray); CD39^{+}CLA^{-}CD103^{-} (black), CD39^{+}CLA^{+} (pink), CD39^{+}CLA^{-}CD103^{+} (blue).

(F) Representative logo plots of clusters of interest. Each symbol represents an individual clonotype. Tumor (red); CD39^{+}CLA^{-}CD103^{-} (blue), CD39^{+}CLA^{+} (green), CD39^{+}CLA^{-}CD103^{+} (cyan). The lower logo shows position-specific frequency of each amino acid within the TCR cluster, and the upper logo plots represent the position-specific information content compared to CDR3β receptors, with the same V- and J-gene usages, randomly sampled from naive repertoires.

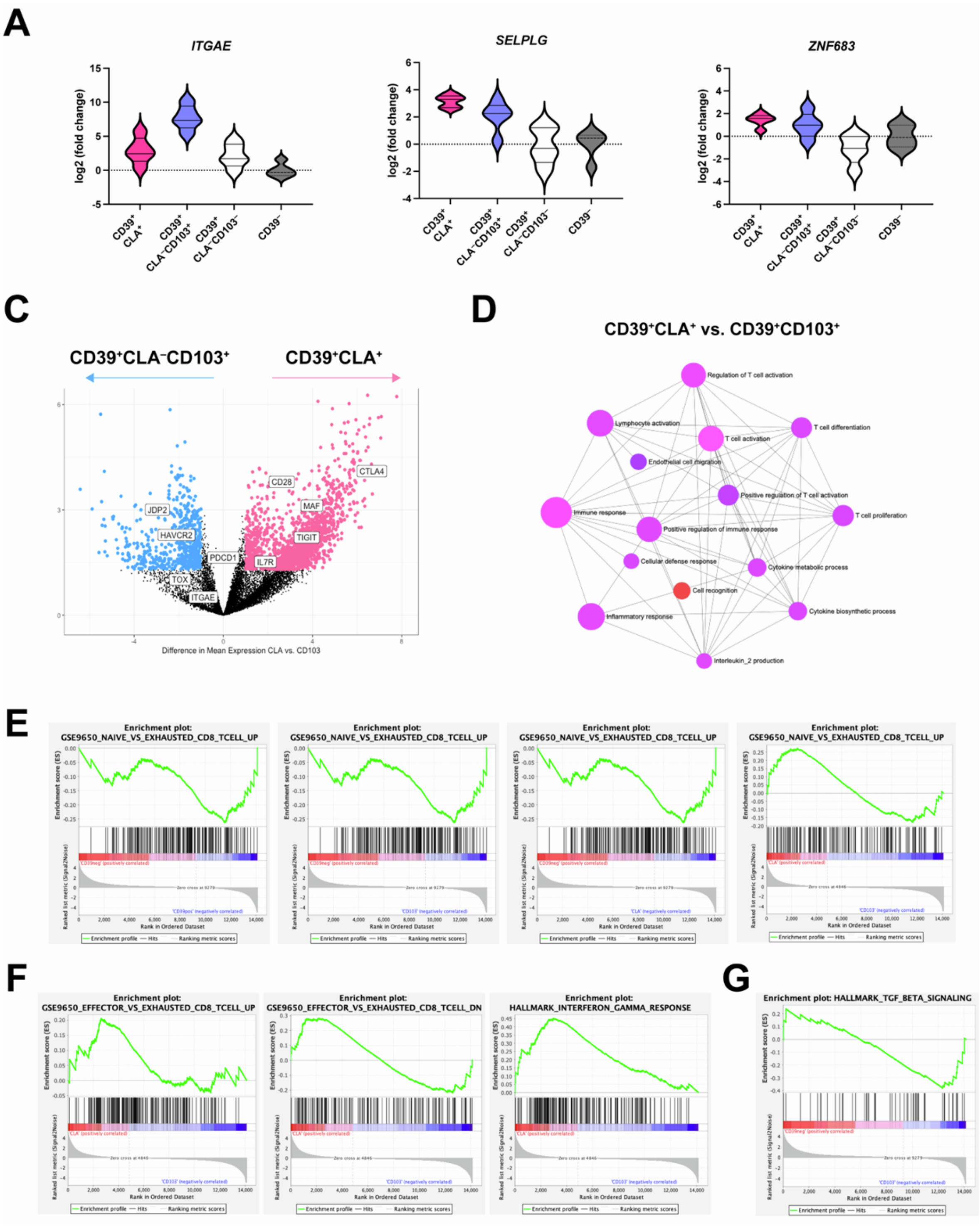

Figure S5. RNA-sequencing analysis of CD39, CLA and CD103 expressing subsets of CD8 T cell from MCC patients, related to Figure 5.

(A) Expression of *ITGAE* (left), *SELPLG* (middle) and *ZNF683* (right) in each CD8 T cell population; results are normalized to those of CD39$^-$.

(B) Volcano plot of CD39$^+$CLA$^+$ and CD39$^+$CLA$^-$CD103$^+$. Each dot corresponds to a specific gene. Red (CD39$^+$CLA$^+$) and blue (CD39$^+$CLA$^-$CD103$^+$) dots represent genes with 2-fold change and p value<0.05.

(C) Gene network analysis of CD39$^+$CLA$^+$ and CD39$^+$CLA$^-$CD103$^+$ CD8 T cells.

(D-F) Gene set enrichment analysis using the Molecular Signature Database. Naïve vs. Exhausted (GSE9650, D), Effector vs. Exhausted (GSE9650, E), Hallmark_Inteferon_gamma (E) and Hallmark_TGF_beta (F) were assessed.

Chapter 4: Circulating tumor-specific CD8 T cells share a transcriptional signature

Saumya Jani, Carolyn Shasha, Tomas Bencomo, Thomas H. Pulliam, Ana Jojic, Candice Church, Ted Gooley, David M. Koelle, Evan W. Newell, Paul Nghiem

CHAPTER SUMMARY: In this chapter, we explore a gene expression-based approach to translate our findings in chapters 2 and 3 to more common, mutationally-driven cancers. By thoroughly profiling antigen-specific CD8 T cells in Merkel cell carcinoma (MCC), we identify 98 genes that are differentially expressed in circulating tumor-specific T cells pre-treatment. We observe that this gene set can comparably identify neoantigen-specific CD8 T cells across mutationally-driven cancers. This suggests that viral oncoprotein and neoantigens elicit similar T cell responses, which would allow us to translate our findings beyond MCC.

Circulating tumor-specific CD8 T cells share a transcriptional signature

Authors
Saumya Jani[1,2], Carolyn Shasha[3], Tomas Bencomo[1], Thomas H. Pulliam[1], Ana Jojic[3], Candice Church[1], Ted Gooley[4], David M. Koelle[2,3,5,6,7], Evan W. Newell[3], Paul Nghiem[1*]

Affiliations
1. Department of Dermatology, University of Washington, Seattle, WA
2. Department of Laboratory Medicine and Pathology, University of Washington, Seattle, WA
3. Vaccine and Infectious Disease Department, Fred Hutchinson Cancer Center, Seattle, WA
4. Clinical Research Division, Fred Hutchinson Cancer Center, Seattle, WA
5. Department of Medicine, University of Washington, Seattle, WA
6. Department of Global Health, University of Washington, Seattle, WA
7. Benaroya Research Institute, Seattle, WA

* Correspondence: pnghiem@uw.edu

Abstract

Recent data suggest that tumor-specific CD8 T cells in the blood are important for and predictive of response to anti-PD-1 therapies. However, as most cancers express patient-specific tumor antigens, identification of tumor-specific CD8 T cells is not routinely feasible. In this study, we characterized tumor-specific CD8 T cells from blood of 17 patients with virus-driven Merkel cell carcinoma. We identified 98 differentially expressed genes (named ‘SPoTT’ for signature of peripheral tumor-specific CD8 T cells) that were important for discriminating tumor-specific CD8 T cells from other T cells in treatment-naïve patients. We calculated SPoTT scores for all cells in our training dataset and identified an optimal score cutoff for distinguishing tumor-specific CD8 T cells. When tested in validation cohorts of MCC, as well as more common, mutationally-driven cancers, SPoTT was able to identify tumor-specific CD8 T cells with sensitivity and specificity above 75%. Additionally, SPoTT performed comparably to a gene signature based on neoantigen-specific CD8 T cells, suggesting similar anti-tumor T-cell phenotypes in neoantigen- and virus-driven cancers. Application of SPoTT to identify tumor-specific T cells across multiple cancer types could allow personalization of treatment regimens based on patient-specific T cell characteristics.

Keywords: Merkel cell carcinoma, Merkel cell polyomavirus, Tumor-specific CD8 T cells, PD-1 pathway blockade, Gene signature

Introduction

Immunotherapies that target the PD-1 pathway are an important pillar of cancer treatment. However, only a small subset of patients experiences durable benefit from these treatments. Predicting which patients will respond to PD-1 blockade and identifying the relevant underlying mechanisms are major challenges in immune-oncology. One of the key roadblocks is the difficulty of identifying tumor-specific CD8 T cells. This is because most patient tumors are driven by unique, patient-specific mutations. Thus, identifying anti-tumor CD8 T cells requires either extensive functional testing or whole exome sequencing, prediction of HLA-restricted epitopes, and development of multimer reagents on a per-patient level. These approaches are infeasible for the large cohorts of patients needed to identify mechanisms of resistance. Development of efficient, clinically feasible approaches to identifying cancer-specific T cells could allow personalization of treatment regimens and improved responses to treatment.

Emerging data suggest that the frequency of cancer-specific T-cells in blood can predict anti-PD-1 response[1,2], suggesting an importance of these cells in the response to anti-PD-1. Given that several gene signatures of intratumoral tumor-specific CD8 T cells[3-7]and one gene signature of peripheral anti-tumor CD8 T cells in metastatic disease (NeoTCR$_{\text{PBL}}$)[8] have successfully been identified, we employed analogous approaches to characterize anti-tumor CD8 T cells in 17 treatment-naïve patients with advanced Merkel cell polyomavirus (**MCPyV**)-driven Merkel cell carcinoma (**MCC**). We used virus-driven MCC as a model cancer as it offers significant advantages: (1) it is extremely immunogenic; (2) the viral oncoproteins are relatively small in size and shared across patients; (3) HLA-restricted epitopes have been mapped and multimer reagents developed; and (4) it has a low tumor mutational burden. Thus, with our suite of multimer reagents, we are able to detect a majority of the tumor-specific CD8 T cells across a large cohort of patients.

After characterizing viral oncoprotein-specific CD8 T cells from virus-driven MCC patients, we developed a 98-gene signature that could discriminate peripheral tumor-specific CD8 T cells from all other CD8 T cells prior to immunotherapy (called SPoTT) with high accuracy. We then tested whether SPoTT could be applied to tumor-specific CD8 T cells from mutationally-driven cancers and compared how well it performed relative to an existing neoantigen-specific CD8 T cell-gene signature. We found that SPoTT was able to identify anti-tumor CD8 T cells from a variety of cancer types and performed comparably to NeoTCR$_{\text{PBL}}$, suggesting that tumor-specific CD8 T cells have a unique transcriptional profile regardless of antigen class.

Results

Identification of a transcriptional signature of tumor-reactive CD8 T cells

We performed single-cell cellular indexing of transcriptomes and epitopes (**CITE**) and T-cell receptor (**TCR**) sequencing on flow cytometry-assisted sorting (**FACS**) purified CD8+ T cells from pre-treatment peripheral blood mononuclear cells (**PBMC**) from 17 patients with MCPyV-driven MCC (**Supplementary Table 1**). MCPyV oncoprotein-, CMV-, EBV-, and flu-specific CD8 T cells were identified using a panel of HLA-matched multimer reagents (**Figure 1A; Supplementary Table 2 and Supplementary Figure 1**). CD8 T cells with diverse phenotypes were captured through this assay (**Figures 1B, D**). 80% of MCPyV-specific CD8 T cells were found in cluster 7, which was marked by high expression of cytotoxic markers (e.g., *GZMK*), exhaustion-associated molecules (e.g., *TOX*), and inhibitory markers (e.g., *ENTPD1, PDCD1*); and low expression of stem/memory markers (e.g., *FOS, JUN, and IL7R)* (**Figures 1C, D**). Comparatively, other virus-specific CD8 T cells were enriched in effector-memory (**TEM**) and effector-memory re-expressed CD45RA (**TEMRA**) clusters (**Figures 1C, D**).

To identify genes enriched in MCPyV-specific CD8 T cells, we performed differential gene expression analysis comparing cluster 7 to all other clusters. Genes involved in cell activation, cytotoxic function, metabolism, and mobility were enriched in cluster 7, while genes related to stemness and memory were downregulated (**Figure 2A**). To develop a gene signature that could discriminate tumor-specific CD8 T cells, we took all 208 genes with a log2 fold change (**log2FC**) greater than 0.5 in cluster 7 (**Supplementary Table 3**), calculated a gene enrichment score using UCell[9], and performed receiver operator characteristic (**ROC**) curve analysis using multimer-determined specificity as the gold standard, as this is currently the most accurate way of identifying antigen-specific T cells. Next, we iteratively removed one gene from the list and repeated the gene score enrichment and ROC analysis. All genes that resulted in a lower area under the curve (**AUC**) when removed were retained (**Supplementary Table 4**). This resulted in a 98-gene signature, SPoTT (**Supplementary Table 5**), and improved AUC scores from 0.93 to 0.96 (**Figure 2B**). To confirm that that our gene set enrichment algorithm (AUCell) was able to identify tumor-specific CD8 T cells, we calculated SPoTT scores for all cells in the training dataset. We indeed observed that the SPoTT score was enriched in cluster 7 and MCPyV-specific CD8 T cells (compared to other viral-specific CD8 T cells and those of unknown specificity; **Figures 2C, D**). To apply SPoTT to other cohorts, we used ROC curve analysis to identify an optimal score cutoff. A score cutoff of 0.34 resulted in a specificity of 88% and sensitivity of 94.2%.

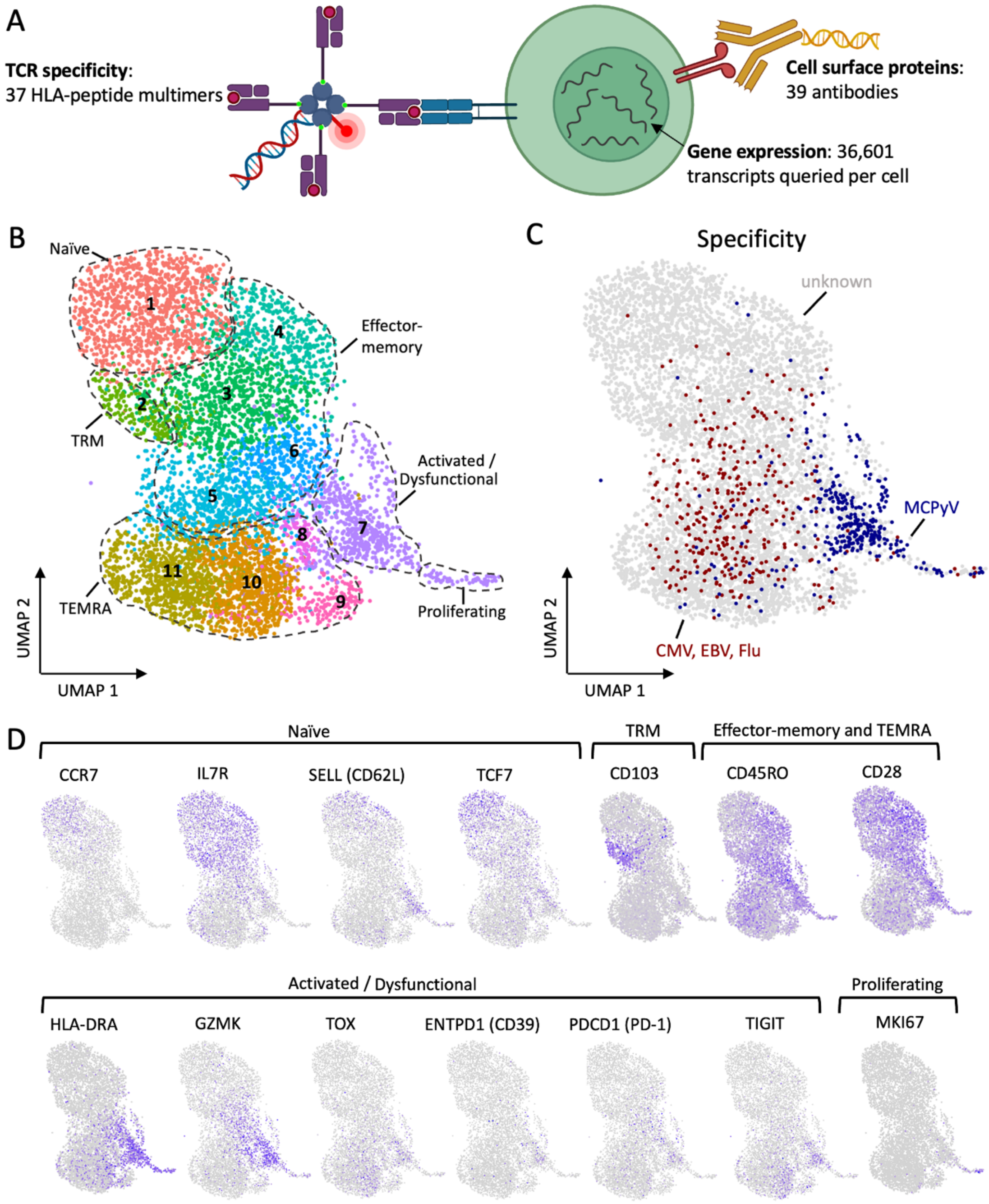

Figure 1. Characterization of peripheral MCPyV-specific CD8 T cells.

A. Pre-treatment PBMC were stained with HLA-matched MCPyV oncoprotein-, CMV-, EBV-, and flu-specific CD8 T cells and DNA barcoded antibodies against cell surface proteins. Tetramer-binding and a subset of non-tetramer binding CD8 T cells were sorted, and single-cell CITE and TCR sequencing was performed.
B. UMAP plot of CD8 T cells with clusters labeled with numbers and specific phenotypic regions labeled.
C. UMAP plot of CD8 T cells colored by T cell specificity (MCPyV = blue; CMV, EBV, or Flu = red; unknown specificity = gray).
D. UMAP plots highlighting expression of key markers used to designate phenotypic regions in panel B.

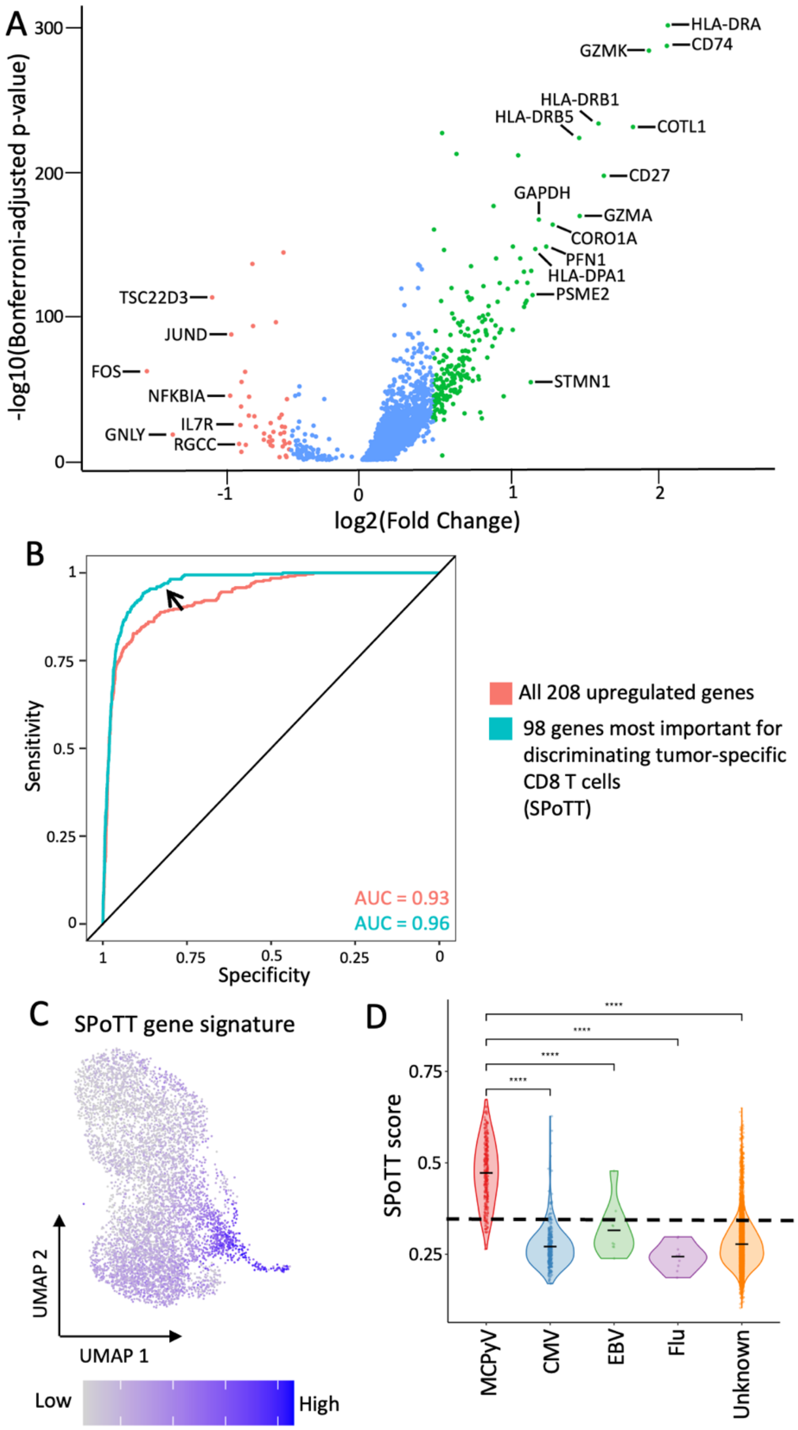

Figure 2. Development of a transcriptional signature (SPoTT) for MCPyV-specific CD8 T cells.

A. Volcano plot of genes upregulated and downregulated in cluster 7 (compared to all other clusters).
B. Improvement in ROC curves after narrowing down 208 upregulated genes to 98 genes most important for discriminating tumor-specific CD8 T cells (termed ‘SPoTT’).
C. UMAP plot colored by gene expression score.
D. Violin plots of gene expression score across CD8 T cell specificities (**** p-value < 0.0001)

Validation of SPoTT in independent cohorts of patients with MCC

To test how well SPoTT performed in independent patient cohorts, we used previously published single-cell RNA sequencing data from 8 virus-driven MCC patients[1]. We calculated a SPoTT score for each CD8 T cell and observed enrichment of SPoTT in cells that bound to MCPyV oncoprotein-specific multimers in the blood, but not in the tumor (compared to CMV-specific CD8 T cells or those of unknown specificity; **Figure 3A**). We used our training cohort-determined cutoff to identify SPoTT-predicted tumor-specific CD8 T cells. Using MCPyV oncoprotein multimer-binding as the gold standard, we observed a sensitivity of 84% and specificity of 85% in blood-derived CD8 T cells (**Figure 3B**).In contrast, in tumor-infiltrating CD8 T cells, we observed a sensitivity of 57% and specificity of 49% (**Figure 3B**). Taken together, this suggests that SPoTT is specific for peripheral CD8 T cells.

Next, we sought to determine if SPoTT could recognize tumor-specific CD8 T cells post-immunotherapy treatment. We performed scCITE and TCR sequencing, using multimers to determine T cell specificity, on longitudinal samples taken either 3 or 15 weeks after initiation of pembrolizumab. We observed a significant drop in sensitivity at both timepoints (from 94% at baseline to 67% 3 weeks post-treatment and 39% 15 weeks post-treatment; **Figure 3C)**.

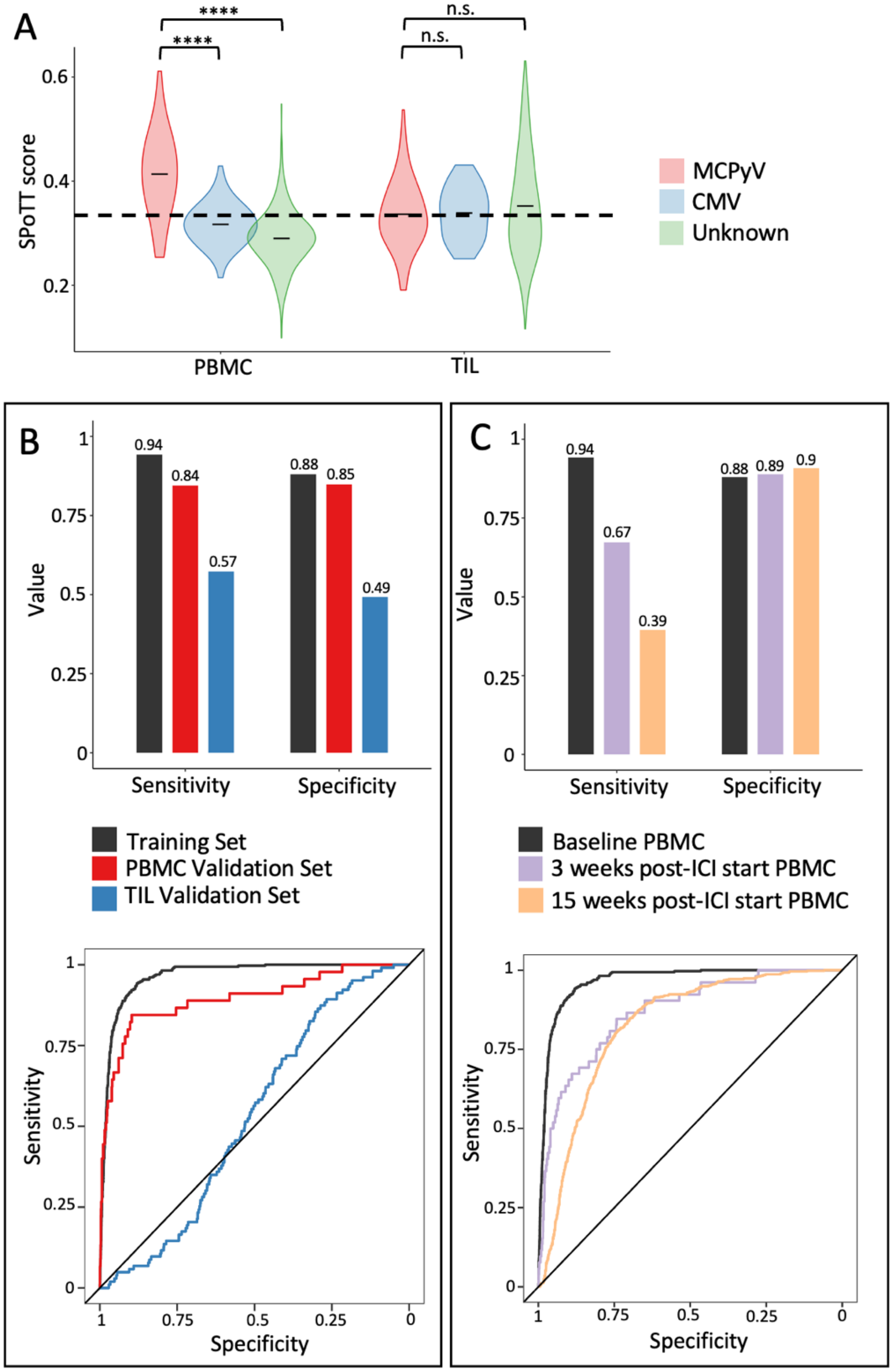

Figure 3. SPoTT is specific to tumor-specific CD8 T cells in pre-treatment blood in MCPyV-driven MCC.

A. Violin plots of gene expression score across CD8 T cell specificities and site of origin in the MCC validation cohort.
B. (Top) Bar charts of true positive (sensitivity) and true negative (specificity) rates for MCC training and validation cohort. (Bottom) ROC curves for MCC training and validation cohort.
C. (Top) Bar charts of true positive (sensitivity) true negative (specificity) rates for at baseline and post-ICI timepoints. (Bottom) ROC curves for baseline and post-ICI timepoints.

**** = p=value < 0.0001, n.s. = p-value > 0.05

SPoTT identifies peripheral neoantigen-specific CD8 T cells in mutationally-driven cancers

In order to test if MCC gene signature could identify tumor-specific CD8 T cells in various mutationally-driven cancers, we used previously published data from PBMC of patients with breast cancer, colon cancer, and rectal cancer[8]. Similar to the MCC validation cohort, we applied SPoTT to identify predicted tumor-specific CD8 T cells. We observed an enrichment of SPoTT in neoantigen-specific CD8 T cells, compared to those of other viral or unknown specificity (**Figure 4A**). When SPoTT predictions (based on the MCC training cohort-determined cutoff) were compared to neoantigen-specific CD8 T cells, we observed that SPoTT identified neoantigen-specific CD8 T cells with a sensitivity of 80% and a specificity of 76% (compared to a sensitivity of 84% and a specificity of 85% in the MCC validation cohort; **Figure 4B**). We then compared performance of SPoTT to a gene expression signature developed from this dataset, $\text{NeoTCR}_{\text{PBL}}$.[8] $\text{NeoTCR}_{\text{PBL}}$ is able to identify MCPyV-specific CD8 T cells with a sensitivity of 66% and a specificity of 88% (compared to a sensitivity of 72% and a specificity of 92% in the $\text{NeoTCR}_{\text{PBL}}$ training cohort; **Figure 4C**). When applied to both the $\text{NeoTCR}_{\text{PBL}}$ training dataset and SPoTT training and validation datasets, we observed comparable accuracy (**Figures 4D and E**). Finally, we compared the scores from both SPoTT and $\text{NeoTCR}_{\text{PBL}}$ per cell and observed significant correlation (i.e., both algorithms assign low scores to the same cells and high scores to the same cells; **Figures 4F and G**). This suggests that viral oncoprotein- and neoantigen-specific CD8 T cells have similar anti-tumor functional capacities that can be detected via gene expression levels.

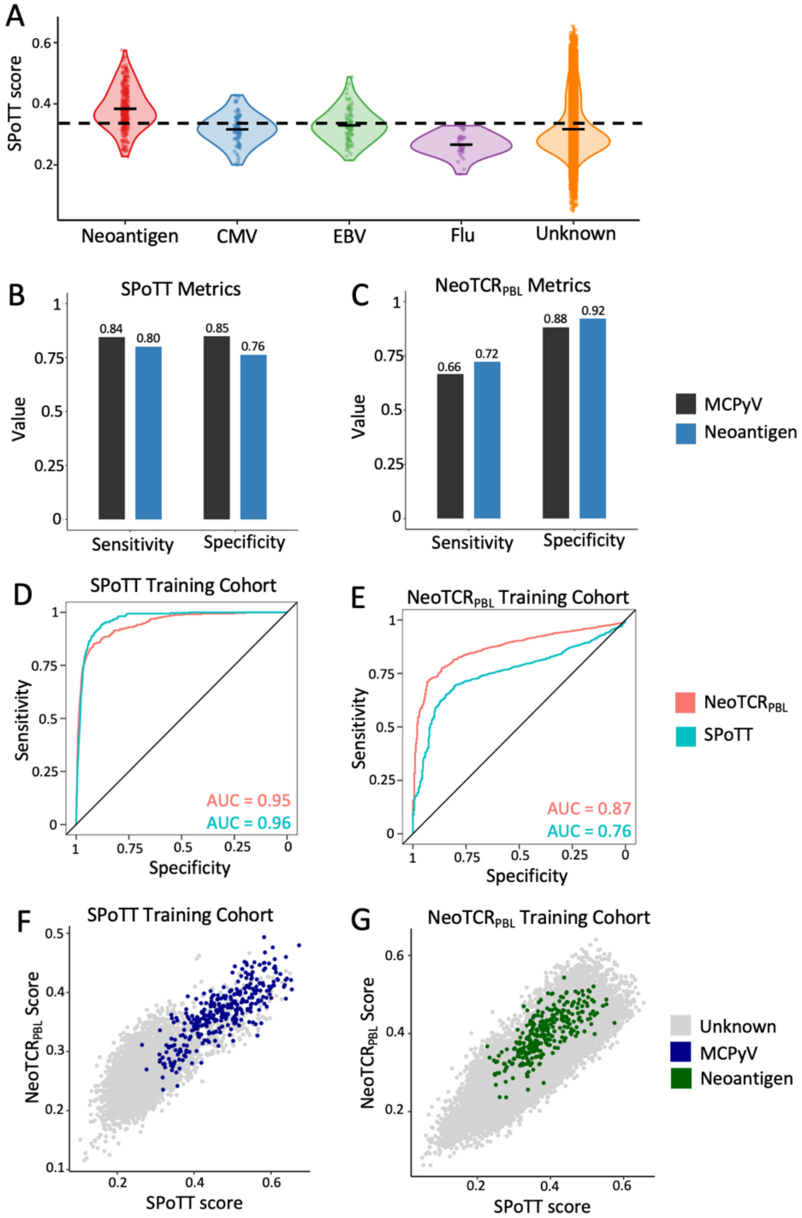

Figure 4. SPoTT recognizes neoantigen-specific CD8 T cells from mutationally-driven cancers.

A. Violin plots of gene expression score across CD8 T cell specificities in a mutationally-driven cancer cohort.
B. Bar charts of true positive (sensitivity) and true negative (specificity) rates for MCC validation and mutationally-driven cancer cohorts using SPoTT.
C. Bar charts of true positive (sensitivity) and true negative (specificity) rates for MCC validation and mutationally-driven cancer cohorts using NeoTCR$_{PBL}$.
D. ROC curves comparing NeoTCRPBL and SPoTT in identifying neoantigen-specific CD8 T cells in NeoTCRPBL training cohort.
E. ROC curves comparing NeoTCRPBL and SPoTT in identifying MCPyV-specific CD8 T cells in SPoTT training cohort.
F. Dot plots comparing SPoTT and NeoTCR$_{PBL}$ scores in the SPoTT training cohort.
G. Dot plots comparing SPoTT and NeoTCR$_{PBL}$ scores in the NeoTCR$_{PBL}$ training cohort.

Conclusion

Summary

Unlike most T cells that are transiently activated and then contract once the infection is cleared, tumor-specific CD8 T cells are persistently activated by tumor cells. This chronic exposure to their cognate antigens results in activation of distinct cellular programs, which can be assessed by transcriptomic analyses. Along the same lines, tumor-specific CD8 T cells that predominantly reside in the tumor vary in phenotype and function from those found in the blood[1,8]. While many groups have characterized intratumoral tumor-specific CD8 T cells[3-7], the phenotype of peripheral tumor-specific CD8 T cells has only been studied via single-cell RNA sequencing in the context of metastatic disease[8]. This is largely because tumor-specific CD8 T cells are found at much lower frequencies in the blood compared to the tumor and are thus more difficult to detect. In this study, we profiled peripheral tumor-specific CD8 T cells from 17 patients with virus-driven MCC prior to immunotherapy. We observed that peripheral tumor-specific CD8 T cells were phenotypically similar (**Figure 1C**) and marked by high expression of cytotoxic effector functions, exhaustion-associated molecules, and inhibitory receptors, as well as low expression of stemness and memory markers (**Figure 2A**). This profile may be a result of (1) lymph node-activated T cells that are trafficking to the tumor (e.g., SELL (L-selectin) is upregulated on these tumor-specific CD8 T cells); (2) T cells transiently activated by material shed by tumor cells; or (3) T cells re-circulating from the tumor.

Via differential gene expression analysis, we identified 98 genes (SPoTT) that could discriminate tumor-specific CD8 T cells from all other CD8 T cells with a sensitivity and specificity of 84% and 85% in an independent, validation cohort of MCC patients (**Figure 3B**). We additionally determined that SPoTT could not identify tumor-specific CD8 T cells in the tumor or at post-immunotherapy timepoints (**Figure 3**), establishing specificity for baseline, peripheral anti-MCC CD8 T cells. This also suggests that immunotherapy induces transcriptional changes that result in a different T cell phenotype.

Additionally, SPoTT was able to identify neoantigen-specific CD8 T cells in tumor samples from multiple mutationally-driven cancers with comparable accuracy to NeoTCR$_{PBL}$ (**Figure 4**). Incorporation of this gene set into transcriptomic studies can allow direct study of the numerically lower, but more relevant tumor-specific CD8 T cell population in transcriptomic studies. Additionally, in combination with TCR sequencing, it can also allow high-throughput identification of tumor-specific TCRs for adoptive cell therapies, as well as TCR bispecific and TCR mimic drugs.

Future directions

While our study can enhance cancer immunology research, single-cell RNA sequencing techniques cannot yet be applied in a clinical setting. We can, however, take advantage of the relatively unbiased nature of transcriptomic analyses to develop flow cytometry panels, informed by our tumor-specific T cell gene set, that can be implemented in a clinical lab. Promisingly, two studies of neoantigen-specific CD8 T cells[8] and viral oncoprotein-specific CD8 T cells[2] identified high expression of CD45RO, CD39, HLA-DRA, and PD-1 via CITEseq and CyTOF, respectively. Validation and incorporation of additional cell surface markers may allow us to efficiently quantify tumor-specific CD8 T cells.

Additionally, a comparison of differentially expressed genes reported in intratumoral vs. peripheral tumor-specific CD8 T cells may allow identification of novel immune checkpoints and therapeutic targets. A comparison of the gene sets discussed here (our MCC gene set and those previously published) identified the following genes as being present in tumor-derived signatures, but absent in blood-derived signatures: *KLRD1, TNFRSF1B, RAB27A, SYTL3, SAMSN1, BATF, CCL3, PHLDA1, CRTAM, CXCR6, TPI1, GAPDH,* and *CXCL13*. While some of these have been extensively reported to be expressed on intratumoral tumor-specific CD8 T cells (e.g., *CXCL13*[10-15]), others have been less studied and could be candidates for further investigation. As an example, *TNFRSF1B* was recently reported as a T cell exhaustion marker associated with poor prognosis in ovarian cancer[16]. Mouse studies demonstrated that *TNFRSF1B* suppressed interferon-γ production and promoted tumor growth. Similar analyses could identify other genes critical to immunotherapy response.

While the differentially expressed gene list was chosen based on a log2-fold change > 0.5, it is possible that subtle fold-changes in some genes could be more important than large fold-changes in irrelevant genes. Rapidly advancing machine learning technologies could be used in the future to refine tumor-specific gene sets in a more unbiased manner. Additionally, we did not observe a significant improvement in predictive capability when downregulated genes were included, though it is possible that their use with upcoming technologies could prove beneficial. Further refinement of the gene set could allow a more quantitative assessment of tumor-specific CD8 T cells and allow us to estimate the frequency of these cells in a patient. Previous reports have suggested an association between frequency of tumor-specific CD8 T cells in blood pre-treatment and response to anti-PD-(L)1[1,2]. Thus, with further refinement, it may be possible to develop a clinical assay that can rationally stratify patients for immunotherapy and prioritize patients unlikely to respond for alternate or synergistic treatments. Additionally, it may also allow us to track T cell response to therapeutic vaccinations and other T cell modulating treatments.

Limitations of study

While relatively large in comparison to other tumor immunology studies that characterize patient samples at single-cell resolution, this study is nevertheless limited by sample size. Although we observed similar phenotypes in tumor-specific CD8 T cells from 25 MCC patients (17 in the training cohort and 8 in the validation cohort) and 6 patients with mutationally-driven cancers (from a previously published study), these are still relatively small numbers compared to the entire cancer patient population. Thus, it is possible that the identified gene set will not translate well to all other patients with cancer.

Additionally, our previous work in MCC[17] and many previously published studies relied on activation and/or expansion of T cells to identify HLA-restricted tumor epitopes or tumor-specific TCRs, which were then used to assign tumor-specificity in the analyzed studies. Thus, these studies could be biased towards T cells that are at an earlier stage of exhaustion and have not lost their ability to response to stimulation by their cognate antigen. Additionally, while multimer reagents have been shown to correlate with cytotoxicity, we do observe an increase in non-specific staining when these reagents are conjugated with DNA oligomers. For both of these reasons, tumor-specific CD8 T cells could have been labeled “unknown,” or non-tumor-specific CD8 T cells designated “tumor-specific,” confounding the sensitivity and specificity values reported in this study. While we have observed that our chosen score cutoff is translatable for other datasets, it is possible that the chosen cutoff of 0.34 is not the most appropriate if datasets are processed differently and/or if different gene set enrichment methods are used. Should this be a problem for any potential users of this gene set, our training dataset can be integrated with their data and a cutoff can be chosen based on ROC curve analysis (using our multimer-based specificity assignments as the gold standard).

Methods

Study participant details

The samples in the training cohort were collected as part of a pembrolizumab trial (NCT02267603[18,19]) and analyzed per IRB protocol #6585 (Fred Hutch Cancer Center). Briefly, eligibility criteria included: (1) at least 18 years old; (2) unresectable metastatic or recurrent locoregional MCC; (3) an Eastern Cooperative Oncology Group performance score of 0 or 1; (4) normal organ and bone marrow function; (5) no history of previous systemic treatment for MCC; (6) no immunosuppression, autoimmune disease, or concurrent second cancer.

Blood collection and processing

PBMC were isolated from whole blood by routine Ficoll density gradient centrifugation and cryopreserved in liquid nitrogen at the Specimen Processing Lab (FHCC).

Single-cell RNA sequencing sample preparation

Single cell suspensions of PBMC samples were analyzed by cellular indexing of transcripts and epitopes by sequencing (CITEseq). Frozen PBMC tubes were thawed at 37 C for 2 minutes. 1 ml of complete media (RPMI, 10% Fetal bovine serum, 1x penicillin/streptomycin, 1x l-glutamine) was then added in a dropwise manner. The samples were then transferred to 50-ml conical tubes and equal volume of complete media was continuously added 4 additional times (dropwise with gentle mixing in between additions (total volume of 32 ml). Cells were then washed twice with phosphate-buffered saline (**PBS**) and transferred to FACS tubes (Fisher Scientific). Cells were then stained with a viability marker (FVS780; BD Biosciences) and blocking buffer (0.5% BSA, 5% TruStain FcX buffer (Biolegend), 100 nM dasatinib, and 0.05mM of biotin). After a 10-minute incubation on ice, DNA barcode-labeled HLA-matched HLA-I multimers (custom ordered from Immudex) were added. After a 5-minute incubation of ice, the following reagents were added: (1) fluorophore-labeled antibodies to allow sorting of live, CD8+ T cells; (2) hashtag antibodies to deconvolute sample of origin from sequencing data after subsequent pooling steps, and DNA barcode-labeled antibodies for measurement of cell surface proteins. Cells were then incubated on ice for 30 minutes and washed three times. An Aria II Cell sorter (BD Biosciences) was used to sort live, CD3+CD8+ lymphocytes into cold complete media. All multimer-binding CD8 T cells and a subset of bulk CD8 T cells were sorted from each patient. All samples were pooled and immediately prepared for sequencing.

Library preparation and sequencing

Sorted cells were then counted, aliquoted according to manufacturer specifications, and mixed with the appropriate primers and enzymes (10x Genomics). These suspensions were then loaded into the appropriate microfluidic chip (chip K; 10x Genomics) and run through a Chromium controller to obtain Gel Beads-in-Emulsion (10x Genomics). Libraries single-cell CITE sequencing and paired single-cell V(D)J sequencing for T-cell receptor (TCR) clonotypes were prepared using the 5′ transcriptome kit with feature barcoding (v2; 10x Genomics). The complementary DNA libraries were then sequenced using a NovaSeq S1 instrument (Illumina) with paired-end reads aiming for an average of 20,000 reads per cell for the gene expression library and 5,000 reads per cell for the V(D)J and cell surface libraries.

HLA multimer gating and analysis

To identify antigen-specific CD8 T cells in single-cell RNA sequencing data, HLA-I multimer unique molecular identifiers (UMIs) counts were plotted. Log-transformed counts for each HLA-I multimer were plotted against all other multimers of the same HLA-I allele (**Supplementary Figure 1**). This allowed us to exclude cells that non-specifically bound to the HLA-I allele. Appropriate count cutoffs were then visually assessed for each sample, and independently confirmed by a second person (T.H.P.). TCRβ sequences of multimer-positive cells were then compared to TCRs of known specificity in the VDJ database[20] as validation for our multimer-based specificity calls.

Single-cell RNA sequencing data analysis

Raw sequencing reads were aligned to the hg38 genome using Cell Ranger v.6.1.1. Filtered counts matrices of transcripts and feature barcoding counts were analyzed in R (v4.2.3) using Seurat (v4.3.0.1). Sample of origin was deconvolution using the HTODemux function. Doublets were detected using DoubletFinder (v.2.0.3). Doublets identified via HTODemux and DoubletFinder were excluded from further analysis. Cells that had more than 10% mitochondrial DNA were presumed to be of low quality and removed. Comparisons of excluded and kept cells were performed to ensure no cell populations were disproportionally removed.

Cells from different 10x runs were then combined into a single Seurat object. Gene expression data was batch correction using Harmony[21] (v0.1.1) and data DNA-barcoded antibodies was normalized using the dsb package[22] (v1.0.3). UMAP dimensionality reduction and clustering was performed using the Harmony-corrected values. Differential gene expression analysis was performed using Seurat's FindMarkers function. Cells were scored for gene sets using the UCell (v.2.2.0) package.

Plots were made using Seurat (v.4.3.0.1) or ggplot2 (3.4.4).

Statistics

Two-sided statistical tests were applied unless specified otherwise. T tests were used to compare differences between two groups unless otherwise noted. When comparing more than two groups, the nonparametric Kruskal–Wallis test was used. The Benjamini–Hochberg method was used to correct for multiple tests. ROC curve analysis was used to measure classification accuracy. All statistical analysis was carried out using R v.4.2+.

Acknowledgements

This study was funded by the National Institutes of Health (NIH) National Cancer Institute (NCI) grants P01 CA225517 (PN), F30 CA254168 (THP), T32 CA080416 (SJ), and P30 CA015704 (PN); Odyssey Group Foundation Kelsey Dickson Team Science Courage Research Award: Advancing New Therapies for Merkel Cell Carcinoma (MCC) (A187769) (PN); National Foundation for Cancer Research (PN); and the Merkel cell carcinoma (MCC) patient gift fund at the University of Washington (PN). This research was supported by the Cell Analysis Facility Flow Cytometry Shared Resource Lab in the Department of Immunology at the University of Washington. Some figures were created with BioRender.

Author contributions

- Saumya Jani – conceptualization, methodology, validation, formal analysis, investigation, visualization, writing – original draft, funding acquisition
- Carolyn Shasha – validation, formal analysis
- Tomas Bencomo – formal analysis
- Thomas H. Pulliam – conceptualization, methodology
- Ana Jojic – formal analysis, investigation
- Candice Church – resources
- Ted Goodley – statistical analysis
- David M. Koelle – methodology, supervision
- Evan W. Newell – methodology, supervision
- Paul Nghiem – conceptualization, methodology, supervision, funding acquisition
- All authors – writing – reviewing and editing

Declaration of interests

PN's institution has received grant support from EMD Serono and Bristol Myers Squibb (BMS), as well as honoraria from Merck and EMD-Serono. DMK and PN are co-inventors on institutionally-owned patents concerning MCPyV-specific T cell receptors. No other authors have relevant disclosures.

Data availability

The single-cell CITE and TCR sequencing data obtained in this study has been uploaded to Zenodo (DOI: 10.5281/zenodo.10936415). Any requests for the raw data will be reviewed by the corresponding authors to ensure patient confidentiality is maintained. If possible, the data will be shared under a material transfer agreement. Data previously published and analyzed here are available on GEO with accession number GSE227708 and dbGAP with study number phs003064.v1.p1. Additional data supporting the study's findings can be found in the main text, figures, and supplementary files.

Code availability

Code needed to reproduce any of the analyses will be made available upon reasonable request.

References

1. Pulliam, T., Jani, S., Jing, L., Ryu, H., Jojic, A., Shasha, C., Zhang, J., Kulikauskas, R., Church, C., Garnett-Benson, C., et al. (2024). Circulating cancer-specific CD8 T cell frequency is associated with response to PD-1 blockade in Merkel cell carcinoma. Cell Rep Med, 101412. 10.1016/j.xcrm.2024.101412.
2. Ryu, H., Bi, T.M., Pulliam, T.H., Sarkar, K., Church, C.D., Kumar, N., Mayer-Blackwell, K., Jani, S., Ramchurren, N., Hansen, U.K., et al. (2024). Merkel cell polyomavirus-specific and CD39(+)CLA(+) CD8 T cells as blood-based predictive biomarkers for PD-1 blockade in Merkel cell carcinoma. Cell Rep Med, 101390. 10.1016/j.xcrm.2023.101390.
3. Caushi, J.X., Zhang, J., Ji, Z., Vaghasia, A., Zhang, B., Hsiue, E.H., Mog, B.J., Hou, W., Justesen, S., Blosser, R., et al. (2021). Transcriptional programs of neoantigen-specific TIL in anti-PD-1-treated lung cancers. Nature *596*, 126-132. 10.1038/s41586-021-03752-4.
4. Oliveira, G., Stromhaug, K., Klaeger, S., Kula, T., Frederick, D.T., Le, P.M., Forman, J., Huang, T., Li, S., Zhang, W., et al. (2021). Phenotype, specificity and avidity of antitumour CD8(+) T cells in melanoma. Nature *596*, 119-125. 10.1038/s41586-021-03704-y.
5. Meng, Z., Rodriguez Ehrenfried, A., Tan, C.L., Steffens, L.K., Kehm, H., Zens, S., Lauenstein, C., Paul, A., Schwab, M., Forster, J.D., et al. (2023). Transcriptome-based identification of tumor-reactive and bystander CD8(+) T cell receptor clonotypes in human pancreatic cancer. Sci Transl Med *15*, eadh9562. 10.1126/scitranslmed.adh9562.
6. Lowery, F.J., Krishna, S., Yossef, R., Parikh, N.B., Chatani, P.D., Zacharakis, N., Parkhurst, M.R., Levin, N., Sindiri, S., Sachs, A., et al. (2022). Molecular signatures of antitumor neoantigen-reactive T cells from metastatic human cancers. Science *375*, 877-884. 10.1126/science.abl5447.
7. Hanada, K.I., Zhao, C., Gil-Hoyos, R., Gartner, J.J., Chow-Parmer, C., Lowery, F.J., Krishna, S., Prickett, T.D., Kivitz, S., Parkhurst, M.R., et al. (2022). A phenotypic signature that identifies neoantigen-reactive T cells in fresh human lung cancers. Cancer Cell *40*, 479-493 e476. 10.1016/j.ccell.2022.03.012.
8. Yossef, R., Krishna, S., Sindiri, S., Lowery, F.J., Copeland, A.R., Gartner, J.J., Parkhurst, M.R., Parikh, N.B., Hitscherich, K.J., Levi, S.T., et al. (2023). Phenotypic signatures of circulating neoantigen-reactive CD8(+) T cells in patients with metastatic cancers. Cancer Cell. 10.1016/j.ccell.2023.11.005.
9. Andreatta, M., and Carmona, S.J. (2021). UCell: Robust and scalable single-cell gene signature scoring. Comput Struct Biotechnol J *19*, 3796-3798. 10.1016/j.csbj.2021.06.043.
10. Litchfield, K., Reading, J.L., Puttick, C., Thakkar, K., Abbosh, C., Bentham, R., Watkins, T.B.K., Rosenthal, R., Biswas, D., Rowan, A., et al. (2021). Meta-analysis of tumor- and T cell-intrinsic mechanisms of sensitization to checkpoint inhibition. Cell *184*, 596-614 e514. 10.1016/j.cell.2021.01.002.
11. Panse, J., Friedrichs, K., Marx, A., Hildebrandt, Y., Luetkens, T., Barrels, K., Horn, C., Stahl, T., Cao, Y., Milde-Langosch, K., et al. (2008). Chemokine CXCL13 is overexpressed in the tumour tissue and in the peripheral blood of breast cancer patients. Br J Cancer *99*, 930-938. 10.1038/sj.bjc.6604621.
12. Thommen, D.S., Koelzer, V.H., Herzig, P., Roller, A., Trefny, M., Dimeloe, S., Kiialainen, A., Hanhart, J., Schill, C., Hess, C., et al. (2018). A transcriptionally and functionally distinct PD-1(+) CD8(+) T cell pool with predictive potential in non-small-cell lung cancer treated with PD-1 blockade. Nat Med *24*, 994-1004. 10.1038/s41591-018-0057-z.
13. Tirosh, I., Izar, B., Prakadan, S.M., Wadsworth, M.H., 2nd, Treacy, D., Trombetta, J.J., Rotem, A., Rodman, C., Lian, C., Murphy, G., et al. (2016). Dissecting the multicellular

ecosystem of metastatic melanoma by single-cell RNA-seq. Science *352*, 189-196. 10.1126/science.aad0501.

14. Yang, M., Lu, J., Zhang, G., Wang, Y., He, M., Xu, Q., Xu, C., and Liu, H. (2021). CXCL13 shapes immunoactive tumor microenvironment and enhances the efficacy of PD-1 checkpoint blockade in high-grade serous ovarian cancer. J Immunother Cancer *9*. 10.1136/jitc-2020-001136.
15. Zheng, C., Zheng, L., Yoo, J.K., Guo, H., Zhang, Y., Guo, X., Kang, B., Hu, R., Huang, J.Y., Zhang, Q., et al. (2017). Landscape of Infiltrating T Cells in Liver Cancer Revealed by Single-Cell Sequencing. Cell *169*, 1342-1356 e1316. 10.1016/j.cell.2017.05.035.
16. Gao, Y., Shi, H., Zhao, H., Yao, M., He, Y., Jiang, M., Li, J., Li, Z., Su, S., Liu, T., et al. (2023). Single-cell transcriptomics identify TNFRSF1B as a novel T-cell exhaustion marker for ovarian cancer. Clin Transl Med *13*, e1416. 10.1002/ctm2.1416.
17. Jing, L., Ott, M., Church, C.D., Kulikauskas, R.M., Ibrani, D., Iyer, J.G., Afanasiev, O.K., Colunga, A., Cook, M.M., Xie, H., et al. (2020). Prevalent and Diverse Intratumoral Oncoprotein-Specific CD8. Cancer Immunol Res *8*, 648-659. 10.1158/2326-6066.CIR-19-0647.
18. Nghiem, P.T., Bhatia, S., Lipson, E.J., Kudchadkar, R.R., Miller, N.J., Annamalai, L., Berry, S., Chartash, E.K., Daud, A., Fling, S.P., et al. (2016). PD-1 Blockade with Pembrolizumab in Advanced Merkel-Cell Carcinoma. N Engl J Med *374*, 2542-2552. 10.1056/NEJMoa1603702.
19. Nghiem, P., Bhatia, S., Lipson, E.J., Sharfman, W.H., Kudchadkar, R.R., Brohl, A.S., Friedlander, P.A., Daud, A., Kluger, H.M., Reddy, S.A., et al. (2021). Three-year survival, correlates and salvage therapies in patients receiving first-line pembrolizumab for advanced Merkel cell carcinoma. J Immunother Cancer *9*. 10.1136/jitc-2021-002478.
20. Goncharov, M., Bagaev, D., Shcherbinin, D., Zvyagin, I., Bolotin, D., Thomas, P.G., Minervina, A.A., Pogorelyy, M.V., Ladell, K., McLaren, J.E., et al. (2022). VDJdb in the pandemic era: a compendium of T cell receptors specific for SARS-CoV-2. Nat Methods *19*, 1017-1019. 10.1038/s41592-022-01578-0.
21. Korsunsky, I., Millard, N., Fan, J., Slowikowski, K., Zhang, F., Wei, K., Baglaenko, Y., Brenner, M., Loh, P.R., and Raychaudhuri, S. (2019). Fast, sensitive and accurate integration of single-cell data with Harmony. Nat Methods *16*, 1289-1296. 10.1038/s41592-019-0619-0.
22. Mule, M.P., Martins, A.J., and Tsang, J.S. (2022). Normalizing and denoising protein expression data from droplet-based single cell profiling. Nat Commun *13*, 2099. 10.1038/s41467-022-29356-8.

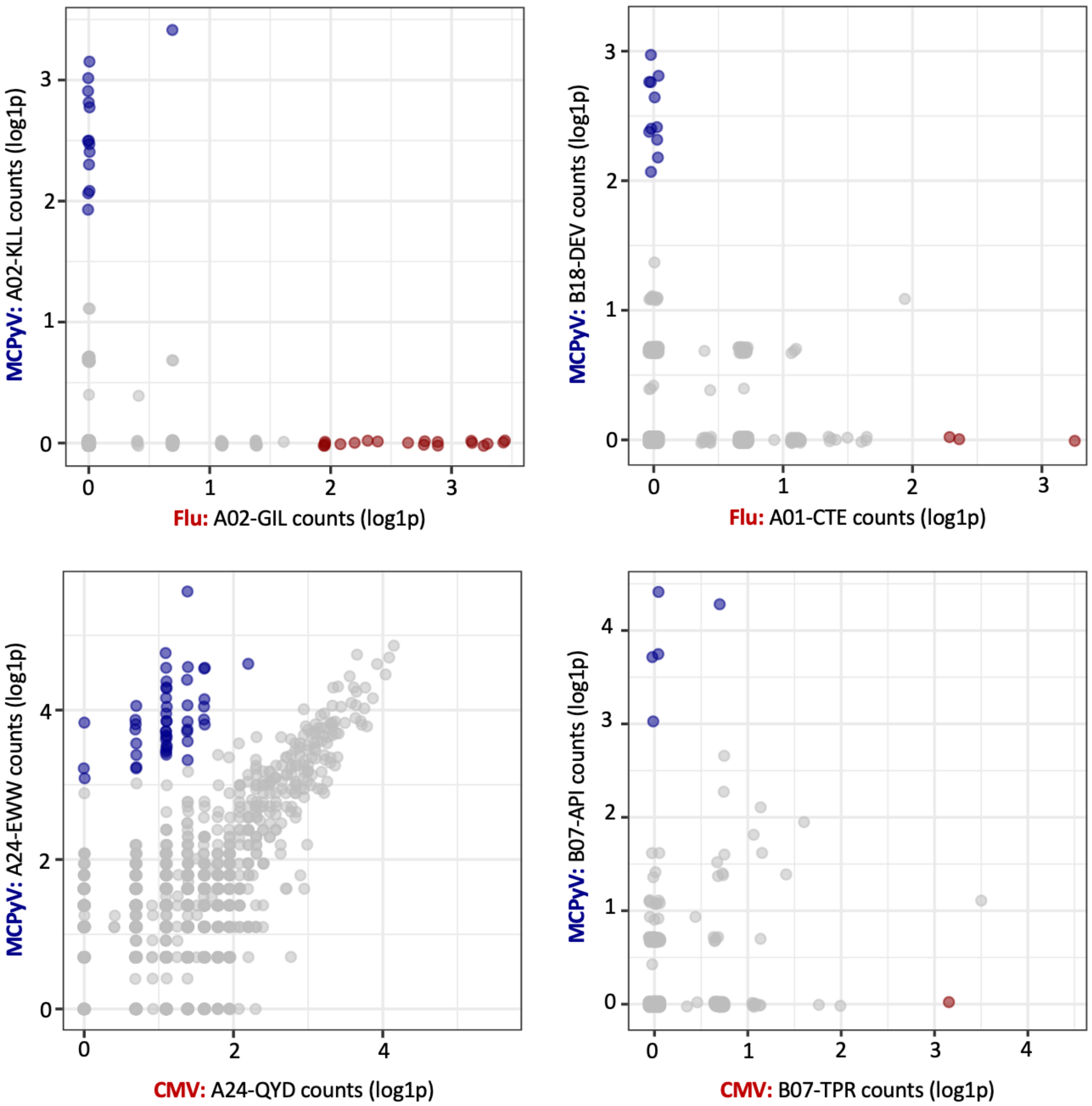

Supplementary Figure 1. Example dot plots assigning tetramer-specificity.
All cells in blue are assigned to the multimer reagent on the y-axis and all cells in red are assigned to the multimer reagent on the x-axis.

Supplementary Table 1. Patients involved in the training cohort

Patient	Publication ID	Viral Status	Best Overall Response	Progression-Free Survival	Overall Survival	HLA Alleles
109-02-003	3	Positive	CR	54.7	56.8	A*01:01, A*24:02, B*08:01, B*44:02
109-02-004	4	Positive	CR	34.5	56.6	A*11:01, A*26:01, B*27:05, B*50:01
109-02-007	6	Positive	CR	50.0	55.8	A*02:01, A*03:01, B*07:02, B*44:02
109-02-010	21	Positive	CR	25.1	50.2	A*01:01, A*24:02, B*07:02, B*35:02
109-05-005	33	Positive	PD	2.8	8.0	A*02:01, B*07:02, B*15:01
109-05-006	38	Positive	PD	2.8	26.8	A*24:02, A*30:02, B*44:02, B*49:01
109-07-001	26	Positive	PR	38.4	46.2	A*01:01, A*68:02, B*53:01, B*57:02
109-10-001	45	Positive	CR	14.1	30.9	A*24:02, A*68:01, B*35:03, B*35:03
109-15-001	46	Positive	CR	29.5	30.9	A*24:02, A*31:01, B*07:02, B*35:01
109-17-009	39	Positive	PD	1.6	19.3	A*02:05, A*32:01, B*44:02, B*50:01
109-17-010	44	Positive	CR	23.4	31.6	A*03:01, A*11:01, B*07:02, B*52:01
109-18-001	8	Positive	PR	8.6	8.6	A*03:01, B*07:02
109-18-003	41	Positive	PD	2.1	3.2	A*02:01, A*26:01, B*39:01, B*45:01
109-21-003	28	Positive	PR	16.8	41.8	A*01:01, A*32:01, B*08:01, B*49:01
109-21-004	47	Positive	PR	9.7	9.7	A*11:01, A*24:02, B*13:01, B*18:01
109-65-001	40	Positive	SD	5.9	16.6	A*01:01, A*03:01, B*35:01, B*57:01
109-65-004	49	Positive	PR	30.2	30.2	A*01:01, A*66:01, B*35:02, B*38:01

Supplementary Table 2. Panel of HLA-restricted MCPyV oncoprotein-specific multimers

			Frequency of multimer-binding cells per patient pre-treatment																
Virus	**HLA**	**Peptide**	**109-02-003**	**109-02-004**	**109-02-007**	**109-02-010**	**109-05-005**	**109-05-006**	**109-07-001**	**109-10-001**	**109-15-001**	**109-17-009**	**109-17-010**	**109-18-001**	**109-18-003**	**109-21-003**	**109-21-004**	**109-65-001**	**109-65-004**
CMV	A0101	VTEHDTLLY	0	0.00417246	0.00864553	0.00307692	0	0	0.24554184	0	0	0.02631579	0	0	0	0.00862069	0	0.01754386	0.04845815
CMV	A0201	NLVPMVATV	0	0	0	0	0	0	0	0	0	0	0	0	0	0	0	0	0
CMV	A0301	KLGGALQAK	0	0	0	0	0	0	0	0	0	0	0	0.00438596	0	0	0	0	0
CMV	A2402	QYDPVAALF	0	0	0	0	0	0	0	0	0	0	0	0	0	0	0	0	0
CMV	B0701	RPHERNGFTVL	0	0	0	0.00769231	0	0	0	0	0	0	0	0	0	0	0	0	0
CMV	B0701	TPRVTGGGAM	0	0	0.00288184	0.20923077	0	0	0	0	0	0	0	0.0372807	0	0	0	0	0.00440529
CMV	B0801	ELRRKMMYM	0	0	0	0	0	0	0	0	0	0	0	0	0	0	0	0	0
CMV	B3501	IPSINVHHY	0	0	0	0	0	0	0	0	0	0	0	0	0	0	0	0.03508772	0
EBV	A0201	GLCTLVAML	0	0.00139082	0.04899135	0	0.00330033	0	0.00274348	0	0.03703704	0	0	0	0.00900901	0	0	0	0
EBV	A0301	RLRAEAQVK	0	0	0	0	0	0	0	0	0	0	0	0	0	0	0	0	0
EBV	B0701	RPPIFIRRL	0	0	0.00864553	0	0.06270627	0	0.00137174	0	0	0	0	0	0	0	0	0	0
EBV	B0801	FLRGRAYGL	0.00131234	0	0	0	0	0	0	0	0	0	0	0	0	0	0	0	0
EBV	B3501	HPVGEADYFEY	0	0	0	0	0	0	0	0	0	0	0	0	0	0	0	0	0
Flu	A0101	CTELKLSDY	0	0	0	0.00307692	0	0	0	0	0	0	0	0	0	0	0	0	0
Flu	A0201	GILGFVFTL	0	0	0.03170029	0	0.01650165	0	0.00548697	0	0	0.01315789	0	0	0.04504505	0	0	0	0
Flu	A0301	ILRGSVAHK	0	0	0	0	0	0	0	0	0	0	0	0	0	0	0	0	0
Flu	A2402	SYINRTGTF	0	0	0	0	0	0	0	0	0	0	0	0	0	0	0	0	0
MCPyV	A0201	KLLEIAPNC	0	0	0.00576369	0	0.00660066	0	0.00137174	0	0	0.01315789	0	0	0	0	0	0	0
MCPyV	A0301	AAFKRSCLK	0	0	0.00576369	0	0.00330033	0	0.00274348	0	0	0	0	0	0	0	0	0	0
MCPyV	A0301	RSGGFSFGK	0	0	0	0	0	0	0.00137174	0	0	0	0	0.07675439	0	0	0	0	0
MCPyV	A1101	RSGGFSFGK	0	0.00556328	0	0	0	0	0	0	0	0	0.00135685	0	0.00900901	0	0.1815562	0	0
MCPyV	A2402	DYCLLHLHLF	0	0	0	0	0	0	0	0	0	0	0	0	0	0	0	0	0
MCPyV	A2402	EWWRSGGFSF	0.39370079	0	0	0.00153846	0	0.20245399	0	0.08888889	0.37037037	0	0.06377205	0.07675439	0.17117117	0	0.11815562	0.11111111	0.13656388
MCPyV	A2402	KFQQNIHKL	0	0	0	0	0	0	0	0	0	0	0	0	0	0	0	0	0
MCPyV	A2402	RTYGTWEDLF	0	0	0	0	0	0	0	0	0	0	0	0	0	0	0	0	0
MCPyV	A6801	STPNGTSVPR	0	0	0	0	0	0	0	0	0	0	0	0	0	0	0	0	0
MCPyV	B0702	APIYGTTKF	0	0.00139082	0.01729107	0	0	0	0.00274348	0	0	0.01315789	0	0.00219298	0	0	0	0	0
MCPyV	B0702	APNCYGNIPL	0	0	0	0	0.00330033	0	0	0	0	0	0	0.00219298	0	0	0	0	0
MCPyV	B0702	HPDKGGNPV	0	0	0	0	0	0	0	0	0	0	0	0	0	0	0	0	0
MCPyV	B0801	LNRKEREAL	0.00131234	0	0	0	0	0	0	0	0	0	0	0	0	0	0	0	0
MCPyV	B1501	FSFGKAYEY	0	0	0	0	0.00330033	0	0	0	0	0	0	0	0	0	0	0	0
MCPyV	B1801	DEVDEAPIY	0	0	0	0	0	0	0	0	0	0	0	0	0	0	0.01152738	0	0
MCPyV	B3501	FSFGKAYEY	0	0	0	0	0	0	0	0	0	0	0.00135685	0.00438596	0.00900901	0	0	0	0
MCPyV	B3502	HPDKGGNPVIM	0	0	0	0	0	0	0	0	0	0	0	0	0	0	0	0	0
MCPyV	B4402	KEWWRSGGF	0.00262467	0	0	0	0	0.00613497	0	0	0	0	0	0	0	0	0	0	0
MCPyV	B5701	FSFGKAYEY	0	0	0	0	0	0	0	0	0	0	0	0	0	0	0	0	0
MCPyV	B5701	GTTKFKEWW	0.60104987	0.98748261	0.870317	0.77538462	0.9009901	0.79141104	0.73662551	0.91111111	0.59259259	0.93421053	0.93351425	0.79605263	0.75675676	0.99137931	0.68876081	0.83625731	0.81057269

Supplementary Table 3 not shown for length.

Supplementary Table 4. ROC metrics for gene lists when one gene was iteratively removed.

Gene removed	Area Under the Curve (AUC)	Specificity	Sensitivity
None	0.932270705	0.90981062	0.82727273
HLA-DRA	0.931712342	0.90142813	0.83030303
CD74	0.931478084	0.90670599	0.82727273
GZMK	0.930783071	0.90204905	0.82727273
HLA-DRB1	0.931468911	0.90717169	0.82727273
COTL1	0.930727564	0.90298044	0.82727273
CDCA7	0.932252124	0.90981062	0.82727273
HLA-DRB5	0.9318457	0.91136293	0.82121212
PCLAF	0.932311159	0.90981062	0.82727273
HLA-DMA	0.932182035	0.9057746	0.82727273
CD27	0.931205724	0.89739211	0.83333333
FABP5	0.93211806	0.90655076	0.82727273
GZMA	0.932857291	0.91074201	0.82727273
GAPDH	0.9323248	0.90950016	0.82727273
CORO1A	0.932362197	0.90779261	0.82727273
TNFRSF9	0.931844994	0.90981062	0.82727273
ANXA5	0.932208612	0.90887923	0.82727273
PFN1	0.932755214	0.90965539	0.82727273
HLA-DPA1	0.931816771	0.90515368	0.82727273
TYMS	0.932319626	0.90981062	0.82727273
DUSP4	0.931228068	0.90981062	0.82424242
HLA-DPB1	0.931830647	0.89025147	0.84545455
HLA-DQA1	0.931914613	0.91058677	0.82424242
UCP2	0.93231845	0.88916486	0.84545455
ACTB	0.932352554	0.90981062	0.82727273
PPP1CA	0.932574111	0.90391183	0.83333333
LIME1	0.931968709	0.90592984	0.82727273
MXD4	0.931941661	0.90655076	0.82727273
ARHGDIB	0.932405003	0.90918969	0.82727273
SIRPG	0.932192854	0.91012108	0.82727273
CFL1	0.932792141	0.90950016	0.82727273
TMSB10	0.932317509	0.90981062	0.82727273
PSME2	0.932615506	0.908724	0.82727273
TALDO1	0.932437461	0.90655076	0.82727273
SH3BGRL3	0.932611508	0.90950016	0.82727273
H3F3A	0.932126763	0.908724	0.82727273
CNN2	0.931891799	0.90887923	0.82424242
CCDC167	0.932307631	0.91012108	0.82727273
YWHAB	0.931793721	0.90453275	0.83030303
ARPC1B	0.932689359	0.90360137	0.83333333
PSME1	0.932571524	0.90856877	0.82727273

ACTG1	0.932627972	0.90934492	0.82727273
MIR4435-2HG	0.932305749	0.90934492	0.82727273
ATP5MF	0.932281994	0.90717169	0.82727273
ARPC3	0.932628207	0.90701645	0.82727273
UBE2L6	0.932218961	0.90608507	0.82727273
TMSB4X	0.932257298	0.90981062	0.82727273
DBI	0.932415117	0.90934492	0.82424242
CLIC1	0.932334208	0.89490841	0.83939394
AP2S1	0.932366666	0.90592984	0.82727273
LSP1	0.932675247	0.90887923	0.82727273
MYL6	0.932219666	0.90918969	0.82727273
ISG15	0.932172627	0.9057746	0.82727273
PARK7	0.932039974	0.90950016	0.82424242
FKBP1A	0.932275409	0.90779261	0.82727273
ITM2A	0.931485846	0.90841354	0.82424242
HMGB2	0.931968709	0.90437752	0.82727273
PSMB10	0.93237725	0.91058677	0.82424242
LIMS1	0.932090307	0.90732692	0.82727273
AC092821.3	0.931544881	0.90996585	0.82424242
TWF2	0.932167217	0.90592984	0.82727273
CCL5	0.931836998	0.90903446	0.82727273
PPIA	0.932305279	0.90856877	0.82727273
PSMB9	0.932540007	0.90561937	0.82727273
IDH2	0.932544241	0.89987581	0.83333333
ARPC2	0.932296341	0.91058677	0.82727273
TIGIT	0.932072902	0.90950016	0.82727273
CAPZB	0.932281759	0.90779261	0.82727273
GMFG	0.932155927	0.88745731	0.84848485
RAC2	0.932632205	0.90608507	0.83030303
COX5A	0.932317274	0.91213909	0.82121212
PSMB3	0.932262002	0.89754735	0.83333333
HLA-DQB1	0.931900972	0.91074201	0.82121212
PYCARD	0.932287639	0.90981062	0.82424242
LIMD2	0.93141364	0.89459795	0.83939394
SIT1	0.932111945	0.90934492	0.82727273
CD3D	0.932068904	0.90763738	0.82727273
JPT1	0.932096422	0.90499845	0.82727273
NDUFA13	0.932199439	0.90515368	0.82727273
PPP1R18	0.932559058	0.91136293	0.82424242
CD52	0.932108182	0.9082583	0.82727273
POLR2G	0.932296812	0.90763738	0.82727273
MT1E	0.932346203	0.91089724	0.82424242
OAZ1	0.932249066	0.90670599	0.82727273

ANXA2	0.93230669	0.90142813	0.83333333
ATP5F1C	0.932191913	0.91043154	0.82424242
TOX	0.932003283	0.91043154	0.82727273
IL2RG	0.932457453	0.90887923	0.82727273
HMGB1	0.931895092	0.90701645	0.82727273
TRAPPC1	0.932413941	0.90530891	0.82727273
LCP1	0.932580932	0.91058677	0.82727273
LSM2	0.932281053	0.91058677	0.82727273
LYST	0.931643664	0.91136293	0.82424242
MPG	0.932300575	0.90670599	0.82727273
COPE	0.932275879	0.90142813	0.83333333
ATP5F1B	0.932373486	0.90468799	0.82727273
SH2D1A	0.932337031	0.91105247	0.82424242
S1PR4	0.932115708	0.91058677	0.82727273
ATP5MC2	0.932221313	0.9082583	0.82727273
ABRACL	0.932274468	0.90887923	0.82727273
CSK	0.932111945	0.9012729	0.83030303
ENO1	0.932374898	0.91198386	0.82727273
NDUFA7	0.932208142	0.91089724	0.82424242
NDUFB9	0.932180623	0.90732692	0.82727273
LAG3	0.932193795	0.90981062	0.82424242
PSMB8	0.932350202	0.90981062	0.82727273
APOBEC3G	0.932494144	0.91136293	0.82424242
EID1	0.931837939	0.90732692	0.82424242
PSMD8	0.932116414	0.91105247	0.82727273
IFI27L2	0.932508255	0.89972058	0.83333333
TAP1	0.932281994	0.90810307	0.82424242
CALM3	0.93223613	0.90034151	0.83333333
COX6C	0.932284816	0.91260478	0.82121212
CYTOR	0.931705051	0.90639553	0.82727273
PTTG1	0.932099715	0.91012108	0.82727273
GBP5	0.932374898	0.91151816	0.82121212
ARPC4	0.932452513	0.91244955	0.82727273
COX8A	0.932629148	0.90282521	0.83333333
ITGB1	0.932338912	0.91213909	0.82424242
ITGA4	0.931623672	0.90701645	0.82727273
LCK	0.932280583	0.90266998	0.83333333
WDR1	0.932131467	0.90934492	0.82727273
PSMA5	0.932125587	0.91074201	0.82727273
SLC25A5	0.93215287	0.9062403	0.82727273
BLOC1S1	0.932582343	0.90111767	0.83333333
CD99	0.932183211	0.90918969	0.82727273
CRIP1	0.932843179	0.90732692	0.83030303

PSMB2	0.932168393	0.91012108	0.82424242
MT1F	0.932422408	0.90950016	0.82727273
ATP5MC3	0.931982586	0.90856877	0.82424242
COX6B1	0.932455101	0.90686122	0.82727273
ATP5MG	0.93227094	0.90763738	0.82727273
PTPRCAP	0.932157809	0.90701645	0.82727273
COX6A1	0.932323389	0.90530891	0.83030303
NDUFA11	0.932619505	0.9057746	0.82727273
PRDX1	0.932165571	0.908724	0.82424242
MYL12B	0.932548239	0.8963055	0.83939394
STMN1	0.93238995	0.91058677	0.82727273
ATP5IF1	0.932220607	0.89025147	0.84242424
LY6E	0.932879399	0.90406706	0.83333333
NDUFC2	0.932535303	0.9062403	0.82727273
PSMA4	0.932000931	0.91167339	0.82121212
BRK1	0.932643495	0.91089724	0.82727273
NDUFB10	0.932359139	0.91151816	0.82727273
TSPO	0.932104889	0.90918969	0.82727273
WAS	0.932293048	0.88869916	0.84545455
ELOB	0.932268117	0.90810307	0.82727273
PLAAT4	0.932355376	0.90981062	0.82424242
ANXA6	0.932588223	0.9012729	0.83333333
CD81	0.932259885	0.90499845	0.83030303
C12orf75	0.93291021	0.9136914	0.82121212
GNAI2	0.932568466	0.90391183	0.83333333
CDC25B	0.932121353	0.89925489	0.83333333
MCUB	0.931453859	0.9032909	0.82727273
UQCR10	0.931913437	0.91058677	0.82121212
FAM160B1	0.931898385	0.90655076	0.82727273
OCIAD2	0.932000696	0.90686122	0.82727273
CLDND1	0.931682472	0.90810307	0.82424242
REEP5	0.932218961	0.90810307	0.82727273
EVL	0.932155457	0.90422229	0.82727273
PPP4C	0.932276114	0.88761254	0.84545455
SELL	0.931955773	0.91089724	0.82121212
H2AFY	0.932307631	0.90950016	0.82727273
MDH2	0.932316333	0.90608507	0.82727273
FLNA	0.932183681	0.90282521	0.83333333
ARF5	0.932394184	0.90965539	0.82424242
SLC9A3R1	0.932278231	0.90763738	0.82727273
CLTA	0.932244362	0.91089724	0.82727273
HMGN2	0.932344322	0.88574977	0.84848485
PKM	0.932430169	0.90918969	0.82424242

SUMO2	0.932133584	0.90779261	0.82727273
CD2	0.932219666	0.9112077	0.82424242
TXN	0.932629853	0.90748215	0.82727273
EMB	0.932116414	0.90748215	0.82727273
COX5B	0.932110769	0.90515368	0.82727273
CACYBP	0.931900031	0.90592984	0.82727273
HSPA8	0.932443811	0.9037566	0.83333333
GNG5	0.932490145	0.90779261	0.82727273
ARPC5	0.932419115	0.90887923	0.82727273
ATP5PB	0.93244875	0.88854393	0.84242424
KRT10	0.932499083	0.89909966	0.83333333
SUB1	0.932416998	0.90391183	0.83030303
ATP5F1D	0.932518604	0.90763738	0.82727273
CD3G	0.932595749	0.90391183	0.83030303
MAP2K2	0.932301516	0.90732692	0.82727273
H2AFV	0.93182806	0.91136293	0.82424242
CAP1	0.932539772	0.90856877	0.82727273
BIN1	0.932271175	0.90856877	0.82424242
TMEM14B	0.932080429	0.90887923	0.82424242
SEM1	0.932595514	0.90841354	0.82727273
PGAM1	0.932258945	0.90981062	0.82424242
NDUFA12	0.932416763	0.90701645	0.82727273
HIGD2A	0.931713989	0.89118286	0.84242424
EIF4A1	0.932008693	0.90608507	0.82727273
CLEC2B	0.932098069	0.9062403	0.82727273
CSNK2B	0.932284816	0.91105247	0.82727273
S100A4	0.932718759	0.90981062	0.82727273
HNRNPA2B1	0.932509196	0.90732692	0.82727273
IL32	0.932874695	0.91012108	0.82727273
ZYX	0.932150518	0.91027631	0.82727273
DUT	0.932385482	0.90686122	0.82727273
GSTK1	0.932173803	0.90608507	0.82727273
DEK	0.932404768	0.91167339	0.82424242
NME2	0.932407355	0.90546414	0.83030303
MYL12A	0.932615977	0.9082583	0.83030303
LGALS1	0.933018402	0.91213909	0.82727273
TPI1	0.932623268	0.90251475	0.83030303
RNF213	0.931849698	0.8987892	0.83333333
TUBB	0.932552002	0.91198386	0.82121212

Supplementary Table 5. List of genes in the transcriptional signature of tumor-specific CD8 T cells

HLA-DRA
CD74
GZMK
HLA-DRB1
COTL1
CDCA7
HLA-DRB5
HLA-DMA
CD27
FABP5
TNFRSF9
ANXA5
HLA-DPA1
DUSP4
HLA-DPB1
HLA-DQA1
LIME1
MXD4
SIRPG
H3F3A
CNN2
YWHAB
UBE2L6
TMSB4X
MYL6
ISG15
PARK7
ITM2A
HMGB2
LIMS1
AC092821.3
TWF2
CCL5
TIGIT
GMFG
PSMB3
HLA-DQB1
LIMD2
SIT1
CD3D
JPT1
NDUFA13
CD52
OAZ1
ATP5F1C
TOX
HMGB1
LYST
S1PR4
ATP5MC2
CSK
NDUFA7
NDUFB9
LAG3
EID1
PSMD8
CALM3
CYTOR
PTTG1
ITGA4
WDR1
PSMA5
SLC25A5
CD99
PSMB2
ATP5MC3
PTPRCAP
PRDX1
ATP5IF1
PSMA4
TSPO
ELOB
CD81
CDC25B
MCUB
UQCR10
FAM160B1
OCIAD2
CLDND1
REEP5
EVL
SELL
FLNA
CLTA
SUMO2
CD2
EMB
COX5B
CACYBP
H2AFV
TMEM14B
PGAM1
HIGD2A
EIF4A1
CLEC2B
ZYX
GSTK1
RNF213

Chapter 5: Progress towards development of a Merkel polyomavirus-specific T cell receptor analysis tool to guide cancer immunotherapy

Saumya Jani

CHAPTER SUMMARY: In this chapter, we explore a T-cell receptor (TCR) sequence-based approach to identify Merkel cell polyomavirus oncoprotein-specific CD8 T cells. This is based on the premise that TCRs that target the same epitopes have structural similarities. We find that tcrdist3, a computational tool that can assign scores quantifying how similar two TCRs are, clusters TCRs that recognize the same epitope together. Training this tool with additional TCR sequences may allow identification of MCC-specific TCRs via commercially-available bulk TCR sequencing, a method compatible with clinical use.

Progress towards development of a Merkel polyomavirus-specific T cell receptor analysis tool to guide cancer immunotherapy

Saumya Jani

Merkel cell carcinoma (**MCC**) is a rare but aggressive neuroendocrine skin cancer. The incidence of MCC in the United States is increasing and is expected to exceed 3,200 cases/year by 2025.[1] MCC typically occurs in older and immunocompromised individuals, which suggests an infectious etiology.[2] While a minority of MCC tumors develop as a result of UV-mediated mutations, 80% of MCC cases indeed arise from clonal integration of the Merkel cell polyomavirus (**MCPyV**) and truncation of its large T-antigen.[2,3] The truncated large T-antigen prevents the virus from replicating, but retains its ability to bind to retinoblastoma-associated protein and promote cell cycle progression.[4] Meanwhile, the small T-antigen inhibits p53 and activates *myc* signaling.[4] Thus, persistent MCPyV oncoprotein expression is necessary for proliferation and survival of virally-driven MCC tumor cells.[4] In addition, virus-positive MCC tumors (**VP-MCC**) have an extraordinarily low tumor mutational burden (13 compared to ~1,121 mutations in virus-negative MCC).[4] Thus, the CD8 T cell response to VP-MCC is composed almost entirely of T-antigen-specific T cells. This makes VP-MCC an attractive test case for tumor immunology and the detailed study of tumor antigen-specific T cell immunity. We have recently observed that the frequency of MCPyV-specific CD8 T cells in patients with VP-MCC can predict response to PD-(L)1 pathway blockade (**see Chapters 2 and 3**). To translate this finding to patients, we explored a bulk TCR sequencing-based approach to quantify tumor-specific CD8 T cells.

CD8 T cells recognize foreign and mutated proteins that are presented on class I human leukocyte antigen (**HLA**) molecules through their T cell receptor (**TCR**). Because the potential range of non-self-antigens is so vast, TCRs also need to be very diverse. TCR diversity is achieved through recombination between V, D, and J gene segments and random insertions and deletions at their junctions, as well as combinatorial αβ chain pairings.[5-10] The measured complexity per person, estimated at $10^8 – 10^9$ unique clonotypes, is lower than the mathematical theoretical level allowed by the above[11]. This may be because of convergent recombination (i.e., some rearrangements are more probable than others) or convergent selection (i.e., high-affinity TCRs proliferate and are selected for after antigen exposure), modulated by thymic positive and negative selection during creation of the naïve repertoire prior to antigen exposure.[12] Along the same lines, it is now recognized that TCRs that recognize the same HLA-restricted epitope in multiple patients have similarities in their TCR sequence (**Figure 1**).

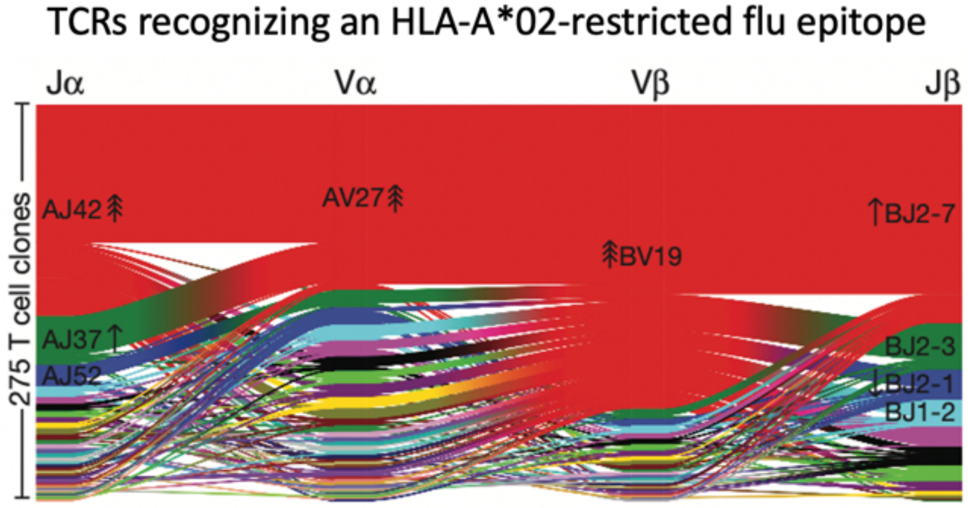

Figure 1. Certain gene segments are overrepresented in epitope-specific repertoires. Analysis of gene usage of 275 flu-specific T cells clones (organized in 4 segments with the most frequent gene segment at the top and in red) reveals that one V and J gene segment in each TCR chain is enriched. Adapted from *Dash et. al.*[13]

The term **“meta-clonotype”** is applied to a group of sequence-similar TCRs recognizing the same peptide-HLA ligand. TCR sequence similarities can be recognized by bioinformatic algorithms, allowing estimation of the likelihood of a previously unseen TCR sequence to bind to a particular HLA/epitope combination.[13-19] Highly sensitive and specific classifiers trained with "**public**" TCRs (TCRs that have the exact same amino acid sequence and are found in multiple individuals) are available to diagnose CMV,[20] SARS-CoV-2,[21] or *Borrelia burgdorferi*[22] infection by sequencing TCR repertoires from patient blood. While exact matching of sequences may be sufficient for detecting prior infection, identifying cancer-specific T cells may require a more detailed assessment of TCR repertoires. This may be possible with the use of algorithms that incorporate the power of TCR cluster analyses to measure the breadth of cancer-specific T cells more fully.

In comparison to previously developed classifiers, we additionally modify our methods in two important ways:

1. <u>Analyzing antigen-specific TCR repertoires with well-validated tumor virus-specific cells using HLA-peptide oligomers</u>: Most current TCR analytical tools[20-22] were developed using antigen-specific T cells identified either through statistical enrichment (i.e., TCRs present in higher numbers in persons with infection compared to healthy individuals) or antigen-specific wet-lab assays (i.e., stimulation of blood with pathogen-specific antigens and TCR sequencing of cells expressing activation markers as a surrogate for pathogen specificity). Both methods lack precision. The statistical method lacks direct demonstration of T cell recognition. Activation methods are susceptible to bystander activation *in vitro* and could fail to detect exhausted T cells that are unresponsive to stimulation. Incorrect TCR inputs introduces bias. In contrast, we used peptide-HLA multimers to identify tumor-specific T cells that identify shared TCR sequence motifs. These tools are typically tetramers of HLA class I-β2M tightly associated with the viral peptide of interest and an identifying molecule(s) such as a fluorescent protein and/or a DNA oligonucleotide to sort and identify cells that bind the tetramer. T cells expressing TCRs that recognize this HLA/epitope combination bind the tetramer. This identifies virus-specific T cells with great specificity and independent of the cell's functional status, though not free of errors[23].

2. <u>Use of both paired TCR α-β and single-chain TCR sequencing</u>: Most previous TCR-based tools have used TCRβ chain sequencing. It is economical, commercially available, and some literature indicates that the TCRβ chain accounts for most of the binding to peptide-HLA. However, both the α and β TCR chains are involved in antigen recognition at the structural level.[24] Each TCR chain possesses three variable regions that bind peptide-HLA, termed complementarity determining regions (**CDRs**).[24] Particularly, the third CDR (**CDR3**) of each chain is heavily involved in antigen binding (**Figure 2**).[24] Indeed, recent comparisons show that the accuracy of bioinformatic tools is enhanced when paired α-β TCR sequences are used (**Figure 3**).[25] Thus, we used paired α-β TCR sequences to identify conserved motifs in antigen-specific repertoires.

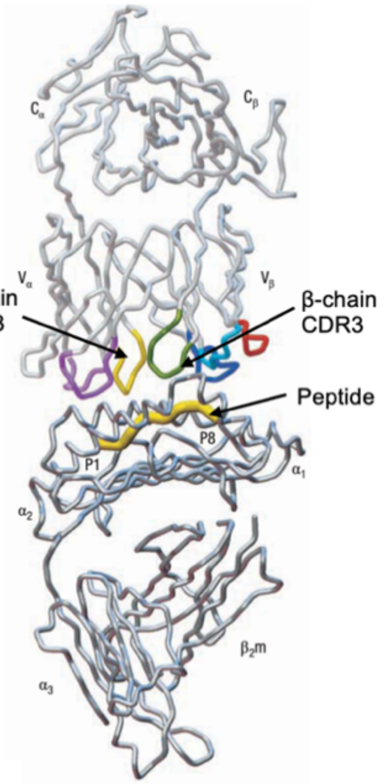

Figure 2. CDR3 of both chains are involved in antigen recognition. The TCR is shown oriented downward, with the α chain CDR3 in yellow and the β chain CDR3 in green. The peptide-HLA complex is shown oriented upwards, with the peptide in yellow. Adapted from *Murphy et. al.*[24]

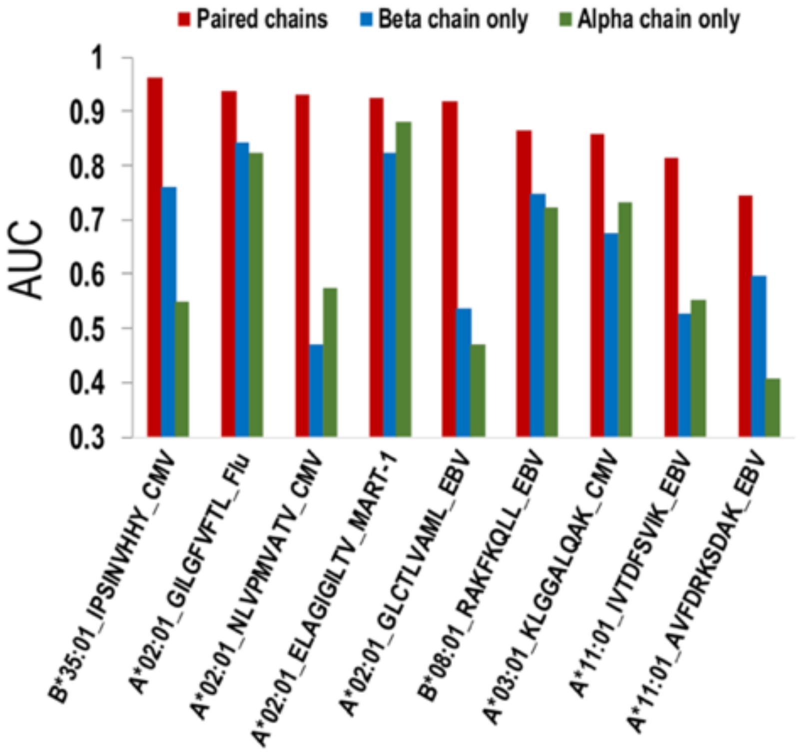

Figure 3. Training a model with α-β paired chain data improves predictive capacity. Tetramer-identified TCRs for multiple HLA/epitope combinations were used to train a predictor. The validation step derived area under the curve (AUC) from receiver operating characteristic curves generated from the true positive and false positive rates of predictor developed using either paired chain, α chain, or β chain data for each of the listed epitopes. As published in *Zhang et al.*[25]

We applied tcrdist3 to datasets generated by N. Miller and T. Pulliam, previous MD/PhD students in the Nghiem lab. The first dataset consisted of 400 TCRβ sequences from T cells that bound to HLA-A*02:01 complexed with the MCPyV peptide KLLEIAPNC (**A02-KLL**) from 12 VP-MCC patients.[26] Previously, we found only one true public TCRβ, shared by 2 patients.[26] Our re-analysis with tcrdist3 identified 19 meta-clonotypes, each of which was shared by anywhere from 2 to 5 patients (3 meta-clonotypes were shared by 5 patients, 3 by 4 patients, 2 by 3 patients, 11 by 2 patients. Overall, 10 of the 12 patients had at least one TCR in one of these newly identified meta-clonotypes. The second dataset consisted of paired α-β TCR sequences from 3 VP-MCC patients that recognized either HLA-B*35:01-HPDKGGNPVIM or HLA-B*37:01-KEWWRSGGF. These TCRs were identified using oligonucleotide-labeled tetramers and 10x Genomics' single cell TCR sequencing workflow. Using tcrdist3, I observed that the TCRs recognizing the distinct epitopes clustered separately in a network plot (**Figure 4**).

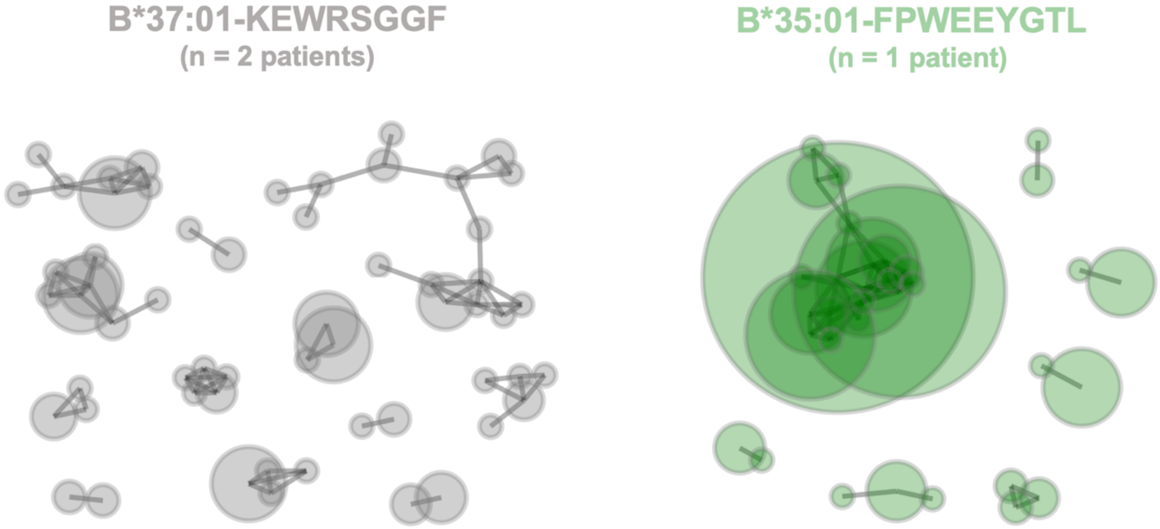

Figure 4. tcrdist3 can successfully group TCRs recognizing different epitopes separately. TCRs specific for a B*37:01 (gray) and a B*35:01 (green) epitope are shown. TCR network formed using a paired α-β multi-CDR TCR distance metric (TCRdist). Edges connect individual clones if their pairwise distance is less than or equal to 150 TCRdist units. Size of nodes are scaled to the counts of each clone. The visualization is spring weighted such that nodes with less sequence divergence are closer together.

Finally, to test whether I could detect MCPyV-specific CD8 T cells using tcrdist3, I trained a computational tool with the two datasets containing tetramer-identified TCRs and applied it to a third dataset (**CITN-09**/KEYNOTE-017 trial NCT02267603).[27,28] In this case, bulk TCRβ chain sequences were obtained from 43 tumor specimens pre-treatment. I used the tcrdist3-based tool to identify MCPyV-specific CD8 T cells in the bulk tissue TCRβ datasets and was able to detect highly-similar TCRs in virally-driven tumors from patients expressing the relevant HLA alleles. However, very few TCRs highly similar to known MCPyV-specific TCRs were identified, suggesting a need for an expanded training set that covers a majority of HLA types and includes more TCRs from more patients.

Further refinement of this tool could yield a clinically implementable way to quantify antigen-specific CD8 T cells, allowing us to stratify patients with detectable amounts of tumor-specific T cells for immunotherapy and those without to interventions that increase the number of CD8 T cells. It could also be used to track changes in tumor-specific T cells over time and in response to different interventions. In **Chapters 6 and 7**, we use these tools to track COVID-specific T cell expansion in response to mRNA vaccination.

References

1. Paulson, K.G., Park, S.Y., Vandeven, N.A., Lachance, K., Thomas, H., Chapuis, A.G., Harms, K.L., Thompson, J.A., Bhatia, S., Stang, A., and Nghiem, P. (2018). Merkel cell carcinoma: Current US incidence and projected increases based on changing demographics. J Am Acad Dermatol *78*, 457-463.e452. 10.1016/j.jaad.2017.10.028.
2. Feng, H., Shuda, M., Chang, Y., and Moore, P.S. (2008). Clonal integration of a polyomavirus in human Merkel cell carcinoma. Science *319*, 1096-1100. 10.1126/science.1152586.
3. Shuda, M., Feng, H., Kwun, H.J., Rosen, S.T., Gjoerup, O., Moore, P.S., and Chang, Y. (2008). T antigen mutations are a human tumor-specific signature for Merkel cell polyomavirus. Proc Natl Acad Sci U S A *105*, 16272-16277. 10.1073/pnas.0806526105.
4. Harms, P.W., Harms, K.L., Moore, P.S., DeCaprio, J.A., Nghiem, P., Wong, M.K.K., Brownell, I., and Group, I.W.o.M.C.C.R.I.W. (2018). The biology and treatment of Merkel cell carcinoma: current understanding and research priorities. Nat Rev Clin Oncol *15*, 763-776. 10.1038/s41571-018-0103-2.
5. Lythe, G., Callard, R.E., Hoare, R.L., and Molina-París, C. (2016). How many TCR clonotypes does a body maintain? J Theor Biol *389*, 214-224. 10.1016/j.jtbi.2015.10.016.
6. Krangel, M.S. (2009). Mechanics of T cell receptor gene rearrangement. Curr Opin Immunol *21*, 133-139. 10.1016/j.coi.2009.03.009.
7. Mahe, E., Pugh, T., and Kamel-Reid, S. (2018). T cell clonality assessment: past, present and future. J Clin Pathol *71*, 195-200. 10.1136/jclinpath-2017-204761.
8. Gascoigne, N.R., Rybakin, V., Acuto, O., and Brzostek, J. (2016). TCR Signal Strength and T Cell Development. Annu Rev Cell Dev Biol *32*, 327-348. 10.1146/annurev-cellbio-111315-125324.
9. Jung, D., and Alt, F.W. (2004). Unraveling V(D)J recombination; insights into gene regulation. Cell *116*, 299-311. 10.1016/s0092-8674(04)00039-x.
10. Jackson, K.J., Kidd, M.J., Wang, Y., and Collins, A.M. (2013). The shape of the lymphocyte receptor repertoire: lessons from the B cell receptor. Front Immunol *4*, 263. 10.3389/fimmu.2013.00263.
11. Bradley, P., and Thomas, P.G. (2019). Using T Cell Receptor Repertoires to Understand the Principles of Adaptive Immune Recognition. Annu Rev Immunol *37*, 547-570. 10.1146/annurev-immunol-042718-041757.
12. Johnson, S.A., Seale, S.L., Gittelman, R.M., Rytlewski, J.A., Robins, H.S., and Fields, P.A. (2021). Impact of HLA type, age and chronic viral infection on peripheral T-cell receptor sharing between unrelated individuals. PLoS One *16*, e0249484. 10.1371/journal.pone.0249484.
13. Dash, P., Fiore-Gartland, A.J., Hertz, T., Wang, G.C., Sharma, S., Souquette, A., Crawford, J.C., Clemens, E.B., Nguyen, T.H.O., Kedzierska, K., et al. (2017). Quantifiable predictive features define epitope-specific T cell receptor repertoires. Nature *547*, 89-93. 10.1038/nature22383.
14. Pogorelyy, M.V., Minervina, A.A., Shugay, M., Chudakov, D.M., Lebedev, Y.B., Mora, T., and Walczak, A.M. (2019). Detecting T cell receptors involved in immune responses from single repertoire snapshots. PLoS Biol *17*, e3000314. 10.1371/journal.pbio.3000314.
15. Glanville, J., Huang, H., Nau, A., Hatton, O., Wagar, L.E., Rubelt, F., Ji, X., Han, A., Krams, S.M., Pettus, C., et al. (2017). Identifying specificity groups in the T cell receptor repertoire. Nature *547*, 94-98. 10.1038/nature22976.
16. Lanzarotti, E., Marcatili, P., and Nielsen, M. (2019). T-Cell Receptor Cognate Target Prediction Based on Paired alpha and beta Chain Sequence and Structural CDR Loop Similarities. Front Immunol *10*, 2080. 10.3389/fimmu.2019.02080.
17. Gielis, S., Moris, P., Bittremieux, W., De Neuter, N., Ogunjimi, B., Laukens, K., and Meysman, P. (2019). Detection of Enriched T Cell Epitope Specificity in Full T Cell Receptor Sequence Repertoires. Front Immunol *10*, 2820. 10.3389/fimmu.2019.02820.
18. Fischer, D.S., Wu, Y., Schubert, B., and Theis, F.J. (2020). Predicting antigen specificity of single T cells based on TCR CDR3 regions. Mol Syst Biol *16*, e9416. 10.15252/msb.20199416.
19. Zhang, H., Liu, L., Zhang, J., Chen, J., Ye, J., Shukla, S., Qiao, J., Zhan, X., Chen, H., Wu, C.J., et al. (2020). Investigation of Antigen-Specific T-Cell Receptor Clusters in Human Cancers. Clin Cancer Res *26*, 1359-1371. 10.1158/1078-0432.CCR-19-3249.
20. Emerson, R.O., DeWitt, W.S., Vignali, M., Gravley, J., Hu, J.K., Osborne, E.J., Desmarais, C., Klinger, M., Carlson, C.S., Hansen, J.A., et al. (2017). Immunosequencing identifies signatures of cytomegalovirus exposure history and HLA-mediated effects on the T cell repertoire. Nat Genet *49*, 659-665. 10.1038/ng.3822.

21. Elyanow, R., Snyder, T.M., Dalai, S.C., Gittelman, R.M., Boonyaratanakornkit, J., Wald, A., Selke, S., Wener, M.H., Morishima, C., Greninger, A.L., et al. (2021). T-cell receptor sequencing identifies prior SARS-CoV-2 infection and correlates with neutralizing antibody titers and disease severity. medRxiv. 10.1101/2021.03.19.21251426.
22. Greissl, J., Pesesky, M., Dalai, S.C., Rebman, A.W., Soloski, M.J., Horn, E.J., Dines, J.N., Gittelman, R.M., Snyder, T.M., Emerson, R.O., et al. (2021). Immunosequencing of the T-cell receptor repertoire reveals signatures specific for diagnosis and characterization of early Lyme disease. medRxiv. 10.1101/2021.07.30.21261353.
23. Altman, J.D., Moss, P.A., Goulder, P.J., Barouch, D.H., McHeyzer-Williams, M.G., Bell, J.I., McMichael, A.J., and Davis, M.M. (1996). Phenotypic analysis of antigen-specific T lymphocytes. Science *274*, 94-96. 10.1126/science.274.5284.94.
24. Murphy, K., and Weaver, C. (2016). Janeway's Immunobiology, Ninth Edition (Garland Science).
25. Zhang, W., Hawkins, P.G., He, J., Gupta, N.T., Liu, J., Choonoo, G., Jeong, S.W., Chen, C.R., Dhanik, A., Dillon, M., et al. (2021). A framework for highly multiplexed dextramer mapping and prediction of T cell receptor sequences to antigen specificity. Sci Adv *7*. 10.1126/sciadv.abf5835.
26. Miller, N.J., Church, C.D., Dong, L., Crispin, D., Fitzgibbon, M.P., Lachance, K., Jing, L., Shinohara, M., Gavvovidis, I., Willimsky, G., et al. (2017). Tumor-Infiltrating Merkel Cell Polyomavirus-Specific T Cells Are Diverse and Associated with Improved Patient Survival. Cancer Immunol Res *5*, 137-147. 10.1158/2326-6066.CIR-16-0210.
27. Nghiem, P., Bhatia, S., Lipson, E.J., Sharfman, W.H., Kudchadkar, R.R., Brohl, A.S., Friedlander, P.A., Daud, A., Kluger, H.M., Reddy, S.A., et al. (2021). Three-year survival, correlates and salvage therapies in patients receiving first-line pembrolizumab for advanced Merkel cell carcinoma. J Immunother Cancer *9*. 10.1136/jitc-2021-002478.
28. Nghiem, P.T., Bhatia, S., Lipson, E.J., Kudchadkar, R.R., Miller, N.J., Annamalai, L., Berry, S., Chartash, E.K., Daud, A., Fling, S.P., et al. (2016). PD-1 Blockade with Pembrolizumab in Advanced Merkel-Cell Carcinoma. N Engl J Med *374*, 2542-2552. 10.1056/NEJMoa1603702.

Chapter 6: Spike-specific T cells are enriched in breastmilk following SARS-CoV-2 mRNA vaccination

Blair Armistead, Yonghou Jiang, Marc Carlson, Emily S. Ford, Saumya Jani, John Houck, Xia Wu, Lichen Jing, Tiffany Pecor, Alisa Kachikis, Winnie Yeung, Tina Nguyen, Rene Coig, Nana Minkah, Sasha E. Larsen, Rhea N. Coler, David M. Koelle, and Whitney E. Harrington

Mucosal Immunology, February 2023

CHAPTER SUMMARY: In this chapter, we compared T cell repertoires in the blood and breastmilk of patients who received SARS-CoV-2 mRNA vaccinations. We found that the breastmilk contained a higher frequency of SARS-CoV-2-specific CD8 T cells than blood, and that these cells expressed higher levels of mucosal-homing markers, suggesting that they did not egress from microtrauma to blood vessels. Additionally, we found that SARS-CoV-2-specific T cells expanded in response to vaccination. Upon comparing T cell repertoires, we observed minimal overlap between blood and breastmilk TCR repertoires. We also applied tcrdist3 (using our experience in Chapter 5) to predict novel SARS-CoV-2-specific CD8 T cells in our data, allowing us to more comprehensively compare repertoires.

SOCIETY FOR MUCOSAL IMMUNOLOGY www.elsevier.com/mi

ARTICLE

Spike-specific T cells are enriched in breastmilk following SARS-CoV-2 mRNA vaccination

Blair Armistead [1,†], Yonghou Jiang [1,†], Marc Carlson [2], Emily S. Ford [3,4], Saumya Jani [4,5], John Houck [1], Xia Wu [4], Lichen Jing [4], Tiffany Pecor [1], Alisa Kachikis [6], Winnie Yeung [1], Tina Nguyen [1], Rene Coig [5], Nana Minkah [1,7], Sasha E. Larsen [1], Rhea N. Coler [1,7,8], David M. Koelle [3,4,5,8,9] and Whitney E. Harrington [1,7,8,✉]

Human breastmilk is rich in T cells; however, their specificity and function are largely unknown. We compared the phenotype, diversity, and antigen specificity of T cells in breastmilk and peripheral blood of lactating individuals who received SARS-CoV-2 messenger RNA (mRNA) vaccination. Relative to blood, breastmilk contained higher frequencies of T effector and central memory populations that expressed mucosal-homing markers. T cell receptor sequence overlap was limited between blood and breastmilk. Overabundant breastmilk clones were observed in all individuals, were diverse, and contained complementarity-determining regions in three sequences with known epitope specificity, including to SARS-CoV-2 spike. SARS-CoV-2 spike-specific T cell receptors were more frequent in breastmilk compared to blood and expanded in breastmilk following a 3rd mRNA vaccine dose. Our observations indicate that the lactating breast contains a distinct T cell population that can be modulated by maternal vaccination with potential implications for passive infant protection.

Mucosal Immunology (2023) 16:39–49; https://doi.org/10.1016/j.mucimm.2023.01.003

INTRODUCTION

The breastfed human infant consumes up to 750,000 maternal leukocytes per day, 5%–10% of which are T cells, the function of which is poorly understood[1,2]. Breastmilk lymphocytes are most abundant at delivery and decline over the 1st month post-partum to a steady state that persists for up to 2 years[1–4]. However, the infant's exposure to breastmilk cells likely remains substantial throughout breastfeeding due to an increase in volume of breastmilk ingested as the infant grows[5]. Breastmilk T cells are phenotypically distinct from peripheral blood T cells, with higher expression of mucosal and effector memory (T_{EM}) markers[6,7]. Cytomegalovirus, Epstein-Barr virus (EBV), influenza, and HIV-specific T cell responses have been detected in breastmilk cells (BMC) at higher frequencies than in peripheral blood mononuclear cells (PBMC)[7–11], and breastmilk T cells may expand in the setting of maternal or infant infection[2,12,13].

The infant stomach pH[14,15] and intestinal permeability[14,16,17] are also highest in the first few weeks of life, and evidence from animal models demonstrates that breastmilk T cells can survive the offspring gastrointestinal tract and traffic into the mesenteric lymph nodes, liver, spleen, and lung as a form of maternal microchimerism[18–20]. In mice, breastmilk-derived maternal helminth-specific T cells were protective in the offspring upon challenge with the same helminth[18], and in lambs, breastmilk-derived tetanus-specific T cells enhanced the response to tetanus vaccination in the offspring[21]. Human breastmilk maternal microchimerism has not been conclusively demonstrated, although we recently found in a cohort of infants that maternal microchimerism increased up to 3 months of age and was positively associated with breastfeeding[22]. These data emphasize the potential for breastmilk-acquired maternal T cells to become resident in the infant and provide an underrecognized form of passive protection.

The full repertoire of breastmilk T cells has not been described, however, and data on maternal vaccine-specific T cells in breastmilk are limited[23]. In the setting of the ongoing pandemic, pregnant and lactating individuals are now widely receiving SARS-CoV-2 (SARS2) vaccines, including the spike protein messenger RNA (mRNA)-based vaccines mRNA1273 (Moderna)[24] and BNT162b2 (Pfizer-BioNTech)[25]. SARS2 mRNA vaccines generate a robust T cell response in peripheral blood[24–27] and induce the expansion of tissue-resident T cell populations in the respiratory mucosa[28]. A recent study reported spike-reactive T cells in breastmilk of mRNA-vaccinated people, although the diversity of their T cell receptor (TCR) usage, relative clonality in breastmilk versus blood, and capacity to directly

---

[1]Center for Global Infectious Disease Research, Seattle Children's Research Institute, Seattle, Washington, USA. [2]Research Scientific Computing, Enterprise Analytics, Seattle Children's Research Institute, Seattle, Washington, USA. [3]Vaccine and Infectious Disease Division, Fred Hutchinson Cancer Research Center, Seattle, Washington, USA. [4]Department of Medicine, University of Washington, Seattle, Washington, USA. [5]Department of Laboratory Medicine & Pathology, University of Washington, Seattle, Washington, USA. [6]Department of Obstetrics & Gynecology, University of Washington, Seattle, Washington, USA. [7]Department of Pediatrics, University of Washington, Seattle, Washington, USA. [8]Department of Global Health, University of Washington, Seattle, Washington, USA. [9]Benaroya Research Institute, Seattle, Washington, USA ✉ email: whitney.harrington@seattlechildrens.org. † Both authors contributed equally.

Received: 7 November 2022 Revised: 20 December 2022 Accepted 7 January 2023

bind antigen were not described. To understand the breadth of maternal T cells consumed by the infant, we characterized the phenotype and diversity of paired breastmilk and peripheral T cells. We further investigated the hypothesis that spike-specific T cells are present in the breastmilk of SARS2 mRNA-vaccinated individuals and expand upon antigen re-encounter.

METHODS

Cohort

The initial cohort was comprised of lactating individuals (*n* = 26, Supplementary Fig. S1) who were recruited as part of the Center for Global Infectious Disease Research Biorepository, approved by the Seattle Children's Research Institute Institutional Review Board (IRB) (STUDY00002048). Participants self-reported as healthy, not pregnant, and weighing > 110 pounds. Demographic data were collected, including age, history of SARS or other serious infections, SARS2 vaccination (brand and dates of doses), sex of infant(s), and parity. All participants reported receipt of two doses of a SARS2 spike mRNA vaccine. No participants reported SARS2 infection, and all were negative for anti-nucleocapsid IgG (Abbott Architect SARS-CoV-2 IgG assay). Breastmilk was pumped by the participants using the method of their choice and transferred fresh to the study team. Blood was obtained from 23 individuals. Twenty individuals were included for experimental analysis based on at least 10^6 BMC recovered (Supplementary Fig. S1). For the pre- and post-3rd mRNA vaccine dose studies, blood and breastmilk were collected before and ~1 week after 3rd mRNA vaccine dose (*n* = 7 PBMC and BMC, *n* = 1 BMC only). Collection interval was based on T cell responses observed in peripheral blood[24,25]. Five participants from the original cohort returned to provide additional specimens, and samples from three additional individuals were added from the maternal immunizations in low and high-risk pregnancies, approved by the University of Washington IRB (STUDY00008491). Participants from both studies provided written informed consent.

Isolation of peripheral blood mononuclear cells from whole blood

Whole blood was collected in ethylenediaminetetraacetic acid (EDTA) Vacutainer tubes (BD Biosciences). Within 4 hours of collection, tubes were centrifuged at 400 x *g* for 10 minutes. The plasma fraction was removed, centrifuged at 800 x *g* for 15 minutes, aliquoted into cryovials, and stored at -80°C. The remaining blood was diluted in sterile phosphate-buffered saline (PBS), layered onto Lymphocyte Separation Medium (Corning), and centrifuged at 800 x *g* for 20 minutes at room temperature with no break. The resulting buffy coat layer was removed and washed two to three times in PBS. Cells were counted using a C-Chip hemocytometer (INCYTO), resuspended in freezing medium [50% fetal bovine serum (FBS), 40% RPMI with L-glutamine, 10% DMSO (Millipore Sigma)] at 5 to 10 million cells/ml, and aliquoted into cryovials for storage in liquid nitrogen.

Isolation of breastmilk cells

Milk was centrifuged at 400 x *g* for 15 minutes at 4°C, and the aqueous fraction was aliquoted into cryovials and stored at -80°C. The cell pellet was washed three times in 40 ml sterile PBS with 2% FBS. As above, cells were counted using a C-Chip hemocytometer (INCYTO), resuspended in freezing medium at 1 to 3 million cells/ml, aliquoted into cryovials, placed in a 1°C cryogenic freezing container at -80°C overnight, and then transferred to liquid nitrogen.

Phenotyping and cell sorting by flow cytometry

PBMC or BMC were thawed at 37°C and added to pre-warmed thaw medium (RPMI with L-glutamine, 20% FBS) and centrifuged at 400 x *g* for 5 minutes. Cell pellets were resuspended in 5 ml complete medium (RPMI with L-glutamine, 10% FBS, 100 U/ml penicillin, 100 µg/ml streptomycin), counted, and assessed for viability. Cells were stained with 100 µl of master mix containing fluorophore-conjugated antibodies and viability dye (Supplementary Table S7; Panel 1) in Brilliant Stain Buffer (BD Biosciences) for 30 minutes at room temperature. Stained cells were washed and resuspended fluorescence-activated cell sorting (FACS) buffer. Cells were run on a FACSMelody Cell Sorter (BD Biosciences) or a FACSAria II Cell Sorter (BD Biosciences), and for BMC CD45+ cells were collected. Single-stained CompBeads (ThermoFisher) were used as compensation controls, and unstained or fluorescence-minus-one stained cells were used to set fluorescence gates. Data were analyzed on FlowJo version 10 (BD Biosciences). CD45RO+/CCR7- T cells were designated as T_{EM}, CD45RO+/CCR7+ T cells were designated as T_{CM}, and CD45RO-/CCR7+ T cells were designated as naïve-like ($T_{N\text{-}like}$). Gating strategy is shown in Supplementary Fig. S6. In addition, data were used to anticipate the frequency of T cells (CD3+) in the collected CD45+ population from BMC to optimize subsequent genomic DNA extraction.

Tetramer generation

YLQPRTFLL (i.e. YLQ peptide), LTDEMIAQY (i.e. LTD peptide), and NYNYLYRLF (i.e. NYN peptide) were synthesized by GenScript Biotech (Piscataway, New Jersey). YLQ peptide (400 µM) was mixed 1:1 (v/v) with 200 µg/ml Flex-T HLA-A*02:01 ultraviolet exchange UVX monomer (BioLegend) and treated with UV irradiation (368 nm) for 30 minutes using a UV crosslinker (Fisher Scientific) to remove the UV-liable peptide. The mixture was incubated at 37°C for 30 minutes to form YLQ monomers, which were then tetramerized through the addition of 200 µg/ml streptavidin-APC (BD Biosciences) and incubation on ice for 30 minutes. Excess streptavidin was blocked with PBS + 0.4 µM D-Biotin + 0.3% (w/v) NaN_3 overnight at 4°C. HLA-A*01_LTD-APC and HLA-A*24_NYN-APC tetramers were generated by the National Institutes of Health Tetramer Core Facility (Emory University, Atlanta, GA).

Tetramer staining and flow cytometry analysis

Cells were thawed and washed as described above and then stained with HLA-A*02_YLQ-APC, HLA-A*01_LTD-APC, or HLA-A*24_NYN-APC tetramer (1:100) for 30 minutes at 4°C. Cells were washed with FACS buffer and then stained with antibody mix containing the optimal dilutions of all antibodies and viability dye in Brilliant Staining Buffer (Supplementary Table S8; Panel 2) for 30 minutes at room temperature, protected from light. Stained cells were washed in FACS buffer and run on a FACSAria II Cell Sorter (BD Biosciences) with single-stained CompBeads (ThermoFisher) as compensation controls. Data were analyzed on FlowJo version 10 (BD Biosciences). HLA-A*02_YLQ tetramer performance was validated with YLQ-specific CD8+ T cells expanded from an HLA-A*02:01 SARS2 convalescent donor spiked into an HLA-A*02:01 negative donor with PBMC collected prior to 2019 (Supplementary Fig. S7). HLA-A*01_LTD and HLA-A*24_NYN tetramer performance was validated using HLA-matched PBMC from donors predicted to have TCRs specific to these epitopes from TCRβ sequencing data and HLA-unmatched PBMC as negative controls. Tetramer-positive cells from BMC and PBMC were gated as follows: lymphocyte cloud (FSC-A by SSC-A) → single cells (FSC-A by FSC-H) → live cells (live/dead Aqua by FSC-H) → CD45+/ CD3+ → CD8+ → tetramer+.

Human leukocyte antigen typing

Genomic DNA was extracted from participants' PBMC with the QIAamp® DNA Blood Mini Kit per manufacturer instructions, and HLA class I genotyping was performed via direct sequencing (Sisco Genetics, Seattle, WA).

T cell receptor beta chain sequencing

Flow-sorted BMC (CD45+) expected to contain T cells underwent genomic DNA extraction using a protocol modified to recover low-yield DNA. Briefly, sorted BMC were pelleted in their collection tubes at 400 x *g* for 10 minutes. Cell pellets were processed in collection tubes using 30 µl of Qiagen Protease (Qiagen) and incubated at 70°C for 20 minutes. Then, 1.5 µg of carrier RNA (Qiagen) and 300 µl of Buffer AL (Qiagen) were added. Samples were incubated for another 20 minutes at 70°C. To recover DNA, 300 µl of 100% ethanol was added to the sample and transferred to a QIAamp® Mini spin column followed by the manufacturer's standard protocol from the QIAamp® DNA Blood Mini Kit. DNA was eluted in water. To assess DNA yield, a quantitative polymerase chain reaction (qPCR) assay targeting the β-globin gene was performed, and only samples anticipated to contain at least 1000 T cells were sent for TCRβ sequencing. Maternal PBMC underwent genomic DNA extraction using the standard protocol provided in the QIAamp® DNA Blood Mini Kit (Qiagen), and 3.4 µg of total genomic DNA was sent for TCRβ sequencing. Samples were sent in batches to Adaptive Biotechnologies (Seattle, WA, USA) and assayed using their ImmunoSEQ® hsTCRBB[46] service pipeline at a survey level.

T cell receptor sequence analysis

TCRβ sequence data were analyzed using the immunoSEQ® Analyzer software and/or exported to R for analysis with the package immunoArch or divo. Repertoire overlap between blood and breastmilk was assessed using the Morisita index (immunoSEQ Analyzer®) and the power geometric index (divo), which are relatively protected from differences in sampling depth[29]. To identify overabundant clones in the breastmilk, frequencies of TCR clonotype nucleotide sequences in the breastmilk were compared to those in peripheral blood using the Differential Abundance tool in immunoSEQ® Analyzer using the binomial statistical method with Benjamini–Hochberg correction and a lower limit of detection of 10.

The CDR3β amino acid sequence of each overabundant clone was compared to that of all other overabundant clones within each participant using tcrdist3[31,32]. Similarly, CDR3β amino acid sequences of overabundant clones across all participants were compared to one another using tcrdist3[31,32]. To identify epitope specificity of overabundant breastmilk clones, TCRβ sequences were matched by CDR3 amino acid and V gene identification against several public databases of TCRβ epitope specificity, namely ImmuneCODE[35] (https://clients.adaptivebiotech.com/pub/covid-2020), VDJdb (https://vdjdb.cdr3.net)[47], TCRBdb (http://bioinfo.life.hust.edu.cn/TCRdb/#/)[48], McPAS-TCRB (http://friedmanlab.weizmann.ac.il/McPAS-TCRB/)[49], and IEDB (http://www.iedb.org/home_v3.php). Epitope matches were considered a direct match if the CDR3 amino acid and TRBV gene were identical and were considered a predicted match if the CDR3 amino acid sequences were identical, but V gene usage was mismatched. All overabundant breastmilk clones were also queried using the IEDB TCRMatch Tool (http://tools.iedb.org/tcrmatch/) with a score threshold of 0.97 to identify closely related epitope restrictions.

TCRβ sequences from both breastmilk and PBMC were evaluated for candidate spike-specific restriction using the COVID Search Tool in immunoSEQ® Analyzer, which utilizes TCRβ sequences assigned as specific for SARS-CoV-2 from the ImmuneCODE database[35,41]. For comparison of clonality metrics only, the full dataset of paired breastmilk and PBMC TCRβ sequences was down-sampled to the lowest productive template frequency. Candidate spike-specific TCRβ in breastmilk and PBMC were further validated by comparing CDR3β amino acid sequences, V gene usage, epitope HLA restriction, and participant HLA concordance to an internally vetted dataset of published TCRβ sequences obtained via spike-epitope-loaded tetramer or multimer-based experiments[36–40]. An exact match at the TCRβ CDR3 sequence was required for these analyses. The internally vetted dataset[36–40] was used to train the tcrdist3 algorithm[31,32] with a distance unit threshold of 10 to identify additional potential spike-specific TCRβ in breastmilk.

Enzyme-linked immunosorbent assay

Enzyme-linked immunosorbent assays (ELISA) were conducted as previously described[50]. Briefly, 384-well plates were coated with SARS-CoV-2 spike protein (Institute for Protein Design, University of Washington). Wells were blocked and washed, and samples were added according to the parameters in Supplementary Table S9. Aqueous breast milk fractions were diluted 1:2, and plasma samples were diluted 1:20 in assay diluent. Each sample was then serially diluted 1:5 across the plate. The average optical density value for all dilutions of the negative sample was used to set a minimum cutoff value for each plate, and each sample's endpoint titer was calculated.

Statistical approach

To assess the primary difference between cellular phenotypic frequency (e.g. % CCR9+ of CD4+ T cells) in BMC versus PBMC, we built a linear regression model for each outcome with sample type as the predictor, adjustment for time since delivery, and clustering by individual to account for the correlation of individuals contributing paired BMC and PBMC. Due to the difference in sampling depth in the two compartments, negative binomial models were used to compare the frequency of spike-specific templates in BMC versus PBMC, accounting for both the number of total SARS2-specific templates identified (viral genome-wide) and the number of spike-specific templates identified to determine the enrichment of spike above background reactivity to non-SARS2 coronaviruses and/or TCRs present in the naïve repertoire, and adjusting for time since delivery. The negative binomial model generates an incidence rate ratio which represents the number of spike-specific templates found in the experimental group (e.g. BMC) for every template identified in the control group (e.g. PBMC). The phenotype and frequency of tetramer-positive T cells in the BMC of individuals pre- and post-3rd dose were compared with paired t tests. A p value less than 0.05 was considered significant.

RESULTS

Breastmilk is enriched for mucosal memory T cells

We collected paired blood and breastmilk from lactating individuals who had received two doses of BNT162b2 or mRNA1273, had no history of SARS2 infection, and were nucleocapsid protein seronegative (Supplementary Fig. S1; Table 1). We characterized cell phenotype by flow cytometry in paired samples with at least 1,000,000 total BMC recovered and at least 100 cells in both the CD4+ and CD8+ T cell populations (n = 17). Breastmilk contained a low but detectible frequency of T cells, and the frequency of CD4+ T cells was similar in BMC and PBMC, whereas the frequency of CD8+ T cells was somewhat lower in BMC than PBMC (24% *vs.* 30%, p = 0.03; Supplementary Fig. S2). Next, we identified naïve and memory T cell subsets in BMC and PBMC through surface expression of CD45RO and CCR7. We found a significant enrichment of CD45RO+/CCR7- T_{EM} and CD45RO+/CCR7+ central memory (T_{CM}) CD4+ T cell populations in BMC versus PBMC (Figs 1A and 1B). Within the CD8+ population, there was also a higher frequency of T_{EM} but not T_{CM} in BMC relative to PBMC (Figs 1A and 1B). These data emphasize that breastmilk is highly enriched for memory T cell populations relative to peripheral blood.

We next investigated the expression of mucosal-homing markers CCR9 and CD103 on T cells within BMC and PBMC. The CD4+ population within BMC versus PBMC had a higher frequency of CCR9+ and CD103+ cells and a higher frequency of double-positive CCR9+/CD103+ cells (Figs 1C and 1D). Similarly, the CD8+ population within BMC versus PBMC had a higher frequency of CCR9+ and CD103+ cells, as well as a higher frequency of CCR9+/CD103+ cells (Figs 1C and 1D). These data emphasize that the T cells in breastmilk express high levels of mucosal-homing markers.

Restricted T cell receptor repertoire overlap between peripheral blood and breastmilk

Because of the high frequency of memory populations, we next investigated the composition and diversity of the TCR repertoire in BMC. BMC were enriched for hematopoietic lineage cells (CD45+) using flow cytometry cell sorting and sorted BMC for which > 1000 DNA genomic equivalents were recovered (n = 16) and underwent bulk TCR beta chain (TCRβ) sequencing. Among BMC samples for which > 1000 TCR templates were recovered, we compared the degree of TCR overlap with matched peripheral blood (n = 11) and surprisingly observed relatively low sequence similarity in all pairs, as measured by the Morisita and power geometric indices[29] (Fig. 2, Supplementary Table S1), indicating that BMC and PBMC have distinct TCR repertoires at the sequence level. In contrast, we observed a high degree of overlap in the PBMC TCR repertoire from one individual at two time points (9 and 17 days post-2nd vaccine dose) utilized as a positive control (Fig. 2, Supplementary Table S1). Neither the Morisita index nor the power geometric index between paired BMC and PBMC was related to the number of productive templates in the BMC (R^2 = 0.4, p = 0.3; R^2 = 0.3, p = 0.4 respectively), suggesting that the low sequence overlap between BMC and PBMC was independent of sampling depth of the BMC. Within each participant, we compared the frequency of clonotypes across the two compartments using the immunoSEQ® Differential Abundance tool[30]. In all individuals, there were select clonotypes that were statistically significantly overabundant in BMC relative to PBMC (Fig. 2; Supplementary Table S1). In contrast, the Simpson Clonality and maximum clone frequency—two metrics of absolute clonality rather than relative clonality—did not differ in BMC and PBMC (Supplementary Table S1), indicating that the two compartments were similarly diverse in each participant. These data indicate that although the TCR repertoire of BMC is as diverse as that of the PBMC, it is composed of a distinct TCR repertoire at the sequence level with select overabundant clonotypes relative to PBMC.

Table 1. Cohort characteristics.

Demographics	Total (n = 20)
Maternal age, years, median (range)	37 (29-39)
Maternal vaccine type, n (%)	
Pfizer-BioNTech	17 (85%)
Moderna	3 (15%)
Time since delivery, weeks, median (range)	26 (2-56)
Time since 2nd SARS2 mRNA dose, weeks, median (range)	11 (0.7-24)
Parity, median (range)	1.5 (1-3)
Infant sex, n (%)	
Female	7 (33%)
Male	14 (67%)

Characterization of breastmilk overabundant T cell clonotypes

We next explored the diversity of the overabundant T cell clonotypes in breastmilk. We analyzed each participant's BMC T cell repertoire using a TCR distance metric, tcrdist3[31,32], which clusters TCRβs based on structural and functional similarities of amino acids within complementarity-determining regions (CDR). In all participants, overabundant clones were broadly distributed across the BMC TCRβ repertoire (Fig. 3A, Supplementary Fig. S3). We additionally evaluated how overabundant clones clustered across all individuals. Most clones were unique to a single individual (i.e. they were "private"), and the clonotypes did not segregate by individual (Fig. 3B), reflecting the diversity of each participant's overabundant clonotypes.

To determine potential antigen specificity, we compared CDR3 amino acid sequences of the overabundant breastmilk clones from all individuals to TCRβ sequence databases populated by validated epitope-specific TCRs. We identified five direct matches from two participants with CDR3 amino acid sequences and identical V gene usage, two of which were reported to bind SARS2 spike epitopes (Fig. 3B, Supplementary Fig. S4, Supplementary Table S2). Notably, the two spike-specific clones had also previously been reported to bind influenza M1[33,34]. Other direct matches included epitopes derived from influenza, *Mycobacterium tuberculosis* lysate, and EBV (Fig. 3B, Supplementary Fig. S4, Supplementary Table S2). Additional clones with identical CDR3 sequences but non-identical V gene usage were reported to bind epitopes from SARS2, EBV, and *M. tuberculosis* (Fig. 3B, Supplementary Fig. S4, Supplementary Table S2). CDR3 sequences with previously published specificity clustered together, irrespective of individual (Fig 3B). Finally, we used the Immune Epitope Database and analysis Resource (IEDB) TCRMatch Tool to predict TCR epitope specificity based on sequence similarity to published TCR sequences, which identified TCR clones with potential specificity to a variety of viral epitopes (Supplementary Table S3). These data indicate that overabundant breastmilk T cell clones are diverse and respond

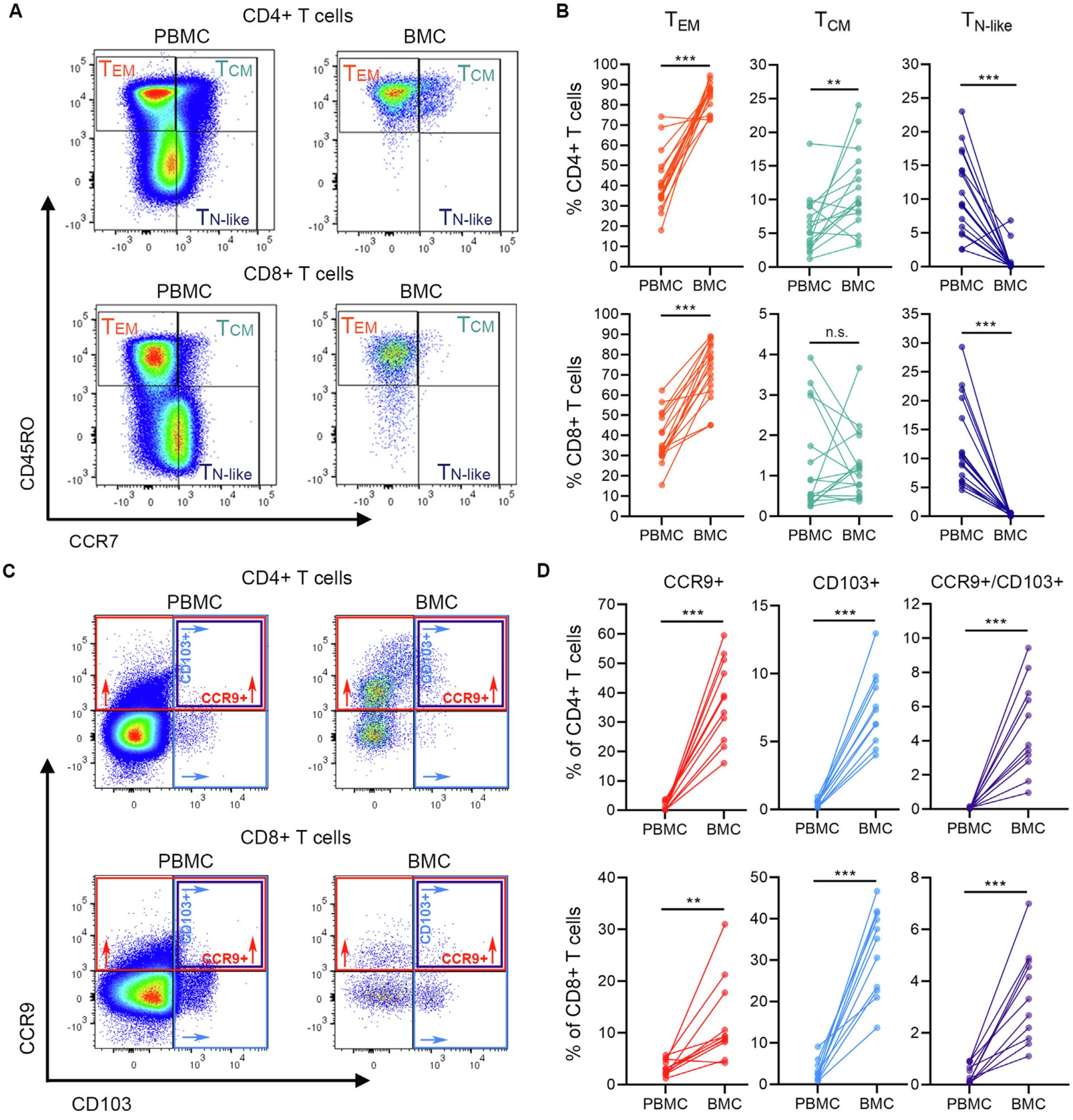

Fig. 1 Antigen-experienced and mucosal-homing T cells are enriched in breastmilk. PBMC and BMC were analyzed by flow cytometry. Comparisons made with linear regression and clustering by individual, ***$p < 0.001$, **$p < 0.01$, *$p < 0.05$. (A) Scatter plots showing expression of CD45RO and CCR7 in CD4+ and CD8+ T cells from PBMC and BMC in one representative participant; (B) Frequencies of T_{EM}, T_{CM}, and $T_{N\text{-like}}$ CD4+ and CD8+ T cells in PBMC and BMC ($n = 17$): CD4+ T_{EM}: 41% versus 84%, $p < 0.001$, CD4+ T_{CM}: 6% versus 11%, $p = 0.006$, CD4+ $T_{N\text{-like}}$: 11% versus 1%, $p < 0.001$; CD8+ T_{EM}: 38% versus73%, $p < 0.001$, CD8+ T_{CM}: 1% versus 1%, p = n.s., CD8+ $T_{N\text{-like}}$: 12% versus 0.2%, $p < 0.001$; (C) Scatter plots showing expression of CCR9 and CD103 in CD4+ and CD8+ T cells from PBMC and BMC in one representative participant; (D) Expression of CCR9 and CD103 within CD4+ and CD8+ T cell populations in PBMC and BMC: CD4+/CCR9+ ($n = 11$): 4% versus 38%, $p < 0.001$, CD4+/CD103+: 0.4% versus 7%, $p < 0.001$, CD4+/CCR9+/CD103+: 0.1 versus 5%, $p < 0.001$, CD8+/CCR9+: 3% versus 12%, $p = 0.005$; CD8+/CD103+: 3% versus 32%, $p < 0.001$, CD8+/CCR9+/CD103+: 0.4% versus 3%, $p < 0.001$. BMC = breastmilk cells; PBMC = peripheral blood mononuclear cells; n.s. = not significant; T_{CM} = central memory T cells; T_{EM} = T cell effector memory T cells; $T_{N\text{-like}}$ = naïve-like T cells.

to a range of pathogen-specific epitopes, although the specificity of the vast majority of these clones is unknown.

SARS2 spike-restricted T cell receptor beta chains are present in breastmilk T cells

Because all participants had received SARS2 spike mRNA vaccination, we next investigated the presence of spike-specific clones in BMC T cells more broadly. We utilized the immunoSEQ® COVID Search Tool[35] to identify candidate Spike-specific TCRβ in all sequenced BMC and PBMC samples ($n = 30$). All PBMC ($n = 14$) contained candidate spike-specific TCRβ, though their predicted epitope specificity was distributed across the entire spike protein with low frequency, suggesting that some of the TCRβ may represent clones in the naïve repertoire rather than expanded vaccine-specific populations (Fig. 4A). Thirteen of the 16 BMC samples contained TCRβ predicted to be spike-specific. In the pairs where both BMC and PBMC were sampled, and at least one clone in each compartment was predicted to be SARS2-specific (*n* = 13 pairs), overall spike-specific TCRβs were nearly 2-fold enriched in BMC versus PBMC (Fig. 4B). However, across participants there was heterogeneity in response with most individuals demonstrating enrichment (*n* = 7), some with similar frequency (*n* = 4), and two with lower frequency of spike-specific T cells in the BMC relative to PBMC. The frequency of spike-specific TCRβs was not strongly correlated with spike-specific immunoglobulin (Ig) G or IgA in breastmilk or blood (Supplementary Fig. S5).

To further validate the presence of spike-specific T cells in breastmilk, we cross-referenced each participant's BMC and PBMC TCRβ CDR3 amino acid sequences and V gene usage against publicly available TCRβ datasets from spike-epitope-loaded tetramer or multimer experiments[36–40]. We identified high-quality CDR3 sequence matches in half of all breastmilk samples, with five samples also containing hits with identical V gene usage (Supplementary Table S4). All PBMC contained clones with identical CDR3 sequence and V gene usage to those published previously (Supplementary Table S5). Consistent with prior studies of PBMC[36–38,41], sequences specific to the spike peptide YLQPRTFLL were prominent in the breastmilk and blood of individuals known to be human leukocyte antigen (HLA)-A*02:01 positive. In addition, clones specific to the A*01:01-restricted spike peptide LTDEMIAQY and the B*15:01-restricted spike peptide NQKLIANQF were present in the breastmilk and blood of HLA concordant participants (Supplementary Tables S4 and S5), suggesting shared epitope specificity following vaccination. Finally, we utilized the list of spike-specific TCRβs in conjunction with the tcrdist3 algorithm[31,32] to identify novel potential spike-specific T cell clones in the BMC (Table S6). Together, these observations demonstrate the presence of spike-specific T cells in breastmilk following mRNA vaccination.

Spike-specific T cells in breastmilk expand after SARS2 mRNA vaccine

To understand whether spike-specific clones in breastmilk were responsive to antigen re-exposure, we took advantage of a natural restimulation experiment in which participants (*n* = 8) donated breastmilk pre- and approximately 1-week post-3rd vaccine dose for in-depth phenotyping and staining with HLA class I tetramers loaded with immunodominant spike epitopes, specifically HLA-A*02_YLQ, HLA-A*01_LDT, and HLA-A*24_NYN (Table 2, Figs 5A–C)[36–38,41]. The proportion of spike tetramer-positive CD8+ T cells of all CD8+ T cells significantly increased in breastmilk between the pre- and post-3rd dose samples (0.8-2.8%, *p* = 0.03), whereas tetramer-positive CD8+ T cells in PBMC showed minimal response (0.04-0.04%, *p* = 0.9) (Fig. 5D). The expression of activation markers on tetramer+ CD8+ T cells was consistently high but did not vary between pre- and post-3rd dose samples including CD69 (51% *vs.* 50%, *p* = 0.9), CD137 (61% *vs.* 42%, *p* = 0.3), and CCR5 (89% *vs.* 84%, *p* = 0.4). The proportion of tetramer+ CD8+ T cells expressing CCR9 and CD103 was similar to our earlier bulk analysis and did not vary between pre- and post-3rd dose (CCR9: 50% *vs.* 31%, *p* = 0.3; CD103: 18% *vs.* 7%, *p* = 0.4; CCR9/CD103: 1.4% *vs.* 3.4%, *p* = 0.3). A proportion of tetramer+ cells pre- and post-3rd dose also expressed the lymphocyte integrin α4β7, which regulates T cell migration to the intestine (21% *vs.* 16%, *p* = 0.7). These data demonstrate that SARS2 spike-specific cells in breastmilk respond *in vivo* upon antigen restimulation.

DISCUSSION

We present a comprehensive comparison of the T cells present in breastmilk relative to peripheral blood, considering phenotype, diversity, and antigen specificity. We find that T cells in breastmilk are nearly uniform memory populations and have high expression of mucosal-homing markers. Their TCRβ repertoire is diverse yet distinct from paired PBMC and with select overabundant clones. Further, we identify SARS2 spike-specific clones in the breastmilk of mRNA-vaccinated individuals, emphasizing that vaccine-specific T cells are present at mucosal sites such as the breast, with important implications for both maternal and infant health.

Breastmilk T cells were enriched for T_{EM} populations, indicating that breastmilk T cells may be poised to respond rapidly following antigen re-encounter[42]. Further, breastmilk T cells displayed high levels of mucosal-homing markers, consistent with earlier reports in individuals living with or without HIV[7]. These data suggest that breastmilk T cells may be derived from a tissue-resident population in the breast[43] rather than vessel microtrauma and contamination by peripheral blood. The high expression of both CCR9 and CD103 by breastmilk T cells also supports the notion of an entero-mammary axis[44]. Future studies should investigate whether breastmilk T cells traffic to the infant respiratory and gastrointestinal tracts when consumed and enhance cellular immunity to pathogens, as has been shown in helminthic infection in mice[18], or amplify infant response to homologous vaccination, as has been shown with tetanus vaccination in lambs[21].

Fig. 2 The TCR repertoires in breastmilk and peripheral blood are distinct. Bulk TCRβ sequencing from BMC and PBMC individuals who had paired samples available and at least 1,000 TCRβ templates in the BMC sample (*n* = 11). Each clone is represented as a dot, with the relative frequency in BMC represented on the X axis and relative frequency in PBMC on the Y axis. TCRβ repertoire overlap was analyzed using the M.I. (value inset), with a value of 0 representing no repertoire overlap and a value of 1 representing complete overlap of the repertoires. The frequencies of each individual TCRβ clonotype in the two compartments were statistically compared using the immunoSEQ® Differential Abundance Tool. Gray dashed line indicates frequency equality in the two compartments. Blue dots represent clonotypes that are significantly more abundant in BMC relative to PBMC. Orange dots represent clonotypes that are significantly more abundant in PBMC relative to BMC. Gray dots represent clonotypes that were not significantly different in frequency between the two compartments. Pale gray dots represent clonotypes that fell below the frequency for valid statistical comparison. As a control, TCRβ clonotypes from an individual's PBMC obtained nine days and 17 days after 2nd mRNA vaccine dose were compared (upper left plot), demonstrating a high degree of repertoire overlap and only a few clones expanded at the 2nd time point relative to the 1st. BMC = breastmilk cells; M.I. = Morisita index; PBMC = peripheral blood mononuclear cells; TCR = T cell receptor; TCRβ = TCR beta chain.

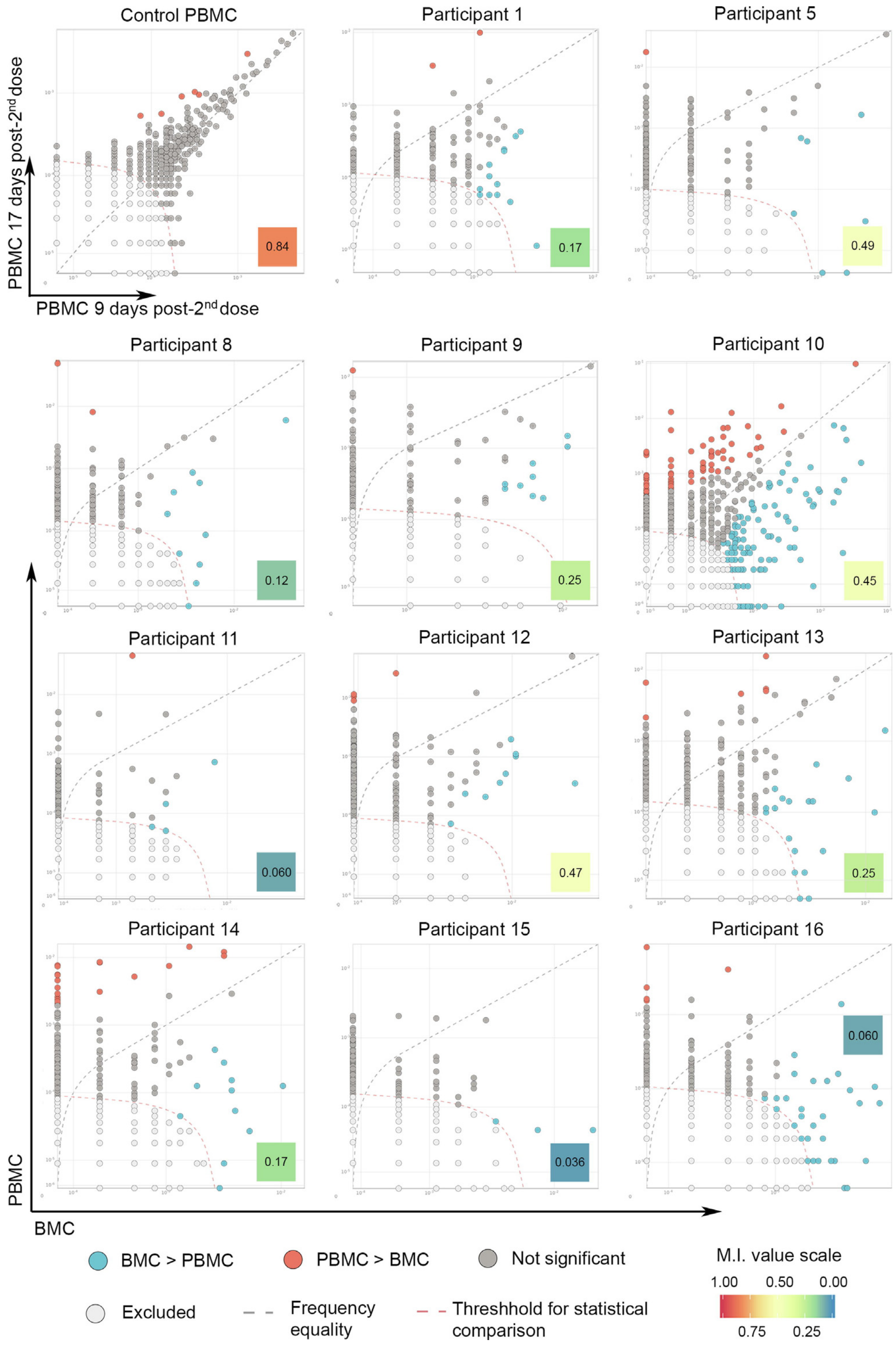

The TCRβ repertoire in BMC was diverse and had uniquely expanded clonotypes relative to paired PBMC. To date, studies have focused on T cell responses to specific pathogens[7–12] rather than capturing the full diversity of the compartment. The low degree of TCRβ repertoire overlap between the BMC and PBMC may reflect a difference in the distribution of naïve versus antigen-experienced T cells. However, the absolute clonality was similar, and there was evidence of high-frequency clonotypes, likely memory cells, that were differentially abundant, suggesting distinct T cell responses in the two compartments independent of the naïve population. The observation of overabundant clones in the BMC is consistent with prior reports of enrichment of virus-specific responses in breastmilk relative to PBMC[7–10], although in our paired TCRβ analysis, only one individual had cytomegalovirus-specific TCRβ and none reported HIV infection, emphasizing that this breast-specific enrichment is not restricted to clones specific to these viruses. In addition, within each individual, overabundant clones were diverse.

To identify antigen specificity of BMC T cells, we used a combination of prior published TCRβ specificities and predictive

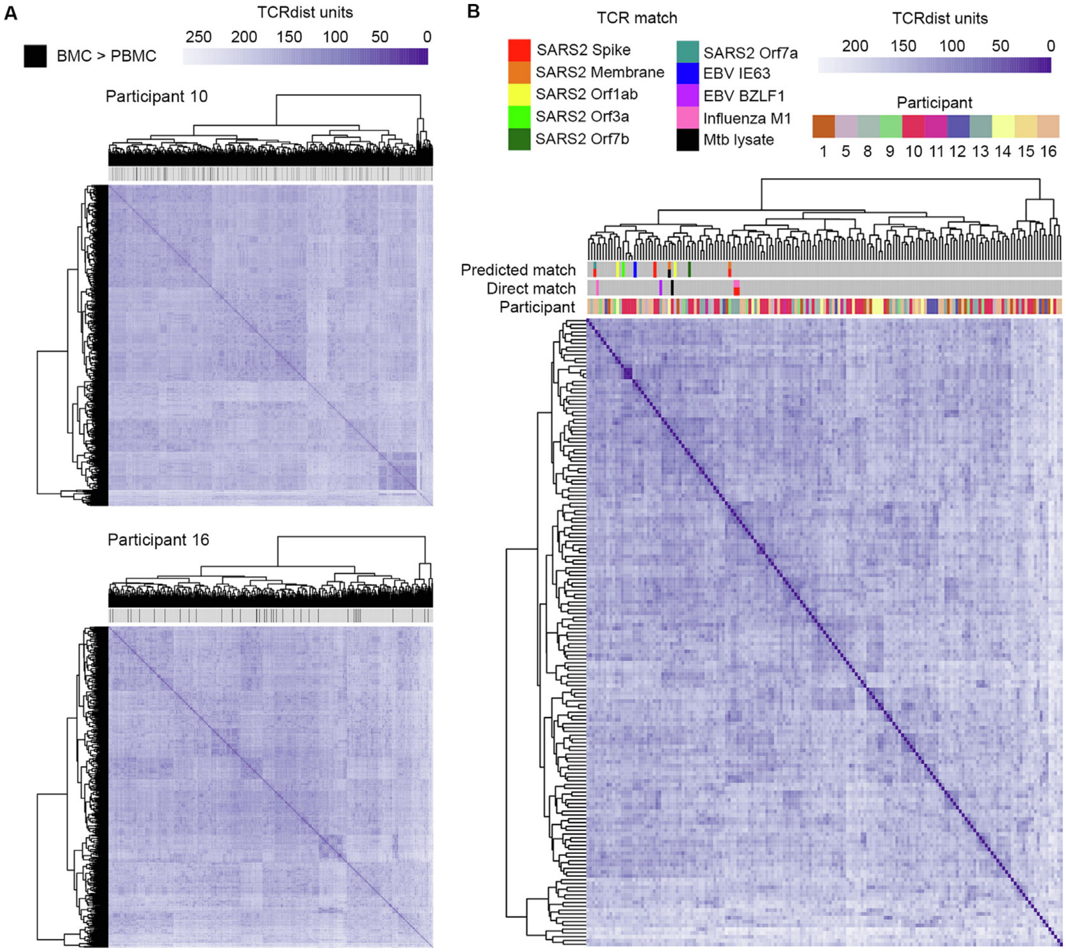

Fig. 3 Overabundant TCR clones in breastmilk are diverse. (A) For each individual participant with paired PBMC available (*n* = 11), all TCRβ CDR3 amino acid sequences obtained from the BMC were compared to one another using tcrdist3; representative plots from two individuals are displayed. Black ticks denote TCRβ sequences significantly overabundant in BMC relative to PBMC, demonstrating that overabundant clones were distributed across the full breastmilk TCR repertoire for each individual (i.e. did not cluster by sequence); (B) Overabundant BMC TCRβ CDR3 amino acid sequences from 11 participants were compared to one another across participants using tcrdist3. Overabundant clones did not cluster by individual, and most clones were private, emphasizing the diversity of overabundant clones across individuals. Overabundant TCRβ clones were further compared by CDR3 amino acid sequence and V gene usage against available public databases of known TCR epitope specificity. Clones matching pathogen-specific epitopes are marked with colored ticks. Epitope matches were considered a direct match if the CDR3 amino acid and TRβV gene were identical and were considered a predicted match if the CDR3 amino acid sequences were identical, but V gene usage was mismatched. Only the minority of clone specificity could be assigned, and characterized clones were tightly clustered across all individuals. For participant 10, only CDR3 amino acid sequences enriched by a factor ≥ 50 relative to PBMC or with epitope specificity were included to reduce data skewing from this participant. BMC = breastmilk cells; CDR = complementarity-determining regions; EBV = Epstein-Barr virus; Orf = open reading frame; Mtb = *Mycobacterium tuberculosis*; PBMC = peripheral blood mononuclear cells; TCR = T cell receptor; TCRβ = TCR beta chain.

algorithms. Although the specificity of the vast majority of BMC overabundant clones remained elusive, we were able to detect SARS2 spike-specific clones with high confidence in most individuals. Consistent with previous observations of convergent epitope specificity across HLA concordant individuals following SARS2 mRNA vaccination[36], we found identical spike-specific CDR3 sequences in BMC of several individuals. This observation, along with the approval of 3rd mRNA vaccine doses, provided a unique opportunity to observe the dynamics of spike-specific CD8+ T cells in the breastmilk after antigen re-encounter using well-validated HLA class I tetramers loaded with spike epitopes[36–38,41]. In contrast to blood-derived CD8+ T cells, the frequency of tetramer-positive CD8+ T cells in breastmilk significantly increased after the 3rd SARS2 mRNA vaccine dose, suggesting that T cells in the lactating breast may be particularly poised to respond to maternal mRNA vaccination. These expanded populations may reflect increased trafficking from the periphery or local antigen re-exposure, consistent with recent reports of detectable SARS2 mRNA vaccine in breastmilk[45]. Tetramer+ CD8+ T cells in breastmilk had high expression of activation and mucosal-homing markers, emphasizing their functional potential[28].

In addition to the potential benefit provided to the infant, the recognition of the breast as a site of mucosal immunity distinct from peripheral immunity has important implications for the study of vaccine responses. Prior work on the response to SARS2

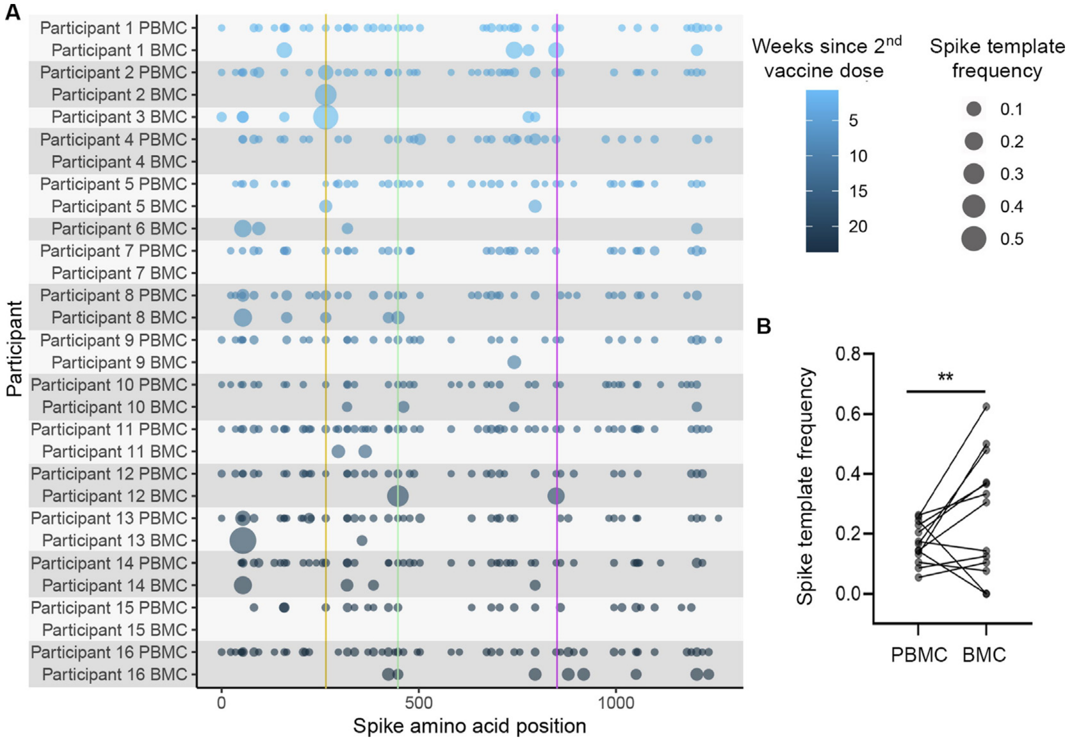

Fig. 4 Candidate SARS2 spike-specific T cells are enriched in the breastmilk relative to the peripheral blood of vaccinated individuals. The frequency of candidate spike-specific clones in all sequenced PBMC and BMC ($n = 14$ paired, $n = 2$ BMC only) was expressed relative to all clones predicted to bind to SARS2 antigens. Spike template frequency was compared using a negative binomial model, $^{**}p < 0.01$. (A) TCRβ sequences predicted to bind to SARS2 were identified in BMC and PBMC using the ImmunoSEQ® T-MAP COVID Search Tool and are mapped by their epitope binding location on the spike protein. Gold line indicates the amino acid position of the spike peptide pool that includes the YLQPRTFLL epitope (HLA-A*02 restricted), green line indicates the position of the NYNYLYRLF epitope (HLA-A*24 restricted), and purple line indicates the position of the LTDEMIAQY epitope (HLA-A*01 restricted); (B) Spike-specific TCRβ templates are enriched in BMC relative to PBMC, incident rate ratio = 1.66, $p = 0.004$. BMC = breastmilk cells; CDR = complementarity-determining regions; HLA = human leukocyte antigen; PBMC = peripheral blood mononuclear cells; TCRβ = T cell receptor beta chain.

Table 2. Spike epitope-loaded tetramers.

SARS2 spike epitope sequence	Sequence position within spike protein	HLA class I restriction
YLQPRTFLL	269-277	HLA-A*02:01
NYNYLYRLF	448-456	HLA-A*24:02
LTDEMIAQY	865-873	HLA-A*01:01

HLA = human leukocyte antigen.

mRNA vaccines has primarily focused on both CD4+ and CD8+ T cell responses present in peripheral blood[24,25] with limited study of T cell responses at mucosal sites. One recent study found that SARS2 mRNA vaccination induces the expansion of resident CD8+ T cells in the upper respiratory tract[28], suggesting that SARS2 mRNA vaccines promote robust T cell responses in the mucosa. In addition, a recent study reported an increase in spike peptide-reactive T cells in breastmilk following mRNA vaccination[23], consistent with our observations. Notably, lower respiratory tract responses are difficult to access in human populations, whereas the collection of breastmilk in lactating individuals is non-invasive. While the association between respiratory tract and breastmilk T cell responses merits further investigation, measuring immune responses in breastmilk may allow for characterization of mucosal immunity more broadly following vaccination.

Our study had several limitations. BMC T cells were low frequency, and although we designed our experimental approach to maximize the information obtained from each sample, the sampling depth between BMC and PBMC differed. However, we took advantage of several computational solutions to overcome this challenge, including repertoire analysis utilizing tools less susceptible to bias with differences in sampling depth and down-sampling for clonality analysis. We were further limited to bulk TCRβ sequencing of combined CD4+ and CD8+ populations, as the number of each sub-population was too small to meet technical requirements to analyze separately. Future work should consider the use of single-cell RNA sequencing to investigate the two populations separately. The number of T cells recovered from each breastmilk sample limited our ability to conduct functional analyses. However, we took advantage of individuals who received a 3rd dose of SARS2 mRNA vaccine to demonstrate expansion of spike-specific T cells with tetramer staining. We utilized previously frozen and thawed BMC and PBMC, which may have biased recovery of cell populations, particularly in breastmilk. Future studies should consider detailed analysis of fresh BMC if possible. Finally, initiation and support for breastfeeding vary by demographic groups, including socioeconomic status, and future work should address a more diverse population of lactating people.

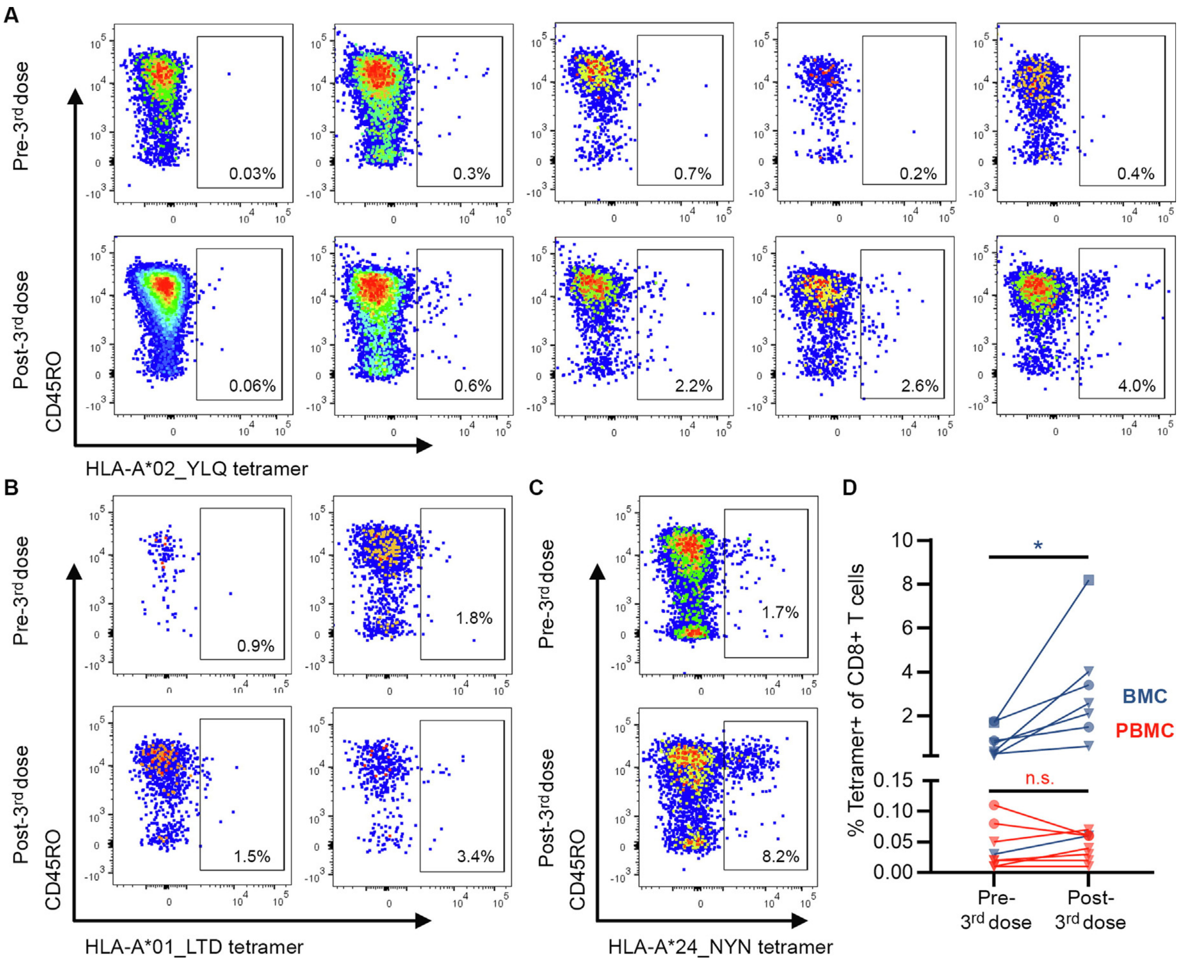

Fig. 5 SARS2 spike-specific T cells expand in breastmilk following 3rd mRNA vaccine dose. BMC and PBMC from before and ∼ 1 week after receipt of the 3rd dose of SARS2 mRNA vaccine were stained with SARS2 spike epitope-loaded class I tetramers and analyzed by flow cytometry to quantify spike-specific CD8+ T cells. Comparisons made with paired t tests, * $p < 0.05$. Scatter plots of (A) HLA-A*02_YLQ-positive ($n = 5$); (B) HLA-A*01_LTD-positive ($n = 2$); and (C) HLA-A*24_NYN-positive ($n = 1$) CD8+ T cells in breastmilk obtained before (top) and after (bottom) 3rd mRNA vaccine dose are shown from HLA concordant individuals. Frequencies of tetramer+ cells of CD8+ T cells inset; (D) Frequencies of tetramer+ cells of CD8+ T cells in BMC ($n = 8$, blue) and PBMC ($n = 7$, red). Triangle = HLA-A*02_YLQ, circle = HLA-A*01_LTD, square = HLA-A*24_NYN. BMC: 0.8-2.8%, $p = 0.03$; PBMC: 0.04-0.04%, $p = 0.9$. BMC = breastmilk cells; CDR = complementarity-determining regions; HLA = human leukocyte antigen; mRNA = messenger RNA; n.s. = non-significant; PBMC = peripheral blood mononuclear cells; TCRβ = T cell receptor beta chain.

We demonstrate that breastmilk T cells are highly diverse and enriched for mucosal memory populations, emphasizing that the lactating breast represents a key site of mucosal immunity that warrants additional study. Further, we identify SARS2 spike-specific T cells in mRNA-vaccinated individuals, a critical demonstration of vaccine-specific T cells in breastmilk. This observation may have important implications for both the study of vaccine-induced T cell responses in the vaccinated individual as well as for passive infant protection.

AUTHOR CONTRIBUTIONS

Conceptualization: BA, YJ, and WEH. Methodology: YJ, MC, ESF, SJ, JH, XW, LJ, TP, SEL, RNC, DMK, and WEH. Participant enrollment: AK, WY, TN, and WEH. Investigation: BA, YJ, MC, ESF, SJ, JH, XW, LJ, TP, DMK, and WEH. Visualization: BA, RC, MC, and WEH. Funding acquisition: BA, ESF, SJ, AK, RNC, DMK, and WEH. Supervision: NM, RNC, DMK, and WEH. Writing –draft: BA, YJ, and WEH. Writing – critical review/editing: BA, YJ, ESF, SJ, XW, NM, SEL, DMK, and WEH.

DECLARATION OF COMPETING INTEREST

The authors have no competing interests to declare.

FUNDING

Funding was provided by National Institute of Health (NIH) grants T32AI007509 (BA), K08AI148588 (ESF), T32CA080416 (SJ), K23AI153390-01 (AK), 1UM1AI148373-01 (RNC), 3UM1 AI148373-01S1 (RNC), R21AI163999 (DMK), K08AI135072 (WEH); NIH contract 75N93019C00063 (DMK); Burroughs Wellcome Fund Career Award for Medical Scientists grant 1017213 (WEH); and University of Washington and Seattle Children's Research Institute (WEH).

DATA AVAILABILITY

All flow cytometry data are available in the Primary Data Table (Table S1), and all TCR sequencing data will be deposited in immuneACCESS®.

ACKNOWLEDGMENTS

We thank all those who donated blood and breastmilk for this work, as well as Drs Christine Johnston and Anna Wald for providing control specimens and the National Institute of Health Tetramer Core Facility for synthesizing the human leukocyte antigen (HLA)-A*01_LTD-APC and HLA-A*24_NYN-APC tetramers.

APPENDIX A. SUPPLEMENTARY DATA

Supplementary data to this article can be found online at https://doi.org/10.1016/j.mucimm.2023.01.003.

REFERENCES

1. Hassiotou, F., Geddes, D. T. & Hartmann, P. E. Cells in human milk: state of the science. *J. Hum. Lact.* **29**, 171–182 (2013).
2. Hassiotou, F. et al. Maternal and infant infections stimulate a rapid leukocyte response in breastmilk. *Clin. Transl. Immunol.* **2**, e3 (2013).
3. Goldman, A. S., Garza, C., Nichols, B. L. & Goldblum, R. M. Immunologic factors in human milk during the first year of lactation. *J. Pediatr.* **100**, 563–567 (1982).
4. Trend, S. et al. Leukocyte populations in human preterm and term breast milk identified by multicolour flow cytometry. *PLoS One* **10**, e0135580 (2015).
5. Kent, J. C. How breastfeeding works. *J. Midwifery Womens Health* **52**, 564–570 (2007).
6. Kourtis, A. P. et al. Breast milk CD4+ T cells express high levels of C chemokine receptor 5 and CXC chemokine receptor 4 and are preserved in HIV-infected mothers receiving highly active antiretroviral therapy. *J. Infect. Dis.* **195**, 965–972 (2007).
7. Sabbaj, S. et al. Breast milk-derived antigen-specific CD8+ T cells: an extralymphoid effector memory cell population in humans. *J. Immunol.* **174**, 2951–2956 (2005).
8. Sabbaj, S. et al. Human immunodeficiency virus-specific CD8(+) T cells in human breast milk. *J. Virol.* **76**, 7365–7373 (2002).
9. Moylan, D. C. et al. Breast milk human Cytomegalovirus (CMV) viral load and the establishment of breast milk CMV-pp65-specific CD8 T cells in human CMV infected mothers. *J. Infect. Dis.* **216**, 1176–1179 (2017).
10. Lohman, B. L. et al. Prevalence and magnitude of human immunodeficiency virus (HIV) type 1-specific lymphocyte responses in breast milk from HIV-1-seropositive women. *J. Infect. Dis.* **188**, 1666–1674 (2003).
11. Ruben, F. L., Holzman, I. R. & Fireman, P. Responses of lymphocytes from human colostrum or milk to influenza antigens. *Am. J. Obstet. Gynecol.* **143**, 518–522 (1982).
12. Bryan, D. L., Hart, P. H., Forsyth, K. D. & Gibson, R. A. Immunomodulatory constituents of human milk change in response to infant bronchiolitis. *Pediatr. Allergy Immunol.* **18**, 495–502 (2007).
13. Riskin, A. et al. Changes in immunomodulatory constituents of human milk in response to active infection in the nursing infant. *Pediatr. Res.* **71**, 220–225 (2012).
14. Molès, J. P. et al. Breastmilk cell trafficking induces microchimerism-mediated immune system maturation in the infant. *Pediatr. Allergy Immunol.* **29**, 133–143 (2018).
15. Miller, R. A. Observations on the gastric acidity during the first month of life. *Arch. Dis. Child.* **16**, 22–30 (1941).
16. Catassi, C., Bonucci, A., Coppa, G. V., Carlucci, A. & Giorgi, P. L. Intestinal permeability changes during the first month: effect of natural versus artificial feeding. *J. Pediatr. Gastroenterol. Nutr.* **21**, 383–386 (1995).
17. Kalach, N., Rocchiccioli, F., de Boissieu, D., Benhamou, P. H. & Dupont, C. Intestinal permeability in children: variation with age and reliability in the diagnosis of cow's milk allergy. *Acta Paediatr.* **90**, 499–504 (2001).
18. Darby, M. G. et al. Pre-conception maternal helminth infection transfers via nursing long-lasting cellular immunity against helminths to offspring. *Sci. Adv.* **5**, eaav3058 (2019).
19. Ma, L. J., Walter, B., Deguzman, A., Muller, H. K. & Walker, A. M. Trans-epithelial immune cell transfer during suckling modulates delayed-type hypersensitivity in recipients as a function of gender. *PLoS One* **3**, e3562 (2008).
20. Zhou, L. et al. Two independent pathways of maternal cell transmission to offspring: through placenta during pregnancy and by breast-feeding after birth. *Immunology* **101**, 570–580 (2000).
21. Tuboly, S., Bernáth, S., Glávits, R., Kovács, A. & Megyeri, Z. Intestinal absorption of colostral lymphocytes in newborn lambs and their role in the development of immune status. *Acta Vet. Hung.* **43**, 105–115 (1995).
22. Balle, C. et al. Factors influencing maternal microchimerism throughout infancy and its impact on infant T cell immunity. *J. Clin. Invest.* **132**, e148826 (2022).
23. Gonçalves, J. et al. Secretory IgA and T cells targeting SARS-CoV-2 spike protein are transferred to the breastmilk upon mRNA vaccination. *Cell Rep. Med.* **2**:100468.
24. Jackson, L. A. et al. An mRNA vaccine against SARS-CoV-2 – Preliminary Report. *N. Engl. J. Med.* **383**, 1920–1931 (2020).
25. Polack, F. P. et al. Safety and efficacy of the BNT162b2 mRNA COVID-19 vaccine. *N. Engl. J. Med.* **383**, 2603–2615 (2020).
26. Collier, A. Y. et al. Immunogenicity of COVID-19 mRNA vaccines in pregnant and lactating women. *JAMA* **325**, 2370–2380 (2021).
27. Skelly, D. T. et al. Two doses of SARS-CoV-2 vaccination induce robust immune responses to emerging SARS-CoV-2 variants of concern. *Nat. Commun.* **12**, 5061 (2021).
28. Ssemaganda, A. et al. Expansion of cytotoxic tissue-resident CD8+ T cells and CCR6+CD161+ CD4+ T cells in the nasal mucosa following mRNA COVID-19 vaccination. *Nat. Commun.* **13**, 3357 (2022).
29. Rempala, G. A. & Seweryn, M. Methods for diversity and overlap analysis in T-cell receptor populations. *J. Math. Biol.* **67**, 1339–1368 (2013).
30. Rytlewski, J. et al. Model to improve specificity for identification of clinically-relevant expanded T cells in peripheral blood. *PLoS One* **14**, e0213684 (2019).
31. Dash, P. et al. Quantifiable predictive features define epitope-specific T cell receptor repertoires. *Nature* **547**, 89–93 (2017).
32. Mayer-Blackwell, K. et al. TCR meta-clonotypes for biomarker discovery with *tcrdist3* enabled identification of public, HLA-restricted clusters of SARS-CoV-2 TCRs. *Elife* **10**, e68605 (2021).
33. Gil, A., Yassai, M. B., Naumov, Y. N. & Selin, L. K. Narrowing of human influenza A virus-specific T cell receptor alpha and beta repertoires with increasing age. *J. Virol.* **89**, 4102–4116 (2015).
34. Chen, G. et al. Sequence and structural analyses reveal distinct and highly diverse human CD8+ TCR repertoires to immunodominant viral antigens. *Cell Rep.* **19**, 569–583 (2017).
35. Nolan, S. et al. A large-scale database of T-cell receptor beta (TCRβ) sequences and binding associations from natural and synthetic exposure to SARS-CoV-2. *Research Square* 2020. https://doi.org/10.21203/rs.3.rs-51964/v1.
36. Minervina, A. A. et al. SARS-CoV-2 antigen exposure history shapes phenotypes and specificity of memory CD8+ T cells. *Nat. Immunol.* **23**, 781–790 (2022).
37. Shomuradova, A. S. et al. SARS-CoV-2 epitopes are recognized by a public and diverse repertoire of human T cell receptors. *Immunity* **53**, 1245–1257.e5 (2020).
38. Agerer, B. et al. SARS-CoV-2 mutations in MHC-I-restricted epitopes evade CD8+ T cell responses. *Sci. Immunol.* **6**, eabg6461 (2021).
39. Dykema, A. G. et al. Functional characterization of CD4+ T cell receptors crossreactive for SARS-CoV-2 and endemic coronaviruses. *J. Clin. Invest.* **131**, e146922 (2021).
40. Nguyen, T. H. O. et al. CD8+ T cells specific for an immunodominant SARS-CoV-2 nucleocapsid epitope display high naive precursor frequency and TCR promiscuity. *Immunity* **54**, 1066–1082.e5 (2021).
41. Snyder, T. M. et al. Magnitude and dynamics of the T-cell response to SARS-CoV-2 infection at both individual and population levels. *medRxiv* 2020. https://doi.org/10.1101/2020.07.31.20165647.
42. Lefrançois, L. & Marzo, A. L. The descent of memory T-cell subsets. *Nat. Rev. Immunol.* **6**, 618–623 (2006).
43. Goff, S. L. & Danforth, D. N. The role of immune cells in breast tissue and immunotherapy for the treatment of breast cancer. *Clin. Breast Cancer* **21**, e63–e73 (2021).
44. Ramanan, D. et al. An immunologic mode of multigenerational transmission governs a gut Treg setpoint. *Cell* **181**, 1276–1290.e13 (2020).
45. Hanna, N. et al. Detection of messenger RNA COVID-19 vaccines in human breast milk. *JAMA Pediatr.* **176**, 1268–1270 (2022).
46. Robins, H. S. et al. Comprehensive assessment of T-cell receptor beta-chain diversity in alphabeta T cells. *Blood* **114**, 4099–4107 (2009).
47. Bagaev, D. V. et al. VDJdb in 2019: database extension, new analysis infrastructure and a T-cell receptor motif compendium. *Nucleic Acids Res.* **48**, D1057–D1062 (2020).
48. Chen, S. Y., Yue, T., Lei, Q. & Guo, A. Y. TCRdb: a comprehensive database for T-cell receptor sequences with powerful search function. *Nucleic Acids Res.* **49**, D468–D474 (2021).
49. Tickotsky, N., Sagiv, T., Prilusky, J., Shifrut, E. & Friedman, N. McPAS-TCR: a manually curated catalogue of pathology-associated T cell receptor sequences. *Bioinformatics* **33**, 2924–2929 (2017).
50. Larsen, S. E. et al. Qualification of ELISA and neutralization methodologies to measure SARS-CoV-2 humoral immunity using human clinical samples. *J. Immunol. Methods* **499**:113160.

Supplementary Material

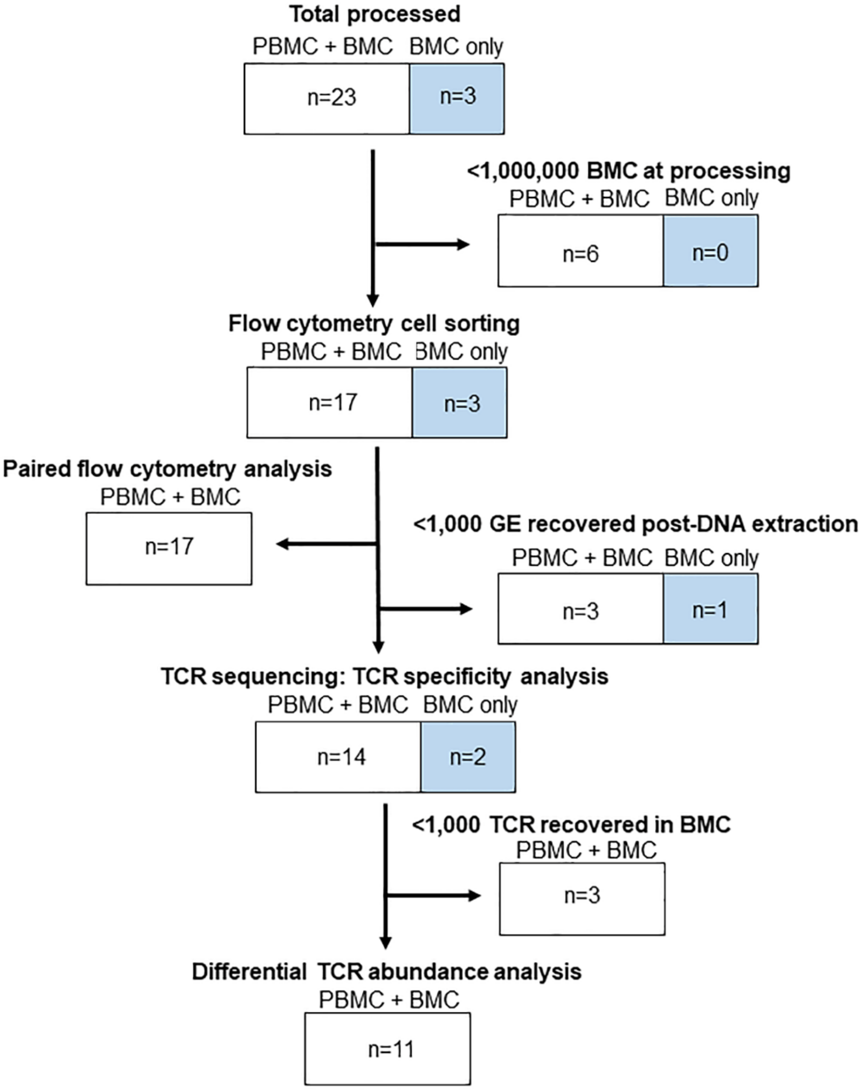

Fig. S1. Inclusion criteria for study analyses. Breastmilk was collected from n=26 individuals, n=23 of which also contributed blood samples. Breastmilk and blood were processed for breastmilk cells (BMC) and peripheral blood mononuclear cells (PBMC), respectively. Individuals (n=6) were excluded from study analyses if <1,000,000 BMC were recovered at processing. Flow cytometry cell sorting was performed for n=20 individuals. Paired flow cytometry analysis was performed on samples for which both BMC and PBMC were available and at least 100 CD4+ and

CD8+ T cells were recorded (n=17). If <1,000 DNA genomic equivalents (GE) were recovered from sorted BMC, individuals (n=4) were excluded from TCR sequencing and TCR specificity analysis (n=16 included). If TCR sequencing yielded fewer than 1,000 TCR templates, individuals (n=3) were excluded from differential TCR abundance analysis. Individuals which met the above criteria and had both BMC and PBMC available (n=11) were included in differential TCR abundance analysis. Spike tetramer staining on pre- and post-3rd SARS2 mRNA vaccine dose samples was performed for n=5 individuals who returned from the original cohort and n=3 newly enrolled individuals.

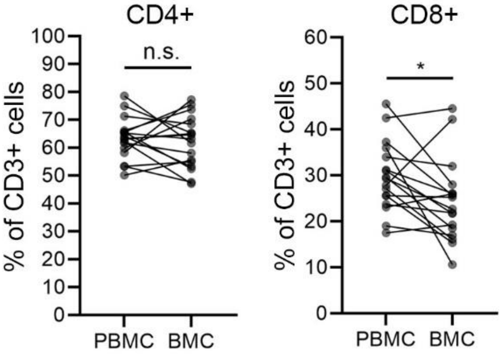

Fig. S2. CD4+ and CD8+ T cell relative frequency in breastmilk and peripheral blood. Frequencies of CD4+ and CD8+ among CD3+ cells in BMC and PBMC were determined by flow cytometry (n=17). Comparisons made with linear regression and clustering by individual, *$p < 0.05$, n.s. (not significant). CD4+ (PBMC vs. BMC): 63% vs. 62%, p=0.6; CD8+ (PBMC vs. BMC): 30% vs. 24%, p=0.03.

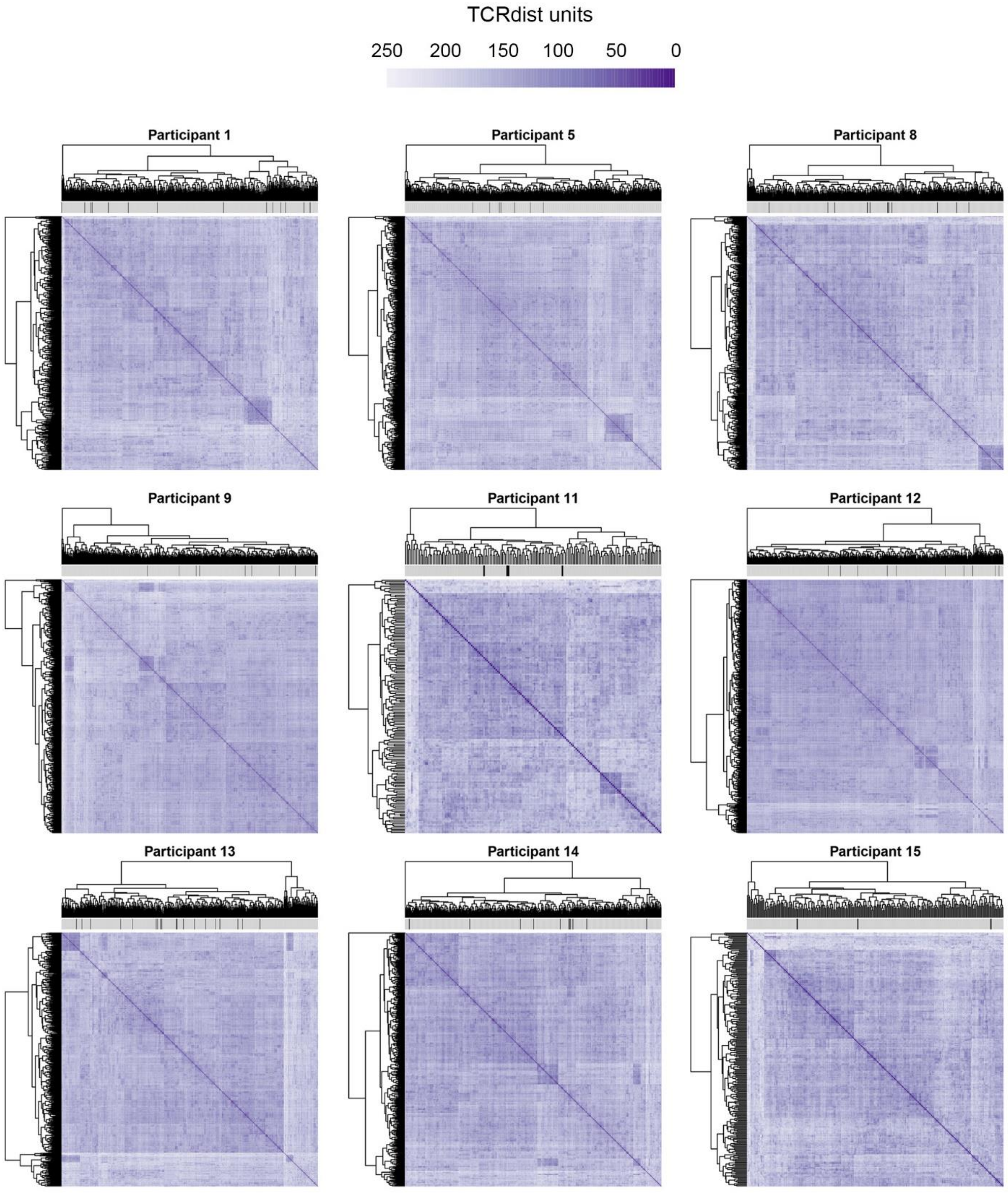

Fig. S3. Overabundant TCR clones in breastmilk are diverse. Each TCRβ CDR3 amino acid sequence obtained from a participant's BMC was compared to all other TCRβ CDR3 amino acid sequences within that participant's BMC using tcrdist3 (n=11, n=9 shown here and n=2 presented in **Fig. 3A**). Heatmaps depict distance units and clustering within each participant's breastmilk T cell repertoire. Black ticks denote TCRβ sequences that were significantly enriched in BMC relative to PBMC in this participant.

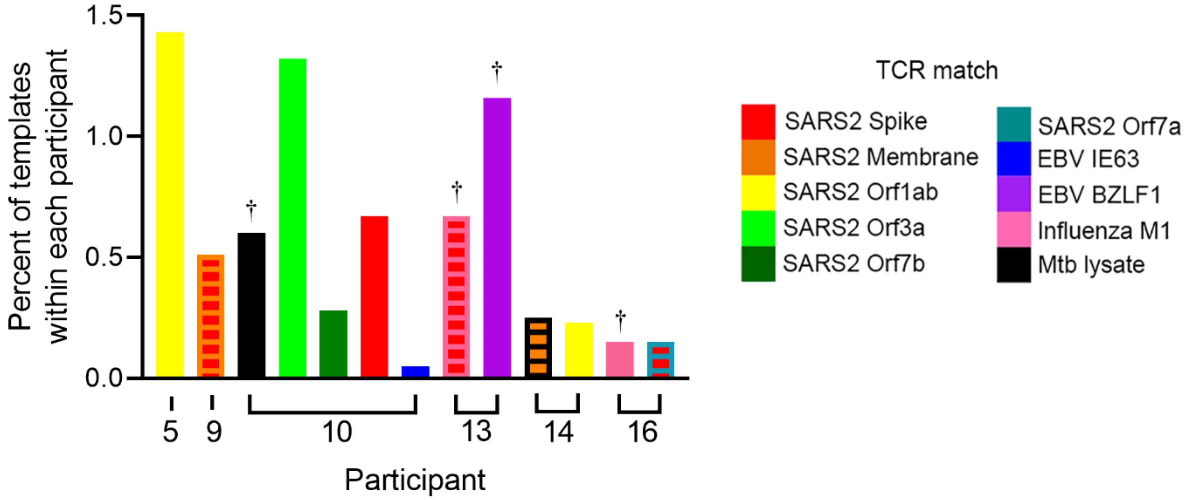

Fig. S4. Pathogen-specific TCR clonotypes are present in overabundant breastmilk T cell clonotypes. CDR3 amino acid sequences of overabundant breastmilk clones from all participants were compared to TCRβ sequence databases populated by validated epitope-specific TCRs. Epitope matches were considered a direct match (marked with †) if the CDR3 amino acid and TRBV gene were identical and were considered a predicted match if the CDR3 amino acid sequences were identical but V gene usage was mismatched. The proportion of individual pathogen-specific T cell templates among all T cell templates within each participant is shown. Dual color striped bars indicate that the TCR has been reported to have specificity to two epitopes.

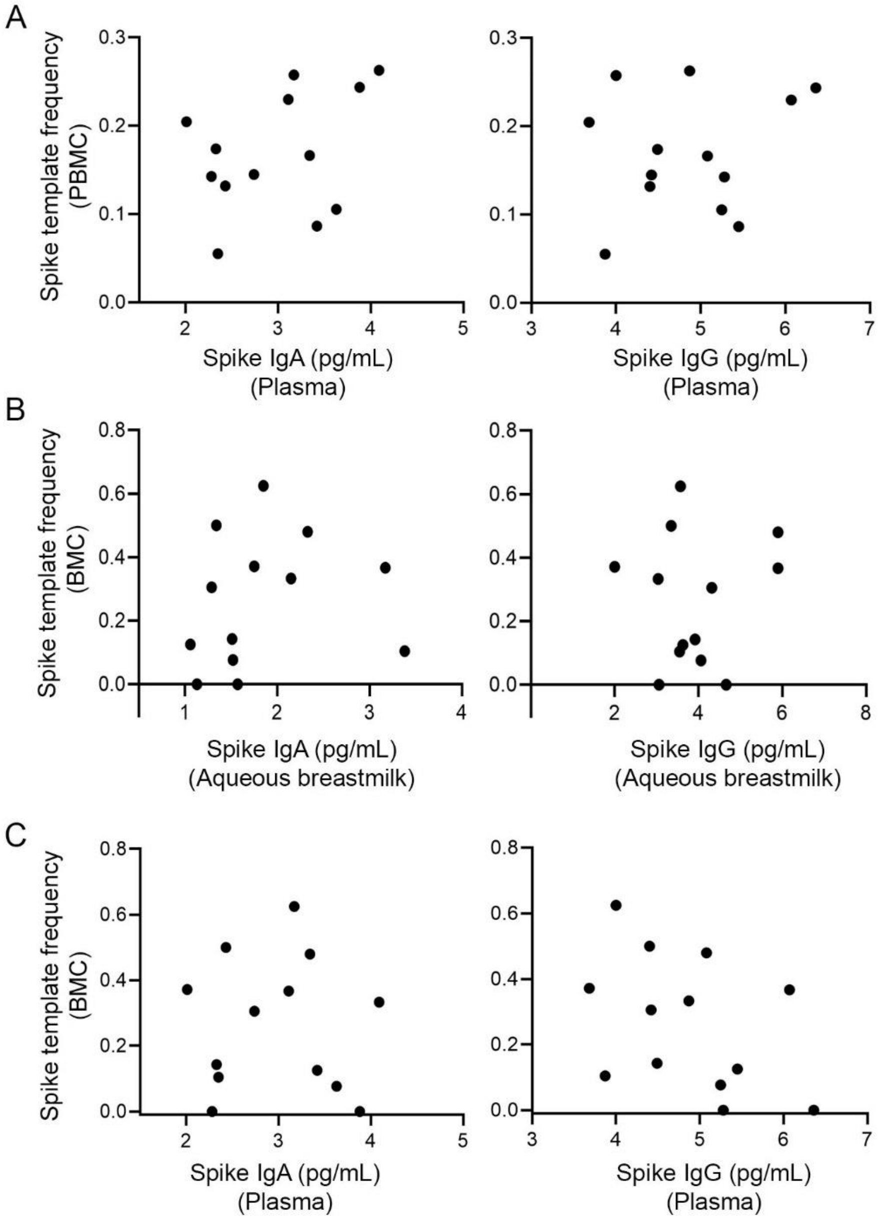

Fig. S5. Spike-specific antibody levels and the frequency of spike-specific T cells were not strongly correlated. Data were analyzed using a negative binomial regression model adjusting for time since delivery (n=13). (**A**) The frequency of Spike-predicted TCRβ templates in PBMC are shown as a function of Spike-specific IgA level (left) and IgG level (right) in the plasma. Spike-specific IgA by Spike-specific TCR frequency: IRR=1.1, 95% C.I. (0.85-1.5), p=0.4; Spike-specific IgG by spike-specific TCR frequency: IRR=1.1, 95% C.I. (0.90-1.3), p=0.4 (**B**) The frequency of

Spike-predicted TCRβ templates in BMC are shown as a function of Spike-specific IgA level (left) and IgG level (right) in aqueous breastmilk. Spike-specific IgA by Spike-specific TCR frequency: IRR=0.95, 95% C.I. (0.66-1.4), p=0.8; spike-specific IgG by spike-specific TCR frequency: IRR=0.97, 95% C.I. (0.88-1.1), p=0.6. (**C**) The frequency of spike-predicted TCRβ templates in BMC are shown as a function of Spike-specific IgA level (left) and IgG level (right) in the plasma. Spike-specific IgA by Spike-specific TCR frequency: IRR=0.86, 95% C.I. (0.59-1.3), p=0.4; spike-specific IgG by spike-specific TCR frequency: IRR=0.9, 95% C.I. (0.68-1.1), p=0.3.

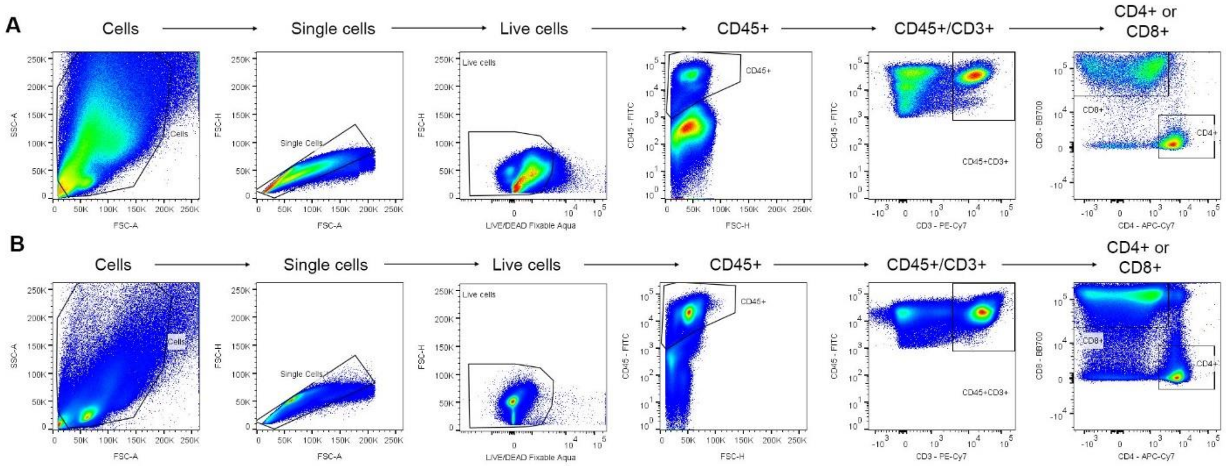

Fig. S6. Gating strategy for phenotyping BMC and PBMC. The gating strategy used to analyze (**A**) BMC and (**B**) PBMC that were stained with flow cytometry panel 1.

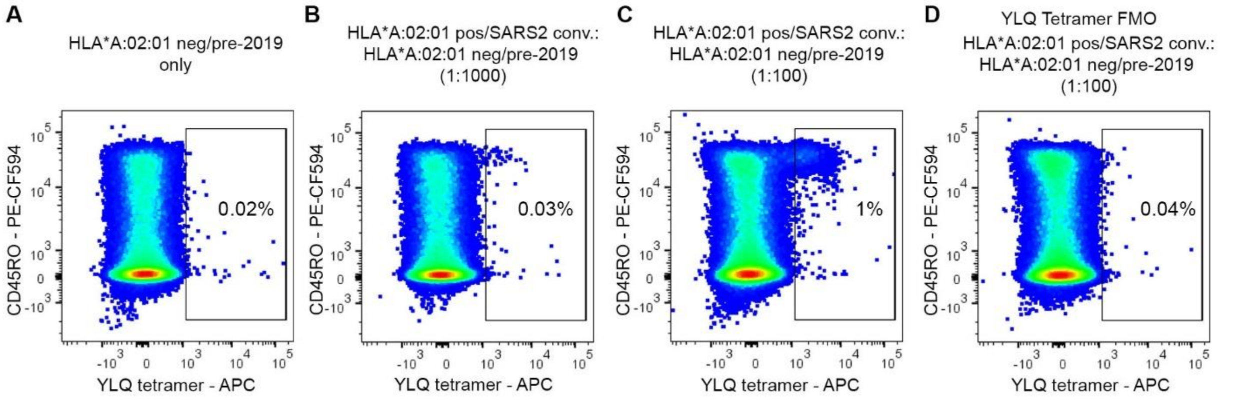

Fig. S7. Validation of Spike-loaded tetramer HLA*A02_YLQ. Positive and negative controls were analyzed for HLA-A*02:01-YLQ tetramer positive cells. (**A**) PBMC from an HLA-A*02:01 negative donor obtained prior to 2019. (**B**) PBMC from an HLA-A*02:01 positive, SARS2 convalescent donor were mixed with PBMC from an HLA-A*02:01 negative donor obtained prior to 2019 at a ratio of 1:1000. (**C**) PBMC from an HLA-A*02:01 positive, SARS2 convalescent donor were mixed with PBMC from an HLA-A*02:01 negative donor obtained prior to 2019 at a ratio of 1:100. (**D**) The fluorescence minus one (FMO) HLA-A*02:01-YLQ tetramer control for the PBMC mixture described in (**C**) is shown.

Chapter 7: Repeated mRNA vaccination sequentially boosts SARS-CoV-2-specific CD8$^+$ T cells in persons with previous COVID-19

Emily S. Ford, Koshlan Mayer-Blackwell, Lichen Jing, Kerry J. Laing, Anton M. Sholukh, Russell St. Germain, Emily L. Bossard, Hong Xie, Thomas H. Pulliam, Saumya Jani, Stacy Selke, Carlissa J. Burrow, Christopher L. McClurkan, Anna Wald, Alexander L. Greninger, Michael R. Holbrook, Brett Eaton, Elizabeth Eudy, Michael Murphy, Elena Postnikova, Harlan S. Robins, Rebecca Elyanow, Rachel M. Gittelman, Matyas Ecsedi, Elise Wilcox, Aude G. Chapuis, Andrew Fiore-Gartland, David M. Koelle

Nature Immunology, January 2024

CHAPTER SUMMARY: In this chapter, we studied the kinetics of SARS-CoV-2-specific CD8 T cells in response to vaccinations. We observed that vaccination led to large expansions in spike-reactive T-cells. Additionally, using tcrdist3, we identified clusters of T cells with similar T cell receptors that were activated by and expanded in response to *ex vivo* stimulation. By focusing on clusters with similar TCRs from multiple patients with shared HLA types, we were able to de-orphan peptide-HLA-TCR pairs and identify novel TCRs that identify an immunodominant A03-restricted spike epitope.

nature immunology

Resource

https://doi.org/10.1038/s41590-023-01692-x

Repeated mRNA vaccination sequentially boosts SARS-CoV-2-specific CD8$^+$ T cells in persons with previous COVID-19

Received: 8 October 2022

Accepted: 27 October 2023

Emily S. Ford[1,2,12], **Koshlan Mayer-Blackwell**[2,12], **Lichen Jing**[1,12], **Kerry J. Laing**[1], **Anton M. Sholukh**[2], **Russell St. Germain**[2], **Emily L. Bossard**[2], **Hong Xie**[3], **Thomas H. Pulliam**[1], **Saumya Jani**[1,3], **Stacy Selke**[3], **Carlissa J. Burrow**[1], **Christopher L. McClurkan**[1], **Anna Wald**[1,2,3,4], **Alexander L. Greninger**[2,3], **Michael R. Holbrook**[5], **Brett Eaton**[5], **Elizabeth Eudy**[5], **Michael Murphy**[5], **Elena Postnikova**[5], **Harlan S. Robins**[6], **Rebecca Elyanow**[6], **Rachel M. Gittelman**[6,10], **Matyas Ecsedi**[7,11], **Elise Wilcox**[7], **Aude G. Chapuis**[1,7], **Andrew Fiore-Gartland**[2] & **David M. Koelle**[1,2,3,8,9] ✉

Severe acute respiratory syndrome coronavirus 2 (SARS-CoV-2) hybrid immunity is more protective than vaccination or previous infection alone. To investigate the kinetics of spike-reactive T (T_S) cells from SARS-CoV-2 infection through messenger RNA vaccination in persons with hybrid immunity, we identified the T cell receptor (TCR) sequences of thousands of index T_S cells and tracked their frequency in bulk TCRβ repertoires sampled longitudinally from the peripheral blood of persons who had recovered from coronavirus disease 2019 (COVID-19). Vaccinations led to large expansions in memory T_S cell clonotypes, most of which were CD8$^+$ T cells, while also eliciting diverse T_S cell clonotypes not observed before vaccination. TCR sequence similarity clustering identified public CD8$^+$ and CD4$^+$ TCR motifs associated with spike (S) specificity. Synthesis of longitudinal bulk ex vivo single-chain TCRβ repertoires and paired-chain TCRαβ sequences from droplet sequencing of T_S cells provides a roadmap for the rapid assessment of T cell responses to vaccines and emerging pathogens.

Hybrid immunity from natural infection and vaccination is more protective against SARS-CoV-2 infection than either alone[1–3]. Vaccination after SARS-CoV-2 infection increases the abundance of virus-specific memory T (T_M) cells[4–7] and diversifies the spike (S)-specific T_M cell pool[8,9], two potential mechanisms by which hybrid immunity is protective against severe disease[10], despite antigenic escape from neutralizing antibodies (nAbs) by variants of concern (VOCs)[11]. In most individuals, the recognition of multiple T cell epitopes[12,13] largely preserves T cell responses despite VOC evolution[14], although T cell escape has been observed[15]. To profile the development of hybrid immunity,

---

[1]Department of Medicine, University of Washington, Seattle, WA, USA. [2]Vaccine and Infectious Disease Division, Fred Hutchinson Cancer Center, Seattle, WA, USA. [3]Department of Laboratory Medicine and Pathology, University of Washington, Seattle, WA, USA. [4]Department of Epidemiology, University of Washington, Seattle, WA, USA. [5]Integrated Research Facility, Division of Clinical Research, National Institute of Allergy and Infectious Diseases, National Institutes of Health, Fort Detrick, Frederick, MD, USA. [6]Adaptive Biotechnologies, Seattle, WA, USA. [7]Clinical Research Division, Fred Hutchinson Cancer Center, Seattle, WA, USA. [8]Department of Global Health, University of Washington, Seattle, WA, USA. [9]Department of Translational Research, Benaroya Research Institute, Seattle, WA, USA. [10]Present address: Guardant Health, Redwood City, CA, USA. [11]Present address: Takeda Oncology, Cambridge, MA, USA. [12]These authors contributed equally: Emily S. Ford, Koshlan Mayer-Blackwell, Lichen Jing. ✉e-mail: dkoelle@medicine.washington.edu

we collected 259 longitudinal peripheral blood mononuclear cell (PBMC) samples and 46 nasal swabs from 54 persons, from COVID-19 convalescence through three mRNA vaccinations.

To investigate the diversity and kinetics of T_S cells, we identified T cells that expressed the activation-induced markers (AIMs) CD69 and CD137 on S peptide stimulation of PBMCs, defined their $CD4^+$ and $CD8^+$ T cell phenotypes with barcoded monoclonal antibodies (mAbs) and obtained paired-chain T cell receptor-αβ (TCRαβ) by single-cell sequencing (hereafter $CD69^+CD137^+$ AIM-scTCRαβ-seq). We also identified activated S-reactive $CD4^+$ *TRB* clonotypes from PBMCs expressing either one of CD69 or CD137 plus at least one of the AIM CD134 or CD154 using single-chain *TRB* locus sequencing ($CD4^+$AIM-TCRβ-seq). To track T_S cells longitudinally, we matched the TCRβ sequences from $CD69^+CD137^+$ AIM-scTCRαβ-seq and $CD4^+$ AIM-TCRβ-seq to the *TRB* locus sequences from bulk PBMCs (hereafter TCRβ-seq) obtained at six intervals between convalescence from SARS-CoV-2 infection and receipt of three mRNA vaccinations. By tracking the frequency of index $CD69^+CD137^+$ AIM-scTCRαβ-seq T_S clones within bulk repertoires at all time points and matching to pre-vaccine memory subset repertoires, we were able to measure the recruitment and expansion of T_S cell clonotypes as hybrid immunity developed. We observed divergent clonotype-level kinetics between S-reactive circulating $CD8^+$ and $CD4^+$ T cells. Sequence similarity clustering of paired-chain TCRs, identified by $CD69^+CD137^+$ AIM-scTCRαβ-seq, permitted inference of the restricting HLA alleles for many S-specific TCR motifs. Taken together, integration of bulk and single-cell TCR sequencing with HLA information provides a broadly applicable roadmap to 'de-orphan' pathogen-specific TCR sequences without a priori knowledge of epitope-level specificity.

Results

Vaccination provokes heterogeneous clonal expansions

To investigate heterogeneity in T cell response to vaccination after COVID-19, we performed bulk TCRβ-seq on PBMCs from 54 adults (28 females and 26 males, median age = 60.3 years, range = 31.4–73.5 years) who were infected with SARS-CoV-2 between April and August 2020, when the ancestral-like D614G strain prevailed[16]. The cohort contained 35 participants with mild or moderate (World Health Organization (WHO) severity scale 1–2)[17] and 19 with severe (WHO severity scale 3–7) COVID-19 (Supplementary Table 1)[18–21]. Blood samples were obtained at six visits. Visit E00 ($n = 54$) occurred at day 78.5 (median, interquartile range (IQR) = 56–105) after COVID-19 diagnosis. Visit E00.5 ($n = 16$, 12 with severe COVID-19) occurred at day 146 (median, IQR 139–147) days after COVID-19 diagnosis. Visit E01 ($n = 34$, 16 with severe COVID-19) occurred immediately before vaccine dose 1 (BNT162b2 or mRNA-1273), corresponding to day 369 (median, IQR = 333–390) after symptom onset. Visit E02 ($n = 52$) occurred at day 19.5 (median, IQR = 15–24) after dose 1 and before dose 2. Visit E03 ($n = 53$) occurred at day 24 (median, IQR = 20–28) after dose 2. Visit E04 ($n = 7$, 2 with severe COVID-19) occurred before dose 3, at day 274 (median, IQR = 251–308). Visit E05 ($n = 44$, 15 with severe COVID-19) occurred at day 41.5 (median, IQR = 26–69) after dose 3 (Fig. 1a and Extended Data Fig. 1).

Before evaluating T cell specificity directly, we examined the kinetics of all unique TCRβ sequences (hereafter, *TRB* clonotypes) detectable in blood. To assess the impact of vaccination on the structure of the T cell repertoire, we compared the frequency of *TRB* clonotypes across the E01–E05 time points using pairwise differential relative abundance in the bulk *TRB* repertoire at each time point in 32 participants (Fig. 1a, Extended Data Fig. 2 and Supplementary Table 2). Among participants with the E01 and E03 repertoires, 21 of 32 had large expansions (1,000-fold or greater) of individual *TRB* clonotypes at E03 (after dose 2) compared to E01 (before vaccine) (Extended Data Fig. 2). To track the kinetics of potentially vaccine-expanded *TRB* clonotypes over the course of the study, we identified clones increasing by a $\log_2$ fold change > 2 and a statistically significant change in frequency between serial visits and between E01 and E03 (hereafter E01–E03 expanded), when evaluated using a Fisher's exact test with correction for multiple hypotheses (false discovery rate (FDR)-adjusted $q < 0.05$) (Fig. 1a and Supplementary Tables 3 and 4).

When assessing the clonal expansions induced by the first and second mRNA vaccinations, a median of 38 (IQR = 21–80, $n = 28$) and 44 (IQR = 29–69, $n = 32$) statistically significant clonal expansions occurred across the intervals E01–E02 and E02–E03, respectively (Supplementary Table 4). Cumulatively, a median of 72 (IQR = 51–104) statistically significant E01–E03 expanded *TRB* clonotypes were detected per participant, representing a median of 1.8% (IQR = 0.9–3.5%) of the circulating T cell repertoire in each participant (Supplementary Table 4). To assess the contribution of T cells established during infection to the vaccine response, we tracked *TRB* clonotypes that were either detected at E00 or E01 (post-infection *TRB* clonotypes, hereafter *TRB*-PI) or detected exclusively starting at E02 (post-vaccination *TRB* clonotypes, hereafter *TRB*-PV) (Fig. 1b). At E02 and E03, the total frequencies of E01–E03 expanded *TRB* clonotypes ranged from 0.001% to 11% and 1% to 26%, respectively (Fig. 1c). At E03, the combined abundance of E01–E03 expanded *TRB*-PI represented 0.1% to 25% of each participant's repertoire while *TRB*-PV represented 0.01% to 3% (Fig. 1c,d and Extended Data Fig. 3a). *TRB*-PI were numerically dominant (Fig. 1f); however, the proportion of unique *TRB* clonotypes was balanced between *TRB*-PI and *TRB*-PV (Fig. 1e,g).

The repertoires of participants with E01–E03 expanded clones exceeding 5% of their total repertoire at E03 (P673, P582, P836, P761 and P581) were characterized by a strong polyclonal expansion of clonotypes detected after infection (Fig. 1f). The breadth (that is, diversity) of *TRB*-PV increased after dose 2 (E03) compared to dose 1 (E02) (Fig. 1g), indicating that successive doses increased the frequency and diversity of expanded clones. Most E01–E03 expanded *TRB*-PV persisted in participant repertoires through to E05, but these clonotypes were not as likely to persist as expanded clonotypes detected after infection (Extended Data Fig. 3b).

Next, to evaluate the memory phenotype of clonotypes detected before the start of the vaccine series, we performed TCRβ-seq on sorted, pooled $CCR7^-CD45RA^+$, $CCR7^+CD45RA^-$ and $CCR7^-CD45RA^-$ ($CD4^+$ and $CD8^+$ combined) T_M cells (Methods) from PBMCs isolated at E00 in seven participants (median age = 66.6, 2 female, 2 with severe COVID-19) (Supplementary Fig. 1 and Supplementary Table 5). Cross-referencing *TRB* sequences from E00 T_M cells against E01–E03 expanded *TRB* clonotypes indicated that at least 25–84% (median = 66%) of vaccine-expanded *TRB*-PI had a T_M cell phenotype before vaccination (Supplementary Fig. 2a,b). Thus, serial bulk PBMC *TRB* sequencing identified clonotype expansions across each of two mRNA vaccine doses approximately 1 year after COVID-19, with a substantial contribution of confirmed T_M cells.

Vaccination strongly expands $CD8^+$ T cells in blood

To obtain paired TCRαβ sequences and determine the $CD4^+$ versus $CD8^+$ T cell phenotype of E01–E03 expanded *TRB* clonotypes, we sorted T cells that coexpressed the activation-induced markers CD69 and CD137 after 18-h stimulation with peptides spanning the SARS-CoV-2 S protein (hereafter S peptides) from the E03 PBMCs of 17 participants (median age = 60.6 years, range = 40.9–73.5, 4 with severe COVID-19, 6 female) with at least 50 E01–E03 expanded *TRB* clonotypes (Supplementary Table 4). Droplet single-cell TCR sequencing of $CD69^+CD137^+$ double-positive T cells ($CD69^+CD137^+$ AIM-scTCRαβ-seq) was then used to define T_S TCRs. *TRB* clonotypes from bulk TCRβ-seq were classified as T_S if the frequency of the *TRB* rearrangement was enriched by $CD69^+CD137^+$ AIM-scTCRαβ-seq compared to unsorted bulk TCRβ-seq at the same time point (Methods). The clonotype frequency of T_S cells in $CD69^+CD137^+$ AIM-scTCRαβ-seq was correlated with the frequency in the bulk repertoires (Methods and Extended

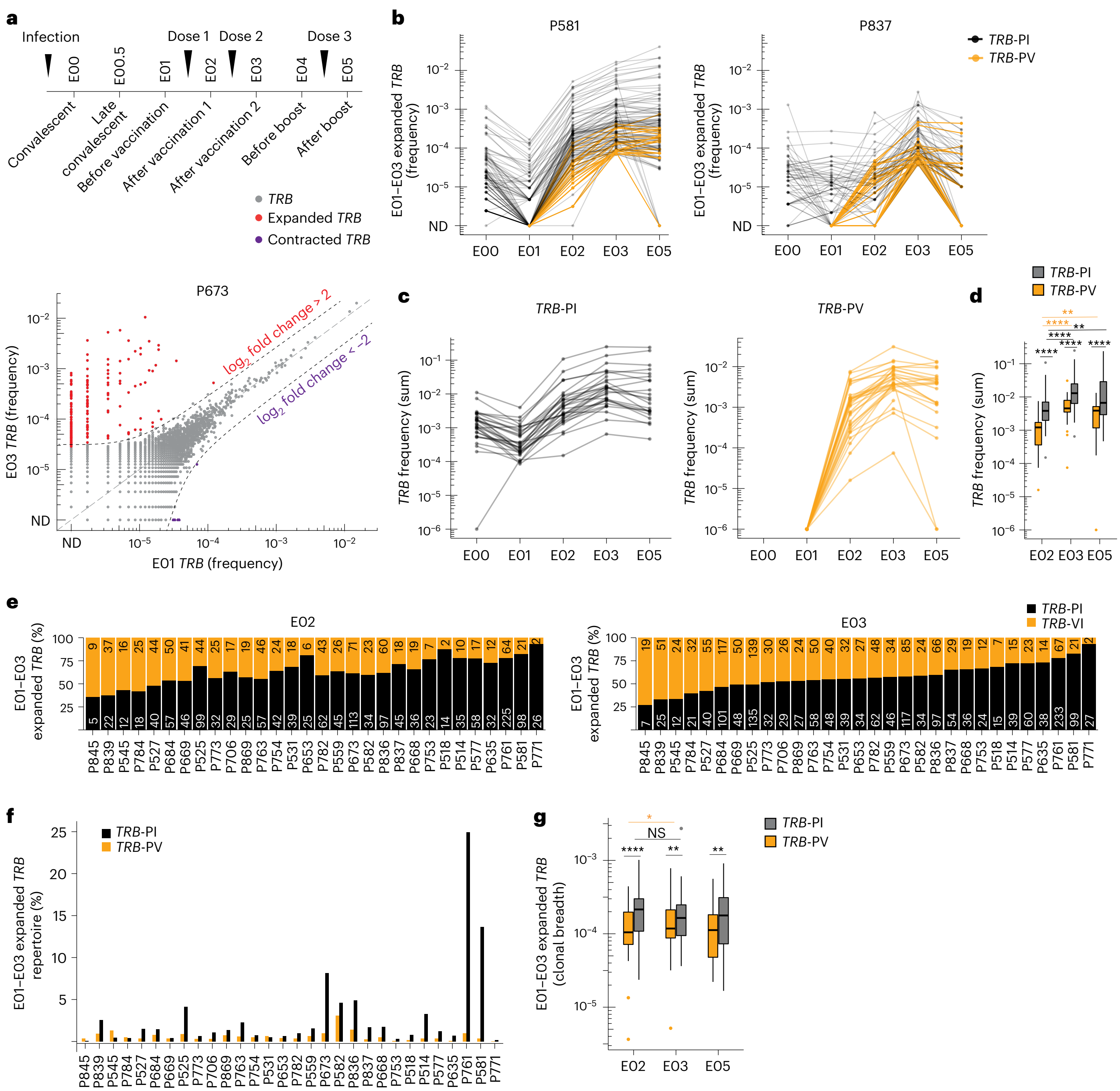

Fig. 1 | Vaccines expand previously detected and low-abundance clonotypes. **a**, Timing of PBMC sampling and frequency (fraction of the bulk *TRB* repertoire) of individual clonotypes in E01 versus E03 in one representative participant (P673). Expanded (or contracted) clonotypes were defined as a log$_2$ fold change > 2 (or <0.5) and Fisher's exact test FDR-adjusted $P < 0.05$. **b**, Frequency of E01–E03 expanded clonotypes from E00 through E05 in two representative participants (P581 and P837). **c**, Sum of E01–E03 expanded *TRB* clonotype frequency (abundance) per participant detected at E00 and E01 (*TRB*-PI) or detected exclusively starting at E02 (*TRB*-PV, $n = 28$). **d**, Comparison of abundance of E01–E03 expanded *TRB*-PI and *TRB*-PV at E02 ($n = 30$), E03 ($n = 30$) and E05 ($n = 28$) relative to E01. **e**, Number of unique E01–E03 expanded *TRB*-PI and *TRB*-PV clonotypes detected at E02 (after dose 1) and E03 (after dose 2), ranked according to the *TRB*-PI fraction of expanded clonotypes at E03. **f**, Breadth of E01–E03 expanded *TRB*-PI and *TRB*-PV clonotypes at E02 ($n = 30$), E03 ($n = 30$) and E05 ($n = 28$). **g**, Percentage of repertoire composed of E01–E03 expanded *TRB* clonotypes at E02 ($n = 30$), E03 ($n = 30$) and E05 ($n = 28$). In **d**, **f** and **g**, the level of statistical significance calculated using a Wilcoxon rank-sum test between groups or Wilcoxon signed-rank test within groups between time periods is indicated. NS, not significant, $^{*}P < 0.05$, $^{**}P < 0.01$, $^{****}P < 0.0001$. The box plots represent the median, IQR and whiskers (1.5 times the IQR). All tests were two-sided.

Data Fig. 4). We identified 5,733 unique S-activated, paired TCRαβ clonotypes (Methods and Supplementary Table 6), with roughly equal numbers of CD4$^+$ and CD8$^+$ TCRαβ clonotypes (Supplementary Table 7). TCRβ-seq of nasal swabs at E05 (after dose 3) showed that T$_S$ identified by CD69$^+$CD137$^+$ AIM-scTCRαβ-seq were detected in the nasal mucosa in 13 of 14 participants with CD69$^+$CD137$^+$ AIM-scTCRαβ-seq data who performed nasal swabs (Extended Data Fig. 5).

There was substantial overlap between CD69$^+$CD137$^+$ AIM-scTCRαβ-seq clones and E01–E03 expanded *TRB* clonotypes (Fig. 2a and Extended Data Fig. 6). In 12 participants with both

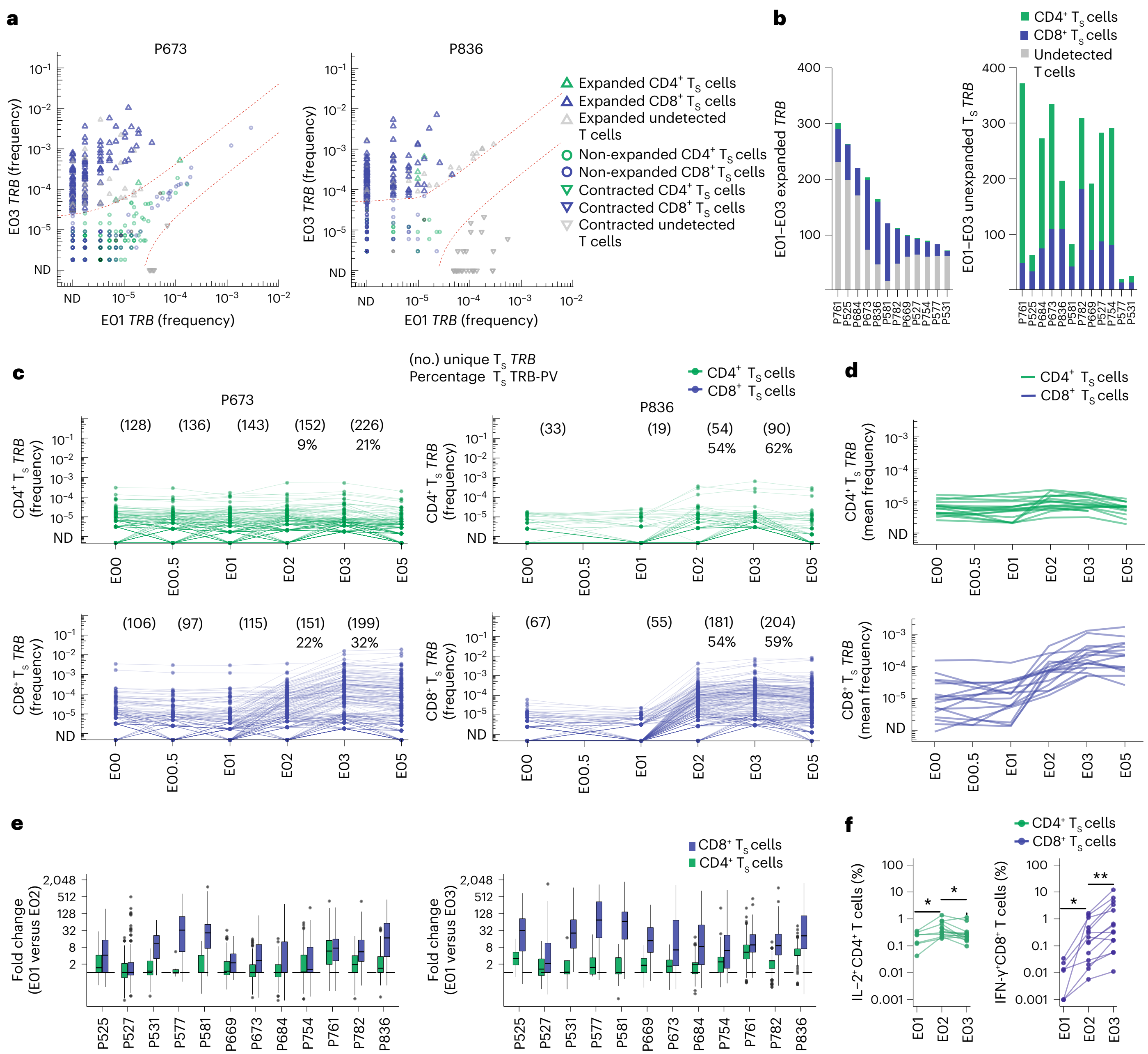

Fig. 2 | Longitudinal kinetics of S-reactive clonotypes defined by AIM-scTCRαβ-seq from after infection to before vaccination. a, Overlay of *TRB* sequences from CD69$^+$CD137$^+$ AIM-scTCRαβ-seq of T$_S$ cells onto bulk *TRB* clonotype frequency at E01 and E03 in two representative participants. E01–E03 expanded, non-expanded or contracted *TRB* clonotypes for *TRB* sequences matching CD69$^+$CD137$^+$ AIM-scTCRαβ-seq (T$_S$) and unmatched *TRB* sequences (undetected) are shown. **b**, Numbers of expanded or non-expanded PBMC *TRB*-defined clonotypes matching CD8$^+$ or CD4$^+$ T$_S$ clonotypes in 12 participants also with E01–E03 samples. **c**, Longitudinal tracking of CD69$^+$CD137$^+$ AIM-scTCRαβ-seq-identified CD4$^+$ and CD8$^+$ T$_S$ *TRB* clonotype abundance in the PBMCs of two representative participants. The number of unique CD69$^+$CD137$^+$ AIM-scTCRαβ-seq *TRB* clonotypes from E03 detected at each time point are shown. The percentages represent CD69$^+$CD137$^+$ AIM-scTCRαβ-seq *TRB*-PV clonotypes for the E02 and E03 time points. **d**, Mean abundances of S-reactive CD4$^+$ and CD8$^+$ T cell clonotypes identified by CD69$^+$CD137$^+$ AIM-scTCRαβ-seq in 17 participants at E00–E05. **e**, Distribution of fold changes (median, box (IQR) and whiskers (1.5 times the IQR)) observed for S-reactive CD4$^+$ or CD8$^+$ T cell clonotypes between E01 and E02 and E01 and E03. **f**, Intracellular cytokine staining after stimulation of PBMCs isolated at E01 ($n = 7$), E02 ($n = 14$) and E03 ($n = 14$) with S peptides. The level of statistical significance calculated using a paired, two-sided Wilcoxon signed-rank test is indicated. *$P < 0.05$, **$P < 0.01$.

datasets (median age = 62.2 years, range = 47.7–73.5, 3 female, 2 with severe COVID-19), a median of 34% (IQR = 26–53%) of CD69$^+$CD137$^+$ AIM-scTCRαβ-seq index TCRs matched E01–E03 expanded *TRB* sequences (Fig. 2b). Despite recovering similar numbers of CD4$^+$ and CD8$^+$ T cell clonotypes, 93% of the robustly E01–E03 expanded *TRB* matching CD69$^+$CD137$^+$ AIM-scTCRαβ-seq TCRαβ clonotypes were CD8$^+$ T cells (Fig. 2b). Most CD69$^+$CD137$^+$ AIM-scTCRαβ-seq-identified S-reactive CD4$^+$ TCRαβ clonotypes did not expand as markedly in response to vaccination as S-reactive CD8$^+$ TCRαβ clonotypes (Fig. 2c,e and Extended Data Fig. 6). Comparison of the mean trajectories (Fig. 2d) and median fold expansion (Fig. 2e) of the abundance of the CD69$^+$CD137$^+$ AIM-scTCRαβ-seq-generated S-reactive clonotypes

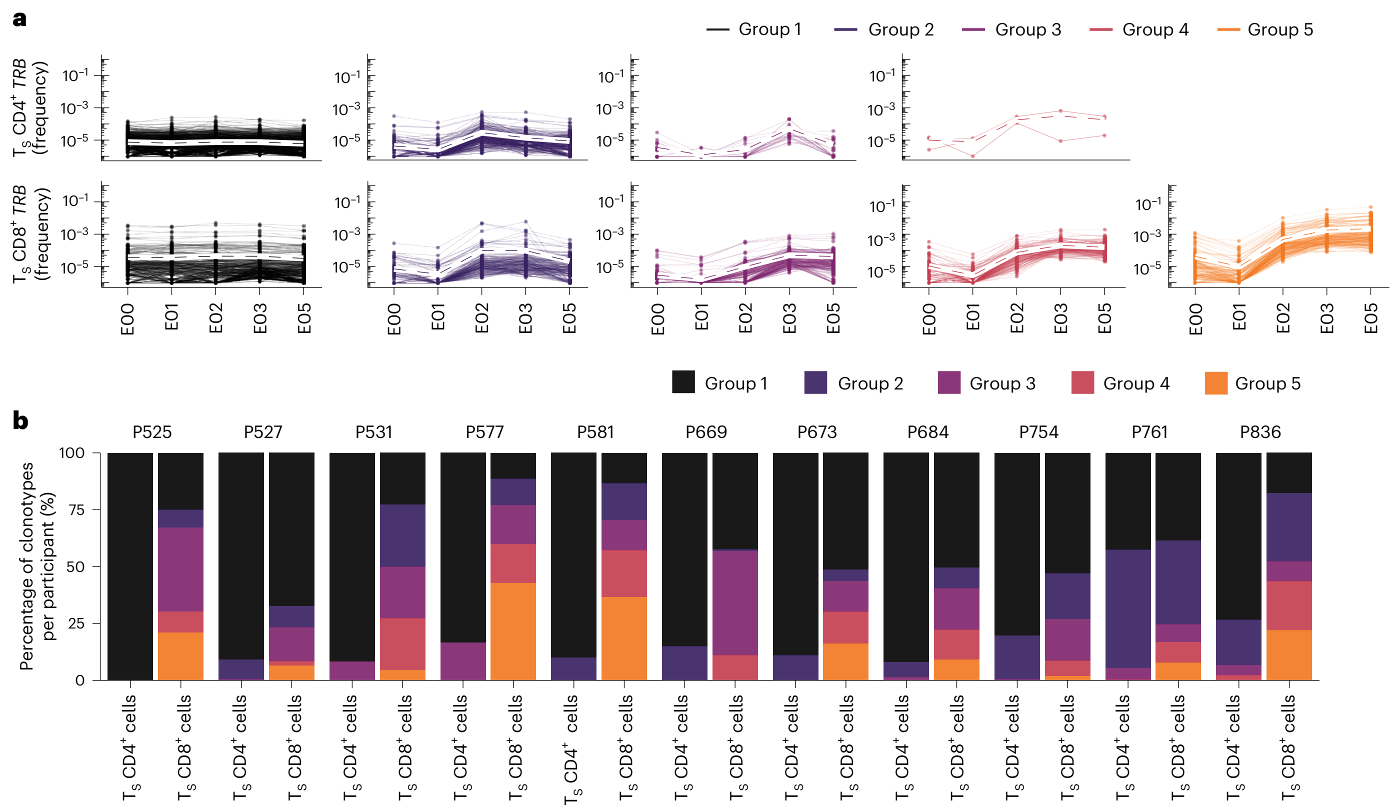

Fig. 3 | Trajectories of S-reactive clonotypes defined by AIM-scTCRαβ-seq differentiate CD4$^+$ and CD8$^+$ T cells. a, Unsupervised hierarchical clustering of S-reactive clonotypes identified by CD69$^+$CD137$^+$ CD69$^+$CD137$^+$ AIM-scTCRαβ-seq based on cosine similarity of their E00, E01, E02, E03 and E05 log productive frequency showing five major trajectory types: minimal proliferation (group 1); proliferation at E02 followed by contraction (group 2); proliferation at E03 (group 3); proliferation at E02 without contraction (group 4); or proliferation at E02 and E03 (group 5). The mean trajectory with each group is shown as a dashed line. **b**, The percentage of clonotypes per participant according to trajectory group for CD4$^+$ and CD8$^+$ T$_S$ cells in the 11 participants with CD69$^+$CD137$^+$ AIM-scTCRαβ-seq phenotyping and PBMC sampling at all five visits (E00–E05).

in all 17 samples indicated greater expansion of CD8$^+$ than CD4$^+$ T cells after vaccination.

Focusing on CD8$^+$ T$_S$ cells, we analyzed the recruitment of rare versus abundant clonotypes by the first two vaccine doses. A median of 50% (IQR = 33–61%) of the CD8$^+$ CD69$^+$CD137$^+$ AIM-scTCRαβ sequences matching bulk *TRB* clonotypes at E03 were not detected at either E00 or E01 (Extended Data Fig. 7). A median of 20% (IQR = 11–32%) of the S-reactive CD8$^+$ *TRB* clonotypes found at E03 were not detected at E02 (Extended Data Fig. 7), showing that the second dose of the vaccine entrained previously undetected CD8$^+$ T$_S$ into the repertoire between E02 and E03 (Fig. 2c, Extended Data Fig. 7 and Supplementary Fig. 2). Thus, even in persons with an appreciable preexisting S-reactive CD8$^+$ T$_M$ cell population due to SARS-CoV-2 infection, the second dose of mRNA vaccine expanded preexisting CD8$^+$ T$_M$ and recruited previously naive or extremely rare CD8$^+$ T$_M$ cell clonotypes, potentially broadening S recognition.

Vaccine kinetics of CD4$^+$ and CD8$^+$ T$_S$ cells diverge

To compare CD4$^+$ and CD8$^+$ T$_S$ trajectories using an independent method, we performed intracellular cytokine staining in PBMCs from E01 ($n = 7$), E02 ($n = 14$) and E03 ($n = 14$) visits from participants with E03 CD69$^+$CD137$^+$ AIM-scTCRαβ-seq data using S peptides. We observed that the kinetics of interleukin-2 (IL-2)$^+$CD4$^+$ and interferon-γ (IFN-γ)$^+$CD8$^+$ T cell responses to S peptide stimulation at E03, relative to E02 and E01, were consistent to those tracked with CD69$^+$CD137$^+$ AIM-scTCRαβ-seq (Fig. 2d,f and Supplementary Table 8). Before vaccination, at E01, S-reactive IL-2$^+$CD4$^+$ T cells were detected at higher frequencies (median 0.25%) than S-reactive IFN-γ$^+$CD8$^+$ T cells (median = 0.012%) (Fig. 2f). The frequency of S-reactive IL-2$^+$CD4$^+$ T cells in blood increased from E01 to E02 (Fig. 2f). The frequency of IFN-γ$^+$CD8$^+$ T cells increased stepwise from the previous visit after each vaccine dose at E02 and E03 in 12 of 14 participants (Fig. 2f). These data indicated a distinct pattern of expansion in CD4$^+$ and CD8$^+$ T cells in response to the second vaccine dose.

To examine the kinetics of CD4$^+$ and CD8$^+$ CD69$^+$CD137$^+$ AIM-scTCRαβ-seq clonotypes in response to each vaccine dose, we performed unsupervised clustering of clonotype-level trajectories in 12 participants (as above) with matching bulk TCRβ-seq repertoire sequencing at E00, E01, E02, E03 and E05. Five classifications described the expansion or contraction trajectory of these T cell clonotypes: minimal proliferation (group 1), proliferation at E02 followed by contraction (group 2), proliferation at E03 (group 3), proliferation at E02 without contraction (group 4) or proliferation at E02 and E03 (group 5) (Fig. 3a). In all 12 participants, many S-reactive CD8$^+$ clonotypes proliferated at both E02 and E03 (group 5) (Fig. 3b). In contrast, most S-reactive CD4$^+$ T cell clonotypes had minimal expansion (76% in group 1) or proliferated at E02 followed by contraction (21% in group 2), with few showing expansion in response to dose 2 (groups 3, 4 and 5) (Fig. 3a).

Activated CD4$^+$ T cells can express diverse combinations of cell surface markers beyond CD69 and CD137 (ref. 22) (Supplementary Fig. 3). We therefore performed TCRβ-seq from sorted CD4$^+$ T cells from PBMCs at E03 expressing either CD69 or CD137 and at least one of the activation markers CD134 or CD154 (CD69$^+$(CD134/CD154)$^+$ and CD137$^+$(CD134/CD154)$^+$) after incubation with S peptides (hereafter CD4$^+$AIM-TCRβ-seq) in seven participants (median age = 66.6, 2 female, 2 with severe COVID-19) (Supplementary Table 9). CD69$^+$(CD134/CD154)$^+$ and CD137$^+$(CD134/CD154)$^+$CD8$^+$ AIM identified very few CD8$^+$ T cells (Supplementary Fig. 4 and Supplementary Table 10), but CD4$^+$AIM-TCRβ-seq identified nearly twice as many S-reactive CD4$^+$ *TRB* clonotypes as identified by CD69$^+$CD137$^+$CD4$^+$AIM-TCRβ-seq (Extended Data Fig. 8). However, the expansion kinetics of the S-reactive CD4$^+$ clonotypes identified by CD69$^+$CD137$^+$ AIM-scTCRαβ-seq and CD4$^+$AIM-TCRβ-seq were similar (Supplementary Fig. 5). To further investigate the expansion of CD4 clonotypes from E01 to E03, we sorted bulk CD4$^+$ T cells from both time points and compared clonotype expansion in these cells to that observed in whole PBMCs. Few E01–E03 expanding clonotypes could be confirmed as CD4$^+$ T cells (Fig. 2, Extended Data Figs. 6 and 8, and Supplementary Fig. 5). Overall, these experiments suggested that at the clonotype level, independent of method, CD4$^+$ T_S cells expanded only modestly in our cohort after mRNA vaccination.

Hybrid immunity elicits highly public T_S TCR motifs

TCRs that recognize a common ligand often exhibit convergent sequence features[23,24] in the CDR3 residues, which directly contact the peptide, and in CDR1 and CDR2, which can also contact peptide HLA. Using TCRdist—a multi-CDR position-weighted, biochemical distance metric—we computed pairwise sequence divergence among the 5,733 unique S-reactive TCRαβ clonotypes recovered using CD69$^+$CD137$^+$AIM-scTCRαβ-seq from 17 participants (Methods) to define public TCR clusters[24]. A similarity graph was constructed from the 1,458 clonotypes that had at least one other similar TCR in the dataset, with edges joining sufficiently similar TCRs (a TCRdist metric ≤ 100 generally corresponds to similar *TRBV* and *TRAV* gene usage and 1–4 amino acid substitutions or deletions within CDR3α and CDR3β). This identified 284 TCR clusters (Fig. 4a), often characterized by distinct CDR3 motifs, which were consistently expanded by mRNA vaccination from E01 to E03 across participants with a common HLA (Fig. 4b–h). The ten largest clusters (clusters 0–9) contained TCRs from 3–11 participants and between 25 and 144 unique clonotypes (Fig. 4b–h and Supplementary Fig. 6). More than 97% of edges within TCR clusters connected clonotypes with matching CD4$^+$ or CD8$^+$ assignments (Fig. 4a); many public TCR clusters were formed from groups of individuals expressing a shared HLA class I or class II allele (Supplementary Fig. 7 and Supplementary Table 11), suggesting common specificity for a peptide ligand restricted by this allele.

Cluster analyses identified many public TCRαβ paired motifs with matching *TRB* clonotypes expanded by vaccination, most notably in individuals expressing the HLA-A*02:01, A*03:01 or A*11:01 alleles (Fig. 4 and Supplementary Figs. 6 and 7). Two large public clusters (clusters 0 and 1) corresponded to previously identified NTGEL-*TRBJ2-2* (Fig. 4b) and PDIE (Fig. 4c) motifs, which recognize the HLA-A*02:01-restricted epitope YLQPRTFLL (amino acid 269–277 in S, $S_{269-277}$)[9,14,25–29]. While TCRs from clusters 0 and 1 were ubiquitous among HLA-A*02:01 participants after infection (E00) and after dose 1 (E02 and later), a related HLA-A*02:01-assigned motif (cluster 8) was only commonly observed after dose 1 (E02 and later) (Fig. 4d). Cluster 8 TCRs were distinguished by longer CDR3α (14 amino acids) and CDR3β (16 amino acids) and strict *TRAV12-1*/*TRBV29-1* usage compared to cluster 0 TCRs (Fig. 4b,d). Cluster 8 TCRs had a much lower probability of being generated[30,31] (median Pgen CDR3α = 5.1×10^{-9}, CDR3β = 9.7×10^{-11}) compared to cluster 0 TCRs (median Pgen CDR3α = 2.2×10^{-8}, CDR3β = 1.5×10^{-8}) (Fig. 4b,d), yet cluster 8 TCRs were expanded from E01 compared to E03 in 8 of 11 HLA-A*02:01 participants (Fig. 4d). This suggests that vaccination may diversify the set of circulating TCRs targeting immunodominant epitopes.

We observed highly public HLA-A*03:01-associated TCR clusters, with sequence motifs found in at least six of the seven HLA-A*03:01-expressing participants (Fig. 4e–g). Two large HLA-A*03:01-associated clusters (clusters 4 and 5) shared CDR3α junctions with central NNNAG residues paired with distinct and *V* gene-biased CDR3β receptor motifs in cluster 4 (*TRBV19*-dominated) and cluster 5 (*TRBV9*-dominated) (Fig. 4e,f). The cluster 4 and 5 CDR3β motifs shared similar central junctional residues, such as SIKGG (Fig. 4e) and SPWGG (Fig. 4f), with a hydrophobic residue preceding diglycine residues (Fig. 4e,f). This pattern also appeared within the CDR3β motif of public HLA-A*03:01-associated cluster 6 (Fig. 4g). A prevalent HLA-A*11:01-associated receptor motif was found in 4 of 6 HLA-A*11:01 participants (Fig. 4h). CD69$^+$CD137$^+$ AIM-scTCRαβ-seq groupings also included two large clusters (clusters 2 and 3) using the *TRAV1-2* and *TRAJ33* genes (Supplementary Fig. 6), characteristic of mucosal-associated invariant T (MAIT) cells[32–34]. Clonotypes in these MAIT clusters did not expand after vaccination in most participants (Supplementary Fig. 6). Together, this analysis linked clusters of similar TCRs with likely shared peptide reactivity to a potentially restricting HLA allele for experimental investigation.

AIM-scTCRαβ public cluster members are S-specific

To confirm the ligands of representative TCRs assigned to HLA-A*03:01, we expressed six TCRαβ identified with CD69$^+$CD137$^+$ AIM-scTCRαβ-seq from participant P673 in Jurkat cells that expressed mNeonGreen after TCR engagement (hereafter Jurkat reporter cells) (Fig. 5a). The TCRs selected were strongly expanded after vaccination (Fig. 5b) and representative of the AIM-scTCRαβ clonotypes found in the TCR clusters (Fig. 4a). All six TCRs showed reactivity with peptide S378–387 (KCYGVSPTKL), an HLA-A*03:01-restricted epitope (Fig. 5c). Strong activation of Jurkat reporter cells was observed for each TCR in the presence of artificial antigen presenting cells (APCs) coexpressing HLA-A*03:01 and full-length S from the ancestral strain Wuhan-1 (Wu-1) (Fig. 5d). Control artificial APCs expressing other HLA-A or HLA-B from participant P673 with S, or HLA-A*03:01 alone, did not activate the Jurkat reporter cells (Fig. 5d). While this core epitope is invariant in Omicron variants of SARS-CoV-2, flanking amino acid residues can influence antigen processing[35]. Near full-length S and relevant peptides from Omicron BA.1, BA.2 or BA.4 SARS-CoV-2 also activated each TCR (Fig. 5d and Supplementary Fig. 8). We observed potential differences in the ligand requirements of the TCRs (Fig. 5c,e), indicating that TCRdist may cluster TCRs into functionally meaningful groups. TCR1 and TCR4, from clusters 269 and 6, respectively, recognized the 10-mer peptide S378–387 (KCYGVSPTKL), but not the internal 9-mers (KCYGVSPTK or CYGVSPTKL) (Fig. 5c). In contrast, TCR3 was versatile and equally recognized the parent 10-mer and each 9-mer (Fig. 5c). TCR2 optimally recognized $S_{378-387}$ and partially recognized the internal 9-mers (Fig. 5c).

Fig. 4 | TCRαβ sequence similarity network shows public CD8$^+$ T cell responses among sequences recovered by AIM-scTCRαβ-seq. a, Sequence similarity graph with 1,448 paired TCRαβ clonotypes and 248 convergent CD8$^+$ and CD4$^+$ T cell clusters of two or more S-reactive clonotypes recovered from 17 individuals at E03. Edges are formed between similar receptors (TCRdist ≤ 100). Edges indicate connections between TCRs observed in multiple or single participants. The circle size represents the relative frequency of each TCRαβ clonotype. Equivalent TCRαβ amino acid sequences may be included more than once if found in multiple participants. **b**–**h**, Logo plots for representative clusters (cluster 0 (**b**); cluster 1 (**c**); cluster 8 (**d**); cluster 4 (**e**); cluster 5 (**f**); cluster 6 (**g**); cluster 17 (**h**)) indicated by integers in **a** with inferred restricting HLA class I alleles (Methods), the number of participants contributing to each cluster with the matching HLA allele and graphs showing the sum of clonal frequency of the *TRB* sequences in each cluster in the longitudinal PBMC repertoires for each participant. For each CDR3 motif, the lower sequence logo shows the probability of each amino acid residue at each CDR3 position, while the upper sequence logo depicts the information content in bits comparing residue usage to a set of randomly selected CDR3 with the same V and J gene usage as the sequence cluster (Methods).

Peptide titration confirmed differences in peptide length requirements between TCRs (Fig. 5e and Supplementary Table 12).

To confirm that CD69$^+$CD137$^+$ AIM-scTCRαβ-seq can identify antigen-specific CD4$^+$ T cells, we expressed representative CD4$^+$ TCRs in autologous polyclonal CD4$^+$ T cells (Methods) and tested activation by S protein and peptides (Supplementary Fig. 9 and Supplementary Tables 13 and 14). We further queried the clusters of CD4$^+$ T$_S$ cells recovered using CD69$^+$CD137$^+$ AIM-scTCRαβ-seq against previously

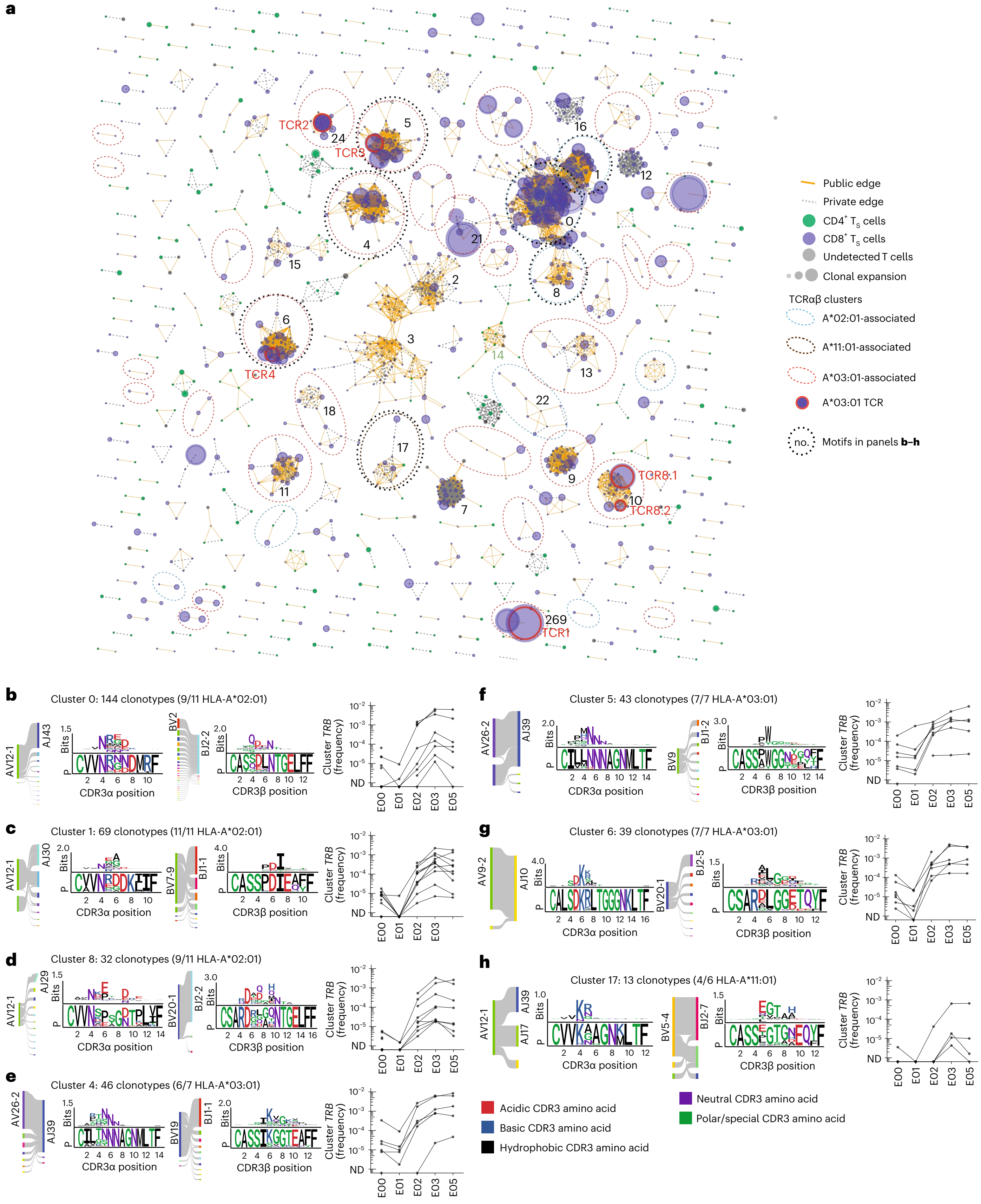

https://doi.org/10.1038/s41590-023-01692-x

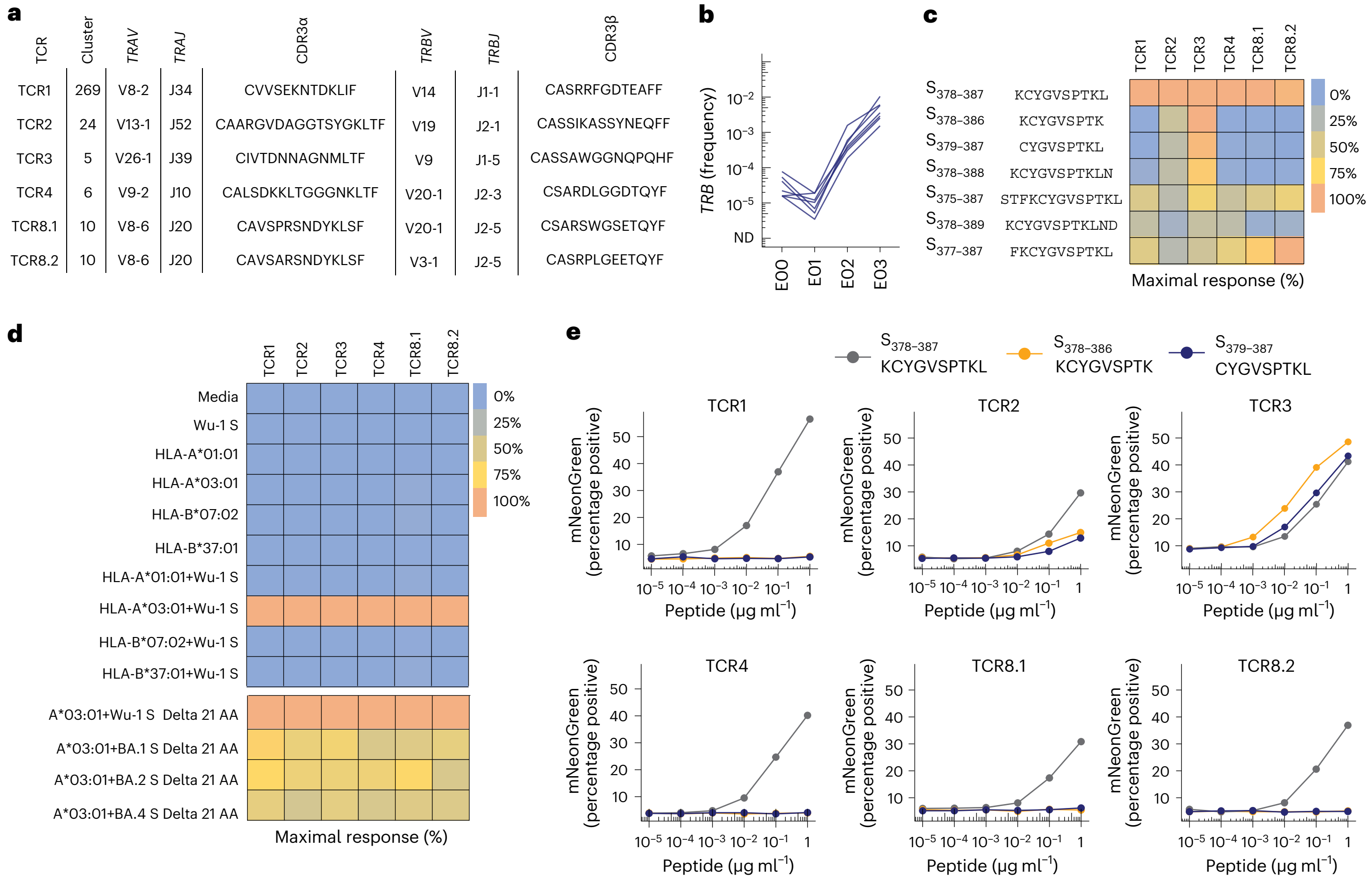

a

TCR	Cluster	*TRAV*	*TRAJ*	CDR3α	*TRBV*	*TRBJ*	CDR3β
TCR1	269	V8-2	J34	CVVSEKNTDKLIF	V14	J1-1	CASRRFGDTEAFF
TCR2	24	V13-1	J52	CAARGVDAGGTSYGKLTF	V19	J2-1	CASSIKASSYNEQFF
TCR3	5	V26-1	J39	CIVTDNNAGNMLTF	V9	J1-5	CASSAWGGNQPQHF
TCR4	6	V9-2	J10	CALSDKKLTGGGNKLTF	V20-1	J2-3	CSARDLGGDTQYF
TCR8.1	10	V8-6	J20	CAVSPRSNDYKLSF	V20-1	J2-5	CSARSWGSETQYF
TCR8.2	10	V8-6	J20	CAVSARSNDYKLSF	V3-1	J2-5	CASRPLGEETQYF

Fig. 5 | Transgenic CD8$^+$ T cell-origin TCRs from five public clusters are activated in the context of HLA-A*03:01 and the KCY epitope. a, *TRA* and *TRB* gene usage and CDR3 sequences of transgenic TCRs from five public sequence similarity clusters expressed in Jurkat reporter cells (Methods). **b**, Frequency in the PBMCs of selected clonotypes in the bulk TCRβ-seq datasets from E00 to E03. **c**, Heatmap showing the percentage of maximal response for each TCR expressed in the Jurkat reporter cells cultured with HLA-A*03:01-expressing APC exposed to peptides of varying lengths in the region of residues 378–386 of S protein (1 μg ml^{-1}) within a single experiment. **d**, Heatmap showing the percentage of maximal response for each TCR expressed in Jurkat reporter cells stimulated with HLA class I-expressing artificial APCs with or without cotransfection of full-length S from SARS-CoV-2 strain Wu-1 within a single experiment. Controls include APCs treated with media or S alone. The last four rows of the heatmap represent a separate experiment, whereby each TCR was tested with HLA-A*03:01 and Wu-1 S or Omicron variants BA.1, BA.2 and BA.4. **e**, Peptide titration (10^{-5} to 1 μg ml^{-1}) with SARS-CoV-2 S 10-mer (KCYGVSPTKL) and internal 9-mers (KCYGVSPTK and CYGVSPTKL) tested with TCR-transduced Jurkat reporter cells cultured with lymphoblastoid cell lines known to express HLA-A*03:01. The *y* axis shows the percentage of reporter cells with mNeonGreen fluorescence.

identified T$_S$ motifs. The CD69$^+$CD137$^+$ AIM-scTCRαβ-seq clusters of CD4$^+$ T$_S$ clonotypes overlapped with published CD69$^+$CD154$^+$CD4$^+$TCR-seq single-chain TRA and TRB of CD4$^+$ T cells responsive to mRNA vaccines in SARS-CoV-2-naive individuals[36] (Supplementary Fig. 10a). In addition, CD69$^+$CD137$^+$ AIM-scTCRαβ-seq cluster 49 matched the *TRAV35*-NYGGSQ motif found enriched in the draining lymph nodes of DPA1*01:03/DPB1*04:02 individuals in response to an immunodominant S$_{167–180}$ class II epitope[37] (Supplementary Fig. 10b). The CDR3β of cluster 49 TCRs contained the S*RG**GY-TRBJ1-2 motif proposed to commonly pair with the *TRAV35*-NYGGSQ motif to form S$_{167–180}$-reactive receptors[38]. Thus, the publicity of T$_S$ TCR motifs, the experimental confirmation of selected CD4$^+$ and CD8$^+$ T cell-origin TCRs and the recovery of TCRs similar to those previously identified as SARS-CoV-2-specific validated the use of AIM to discover antigen-specific receptors without previous epitope knowledge.

Severe disease imprints CD4$^+$ T$_S$ cells

To further assess the participant-level heterogeneity and longitudinal dynamics of SARS-CoV-2-reactive CD4$^+$ T cells, we computed the breadth of clones in the E00–E05 samples that matched a diagnostic set of CD4$^+$ T cell-associated *TRB* sequences reported to be enriched in SARS-CoV-2 convalescent compared to healthy control repertoires[39] as a measure of antigen-specific TCR diversity (hereafter diagnostic clonal breadth). These *TRB* sequences[40–43] were previously assigned to S (n = 917) or non-S (n = 1,564) SARS-CoV-2 antigens[42] (Methods). To examine if COVID-19 severity resulted in differential imprinting of the T cell repertoire, we compared the diagnostic breadth of patients with mild or moderate and severe COVID-19 (Fig. 6a and Supplementary Table 15). Severe infection was associated with greater overall SARS-CoV-2-specific *TRB* repertoire diversity after infection[18,44]. We observed greater diagnostic breadth of S-reactive CD4$^+$ T cells in patients with severe COVID-19 compared to patients with only mild or moderate infection at E00 (0.014 versus 0.006%; Fig. 6a), but this difference was not detected at E01 or E02 (Fig. 6a). Diagnostic S-reactive CD4$^+$ T cell breadth was elevated in participants with severe COVID-19 compared to those with mild or moderate disease at E03 (0.012 versus 0.008%) and E05 (0.009% versus 0.005%) (Fig. 6a). In contrast, the breadth of E01–E03 expanded *TRB* clonotypes at E03 did not correlate with the severity of previous infection (Fig. 6b). The diagnostic breadth of S and non-S CD4$^+$ T cells weakly correlated (rank correlation ρ = 0.38, P = 0.019) at E00 (Fig. 6c). The diagnostic breadth of S-reactive CD4$^+$ T cells increased promptly at E02 and slowly declined at E03

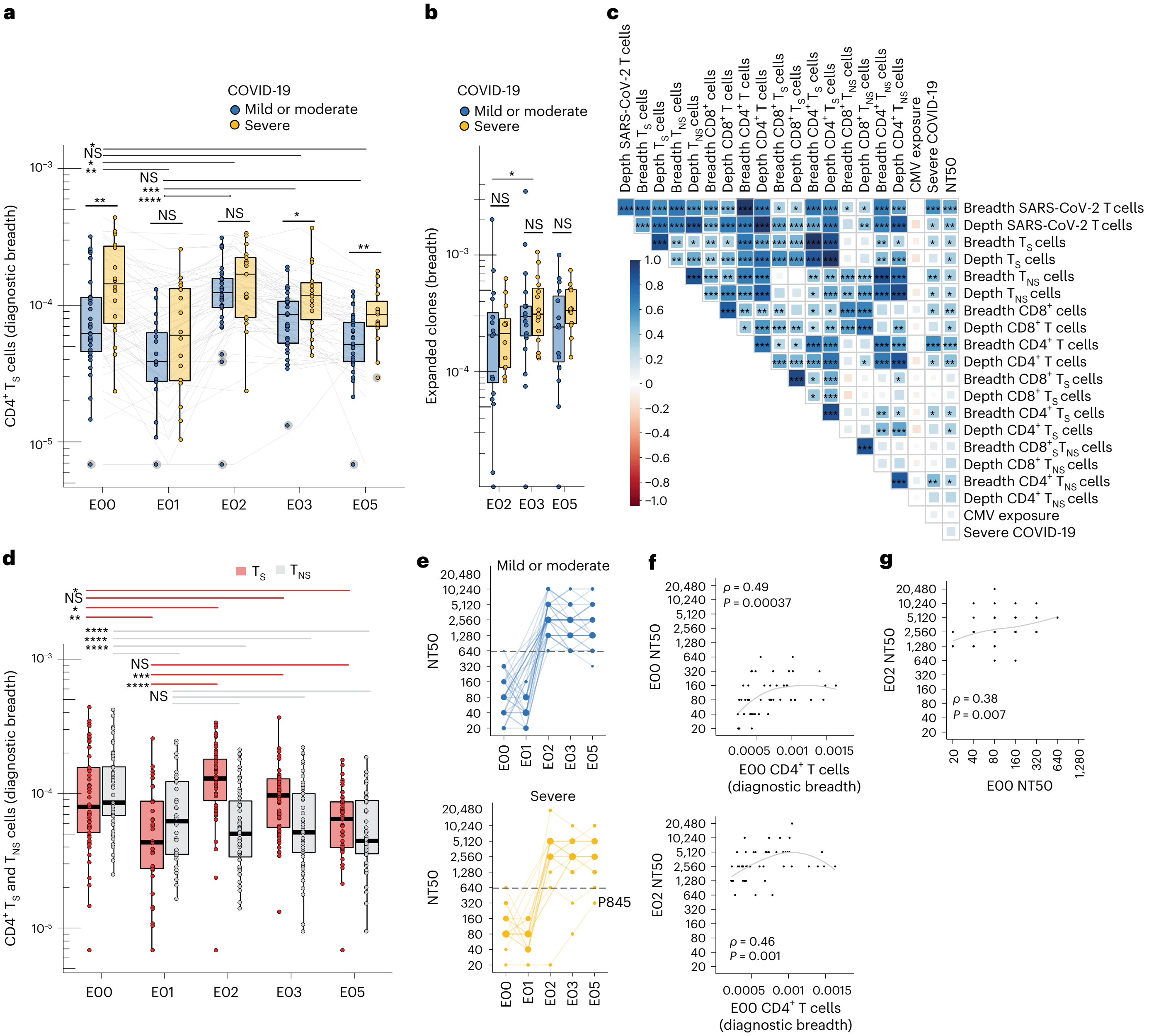

Fig. 6 | *TRB* sequence-defined metrics and nAbs are associated with disease severity before and after mRNA vaccination. a, Comparison of diagnostic CD4$^+$ T$_S$ breadth (Methods) between participants with mild or moderate COVID-19 at E00 ($n = 35$), E01 ($n = 18$), E02 ($n = 35$), E03 ($n = 35$) and E05 ($n = 29$) and severe COVID-19 at E00 ($n = 19$), E01 ($n = 16$), E02 ($n = 17$), E03 ($n = 18$) and E05 ($n = 15$). **b**, Breadth of E01–E02, E01–E03 and E01–E05 expanded clonotypes in mild or moderate COVID-19 at E02 ($n = 17$), E03 ($n = 18$) and E05 ($n = 16$), and severe COVID-19 at E02 ($n = 12$), E03 ($n = 15$) and E05 ($n = 12$). **c**, Rank correlation of diagnostic sequence-defined metrics (S, non-S) with severity and neutralization titers (NT50) at E00 ($n = 51$). CMV exposure was imputed from the *TRB* repertoire (Methods). Shading represents the strength of the correlation (ρ correlation coefficient); the asterisks represent the level of statistical significance. **d**, Breadth of inferred CD4$^+$ T$_S$ and T$_{NS}$ *TRB* sequences from PBMCs at E00 ($n = 54$), E01 ($n = 34$), E02 ($n = 52$), E03 ($n = 53$) and E05 ($n = 44$). **e**, NT50 of serum antibodies in mild or moderate ($n = 35$) and severe COVID-19 ($n = 19$) at E00, E01, E02, E03 and E05. **f**, Association of CD4$^+$ T cell diagnostic breadth at E00 with nAb NT50 at E00 and E02 ($n = 52$). **g**, Association between E00 nAb NT50 and E02 nAb NT50 ($n = 52$) in participants with previous SARS-CoV-2 infection. In **a**,**b** and **d**, the tests between time points were paired Wilcoxon signed-rank tests; the tests between groups with different severity were unpaired Wilcoxon rank-sum tests. The median, IQR and whiskers (1.5 times the IQR) are shown. The level of two-sided statistical significance is as indicated. *$P < 0.05$, **$P < 0.01$, ***$P < 0.001$, ****$P < 0.0001$.

and E05, in contrast to the non-S-reactive CD4$^+$ T cell breadth, which remained stable from E01 to E05 after the initial decline from E00 to E01 (Fig. 6d). Cytomegalovirus (CMV) infection has been reported to impact immune parameters related to SARS-CoV-2 infection or vaccine[45,46]. We did not observe any associations between imputed CMV infection status[47] and the parameters of SARS-CoV-2-specific *TRB* repertoires at E00 (Fig. 6c).

To examine a potential correlation between T cell and humoral responses in this cohort, we measured nAb titers (NT50) in all participants. NT50 declined after SARS-CoV-2 infection (median = 80, IQR = 50–160 at E00; median = 60, IQR = 40–80 at E01), but was boosted in 51 of 52 participants at E02 (median = 2,560, IQR = 2,250–5,120; Fig. 6e). In contrast to dose-dependent serial boosting of CD8$^+$ T cells from E02 to E03, little to no further increase in NT50 was observed from

E02 to E03 (Fig. 6e). The after infection diagnostic breadth of CD4$^+$ T cells at E00 was correlated with both NT50 at E00 ($\rho = 0.49$, $P = 0.00004$; Fig. 6f) and after vaccination at E02 ($\rho = 0.46$, $P < 0.001$; Fig. 6f), and NT50 at E00 was correlated with NT50 at E02 ($\rho = 0.38$, $P = 0.007$; Fig. 6g). These data were consistent with CD4$^+$ T cell help to B cells and possible detection of S-specific circulating follicular helper-like T cells, which have been positively associated with nAb titers[48]. These results suggested that in hybrid immunity severe disease imprints a more diverse and persistent CD4$^+$ T$_S$ cell population, which was maintained after repeated antigen exposure.

Discussion

In this study, we longitudinally profiled the cellular and humoral immunity in a cohort of adults from after SARS-CoV-2 infection through to three doses of mRNA vaccine. We used CD69$^+$CD137$^+$ AIM-scTCRαβ-seq and CD4$^+$ AIM-TCRβ-seq to obtain index T$_S$ clonotypes to track in serial bulk *TRB* repertoires. This revealed divergent vaccine response kinetics between CD4$^+$ and CD8$^+$ T$_S$ cells. In persons with previous SARS-CoV-2 infection, mRNA vaccines induced profound, albeit variable, expansion of preexisting circulating T$_M$ cell clones. We observed that the first two doses of the vaccine augmented S-reactive clonotypic diversity in the blood, which is consistent with observations in peptide–HLA oligomer-sorted T cells after repeated antigen exposure[9]. These doses lead to strong expansion in CD8$^+$ T$_S$ clonotypes measured using both CD69$^+$CD137$^+$ AIM-scTCRαβ-seq and intracellular cytokine staining. Rapid expansion of CD8$^+$ T cells after the first mRNA vaccination has also been described in SARS-CoV-2-naive individuals[25].

In contrast to our results, a study that measured the percentage of AIM$^+$CD4$^+$ T$_S$ or AIM$^+$CD8$^+$ T$_S$ cells (AIM$^+$ defined as four of the five activation markers CD200, CD154, CD137, CD107a and IFN-γ) in the blood of 11 individuals with previous SARS-CoV-2 infection found prominent CD4$^+$ T$_S$ cell expansion, but little increase in CD8$^+$ T$_S$ cells[49]. Differences in study design (the cohort was younger, median age = 34.7 compared to 60.7 years in our study; shorter intervals between infection, vaccination and PBMC sampling[49]; and an emphasis on specificity over sensitivity) may account for these divergent conclusions. The CD8$^+$ T$_S$ cell selection[49] was more restrictive than ours and included CD154, which is seldom expressed on activated CD8$^+$ T cells[50,51]. The different results could also stem from an incomplete coverage of S protein when measuring CD8$^+$ T cell responses[49,52]. To increase sensitivity, we used CD69$^+$CD137$^+$CD8$^+$ to identify vaccine-responsive CD8$^+$ T$_S$ cells and two methods to identify vaccine-responsive CD4$^+$ T$_S$ cells (CD69$^+$CD137$^+$ and (CD69/CD137)$^+$(CD134/CD154)$^+$). We further used intracellular cytokine staining to compare CD4$^+$ and CD8$^+$ T$_S$ cells after the first and second vaccine doses. With all approaches, we found robust CD8$^+$ T cell expansion and a more modest CD4$^+$ T cell expansion after the second vaccination.

This report builds on previous work describing longitudinal dynamics in TCR repertoires in general, and the response to SARS-CoV-2 infection and vaccination in particular. A foundational study identified vaccine-expanded *TRB* sequences after yellow fever vaccination in naive individuals to link yellow fever-associated *TRB* sequences and shared HLA alleles to T cell clones of unknown specificity[53,54]. Previous work defined many individual TCRs and TCR clusters in the context of T$_M$ cell contraction after COVID-19 (ref. 55) or SARS-CoV-2 vaccination in naive individuals[56] by peptide–HLA oligomer-sorted T cells or statistical enrichment versus a control (often historical) population. Our work used AIM with statistical filters to assign S specificity to individual TCRs. We recovered thousands of paired-chain TCRαβ sequences with S reactivity to augment public databases[57] for characterizing T cell responses to vaccines[58,59] and reveal both α-chain and β-chain sequence features contributing to epitope specificity. We report a large set of experimentally validated public CDR3 sequence motifs for an immunodominant A*03:01-restricted S epitope. Through experimental validation of proposed S-specific TCRs within sequence-similar clusters, we successfully de-orphaned TCR–peptide–HLA ligand pairings without previous knowledge of epitopes or restricting HLA.

Our study has several limitations. We studied heterologous exposure only in the context of infection before vaccination. The order of serial antigen exposure may differentially shape the TCR repertoire. Our study was not structured to detect associations of TCR clonotypes with functional profiles or with COVID-19 severity. Because our participants were infected early in the pandemic and were generally older (median age = 60.6 years), our findings may not directly translate to younger individuals. Another limitation is the inability to infer directly whether E01–E03 expanded clonotypes that were below the limit of detection at all time points before vaccination came from either very rare T$_M$ or naive T cell populations. However, we showed that both doses of mRNA vaccination can expand low-abundance CD8$^+$ T cell clonotypes that were undetectable after SARS-CoV-2 infection. Synthesis of serial bulk TCRβ with single-cell TCRαβ sequencing provides insights into the spectrum of mRNA vaccine potency across doses and a tool to efficiently focus research attention on antigen-specific TCRs for detailed assignment of epitope specificity. Further research is required to determine how the phenotype, durability and distribution of CD4$^+$ and CD8$^+$ T cells elicited by hybrid exposure compare to responses elicited by infection or vaccination alone.

Online content

Any methods, additional references, Nature Portfolio reporting summaries, source data, extended data, supplementary information, acknowledgements, peer review information; details of author contributions and competing interests; and statements of data and code availability are available at https://doi.org/10.1038/s41590-023-01692-x.

References

1. Goldberg, Y. et al. Protection and waning of natural and hybrid immunity to SARS-CoV-2. *N. Engl. J. Med.* **386**, 2201–2212 (2022).
2. Suarez Castillo, M., Khaoua, H. & Courtejoie, N. Vaccine-induced and naturally-acquired protection against Omicron and Delta symptomatic infection and severe COVID-19 outcomes, France, December 2021 to January 2022. *Euro Surveill.* **27**, 2200250 (2022).
3. Qu, P. et al. Durability of booster mRNA vaccine against SARS-CoV-2 BA.2.12.1, BA.4, and BA.5 subvariants. *N. Engl. J. Med.* **387**, 1329–1331 (2022).
4. Lim, J. M. E. et al. SARS-CoV-2 breakthrough infection in vaccinees induces virus-specific nasal-resident CD8$^+$ and CD4$^+$ T cells of broad specificity. *J. Exp. Med.* **219**, e2020780 (2022).
5. Peng, Y. et al. Broad and strong memory CD4$^+$ and CD8$^+$ T cells induced by SARS-CoV-2 in UK convalescent individuals following COVID-19. *Nat. Immunol.* **21**, 1336–1345 (2020).
6. Tavukcuoglu, E., Horzum, U., Cagkan Inkaya, A., Unal, S. & Esendagli, G. Functional responsiveness of memory T cells from COVID-19 patients. *Cell. Immunol.* **365**, 104363 (2021).
7. Rodda, L. B. et al. Functional SARS-CoV-2-specific immune memory persists after mild COVID-19. *Cell* **184**, 169–183 (2021).
8. Dykema, A. G. et al. SARS-CoV-2 vaccination diversifies the CD4$^+$ spike-reactive T cell repertoire in patients with prior SARS-CoV-2 infection. *eBioMedicine* **80**, 104048 (2022).
9. Minervina, A. A. et al. SARS-CoV-2 antigen exposure history shapes phenotypes and specificity of memory CD8$^+$ T cells. *Nat. Immunol.* **23**, 781–790 (2022).
10. Kared, H. et al. Immune responses in Omicron SARS-CoV-2 breakthrough infection in vaccinated adults. *Nat. Commun.* **13**, 4165 (2022).
11. Altarawneh, H. N. et al. Effects of previous infection and vaccination on symptomatic Omicron infections. *N. Engl. J. Med.* **387**, 21–34 (2022).

12. Keeton, R. et al. T cell responses to SARS-CoV-2 spike cross-recognize Omicron. *Nature* **603**, 488–492 (2022).
13. Gao, Y. et al. Ancestral SARS-CoV-2-specific T cells cross-recognize the Omicron variant. *Nat. Med.* **28**, 472–476 (2022).
14. Dolton, G. et al. Emergence of immune escape at dominant SARS-CoV-2 killer T cell epitope. *Cell* **185**, 2936–2951 (2022).
15. Naranbhai, V. et al. T cell reactivity to the SARS-CoV-2 Omicron variant is preserved in most but not all individuals. *Cell* **185**, 1041–1051 (2022).
16. Müller, N. F. et al. Viral genomes reveal patterns of the SARS-CoV-2 outbreak in Washington State. *Sci. Transl. Med.* **13**, eabf0202 (2021).
17. Mueller, Y. M. et al. Stratification of hospitalized COVID-19 patients into clinical severity progression groups by immuno-phenotyping and machine learning. *Nat. Commun.* **13**, 915 (2022).
18. Elyanow, R. et al. T cell receptor sequencing identifies prior SARS-CoV-2 infection and correlates with neutralizing antibodies and disease severity. *JCI Insight* **7**, e150070 (2022).
19. Zhang, J. Z. et al. Thermodynamically coupled biosensors for detecting neutralizing antibodies against SARS-CoV-2 variants. *Nat. Biotechnol.* **40**, 1336–1340 (2022).
20. Johansson, A. M. et al. Cross-reactive and mono-reactive SARS-CoV-2 CD4$^+$ T cells in prepandemic and COVID-19 convalescent individuals. *PLoS Pathog.* **17**, e1010203 (2021).
21. Boonyaratanakornkit, J. et al. Clinical, laboratory, and temporal predictors of neutralizing antibodies against SARS-CoV-2 among COVID-19 convalescent plasma donor candidates. *J. Clin. Invest.* **131**, e144930 (2021).
22. Reiss, S. et al. Comparative analysis of activation induced marker (AIM) assays for sensitive identification of antigen-specific CD4 T cells. *PLoS ONE* **12**, e0186998 (2017).
23. Glanville, J. et al. Identifying specificity groups in the T cell receptor repertoire. *Nature* **547**, 94–98 (2017).
24. Dash, P. et al. Quantifiable predictive features define epitope-specific T cell receptor repertoires. *Nature* **547**, 89–93 (2017).
25. Oberhardt, V. et al. Rapid and stable mobilization of CD8$^+$ T cells by SARS-CoV-2 mRNA vaccine. *Nature* **597**, 268–273 (2021).
26. Francis, J. M. et al. Allelic variation in class I HLA determines CD8$^+$ T cell repertoire shape and cross-reactive memory responses to SARS-CoV-2. *Sci. Immunol.* **7**, eabk3070 (2022).
27. Shomuradova, A. S. et al. SARS-CoV-2 epitopes are recognized by a public and diverse repertoire of human T cell receptors. *Immunity* **53**, 1245–1257 (2020).
28. Szeto, C. et al. Molecular basis of a dominant SARS-CoV-2 spike-derived epitope presented by HLA-A*02:01 recognised by a public TCR. *Cells* **10**, 2646 (2021).
29. Ferretti, A. P. et al. Unbiased screens show CD8$^+$ T cells of COVID-19 patients recognize shared epitopes in SARS-CoV-2 that largely reside outside the spike protein. *Immunity* **53**, 1095–1107 (2020).
30. Robins, H. S. et al. Overlap and effective size of the human CD8$^+$ T cell receptor repertoire. *Immunology* **2**, 47ra64 (2010).
31. Sethna, Z. et al. OLGA: fast computation of generation probabilities of B- and T-cell receptor amino acid sequences and motifs. *Bioinformatics* **35**, 2974–2981 (2019).
32. Flament, H. et al. Outcome of SARS-CoV-2 infection is linked to MAIT cell activation and cytotoxicity. *Nat. Immunol.* **22**, 322–335 (2021).
33. Parrot, T. et al. MAIT cell activation and dynamics associated with COVID-19 disease severity. *Sci. Immunol.* **5**, eabe1670 (2020).
34. Boulouis, C. et al. MAIT cell compartment characteristics are associated with the immune response magnitude to the BNT162b2 mRNA anti-SARS-CoV-2 vaccine. *Mol. Med.* **28**, 54 (2022).
35. Le Gall, S., Stamegna, P. & Walker, B. D. Portable flanking sequences modulate CTL epitope processing. *J. Clin. Invest.* **117**, 3563–3575 (2007).
36. Saggau, C. et al. The pre-exposure SARS-CoV-2-specific T cell repertoire determines the quality of the immune response to vaccination. *Immunity* **55**, 1924–1939 (2022).
37. Mudd, P. A. et al. SARS-CoV-2 mRNA vaccination elicits a robust and persistent T follicular helper cell response in humans. *Cell* **185**, 603–613 (2022).
38. Pogorelyy, M. V. et al. Resolving SARS-CoV-2 CD4$^+$ T cell specificity via reverse epitope discovery. *Cell Rep. Med.* **3**, 100697 (2022).
39. Gittelman, R. M. et al. Longitudinal analysis of T cell receptor repertoires reveals shared patterns of antigen-specific response to SARS-CoV-2 infection. *JCI Insight* **7**, e151849 (2022).
40. Carlson, C. S. et al. Using synthetic templates to design an unbiased multiplex PCR assay. *Nat. Commun.* **4**, 2680 (2013).
41. Robins, H. S. et al. Comprehensive assessment of T-cell receptor β-chain diversity in α-β T cells. *Blood* **114**, 4099–4107 (2009).
42. Xu, A. M. et al. Differences in SARS-CoV-2 vaccine response dynamics between class-I- and class-II-specific T-cell receptors in inflammatory bowel disease. *Front. Immunol.* **13**, 880190 (2022).
43. Robins, H. et al. Ultra-sensitive detection of rare T cell clones. *J. Immunol. Methods* **375**, 14–19 (2012).
44. Xu, J. et al. T cell receptor β repertoires in patients with COVID-19 reveal disease severity signatures. *Front. Immunol.* **14**, 1190844 (2023).
45. Pothast, C. R. et al. SARS-CoV-2-specific CD4$^+$ and CD8$^+$ T cell responses can originate from cross-reactive CMV-specific T cells. *eLife* **11**, e82050 (2022).
46. Jo, N. et al. Aging and CMV infection affect pre-existing SARS-CoV-2-reactive CD8$^+$ T cells in unexposed individuals. *Front. Aging* **2**, 719342 (2021).
47. Emerson, R. O. et al. Immunosequencing identifies signatures of cytomegalovirus exposure history and HLA-mediated effects on the T cell repertoire. *Nat. Genet.* **49**, 659–665 (2017).
48. Boppana, S. et al. SARS-CoV-2-specific circulating T follicular helper cells correlate with neutralizing antibodies and increase during early convalescence. *PLoS Pathog.* **17**, e1009761 (2021).
49. Painter, M. M. et al. Rapid induction of antigen-specific CD4$^+$ T cells is associated with coordinated humoral and cellular immunity to SARS-CoV-2 mRNA vaccination. *Immunity* **54**, 2133–2142 (2021).
50. Ngalamika, O., Kawimbe, M. & Mukasine, M. C. Expression of CD40L on CD4$^+$ T cells distinguishes active versus inactive HIV-associated Kaposi's sarcoma. *Cancer Treat. Res. Commun.* **27**, 100361 (2021).
51. Curato, C. et al. Frequencies and TCR repertoires of human 2,4,6-trinitrobenzenesulfonic acid-specific T cells. *Front. Toxicol.* **4**, 827109 (2022).
52. Sette, A. & Crotty, S. Adaptive immunity to SARS-CoV-2 and COVID-19. *Cell* **184**, 861–880 (2021).
53. DeWitt, W. S. et al. Dynamics of the cytotoxic T cell response to a model of acute viral infection. *J. Virol.* **89**, 4517–4526 (2015).
54. Pogorelyy, M. V. et al. Precise tracking of vaccine-responding T cell clones reveals convergent and personalized response in identical twins. *PNAS* **115**, 12704–12709 (2018).
55. Minervina, A. A. et al. Longitudinal high-throughput TCR repertoire profiling reveals the dynamics of T-cell memory formation after mild COVID-19 infection. *eLife* **10**, e63502 (2021).
56. Meckiff, B. J. et al. Imbalance of regulatory and cytotoxic SARS-CoV-2-reactive CD4$^+$ T cells in COVID-19. *Cell* **183**, 1340–1353 (2020).

57. Goncharov, M. et al. VDJdb in the pandemic era: a compendium of T cell receptors specific for SARS-CoV-2. *Nat. Methods* **19**, 1017–1019 (2022).
58. Alter, G. et al. Immunogenicity of Ad26.COV2.S vaccine against SARS-CoV-2 variants in humans. *Nature* **596**, 268–272 (2021).
59. Swanson, P. A.2nd et al. AZD1222/ChAdOx1 nCoV-19 vaccination induces a polyfunctional spike protein-specific T_H1 response with a diverse TCR repertoire. *Sci. Transl. Med.* **13**, eabj7211 (2021).

Methods

Participants and specimens

Persons with a self-reported history of PCR-confirmed COVID-19 were recruited through local advertising from April through to August 2020 in the Seattle area for convalescent plasma donation (ClinicalTrials.gov registration: NCT04338360, NCT04344977). Participants provided written informed consent to the University of Washington institutional review board-approved protocol STUDY00004312 'Protocol for the Collection of Laboratory Research Specimens'. Participant data were collected and managed in RedCap, a protected health information-secure data collection and management resource (hosted at the University of Washington Institute of Translational Health Sciences)[60]. PBMCs were cryopreserved at 5–10 × 10^6 cells per vial in 10% dimethylsulfoxide (DMSO), 50% human serum, 40% Roswell Park Memorial Institute (RPMI) 1640 in LN$_2$. Plasma from heparin-anticoagulated blood or serum was frozen at −20 °C.

Study cohort

Fifty-seven individuals agreed to observational PBMC samples from disease convalescence through to vaccination. No statistical methods were used to determine sample sizes. Two individuals without an E00 or E03 sample were excluded, as was one individual who did not receive an mRNA vaccine. Of the remaining 54 participants, 35 had mild or moderate and 19 severe COVID-19 requiring hospitalization and oxygen support. Eight had critical illness requiring intensive care unit admission. All individuals attested to a diagnostic PCR sample confirming SARS-CoV-2 infection; 50 were confirmed. Twenty-eight were female. The median age was 60.3 years, range 31.4–73.5 years. Comorbidities that did not preclude blood or plasma donation included a history of cancer ($n = 8$), heart disease ($n = 9$), renal disease ($n = 4$), hypertension ($n = 9$), hyperlipidemia ($n = 10$), lung disease ($n = 9$) and diabetes ($n = 9$). One participant (P845) was serologically naive before vaccination and was excluded from the statistical analyses (Supplementary Fig. 11). Three participants (P545, P664 and P669) had breakthrough infections between the second and third mRNA vaccine doses and the E05 samples were excluded from the statistical analyses (Extended Data Fig. 1 and Supplementary Table 16). Data collection and analysis were not performed blinded to the conditions of the experiments.

SARS-CoV-2 and CMV infection status

Plasma nAbs to the SARS-CoV-2 strain WA1 were measured using microfluorescence[61] and resulted as the reciprocal dilution inhibiting infection by 50% (NT50). The antibodies used in the neutralization assay were an anti-SARS rabbit monoclonal nucleocapsid antibody (1:8,000 dilution, catalog no. 40143-R001, Sino Biological), Alexa Fluor 594-conjugated goat anti-rabbit IgG secondary antibody (1:2,500 dilution, catalog no. A11037, Thermo Fisher Scientific) and Hoechst 33342 nuclear stain (catalog no. H3570; Thermo Fisher Scientific). Plasma SARS-CoV-2 anti-strain Wu-1 S and anti-N IgG were measured using a microbead-based binding assay[62] and are reported as µg ml^{-1}. CMV infection status was imputed from the analysis of whole PBMC *TRB* repertoires from the first available sample from each individual using the CMV classifier tool (Adaptive Biotechnologies), an update of published methods[47] (Supplementary Table 1).

Isolation of memory and naive T cell subsets

From the earliest available time point (E00), for selected individuals, cryopreserved PBMCs (2 × 10^7) were thawed and stained with anti-human CCR7-PE (1.25:100 dilution, clone G043H7, BioLegend), anti-human CD95 Pacific Blue (2.5:100 dilution, clone DX2, BioLegend), anti-human CD45RA-APC (1.25:100 dilution, clone HI100, BioLegend), anti-human CD4 Brilliant Violet 510 (2.5:100 dilution, clone A161A1, BioLegend), anti-human CD8-FITC (5:100 dilution, clone 3B5, Thermo Fisher Scientific), anti-human CD3-ECD (2:100 dilution, clone UCHT1, BD Biosciences) and 7-AAD (1:10 dilution, BD Biosciences). Among gated, live CD3$^+$ single cells, single-positive CD4$^+$CD8$^-$ and CD4$^-$CD8$^+$ cells were identified and double-negative or double-positive cells were excluded. CD4$^+$CD8$^-$ and CD4$^-$CD8$^+$ cells were analyzed separately for CCR7 and CD45RA. CCR7$^+$/CD45RA$^+$ cells were separated from cells expressing one or neither marker. CD45RA-intermediate and CCR7-intermediate cells (<5% of total CD3$^+$ T cells) were excluded. Among pooled CCR7$^+$/CD45RA$^+$ central memory, CCR7$^-$CD45RA$^-$ effector memory cells re-expressing CD45RA and CCR7$^-$/CD45RA$^+$ effector memory cells, most (>99%) were CD95$^+$. Among CCR7$^+$CD45$^+$ cells preliminarily assigned as naive, cells with CD95 expression below the lower limit of CD95 expression among memory cells were defined as naive. Thus, specificity for memory or naive subsets was emphasized over cell inclusion in the gating scheme. CD4$^+$ and CD8$^+$ cells were pooled for memory and naive *TRB* repertoire analyses. A representative gating scheme is shown in Supplementary Fig. 1; participant and raw sequencing results are shown in Supplementary Table 5.

AIM detection and sorting of SARS-CoV-2-reactive T cells

PBMCs were thawed and cultured at 4 × 10^6 cells per well in 2 ml per well T cell medium (TCM)[63] in 2–3 wells of a 24-well plate with 1 µg ml^{-1} of each peptide covering SARS-CoV-2 strain Wu-1 S (PM-WCPV-S-1, JPT Peptide Technologies) at a final concentration of 0.2% DMSO or DMSO negative control. Peptides were 15-amino-acid-long with an 11 amino acid overlap. After 18 h, cells were recovered by centrifugation into 50 µl PBS with 1% BSA and incubated with 5 µl TruStain FcX blocking reagent (BioLegend) for 10 min on ice, followed by the addition of 50 µl of a cocktail (Supplementary Table 17) of oligonucleotide-labeled mAbs (TotalSeq-C, BioLegend) for 5 min on ice. Cells were then stained with anti-CD3-FITC (3:200 dilution, clone SK7, BioLegend), anti-CD69 Brilliant Violet 421 (3:100 dilution, clone FN50, BioLegend), anti-CD137-APC (2:10 dilution, clone 4B4-1, BD Biosciences) and 7-AAD (1:10 dilution, BD Biosciences), washed and resuspended in 1 ml TCM. Live, single, CD3$^+$ cells expressing CD69 and CD137 were sorted (FACSAria II, BD Biosciences) from S-stimulated PBMCs for subsequent CD69$^+$CD137$^+$ AIM-scTCRαβ-seq (for a representative gating tree, see Supplementary Fig. 12a).

To study the AIM combinations, we investigated both the abundance and *TRB* repertoire of CD4 T cells staining for various markers. PBMCs were stimulated and stained with anti-CD3-PE (1:200 dilution, clone UCHT1, BioLegend), anti-CD4-APC-H7 (1:40 dilution, clone RPA-T4, BD Biosciences), anti-CD8-FITC (1:20 dilution, clone 3B5, Thermo Fisher Scientific), anti-CD25-PE-Cy7 (1:50 dilution, clone BC96, BioLegend), anti-CD134 Brilliant Violet 480 (1:50 dilution, clone L106, BD Biosciences), anti-CD69 Brilliant Violet 421 (3:100 dilution, clone FN50, BioLegend), anti-CD137-APC (1:5 dilution, clone 4B4-1, BD Biosciences), anti-CD154 Brilliant Violet 711 (1:50 dilution, clone 24-31, BioLegend) and 7-AAD. After washing, data were acquired on a FACSAria III in analytical mode. Gating and Boolean analyses used FlowJo v.10.7.1 (FlowJo LLC). Gating schemes are shown in Supplementary Fig. 12. We investigated the activation of CD4$^+$ T cells by measuring the tumor necrosis factor (TNF) receptor (TNFR) family members CD134 (OX40L), CD137 (4-1BB) and CD154 (CD40L), CD25 (IL-2 receptor subunit) and CD69. We considered five pairs of activation markers, that is, CD69/CD137, CD25/CD134, CD134/CD137, CD134/CD154 and CD137/CD154, and set the sum of cells expressing at least two markers to 100%. For CD8$^+$ T cells, CD69/CD137 detected a median of 85.7% of all activated cells, with CD134 and CD154 showing very little activation (Supplementary Figs. 2 and 12). For CD4$^+$ T cells, the sensitivity to detect peptide activation using CD69/CD137 was more limited (median = 21.1%). However, no AIM molecule pair was consistently the most sensitive. CD69/CD137 showed better sensitivity than combinations of two TNFRs and was used for AIM-scTCRαβ-seq to identify both CD4$^+$ and CD8$^+$ T cell activation using peptide stimulation. To study the relationship between selection markers and TCR repertoires, we selected seven individuals with PBMC availability at the E03 time point (Supplementary Table 10).

We sequentially sorted live, single, CD3$^+$ and CD8$^-$ T cells stimulated for 18 h with S peptides, first selecting all CD69$^+$/CD137$^+$ cells (fraction 1, black gates), and then selecting any residual CD69$^+$ cells expressing CD134 or CD154 (fraction 2, blue gates). Finally any residual CD137$^+$ cells expressing CD134 or CD154 (fraction 3, red gates) (representative gating scheme, Supplementary Fig. 4) were sorted live. Fraction 1 and pooled fractions 2 and 3 were submitted (separately) for bulk TCRβ-seq.

Intracellular cytokine staining

Cryopreserved PBMCs were thawed and rested overnight. PBMCs (1×10^6 per well) were stimulated with a SARS-CoV-2 S overlapping peptide pool (1 µg ml^{-1} each peptide, JPT Peptide Technologies; 0.4% final DMSO concentration), 0.4% DMSO as a negative control or PHA-P (1.6 µg ml^{-1} final concentration, Remel) as a positive control, in the presence of anti-CD28 (1:1,000 dilution, clone L293, BD Biosciences) and anti-CD49d (1:1,000 dilution, L25, BD Biosciences) antibodies at 37 °C for 6 h. Brefeldin A (Sigma-Aldrich) was added after 2 h. Cells were stained with LIVE/DEAD Fixable Near-IR dye (1:250 dilution, Invitrogen), treated with FACS lyse (BD Biosciences) and frozen at −80 °C. For staining, cells were thawed, washed and permeabilized with Permeabilizing Solution 2 (BD Biosciences), then stained with fluorochrome-labeled mAbs to anti-human CD3-PE-Texas Red (1:40 dilution, clone UCHT1, Beckman Coulter), anti-human CD4 Brilliant Violet 510 (1:83 dilution, clone SK3, BioLegend), anti-human CD8-PerCP-Cy5.5 (1:33 dilution, clone SK1, BD Biosciences) and the activation markers anti-human CD40L Brilliant Violet 421 (1:167 dilution, clone TRAP1, BD Biosciences), anti-human IFN-γ-PE (1:500 dilution, 4S.B3, BD Biosciences), anti-human IL-2-APC (1:250 dilution, clone MQ1-17H12, BD Biosciences) and anti-human TNFα-FITC (1:400 dilution, clone Mab11, BD Biosciences). Events were recorded with a BD Fortessa and analyzed with FlowJo (v.10 for Mac).

Bulk TCR sequencing

Genomic DNA was extracted from frozen PBMC samples using the QIAGEN DNeasy Blood Extraction Kit. Immunosequencing of the CDR3 regions of the TCRβ chains used the immunoSEQ Assay (Adaptive Biotechnologies). Input DNA was amplified in a bias-controlled multiplex PCR, followed by high-throughput sequencing. Sequences were collapsed and filtered to identify and quantitate the absolute abundance of each unique TCRβ CDR3 region for further analysis, as described elsewhere[40,41,43]. Blood *TRB* sequencing recovered a median of 429,661 productive *TRB* templates and 242,861 unique productive *TRB* rearrangements (clonotypes) per sample (Supplementary Table 2). For the analyses of bulk repertoires, the term clonotype was used for a unique *TRB* sequence: a CDR3 nucleotide sequence and associated *TRBV* and *TRBJ* genes. These generally distinguish a unique T cell clonotype; occasionally, a single *TRB* may pair with more than 1 *TRA* in distinct T cell clonotypes. To assist the assessment of expanded or AIM-selected T cell clonotypes as CD4$^+$ T cells, we stained cells with anti-human CD3-PE-Texas Red (1:40 dilution, clone UCHT1, Beckman Coulter), anti-human CD4 Brilliant Violet 510 (1:83 dilution, clone SK3, BioLegend) and anti-human CD8-PerCP-Cy5.5 (1:33 dilution, clone SK1, BD Biosciences). We then sorted unstimulated live single CD3$^+$CD4$^+$CD8$^-$ cells from the E03 after vaccine time point for bulk TCR sequencing (for a representative gating scheme, see Supplementary Fig. 4a), selecting the same individuals used to study CD4$^+$ T cell AIM selection conditions, and memory and naive cells (cells sorted per individual; Supplementary Table 10).

Single-cell TCR sequencing

Sorted single cells were segregated into nanoliter droplets (Chromium Next GEM Single Cell 5′ Kit v2, PN-1000263; Chromium Next GEM Chip K Single Cell Kit, PN-1000286; and Chromium Controller; 10X Genomics). The VDJ and antibody feature barcode libraries were made according to the user guide (CG000330 Rev C, 10X Genomics). Library quality was measured using a TapeStation (Agilent Technologies). Library DNA quantification was measured using a Qubit 3.0 Fluorometer (Thermo Fisher Scientific). Sequencing depth was 5,000 paired reads per cell with 26, 10, 10 and 150 configurations, assuming 10,000 cells per library. Sequencing used the NovaSeq 6000 System (Illumina) and SP200 Kit (Illumina).

Single-cell VDJ sequencing and feature barcode data analysis and alignment

Raw sequencing data were processed with the Cell Ranger v.6.1.0 (10X Genomics) pipeline. Demultiplexing from raw BCL data and conversion to FASTQ data used Cell Ranger mkfasq. The surface feature barcode antibody binding analyses used Cell Ranger counts with the reference feature barcode library (Supplementary Table 17). Initial TCR VDJ analyses used the Cell Ranger VDJ module and GRCh-Alts-ensembl-5.0.0.

CD4$^+$ and CD8$^+$ assignments

For the analyses of single-cell data, we computed the percentage of unique molecular identifier (UMI) counts corresponding to the DNA barcodes for CD8 and CD4 assigned to each marker. To assign a phenotype per cell, we computed a score based on the natural logarithm of total CD8 divided by the total CD4 counts. A score greater than 1 was classified as CD8 and a score less than −1 was classified as CD4. Cells with fewer than ten UMIs or values between 1 and −1 were considered ambiguous and were not assigned a T cell phenotype. When a TCR clonotype (cells with identical *TRA* and *TRB* nucleotide sequences) was present in multiple droplets, the median score was used to classify that clonotype. For bulk *TRB* analyses of AIM-selected total CD4$^+$ T cells, we considered *TRB* sequences that were present and enriched in the flow-sorted (bulk) CD4$^+$ T cell population compared to unselected PBMCs to be CD4$^+$. For the bulk CD4$^+$ *TRB* analyses, *TRB* sequences that were enriched in the bulk CD4$^+$ T cell population compared to unselected PBMCs were assigned to be CD4$^+$.

Longitudinal analysis of S-reactive clones

We tested for enrichment of S-reactive (T_S) clones in the AIM assay using a statistical test. The observed frequency of each AIM$^+$ clonotype among the total AIM$^+$ cells was compared with an expectation from a null model based on each clonotype's frequency in the bulk-sequenced repertoire from the same visit. The *P* value of the observed counts of each AIM$^+$ clonotype under the null model was computed from the complement of the binomial cumulative distribution function:

$$1 - \Pr(X < k - 1) = 1 - \sum_{i=0}^{k-1} \binom{n}{i} p^i (1-p)^{n-i}$$

From the binomial cumulative distribution function, we computed the chance of observing k single cells of a given clonotype in a pool of n total AIM$^+$ single cells, with the null success probability p equal to the fraction of the matching *TRB* in the unsorted bulk repertoire. We then applied a multiple hypothesis correction using the Benjamini–Hochberg procedure to compute an FDR-adjusted q for each AIM$^+$ clonotype. We designated clonotypes with a $q < 0.05$ as stringently enriched by the AIM sort and thus high-confidence S-reactive clones. These highest-confidence S-reactive clonotypes were used for trajectory analysis and estimation of the total fraction of the repertoire consisting of S-reactive CD4$^+$ and CD8$^+$ T cells, respectively.

TCR sequence clustering

To compare and cluster paired *TRA*/*TRB* sequences between cells, we first filtered sequences from CD69$^+$CD137$^+$ AIM-scTCRαβ-seq to those with a matching *TRB* from the deeply sequenced bulk blood repertoire from the same individual and time point. Next, we filtered out sequences with *TRB* occurring at a lower frequency in the set of clonotypes expressing AIM markers than in the bulk repertoire, that is, clonotypes that had not been enriched by AIM. Non-enriched clonotypes were assumed to have been sorted after bystander activation and were not considered further. Next we computed pairwise dissimilarity between 5,569 participant-unique *TRA*/*TRB* clonotypes using the TCRdist distance metric[24] as implemented using default parameters in tcrdist3 v.0.2.2 (ref. 64). By pruning the pairwise distance matrix to include connections between sequences within 100 TCRdist units, we formed a sequence graph.

When selecting samples to analyze using TCRdist, we restricted analyses to samples to include two or more individuals with prevalent HLA alleles, such that the subcohort studied included persons with HLA-A*02:01 ($n = 11$), HLA-A*03:01 ($n = 7$), HLA-A*11:01 ($n = 6$), HLA-B*07:02 ($n = 6$), HLA-B*15:01 ($n = 4$), HLA-B*35:01 ($n = 4$), HLA-C*07:02 ($n = 8$), HLA-C*03:04 ($n = 3$) and HLA-A*24:02 ($n = 2$) (Supplementary Tables 1, 2 and 11). To examine whether connected components within the graph (that is, any subgraph where a pair of nodes was connected with each other via an edge path) might recognize an HLA-restricted epitope, we used a graph walking approach to discover minimal sets of feasible HLA alleles that participants shared within closely connected nodes. Briefly, for each node, we sorted nodes in ascending order using TCRdist to all other nodes with its largest connected component. Starting at the closest public node found in another HLA genotyped participant, we took the intersection of the set of all class I (CD8$^+$ nodes) or class II (CD4$^+$ nodes) before moving on to the next-nearest connected node and taking the next stepwise intersection. If possible, the algorithm continues to narrow the set of feasible presenting HLA alleles to a minimal possible set. We inferred feasible HLA alleles; in many cases only one allele was shared among closely connected S-reactive TCR sequences. This allele was assigned to the corresponding TCR cluster. The code used to assign feasible HLA restriction from TCR sequence similarity analyses and graphs is provided in the 'Code availability' statement using custom scripts run in Python v.3.8. Sequence similarity networks were visualized with the Networkx v.2.8.6 package[65].

TCR motif visualization

From the weighted sequence similarity graphs formed from all CD69$^+$CD137$^+$ AIM-scTCRαβ-seq S-reactive clones, we identified clusters of similar sequences using the Louvain community detection algorithm with the communities v.3.0.0 package in Python. For each public sequence cluster with sequences donated from three or more participants, we depicted selected TCR clusters using six graphical elements, with the CDR3α and CDR3β junctions on the left and right, respectively (Fig. 3b–h). The lower sequence logo shows the observed position-specific frequency of each amino acid within the TCR cluster; the upper logo plots represent the position-specific information content in bits (that is, a signal of selection) compared to the CDR3α and CDR3β receptors, with the same *V* and *J* gene use, randomly sampled from naive repertoires[64,66]. The Sankey flow diagrams to the left of the CDR3 motifs show the frequencies of *TRAV*/*TRAJ* and *TRBV*/*TRJV* gene use within each cluster. Motifs were aligned and computed in palmotif v.0.4 and the graphics were rendered using ggplot2 and ggseqlogo[67] in R v.4.1.2.

TRB repertoire analyses

The breadth of *TRB* sequences significantly expanding (or contracting) between serially collected blood specimens was calculated as the fraction of unique clonotypes meeting the significance criteria. Briefly, to determine longitudinal persistence and previous detection, *TRB* were filtered for productive sequences and analyzed at the nucleotide level (*CDR3*, *TRBV*, *TRBJ*). *TRB* from bulk sequencing data were defined as expanded if their $\log_2$ fold change was greater than 2 relative to the E01 time point and met a second criteria for a statistically significant change in counts between samples using Fisher's exact test with correction for multiple hypotheses (FDR-adjusted $q < 0.05$). The analysis used custom R and Python scripts detailed in the 'Code availability' statement. The CDR3 amino acid sequence with *V* and *J* gene use and HLA restriction (if published) was used to determine whether a clonotype was previously associated with a known antigen.

Separately, *TRB* CDR3 assigned to SARS-CoV-2 were generated by statistically comparing *TRB* CDR3 sequences from whole-blood immunosequenced *TRB* repertoires between persons with documented SARS-CoV-2 infection and healthy controls. Sequences were assigned as likely to represent CD4$^+$ T cells based on publicity between individuals sharing HLA class II alleles, or as likely to represent CD8$^+$ T cells based on publicity between individuals sharing HLA class I alleles. Assignment to SARS-CoV-2 S or non-S specificity was performed using the output of multiplexed antigen restimulation assays[68–70]. Briefly, the defined SARS-CoV-2 antigens were used to stimulate expanded PBMCs from SARS-CoV-2-infected individuals; sorted CD4$^+$ or CD8$^+$ T cells expressing activation markers were bulk-sequenced at the *TRB* locus. Further refinements were performed to exclude non-SARS-CoV-2-specific *TRB* sequences associated with ubiquitous antigens such as CMV or Epstein–Barr virus, or with *TRB* sequences nonspecifically associated with HLA alleles in a cohort of healthy controls[18]. Multiplexed antigen restimulation assay-enriched and statistically SARS-CoV-2-associated *TRB* sequences were coanalyzed to create sets of *TRB* sequences spanning CDR3 and assigned, when possible, as CD4$^+$ or CD8$^+$, or as S-specific or non-S-specific. The diagnostic breadth of the blood *TRB* repertoires was calculated as described[18,71] and represent the proportion of productive *TRB* clonotypes present in a repertoire that were assigned as SARS-CoV-2-specific.

CD8$^+$ T cell-origin TCR reporter cell lines

TCR CDR3 sequences from CD69$^+$CD137$^+$ AIM-scTCRαβ-seq were integrated into assigned *TRA* and *TRB* genomic variable genes using ImMunoGeneTics[72]. Codon-optimized TCR lentiviral expression constructs (GenScript) were cloned into pRRLSIN.cPPT.MSCV/GFP.WPRE[73]. *TRB* is an N-terminal polypeptide within a fusion protein separated from *TRA* by a porcine echovirus P2A sequence, with both TCR-constant regions of murine origin and extra cysteine residues to promote pairing[74]. Lentiviral particles were expressed in HEK 293 cells (CRL-1573, ATCC) by cotransfection with packaging plasmids[75]. Lentivirus was concentrated (Lenti-X, Takara Bio). The NR4A1 mNeonGreen TCR reporter cell line has been described elsewhere[76]. Briefly, mNeonGreen was integrated in-frame into the *NR4A1* locus using CRISPR-induced homology-directed repair into Jurkat clone E6-1 cells (ATCC). Cells were additionally modified to knock out endogenous TCR expression. CD8αβ were also inserted using CRISPR to create NR4A1_mNeonGreen_035 (Jurkat_035) cells. Jurkat_035 were maintained in TCM. A total of 1×10^6 Jurkat_035 cells were transduced with 200–300 μl of lentiviral stock based on analysis for p24 antigen protein (Lenti-X GoStix, Takara Bio) for an estimated five infectious units per cell. Five days or longer after transduction, flow cytometry routinely showed more than 80% TCR expression as measured with anti-murine *TRB* clone H57-597-APC (eBioscience).

CD8$^+$ T cell-origin TCR specificity, HLA restriction and dose responsiveness

To evaluate specificity, Cos-7 cells were transfected as described elsewhere[77] in 96-well flat-bottom plates with HLA class I complementary DNA (cDNA), SARS-CoV-2 full-length S from strain Wu-1 cloned into pDEST103, HLA and S, or neither. Details of HLA cDNA and S cloning were published elsewhere[19,77–79]. HLA and S were sequence-confirmed. At 48 h, TCR-expressing Jurkat_035 cells were stained with CellTrace Violet (CTV) (Invitrogen), washed and added to Cos-7 cells at 3×10^5 per well. To determine the peptide epitopes, TCR-expressing Jurkat_035 cells were cocultured with B-lymphoblastoid cell lines (B-LCLs) (1×10^5 each) and pools of 1 μg ml^{-1} each 15-amino-acid peptide covering either the N or C terminal halves of SARS-CoV-2 Wu-1 S (PM-WCPV-S-1, JPT Peptide Technologies) in 200 µl TCM in round-bottom plates. Next, HLA-transfected Cos-7 artificial APC and 2×10^5 per well Cell Trace Violet-labeled Jurkat_035 cells were incubated with S peptides, 13-amino-acid-long with a 9-amino-acid overlap covering the full-length SARS-CoV-2 strain Wu-1, arrayed in rectangular matrices with row or column pool complexities of 8–12 peptides as reported elsewhere[19]. Peptides at the intersection of positive rows and columns, or internal shorter peptides, were repeated in the follow-up experiments. Subsequent experiments used fresh synthesis of selected single peptides and truncated internal peptides in the vicinity of the active peptide, at 1 µg ml^{-1} (70% purity, GenScript). For some peptide experiments, the APCs used were autologous Epstein–Barr virus-transformed B-LCLs. These were cultured as described by Tigges et al.[80] and CTV-labeled; Jurkat_035 responder cells were not CTV-labeled. To determine the dose responsiveness of confirmed KCY epitope-specific CD8 TCRs, SARS-CoV-2 S 10-mer (KCYGVSPTKL) and internal 9-mers (KCYGVSPTK and CYGVSPTKL) were tested independently against six Jurkat-based reporter lines with TCRs recognizing SARS-CoV-2 S in the context of HLA-A*03:01. B-LCLs known to express HLA-A*03:01 were used as APCs with the supplied peptide concentration ranging from 10^{-5} to 1 µg ml^{-1}. To study S variants, Cos-7 artificial APCs were cotransfected with HLA-A*03:01 and S plasmid constructs representing the Wu-1 or SARS-CoV-2 Omicron BA.1, BA.2 and BA.4 variants, each with 21-amino-acid C-terminal deletions. Regardless of APC and antigen, after 24 h cells were analyzed using flow cytometry (LSR II, BD Biosciences); the percentage of gated Jurkat cells, either CTV^{hi} or CTV^{lo}, expressing mNeonGreen was analyzed.

CD4$^+$ T cell-origin TCR reporter cells

To test the CD4$^+$ T cell-origin candidate TCRs, engineered reporter T cells were generated by transduction of autologous CD4$^+$ T cells using lentiviruses with candidate-paired TCR expression cassettes. Autologous CD4$^+$ T cells were immunomagnetically enriched (catalog no. 19662, STEMCELL Technologies) according to the manufacturer, seeded at 5×10^5 per well in 48-well plates in 1 ml TCM, and activated with anti-CD3/anti-CD28 Dynabeads (catalog no. 11131D, Invitrogen) at a bead:cell ratio of 3:1. Recombinant human IL-2 (50 U ml^{-1}, Miltenyi Biotec) was added. After a 24-h incubation, T cells were transduced with 200–300 µl of concentrated lentiviral stock. On day 4, the beads were removed. Cells were further expanded for 10 days in TCM containing recombinant IL-2, washed and counted. To evaluate the specificity of CD4$^+$ T cell-origin TCRs, 10^5 TCR-transduced reporter cells were cultured in 96-well round-bottom plates in 200 µl TCM containing 10^5 autologous, irradiated PBMCs as APC and SARS-CoV-2 S protein (D614G mutation, catalog no. 10587-CV-100, R&D Systems) at 0.1 µg ml^{-1}. Other stimuli included pooled SARS-CoV-2 S1 or S2 peptide pools from the N-terminal or C-terminal regions of S, respectively (PM-WCPV-S-1, JPT Peptide Technologies) at a final concentration of 1 µg ml^{-1} for each peptide, TCM or 0.1% DMSO as negative controls, or 1.6 µg ml^{-1} PHA-P as a positive control. On day 3, supernatants were evaluated for IFN-γ secretion by ELISA.

HLA typing

HLA class I and II allotypes were determined using next-generation sequencing at Scisco[21].

Statistics

Statistical comparison between paired samples was tested using Wilcoxon signed-rank tests; comparisons between groups were tested using Wilcoxon rank-sum tests. Tests used a two-sided alternative hypothesis. Associations among immunological parameters were measured with Spearman rank correlation. Statistical significance is represented by $^*P < 0.05$, $^{**}P < 0.01$, $^{***}P < 0.001$ and $^{****}P < 0.0001$. *TRB* from bulk sequencing data were defined as expanded if their $\log_2$ fold change was greater than 2 relative to the E01 time point and met a second criteria for a statistically significant change in counts between samples using Fisher's exact test with correction for multiple hypotheses (FDR-adjusted $q < 0.05$). Statistical testing was performed in R v.4.1.2. and Python v3.8. Repertoires were generated from distinct samples collected longitudinally.

Biological material availability

Please contact the corresponding author. Biological materials may be available after institutional review board or technology transfer office approval from sending and receiving institutions and execution of a material transfer agreement.

Reporting summary

Further information on research design is available in the Nature Portfolio Reporting Summary linked to this article.

Data availability

The whole PBMC and nasal *TRB* repertoires are available at https://doi.org/10.5281/zenodo.7698787. Sorted naive and memory PBMC T cell subset *TRB* repertoires from the time point E00, sorted total CD4$^+$ T cells and AIM-sorted CD4$^+$ T cell subsets from the time point E03 are available at https://doi.org/10.5281/zenodo.7686500. Processed single-cell CD69$^+$CD137$^+$ AIM-scTCRαβ-seq and feature barcode oligonucleotide-labeled mAb data are available at https://zenodo.org/record/6909380. The flow cytometry results from the intracellular cytokine staining of CD4$^+$ and CD8$^+$ S-reactive T cells are available at https://doi.org/10.5281/zenodo.8088178. The sequences of CD8$^+$ and CD4$^+$ T cell-origin TCRs expressed in reporter cells are available from GenBank (OP245920-OP245935 and OR239787-OR239798, respectively). The reference dataset for Cell Ranger used was GRCh-Alts-ensembl-5.0.0 and is available at 10xgenomics.com/support/software/cell-ranger/downloads. Source data are provided with this paper.

Code availability

The code used to analyze and present the data is based on Python v.3.8 or R v.4.1.2 and is available at https://github.com/kmayerb/NIA34780B. The availability of the tool used to classify PBMC *TRB* repertoires for evidence of CMV infection is discussed at https://www.immunoseq.com/cmv-classifier/.

References

60. Harris, P. A. et al. Research electronic data capture (REDCap)—a metadata-driven methodology and workflow process for providing translational research informatics support. *J. Biomed. Inform.* **42**, 377–381 (2009).
61. Bennett, R. S. et al. Scalable, micro-neutralization assay for assessment of SARS-CoV-2 (COVID-19) virus-neutralizing antibodies in human clinical samples. *Viruses* **13**, 893 (2021).
62. Sholukh, A. M. et al. Evaluation of cell-based and surrogate SARS-CoV-2 neutralization assays. *J. Clin. Microbiol.* **59**, e0052721 (2021).
63. Koelle, D. M. Expression cloning for the discovery of viral antigens and epitopes recognized by T cells. *Methods* **29**, 213–226 (2003).
64. Mayer-Blackwell, K. et al. TCR meta-clonotypes for biomarker discovery with *tcrdist3* enabled identification of public, HLA-restricted clusters of SARS-CoV-2 TCRs. *eLife* **10**, e68605 (2021).
65. Hagberg, A. A., Schult, D. A. & Swart, P. J. Exploring network structure, dynamics, and function using NetworkX. In *Proc. 7th Python in Science Conference (SciPy2008)* (eds Varoquaux, G. et al.) 11–15 (SciPy, 2008).
66. Britanova, O. V. et al. Age-related decrease in TCR repertoire diversity measured with deep and normalized sequence profiling. *J. Immunol.* **192**, 2689–2698 (2014).

67. Wagih, O. ggseqlogo: A versatile R package for drawing sequence logos. *Bioinformatics* **33**, 3645–3647 (2017).
68. Snyder, T. M. et al. Magnitude and dynamics of the T-cell response to SARS-CoV-2 infection at both individual and population levels. Preprint at *medRxiv* https://doi.org/10.1101/2020.07.31.20165647 (2020).
69. Nolan, S. et al. A large-scale database of T-cell receptor beta (TCRβ) sequences and binding associations from natural and synthetic exposure to SARS-CoV-2. Preprint at *Research Square* https://doi.org/10.21203/rs.3.rs-51964/v1 (2020).
70. Klinger, M. et al. Multiplex identification of antigen-specific T cell receptors using a combination of immune assays and immune receptor sequencing. *PLoS ONE* **10**, e0141561 (2015).
71. Li, D. et al. The T-cell response to SARS-CoV-2 vaccination in inflammatory bowel disease patients is augmented with anti-TNF therapy. *Inflamm. Bowel Dis.* **28**, 1130–1133 (2022).
72. Lefranc, M.-P. et al. IMGT, the international ImMunoGeneTics information system 25 years on. *Nucleic Acids Res.* **43**, D413–D422 (2015).
73. Schmitt, T. M. et al. Generation of higher affinity T cell receptors by antigen-driven differentiation of progenitor T cells in vitro. *Nat. Biotechnol.* **35**, 1188–1195 (2017).
74. Linnemann, C. et al. High-throughput identification of antigen-specific TCRs by TCR gene capture. *Nat. Med.* **19**, 1534–1541 (2013).
75. Jing, L. et al. Extensive CD4 and CD8 T cell cross-reactivity between alphaherpesviruses. *J. Immunol.* **196**, 2205–2218 (2016).
76. Ford, E. S. et al. Expansion of the HSV-2-specific T cell repertoire in skin after immunotherapeutic HSV-2 vaccine. Preprint at *medRxiv* https://doi.org/10.1101/2022.02.04.22270210 (2022).
77. Jing, L. et al. Cross-presentation and genome-wide screening reveal candidate T cells antigens for a herpes simplex virus type 1 vaccine. *J. Clin. Invest.* **122**, 654–673 (2012).
78. van Velzen, M. et al. Local CD4 and CD8 T-cell reactivity to HSV-1 antigens documents broad viral protein expression and immune competence in latently infected human trigeminal ganglia. *PLoS Pathog.* **9**, e1003547 (2013).
79. Jing, L. et al. Prevalent and diverse intratumoral oncoprotein-specific $CD8^+$ T cells within polyomavirus-driven Merkel cell carcinomas. *Cancer Immunol. Res.* **8**, 648–659 (2020).
80. Tigges, M. A. et al. Human $CD8^+$ herpes simplex virus-specific cytotoxic T-lymphocyte clones recognize diverse virion protein antigens. *J. Virol.* **66**, 1622–1634 (1992).

Acknowledgements

We thank: the participants; the Virology Research Clinic, University of Washington for collecting the specimens and data; D. Geraghty and C.-W. Pyo at the Fred Hutchinson Cancer Center (FHCC) for HLA typing; L. Stamatatos, FHCC, for the SARS-CoV-2 S protein with stabilizing proline substitutions used in the antibody assays; J. Bloom, FHCC, for the expression plasmids encoding the SARS-CoV-2 S protein from strain Wu-1, or Omicron BA.1, BA.2 and BA.4, with 21-amino-acid C-terminal deletions. D.M.K. received support from a National Institutes of Health (NIH) National Institute of Allergy and Infectious Diseases (NIAID) contract no. 75N93019C00063 (D.M.K.). The study has received support from NIH grant nos. AI163999 (D.M.K.), K08 AI148588 (E.S.F.), R01 AI136514 (K.M.-B. and A.F.-G.), F30 CA254168 (T.H.P.), T32 CA080416 (S.J.), P01 CA225517 (A.G.C., D.M.K., L.J., T.H.P. and S.J.), R01 AI134878 (A.M.S., E.L.B. and R.S.G.) and UM1 AI068614 (A.M.S., E.L.B. and R.S.G.). The scientific computing infrastructure at the FHCC was funded by an NIH Office of Research Infrastructure Programs grant no. S10 OD028685 (K.M.-B., A.F.-G. and E.S.F.). The Bill and Melinda Gates Foundation provided support via grant no. INV-027499 (A.F.-G. and K.M.-B.). This study was funded in part with Federal funds from the NIAID, NIH and Department of Health and Human Services under NIH contract no. HHSN272201800013C.

Author contributions

D.M.K., E.S.F., K.M.-B., A.F.-G., L.J. and K.J.L. conceptualized the study. A.M.S., E.L.B., R.S.G., M.R.H., B.E., E.E., M.M. and E.P. designed and performed the serological assays. L.J., C.J.B., H.X., T.H.P., K.J.L., H.S.R., R.M.G., R.E. and A.L.G. designed and performed the cellular immunity and sequencing assays. A.G.C., E.W. and M.E. provided the specialty reagents enabling the TCR functional assays. S.S. and C.L.M. processed and managed the specimen and demographic data. A.W. organized the clinical cohort. K.M.-B., E.S.F., K.J.L, L.J., S.J. and A.F.-G. carried out the bioinformatic and statistical analyses. E.S.F., K.M.-B., K.J.L., A.F.-G., L.J. and D.M.K. wrote the manuscript. The funders had no role in study design, data collection and analysis, decision to publish or preparation of the manuscript.

Competing interests

H.S.R. and R.E. are employees of Adaptive Biotechnologies. B.E., E.E. and M.R.H. performed this work as employees of Laulima Government Solutions. M.M. and E.P. are subcontractors to Laulima Government Solutions; they performed this work as employees of Tunnell Government Services. The other authors declare no competing interests.

Additional information

Extended data is available for this paper at https://doi.org/10.1038/s41590-023-01692-x.

Supplementary information The online version contains supplementary material available at https://doi.org/10.1038/s41590-023-01692-x.

Correspondence and requests for materials should be addressed to David M. Koelle.

Peer review information *Nature Immunology* thanks Tao Dong and the other, anonymous, reviewer(s) for their contribution to the peer review of this work. Peer reviewer reports are available. Primary Handling Editor: Ioana Visan in collaboration with the *Nature Immunology* editorial team.

Reprints and permissions information is available at www.nature.com/reprints.

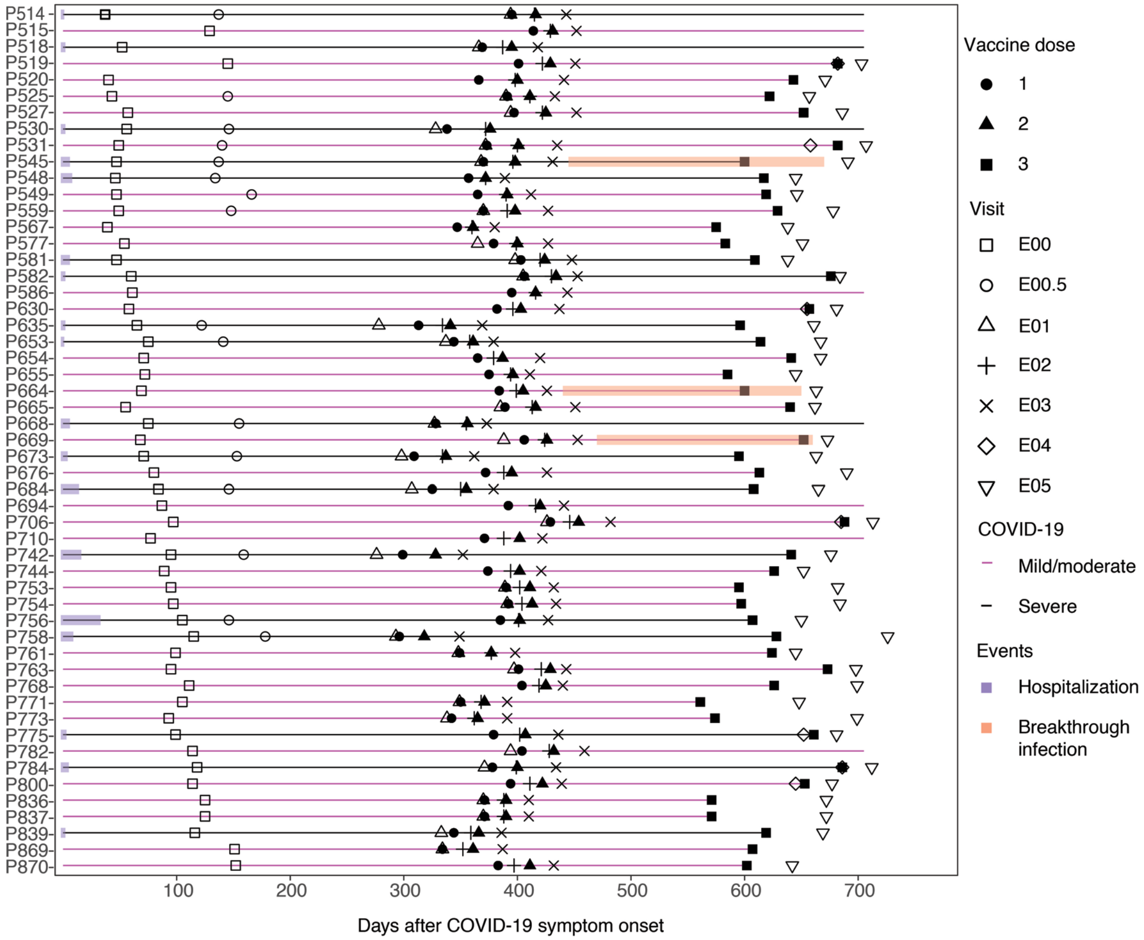

Extended Data Fig. 1 | Schedule of infection, vaccination, and sample collection. Fifty-three study participants with prior SARS-CoV-2 infection as documented by seropositivity to S and N proteins and participant P845 who was seronegative prior to vaccination received either BNT162 or mRNA-1273 1st dose (closed circle), 2nd dose (closed triangle), and booster (3rd) dose (closed square) on the days after symptom onset as shown. Persons with mild or moderate COVID-19 are shown in magenta, persons with severe COVID-19 in black. Duration of hospitalization in persons with severe COVID-19 is shown in purple. PBMC were obtained at exam visits convalescence (E00, n = 54), late convalescence (E00.5, n = 16), pre-dose 1 (E01, n = 34), post-dose 1 (E02, n = 52), post-dose 2 (E03, n = 53), pre-boost (E04, n = 7), and post-boost (E05, n = 44). 33 persons had samples at E00, E01 and E03, 31 had samples at E00, E01, E02, and E03, and 26 had samples at all of E00, E01, E02, E03, and E05. Three participants were observed to have breakthrough COVID-19 infection based on boosting of anti-nucleocapsid antibody levels at visit E05 (P545, P664, P669), indicated in orange. All participants received primary vaccination but not all received a booster dose.

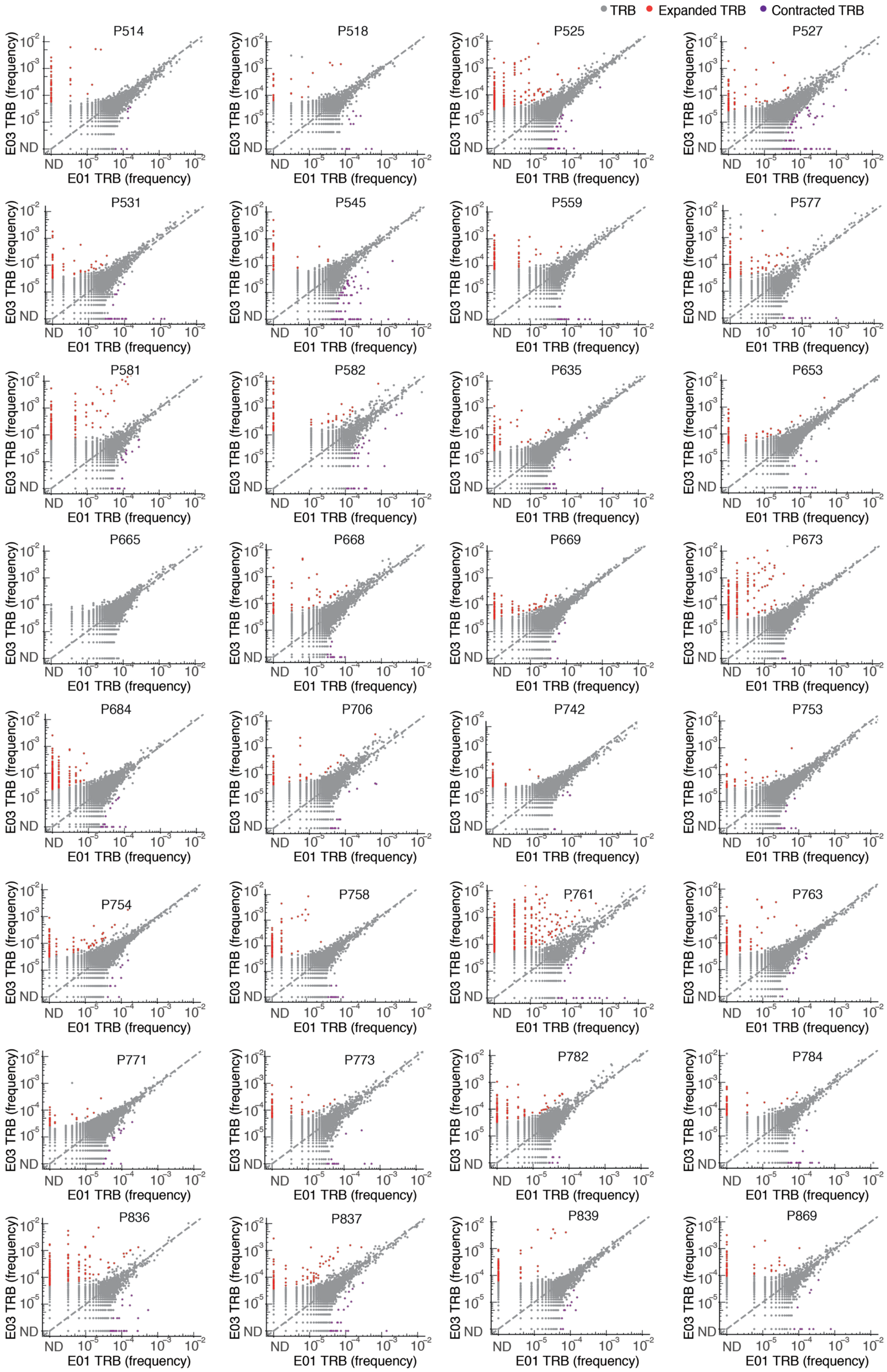

Extended Data Fig. 2 | Primary vaccination led to expansion in specific TCR clonotypes in vaccinated persons. Frequency (% of bulk *TRB* repertoire) of individual clonotypes in E01 vs. E03 in 32 persons with both samples. Expanded (red) (or contracted, purple) clonotypes were defined as $\log_2$(fold change) > 2 (or < 0.5) and Fisher's exact test FDR-adjusted p value < 0.05. Dotted line indicates y = x. Participant ID at top of each graph. ND = not detected. Serologically-naive Participant P845 is not shown.

https://doi.org/10.1038/s41590-023-01692-x

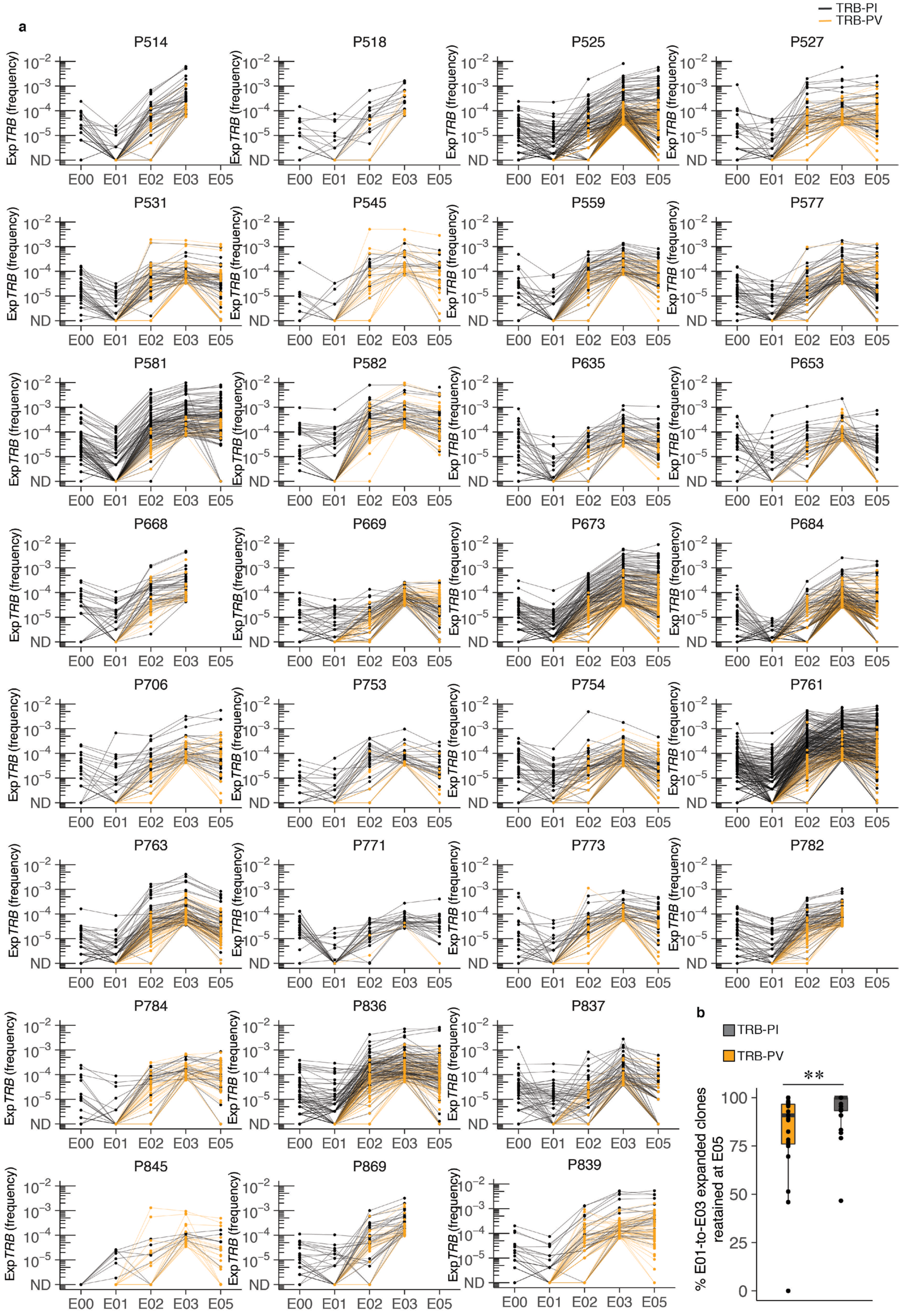

Extended Data Fig. 3 | See next page for caption.

Extended Data Fig. 3 | Frequency of E01-E03 expanded clonotypes from E00 through E05. (a) E01-E03 expanded clonotype frequency (abundance) over the course of the study. Each line is an individual clonotype. TRB-PI are shown in black, TRB-PV are in orange (n = 30). ND = not detected. **(b)** Boxplot at lower right shows the percent of TRB-PI and TRB-PV for each participant that were detectable after a 3rd vaccine dose (E05) (n = 26). Median, IQR and whiskers (1.5*IQR) are noted. Comparison between groups is by two-sided Wilcoxon rank sum test, p = 0.0023. Participants P742 and P758 were not sampled at E02 and trajectories are not shown. Participant P665 had no expanded clonotypes and is not shown. Participant P845 was serologically naive at E00. Participants P545 and P669 experienced breakthrough infection between the E03 and the E05 timepoints and so repertoires at E05 represent both repeat natural infection as well as mRNA booster vaccine dose.

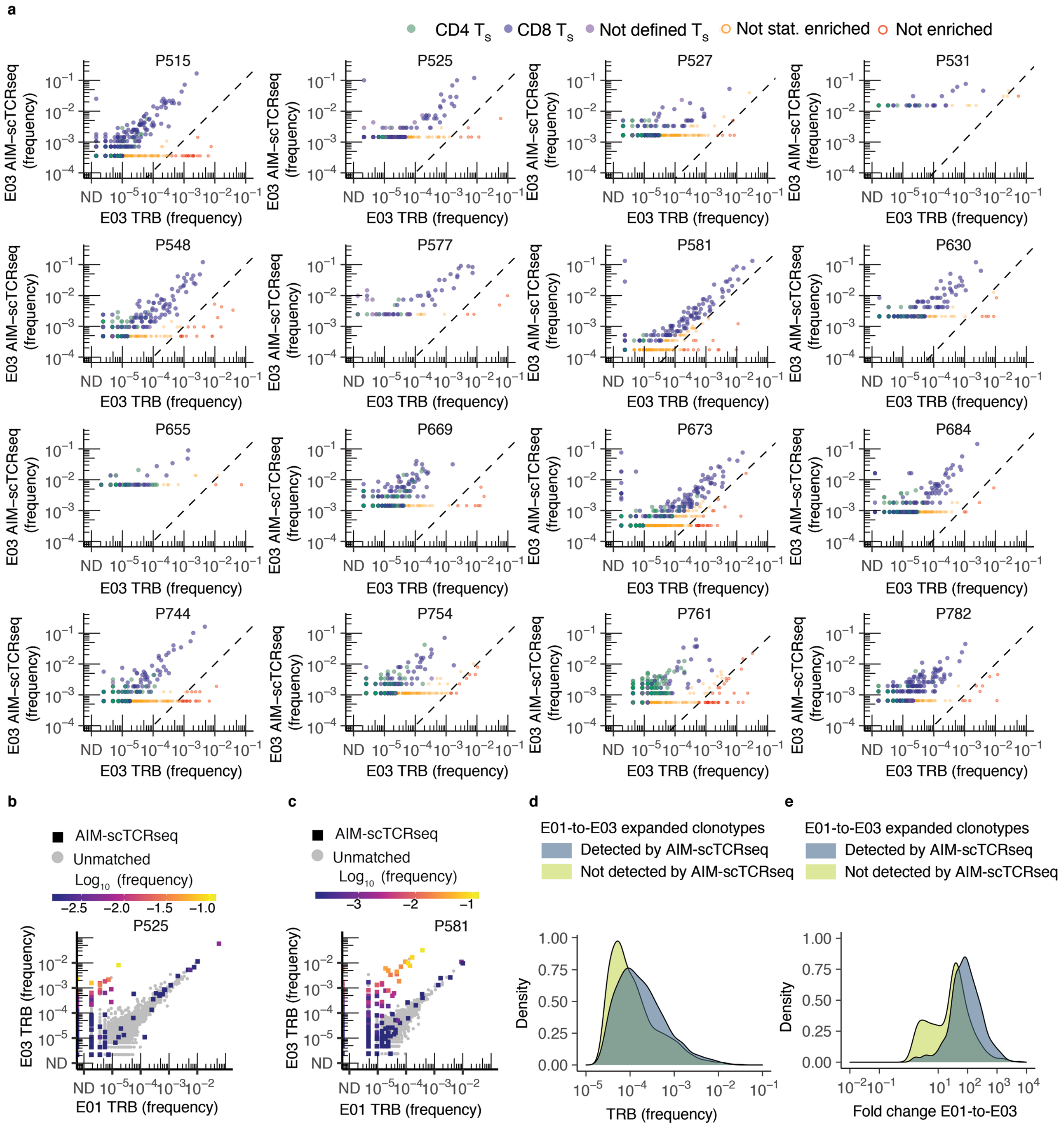

Extended Data Fig. 4 | AIM-scTCRαβ-seq enriches a complex set of clonotypes from PBMC after mRNA vaccination of previously SARS-CoV-2 infected persons. (a) Frequency of clonotypes detected by CD69^{+}CD137^{+} AIM-scTCRαβ-seq plotted against the productive frequency of *TRB*-matched templates in bulk *TRB* sequencing at E03. Cell types defined by oligonucleotide-labeled mAbs are shown as CD4^{+} (green), CD8^{+} (blue), or phenotype not defined (purple) T cells. Clonotype enrichment in CD69^{+}CD137^{+} AIM-scTCRαβ-seq was determined by cumulative distribution function (CDF) with false discovery rate (FDR) correction (Methods). Clonotypes that were detected, but not enriched, in CD69^{+}CD137^{+} AIM-scTCRαβ-seq are shown in red (n = 180) and were omitted from CDR3 motif discovery analysis. ND indicates clonotypes that could not be assigned a *TRB* unambiguously. **(b,c)** Productive frequency of CD69^{+}CD137^{+} AIM-scTCRαβ-seq detected clonotypes in relation to change in productive frequency from E01 to E03 in bulk TCR-β-seq is shown for 2 representative participants, including one with a lower proportion of representation in CD69^{+}CD137^{+} AIM-scTCRαβ-seq of their significantly expanded clonotypes (P525, **b**) and another with a higher proportion of significantly expanded clonotypes also seen by CD69^{+}CD137^{+} AIM-scTCRαβ-seq (P581, **c**). **(d, e)** Density plots show proportion of unique, expanded clonotypes by frequency at E03 (**d**) or fold change from E01 to E03 (primary vaccination) (**e**) by detection in CD69^{+}CD137^{+} AIM-scTCRαβ-seq at E03 amongst 12 participants with both paired E01/E03 bulk TCR-β-seq and CD69^{+}CD137^{+} AIM-scTCRαβ-seq.

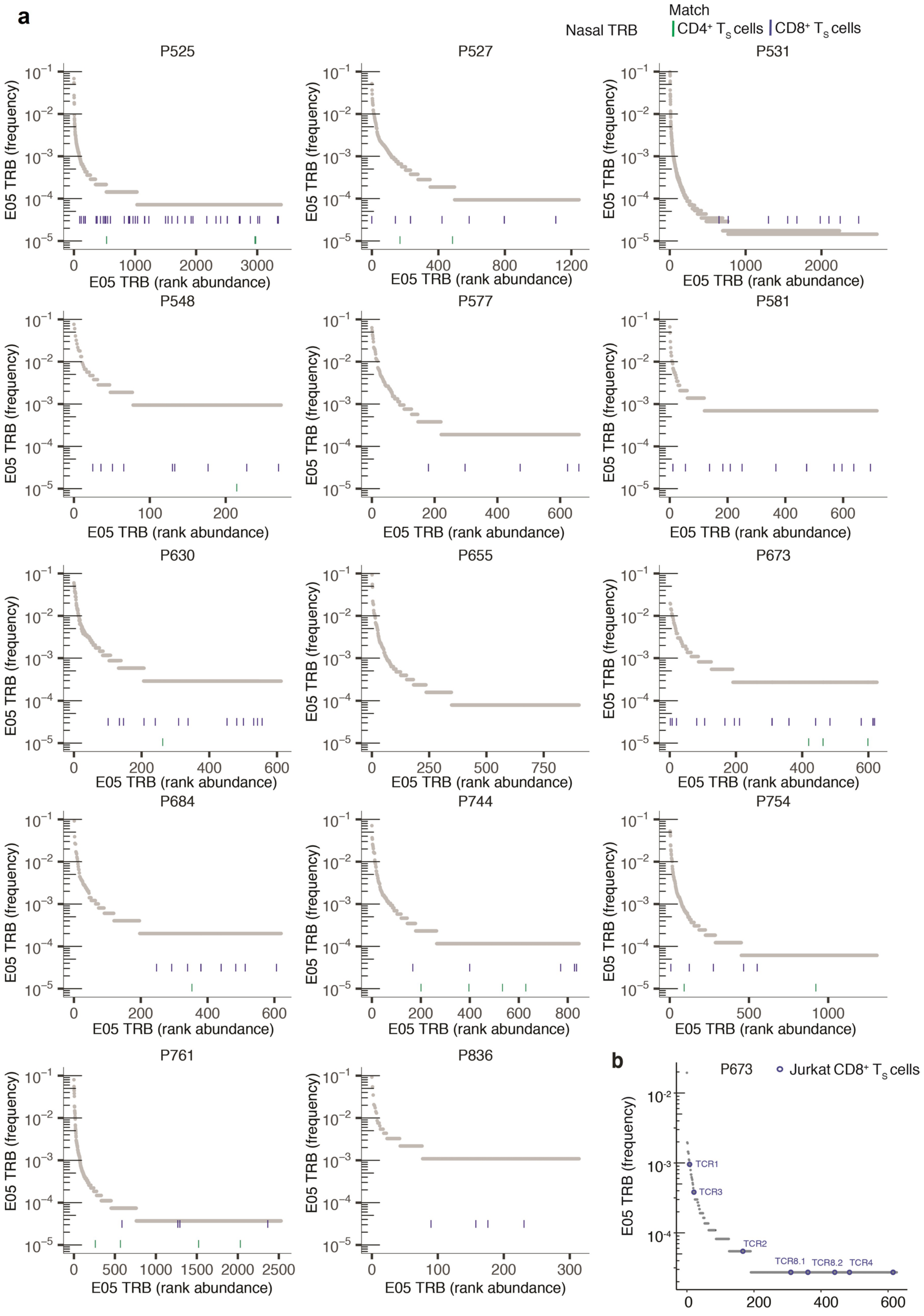

Extended Data Fig. 5 | T_S from CD69⁺CD137⁺ AIM-scTCRαβ-seq matching *TRB* clonotypes from nasal swabs in 14 participants at E05. (a) Rank abundance plots of *TRB* clonotypes in nasal samples in 14 participants, where blue (CD8⁺) and green (CD4⁺) dashes indicate rank of clones identified in the same participant's blood by CD69⁺CD137⁺ AIM-scTCRαβ-seq at E03. **(b)** In participant P673, rank abundance plot of *TRB* clonotypes in nasal samples collected at E05. Clones labeled TCR1, TCR2, TCR3, TCR4, TCR8.1 and TCR8.2 indicate *TRB* clonotypes with exact sequence match to experimentally-confirmed receptors shown to recognize HLA-A*03:01 S epitopes.

https://doi.org/10.1038/s41590-023-01692-x

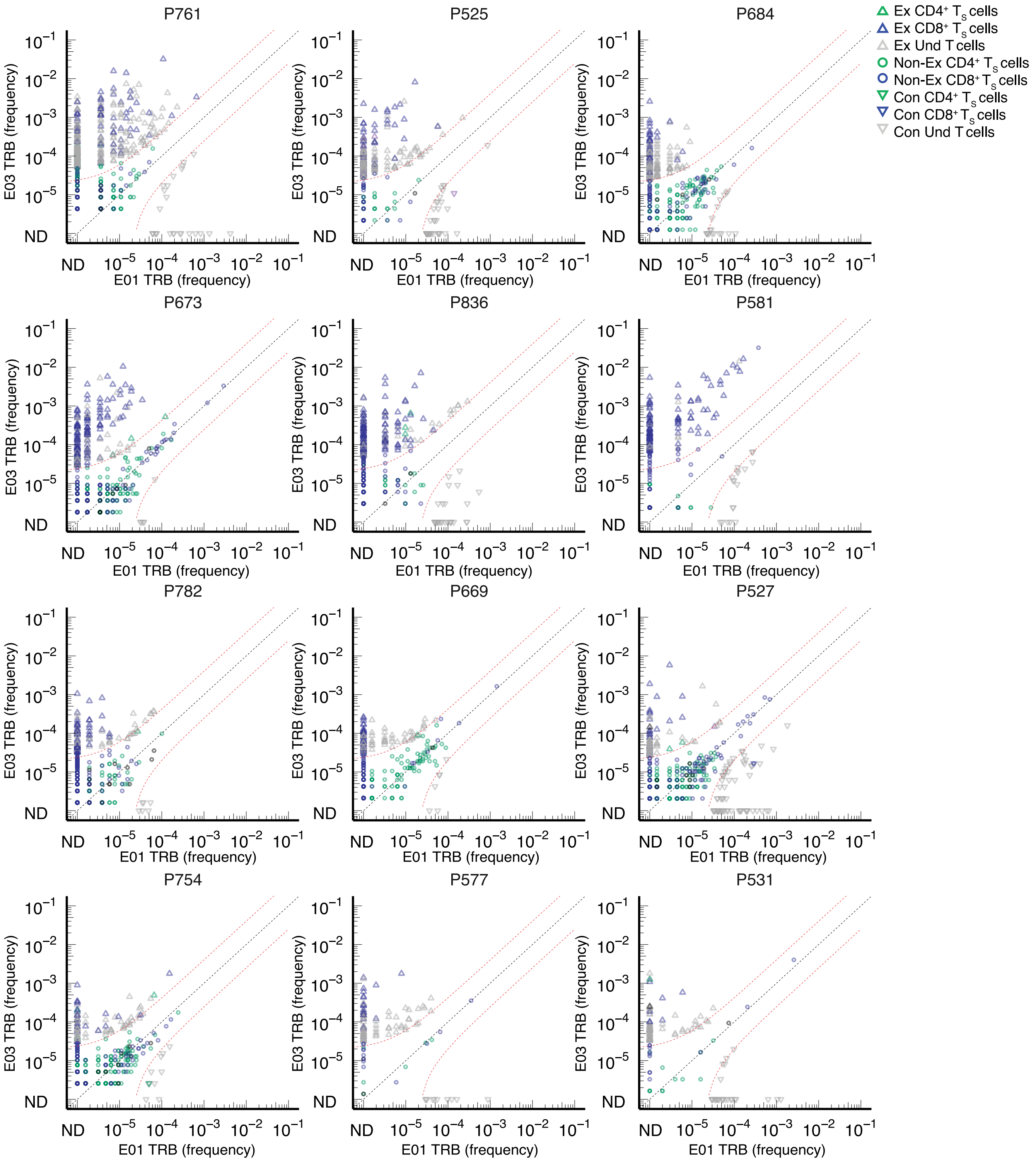

Extended Data Fig. 6 | T_S and vaccine-expanded clonotypes. Overlay of *TRB* sequences from CD69⁺CD137⁺ AIM-scTCRαβ-seq of T_S cells onto bulk *TRB* clonotype frequency at E01 and E03 in two representative participants. E01-to-E03 expanded (Ex) or contracted (Con), *TRB* clonotypes are shown, with TRB matching a CD69⁺CD137⁺ AIM-scTCRαβ-seq (T_S) shown in color and unmatched TRB are shown in gray (Und). Among clonotypes that neither expanded nor contracted (Non-Ex), only CD69⁺CD137⁺ AIM-scTCRαβ-seq *TRB*-matched clonotypes are shown between red dashed lines. Frequencies of *TRB* clonotypes pre- and post-vaccine are as resolved by bulk TCR-β-seq. ND = not detected.

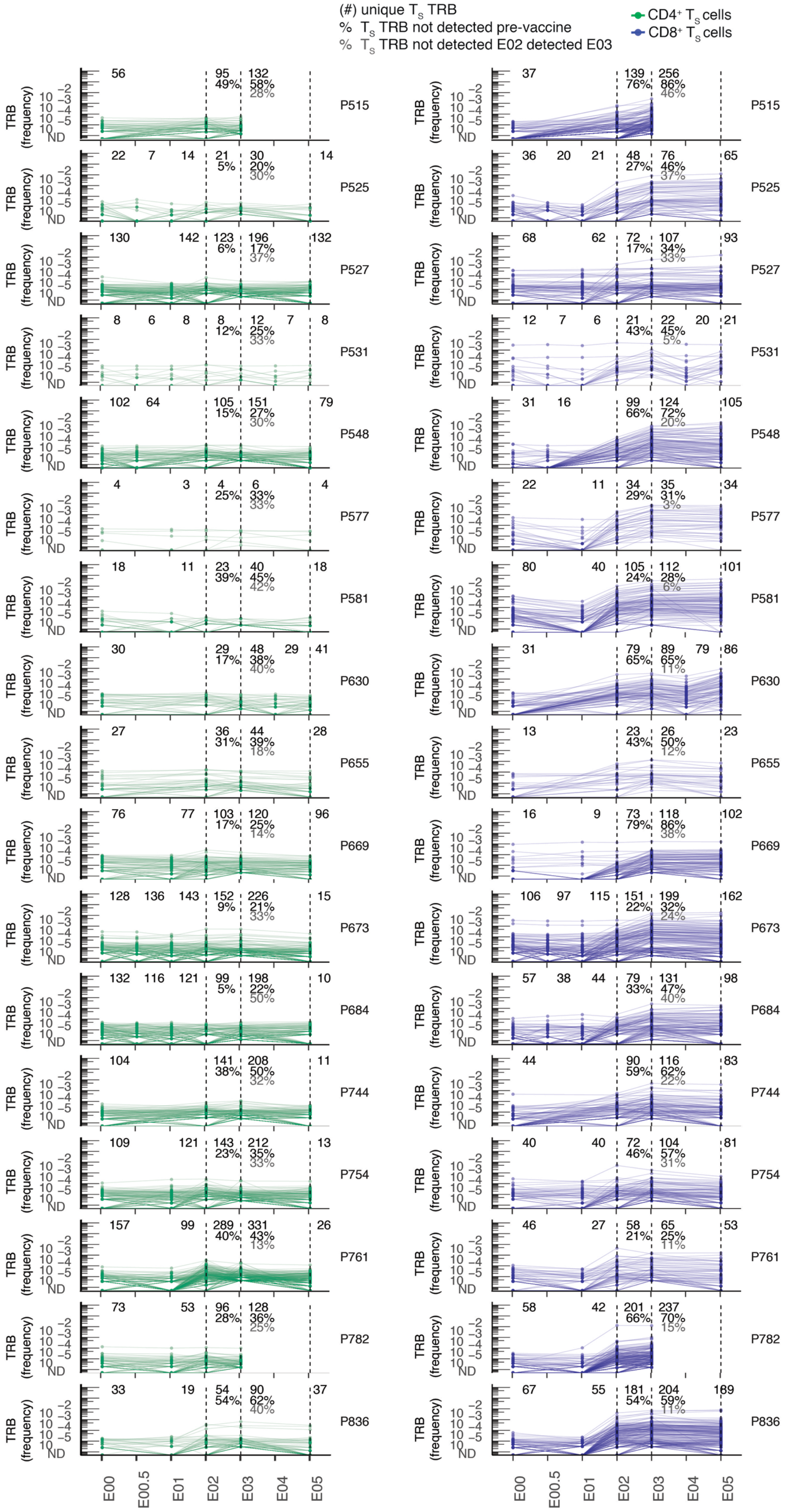

Extended Data Fig. 7 | See next page for caption.

Extended Data Fig. 7 | Abundance of T_S clonotypes by TCRβ-seq over time. Longitudinal tracking of abundance of $CD69^+CD137^+$ AIM-scTCRαβ-seq-identified $CD4^+$ and $CD8^+$ T_S *TRB* clonotypes in PBMC by TCRβ-seq in all participants with AIM-scTCRαβ-seq. Numbers in top rows indicate the number of unique $CD69^+CD137^+$ AIM-scTCRαβ-seq *TRB* clonotypes from E03 detected at each time point. Percentages refer to the fraction of $CD69^+CD137^+$ AIM-scTCRαβ-seq clonotypes detected at the E02 and E03 timepoints, respectively, detected only post-vaccination. Percentages in gray are the fraction of unique clones detected at E03 that are below the level of detection at E02. Not all participants had samples at each time point, indicated by absence of dot symbols at those samples. Participant P669 had SARS-CoV-2 infection between E03 and E05 timepoints and so this E05 repertoire reflects repeat SARS-Co-2 infection and mRNA booster vaccine.

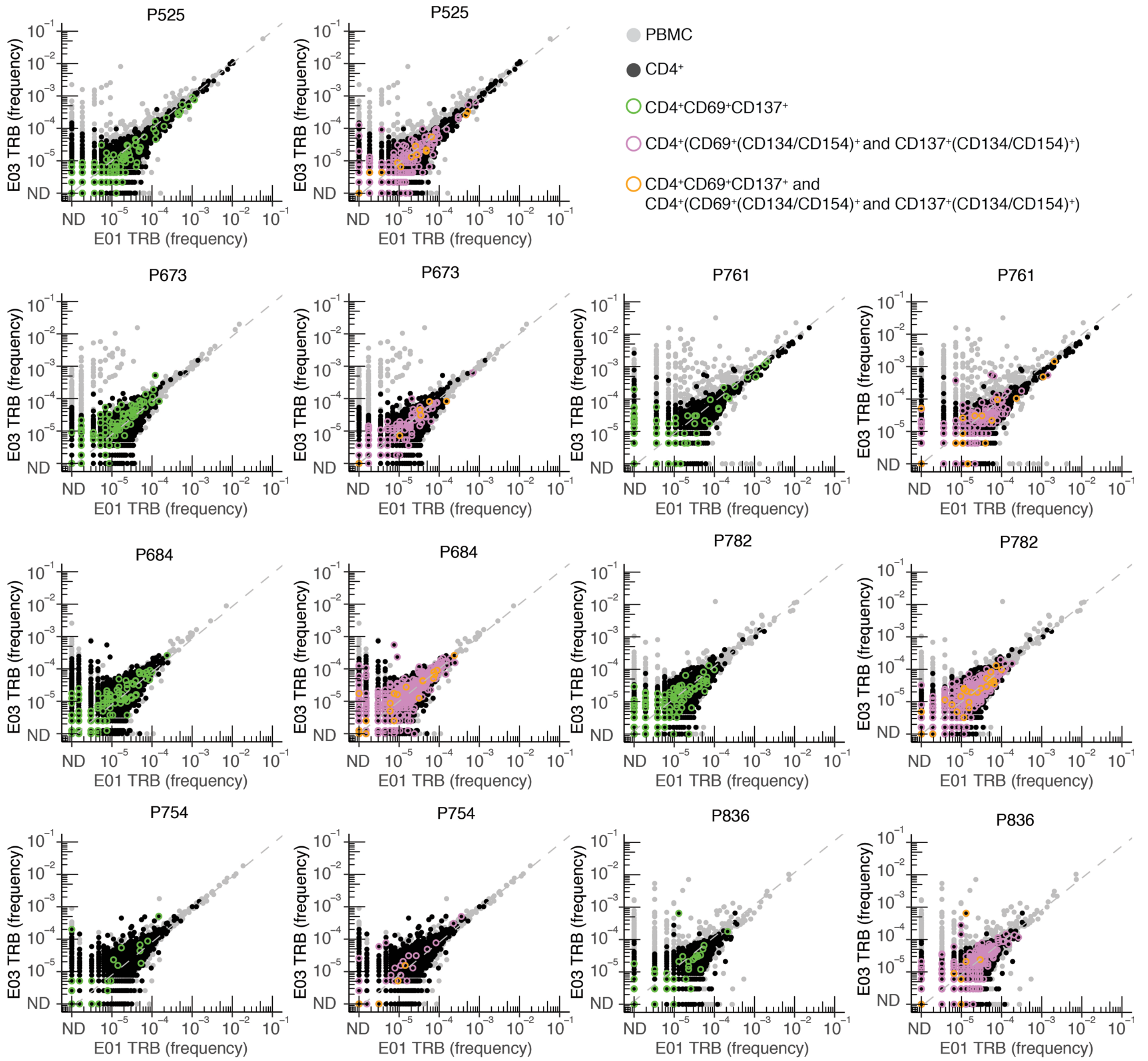

Extended Data Fig. 8 | Selection of AIM-scTCRαβ-seq T cells using CD69, CD137, and CD134/ CD154 marker sets compared to bulk TCRβ-seq and sorted CD4 TCRβ-seq from PBMCs over primary vaccination. Frequency (% of bulk *TRB* repertoire) of individual clonotypes in E01 vs. E03 in 7 persons studied by CD69$^+$CD137$^+$ AIM-scTCRαβ-seq and (CD69/CD137)$^+$(CD134/CD154)$^+$ CD4$^+$ AIM-TCRβ-seq. Dotted line indicates y = x. Participant ID at top of each pair of graphs. ND = not detected. All PBMC are shown. Clonotypes found in the total CD4$^+$ sorted fraction are shown in black. Clonotypes present in the total CD4$^+$ sorted fraction and also enriched in sequential sorting of CD4$^+$CD69$^+$CD137$^+$ (green) cells are overlaid with CD4$^+$CD69$^+$(CD134/CD154)$^+$ and CD4$^+$CD137$^+$ (CD134/CD154)$^+$ (pink) cells in the left and right panels, respectively, for seven participants. Clonotypes in all three fractions (total CD4$^+$, CD4$^+$CD69$^+$CD137$^+$, and CD4$^+$CD69$^+$(CD134/CD154)$^+$ and CD4$^+$CD137$^+$(CD134/CD154)$^+$) are shown in orange. Gray shaded clonotypes were not identified as CD4$^+$ by any of these methods.

nature immunology

Resource

https://doi.org/10.1038/s41590-023-01692-x

Repeated mRNA vaccination sequentially boosts SARS-CoV-2-specific CD8$^+$ T cells in persons with previous COVID-19

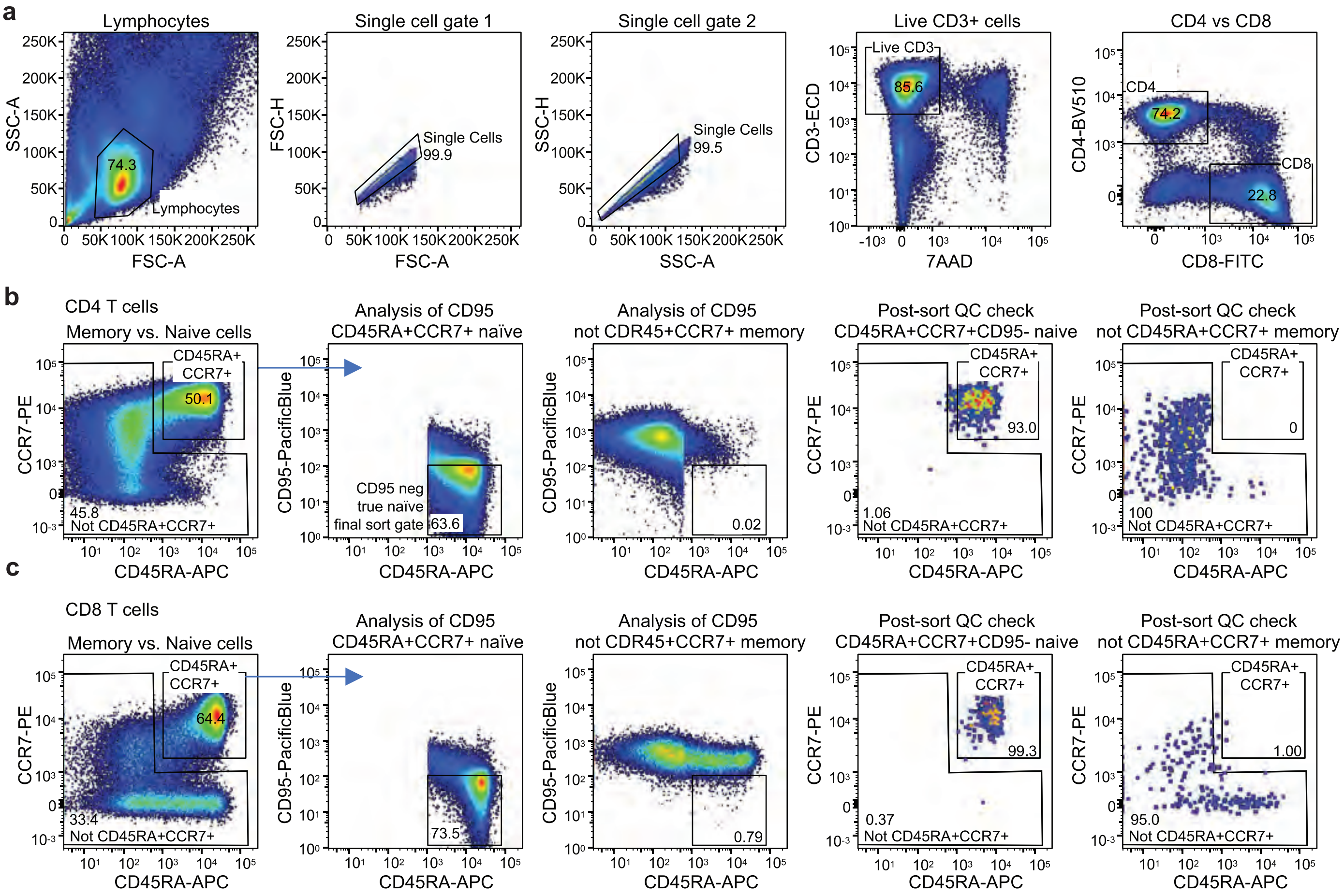

Supplementary Data Fig. 1. (**a**) Representative gating for evaluation of memory/naive phenotype at pre-vaccine timepoint E00. In the top row, PBMC were gated for single live CD4$^+$CD8$^-$ or CD4$^-$CD8$^+$ T cells. (**b**) Gated CD4$^+$ T cells were stained for CD45RA vs. CCR7 to preliminarily identify memory vs. naïve cells. The third dot plot illustrates CD95 expression for memory CD4$^+$ T cells. The same indicated gate for CD95$^-$ cells was applied to the second dot plot containing preliminarily identified naïve CD4$^+$ T cells. Cells within the square gate were retained as final naïve CD4$^+$ T cells. (**c**) A similar process was applied to CD8$^+$ T cells in the third row. The right two dot plots in (**b**) and (**c**) represent post-sort quality control checks of sorted CD4$^+$ and CD8$^+$ final naïve and memory cells. Numbers in boxed areas are percent of total cells in indicated gates.

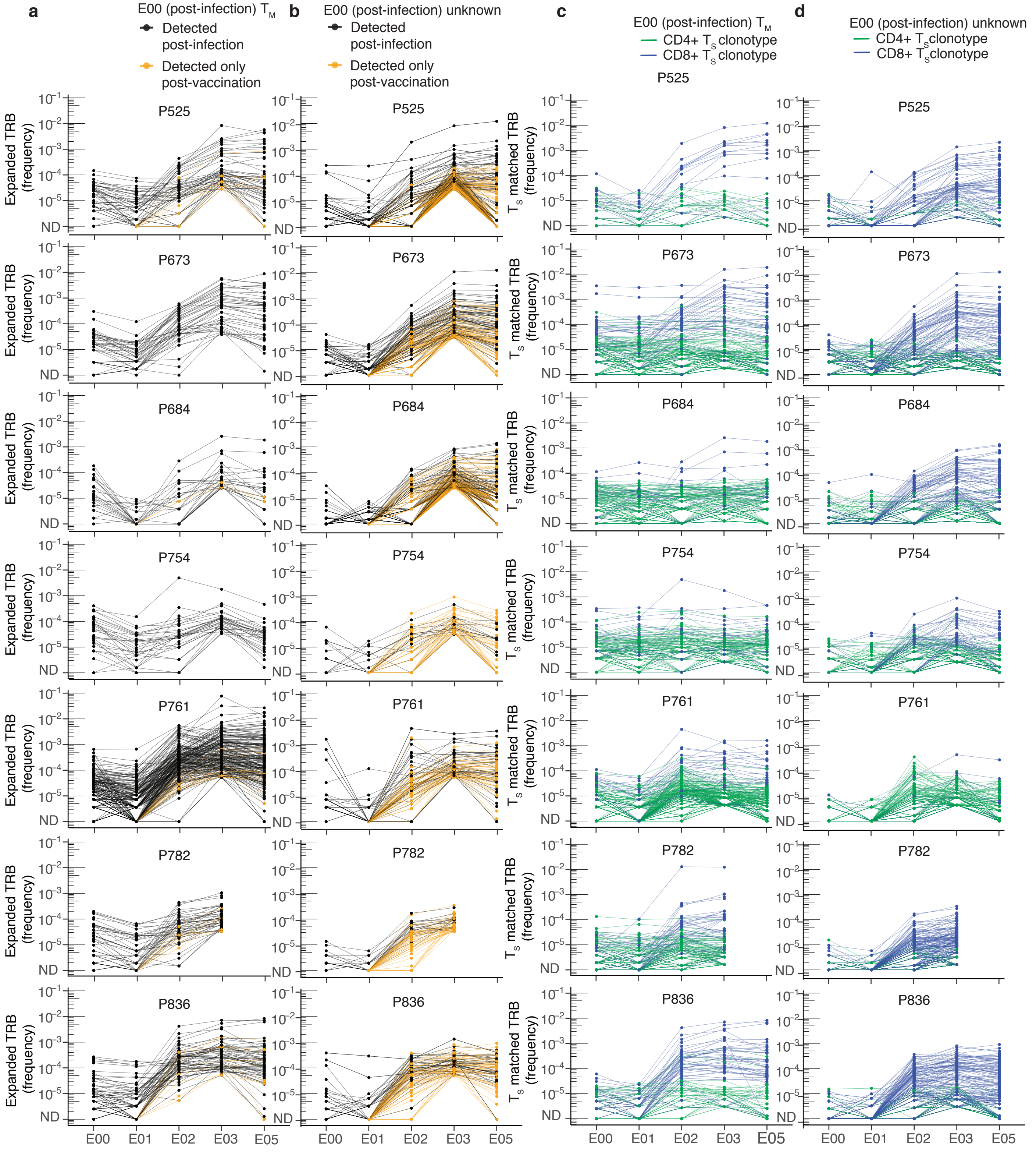

Supplementary Data Fig. 2. (**a**) Trajectories of clonotypes with confirmed pre-vaccine memory or unknown phenotypes among vaccine-expanded and AIM$^+$ S-reactive clonotypes. Deep TRB sequencing was performed after sorting PBMCs into memory and naïve subsets at time point E00 shortly after infection. Clonotypes with a confirmed memory phenotype prior to vaccination that were vaccine-expanded (log2(fold change) > 2 and Fisher's Exact Test q-value < 0.05 between pre-vaccine and post-vaccine repertoires). Black clonotypes were also detected in bulk PBMC repertoires prior to vaccination. Many clones decreased in the year after infection (E00 to E01). A few clonotypes (orange) were not detected prior to initiation of vaccination, but were detected in sorted phenotypic memory cells from E00. (**b**) Vaccine-expanded clones that were not detected amongst memory cells from E00. A few clonotypes were detectable during convalescence (black), but could not be confirmed as memory in (**a**). In general, there are far fewer of such clonotypes per subject than those confirmed as memory in (**a**). Orange clonotypes were not seen in pre-vaccine bulk PBMC, not detected as memory cells at E00, and were only noted after vaccination. (**c**) Spike-activated clonotypes (CD69$^+$CD137$^+$) with a documented memory phenotype at E00 shortly after infection. (**d**) Spike-activated clonotypes that were not detected amongst memory cells at E00. Comparing (**c**) and (**d**), confirmed CD8$^+$ T cell S-reactive clonotypes exhibited stronger vaccine-related expansion than did CD4$^+$ T cell clonotypes, regardless of evidence of memory status.

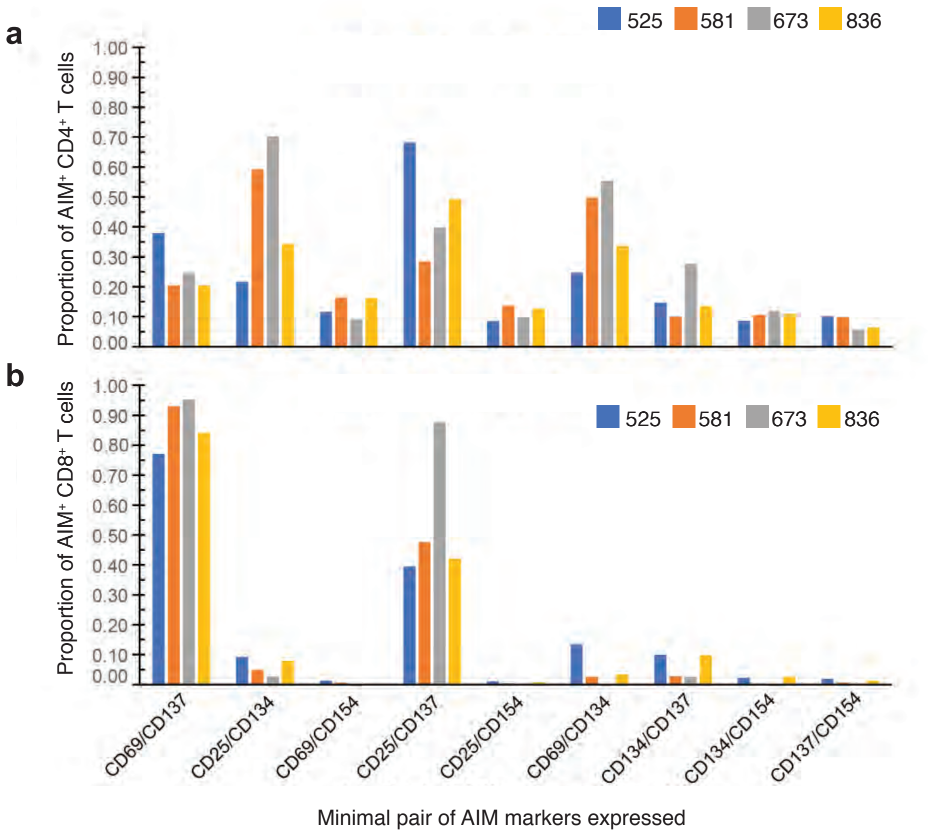

Supplementary Data Fig. 3. Sensitivity of different combinations of activation markers for detection of SARS-CoV-2 S peptide-reactive CD4 and CD8 T cells. E03 PBMC from 4 participants (P525, P581, P673, P836) were gated for **(a)** live, single CD3$^+$CD4$^+$CD8$^-$ T cells or **(b)** live, single CD3$^+$CD4$^-$CD8$^+$ lymphocytes. Bars are colored by participant. Net percentages of cells expressing each combination of activation induced markers (AIM) were calculated by subtracting values of DMSO-exposed samples from values of S peptides-exposed samples. Total AIM$^+$ CD4$^+$ and total AIM$^+$ CD8$^+$, calculated from net percentages, represents the sum of the cells expressing any combination of 2 or more AIM (except for CD25$^+$CD69$^+$) and is set to 100%. The y-axis shows the proportion of total CD4$^+$ or CD8$^+$ AIM$^+$ cells detected per AIM pair indicated on the x-axis. The number of CD4$^+$ T cells analyzed per condition ranged from 10,190 to 95,833 for DMSO and from 27,368 to 112,383 for S peptide pool. Bars represent results from single flow cytometry experiments.

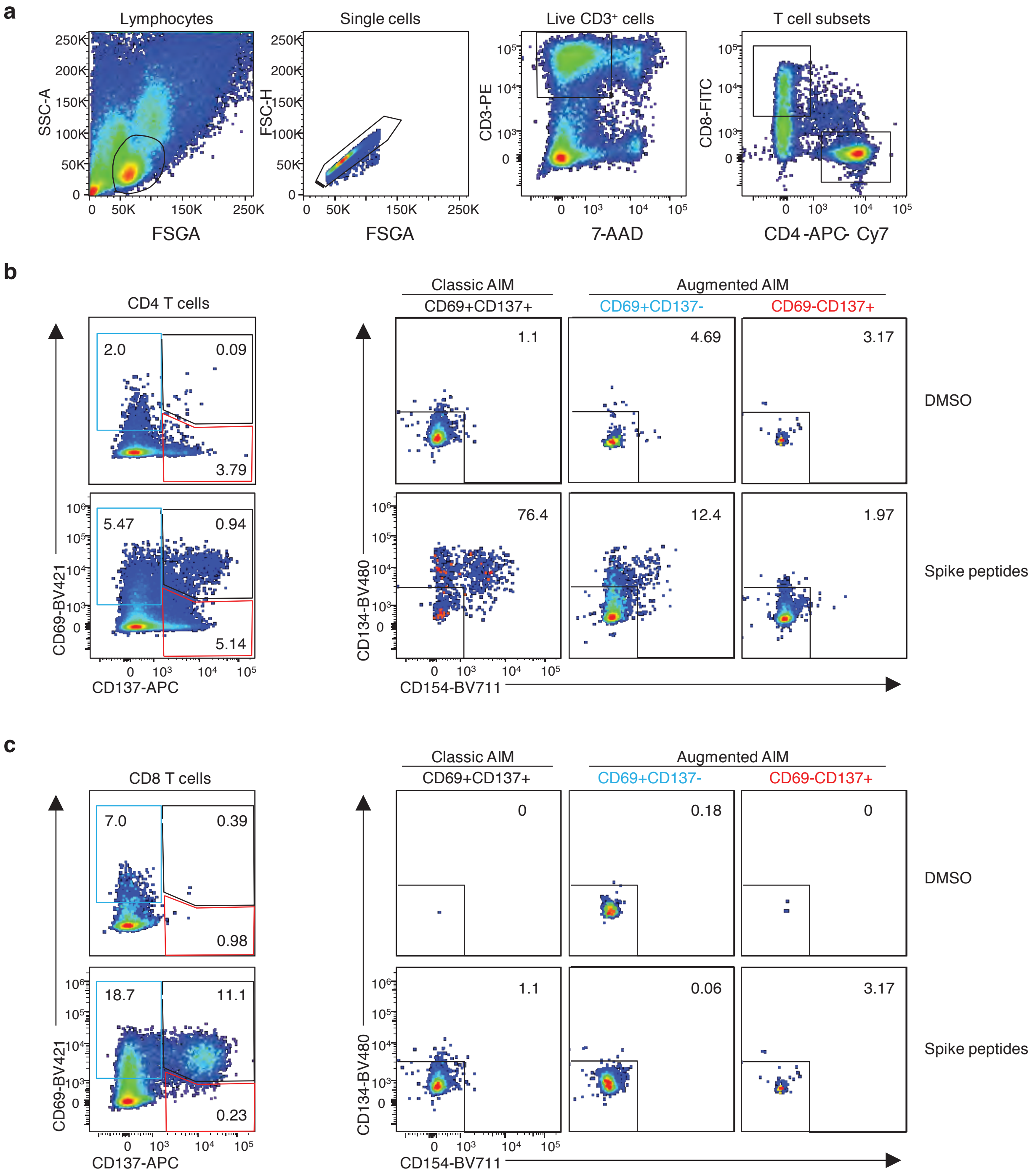

Supplementary Data Fig. 4. Representative gating scheme for sorting of CD69^{+} CD137^{+} and CD69^{+} or CD137^{+} plus CD134^{+} and/or CD154^{+} activation induced marker (AIM) cell fractions to investigate AIM identification of S-reactive clonotypes via bulk TCRβ-seq. PBMC from E03 were stimulated with S peptides or DMSO for 18 hours and stained for expression of the indicated markers. (**a**) Preliminary gating for live CD4^{+} and CD8^{+} T cells. (**b, c**) show the same scheme in CD4^{+} (**b**) and CD8^{+} (**c**) T cells, respectively. Left dot plots show expression of CD69^{+} and CD137^{+} CD4^{+} and CD8^{+} T cells in the CD69^{+} CD137^{+} double positive (black) gate, were collected for CD4^{+} TCRβ-seq as 'classic' AIM (black gate). The right three columns of dot plots show expression of additional activation markers for cells in the indicated quadrants in the CD69/CD137 plots. CD4^{+} T cells expressing either CD134 and/or CD154 from the CD69^{+} CD137^{-} (blue) and CD69^{-} CD137^{+} (red) gates were pooled for CD4^{+} TCRβ-seq as 'augmented' AIM^{+} cells. In this representative person, 76.4% of CD69^{+} CD137^{+} CD4+ T cells were positive for CD134 and/or CD154. However, 12.4% of CD69^{+} CD137^{-} CD4^{+} T cells and 2.0% of CD69^{-} CD137^{+} CD4 T cells were positive for these additional markers. Few CD8^{+} T cells from the CD69^{+} CD137^{-} and CD69^{-} CD137^{+} gates expressed either CD134 and/or CD154 and so these were not sequenced by TCRβ-seq.

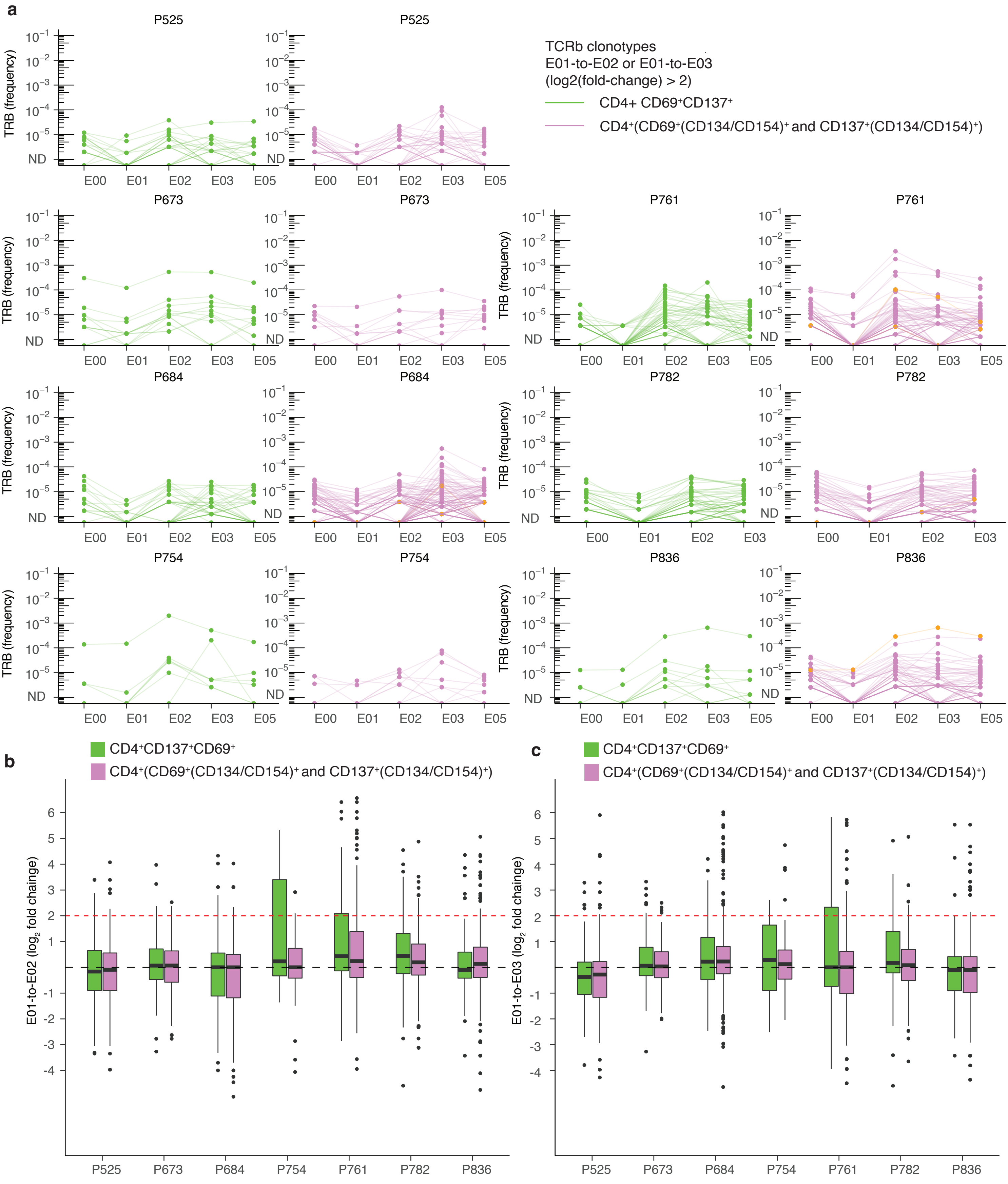

Supplementary Data Fig. 5. Longitudinal kinetics and fold change distribution of AIM-scTCRαβ-seq selected T cells comparing CD69, CD137, and CD134/ CD154 marker sets in 7 persons. (**a**) The frequency of each expanding ($\log_2$(FC) > 2) TRB clonotype is tracked from E00 to E05. Clonotypes shown were those enriched in the total CD4+ sort and enriched in subsequent split sample sorts for $CD69^{+}CD137^{+}$ (green) or augmented CD69/137 single positive $CD134^{+}$ and/or $CD154^{+}$ (pink, 'augmented'), or both (orange). Among all TS cells identified using either marker set, 12-49% (median 27%) TRB clonotypes were $CD69^{+}CD137^{+}$ double positive and 48-86% (median 69%) were CD69/CD137 single positive plus $CD134^{+}$ and/or $CD154^{+}$. A small fraction of TRB sequences, 2-12% (median 4%) were identified in both AIM+ populations. **(b, c)** Distribution of fold change of all AIM^{+} $CD4^{+}$ TRB clonotypes between pre-vaccine E01 and E02 (b) and E01 and E03 (c). Median, box (IQR), and whiskers (1.5 * IQR) indicate distribution of fold changes. Clonotypes falling above the red line in either **(b)** or **(c)** are those with expansion of $\log_2$(fold-change) > 2 relative to E01.

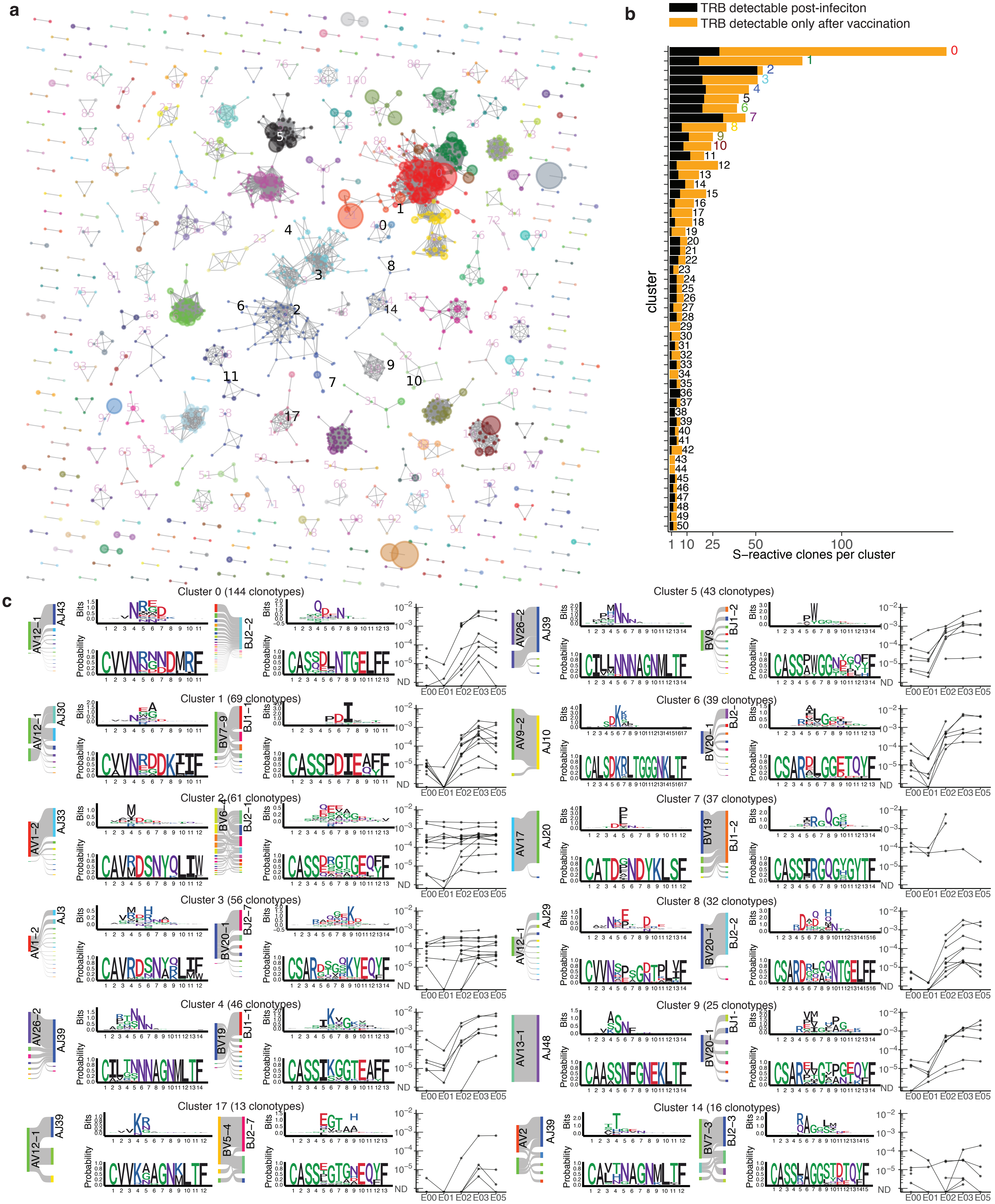

Supplementary Data Fig. 6. Selected TS clonotype clusters by CD69+CD137+ AIM-scTCRαβ-seq. (**a**) Sequence similarity graph with 1,448 clones and 248 convergent clusters of two or more TS clonotypes recovered from 17 individuals at E03. Circle size represents the relative frequency of each TCRαβ clonotype. Equivalent TCRαβ AA sequences may be included more than once if found in multiple participants. Color is by cluster number. (**b**) The number of clones comprising each cluster that had a corresponding TRB detectable post-infection (black) or only post-vaccination (orange) for the top 50 clusters. (**c**) Logo plots for representative clusters indicated by integers in (**a**) with inferred restricting HLA class I alleles (Methods), if able to be defined. For each CDR3 motif, the lower sequence logo shows the probability of each amino acid residue at each CDR3 position and the upper sequence logo depicts the information content in bits comparing the residue usage to a set of randomly selected CDR3 with the same V and J gene usage as the sequence cluster (Methods). Residue color indicates chemistry: acidic (red), basic (blue), hydrophobic (black), neutral (purple), polar (green). Line graphs show the sums of the abundances of the TRB sequences in each cluster in longitudinal PBMC repertoires for each participant contributing sequences to the cluster. Clusters 2 and 3 have many members with characteristic MAIT cell V-J gene usage (*TRAV1-2* with *TRAJ33*, *TRAJ20*, or *TRAJ12*).

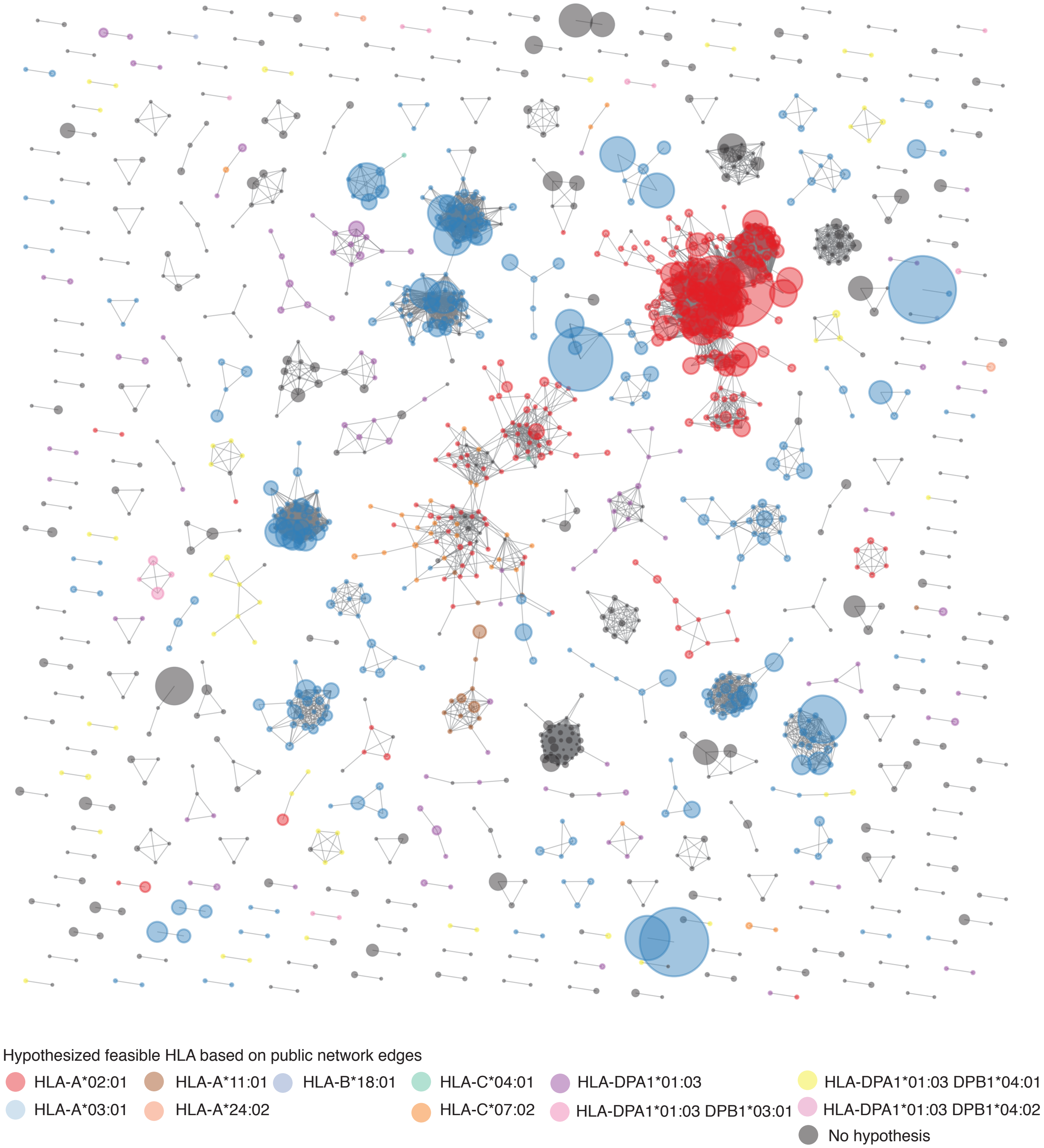

Supplementary Data Fig. 7. Feasible cognate HLA alleles (Feasible indicating clusters formed from groups of persons expressing a shared HLA class I or class II allele, suggesting common specificity for a peptide ligand restricted by this allele.) T cells co-expressing CD69 and CD137 after 18 hour stimulation with S peptides we e sorted and TRA/TRB sequences recovered by AIM-scTCRαβ-seq (see Methods). Sequence similarity graph of paired TRA/TRB sequences with 1,448clones and 248 convergent clusters of two or more S-reactive clones recovered from 17 individuals following second immunization. HLA feasibility analysis (see Methods) was used to assess feasible shared HLA allele among participants contributing TCRs to convergent sequence clusters. U indicates the feasible allele could not be narrowed down to two or fewer candidates (see Methods).

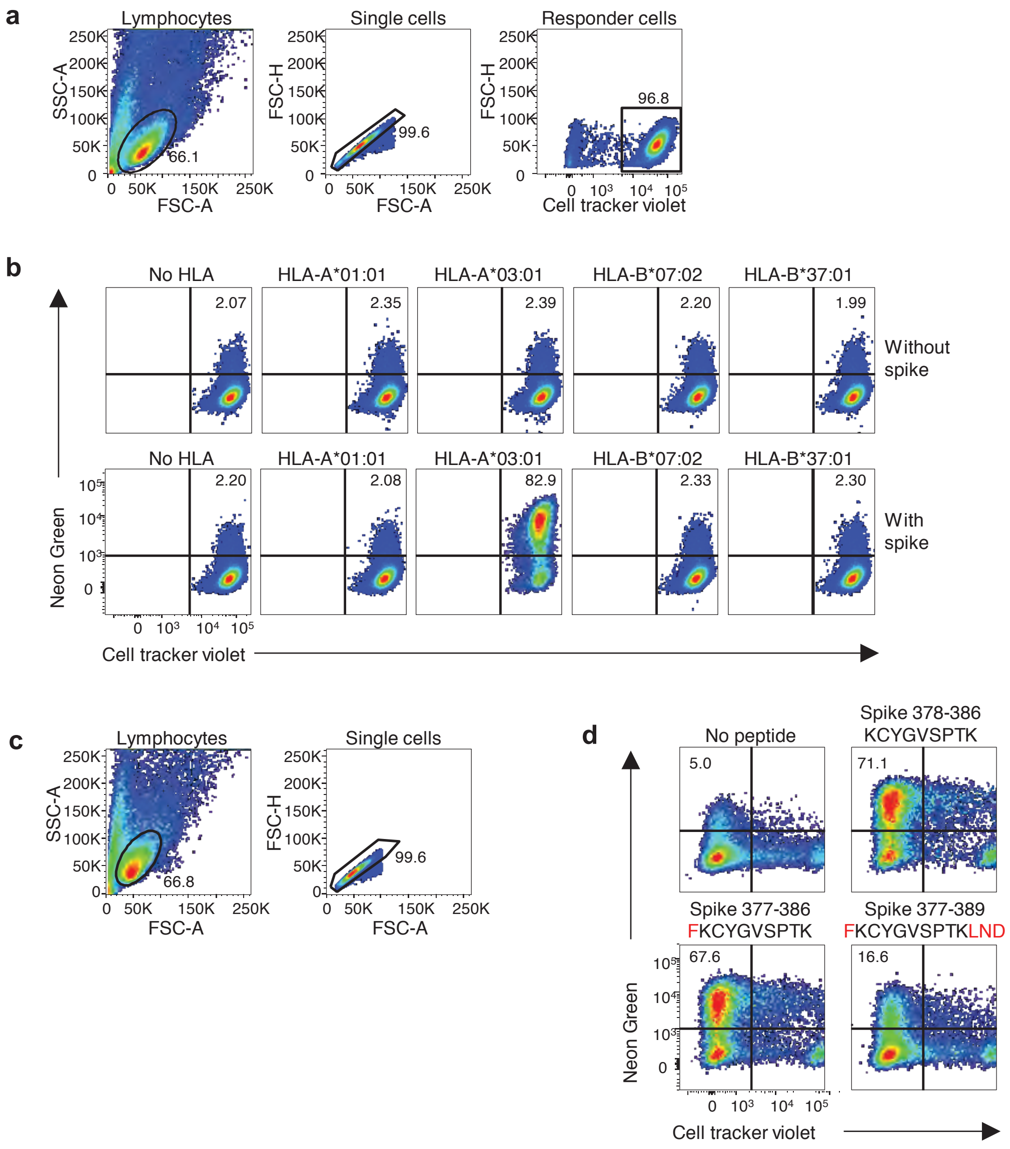

Supplementary Data Fig. 8. Evaluation of specificity of cluster-identified TCR for SARS-CoV-2 S. Representa-tive example shows evaluation of Spike-specificity of TCR3 from subject P673. (**a**) Representative gating strategy shows selection of CTV- labeled TCR3-transduced reporter cells after incubation with artificial antigen presenting cells expressing SARS-CoV-2 spike and each subject-specific HLA-A or HLA-B. (**b**) T cell activation was determined by measuring the percentage of mNeonGreen expression on TCR3-transduced reporter cells for each of the indicated HLA allelic variants. (**c**) Gating scheme for peptide specificity workup with EBV-LCL used as antigen presenting cells. (**d**) Cell tracker violet stained EBV-LCL were de-gated, and percent mNeonGreen expression determined on TCR3-transduced reporter cells. Amino acids lateral to the core 9 amino acid antigenic peptide recognized by TCR3 are shown in red. Numbers are percent of cells in indicated gates.

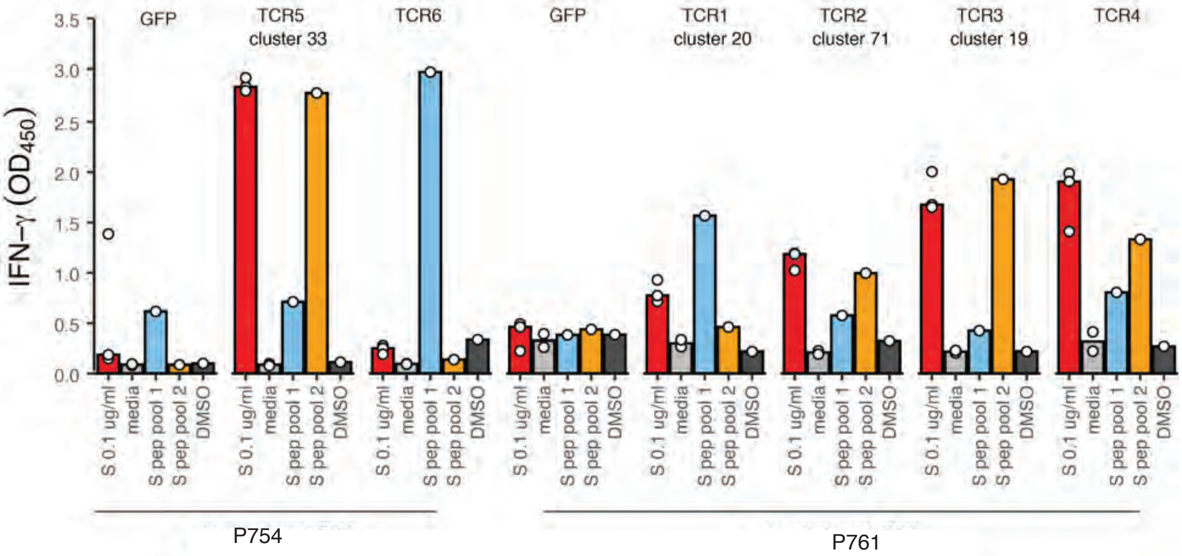

Supplementary Data Fig. 9. Confirmation of S-specificity of CD4+ TCRs identified by AIM-scTCRα β-seq. IFNɣ response of reporter T cells with engineered TCRs selected from public clusters after stimulation with 0.1µg/ml whole S protein (red) or overlapping 15-mer peptides (1µg/ml each) spanning S protein amino terminal domain S1 (light blue) and carboxy terminal domain S2 (orange). The height of each bar represents the mean of three replicates (individual dots are shown). The negative control level of activation of $CD4^+$ T cells lentivirus-transduced with the control GFP gene is also shown.

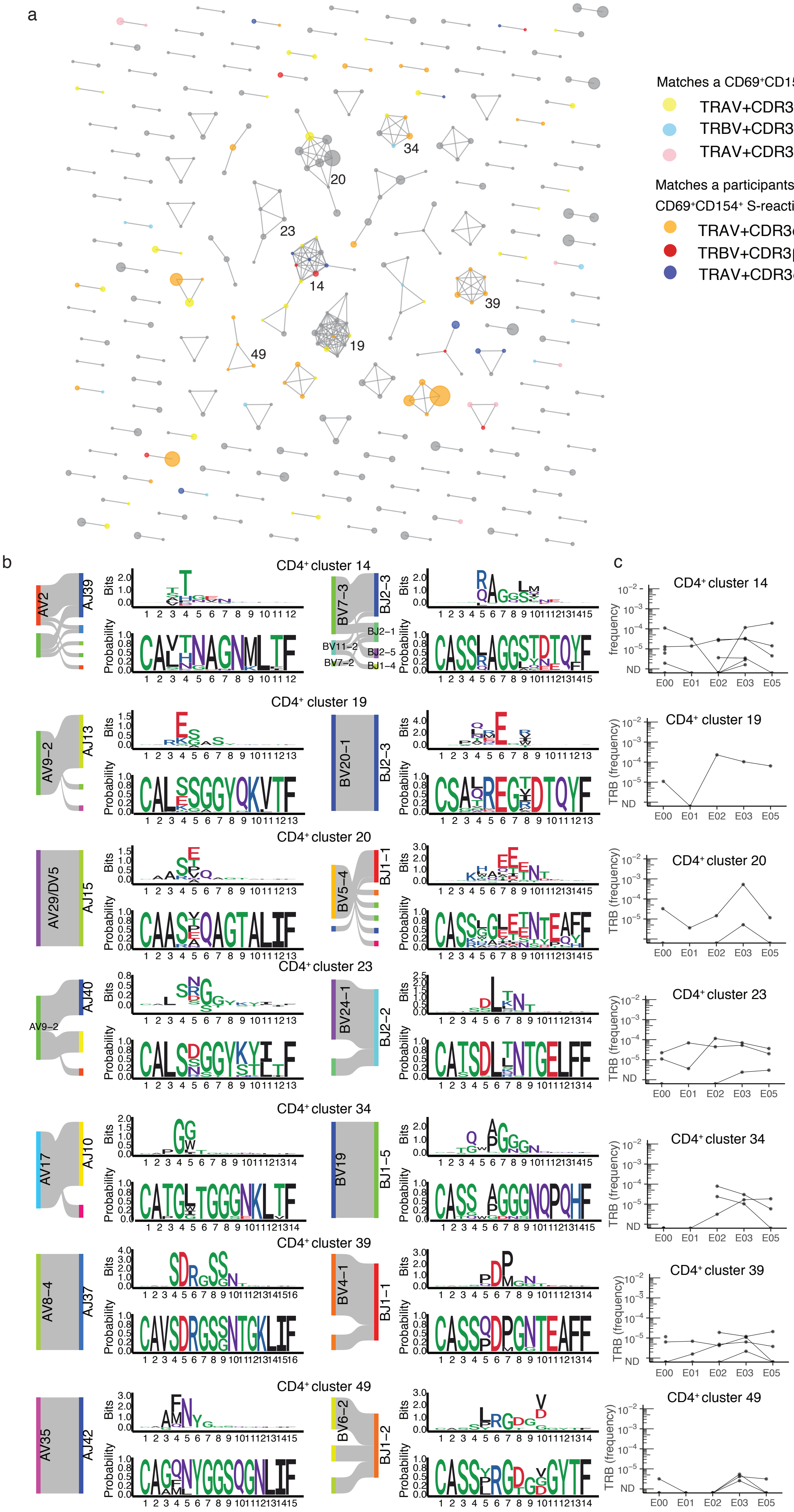

Supplementary Data Fig. 10. Selected S-reactive CD4⁺ TRA/TRB clonotype clusters. (**a**) Sequence similarity graph of CD4⁺ TS from CD69⁺CD137⁺ AIM-scTCRαβ-seq. Each circle is a unique clonotype and the size is proportional to the number of cells with that clonotype at the post-vaccine (E03) time point. Colors indicate exact V-gene and CDR3 amino acid-level match to S- reactive CD69⁺CD154⁺ single-chain receptor sequences identified previously (see text). (**b**) Corresponding cluster-associated CDR3α and CDR3β sequence motifs, *TRAV/J* and *TRBV/J* gene usage plots, and (**c**) clonotype trajectories demonstrating the observed stable kinetics over the course of vaccination in persons with hybrid immunity.

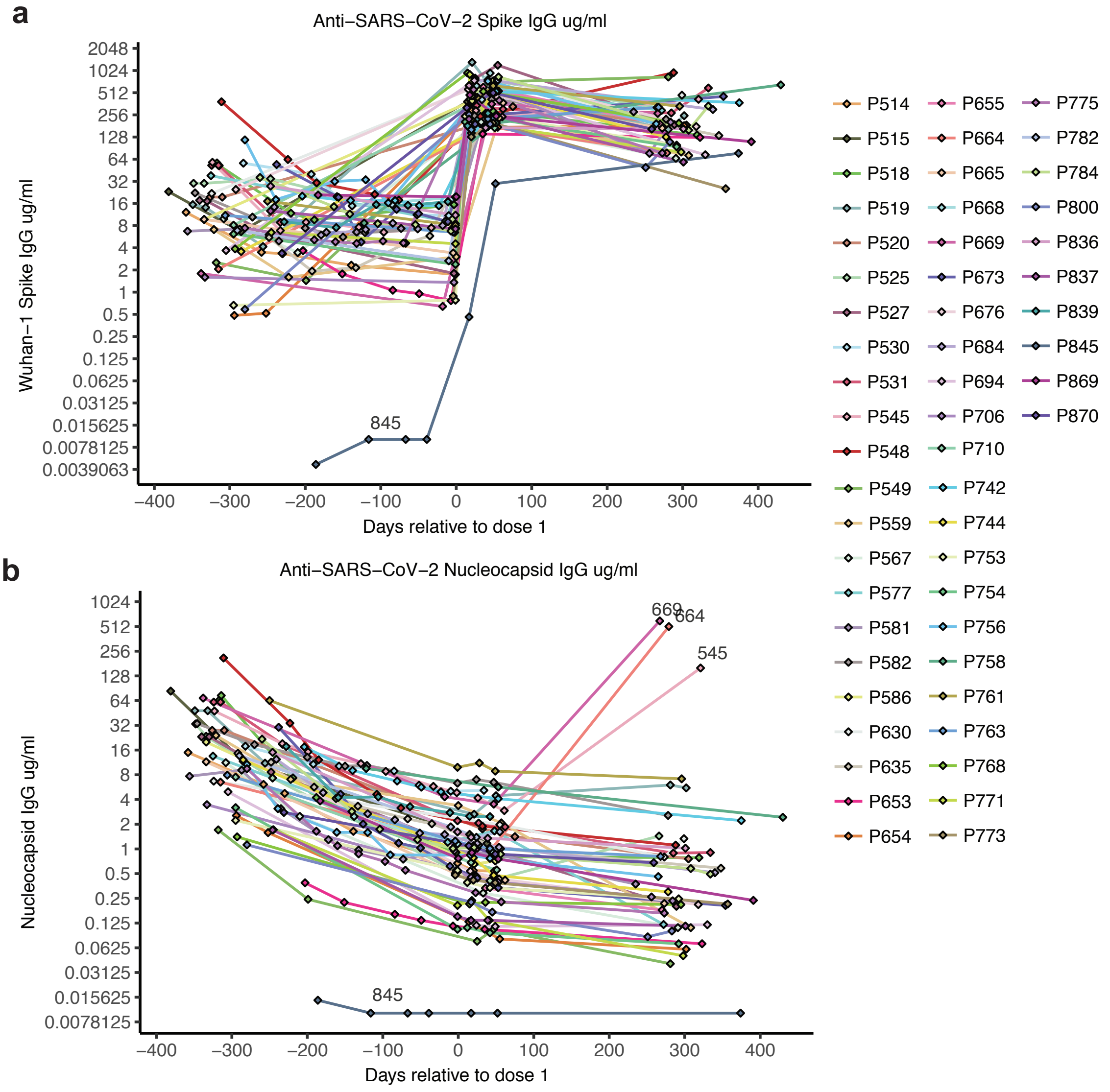

Supplemental Data Fig. 11. Serial anti-SARS-CoV-2 plasma IgG levels over time from convalescence to vaccine booster. (**a**) Anti-spike and (**b**) anti-nucleocapsid antibodies. Day 0 on X axis is date of first mRNA vaccination. Participant P845, who was seronegative for both anti-nucleocapsid and anti-S at study entry and seroconverted (anti-S only) with vaccination, is shown. Participants with breakthrough infections (P545, P664, P669) are indicated by increase in anti-nucleocapsid antibodies between E03 and E05. Participant numbers and color codes for both graphs are provided.

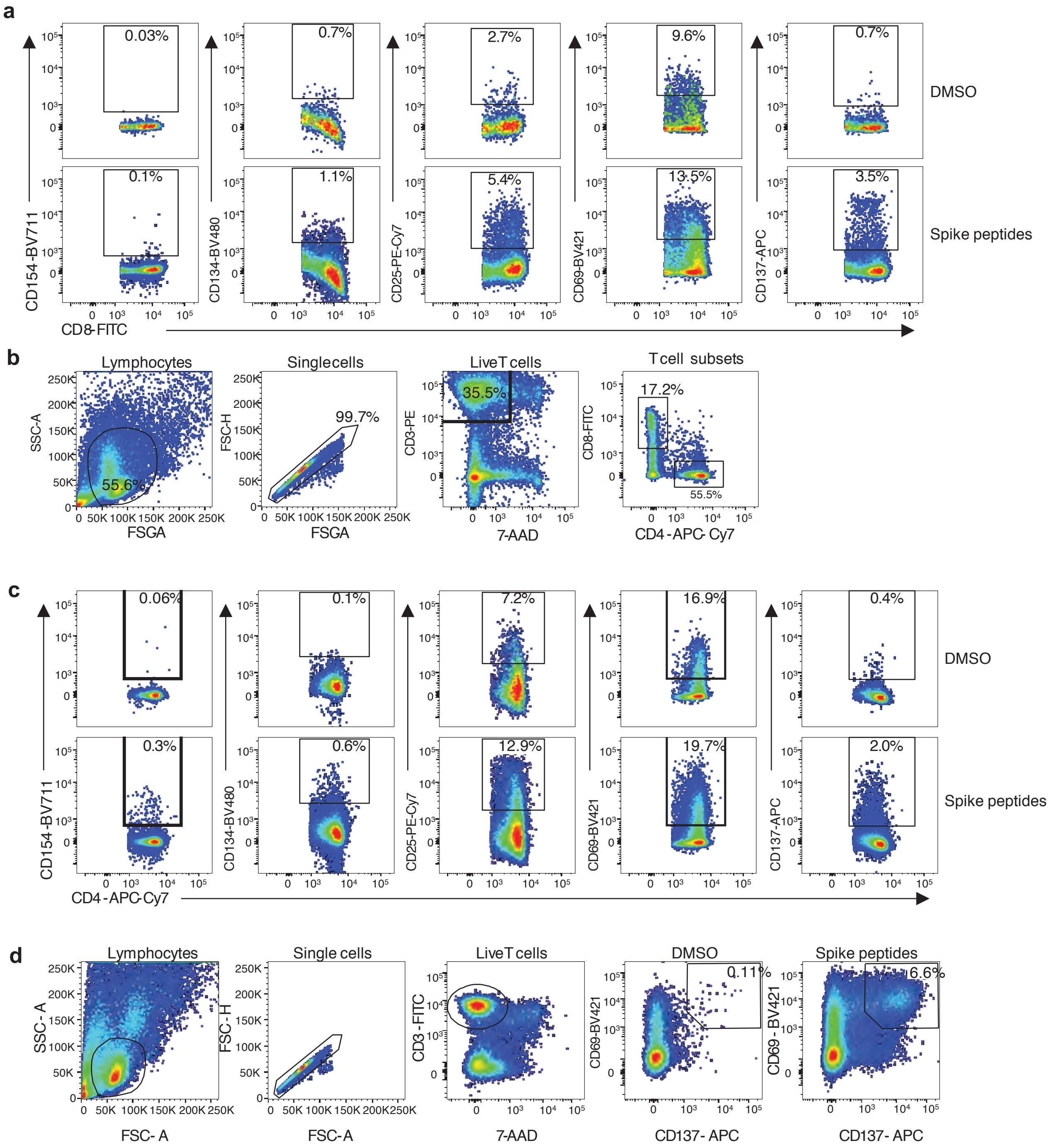

Supplementary Data Fig. 12 | Gating scheme for comparison of AIM candidates. (**a**) Representative results for person with hybrid immunity after stimulation with DMSO negative control or SARS-CoV-2 spike peptide pool for CD3^{+} T cells expressing activation markers CD69 and CD137. (**b**) Gating on single live CD4^{+} or CD8^{+} cells. (**c, d**) Representative results of gated CD4^{+} T cells (**c**) or CD8^{+} T cells (**d**) after stimulation with DMSO negative control (top) or S peptides (bottom) for five indicated candidate activation markers. Numbers are percent of CD4^{+} or CD8^{+} T cells in indicated gates.

Chapter 8: A STING agonist-mediated durable clinical response in an anti-PD-L1 refractory patient: Mechanisms revealed by single cell analyses including tumor antigen-specific T cells

Thomas H. Pulliam, Peter H. Goff, Saumya Jani, Rashmi Bhakuni, Shira Tabachnick-Cherny, Kimberly S. Smythe, Brandon Seaton, Lisa Tachiki, Rima Kulikauskas, Candice Church, David M. Koelle, Paul Nghiem, Shailender Bhatia

CHAPTER SUMMARY: In this chapter, we investigate a case of secondary resistance (initial response followed by disease relapse) to anti-PD-(L)1 treatment that experienced a partial, abscopal response to Stimulator of Interferon Genes (STING) agonism. This was puzzling because MCC tumor cells do not express STING. Through multiplexed immunohistochemistry, Western blots, and single-cell RNA sequencing, we demonstrate that infiltrating stromal and immune cells express STING, can release interferon into the tumor microenvironment, and upregulate HLA-I expression on tumor cells. This increased antigen presentation allows existing tumor-specific T cells to recognize the tumor and exert anti-tumor effects.

A STING agonist-mediated durable clinical response in an anti-PD-L1 refractory patient: Mechanisms revealed by single cell analyses including tumor antigen-specific T cells

Authors:
Thomas H. Pulliam[1],
Peter H. Goff[1,2,3],
Saumya Jani[1],
Rashmi Bhakuni[1],
Shira Tabachnick-Cherny[1],
Kimberly S. Smythe[2],
Brandon Seaton[2],
Lisa Tachiki[2, 4],
Rima Kulikauskas[1],
Candice Church[1],
David Koelle[5,6,7,8],
Paul Nghiem[1,2],
Shailender Bhatia[2,4,9]

Affiliations:
1. Division of Dermatology, Department of Medicine University of Washington, Seattle, WA
2. Fred Hutchinson Cancer Center, Seattle WA
3. Department of Radiation Oncology, University of Washington, Seattle, WA
4. Division of Medical Oncology, Department of Medicine, University of Washington School of Medicine, Seattle, WA
5. Department of Laboratory Medicine and Pathology, University of Washington, Seattle, WA
6. Department of Medicine, University of Washington, Seattle, WA
7. Department of Global Health, University of Washington, Seattle, WA
8. Benaroya Research Institute, Seattle, WA
9. Corresponding author at:
825 Eastlake Ave E
Seattle, WA 98109
phone (855) 557-0555
email sbhatia@uw.edu

Key Words:
Immunity, Innate, adaptive immunity; immunity, cellular; immunotherapy; skin neoplasms

Abstract

Background: Antibodies blocking programmed death (PD)-1 or its ligand (PD-L1) have revolutionized cancer care, but many patients do not experience durable benefit. Novel treatments to stimulate anti-cancer immunity are needed in PD-(L)1 refractory setting. The Stimulator of Interferon Genes (STING) protein, an innate sensor of cytoplasmic DNA, is a promising target with several agonists in development. However, response rates in most recent clinical trials have been low and mechanisms of response and failure remain unclear. We report detailed biomarker analyses in a patient with anti-PD-(L)1 refractory, Merkel cell polyomavirus (MCPyV)-positive, metastatic Merkel cell carcinoma (MCC) who was treated with intralesional STING agonist (ADU-S100) plus intravenous anti-PD-1 antibody (spartalizumab) and experienced a durable objective response with regression of both injected and non-injected lesions.

Methods: We analyzed pre- and post-treatment tumor biopsies and peripheral blood with single cell RNA sequencing, 27-color flow cytometry, T cell receptor sequencing and multiplexed immunohistochemistry (mIHC; post treatment tumor specimen only). We used MHC-I tetramers containing MCPyV peptides to identify cancer-specific CD8 T cells. We also analyzed STING expression and signaling in MCC cell lines and tumor specimens from 88 additional MCC tumors.

Results: We observed high levels of cancer-specific T cells (12% of T cells recognized an MCPyV epitope) in our patient's tumor at baseline. These MCPyV-specific CD8 T cells exhibited characteristics of exhaustion including high TOX and low TCF1. Following treatment with STING-agonist plus anti-PD-1, MCPyV-specific CD8 T cells expanded 3-fold. We also observed increased antigen presentation on MCC cancer cells (>4-fold increase of MHC-I-positive cancer cells). This was likely not a result of STING-agonist acting directly on cancer cells, as mIHC analysis confirmed little or no STING expression in cancer cells in the treated tumor or 88 other MCC tumors. However, high STING expression on infiltrating immune and stromal cells was observed. Further *in vitro* studies showed MCPyV-positive MCC cell lines are STING deficient, and exposure to STING-agonist did not induce interferon.

Conclusions: Our results suggest that STING agonists upregulate cancer cell antigen presentation and also reinvigorate the anti-cancer response from pre-existing cancer-specific T cells. Thus, patients with anti-PD-(L)1-refractory disease showing downregulation of antigen-presentation may benefit from intralesional STING agonists.

Introduction

MCC is a rare neuroendocrine cancer associated with Merkel cell polyomavirus (MCPyV) and/or ultraviolet (UV) radiation exposure, and usually occurs in elderly and/or immunosuppressed patients[1]. Both MCPyV-positive (VP) and MCPyV-negative (VN) MCC tumors are considered immunogenic with excellent prognosis in patients with brisk IT infiltration of CD8 T cells into MCC tumors[2], and a particularly high response rate to PD-1/PD-L1 pathway blockade with around half of patients experiencing durable responses[3-6]. There is a strong unmet need for effective therapies in PD-(L)1 refractory MCC tumors. Unlike most other cancers, VP-MCC allows unique opportunities to study cancer-specific immune responses through MCPyV-specific CD8 T cells, which can be helpful to uncover mechanisms of response and failure of novel immunotherapies.

Innate immune sensors of pathogen associated molecular patterns (PAMPs) represent an important host defense mechanism against infectious agents and have been employed as targets in several oncology clinical trials to stimulate anti-cancer immunity[7]. Stimulator of interferon genes (STING) is one such promising PAMP sensor that has shown promise in pre-clinical mouse models[8-11]. The STING pathway senses cytoplasmic DNA through cyclic GMP-AMP synthase (cGAS), which then produces cyclic GMP-AMP as second messenger. This in turn acts on STING to induce transcription of type I interferons and inflammatory cytokines via nuclear factor kB (NF-kB) and interferon regulatory factor 3 (IRF3). The STING pathway is thought to have evolved to protect against DNA viruses that replicate in the cytoplasm of cells; however, it can also be engaged by DNA damaging chemotherapies and radiation that cause DNA release into the cytoplasm. Murine models have shown that these DNA damaging therapies lead to adaptive anti-cancer immune responses, primarily through activation of STING in dendritic cells in the tumor microenvironment (TME)[12,13]. Based on these findings, several novel agents designed to directly engage STING have been developed. These STING agonists, when delivered intratumorally, appear to increase intratumoral (IT) NK cells, activate CD8 T cells[14,15] and facilitate both local and systemic anti-cancer responses.

While IT administration of STING agonists has been successful in murine models, recent clinical trials have yielded disappointing results. In a clinical trial (NCT02675439) of IT ADU-S100 in 47 patients with metastatic cancers, only one patient had a confirmed response[16]. Of note, the only responding patient had a diagnosis of Merkel cell carcinoma (MCC). In a separate trial (NCT03172936) of IT ADU-S100 in combination with intravenous (IV) anti-PD-1 (spartalizumab) in 106 patients, only 11 patients responded (objective response rate of 10%) with 10 patients achieving a partial response (PR) and 1 patient receiving a complete response (CR)[17]. One of those 11 responders also had a diagnosis of MCC and is the subject of this report.

Herein, we describe the clinical course along with detailed biomarker analyses of this patient with metastatic VP-MCC, refractory to avelumab (anti-PD-L1 antibody) treatment, who experienced durable clinical response in both injected and non-injected lesions with combination treatment with IT STING-agonist (ADU-S100) plus IV anti-PD-1 (spartalizumab). To further assess the relevance of our findings to MCC patients in general, we also queried STING expression and activity in other MCC tumor samples and cell lines.

Results

Clinical MCC History and Response to STING agonist and anti-PD-1

A 63-year-old man presented with a MCPyV-positive primary MCC on the left knee with inguinal lymph node metastasis, which were initially treated with surgery and adjuvant radiotherapy (54 Gy to the primary and 50 Gy to inguinal nodes) (**Figure 1a**). One month later, he developed distant metastatic disease in the left elbow region, which prompted systemic treatment with IV avelumab. This was associated with a complete response (CR), and avelumab was electively discontinued after 1 year of therapy. Nine months later, the patient developed recurrence with multi-focal MCC metastases in the left lower extremity, which were refractory to rechallenge with avelumab.

The patient was subsequently enrolled on the above-mentioned clinical trial (NCT03172936) and received intratumoral injections of the STING agonist (ADU-S100) with IV spartalizumab, both administered every 4 weeks. Both injected and non-injected lesions regressed leading to an overall partial response (43% reduction in tumor burden in index lesions; **Figure 1b**). Two months after initiating trial therapy, no injectable lesions were clinically apparent. After experiencing disease control for ~1 year, the patient experienced MCC progression again with new metastases in the left lower extremity (**Figure 1b)**.

During the course of his treatment, we collected serial tumor biopsies and peripheral blood specimens to characterize this patient's anti-cancer response via detailed immunophenotyping of the tumor and immune cells, including cancer-specific CD8 T cells, both in the TME and systemically.

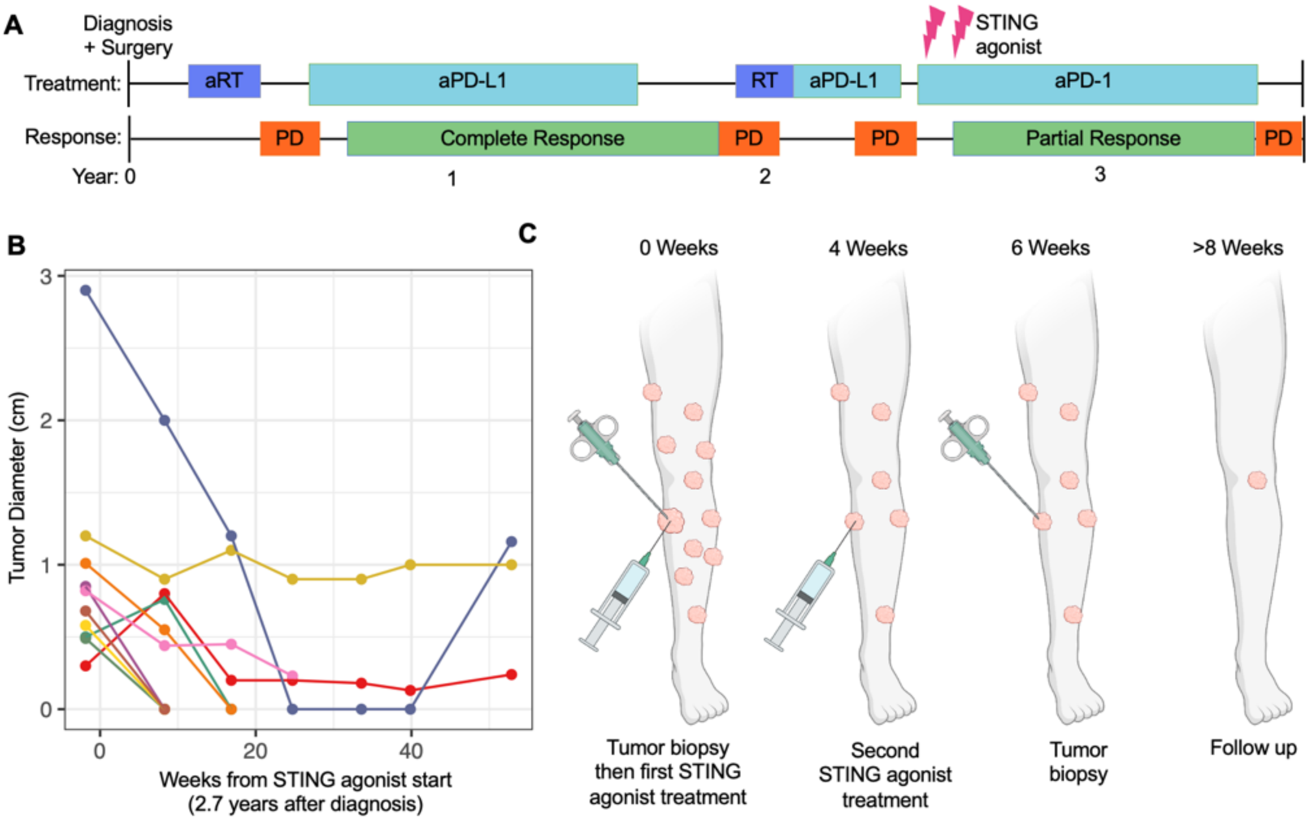

Figure 1. Clinical course of a 63-year-old man with metastatic, PD-1 refractory MCC who experienced an objective response with intralesional STING agonist +intravenous anti-PD-1 therapy.

A. Clinical course over time (in years) after MCC diagnosis
B. Changes in size of MCC tumors on the left lower extremity (LLE), including both injected and non-injected lesions, during the trial treatment. The patient experienced a partial response per RECIST with 43% decrease in target lesions.
C. Representative schematic of MCC tumors on the lesions, including both injected and biopsied lesions, at baseline, post-treatment, and at the time of disease progression.

Intralesional STING treatment increases intratumoral T cell infiltration

We first performed single cell RNAseq with feature barcoding (CITEseq) on pre- and post-treatment tumor and blood specimens in an unbiased approach to study cell populations and gene expression profile at various timepoints. DNA barcoded MHC-I tetramers containing MCPyV or CMV and EBV peptides were used to identify antigen-specific T cells (**Figure 2**). These data were then used to create a 27-color flow cytometry panel to study major cell populations observed in the scRNAseq data and rare cell populations that could have been missed due to the low-throughput nature of CITEseq (**Figure 2a**).

Unbiased clustering and dimensionality reduction in the pre-treatment (baseline) tumor biopsy revealed the TME composition of 70% cancer cells and 28% immune cells, with the remaining 2% of cells bearing markers of stromal/endothelial cells including CD34. 95% of immune cells were in the T cell, NK cell or dendritic cell clusters with B cells, tumor associated macrophages and neutrophils being rare. Meanwhile, cancer cells primarily grouped into two distinct clusters which were differentiated by Ki67 expression indicating proliferating and non-proliferating cells. Following intralesional STING agonist injection, cancer cells decreased to 49% of the TME, which was accompanied by a 2-fold increase in T cells from 18% to 36% (**Figure 2b, 2c**). Further sub-clustering of cancer, T cell and myeloid populations (**Figure 2, Supplemental Figures S1,S5**) revealed that while all cancer cell populations decreased over the course of immunotherapy, the most dramatic change was in the proliferating tumor cells, which decreased from 17% of all cells in the TME before treatment to 5% following treatment (**Figure 2d**). Sub-clustering of T cells revealed that Memory CD4 T cells, T_{REG}, CLA+ CD8 T cells, progenitor exhausted, and terminally exhausted CD8 T cells all comprised more than 2% of the cells in the TME prior to STING treatment. All T cell populations increased proportionally following treatment (**Figure 2e**). No significant changes were observed in myeloid cells. However, a high portion of myeloid cells were plasmacytoid dendritic cells (2.7% of pre-treatment cells, marked by CD123 expression), which are specialized for sensing PAMPs. An additional 2% of cells in the TME were classical dendritic cells (marked by high CD11c expression). Both dendritic cell populations expressed high levels of STING protein (**Supplemental Figure S5**).

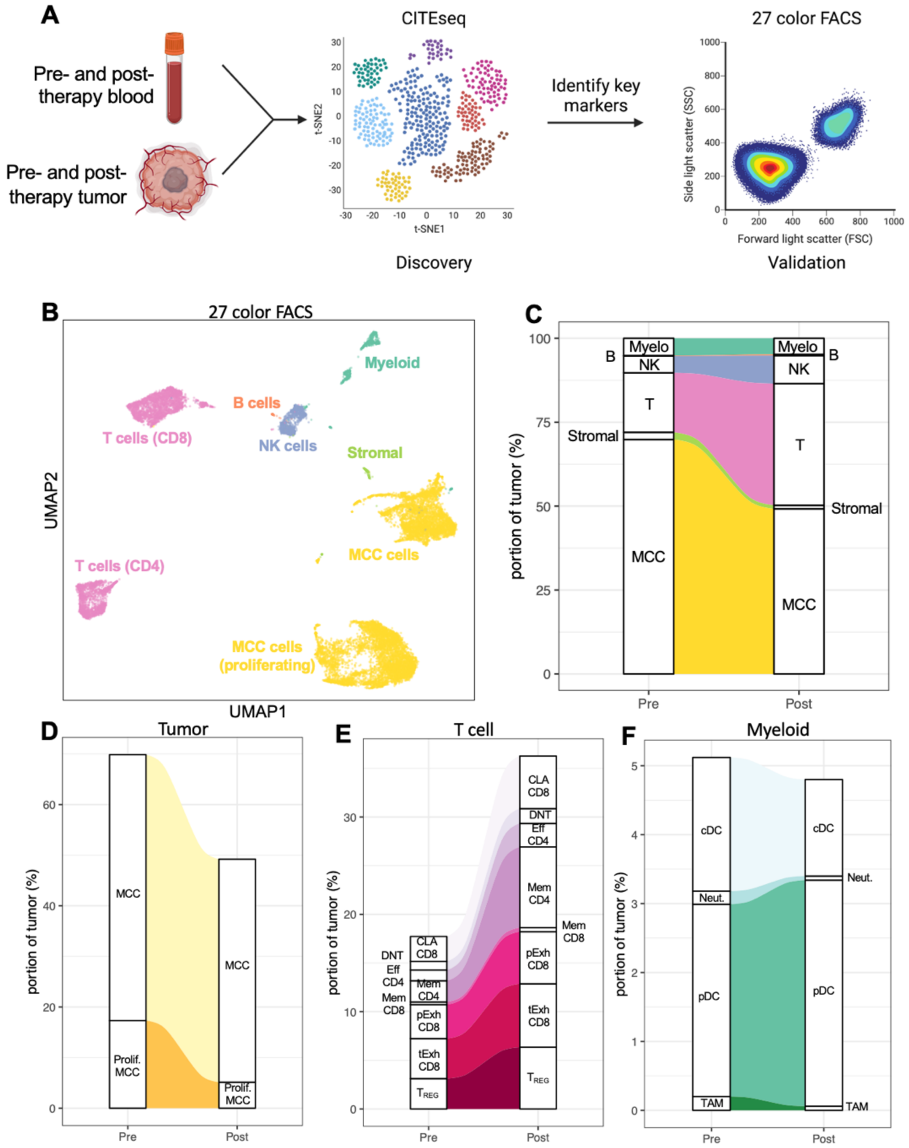

Figure 2. Intratumoral T cells increase following intralesional STING agonism.

a. Experimental overview. CITEseq was performed on pre- and post-treatment tumor and blood specimens for unbiased analyses. Key markers and cell populations were identified and used to design a 27-color flow cytometry panel to validate samples in high throughput fashion to capture rare cell populations.
b. UMAP plot of 27 color flow cytometry data from pre- and post-STING agonist treatment. Each point represents one cell colored by cell lineage. Samples were subsetted to 10,000 cells per time point for visualization purposes.
c. Alluvium plot of tumor composition before and after STING agonism showing expansion of T cells and contraction of cancer cells following treatment with STING agonist.
d. Alluvium plot of cancer cells sub clustered into proliferating MCC and non-proliferating cells showing contraction of both populations.
e. Alluvium plot of T cells showing an expansion of T cells following STING agonism. All T cells expanded similarly regardless of phenotype.
f. Alluvium plot of myeloid cells before and after STING agonist treatment. A predominance of plasmacytoid dendritic cells was noted but minimal changes occurred over the course of therapy.

Abbreviations: FACS: fluorescent activated cells sorting; UMAP: uniform manifold approximation projection; Myelo: Myeloid cells; NK: Natural killer cells; MCC: Merkel cell carcinoma; prolif: proliferating; CLA: cutaneous leukocyte antigen; DNT: double negative T cells; Mem: memory; pExh: progenitor exhausted; tExh: Terminally exhausted; cDC: classical dendritic cells; Neut: Neutrophil; pDC: plasmacytoid dendritic cells; TAM: tumor associated macrophage

Cancer-specific CD8 T cells expand in tumors following intralesional STING agonism

Given the overall increase in T cells observed following STING agonism, we sought to characterize the dynamics of antigen-specific T clones in the tumor and blood utilizing a dual approach schematized in **Figure 3a**. T cell specificity was identified using DNA barcoded MHC-I tetramers (with MCPyV or CMV and EBV peptides) with paired CITEseq and V(D)J sequencing (**Figure 3b**). Gating of multimer positivity was confirmed by visualizing PD-1 positivity in these cells, known to be elevated in MCPyV[18].This resulted in 12 T cell clonotypes specific for MCPyV in a B*37:01 allele. CD8 T cells specific for other MCPyV or other viral epitopes were detected at low levels, and antigen-specific TCRs could not confidently be identified.

T cell frequency was quantified using bulk beta TCRseq and MCPyV-specific T cells were annotated (**Figure 3c**). Only 0.03% of peripheral blood mononuclear cells (PBMC) were MCPyV-specific CD8 T cells prior to STING agonism. The proportion of these cells was ~10 fold higher in the tumor where 0.39% of cells in the TME were MCPyV-specific CD8 T cells before STING agonism. This proportion in the TME increased to 0.93% following STING agonism. Expansion of T cell clones of any specificity in the TME was predominately proportionate with only 8 of 5128 intratumoral clones significantly increasing following treatment and 20 of 5128 clones decreasing as a portion of all T cell ($p<0.01$; beta binomial test; **Supplementary Figure 7**). The results were similar for cancer-specific CD8 T cells where 1 of 12 MCPyV-specific clones expanded following STING treatment and 2 of 12 contracted as a portion of all T cells. Cancer-specific T cells were long-lived in the blood and were detected 1 year after treatment (at the time of recurrence) at frequencies similar to pre-treatment (0.04% of all PBMC).

Cancer-specific CD8 T cells exhibit characteristics of exhaustion

We next sought to phenotype cancer-specific T cells in the tumor and blood. Unbiased clustering of scRNAseq of CD8 T cells yielded clusters of memory, naïve, progenitor exhausted, terminal exhausted, two effector, and two gamma delta populations (**Figure 4a, 4b**). Expression of stem-like and memory genes was higher in CD8 T cells in blood, while genes associated with exhaustion were higher in tumor tissues and highest in MCPyV-specific T cells (**Figure 4c**). MCPyV-specific CD8 T cells in tumors were largely confined to the terminally exhausted population defined by high expression of PDCD1 (PD-1) and CD39 (**Figure 4b, 4d**). The proportion of MCPyV-specific CD8 T cells in the terminally exhausted population decreased slightly following STING agonism but low numbers of MCPyV-specific CD8 T cells in the pre-treatment timepoint limited analyses (**Figure 4d**). To circumvent the low capture efficiency of single cell RNAseq, flow cytometry was subsequently used as a higher throughput technique. These data show high expression of TOX, TCF7 and PD-1 proteins in MCPyV-specific CD8 T cells (99% PD-1+, 99% TOX+, 14% TCF1+, in pre-treatment samples, **Figure 5e**). This was unchanged following STING agonism suggesting that treatment did not induce lasting phenotypic changes in cancer-specific CD8 T cells.

MCC cancer cells are STING deficient

To study the effects of IT ADU-S100 on cancer, immune and stromal cells in the TME, we first analyzed STING expression in the TME by performing multiplexed immunohistochemistry (mIHC) on the studied patient's tumor specimen. Previous studies of STING in MCC have suggested that this pathway is deficient in VP-MCC[19]. We confirmed that the STING protein was indeed absent in the MCC cancer cells, with mIHC staining showed STING expression in immune and stromal cells, but an absence of STING protein in areas of cancer tissue (**Figure 5a**). This pattern of STING expression was then confirmed broadly in further staining of 88 MCC tumors from 68 unique patients (55 VP, 13 VN), which similarly showed an absence of STING staining in cancer cells (**Figure 5b**).

The absence of STING protein on cancer cells suggests that the downstream effects of STING-agonism using ADUS100 are likely mediated by effects on the non-cancer cells rather than the MCC cancer cells in the TME. To independently confirm that MCC cells do not respond to ADU-S100 treatment, 4 VP-MCC cell lines were treated with increasing doses of ADU-S100 (**Figure 5c**). Treatment did not induce production of interferon beta (a downstream target of STING activation) in MCC cell lines, but led to production of interferon beta in control monocytic THP-1 cells (**Figure 5c**). Moreover, none of the virally driven MCC cell lines that were tested produced detectable amounts of STING protein (**Figure 5c**).

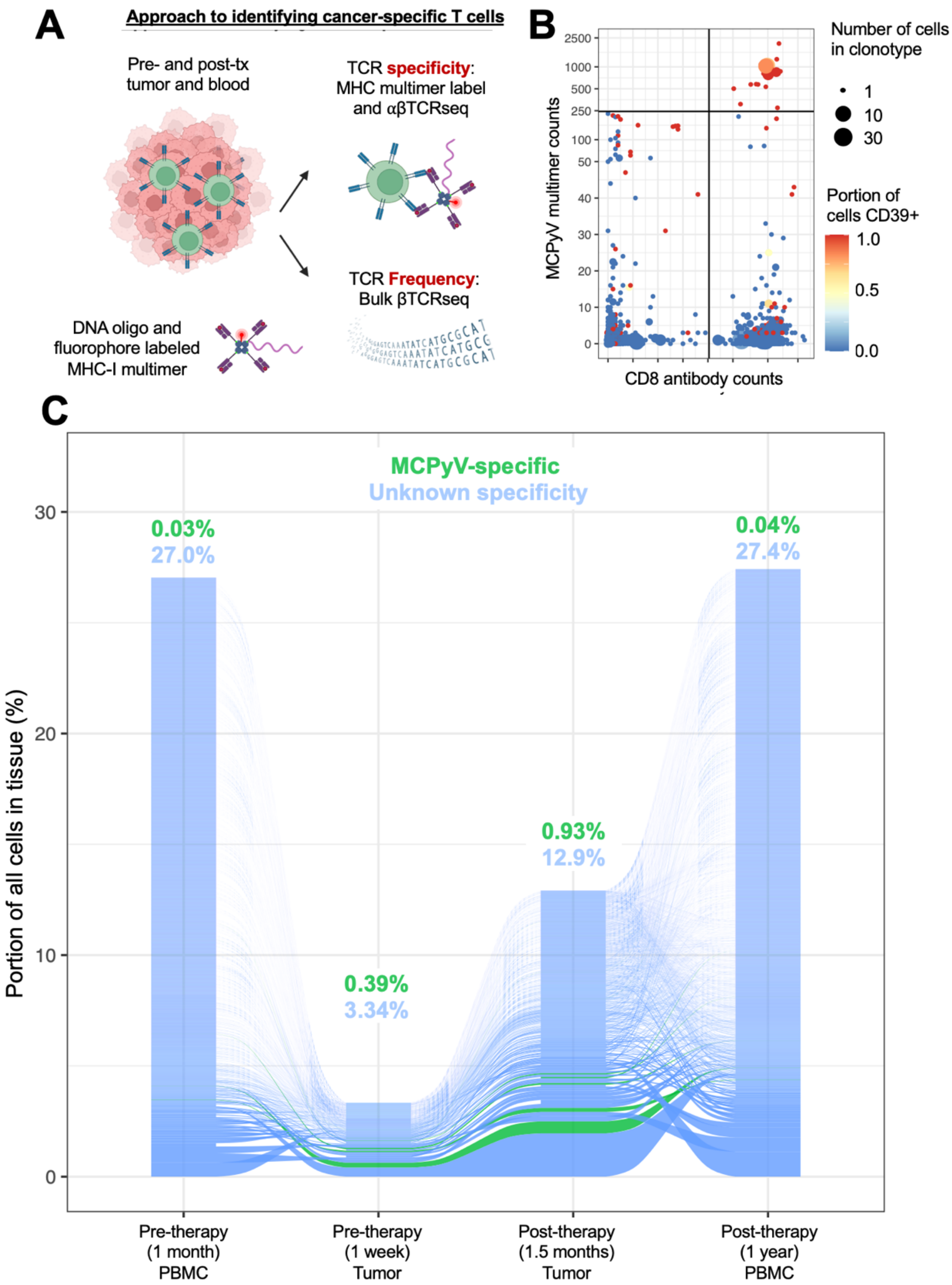

Figure 3. Intralesional STING treatment increases intratumoral T cell infiltration.

a. Schematic of approach to quantifying frequency of MCPyV-specific CD8 T cells in tumor and blood specimens. Tumor or blood specimen were stained with DNA oligo and fluorophore labeled MHC tetramers and CITEseq with V(D)J seq was performed to identify specificity of TCRs. In parallel, beta-TCRseq was performed on tumor and blood specimen to quantify frequency of TCR clonotypes.

b. Gating of MCPyV-specific CD8 T cells via CITEseq. All cells with a single productive alpha and single productive beta TCR are shown. Cells with identical TCR sequences were grouped as clonotypes. X axis represents the median counts of CD8 antibody for each clonotype and y axis represents the median counts of an HLA-B*37:01 multimer containing a T antigen peptide. Cells identified as MCPyV-specific shown in upper right hand quadrant.

c. Frequency of T cell clonotypes in tumor and blood before and after intralesional STING agonism. Alluvium plot where each alluvium represents and individual T cell clonotype. Clonotypes known to be MCPyV-specific are green. MCPyV-specific CD8 T cells were present in tumor and blood of patient.

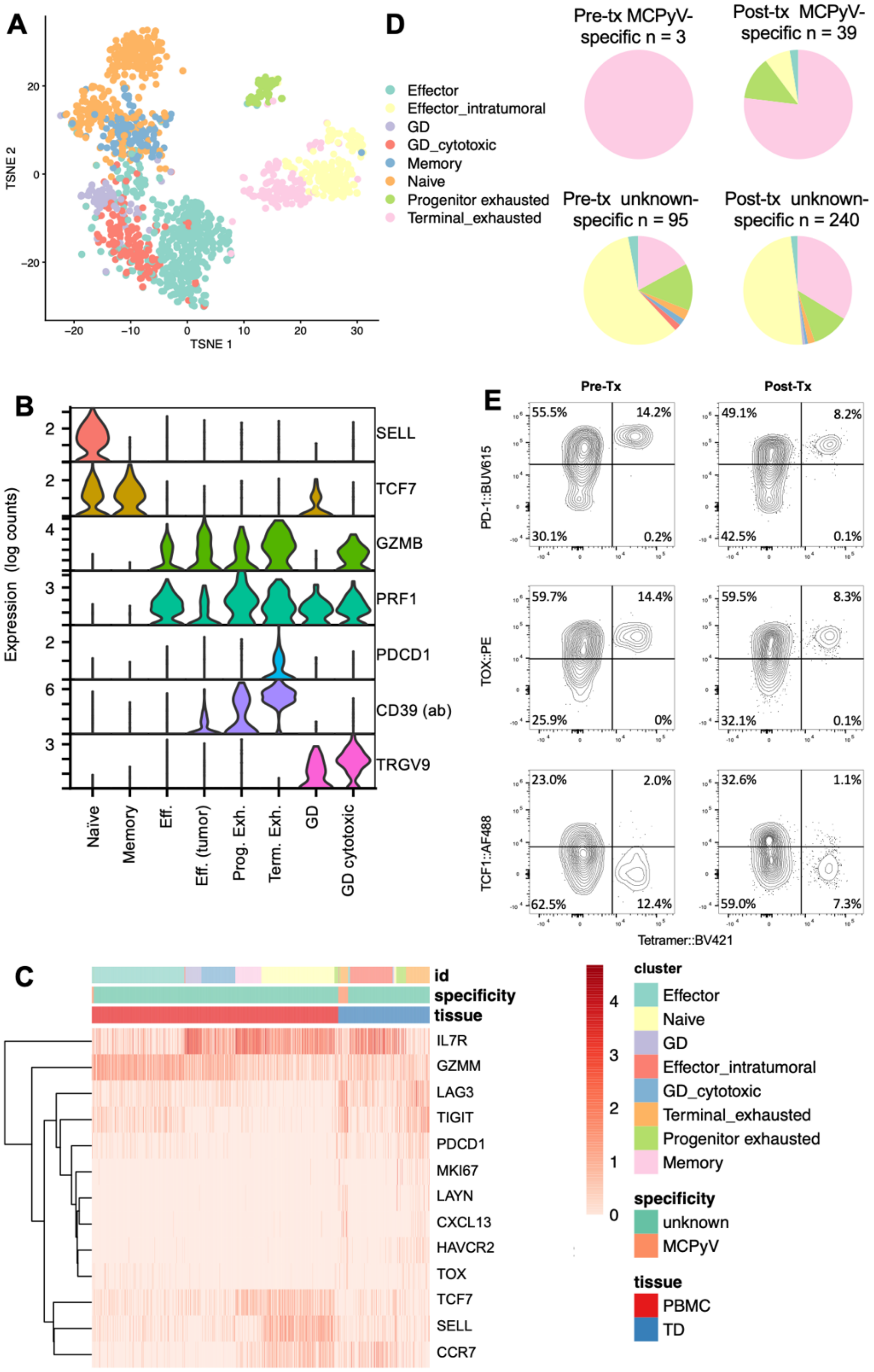

Figure 4. Cancer-specific CD8 T cells exhibit characteristics of exhaustion.

a. TSNE plot of CD8 T cells isolated in silico from single cell RNAseq of patient tumor and blood specimen. Cells are colored by cluster.
b. Violin plots of expression of key genes in each cluster.
c. Heatmap of single cell RNAseq data of CD8 T cells from tumor or blood specimen. Each column represents an individual T cell. T cell specificity, id (cluster) and tissue of origin are indicated on top of heatmap with legend on far right.
d. Portion of MCPyV-specific CD8 T cells in tumors in each of 8 clusters. MCPyV-specific CD8 T cells in top pie charts and CD8 T cells of unknown specificity in bottom charts. Pre-treatment specimen on left hand side and post-treatment on right.
e. FACS plots of CD8 T cells from tumors showing expression of proteins associated with exhaustion or stem like phenotypes in MCPyV-specific T cells.

Abbreviations: GD: Gamma delta T cells, PBMC: peripheral blood mononuclear cells, TD: tumor digest, MCPyV: Merkel cell polyomavirus

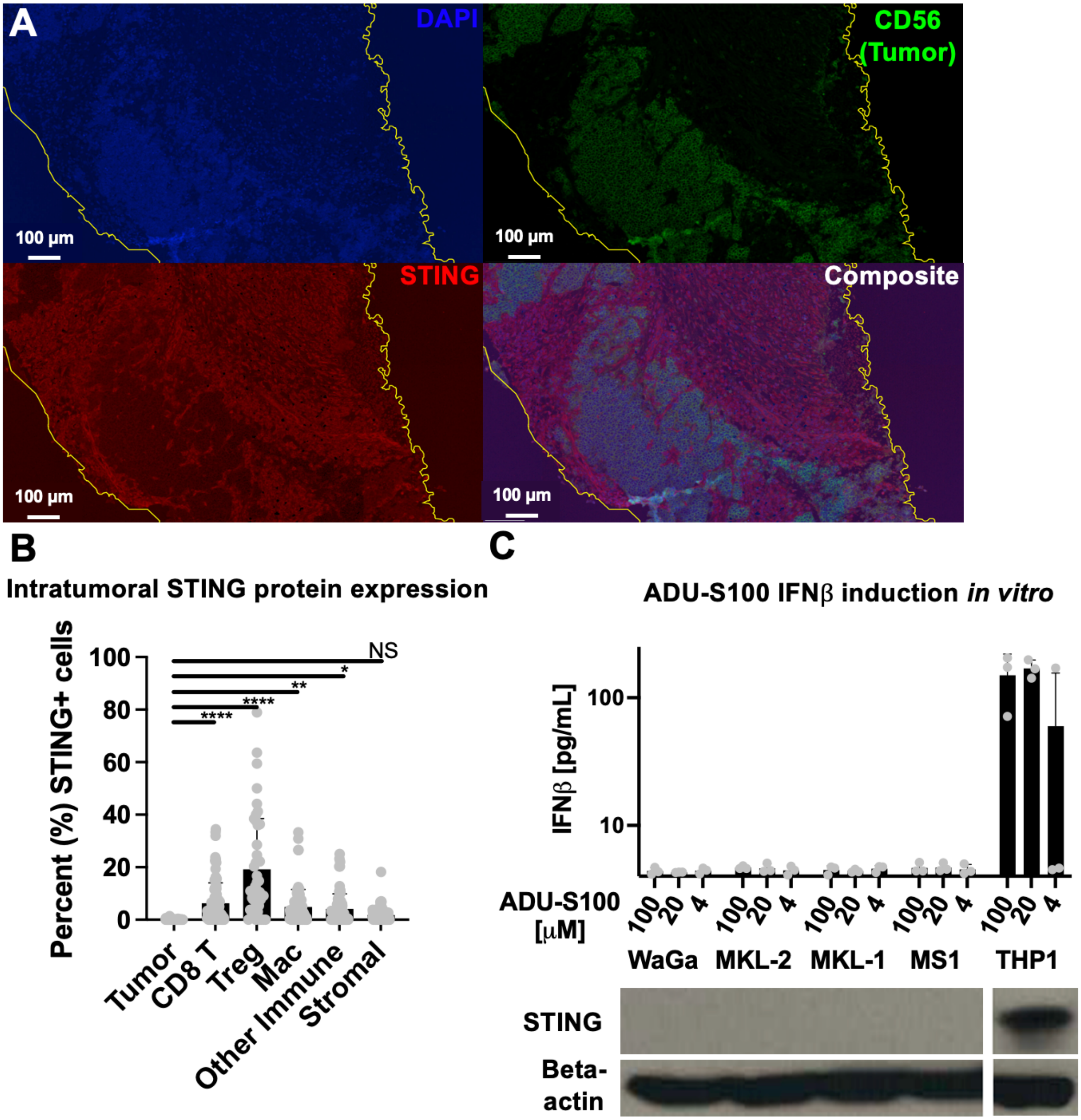

Figure 5. Merkel cell carcinoma are deficient in STING signaling.

a. Multiplexed immunohistochemistry of post-ADU-S100 treated tumor. Areas of CD56 positivity (representing MCC cells) are non-overlapping with STING which is primarily expressed in stromal and immune tissues.
b. Quantification of STING expression. Each point represents 1 of 88 unique tumor specimens on a tissue microarray. STING is universally absent in MCC tumor cells. Cancer cells defined as CD56+, CD45-, CD8 T cells defined as CD8+, Treg cells defined as CD4+, FoxP3+, Macrophages defined as CD68+ or CD163+, Other immune cells defined as CD45+ cells which did not fall into prior categories, stromal cells defined as CD45-, CD56- cells. Statistical comparison with one-way ANOVA compared to tumor expression. *$p<0.05$, **$p<0.01$, ****$p<0.0001$, NS (not significant).
c. MCC cell lines do not produce interferon-beta in response to ADU-S100 treatment. WaGa, MKL-2, MKL-1, MS1 MCC cells and THP1 cells (control human monocytic cells) were all treated with decreasing doses of ADU-S100. None of the MCC cell lines produced detectable interferon-beta at any tested ADU-S100 concentration. These cells were all also deficient in STING protein (western blot, below).

Cancer cells upregulate MHC following STING agonism

To investigate the mechanisms of anti-tumor immune responses following STING agonism, we investigated the expression of genes associated with antigen processing and presentation (**Figure 6a**). cancer and non-cancer cells were isolated *in silico* (**supplemental Figure S2**) and a gene set of 18 genes associated with antigen presentation were used to measure this pathway in aggregate. A 49% increase in this gene signature was observed in cancer cells following STING agonism ($p<10^{-16}$). A more modest 4% increase was observed in non-tumor cells in the TME ($p=0.016$) with higher expression of antigen presentation genes in non-cancer cells than in cancer cells.

Further analyses of these genes showed that most of this increase was driven by beta 2 microglobin (**Supplemental Figure S2**), which was significantly upregulated in cancer cells following STING treatment ($p<10^{-16}$; **Figure 6b**). However, no remarkable change was observed in other cells in the TME. Upregulation of MHC-I was validated at a protein level via FACS, which showed 1.8% of cancer cells positive for MHC-I prior to STING treatment compared to 8.2% following STING treatment. Consistent with these findings, we observed increases in genes associated with interferon gamma or interferon alpha receptor signaling in most cell types in the TME following STING agonism (**Supplemental Figure S3a & S3b**) suggesting that these cytokines were more active in the TME after STING agonism.

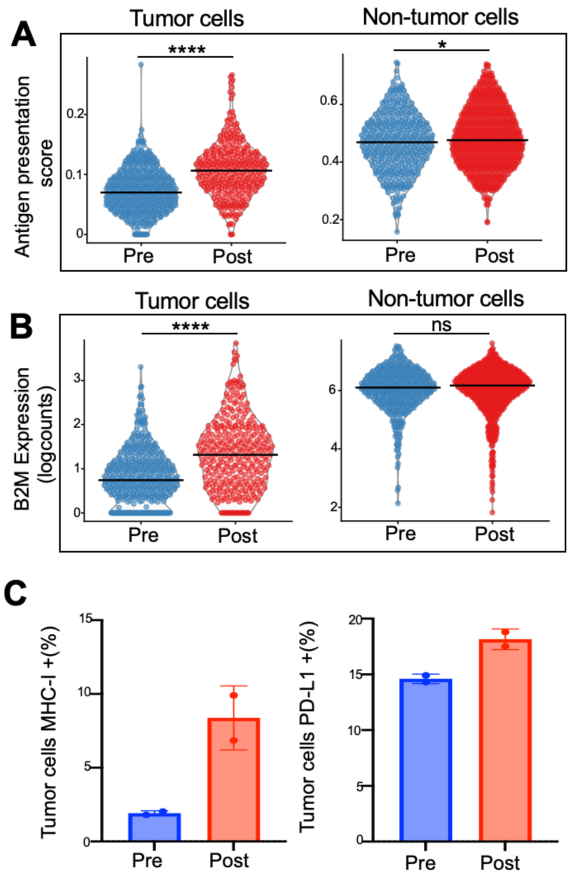

Figure 6. Cancer cells upregulate MHC following STING agonism.

a. scRNAseq data showing upregulation of antigen presentation genes following STING agonism on cancer cells. Cancer or non-cancer cells identified in silico. Antigen presentation score calculated using 16 genes involved in the MHC-I antigen presentation pathway.
b. B2M upregulation in cancer cells but not non-cancer cells following STING agonism.
c. Quantification of MHC-I and PD-L1 expression on cancer cells via flow cytometry. Each data point represents one of two technical replicates.

T tests with bonferoni multiple comparison testing used for statistical significance. p value key: ns = p>0.05, * = p<0.05, ** = p<0.05, * = p<0.01, *** = p<0.001, **** = p<0.0001,

Abbreviations: MHC-I: major histocompatibility complex-I; FMO: Fluorescence minus one

Discussion

STING agonists have shown great promise in pre-clinical models. However, clinical trials have shown limited early efficacy with objective response rates reported between 2% and 10%[16,17]. It is of note that 2 of 4 (50%) MCC patients treated on two large trials of ADU-S100 experienced objective responses compared to 10 of 139 (7%) non-MCC patients. Intrigued by the seemingly higher response rate in MCC, we performed exhaustive biomarker studies on a patient with metastatic MCC tumors that were refractory to anti-PD-L1 therapy. This patient with numerous (>10) metastatic tumors received intratumoral STING-agonist (ADU-S100) in 2 lesions on his lower extremity plus systemic anti-PD-1 therapy and experienced a durable objective response in both injected and distant, non-injected lesions.

Abscopal tumor regression in non-injected lesions in our patient suggested that STING-agonism in the injected tumor may be facilitating an adaptive immune response to lead to systemic immunity. To further interrogate this, we used a panel of MHC-I multimers and the viral etiology of this patient's tumor to study MCPyV-specific (cancer-specific T cells). Indeed, we observed a 2.4 fold increase in cancer-specific T cells in the TME following STING agonism. Using scRNAseq and FACS to further determine the characteristics of this expansion, we found that 93% of MCPyV-specific CD8 T cell clonotypes in the tumor following STING agonism had at least one clonotype present in the pre-treatment tumor. This suggests that novel CD8 T cell priming may not be a major driving factor in the STING driven anti-tumor immune response. Furthermore, minimal changes were detected in MCPyV-specific phenotype or exhaustion status suggesting that a reversal of CD8 T cell exhaustion also does not explain the response seen in this patient. We did however note an increase in MHC-I tumor cells from 1.8% before treatment to 8.2% after treatment consistent with ADU-S100 upregulating antigen-presentation in tumor cells. Since disruption of the antigen-presentation pathway is a well-known immune evasion mechanism in MCC, this may be particularly relevant to the successful clinical response in our patient[20-23].

We then asked if ADU-S100 may be acting directly on the STING pathway in the MCC tumor cells. Since a recent in vitro study had suggested that MCC tumors are likely STING deficient[19], we examined STING expression by mIHC in the patient treated with ADU-S100 and found STING expression to be absent in the MCC cancer cells, but intact in the non-cancer (immune) cells. We then verified the lack of STING expression in MCC cancer cells in a large independent patient cohort (88 MCC tumors in 68 patients, including both VP and VN MCC). It has been proposed that inactivation of STING is an important part of immune evasion by MCPyV, a DNA virus. Indeed, the LxCxE motif that inactivates STING in adenovirus and human papillomavirus[24] is also present in the MCPyV large T antigen[25]. Murine studies of STING's role in anti-cancer immunity have shown that STING activity is vital in dendritic cells, but largely dispensable in cancer cells[12,13]. These dendritic cells would release interferons following STING signaling, which in turn leads to MHC-I upregulation on cancer cells, recruits immune cells into the tumors, stimulates adaptive immunity and mediates tumor regression. We observed a high portion of plasmacytoid dendritic cells in the treated patient's tumor (5% of all cells in the TME prior to treatment). This is compared to only 0.1% (median) of cells expressing pDC markers in a prior study of 22 MCC tumors[26]. We also observed an increase in expression of genes downstream of interferon-alpha and interferon-gamma signaling following STING agonism further suggesting STING treatment induced an inflammatory TME, likely through cytokine production by non-cancer (immune) cells in response to STING-agonism.

Although initial trials of STING agonists have yielded relatively low response rates; herein, we show that these agents can lead to durable immune responses in the PD-(L)1 refractory setting. We show successful anti-cancer immune response via STING-agonism does not need STING-expression in the targeted cancer cells. Our results suggest that STING-agonism is potentially less effective at priming novel anti-cancer CD8 T cell responses and may be particularly effective in tumors that already are infiltrated by inflammatory cells in the TME but are evading immune detection via MHC-I downregulation.

Methods

Study design and participants

Samples were collected with informed consent for research use and were approved by the Fred Hutch Cancer Center institutional review board, in accordance with the Declaration of Helsinki (2013) as part of observational registry studies focusing on Merkel cell carcinoma (Fred Hutch Cancer Center IRB#6585). This patient presented to our institution as part of standard of care. Upon progression on anti-PD-L1, he was evaluated and enrolled in clinical trial with ADU-S100 and spartalizumab antibody (NCT03179236; PMID: 36282874). ADU-S100 was administered at 3200 mcg/injection every four weeks. One lesion was injected the first cycle, and a separate lesion was injected the second cycle. Tumor biopsy was taken 6 weeks after the first lesion was injected. Blood was collected before and 1 year after treatment. Every four weeks, the patient received spartalizumab administered at a dose of 400 mg until progression.

Blood collection and processing

Heparinized whole blood from MCC patients was processed at the Specimen Processing Lab (Fred Hutchinson Cancer Center). Peripheral blood mononuclear cells (PBMC) were isolated by routine Ficoll density gradient centrifugation and cryopreserved in liquid nitrogen.

Tumor digestion processing

Fresh MCC tumor specimens from needle cores, punch biopsies, or surgical excisions were enzymatically digested as described[27]. All single-cell suspensions were cryopreserved in Freezing Medium [50% human serum (Valley Biomedical), 40% RPMI (Corning), and 10% DMSO (Sigma-Aldrich)] in liquid nitrogen.

Flow cytometry

Frozen pre- and post-treatment PBMC and tumor digest samples were analyzed using flow cytometry. Tubes were thawed at 37°C and mixed with complete media (consisting of RPMI, 10% fetal bovine serum, 1x penicillin/streptomycin, and 1x l-glutamine). DNAse I was added at a concentration of 10 units/ml and the tubes were left to rest for an hour. The cells were counted using a hemacytometer and divided into tubes containing 1-3 million cells each. After two washes with PBS, dasatinib (100 nM) and live dead staining buffer (Live dead Blue; ThermoFisher) were added and the cells were incubated at 37°C for 10 minutes. The MHC-I multimers were then added, followed by the addition of antibodies against cell surface receptors (BV605 conjugated anti-E selectin (clone 68-5H11; BD), BUV395 conjugated anti-CD56 (clone NCAM16.2; BD), BUV615 conjugated anti-PD1 (clone EH12.1; BD), BV650 conjugated anti-PDL1 (clone 29E.2A3; Biolegend), PE-Cy7 conjugated anti-CLA (clone HECA-452; Biolegend), BV785 conjugated anti-CD163 (clone GHI/61; Biolegend), BUV805 conjugated anti-CD4 (clone SK3; BD), BV570 conjugated anti-CD8 (clone RPA-T8; Biolegend), BV711 conjugated anti-HLA-DR (clone L243; Biolegend), APC-Fire750 conjugated anti-CD123 (clone S18016F; Biolegend), BUV563 conjugated anti-CD14 (clone MφP9; BD), BB700 conjugated anti-CD19 (clone SJ25C1; BD), BUV496 conjugated anti-HLA-ABC (clone W6/32; BD), V450 conjugated anti-CD66b (clone G10F5; BD), BUV737 conjugated anti-CD86 (clone 2331 (FUN-1); BD), BV510 conjugated anti-CD33 (clone WM53; Biolegend), BV480 conjugated anti-CD45 (clone HI30; BD), BV750 conjugated anti-CD34 (clone 563; BD), APC conjugated anti-CD11c (clone Bu15; Biolegend))were then added and incubated for 30 minutes at room temperature. The cells were washed twice with autoMACS running buffer (Miltenyi) and permeabilized using the Foxp3/Transcription factor staining buffer set (eBioscience), followed by two more washes with the permeabilization buffer. The intracellular antibodies (PE conjugated anti-TOX (clone Invitrogen; Invitrogen), AF488 conjugated anti-TCF7 (clone S33-966; BD), PE-CF594 conjugated anti-STING (clone T3-680; BD), AF532 conjugated anti-CD3 (clone UCHT1; Invitrogen), PE-Cy5 conjugated anti-FoxP3 (clone PCH101; Invitrogen), AF700 conjugated anti-Ki67 (clone Ki-67; Biolegend)) were then added and incubated for 1 hour at room temperature, followed by two washes with permeabilization buffer and fixation in 1% paraformaldehyde. Antibody capture beads or amine reactive beads (ThermoFisher) were used to balance each fluorophore in the experiment. The stained cells were then analyzed using the Cytek Aurora spectral analyzer at the University of Washington's Department of Immunology Cell Analysis Facility. Spectral unmixing was performed using

SpectroFlo software and the initial gating, selecting for single cells, lymphocytes, and live cells, was performed in FlowJo v.10 (FlowJo LLC; Supplementary Figure 4). Further analysis was carried out in R.

Single cell RNAseq sample preparation

Frozen pre- and post-treatment PBMC and tumor digest samples were analyzed by cellular indexing of transcripts and epitopes by sequencing (CITEseq). Frozen tubes were thawed at 37 C, followed by dropwise addition of 1 ml complete media (RPMI, 10% Fetal bovine serum, 1x penicillin/streptomycin, 1x l-glutamine). Complete RPMI media was continuously added dropwise with gentle mixing in between up to a total volume of 32 ml. Cells were then washed twice with PBS, counted using a hemacytometer and transferred to FACS tubes (Fisher Scientific). Live dead stain was then added (FVS780; BD Biosciences), followed by a blocking buffer to bring samples to 0.5% BSA, 5% TruStain FcX buffer (Biolegend), 100 nM dasatinib, and 50 µg salmon sperm. Samples were then incubated on ice for 10 minutes. DNA oligo labeled MHC multimers were then added to patients with matched HLA types. Hashtag antibodies were added to identify sample origin in subsequent pooling steps. Fluorophore labeled antibodies were then added followed by DNA oligo labeled antibodies. Cells were then incubated on ice for 30 minutes and washed three times. Cells were sorted on an Aria II Cell sorter (BD Biosciences). Dead cells and debris were excluded and all live cell were sorted into cold complete media, pooled, and immediately prepared for CITEseq (see below).

scRNA-seq and scV(D)J-seq library preparation and sequencing

Single cell suspensions were collected from either tumor or blood samples as above and counted using a hemacytometer. Single cell suspensions were then loaded into the appropriate microfluidic chip (chip G; 10x Genomics) in a chromium controller (10x Genomics). Resulting cell suspensions then went through a library preparation process for single-cell RNA sequencing (scRNA-seq) along with paired scV(D)J-seq for T-cell receptor (TCR) using the 5′ transcriptome kit with feature barcoding (V1.1; 10x Genomics) following the manufacturer's guidelines. The complementary DNA libraries were then sequenced using a NovaSeq instrument (Illumina) with 2 × 92 base pair paired-end reads aiming for an average of 20,000 reads per cell.

Beta TCR receptor profiling

Frozen peripheral blood mononuclear cells or formalin-fixed paraffin-embedded (FFPE) tumor biopsy material (20 µm thick molecular curls) were used for DNA extraction using QIAamp DNA Blood Mini Kit or QIAamp DNA FFPE tissue kit respectively (Qiagen). Resulting samples were submitted to Adaptive Biotechnologies for TCRβ sequencing and normalization as previously described (PMID: 19706884)

Immunohistochemistry

Formalin-fixed paraffin-embedded tissues were stained on a Leica BOND Rx autostainer using the Akoya Opal Multiplex IHC assay (Akoya Biosciences, Menlo Park, CA) with the following changes: Additional high stringency washes were performed after the secondary antibody and Opal fluor applications using high-salt TBST (0.05M Tris, 0.3M NaCl, and 0.1% Tween-20, pH 7.2-7.6). TCT was used as the blocking buffer (0.05M Tris, 0.15M NaCl, 0.25% Casein, 0.1% Tween 20, pH 7.6 +/- 0.1). All primary antibodies were incubated for 1 hour at room temperature. Antibodies against the following targets were used for staining: CD56 (clone cl123C3.D5; BioSB), CD8 (clone 144Bl; DAKO) STING (clone SP338; Abcam) CD45 LCA clone 2B11+PD7/26; DAKO) FoxP3 (clone 236A/E7; eBioscience), CD163 (clone ERP324; BioSB) CD68 (clone PG-M1; DAKO).

Slides were mounted with ProLong Gold and cured for 24 hours at room temperature in the dark before image acquisition at 20x magnification on the Akoya PhenoImager HT Automated Imaging System. Images were spectrally unmixed using Akoya inForm software.

MHC multimer preparation

MHC tetramers used for scRNAseq were created using MHC-I easYmers (Immunaware. BV421-labeled streptavidin (Biolegend) was used to prepare tetramers for flow cytometry experiments. PE or APC and DNA oligo streptavidins (Biolegend) were used for scRNAseq experiments. Tetramers were titered using samples of known positivity. Tetramers for six epitopes were created matching this patients HLA typing: Influenza A (HLA A*02:01 containing GILGFVFTL peptide),Epstein-Barr virus (HLA A*02:01 containing GLCTLVAML peptide), cytomegalovirus (HLA A*02:01 containing NLVPMVATV peptide), and three MCPyV epitopes (HLA A*02:01 containing KLLEIANPC peptide; HLA A*11:01 containing RSGGFSFGK peptide and HLA A*37:01 containing KEWWRSGGF peptide).

Flow cytometry data analysis

Fcs files of live cells were loaded into a gating set object in R using flowWorkspace (v.4.6.0). Data from fluorescent markers was transform using the biexponential function. Fluorescent-minus-one (FMO) samples were used to draw minimum gates at the 99th percentile Gates were adjusted upward as appropriate based on visual inspection. UMAP dimensionality reduction was performed using uwot (v.0.1.14). clustering was performed using phenograph (v.0.99.1). Visualization was performed using ggplot2 (v.3.4.0) or FlowJo (v.10.8.1).

Single cell RNAseq data analysis

The raw sequencing reads were aligned to the hg38 genome using Cell Ranger v.3.1. The filtered count matrices of transcripts and feature barcoding counts were then loaded into an R (v.4.1.2) SingleCellExperiment object for further analysis. The sample hash deconvolution was carried out using DropletUtils (v.1.14.2) and doublet detection and removal was done through scds (v.1.10.0) in conjunction with the doublets detected during hash deconvolution.
Low-quality cells with fewer than 800 transcript reads, fewer than 250 genes detected, or more than 10% of mitochondrial DNA were excluded from the analysis. A comparison of genes expressed in the removed low-quality cells and kept cells was done to ensure that no cell populations were removed disproportionately. The result showed that only mitochondrial genes, MALAT1 (a transcript associated with dying cells), and hemoglobin genes were disproportionately represented in the removed cells. The cells were size-normalized and log-transformed using scuttle (v.1.4.0).

The cells from different runs were then integrated using the mutual nearest neighbor method through the batchelor package (v1.10.0). UMAP dimensionality reduction was performed with the integrated values. Clustering was done using the integrated transcript values and feature barcoding reads through the walktrap algorithm on a nearest neighbor graph (scran v.1.22.1). The number of clusters was varied by adjusting the number of nearest neighbors (k) during graph construction, followed by analysis using clustree (v.0.5.0).

Clusters were then labeled as the major cell lineages of CD4 T cells, CD8 T cells, B cells, myeloid cells, erythrocytes, NK cells, and cancer cells through the expression of key genes, including MS4A1, CD19, CD4, CD8A, CD3E, CD3D, GZMB, NCAM1, HLA-DRA, PTPRC, NKG7, and the MCPyV oncoproteins. The cluster labels were validated by investigating the portion of the cluster with productive TCR rearrangements. The cell lineages were isolated in silico and split into major lineages, and dimensionality reduction and clustering were re-performed as described above.

The cells were scored for the expression of MHC and Interferon gene sets using the UCell (v.1.99.1) package. Plotting was performed using scater (v.1.22.0), Seurat (v.4.3.0), or ggplot2 (3.4.0).

Gene sets

Genes associated with antigen-presentation were taken from the antigen-presentation and processing dataset from Biocarta[28]. HLA genes B, C, E and F not originally included in the set were added for completeness. Genes associated with Interferon alpha or gamma signatures were taken from the respective hallmark gene sets[29].

ADU-S100 stimulation

To assess MCC cell lines response to STING agonism, the virus positive cell lines WaGa, MKL1, MKL2 and MS-1 as well as a human monocytic cell line (THP1; positive control) were treated with ADU-S100. 100,000 cells were plated in 0.25 ml of media. ADU-S100 (Medchemexpress) was added to bring final concentrations to 100, 20 or 4 micromolar. The concentration of interferon beta was measured in media 48 hours later via ELISA (R&D Systems). All samples run in triplicate.

Western blot

WaGa, MKL1, MKL2, MS-1 and THP-1 cells were seeded in T75 flasks and maintained at 37 °C in a humidified incubator with 5% CO2. Cells were pelleted and lysed in ice-cold buffer containing 150 mM NaCl, 1.0% IGEPAL CA-630, 0.5% sodium deoxycholate, 0.1% SDS, 50 mM Tris (pH 8.0) and protease/phosphatase inhibitor cocktail (1:100; Cell Signaling Technology, USA). Soluble fractions from prepared cell lysates were collected after centrifugation at 13,000 rpm for 10 minutes at 4 °C. Next, normalized cell lysates (quantified using Bradford assay) were separated by 10% SDS-PAGE electrophoresis, transferred onto PVDF membranes, and immunoblotted with STING (1:1000; Cell Signaling Technology, USA) / β-actin (1:10,000; Sigma Aldrich, USA) primary antibody and anti-rabbit (1:2500; Cell Signaling Technology, USA) / anti-mouse (1:2500; Cell Signaling Technology, USA) horseradish peroxidase-conjugated secondary antibody respectively. Blotted proteins were visualized on X-ray films incubated with a high sensitivity ECL reagent (Sigma Aldrich, USA) inside a dark room.

Statistics

The statistical tests applied were two-sided unless specified otherwise. T tests were used to compare differences between two groups unless otherwise noted. When comparing more than two groups, the nonparametric Kruskal–Wallis test or one-way ANOVA was used as indicated. Multiple hypothesis testing was done with the Bonferroni method unless noted differently. Fisher's exact test was used to evaluate differences between two categorical variables. All statistical analysis was carried out using R v.4.1+ or GraphPad Prism v9.5

Acknowledgements

Figure schematics created using biorender.com. This research was supported by the Experimental Histopathology shared resource of the Fred Hutch/University of Washington Cancer Consortium (P30 CA015704).

Support

This work was supported by the National Cancer Institute (NCI) Grants No. P01 CA225517 (PN), F30 CA254168 (TP), and T32 CA080416 (SJ). Scientific computing infrastructure at Fred Hutchinson Cancer Center was funded by US NIH ORIP grant S10 OD028685. This work was also supported by the National Institutes of Health/NCI Cancer Center Support Grant in Seattle Grant No. P30 CA015704. We would like to acknowledge support from the Merkel cell carcinoma (MCC) patient gift fund at the University of Washington, the Kelsey Dickson MCC Challenge Grant from the Prostate Cancer Foundation.

Conflicts of interest

PN reports personal fees from Pfizer, Inc, Bristol Myers Squibb, EMD Serono, Rain Therapeutics, Almirall, and Instill Bio. In addition, PN has pending patents for ‘Merkel cell polyomavirus T antigen-specific TCRs and uses thereof’ and ‘Novel epitopes as T cell targets in Merkel Cell Carcinoma (MCC)’. CC has a pending patent ‘Merkel cell polyomavirus T antigen-specific TCRs and uses thereof’.

Supplemental Figures

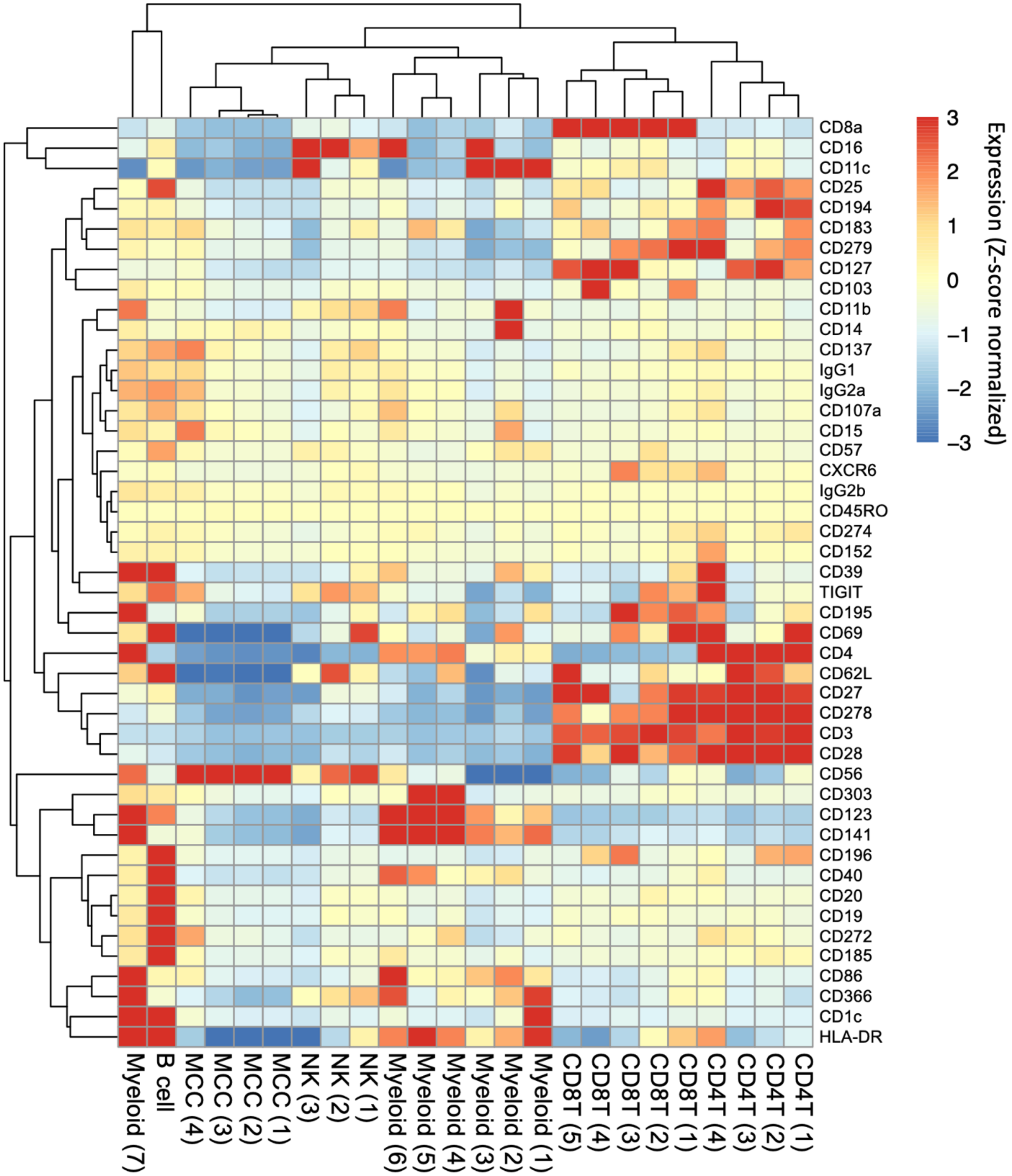

Supplemental Figure 1. Clustering justification of single cell RNAseq. Rows represent proteins measured via CITEseq. Rows represent clusters. Cell color average protein expression for a given protein in each cluster normalized to a Z statistic for each protein.

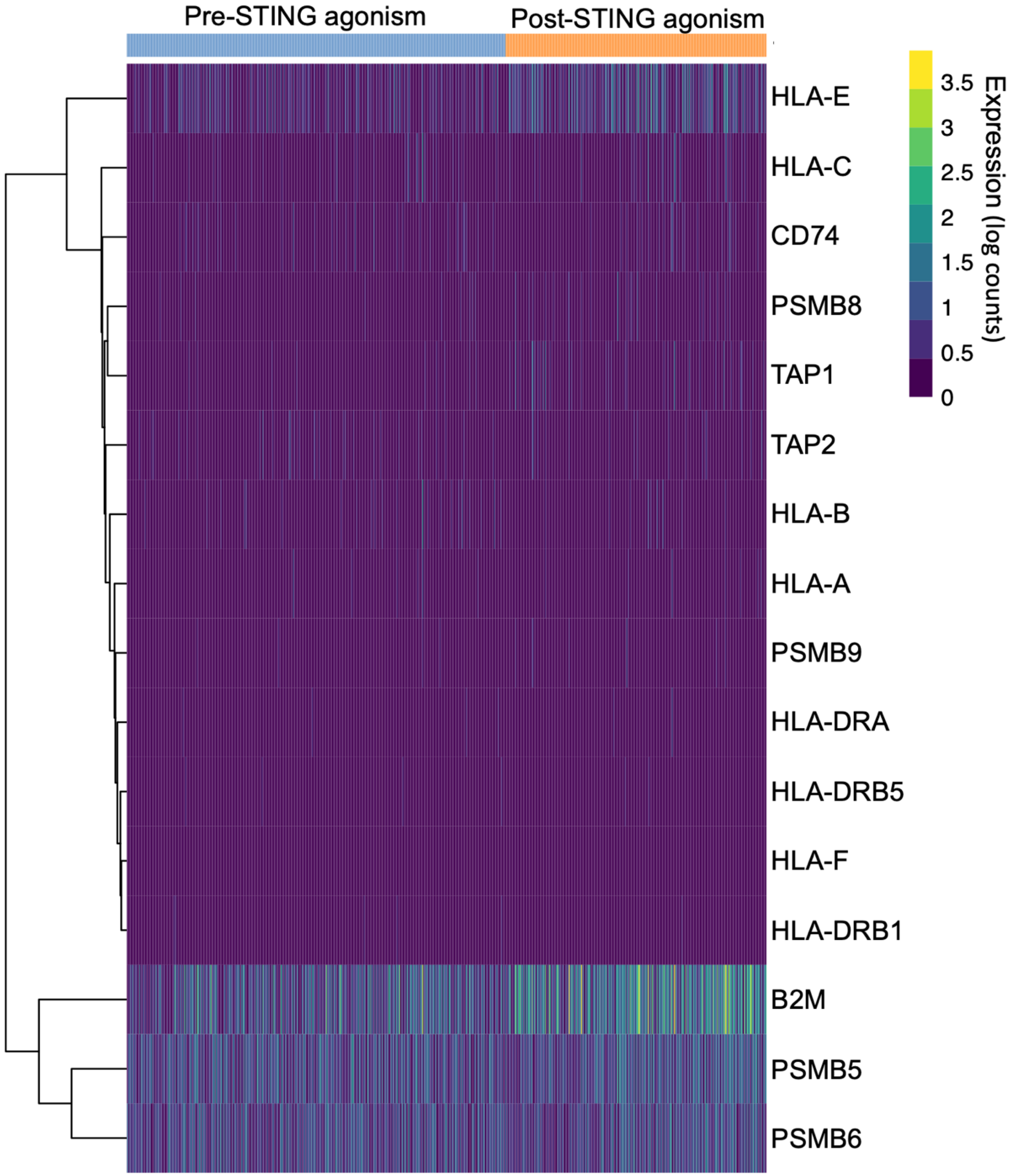

Supplemental Figure 2. Antigen presentation genes increase following STING agonism. Each row represents an individual cancer cell grouped by pre- or post-STING agonism (color on top of heatmap). Genes selected from Biocarta antigen presentation gene set.

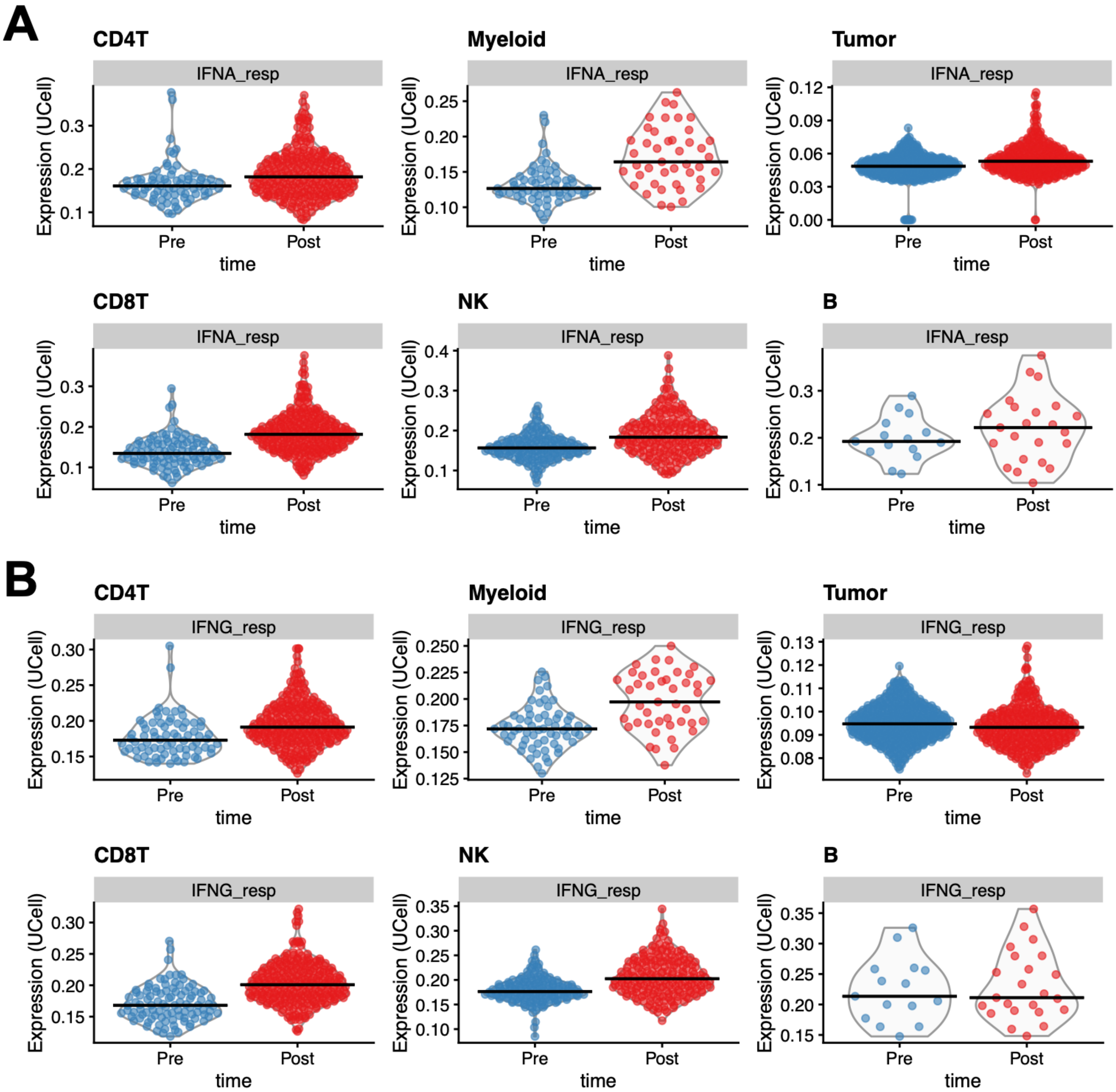

Supplemental Figure 3. Interferon gene signatures are upregulated in cell in the tumor microenvironment following STING agonist treatment. Graphs broken down to show expression for individual cell lineages before (blue) or after (red) STING agonism. Interferon alpha response signature shown in a (top), and interferon gamma signature shown in b (bottom). Hallmark gene sets for interferon alpha or interferon gamma responses used.

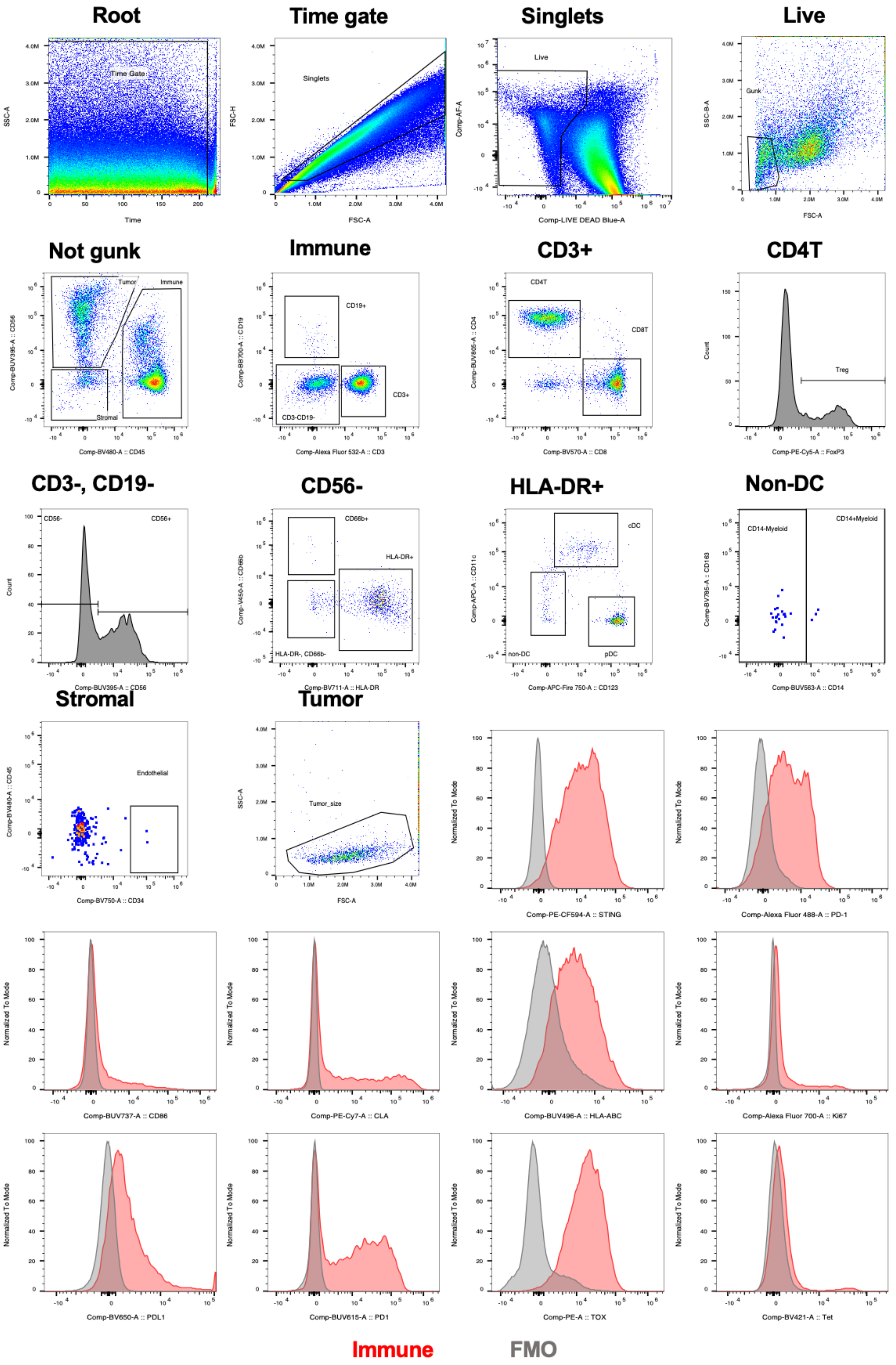

Supplemental Figure 4. Flow cytometry gating strategy. Data shown for one tumor sample. Fluorscence-minus-one (FMO) controls shown in grey histograms with samples in red for relevant markers (bottom panels).

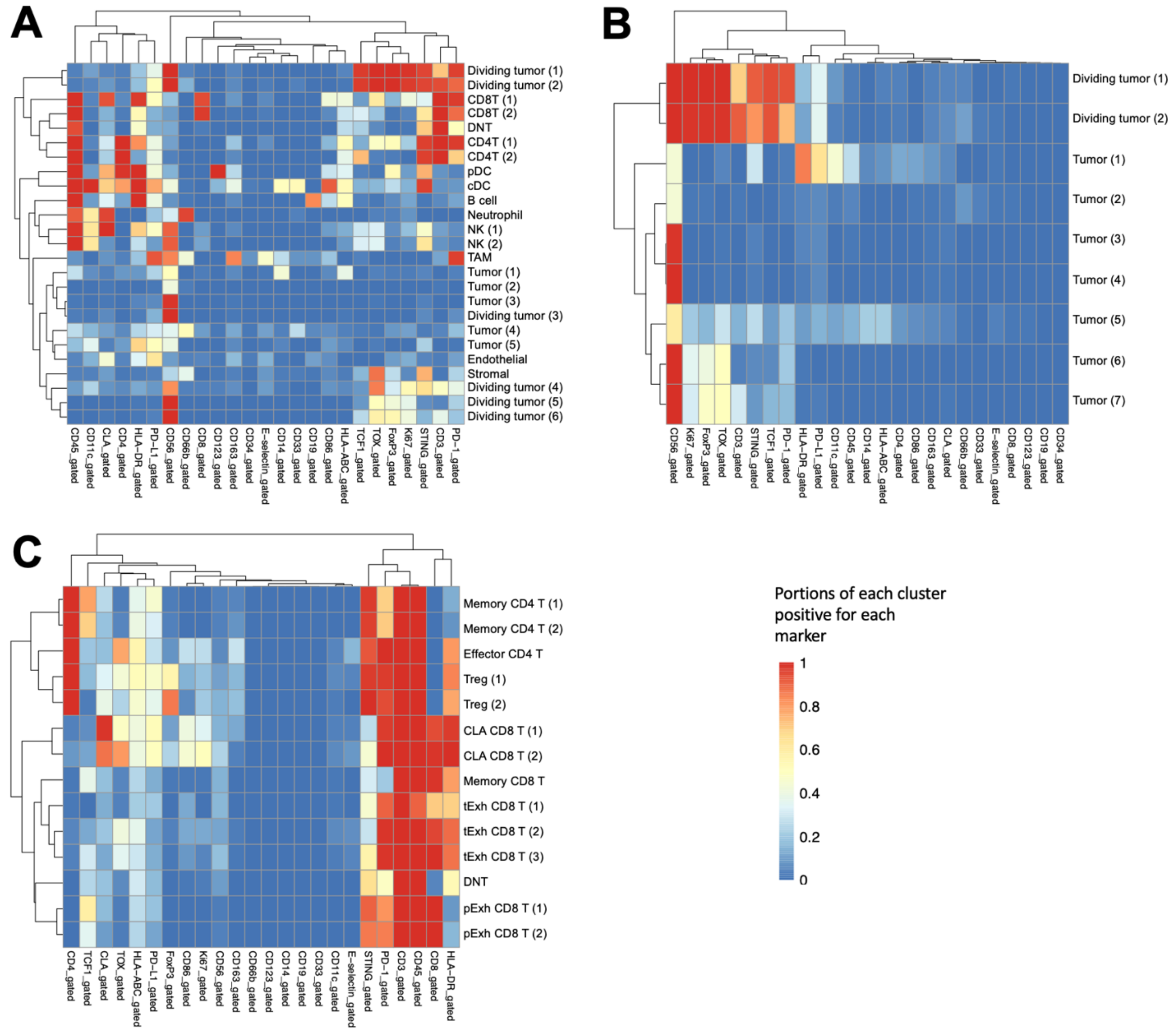

Supplemental Figure 5. Clustering and sub-clustering justification for flow cytometry data. Cells from pre or post-STING agonism were grouped into clusters using phenograph (see methods). Cluster identify was established by calculating mean proportion of cells positive for each protein.

A. Clustering of all live cells from flow cytometry data.
B. Cancer cells isolated *in silico* and reclustered for finer tuned identification.
C. T cells isolated *in silico* and reclustered for finer tuned identification.

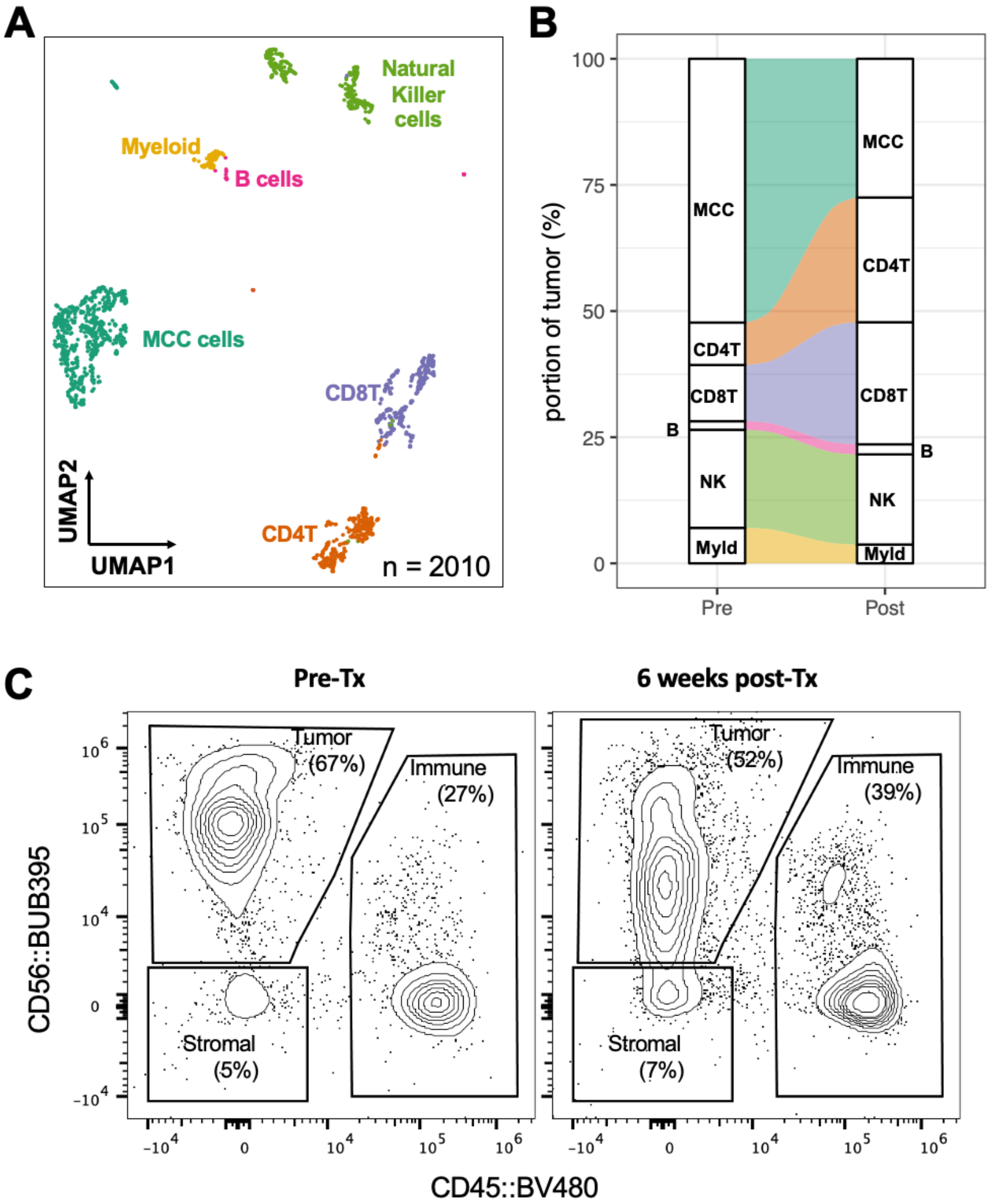

Supplemental Figure 6. T cells increase in tumor following STING agonism as measured via single cell RNAseq.

a. UMAP plot of single cell RNAseq of pre and post-treatment tumor samples.

b. Alluvium plot showing changes in cell populations after treatment.

c. FACS plot confirming trends seen in panel b. Cells gated on live singlets.

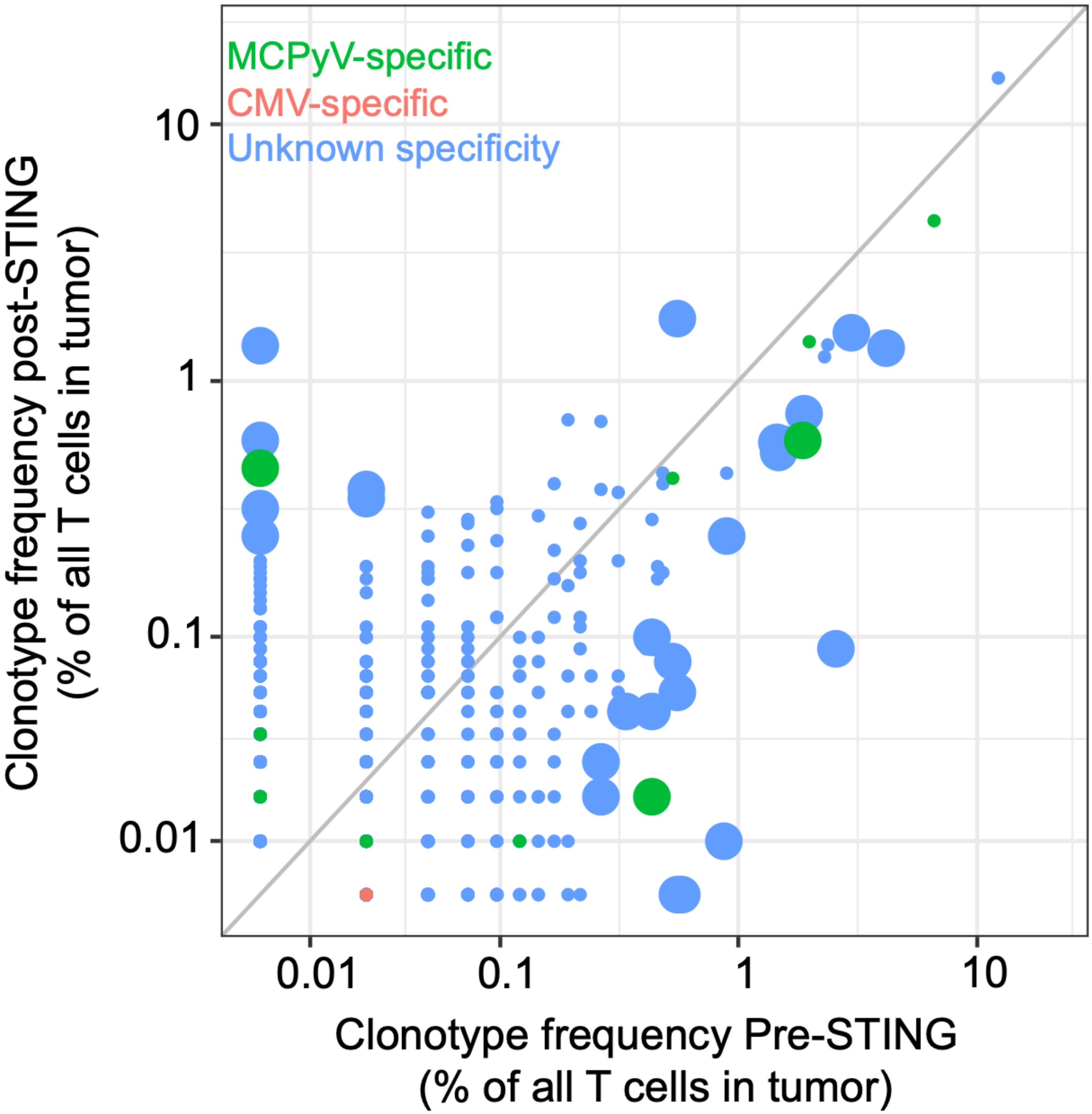

Supplemental Figure 7. MCPyV-specific T cells in tumor increase proportionately after STING agonism. Each point represents an individual T cell clonotype. Clonotypes significantly expanded shown with large points. Clonotypes colored by specificity. Statistical significance assessed using betabinomial test and a p value of less than 0.01.

Citations

1. Harms, P.W., *et al.* The biology and treatment of Merkel cell carcinoma: current understanding and research priorities. *Nat Rev Clin Oncol* **15**, 763-776 (2018).
2. Paulson, K.G., *et al.* Transcriptome-wide studies of merkel cell carcinoma and validation of intratumoral CD8+ lymphocyte invasion as an independent predictor of survival. *J Clin Oncol* **29**, 1539-1546 (2011).
3. Nghiem, P., *et al.* Three-year survival, correlates and salvage therapies in patients receiving first-line pembrolizumab for advanced Merkel cell carcinoma. *J Immunother Cancer* **9**(2021).
4. D'Angelo, S.P., *et al.* First-line avelumab in a cohort of 116 patients with metastatic Merkel cell carcinoma (JAVELIN Merkel 200): primary and biomarker analyses of a phase II study. *J Immunother Cancer* **9**(2021).
5. Bhatia, S., *et al.* Real-world clinical outcomes with avelumab in patients with Merkel cell carcinoma treated in the USA: a multicenter chart review study. *J Immunother Cancer* **10**(2022).
6. Topalian, S.L., *et al.* Neoadjuvant Nivolumab for Patients With Resectable Merkel Cell Carcinoma in the CheckMate 358 Trial. *J Clin Oncol* **38**, 2476-2487 (2020).
7. Samson, N. & Ablasser, A. The cGAS-STING pathway and cancer. *Nat Cancer* **3**, 1452-1463 (2022).
8. Francica, B.J., *et al.* TNFalpha and Radioresistant Stromal Cells Are Essential for Therapeutic Efficacy of Cyclic Dinucleotide STING Agonists in Nonimmunogenic Tumors. *Cancer Immunol Res* **6**, 422-433 (2018).
9. Corrales, L., *et al.* Direct Activation of STING in the Tumor Microenvironment Leads to Potent and Systemic Tumor Regression and Immunity. *Cell Rep* **11**, 1018-1030 (2015).
10. Downey, C.M., Aghaei, M., Schwendener, R.A. & Jirik, F.R. DMXAA causes tumor site-specific vascular disruption in murine non-small cell lung cancer, and like the endogenous non-canonical cyclic dinucleotide STING agonist, 2'3'-cGAMP, induces M2 macrophage repolarization. *PLoS One* **9**, e99988 (2014).
11. Ohkuri, T., *et al.* STING contributes to antiglioma immunity via triggering type I IFN signals in the tumor microenvironment. *Cancer Immunol Res* **2**, 1199-1208 (2014).
12. Woo, S.R., *et al.* STING-dependent cytosolic DNA sensing mediates innate immune recognition of immunogenic tumors. *Immunity* **41**, 830-842 (2014).
13. Deng, L., *et al.* STING-Dependent Cytosolic DNA Sensing Promotes Radiation-Induced Type I Interferon-Dependent Antitumor Immunity in Immunogenic Tumors. *Immunity* **41**, 843-852 (2014).
14. Marcus, A., *et al.* Tumor-Derived cGAMP Triggers a STING-Mediated Interferon Response in Non-tumor Cells to Activate the NK Cell Response. *Immunity* **49**, 754-763 e754 (2018).
15. Sivick, K.E., *et al.* Magnitude of Therapeutic STING Activation Determines CD8(+) T Cell-Mediated Anti-tumor Immunity. *Cell Rep* **25**, 3074-3085 e3075 (2018).
16. Meric-Bernstam, F., *et al.* Phase I Dose-Escalation Trial of MIW815 (ADU-S100), an Intratumoral STING Agonist, in Patients with Advanced/Metastatic Solid Tumors or Lymphomas. *Clin Cancer Res* **28**, 677-688 (2022).
17. Meric-Bernstam, F., *et al.* Combination of the STING Agonist MIW815 (ADU-S100) and PD-1 Inhibitor Spartalizumab in Advanced/Metastatic Solid Tumors or Lymphomas: An Open-Label, Multicenter, Phase Ib Study. *Clin Cancer Res* **29**, 110-121 (2023).
18. Afanasiev, O.K., *et al.* Merkel polyomavirus-specific T cells fluctuate with merkel cell carcinoma burden and express therapeutically targetable PD-1 and Tim-3 exhaustion markers. *Clin Cancer Res* **19**, 5351-5360 (2013).
19. Liu, W., *et al.* Selective reactivation of STING signaling to target Merkel cell carcinoma. *Proc Natl Acad Sci U S A* **117**, 13730-13739 (2020).
20. Lee, P.C., *et al.* Reversal of viral and epigenetic HLA class I repression in Merkel cell carcinoma. *J Clin Invest* **132**(2022).
21. Ritter, C., *et al.* Epigenetic priming restores the HLA class-I antigen processing machinery expression in Merkel cell carcinoma. *Sci Rep* **7**, 2290 (2017).
22. Paulson, K.G., *et al.* Acquired cancer resistance to combination immunotherapy from transcriptional loss of class I HLA. *Nat Commun* **9**, 3868 (2018).
23. Paulson, K.G., *et al.* Downregulation of MHC-I expression is prevalent but reversible in Merkel cell carcinoma. *Cancer Immunol Res* **2**, 1071-1079 (2014).
24. Lau, L., Gray, E.E., Brunette, R.L. & Stetson, D.B. DNA tumor virus oncogenes antagonize the cGAS-STING DNA-sensing pathway. *Science* **350**, 568-571 (2015).

25. Feng, H., Shuda, M., Chang, Y. & Moore, P.S. Clonal integration of a polyomavirus in human Merkel cell carcinoma. *Science* **319**, 1096-1100 (2008).
26. Walsh, N.M.*, et al.* A morphological and immunophenotypic map of the immune response in Merkel cell carcinoma. *Hum Pathol* **52**, 190-196 (2016).
27. Longino, N.V.*, et al.* Human CD4(+) T Cells Specific for Merkel Cell Polyomavirus Localize to Merkel Cell Carcinomas and Target a Required Oncogenic Domain. *Cancer Immunol Res* **7**, 1727-1739 (2019).
28. Rouillard, A.D.*, et al.* The harmonizome: a collection of processed datasets gathered to serve and mine knowledge about genes and proteins. *Database (Oxford)* **2016**(2016).
29. Liberzon, A.*, et al.* The Molecular Signatures Database (MSigDB) hallmark gene set collection. *Cell Syst* **1**, 417-425 (2015).

Chapter 9: Conclusions and Future Directions

Summary of research findings

While immunotherapy has revolutionized cancer treatment, only a small subset of patients experience durable responses[1]. Thus, a major effort in immune-oncology is predicting which patients are likely to respond and identifying targetable mechanisms of resistance. While significant advances have been made (as described in **Chapter 1**), current efforts are impeded by our inability to routinely distinguish the immune cells directly fighting cancer from the rest of the immune milieu. This is because most cancers are driven by private, patient-specific mutations. Identification of the tumor-driving mutations and subsequent identification of T cells targeting these mutations requires large amounts of patient samples and is laborious, making routine use of this approach infeasible. Merkel cell carcinoma (MCC), on the other hand, is driven largely by Merkel cell polyomavirus (MCPyV)[2]. Importantly, the MCPyV oncoproteins are small in size, relatively invariant, and shared across patients[2]. This has allowed us to develop multimer reagents that can identify MCPyV oncoprotein-specific CD8 T cells across many patients (described in **Chapter 1**)[3].

Use of these multimers allowed us to identify two ways to predict response to immunotherapy, as described in **Chapters 2 and 3**. Studies in **Chapter 2** found that detection of circulating MCPyV-specific CD8 T cells at baseline associated with response to neoadjuvant nivolumab. However, no similar trend was observed for intratumoral tumor-specific CD8 T cells. We observed that tumor-specific CD8 T cells in blood were more functional than their intratumoral counterparts, which may account for this discrepancy. In **Chapter 3**, we confirmed our finding that the baseline frequency of MCPyV-specific CD8 T cells in blood corresponds to response in an independent cohort of patients with virus-driven MCC. Additionally, we observed that patients with a higher number of CD39 and CLA co-expressing CD8 T cells had more favorable responses to immunotherapy, while patients with a lower number of CD39 and CD103 co-expressing CD8 T cells had more favorable responses to immunotherapy. Thus, frequency of MCPyV-specific CD8 T cells as identified by multimer reagents and frequency of CD39 and CLA co-expressing CD8 T cells are two ways to predict response to immunotherapy.

To translate these findings to patients with more common, mutationally-driven cancers, we sought to identify an antigen-independent way to identify circulating tumor-specific CD8 T cells. In **Chapter 4**, we use MCPyV oncoprotein multimer-binding cells and single-cell CITE (cellular indexing of transcriptomes and epitopes) sequencing to identify a 98-gene signature that can identify tumor-specific CD8 T cells. We apply this gene signature to CD8 T cells from mutationally-driven cancers and observe that it can identify neoantigen-specific CD8 T cells with comparable accuracy. Additionally, this signature is not enriched in CD8 T cells that target CMV, EBV, flu, or those of unknown specificity. Integration of this signature in single-cell gene expression analyses being routinely performed by cancer immunology labs may allow us to focus on characterizing tumor-specific CD8 T cells without currently available, laborious methods. This may allow identification of additional mechanisms of response and resistance that are currently being masked by non-tumor-specific CD8 T cells in bulk analyses. Although further refinement is likely needed in order to quantify tumor-specific CD8 T cells with enough accuracy to predict response to immunotherapy, especially in tissues where they are not very prevalent.

In **Chapter 5**, we explore a clinically-feasible approach to identify MCPyV oncoprotein-specific CD8 T cells. Previous studies have demonstrated that TCRs that recognize the same HLA-restricted epitope have sequence similarity. We hypothesized that we could use existing computational algorithms to recognize these similarities and identify tumor-specific CD8 T cells from bulk TCR sequence data. To test this, we trained a tcrdist3-based algorithm with TCR sequences of MCPyV multimer-binding CD8 T cells specific to three HLA types. We were able to find similar TCRs in patients with the appropriate HLA types in an independent set of patients. However, we were limited in the number of tumor-specific CD8 T cells we were able to find. SARS-CoV-2-specific CD8 T cells have been identified by numerous groups and available on public databases. Thus, we further tested the algorithm's ability to identify COVID-specific CD8 T cells in **Chapters 6 and 7**.

Much of this thesis has focused on the role of tumor-specific CD8 T cells in immunotherapy response and resistance. Finally, in **Chapter 8**, we investigate a case in which abundant anti-tumor CD8 T cells were present, but the patient's disease relapsed after initial response to immunotherapy. Through single-cell RNA sequencing and multiplexed immunohistochemistry, we demonstrate that this patient had downregulated expression of HLA-I molecules, preventing the present tumor-specific CD8 T cells from recognizing and fighting the tumor. Excitingly, intralesional injection of a STING agonist partially upregulated HLA-I expression and resulted in a partial response. Interestingly, MCC tumor cells do not express STING, implying that the STING agonist was not acting directly on these cells. We provide evidence of STING expression on infiltrating immune and stromal cells, suggest that the drug acted via these cells to induce an inflamed tumor microenvironment. The cytokines from the inflamed cells then acted on the tumor cells to upregulate HLA-I.

Future directions

Identify novel mechanisms of response and resistance to immunotherapy

The studies described in **Chapters 2 and 3** identified absence of tumor-specific CD8 T cells in blood and HLA-I downregulation as mechanisms of resistance to anti-PD-1 treatment. Subsequently, the studies in **Chapter 4** comprehensively characterized tumor-specific CD8 T cells in blood and developed a gene signature for tumor-specific CD8 T cells. Importantly, this gene signature appears to identify neoantigen-reactive CD8 T cells as well. Thus, inclusion of this gene signature in current data analysis pipelines can overcome current challenges in identifying neoantigen-specific T cells in mutationally-driven cancers and allow focus on this more relevant, but less prevalent cell population. It is possible that different in the tumor-specific T cell population are masked by the dominant, non-tumor-specific CD8 T cell population. Thus, this ability to home in on tumor-specific T cells across cancers may allow us to uncover novel mechanisms of response and resistance.

Additionally, the studies in **Chapters 2, 4, and 5** have generated a library of T cell receptors that recognize Merkel cell polyomavirus oncoproteins. Use of this antigen-specific TCR library can allow identification of tumor-specific CD8 T cells in spatial transcriptomic studies. This would allow us to observe proximity of tumor-specific CD8 T cells to other aspects of the tumor microenvironment (e.g., tumor cells, immune cells, stroma, neurons, etc.), as well as interrogate their phenotype. For example, one study has demonstrated that exhausted CD8 T cells are present near adrenergic neurons, which drive their functional state and lead to an impaired response to immunotherapy[4]. Distinguishing tumor-specific CD8 T cells from bystander cells in humans would strengthen and increase confidence in these findings.

Develop clinically useful assays for stratifying patients for immunotherapy

The studies described in **Chapters 2 and 3** suggest that blood is an important reservoir of functional, tumor-specific CD8 T cells that respond to immunotherapy and facilitate tumor regression. This suggests that patients with tumor-specific CD8 T cells in blood should be stratified for immunotherapy, while patients that lack these T cells should receive interventions to increase the frequency of these cells (e.g., therapeutic vaccines, transgenic TCR therapy, TIL therapy, etc.). However, we currently do not have a method of routinely estimating frequency of tumor-specific CD8 T cells. Studies in **Chapters 3 and 4** provide important groundwork for development of clinically implementable assays to quantify tumor-specific CD8 T cells. Studies in **Chapter 3** suggest that the co-expression of CD39 and CLA correlate to the frequency of tumor-specific CD8 T cells. However, the frequency of CD39+CLA+ CD8 T cells is still 10-100-fold higher than the frequency of tumor-specific CD8 T cells as determined by multimer reagents. While existing methods are also prone to errors, the unbiased single-cell RNA sequencing studies described in **Chapter 4** could be used to identify corresponding protein markers that are differentially expressed in tumor-specific CD8 T cells. For example, one study has reported that PD-1 positivity enriches tumor-specific CD8 T cells by 33-fold, while co-expression of CD45RO, HLA-DR, CD39, and CD103 enriched for tumor-specific CD8 T cells by >2,100-fold[5]. This provides proof-of-concept that it is possible to further enrich for tumor-specific CD8 T cells. Single-cell gene expression could also be used to identify T cells with similar functional states as tetramer-binding T cells, and identify previously unknown tumor-specific T cell epitopes. Both approaches could potentially decrease the discrepancy between multimer-determined and existing cell surface marker-determined tumor-specific CD8 T cells.

Additionally, the studies described in **Chapters 5, 6, and 7** provide important groundwork for the development of T cell receptor-based predictors for antigen-specific CD8 T cells. Further development of these tools could allow identification of tumor-specific CD8 T cells from bulk TCR sequencing data, which is commercially available using a small volume of blood and for a reasonable cost. The tools described in this thesis are likely limited to HLA-restricted epitopes for which we can gather a large amount of training data. Excitingly, new artificial intelligence and machine learning-based models (e.g., TAPIR[6] and pMTnet[7]) that do not require antigen-specific training data have also recently been made available for public use. These models can take in bulk or paired-chain TCR sequencing data, along with tumor-specific HLA-restricted epitopes, and predict which TCRs are likely to recognize the queried epitopes. Thus, performance of whole exome sequencing on tumor tissue and utilization of peptide prediction tools[8] (e.g., NetMHC[9]) to identify HLA-restricted epitopes, in conjunction with bulk TCR sequencing, is all that would be needed to utilize these models for quantification of tumor-specific CD8 T cells in the near future.

In conclusion, the studies described here move us closer to efficient identification of tumor-specific CD8 T cells. This would allow us to rationally stratify patients for immunotherapy, prioritize patients unlikely to respond to immunotherapy for alternate or synergistic treatments, and identify T cell receptors for transgenic T cell therapies and TCR-based drugs.

References

1. Yarchoan, M., Hopkins, A., and Jaffee, E.M. (2017). Tumor Mutational Burden and Response Rate to PD-1 Inhibition. N Engl J Med *377*, 2500-2501. 10.1056/NEJMc1713444.
2. Harms, P.W., Harms, K.L., Moore, P.S., DeCaprio, J.A., Nghiem, P., Wong, M.K.K., Brownell, I., and Group, I.W.o.M.C.C.R.I.W. (2018). The biology and treatment of Merkel cell carcinoma: current understanding and research priorities. Nat Rev Clin Oncol *15*, 763-776. 10.1038/s41571-018-0103-2.
3. Jing, L., Ott, M., Church, C.D., Kulikauskas, R.M., Ibrani, D., Iyer, J.G., Afanasiev, O.K., Colunga, A., Cook, M.M., Xie, H., et al. (2020). Prevalent and Diverse Intratumoral Oncoprotein-Specific CD8. Cancer Immunol Res *8*, 648-659. 10.1158/2326-6066.CIR-19-0647.
4. Globig, A.M., Zhao, S., Roginsky, J., Maltez, V.I., Guiza, J., Avina-Ochoa, N., Heeg, M., Araujo Hoffmann, F., Chaudhary, O., Wang, J., et al. (2023). The beta(1)-adrenergic receptor links sympathetic nerves to T cell exhaustion. Nature *622*, 383-392. 10.1038/s41586-023-06568-6.
5. Yossef, R., Krishna, S., Sindiri, S., Lowery, F.J., Copeland, A.R., Gartner, J.J., Parkhurst, M.R., Parikh, N.B., Hitscherich, K.J., Levi, S.T., et al. (2023). Phenotypic signatures of circulating neoantigen-reactive CD8(+) T cells in patients with metastatic cancers. Cancer Cell. 10.1016/j.ccell.2023.11.005.
6. Fast, E., Dhar, M., and Chen, B. (2023). TAPIR: a T-cell receptor language model for predicting rare and novel targets. bioRxiv. 10.1101/2023.09.12.557285.
7. Lu, T., Zhang, Z., Zhu, J., Wang, Y., Jiang, P., Xiao, X., Bernatchez, C., Heymach, J.V., Gibbons, D.L., Wang, J., et al. (2021). Deep learning-based prediction of the T cell receptor-antigen binding specificity. Nat Mach Intell *3*, 864-875. 10.1038/s42256-021-00383-2.
8. Luo, H., Ye, H., Ng, H.W., Shi, L., Tong, W., Mendrick, D.L., and Hong, H. (2015). Machine Learning Methods for Predicting HLA-Peptide Binding Activity. Bioinform Biol Insights *9*, 21-29. 10.4137/BBI.S29466.
9. Lundegaard, C., Lund, O., and Nielsen, M. (2008). Accurate approximation method for prediction of class I MHC affinities for peptides of length 8, 10 and 11 using prediction tools trained on 9mers. Bioinformatics *24*, 1397-1398. 10.1093/bioinformatics/btn128.

Appendix

Appendix A: Blog post to communicate new research findings to a lay audience

Published on Engage blog on April 4, 2022

https://www.engage-science.space/blog

Do we need a psychiatrist for our immune system?

Imagine if you lost the ability to see in one eye or were unable to feel a part of your arm. Either of these things, among others, could happen to you at any time if you had multiple sclerosis (MS). MS is an autoimmune disorder that sporadically damages myelin, the part of brain cells that allows them to respond quickly. When the myelin is gone, signals between your brain and the rest of your body are sent much, much slower. The damaged brain cells are fixed by the body over time and the symptoms disappear over time. But more damage eventually occurs and the symptoms come back, each time different than the last.

But what causes MS in the first place?

A group of scientists from Boston recently found that infection with Epstein-Barr virus (EBV) increases one’s chance of developing MS. Our bodies are filled with and surrounded by approximately 380 trillion viruses – 12 times the number of cells that make up a person. Parts of these viruses could be similar to our cells. And when our immune system learns to fight the viruses, it may inadvertently attack our own cells too. This is presumably what is happening in MS – the virus and the myelin are similar in some way and our immune system is tricked into attacking the myelin on brain cells, believing it is actually EBV.

If we could know who has been infected with EBV, could we monitor them more closely and prevent even the first attack of MS? More broadly, if we could know what viruses are living in us, could we determine which currently unexplained illnesses are caused by viruses? Researchers in Seattle think they can do just this by looking at immune cells.

Our immune system is our first line of defense against infections. While some immune cells act like fences, preventing germs from getting into cells, others act like snipers – eliminating the enemy once it has already made it past the fence. “T cells” are the snipers. When they see harmful viruses in our cells, they react – they make more copies of themselves and then attack the virus-infected cells. Once the threat has been neutralized, the some of the responding T cells become “memory” cells, lying in wait until the same virus comes in again. Just like a psychiatrist tries to identify the root of a person’s problem, we may soon be able to know what viruses we have been infected with by finding out which of our T cells have reacted to a threat.

T cells see viruses that are present in our cells with molecules on their surface called “receptors.” T cell receptors that recognize the same virus are like each other. And we are now increasingly able to detect similar patterns in T cell receptors and predict which virus a T cell is poised to fight. Researchers at the University of Washington and the Fred Hutchinson Cancer Research Center are perfecting a tool that can predict whether a T cell is seeing the virus that causes a deadly skin cancer, Merkel cell carcinoma.

Once refined, similar tools can be developed for other viruses until we can metaphorically ask a T cell what virus triggers it. And if we see many copies of the same T cell, we know that it was once activated and that we have previously come across the virus that it recognizes. With this knowledge, the possibilities for scientific progress are vast, and include identifying viral causes of currently unexplained illnesses and determining how well our immune system is fighting an infection or a virus-driven cancer.

Appendix B: Slides to communicate research in progress to a lay audience

Presented at Town Hall Seattle on April 11, 2022

https://townhallseattle.org/event/caitlin-cruz-saumya-jani-and-miranda-mudge/

https://www.youtube.com/watch?v=C-xi2cJB7KI

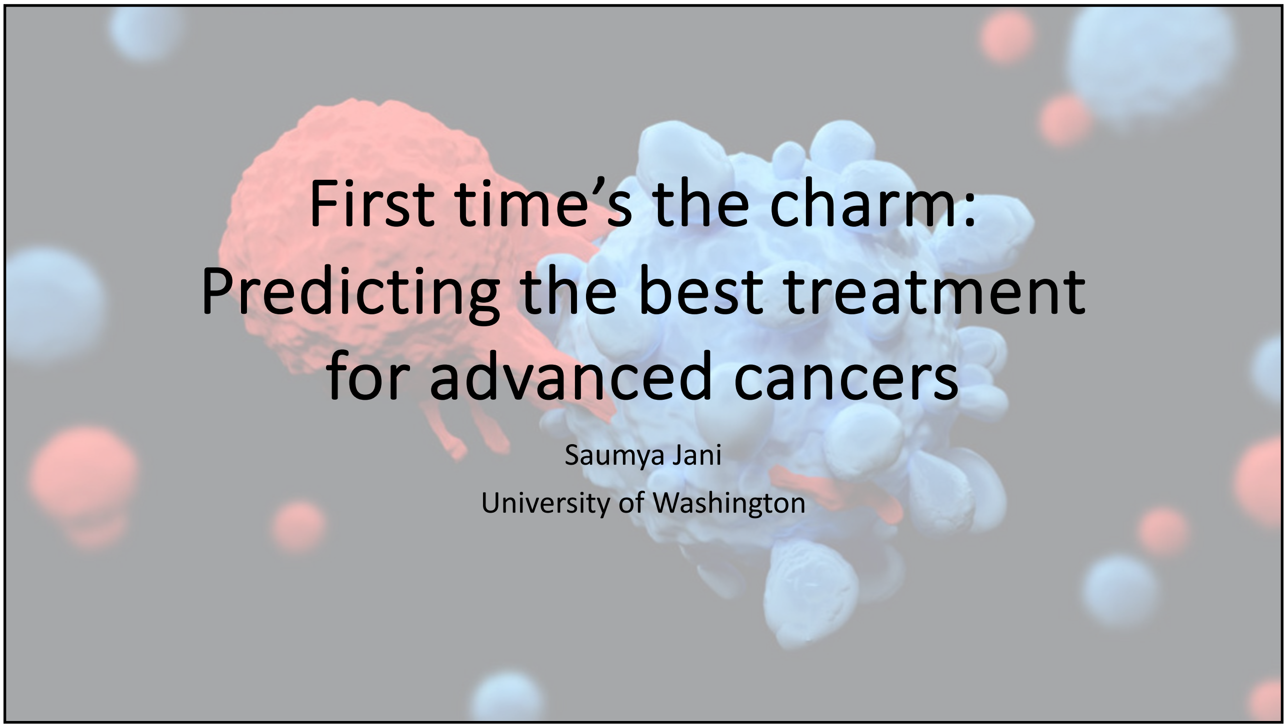

First time's the charm: Predicting the best treatment for advanced cancers

Saumya Jani
University of Washington

Merkel cell carcinoma: A pimple that never stops growing

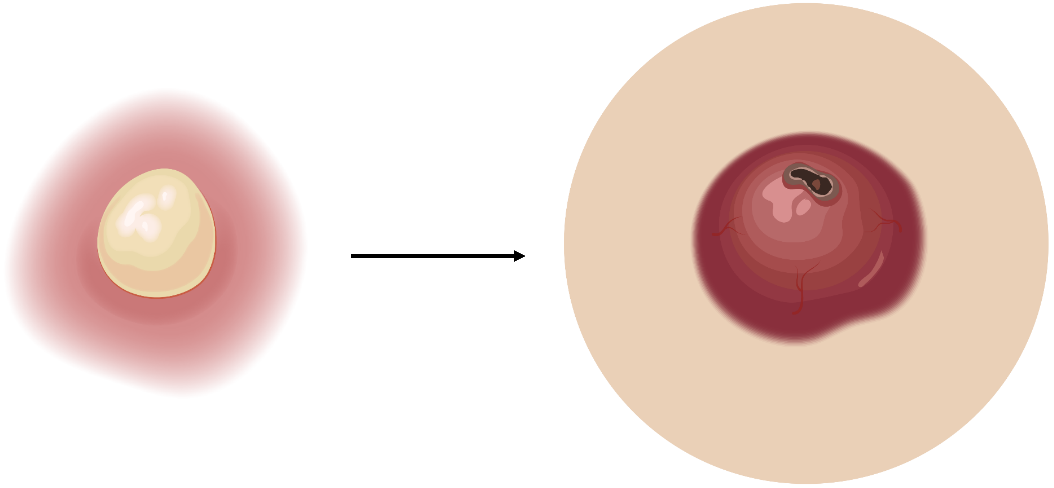

Who gets MCC?

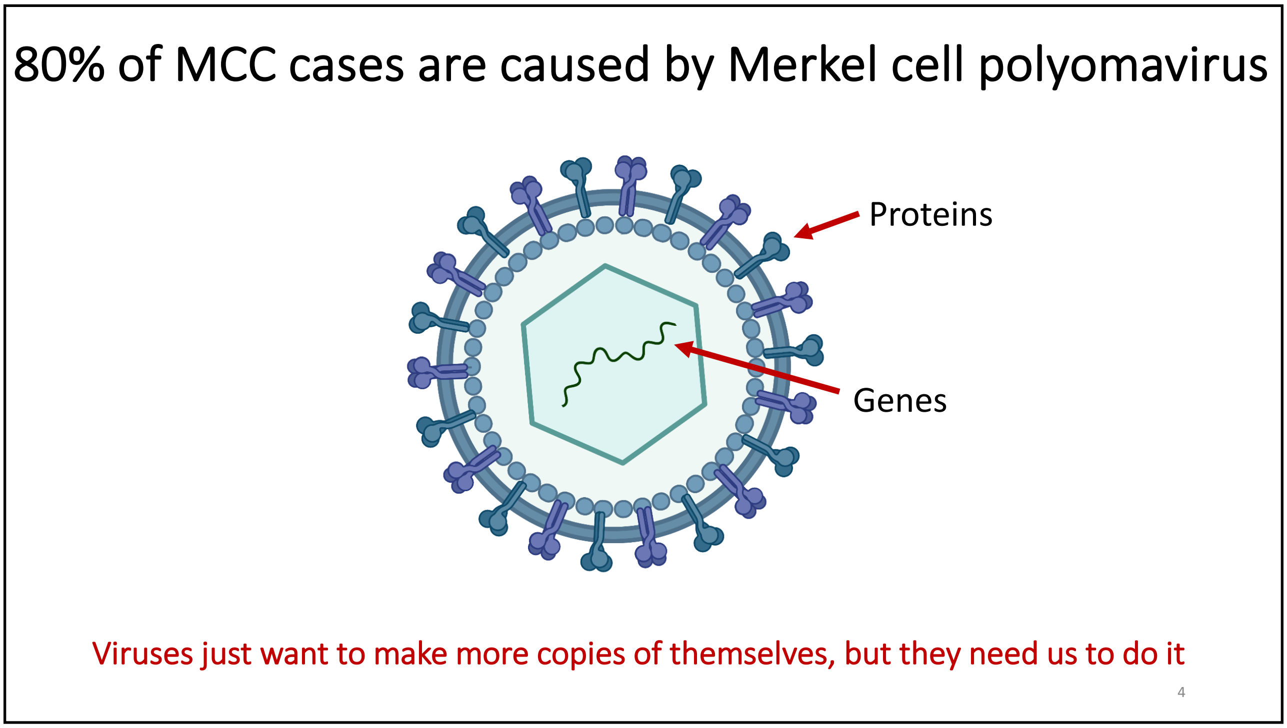

80% of MCC cases are caused by Merkel cell polyomavirus

Viruses just want to make more copies of themselves, but they need us to do it

Merkel virus causes cancer by entering our genes

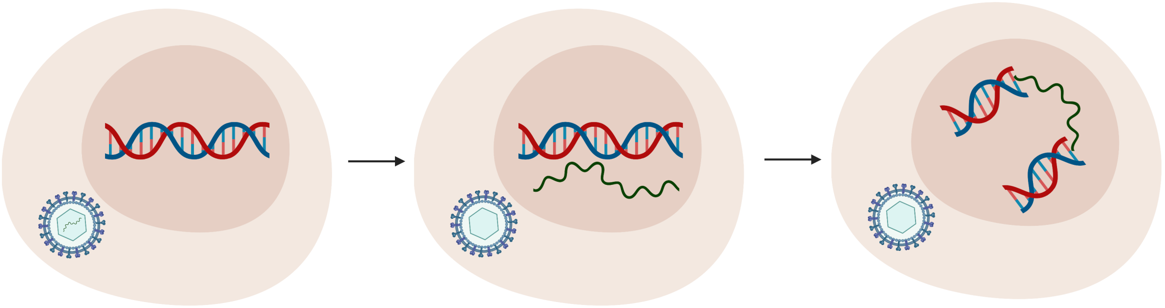

The virus enters our cells

Virus genes go to the same place as our genes

Small part of virus gets into our genes

We don't have a way of preventing this progression, but we may be able to determine the best treatment for each patient

How is MCC treated?

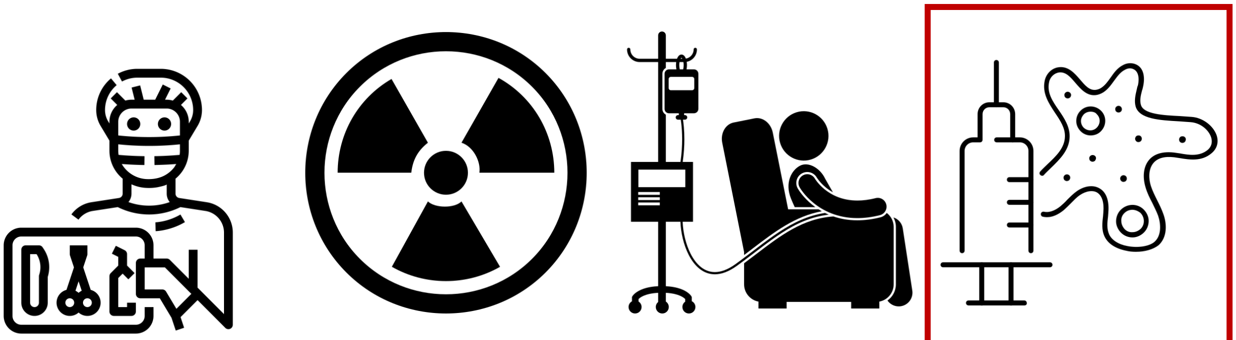

Surgery

Radiation

Chemotherapy

Immunotherapy

Our immune system is our first line of defense

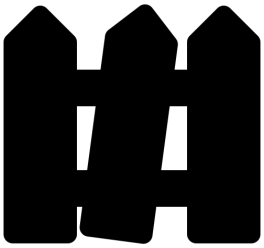

Your skin can prevent germs from getting into your body

“Guard” cells patrol the blood and prevent germs from getting into your cells

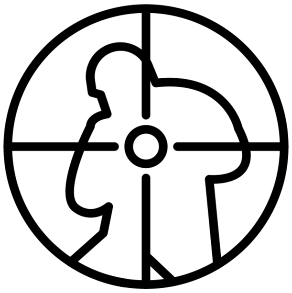

“Sniper” cells see what is in your cells and kill the infected ones

A weak immune system increases your chances for MCC

How do “snipers” see virus-infected and cancerous cells?

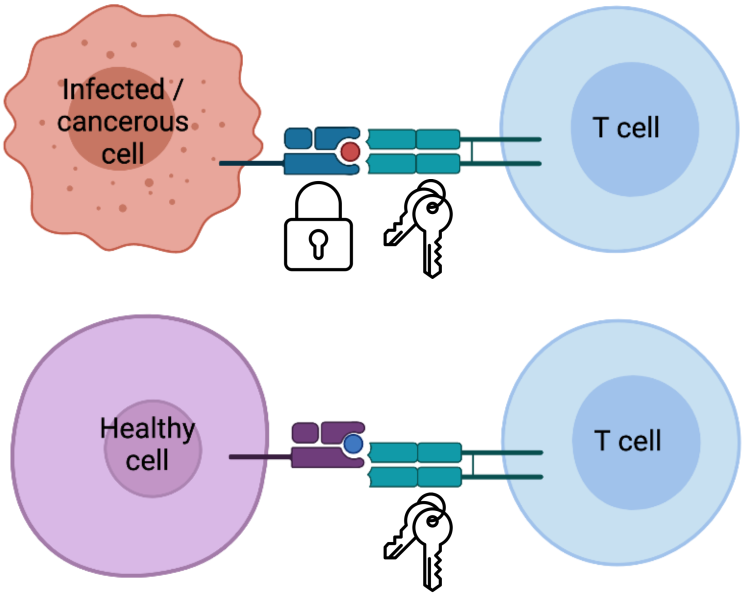

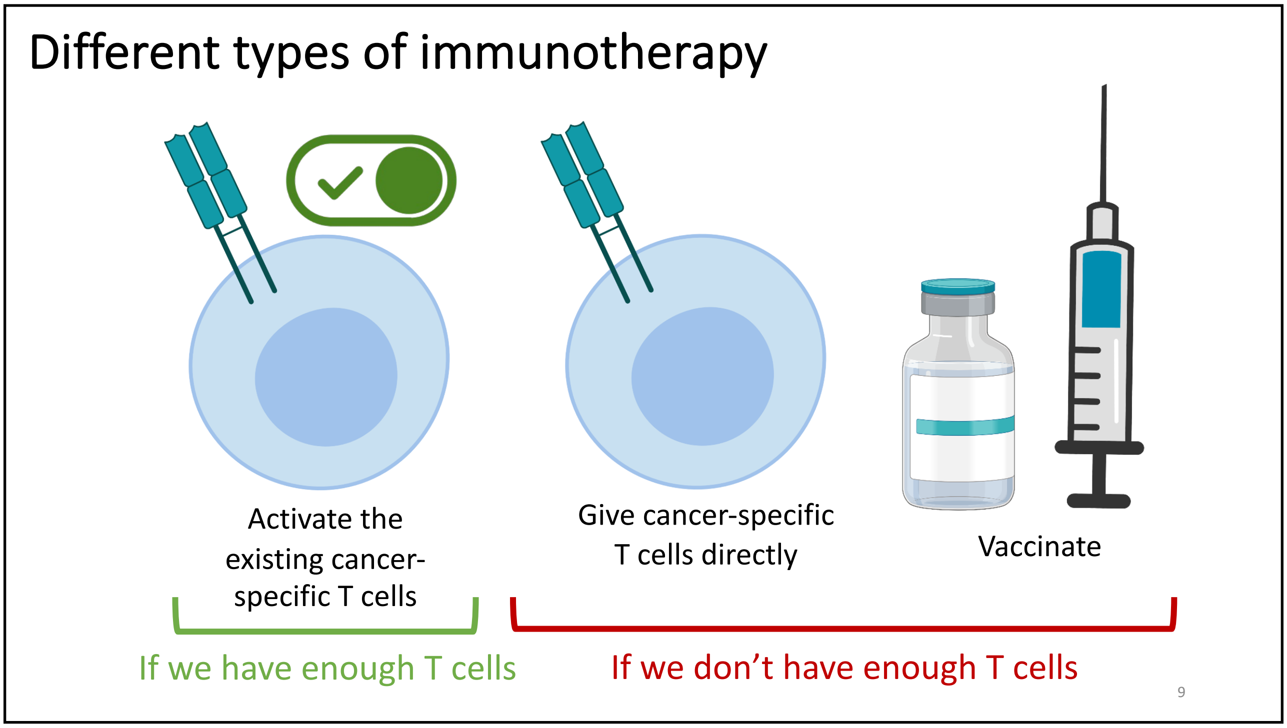

Different types of immunotherapy

Activate the existing cancer-specific T cells

Give cancer-specific T cells directly

Vaccinate

If we have enough T cells

If we don’t have enough T cells

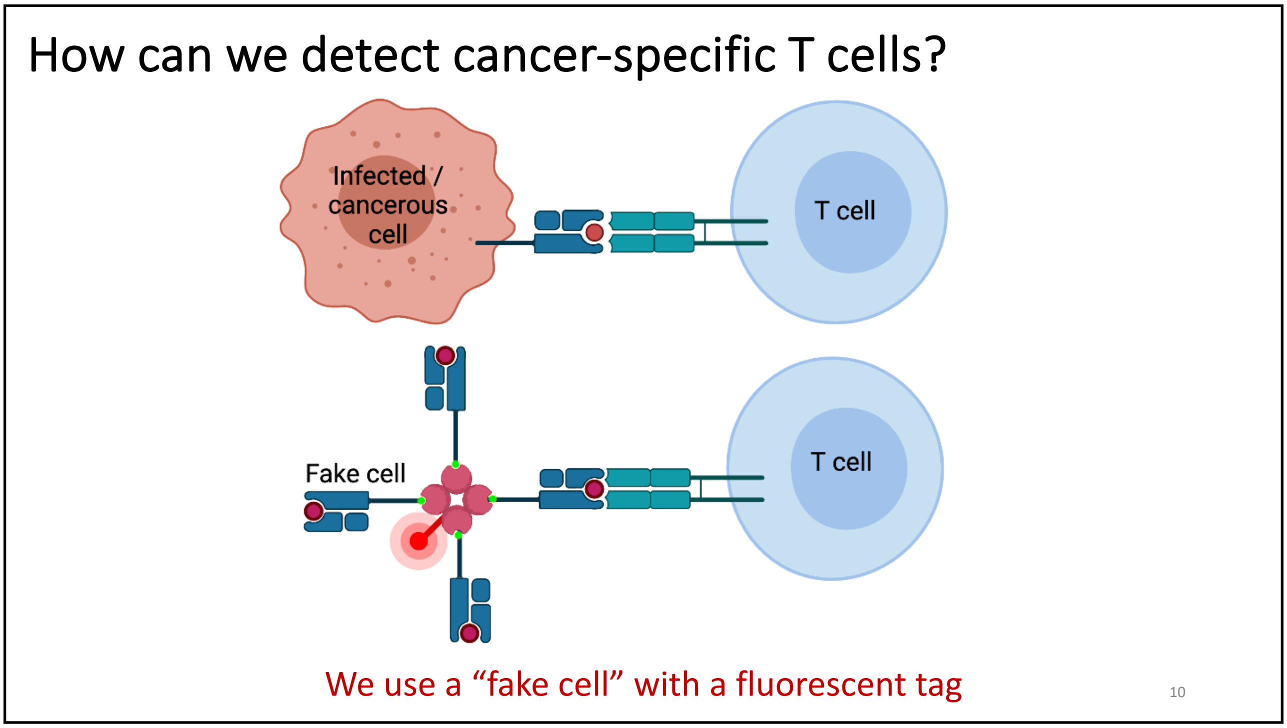

How can we detect cancer-specific T cells?

Infected / cancerous cell

T cell

Fake cell

T cell

We use a “fake cell” with a fluorescent tag

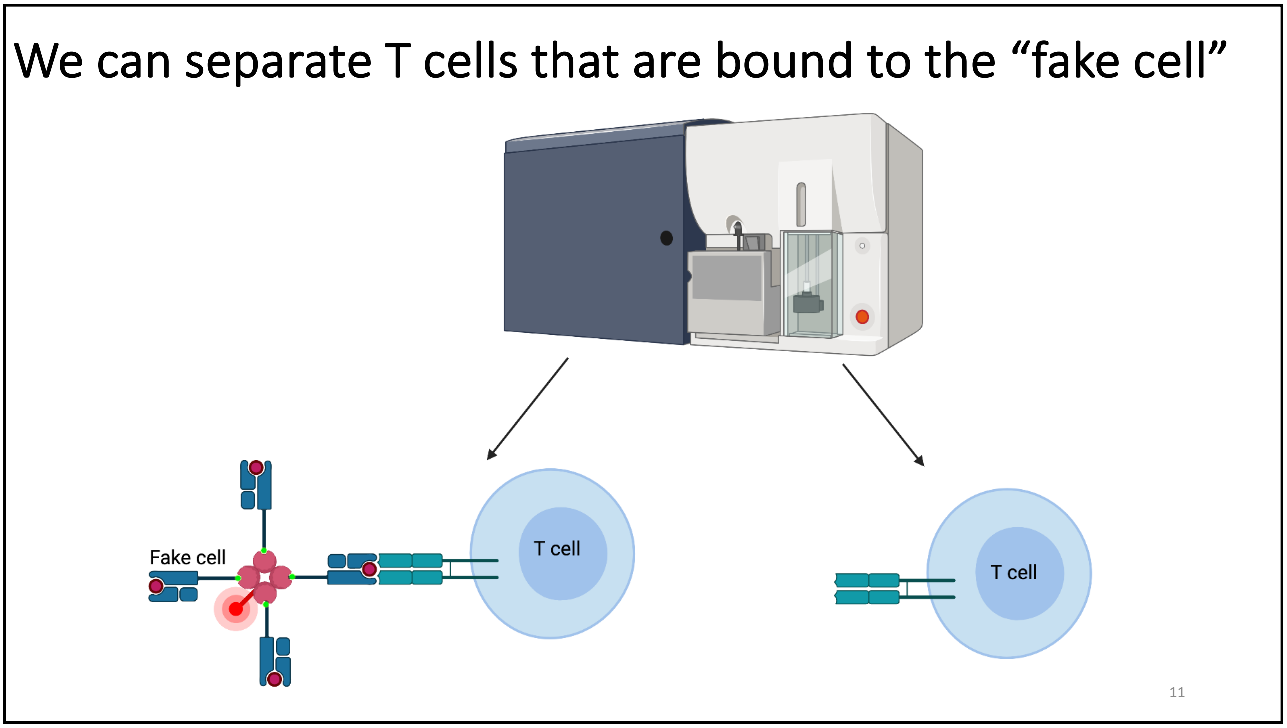

We can separate T cells that are bound to the “fake cell”

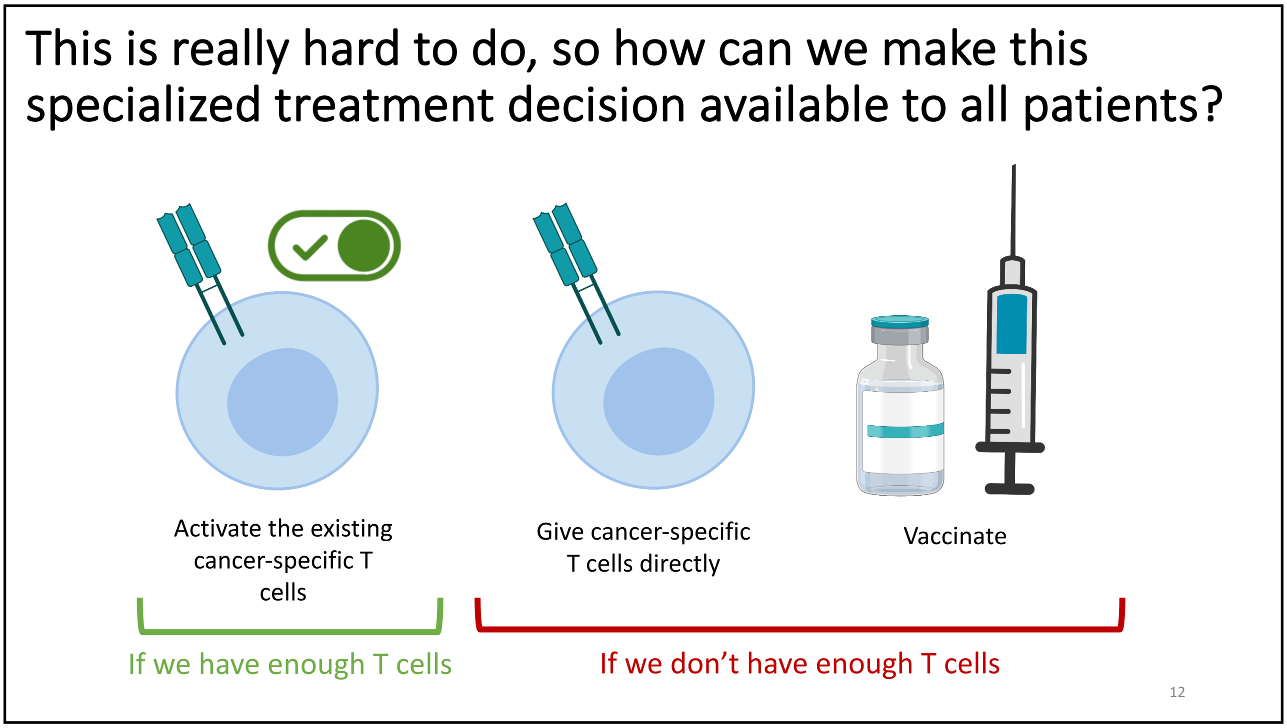

This is really hard to do, so how can we make this specialized treatment decision available to all patients?

Activate the existing cancer-specific T cells

Give cancer-specific T cells directly

Vaccinate

If we have enough T cells

If we don’t have enough T cells

T cell receptor (TCR) are diverse, but not infinitely so

T cell receptors

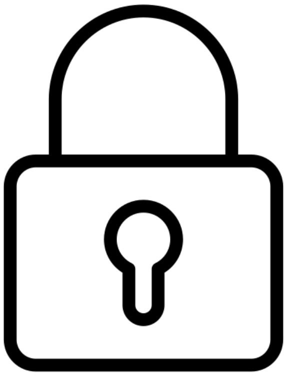

Viruses and cancers

One lock can have multiple keys, but not an infinite amount

Can we read the cell’s instruction manual?

English: 26 letters

Cell’s language: 4 letters

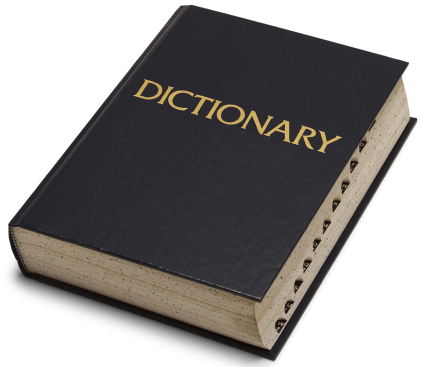

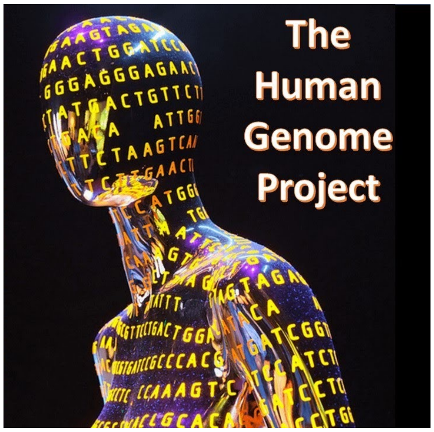

Computers can find patterns that the human eye cannot

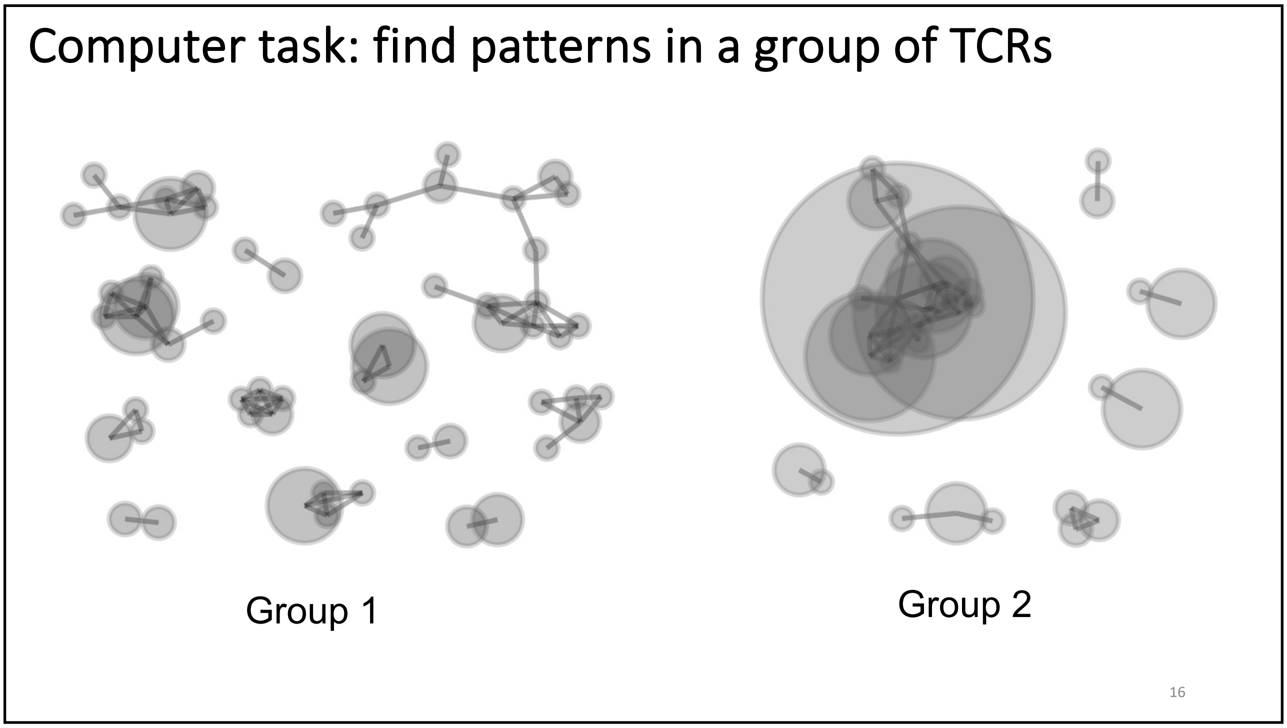

Computer task: find patterns in a group of TCRs

We can find patterns in the sequences!

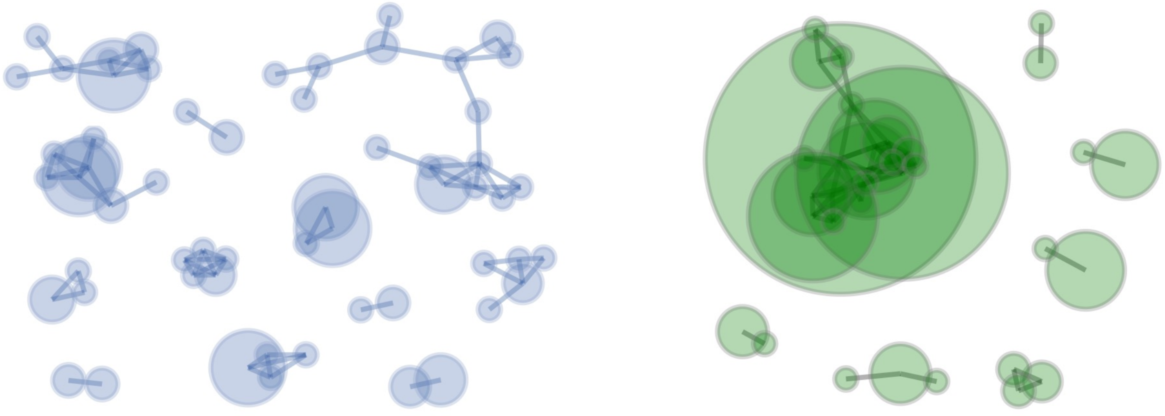

One part of the virus

Second part of the virus

The patterns can be used to quantify virus-specific cells in MCC patients

Ultimate clinical use

Get blood or tumor tissue from patients

Obtain instructions that make T cell receptors

Count how many T cell receptors overlap with those known to be cancer-specific

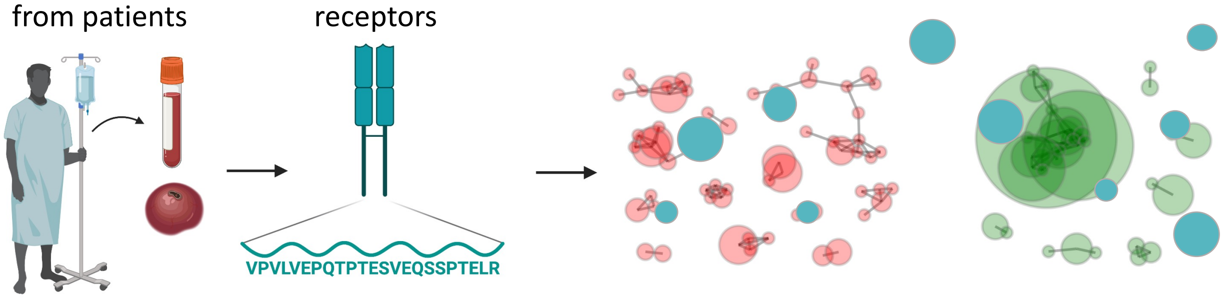

How many “overlapping” T cells are there?

Enough

Too few

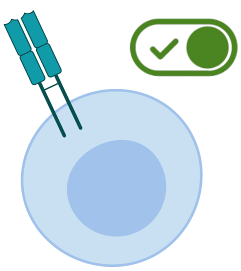

Activate the existing cancer-specific T cells

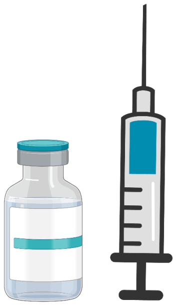

Vaccinate

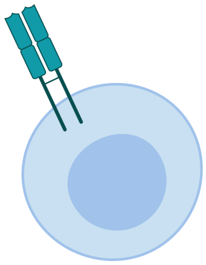

Give cancer-specific T cells directly

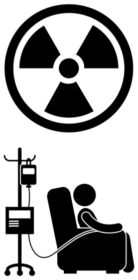

Conventional treatments

What else can this technology help with?

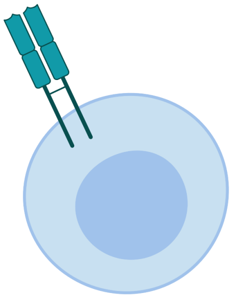

Give cancer-specific T cells directly

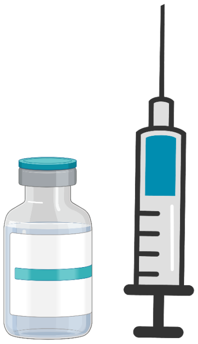

Estimate clinical efficacy of therapeutic vaccines

Acknowledgements

Thank you for your attention!

Appendix C: Slides to teach trainees how to engage with audiences skeptical of science

Presented at Science Talk on April 6, 2023

Communicating Science to Science Skeptics

Science Talk 2023

ENGAGE

Miranda Mudge

Kevin Bishop

Natalie Mastick

Saumya Jani

Communicating Science to Science Skeptics

Goal: Building confidence when communicating to science skeptics

Everything but the content

- Making your science more understandable
- Improv strategies

Connecting with your audience

- Listening
- Responding with empathy and understanding

Fundamental Skills and Strategies

Communicating Science Effectively

1. Know Your Goal(s)

1. Know Your Audience

Communicating Science Effectively

- Lose the Jargon
    - Avoid it
    - Define it

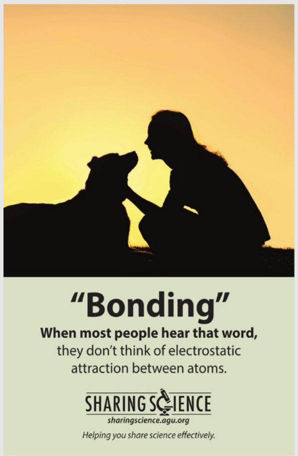

"Bonding"

When most people hear that word, they don't think of electrostatic attraction between atoms.

SHARING SCIENCE
sharingscience.agu.org
Helping you share science effectively.

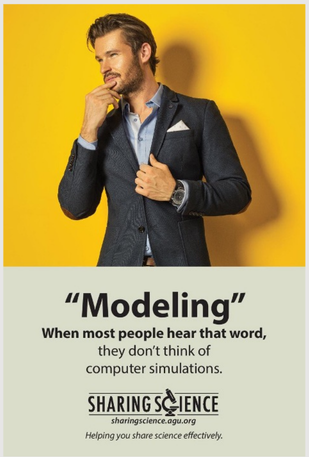

"Modeling"

When most people hear that word, they don't think of computer simulations.

SHARING SCIENCE
sharingscience.agu.org
Helping you share science effectively.

Communicating Science Effectively

- Lose the Jargon
- Practice Distillation

"nutrients" =

Communicating Science Effectively

- Lose the Jargon
- Practice Distillation
- Utilize Storytelling

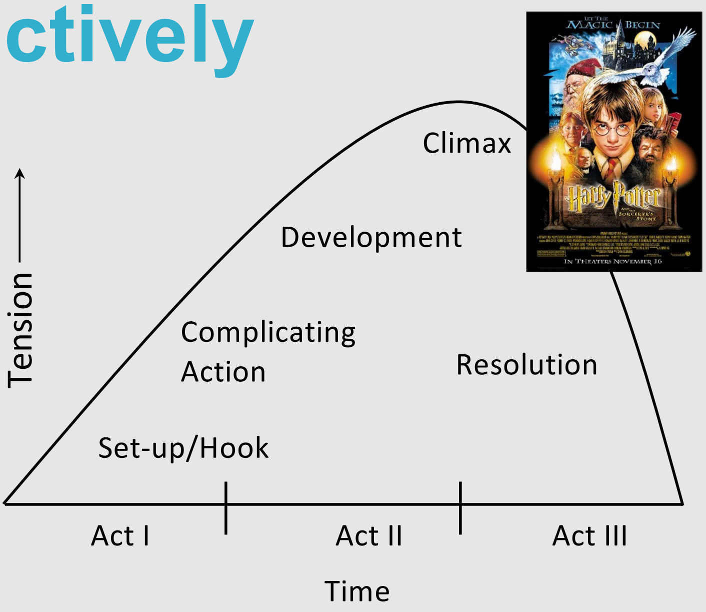

Communicating Science Effectively

- Lose the Jargon
- Practice Distillation
- Utilize Storytelling
- Be Prepared

Communicating Science Effectively

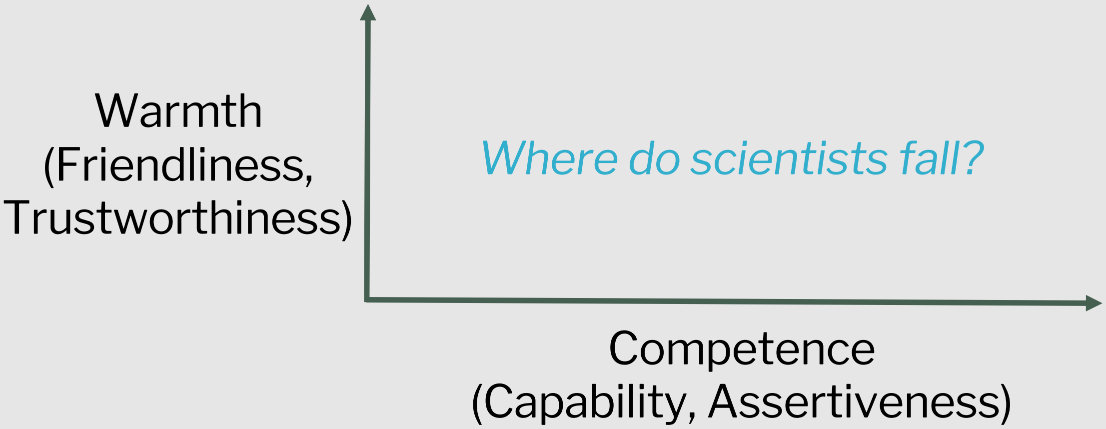

Warmth (Friendliness, Trustworthiness)

Where do scientists fall?

Competence (Capability, Assertiveness)

Communicating Science Effectively

*"Groups stereotyped as **cold but competent…** including rich people, businesspeople, and **technical experts.** People reported that they elicit envy….**they admire such people but also resent them.**"*

Fiske, 2018. Curr Dir Psychol Sci.

Communicating Science Effectively

- Lose the Jargon
- Practice Distillation
- Utilize Storytelling
- Be Prepared
- Convey Warmth

Activity:
Convey tone through gibberish

Activity:
Convey tone through gibberish

1) Pair up with someone in your group
2) Choose an emotion to convey from the cards available
3) Using only gibberish, have a conversation with your partner focusing on tone

Can you guess the emotion your partner is trying to convey?

Would you want to continue this conversation?

Distillation

Distilling vs. Dumbing Down

Leaving out difficult content

“this content is too hard for you to understand”

Distilling vs. Dumbing Down

Making concepts **accessible** to general audience

"Distilling" ideas into relevant, digestible chunks

Leaving out difficult content

"this content is too hard for you to understand"

The Process of Distillation

- What information is absolutely necessary to communicate this concept to my audience?
- Which details are important to my whole story? Which can be left out?
- How complex is this topic? Can I present it with a few words?
- Would an analogy benefit my audience?

Elevator pitches

Why is this useful?

- Communicate your research to non-scientists
- Communicate your research to other scientists

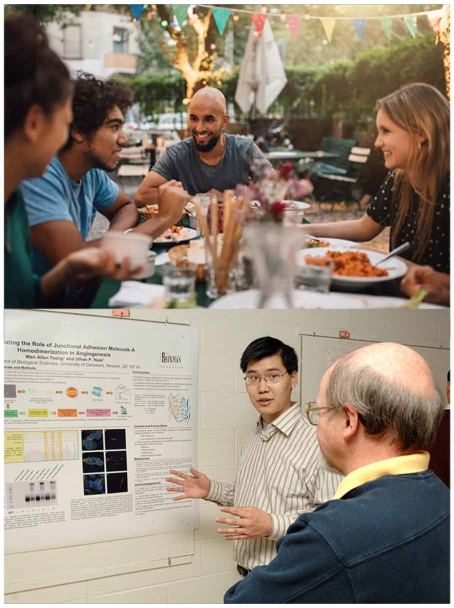

Example: Elevator Pitch

I am a marine parasite ecologist who focuses on the temporal shifts in risk of parasitism in marine mammal populations. Intestinal nematodes of the family Anisakidae have complex life cycles and are trophically transferred to piscivorous marine mammals. With increasing marine mammal populations, the number of definitive hosts available for Anisakidae parasites to exploit increases, increasing reproductive output of the nematodes and potentially increasing the risk to other marine mammal hosts.

Example: Elevator Pitch

I am a marine parasite ecologist who focuses on the temporal shifts in risk of parasitism in marine mammal populations. Intestinal nematodes of the family Anisakidae have complex life cycles and are trophically transferred to piscivorous marine mammals. With increasing marine mammal populations, the number of definitive hosts available for Anisakidae parasites to exploit increases, increasing reproductive output of the nematodes and potentially increasing the risk to other marine mammal hosts.

Commercial whaling, seal hunting, and other forms of exploitation decimated many marine mammal populations. Since these exploits have ended, many marine mammal species have increased, while others still teeter on the brink of extinction. We wanted to know if the parasites that infect the healthy marine mammals could be increasing with their populations, and infecting other, at-risk marine mammals through the fish they eat. We studied the change in parasite infections in fish prey species to see if there's been a change in risk over time.

But…

… you can only hold someone's attention for so long.

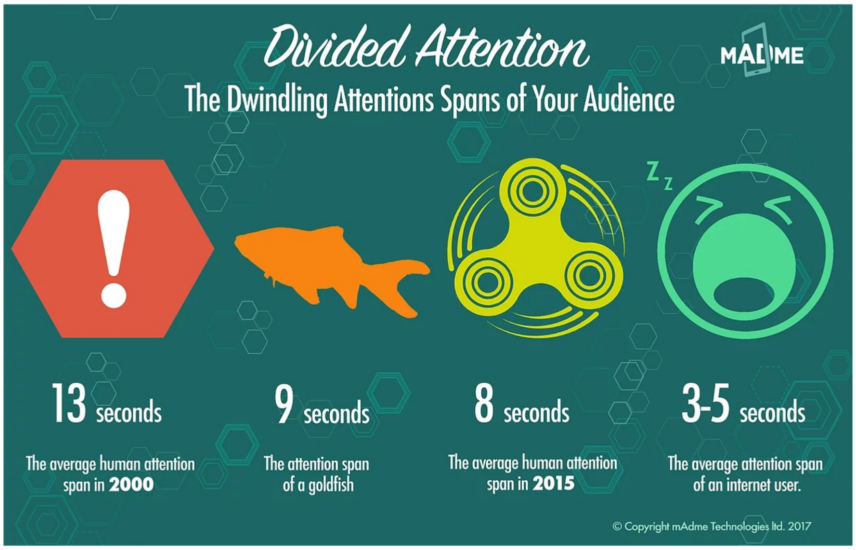

Divided Attention

The Dwindling Attentions Spans of Your Audience

MADME

13 seconds

The average human attention span in **2000**

9 seconds

The attention span of a goldfish

8 seconds

The average human attention span in **2015**

3-5 seconds

The average attention span of an internet user.

Activity: Speed Pitches

Speed Pitches

- Partner with someone in your group
- You'll each get 90 seconds to deliver an elevator pitch about your science or a scientific topic you know a lot about
- After the first iteration, you'll deliver your pitch again, but this time with 60 seconds.
- Then 30 seconds
- Then 15 seconds
- Then 8 seconds
- After the 8 second pitches, talk to your partner! Ask them for feedback, whether you captured their attention, and what they would do differently

Example

From NBC News

Speed Pitches

- Partner with someone in your group
- You’ll each get 90 seconds to deliver an elevator pitch about your science or a scientific topic you know a lot about
- After the first iteration, you’ll deliver your pitch again, but this time with 60 seconds.
- Then 30 seconds
- Then 15 seconds
- Then 8 seconds
- After the 8 second pitches, talk to your partner! Ask them for feedback, whether you captured their attention, and what they would do differently

Skeptical audiences

Some audiences may be hostile to your ideas

About 40% of Americans believe a divinity created humanity in its current form less than 10,000 years ago.[1]

In 2010, over 25% of surveyed parents reported concerns that vaccine ingredients might be unsafe or cause learning disabilities.[2]

[1] Pobiner. 2016. *American Journal of Physical Anthropology.*
[2] Kennedy et al. 2010. *Health Affairs.*

Myths are side effects of evolution

“One of the reasons why [myths] spring up with such regularity is due to our desire to impose structure on the world and incredible ability to recognise patterns.”

“[...] we are social animals and our status in that society is much more important (from an evolutionary standpoint) than being right.”

Lorch. 2017. *The Conversation*.

Basic science education is lacking

Image credit: [normaals]()

Image credit: Adam Hoglund/Shutterstock

How to correct misinformation

- Find common ground
- Focus on your message and replace the myth
- Offer explanations that fit with their world view
- Engage the audience in brainstorming counterarguments

Lorch. 2017. *The Conversation*.
Cook. 2015. *The Conversation.*
Donnelly. 2017. *Shelter.*
Shermer. 2017. *Scientific American.*
Association for Psychological Science. 2017.

Myth busting via “technique rebuttal”

- Science deniers draw on flawed reasoning techniques
- Identifying flawed techniques can mitigate misinformation
- Need to build trust first

From McIntyre, L. “Talking to science deniers and sceptics is not hopeless,” Nature, 5 Aug 2021

Avoid the B’s: ‘backfiring’ and ‘boomerangs’

Backfiring: Myth becomes more memorable than the correction

Boomerang: Correction causes people to develop a stronger dislike for the opposing argument

Lorch. 2017. *The Conversation*.

What does it look like?

“I let them speak, then followed up with questions once the dialogue was rolling. Instead of refuting arguments, I asked, “What evidence might change your mind?” If they said they needed ‘proof’, I asked why existing evidence was insufficient. If they shared a conspiracy theory, I asked why they trusted the evidence for it. By doing that — and not monologuing the facts — I was able to let them wonder why they couldn’t answer my questions.”

- Lee McIntyre, on talking with flat-earthers at a flat-earth conference

From “Talking to science deniers and sceptics is not hopeless,” Nature, 5 Aug 2021

Difficult conversations

Improv game: Yes and…

1) In your groups, build a story one sentence at a time
2) One person starts

“Once there was an angry potato named Hank”

1) The next person continues with Yes and…

“Yes, and one day Hank started yelling at Charlie the broccoli for no reason”

1) Embrace whatever was said before
2) After finishing the circle, someone new starts

Productive conversations...

…find common ground by listening.

…are not held to “win”.

…focus on why the information matters to someone.

First rule of communication: *Know your Audience!*

- **Why** might this person have this perspective?
  Apathy, **skepticism**, **animosity**
- How have this person's **experiences** influenced their thinking?
- How can I connect with this person - what **common goals** do we share?

What **doesn't** work:

I don't want to get my child vaccinated.

But according to the CDC, the number of vaccine-related complications in the US is miniscule. *(Evidence)*

Why should I believe the government? They just want to push vaccines on us that aren't safe. *(Disqualifies evidence)*

But there is no evidence that vaccines aren't safe. The study linking autism to vaccines was debunked.

My friend's child got sick after getting vaccinated. There's no way I'm going to endanger my child.

A Framework for Productive Conversations

Step 1: Get more information - ask questions!

I don’t want to get my child vaccinated.

What concerns do you have about vaccines?

A Framework for Productive Conversations

Step 2: Accurately restate the other person’s viewpoint & try to find common ground.

I’m afraid that vaccines will hurt my child. They are full of chemicals I can’t pronounce and they can have horrible side-effects. My friend’s child got really sick after getting a vaccine.

So you don’t want to vaccinate your child because you want to protect them from harmful side effects. I also want to ensure we give children every resource we can to grow up healthy.

A Framework for Productive Conversations

Step 3: Share your perspective (stories are great!) and consider reframing the problem.

Right, and I've heard terrible stories about how vaccines have hurt children.

Vaccines, like any medical intervention, can have side effects - even though they are very rare. Unfortunately not getting vaccinated can have side effects too. I recently worked with a patient who…

Activity

1) Your will be given envelopes of prompts sorted by field of expertise - grab one prompt from your field but **do not look!**
2) Pair up with someone in your group, and switch prompts with them
3) One person is an expert, the other person has a specific take on something related to your field (range of silly vs. legitimate)
4) Have productive conversation following the framework (remember, your goal is not to "win"!)
5) Discuss what worked well and what did not

Activity

1) Grab a prompt from your field
2) Pair up with someone and switch prompts
3) One person is the expert, one person has a take (on the prompt)
4) Have a productive conversation
5) Discuss

Framework:

Step 1: Get more information - ask questions!

Step 2: Accurately restate the other person’s viewpoint & try to find common ground.

Step 3: Share your perspective (STORIES STORIES STORIES) and consider reframing the problem.

In summary

- Preparation & improv techniques can build confidence for public speaking and responding to unexpected situations
- When trying to correct a myth, don’t challenge their world view and replace the myth with something stickier
- Approach difficult conversations by learning about the person you’re speaking to and trying to find common ground

Thank you SciTalk 2023!

Help us improve our workshop! Follow the QR code below to fill out a survey.

Works Cited

- Association for Psychological Science. (2017). Counterarguments are critical to debunking misinformation.
- Cook, J. (2015). Busting myths: a practical guide to countering science denial. *The Conversation.*
- Corner, A. (2012). Science literacy and climate views. *Nature Climate Change*, *2*(10), 710–711. https://doi.org/10.1038/nclimate1700
- Donnelly, P. (2017). Busting some myths: why myth busting doesn't work. *Shelter*.
- Edwards, V. V. 5 Vocal Warm Ups Before Meetings, Speeches and Presentations. www.scienceofpeople.com/vocal-warm-ups/
- Fiske, S. T. (2018). Stereotype Content: Warmth and Competence Endure. *Curr Dir Psychol Sci.*
- Kahan, D. (2010). Fixing the communications failure. *Nature*, *463*(7279), 296–297. https://doi.org/10.1038/463296a
- Kennedy A., Lavail K., Nowak G., Basket M., and Landry S.: Confidence about vaccines in the United States: understanding parents' perceptions. Health Aff (Millwood) 2011; 30: pp. 1151-1159
- Lorch, M. (2017). Why people believe in conspiracy theories – and how to change their minds. *The Conversation.*
- Lord, C. G., Ross, L., & Lepper, M. R. (1979). Biased assimilation and attitude polarization: The effects of prior theories on subsequently considered evidence. *Journal of Personality and Social Psychology*, *37*(11), 2098–2109. https://doi.org/10.1037/0022-3514.37.11.2098
- Maibach, E. W., Nisbet, M., Baldwin, P., Akerlof, K., & Diao, G. (2010). Reframing climate change as a public health issue: an exploratory study of public reactions. *BMC Public Health*, *10*(1), 299. https://doi.org/10.1186/1471-2458-10-299

Works Cited Con't

- McIntyre, L. "Talking to science deniers and sceptics is not hopeless." 5 Aug 2021, Nature. https://www.nature.com/articles/d41586-021-02152-y
- Munro, G. D., & Ditto, P. H. (1997). Biased Assimilation, Attitude Polarization, and Affect in Reactions to Stereotype-Relevant Scientific Information. *Personality and Social Psychology Bulletin*, *23*(6), 636–653. https://doi.org/10.1177/0146167297236007
- Nyhan, B., & Reifler, J. (2010). When Corrections Fail: The Persistence of Political Misperceptions. *Political Behavior*, *32*(2), 303–330. https://doi.org/10.1007/s11109-010-9112-2
- Pobiner, B. (2016). 'Accepting, understanding, teaching and learning (human) evolution: obstacles and opportunities'. American Journal of Physical Anthropology 159 (S61). Supplement: Yearbook of Physical Anthropology, pp. 232–274. https://doi.org/10.1002/ajpa.22910.
- Shermer, M. (2017). How to convince someone when facts fail. *Scientific American.*
- Wood, T., & Porter, E. (2016). The Elusive Backfire Effect: Mass Attitudes' Steadfast Factual Adherence. *SSRN Electronic Journal*. https://doi.org/10.2139/ssrn.2819073
- Conversational framework based on the work of Dr. Karin Tamerius
- Gibberish image: Image by upklyak on Freepik

Appendix D: Slides to communicate new research findings to patients

Presented at Merkel CELLebration dinner on September 11, 2023

https://www.youtube.com/watch?v=GqavZBPqHbk&t=2184s

Merkel CELLebration Dinner 2023

Welcome...

in-person and online

Online attendees-
please put questions in chat

September 11, 2023
5-6 PM PDT / 8-9 PM EDT

Topics for Today: Future of MCC

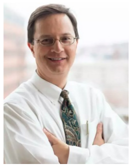

Paul Nghiem
(Herder of Cats)
Overview

Kelsey Cahill
(Research Coordinator)
Newsletter & Website

Patient Story #1

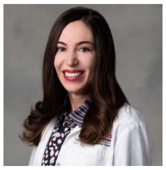

Lisa Zaba
(Stanford Professor)
MCC Blood Tests

Patient Story #2

Saumya Jani
(MD/PhD student)
Insights on Killer T cells

Austin Jabbour & Ariel Finberg
(Clinical Fellows)
Exciting Trials

Patient Story #3

Science updates:

Killer T cells

Diagnosis → Initial Treatment → Surveillance → Recurrence → Refractory

‘Killer T cells’ kill cancer cells

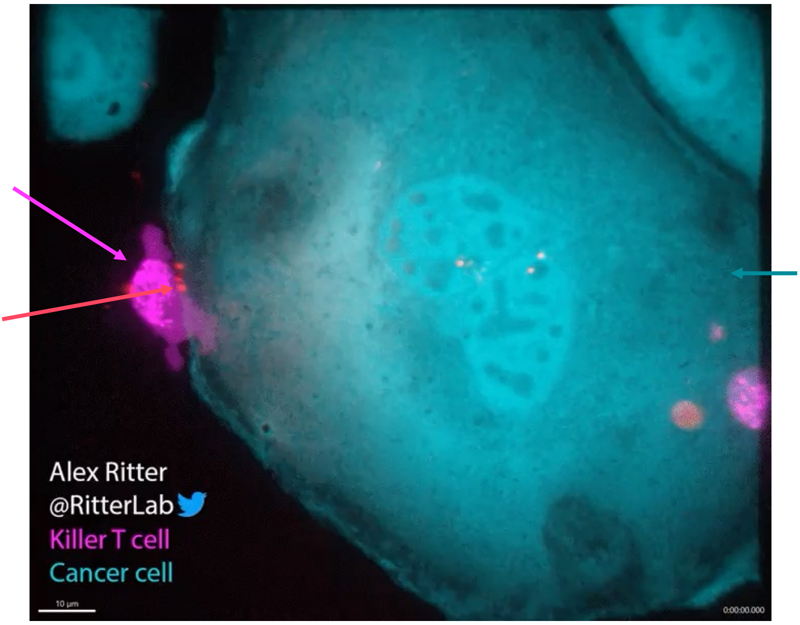

Killer T cell

Cellular ‘grenades’

Cancer cell

(Dying cell)

Killer T cells mission: via T cell receptor

James Bond

Villain

T cell receptor

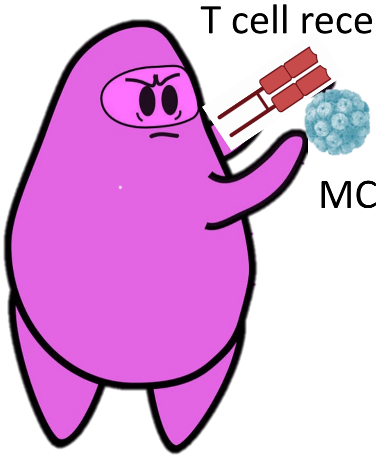

MCC

Killer T cell

Killer T cells travel to tumors through the blood

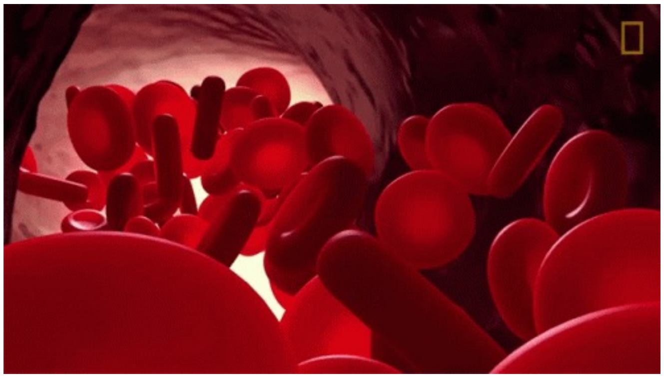

T cells travel through the blood to find tumors

Does a T cell target MCC?

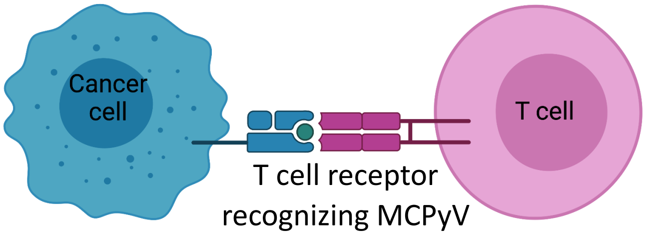

T cell receptor recognizing MCPyV

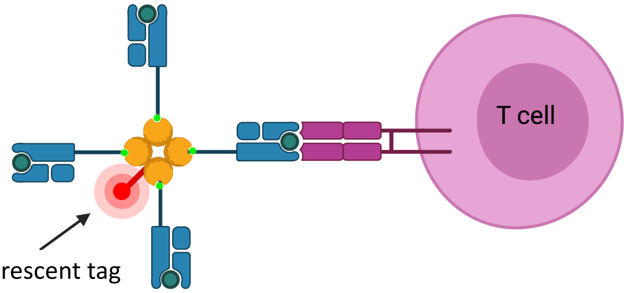

Fluorescent tag

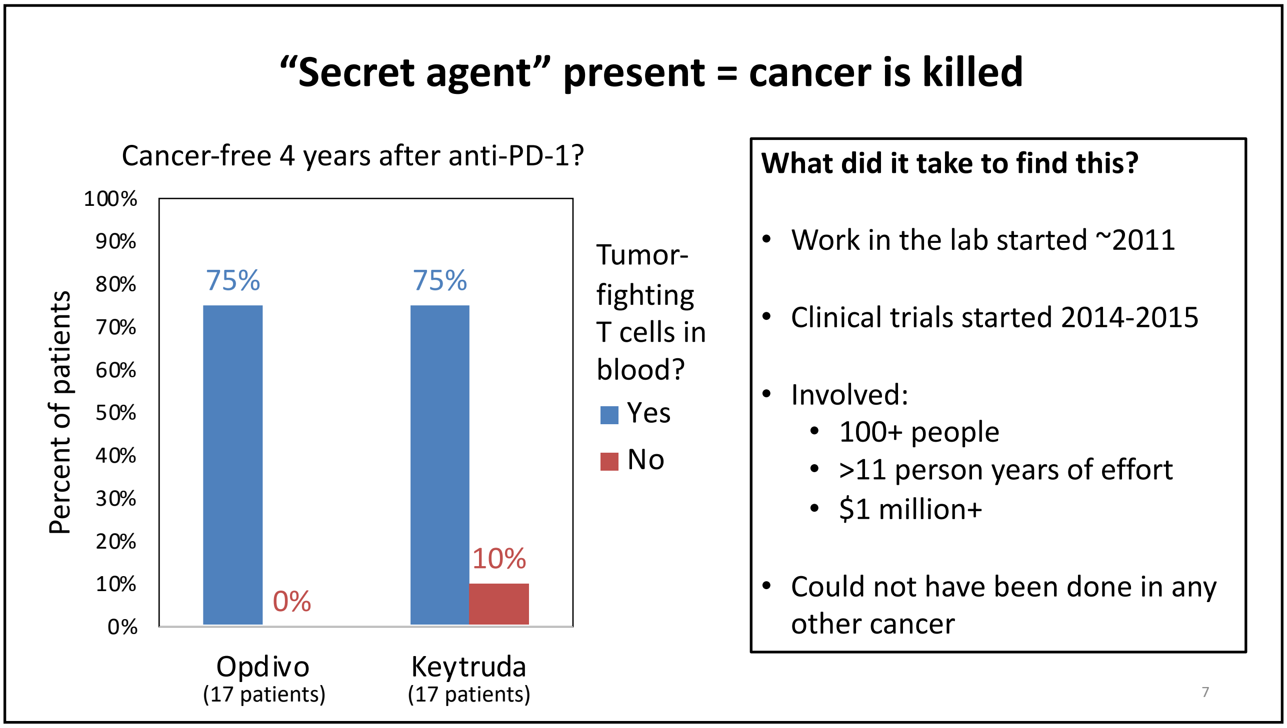

"Secret agent" present = cancer is killed

Cancer-free 4 years after anti-PD-1?

What did it take to find this?

- Work in the lab started ~2011
- Clinical trials started 2014-2015
- Involved:
  - 100+ people
  - >11 person years of effort
  - $1 million+
- Could not have been done in any other cancer

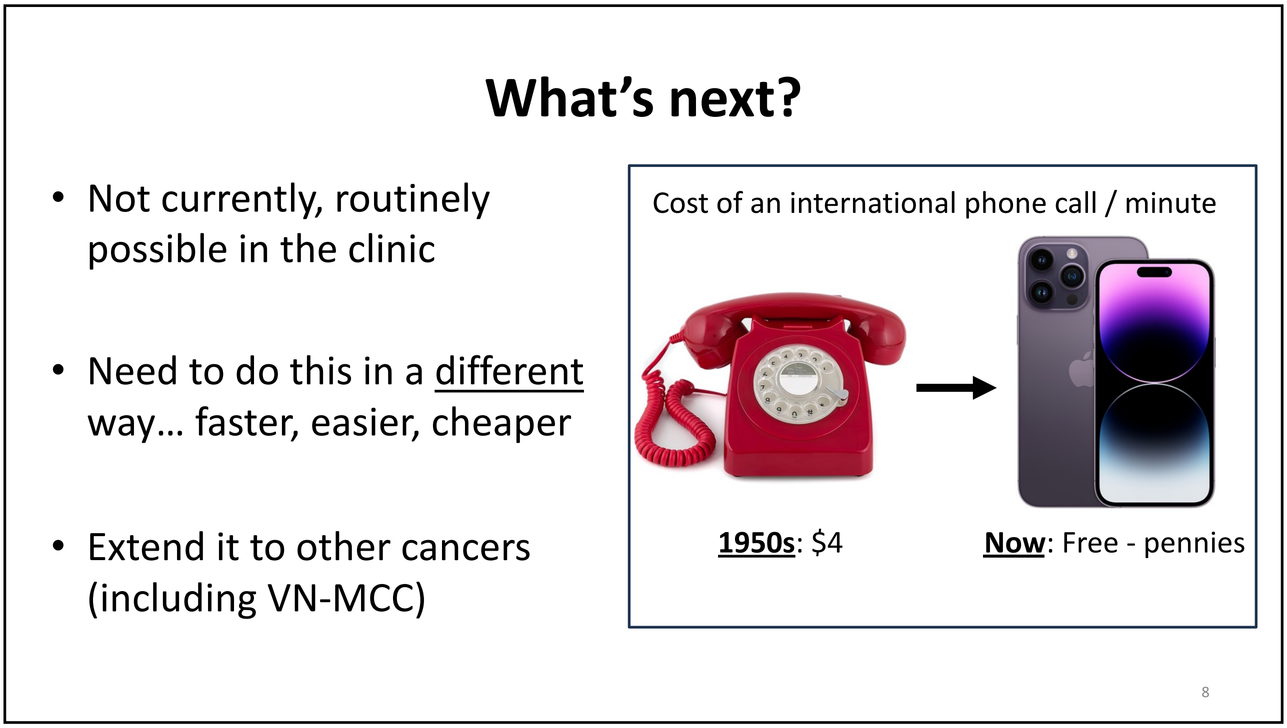

What's next?

- Not currently, routinely possible in the clinic
- Need to do this in a <u>different</u> way… faster, easier, cheaper
- Extend it to other cancers (including VN-MCC)

Cost of an international phone call / minute

<u>1950s</u>: $4

<u>Now</u>: Free - pennies

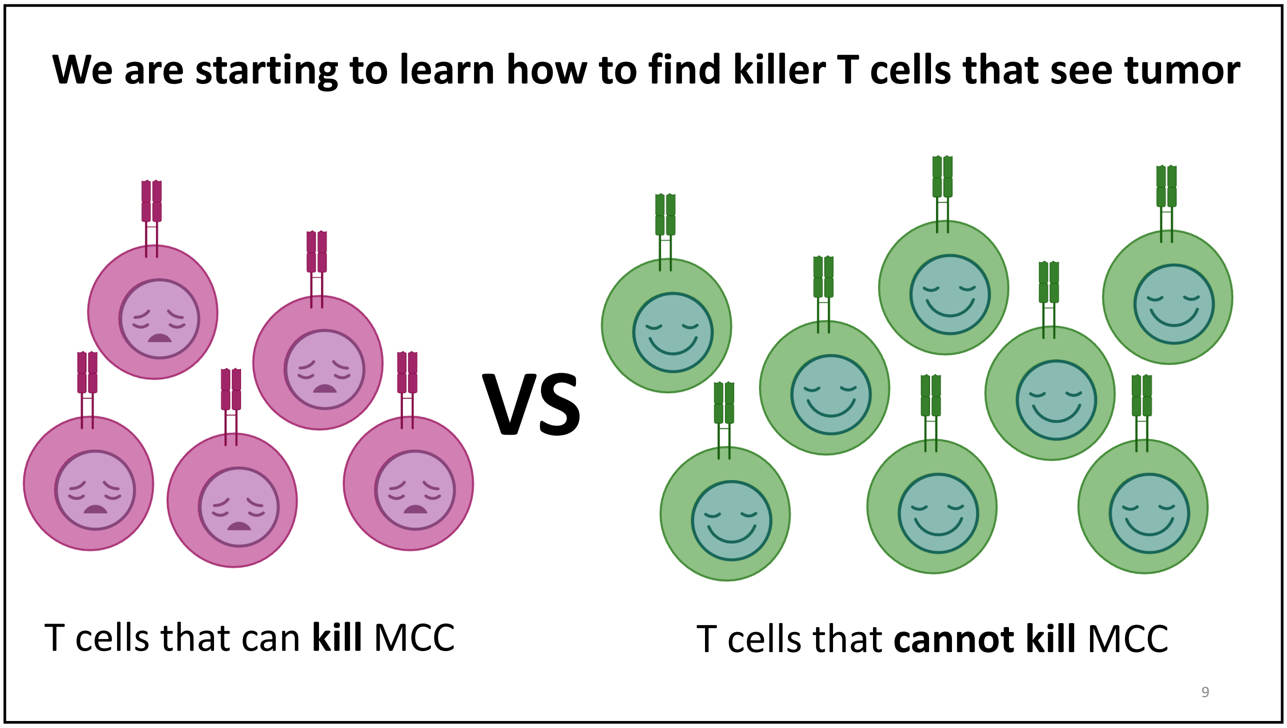

We are starting to learn how to find killer T cells that see tumor

VS

T cells that can **kill** MCC

T cells that **cannot kill** MCC

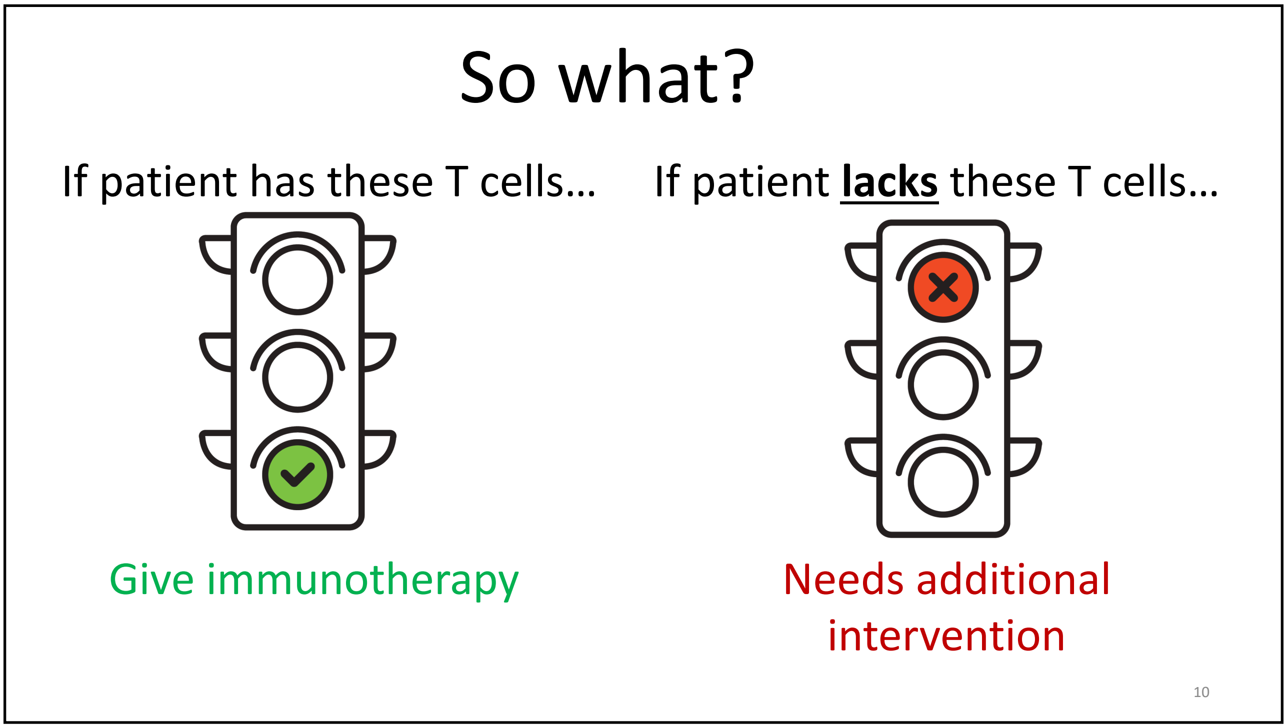

So what?

If patient has these T cells…

If patient **lacks** these T cells…

Give immunotherapy

Needs additional intervention

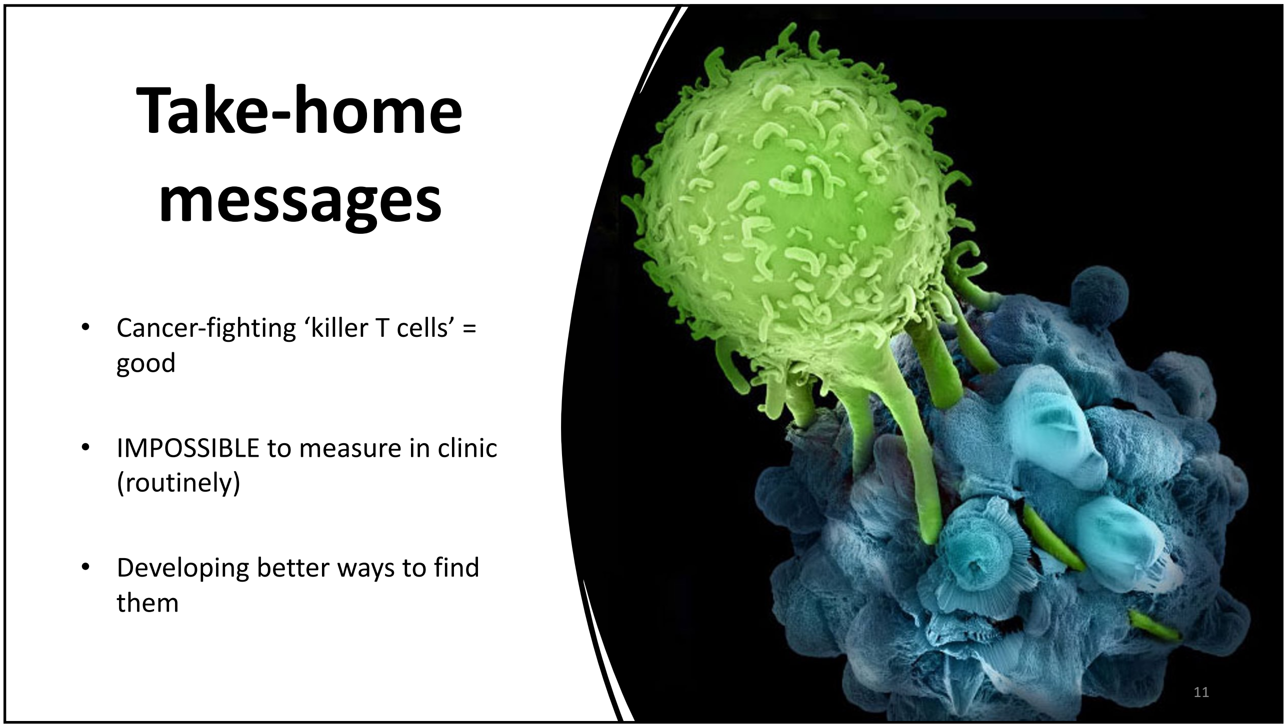

Take-home messages

- Cancer-fighting ‘killer T cells’ = good
- IMPOSSIBLE to measure in clinic (routinely)
- Developing better ways to find them

Thank you!